Solid Mechanics and Its Applications

George Dvorak

Micromechanics of Composite Materials

Springer

Micromechanics of Composite Materials

SOLID MECHANICS AND ITS APPLICATIONS
Volume 186

Series Editors: G.M.L. GLADWELL
Department of Civil Engineering
University of Waterloo
Waterloo, Ontario, Canada N2L 3GI

Aims and Scope of the Series

The fundamental questions arising in mechanics are: *Why?*, *How?*, and *How much?* The aim of this series is to provide lucid accounts written by authoritative researchers giving vision and insight in answering these questions on the subject of mechanics as it relates to solids.

The scope of the series covers the entire spectrum of solid mechanics. Thus it includes the foundation of mechanics; variational formulations; computational mechanics; statics, kinematics and dynamics of rigid and elastic bodies: vibrations of solids and structures; dynamical systems and chaos; the theories of elasticity, plasticity and viscoelasticity; composite materials; rods, beams, shells and membranes; structural control and stability; soils, rocks and geomechanics; fracture; tribology; experimental mechanics; biomechanics and machine design.

The median level of presentation is the first year graduate student. Some texts are monographs defining the current state of the field; others are accessible to final year undergraduates; but essentially the emphasis is on readability and clarity.

For further volumes:
http://www.springer.com/series/6557

George J. Dvorak

Micromechanics of Composite Materials

Springer

George J. Dvorak
Mechanical, Aeronautical and Nuclear
Engineering
Rensselaer Polytechnic Institute
Troy, NY
USA

ISSN 0925-0042
ISBN 978-94-007-4100-3 ISBN 978-94-007-4101-0 (eBook)
DOI 10.1007/978-94-007-4101-0
Springer Dordrecht Heidelberg New York London

Library of Congress Control Number: 2012954814

To the memory of my father
– JUDr. Jiří Dvořák 1899–1973

Preface

Few, if any, accomplishments of solid mechanics research in the second half of the last century can match those associated with modeling of heterogeneous solids, in support of the development of composite materials and their use in numerous structural applications. From their early introduction in high performance aircraft and spacecraft, electronic packaging, and thermal management, boats and sports equipment, to their recent adoption in ship and marine construction, oil exploration and production, bridges, and road and rail vehicles, composite and sandwich structures have not only replaced more traditional materials, but enabled production of entirely new devices and structures.

Among the many subjects in micromechanics, this book outlines several key subjects on modeling of composites reinforced by particles of various shapes, aligned fibers, symmetric laminated plates and metal matrix composites. Solved problems are presented in several parts of the book. The first two chapters on notation and anisotropic solids briefly summarize well know topics, and point out how they should be interpreted in present applications. The third chapter is a collection of different concepts that are useful in understanding properties of heterogeneous media, and of solution strategies, theorems and connections that lead to evaluation of local field averages and of overall property estimates and bounds.

The next Chap. 4 focuses on elastic solutions of strain and stress fields at inclusions, inhomogeneities and cavities embedded either alone or in a dilute distribution in a common matrix. Green's functions, Eshelby tensors as well as the coefficients of the analogous $\boldsymbol{P}$ tensors for common ellipsoidal inclusions shapes and cracks are derived and listed for future use. Potential and interaction energies generated by addition of inhomogeneities, cavities or cracks to uniformly deformed or internally transformed elastic solids are evaluated for several loading conditions in Chap. 5. The next two Chaps. 6 and 7 describe derivation of bounds on and estimates of overall elastic moduli and local field averages of particulate and fibrous composites. Apart from numerous specific results, we emphasize connections between different methods, such as those between the Hashin-Shtrikman bounds and the self-consistent and Mori-Tanaka methods. Restrictions on shape and alignment of constituents of material microstructures that assure diagonal symmetry of overall

stiffness and compliance matrices are examined in detail. Models suitable for more diverse microstructures are based on double inclusion or double inhomogeneity configurations.

A separate Chap. 8 is devoted to analysis of transformation strains, which include eigenstrains caused by thermal, inelastic and other stress-free deformations, and of their effect on phase fields and overall response. Chapter 9 is concerned with local fields at perfect and imperfect interfaces and at different interphases between inhomogeneities or reinforcements and matrix. A connection between local displacement jumps and overall deformation is established by introduction of damage-equivalent eigenstrains.

Application of micromechanical methods to symmetric laminates is discussed in Chap. 10. Many different problems are treated here, such as design of laminates for pressure vessels, dimensionally stable and auxetic laminates, laminates with fiber prestress for damage mitigation or for reduction of free edge stress concentrations, and the role of transverse cracks on stiffness changes in fibrous plies embedded in laminated plates.

Chapter 11 is concerned with elastic-plastic materials. An overview of the incremental plasticity theory, including hardening and flow rules derived from a double surface model leads to matrix form of the instantaneous stiffness and compliance and thermal strain and stress vectors. The final Chap. 12 discusses the transformation field analysis (TFA) of inelastic composites, including unit cell models, yield and loading surfaces, overall response under thermoplastic deformation, and modification of the TFA method by other authors. Experimental results obtained from monitoring the deformation of thin-walled unidirectional boron/aluminum tubes loaded along a complex loading path provide support for certain parts of the bimodal plasticity theory, the preferred analytical model. Numerical implementation of the TFA method shows generally good agreement with observed plastic strains and their directions, but the analytical model can approximate only yield and loading surfaces. Analysis of thermal hardening in two-phase particulate and fiber composites, laminated plates and multiphase systems, is followed by a discussion of the utility of plasticity theories, that completes the last chapter.

The subject is of course much broader and cannot be covered in a single publication. Thousands of papers and several books have been published over the years. However, this text can introduce the reader to many aspects of the field. It is intended to advanced undergraduate and graduate students, researchers and engineers interested and involved in analysis and design of composite structures. Educational background in continuum mechanics, elasticity, fracture mechanics and plasticity should facilitate understanding.

The author is indebted to several former graduate students and collaborators who have read and contributed to the text. Among those are Professor Y. A. Bahei-El-Din of the British University Cairo, Professor Yakov Benveniste of Tel Aviv University, Professor Tungyang Chen of the National Cheng Kung University in Taiwan, who had also drafted parts of Sects. 2.5, 4.5 and 9.1, and Professor

Richard M. Christensen of Stanford University. Special thanks are due to Dr. Alexander P. Suvorov of McGill University who had carefully read the manuscript, offered numerous suggestions and had drawn many new figures. Cooperation of Mr. S. Karthigayan, production manager at www.spi-global.com, in finishing the final manuscript is much appreciated.

Contents

Chapter 1
Tensor Component and Matrix Notations

Derivations and presentations of results in this book will appear in the tensor components, or in the related matrix notation. *In the tensor component or subscript notation,* vectors or first-order tensors are denoted by lower case italics with a single letter subscript, such as n_i or v_j, while second, third and fourth-order tensors are written as ε_{ij}, $\in_{ijk}$, L_{ijkl}, with the number of subscripts indicating the order or rank R of the tensor. The subscripts have a certain assigned range of values, which is i, $j, \ldots = 1, 2, 3$, or $\rho = 3$ for tensorial quantities in the Cartesian coordinates x_i. The number of tensor components is $N = R^\rho$. It is then convenient to write the components of a first, second or fourth order tensors as (3×1), (3×3) or (9×9) arrays, which need not conform to the rules of matrix algebra. The third order tensor can be displayed in three (3×3) arrays.

Relations between tensor quantities must be written in a form that is preserved under coordinate transformations. However, magnitudes of the tensor components depend on the particular orientation of the coordinate system, and they change according to the rules for transformation of Cartesian tensors. Transformations from the current coordinates x_j to the new, primed coordinates x'_i, are described by

$$n'_i = a_{ij} n_j \quad \varepsilon'_{ij} = a_{ik} a_{jl} \varepsilon_{kl} \quad \in'_{ijk} = a_{ip} a_{jq} a_{kr} \in_{pqr} \quad L'_{ijkl} = a_{ip} a_{jq} a_{kr} a_{ls} L_{pqrs} \tag{1.1.1}$$

where $a_{ij} = \cos(x'_i, x_j)$ is an orthogonal (3×3) matrix of directional cosines of angles contained by the new (primed) and current (unprimed) coordinates. The primes are added here for emphasis only. It can be verified that $a_{ik} a_{jk} = a_{ki} a_{kj} = \delta_{ij}$, where δ_{ij} is the Kronecker symbol; $\delta_{ij} = 0$ for $i \neq j$, and $\delta_{ij} = 1$ for $i = j$. These connections can be written using bold Roman letters to denote (3×3) matrices and $\mathbf{I}_3$ for the identity matrix, as $\mathbf{a}\mathbf{a}^{\mathrm{T}} = \mathbf{a}^{\mathrm{T}}\mathbf{a} = \mathbf{I}_3 \Rightarrow \mathbf{a}^{\mathrm{T}} = \mathbf{a}^{-1}$, where $\mathbf{a}$ is the proper ($|\mathbf{a}| = +1$) or improper ($|\mathbf{a}| = -1$) orthogonal rotational matrix. Evaluation of the a_{ij} coefficients in an actual transformation is illustrated in Sect. 2.2.1.

Equations involving tensorial quantities must have identical free or single letter subscripts in all monomials. Repeated subscripts can appear only as pairs of

G.J. Dvorak, *Micromechanics of Composite Materials*, Solid Mechanics and Its Applications 186, DOI 10.1007/978-94-007-4101-0_1,

the same two letters, implying summation over the assigned range; for example, $\delta_{kk} = 3$, $\varepsilon_{kk} = \varepsilon_{ij}\delta_{ij} = \varepsilon_{11} + \varepsilon_{22} + \varepsilon_{33}$. Expressions with three or more identical subscripts in a monomial are not defined.

The tensor component notation can be illustrated with reference to the generalized Hooke's law for homogeneous elastic solids, which connects the symmetric, second order stress and small strain tensors σ_{ij} and ε_{kl} by constant, fourth order stiffness or compliance tensors L_{ijkl} or M_{klij}. The latter symbols, introduced by Hill (1963a, 1964), are frequently used in the micromechanics literature. The kernel letters C and S, that denote the same tensors in classical elasticity, are reserved here for different quantities. For example, S_{ijkl} is the Eshelby tensor in Chap. 4.

In the subscript or tensor component notation associated with the Cartesian coordinates x_i $(i = 1, 2, 3)$, the said Hooke's law is written as

$$\left.\begin{aligned} \sigma_{ij} &= L_{ijkl}\varepsilon_{kl} \left(\text{or } \sigma_{ij} = C_{ijkl}\varepsilon_{kl}\right) \\ \varepsilon_{ij} &= M_{ijkl}\sigma_{kl} \left(\text{or } \varepsilon_{ij} = S_{ijkl}\sigma_{kl}\right) \end{aligned}\right\} \tag{1.1.2}$$

The interior product of the stiffness and compliance matrices is

$$L_{ijpq}M_{pqkl} = I_{ijkl} = \frac{1}{2}\left(\delta_{ik}\delta_{jl} + \delta_{il}\delta_{jk}\right) \tag{1.1.3}$$

where I_{ijkl} is the fourth-order identity tensor.

At all interior points of any volume V, the stresses must satisfy the equations of equilibrium, and on any interior interface or exterior surface ∂V, the traction continuity or boundary conditions

$$\sigma_{ij,j} + F_i = 0 \quad \sigma_{ij}n_j - t_i = 0 \tag{1.1.4}$$

where the comma denotes differentiation with respect to x_j; F_i is the body force, n_j is the normal to ∂V directed to the exterior of V, and t_i is the surface traction on ∂V.

When a displacement field is prescribed in V, that has continuous first derivatives and complies with the displacement boundary conditions on ∂V, the strain and rotation components ε_{ij} and ω_{ij} are the symmetric and antisymmetric parts of the strain gradient $u_{i,j}$ in $(1.1.5)_1$. Rigid body rotation is usually disallowed by the boundary conditions. However, if the strains are derived from an equilibrium stress field, then they must satisfy the St. Venant's equations of compatibility $(1.1.5)_2$, which guarantee existence of a continuous displacement field u_i in V. The said relations are

$$\left.\begin{aligned} u_{i,j} &= \frac{1}{2}\left[\left(u_{i,j} + u_{j,i}\right) + \left(u_{i,j} - u_{j,i}\right)\right] = \varepsilon_{ij} + \omega_{ij} \\ \varepsilon_{ij,kl} &+ \varepsilon_{kl,ij} - \varepsilon_{ik,jl} - \varepsilon_{jl,ik} = 0 \end{aligned}\right\} \tag{1.1.5}$$

Symmetry properties of the stiffness and compliance tensors are derived, in part, from the diagonal symmetry $\sigma_{ij} = \sigma_{ji}$ and $\varepsilon_{ij} = \varepsilon_{ji}$ of the stress and strain tensors, which imply corresponding symmetries in the first and second pairs or subscripts

$$L_{ijkl} = L_{jikl} = L_{ijlk} \quad M_{ijkl} = M_{jikl} = M_{ijlk} \tag{1.1.6}$$

These relations reduce the number of independent stiffness or compliance coefficients from 81 to 36. Therefore, the tensors (1.1.6), and any other fourth-order tensors having the indicated symmetry, can be represented by (6×6) arrays, and the stress and strain tensors by (6×1) column arrays. Moreover, as shown next in Sect. 2.1, analysis of the strain energy density function yields diagonal symmetry of both stiffness and compliance tensors and of their matrix equivalents.

$$L_{ijkl} = L_{klij} = L_{jilk} \quad M_{ijkl} = M_{klij} = M_{jilk} \tag{1.1.7}$$

The matrix notation exploits these and related properties to reproduce relations between tensor quantities, in matrix form that is suitable for numerical evaluations. Second order and fourth order symmetric tensors are replaced by (6×1) vectors and (6×6) matrices. Operations with the matrices can be written in direct form using boldface symbols, e.g., $\boldsymbol{\sigma} = \boldsymbol{L\varepsilon}$, $\boldsymbol{\varepsilon} = \boldsymbol{M\sigma}$, $\boldsymbol{M} = \boldsymbol{L}^{-1}$, or with subscripts and summation rules. In the latter case, the range of subscripts is changed from the i, j, $\ldots = 1, 2, 3$, with $\rho = 3$, used in the tensor component notation, to Greek letter subscripts that have the range $\rho = 6$, with $\alpha, \beta, \ldots = 1, 2, \ldots, 6$. Each ij pair is replaced by a single α or β, using the scheme:

$$11 \to 1,\ 22 \to 2,\ 33 \to 3,\ 23 \text{ or } 32 \to 4,\ 31 \text{ or } 13 \to 5,\ 12 \text{ or } 21 \to 6 \tag{1.1.8}$$

In its (9×1) form, the stress vector contains both σ_{jk} and σ_{kj} when $j \neq k$. However, the contracted (6×1) stress vector is written as

$$\sigma = [\sigma_{11},\ \sigma_{22},\ \sigma_{33},\ \sigma_{23},\ \sigma_{31},\ \sigma_{12}]^{\mathrm{T}} = [\sigma_1,\ \sigma_2,\ \sigma_3,\ \sigma_4,\ \sigma_5,\ \sigma_6]^{\mathrm{T}} \tag{1.1.9}$$

These components transform as those of a rank two tensor.

The (9×1) strain vector has the same $j \neq k$ components as the (9×1) stress vector, but it is reduced to its (6×1) form in two different ways in the solid mechanics literature. Used in most papers on mathematical theory of micromechanics, and where appropriate in this book, is the *contracted tensorial strain vector*

$$\boldsymbol{\varepsilon} = [\varepsilon_{11},\ \varepsilon_{22},\ \varepsilon_{33},\ \varepsilon_{23},\ \varepsilon_{31},\ \varepsilon_{12}]^{\mathrm{T}} = [\varepsilon_1,\ \varepsilon_2,\ \varepsilon_3,\ \varepsilon_4,\ \varepsilon_5,\ \varepsilon_6]^{\mathrm{T}} \tag{1.1.10}$$

The above components transform as a tensor, as they do in (1.1.9). In contrast, the *engineering strain vector*, denoted here only for emphasis by the *EG* subscript or superscript, includes shear strains equal to the angles of change of a square element,

which are twice as large as the tensorial shear strains, e.g., $\varepsilon_4^{EG} = 2\varepsilon_{23} = \gamma_{23}$, etc.

$$\boldsymbol{\varepsilon}_{EG} = [\varepsilon_{11},\ \varepsilon_{22},\ \varepsilon_{33},\ 2\varepsilon_{23},\ 2\varepsilon_{31},\ 2\varepsilon_{12}]^{\mathrm{T}} = \left[\varepsilon_1,\ \varepsilon_2,\ \varepsilon_3,\ \varepsilon_4^{EG},\ \varepsilon_5^{EG},\ \varepsilon_6^{EG}\right]^{\mathrm{T}} \tag{1.1.11}$$

Consequences of the distinct strain notations are further discussed in Sect. 2.2.9 on decomposition of isotropic tensors, and in Sects. 2.3.1, 2.3.2 on engineering and Hill's moduli and on Walpole's notation.

The two forms of the strain vector are connected by (6×6) diagonal matrices

$$\boldsymbol{\varepsilon}_{EG} = \boldsymbol{\Theta}\boldsymbol{\varepsilon} \quad \boldsymbol{\varepsilon} = \boldsymbol{\Theta}^{-1}\boldsymbol{\varepsilon}_{EG} \tag{1.1.12}$$

where

$$\boldsymbol{\Theta} = \mathrm{diag}\,(1,\ 1,\ 1,\ 2,\ 2,\ 2) \quad \boldsymbol{\Theta}^{-1} = \mathrm{diag}\left(1, 1, 1, \frac{1}{2}, \frac{1}{2}, \frac{1}{2}\right) \tag{1.1.13}$$

That invites introduction of two distinct matrix notations, henceforth referred to as the ***contracted tensorial notation*** and ***engineering matrix notation*** (*EG*). The two notations will also be applied to eigenstrains or transformations strains, such as thermal or inelastic strains, which do not depend on current mechanical loads, and will therefore be denoted by the kernel letter $\boldsymbol{\mu}$, as discussed in Sect. 3.6. Since stress components remain unchanged, the stiffness and compliance matrices assume different forms in the two notations, as shown in (1.2.9) below.

It is often useful to *decompose the stress and strain tensors* into their isotropic and deviatoric parts

$$\varepsilon_{ij} = \frac{1}{3}\varepsilon_{kk}\delta_{ij} + e_{ij} \quad \sigma_{ij} = \frac{1}{3}\sigma_{kk}\delta_{ij} + s_{ij} \tag{1.1.14}$$

where the Kronecker tensor $\delta_{ij} = 1$ when $i = j$ and $\delta_{ij} = 0$ when $i \neq j$. The deviators have no isotropic component, $e_{kk} = e_{kj}\delta_{kj} = 0$ and $s_{kk} = s_{kj}\delta_{kj} = 0$. A second order symmetric tensor, such as ε_{ij} or σ_{ij} can be contracted to $\varepsilon_{kk} = \varepsilon_{kl}\delta_{kl} = \varepsilon_{ll}$ or $\sigma_{kk} = \sigma_{kl}\delta_{kl}$, so that $\varepsilon_{kk}\delta_{ij} = \varepsilon_{kl}\delta_{ij}\delta_{kl}$, or $\sigma_{kk}\delta_{ij} = \sigma_{kl}\delta_{ij}\delta_{kl}$.

Then, the above decomposition may be written as

$$\varepsilon_{ij} = \left(J_{ijkl} + K_{ijkl}\right)\varepsilon_{kl} \quad \sigma_{ij} = \left(J_{ijkl} + K_{ijkl}\right)\sigma_{kl} \tag{1.1.15}$$

where

$$\left.\begin{aligned} J_{ijkl} = \frac{1}{3}\delta_{ij}\delta_{kl} \quad K_{ijkl} = \frac{1}{2}\left(\delta_{ik}\delta_{jl} + \delta_{il}\delta_{jk}\right) - J_{ijkl} = I_{ijkl} - J_{ijkl} \\ J_{ijkl}J_{lkpq} = J_{ijpq} \quad K_{ijkl}K_{lkpq} = K_{ijpq} \quad J_{ijkl}K_{lkpq} = K_{ijkl}J_{lkpq} = 0 \end{aligned}\right\} \tag{1.1.16}$$

are the idempotent isotropic and deviatoric projection tensors and I_{ijkl} is the identity tensor (1.1.3).

In the contracted tensorial notation, the above results are reproduced using (6×1) vectors and (6×6) matrices. In particular, $\boldsymbol{\delta} = [1,\ 1,\ 1,\ 0,\ 0,\ 0]^{\mathrm{T}}$ is equivalent to the Kronecker tensor δ_{ij}, and the deviatoric parts of $\boldsymbol{\varepsilon}$ in (1.1.10) and of $\boldsymbol{\sigma}$ in (1.1.9) are denoted by

$$\boldsymbol{e} = [e_1,\ e_2,\ e_3,\ e_4,\ e_5,\ e_6]^{\mathrm{T}} \quad \boldsymbol{s} = [s_1,\ s_2,\ s_3,\ s_4,\ s_5,\ s_6]^{\mathrm{T}} \tag{1.1.17}$$

The decomposition (1.1.14) can be transcribed using isotropic and deviatoric projection matrices $\boldsymbol{J} = \boldsymbol{\delta}\boldsymbol{\delta}^{\mathrm{T}}/3$ and $\boldsymbol{K} = \boldsymbol{I} - \boldsymbol{J}$

$$\boldsymbol{\varepsilon} = \frac{1}{3}\boldsymbol{\delta}\boldsymbol{\delta}^{\mathrm{T}}\boldsymbol{\varepsilon} + \boldsymbol{e} = (\boldsymbol{J} + \boldsymbol{K})\,\boldsymbol{\varepsilon} \quad \boldsymbol{\sigma} = \frac{1}{3}\boldsymbol{\delta}\boldsymbol{\delta}^{\mathrm{T}}\boldsymbol{\sigma} + \boldsymbol{s} = (\boldsymbol{J} + \boldsymbol{K})\,\boldsymbol{\sigma} \tag{1.1.18}$$

Evaluation of $\boldsymbol{J}$ and $\boldsymbol{K}$ yields

$$3\boldsymbol{J} = \begin{bmatrix} 1 & 1 & 1 & 0 & 0 & 0 \\ 1 & 1 & 1 & 0 & 0 & 0 \\ 1 & 1 & 1 & 0 & 0 & 0 \\ 0 & 0 & 0 & 0 & 0 & 0 \\ 0 & 0 & 0 & 0 & 0 & 0 \\ 0 & 0 & 0 & 0 & 0 & 0 \end{bmatrix} \quad 3\boldsymbol{K} = \begin{bmatrix} 2 & -1 & -1 & 0 & 0 & 0 \\ -1 & 2 & -1 & 0 & 0 & 0 \\ -1 & -1 & 2 & 0 & 0 & 0 \\ 0 & 0 & 0 & 3 & 0 & 0 \\ 0 & 0 & 0 & 0 & 3 & 0 \\ 0 & 0 & 0 & 0 & 0 & 3 \end{bmatrix} \tag{1.1.19}$$

The projection matrices have the same properties as the projection tensors (1.1.16), $\boldsymbol{J}\boldsymbol{J} = \boldsymbol{J}$, $\boldsymbol{K}\boldsymbol{K} = \boldsymbol{K}$, $\boldsymbol{J}\boldsymbol{K} = \boldsymbol{K}\boldsymbol{J} = 0$. According to (1.1.13), $\boldsymbol{J}\boldsymbol{\Theta} = \boldsymbol{\Theta}\boldsymbol{J}$, hence the products $\boldsymbol{K}\boldsymbol{\varepsilon}$ and $\boldsymbol{K}\boldsymbol{\varepsilon}_{EG}$ modify only the first three components of the strain vectors. Therefore, the decompositions (1.1.15, 1.1.16, 1.1.17, 1.1.18) apply to both contracted tensorial and engineering strains.

Stiffness and compliance tensors (1.1.7) are represented by (6×6) matrices

$$L_{\alpha\beta} = L_{\beta\alpha} \quad M_{\alpha\beta} = M_{\beta\alpha} \quad \boldsymbol{L} = \boldsymbol{L}^{\mathrm{T}} \quad \boldsymbol{M} = \boldsymbol{M}^{\mathrm{T}} \tag{1.1.20}$$

The generalized Hooke's law (1.1.2) and the identity (1.1.3) can then be written in one of three forms, with $i, j = 1, 2, 3$, or with $\alpha, \beta, \ldots = 1, 2, \ldots, 6$

$$\left.\begin{array}{lll} \sigma_{ij} = L_{ijkl}\varepsilon_{kl} & \varepsilon_{ij} = M_{ijkl}\sigma_{kl} & L_{ijpq}M_{pqkl} = I_{ijkl} \\ \sigma_{\alpha} = L_{\alpha\beta}\varepsilon_{\beta} & \varepsilon_{\alpha} = M_{\alpha\beta}\sigma_{\beta} & L_{\alpha\beta}M_{\beta\gamma} = I_{\alpha\gamma} \\ \boldsymbol{\sigma} = \boldsymbol{L}\boldsymbol{\varepsilon} & \boldsymbol{\varepsilon} = \boldsymbol{M}\boldsymbol{\sigma} & \boldsymbol{L}\boldsymbol{M} = \boldsymbol{I} \end{array}\right\} \tag{1.1.21}$$

where $I_{\alpha\gamma}$ and $\boldsymbol{I}$ are (6×6) identity matrices. In applications, the coefficients of the $\boldsymbol{L}$ and $\boldsymbol{M}$ matrices are evaluated in terms of elastic moduli of specific materials. The tensorial stiffness and compliance components L_{ijkl} and M_{klij} may not have assigned values, but are convenient in certain theoretical derivations.

Connections between the contracted tensorial and engineering (*EG*) stiffness and compliance matrices for the isotropic and certain other material symmetries can be recorded as

$$\left.\begin{array}{ll} \boldsymbol{\sigma} = \boldsymbol{L\varepsilon} = \boldsymbol{L}_{EG}\boldsymbol{\varepsilon}_{EG} = \boldsymbol{L}_{EG}\boldsymbol{\Theta\varepsilon} & \boldsymbol{L} = \boldsymbol{L}_{EG}\boldsymbol{\Theta} \\ \boldsymbol{\varepsilon} = \boldsymbol{M\sigma} = \boldsymbol{\Theta}^{-1}\boldsymbol{\varepsilon}_{EG} = \boldsymbol{\Theta}^{-1}\boldsymbol{M}_{EG}\boldsymbol{\sigma} & \boldsymbol{M} = \boldsymbol{\Theta}^{-1}\boldsymbol{M}_{EG} \end{array}\right\} \tag{1.1.22}$$

where $\boldsymbol{\varepsilon}_r$, $\boldsymbol{L}_r$ and $\boldsymbol{M}_r$ or $\boldsymbol{\varepsilon}, \boldsymbol{L}, \boldsymbol{M}$ are affected by and need to be consistently written in each of the two notations. Since the $\boldsymbol{\Theta}$ matrix operates only on the last three rows of the $\boldsymbol{L}_{EG}$ or $\boldsymbol{M}_{EG}$ matrices, diagonal symmetry of the above $\boldsymbol{L}$ and $\boldsymbol{M}$ is preserved as long as the L_{44}^{EG}, L_{55}^{EG} and L_{66}^{EG}, or M_{44}^{EG}, M_{55}^{EG} and M_{66}^{EG} are the sole nonzero coefficients in the last three rows and columns. *Validity of the above connections is restricted to such matrices.* In Chap. 2, those will be identified with orthotropic, tetragonal, transversely isotropic, cubic and isotropic solids. For example, in the latter, the diagonal coefficients $L_{44} = L_{55} = L_{66} = 2G$ change to $L_{44}^{EG} = L_{55}^{EG} = L_{66}^{EG} = G$, and $M_{44} = M_{55} = M_{66} = 1/(2G)$ to $M_{44}^{EG} = M_{55}^{EG} = M_{66}^{EG} = 1/G$. This subset of five material symmetries accommodates most composite materials and their constituents.

Use of engineering strains has an effect on the relationships between the coefficients of the (9×9) and (6×6) stiffness and compliance matrices written in the engineering matrix notation. In particular, $L_{ijkl} \rightarrow L_{\alpha\beta}^{EG}$ according to (1.1.8). However, the (6×6) engineering compliance matrix $M_{\alpha\beta}^{EG}$ is related to M_{ijkl} by $M_{\alpha\beta}^{EG} = M_{ijkl}$ only for $\alpha, \beta \leq 3$, but $M_{\alpha\beta}^{EG} = 2M_{ijkl}$ for either α or $\beta \leq 3$, and $M_{\alpha\beta}^{EG} = 4M_{ijkl}$ when both $\alpha, \beta > 3$. The engineering stiffness and compliance matrices remain diagonally symmetric at all material symmetries, including the trigonal, monoclinic and triclinic symmetries (Ting 1987).

Those and other distinctions should be kept in mind in interpretation of results that appear in many technical publications, albeit without the *EG* subscripts or reference to the noted connections. It should be emphasized that matrix equivalents of tensorial expressions in both notations need to be carefully selected to preserve original properties of the latter, in order to obtain correct numerical results. In the chapters that follow, we will use the notation appropriate for a particular topic.

Of course, the (6×1) and (6×6) matrices (1.1.9, 1.1.10, 1.1.11) and (1.1.20) do not transform as do Cartesian tensors in (1.1.1), even though both transformations are always defined by the same single matrix of directional cosines $a_{ij} = \cos\left(x_i', x_j\right)$ of angles relating the new to current coordinate systems. Instead, the matrices are transformed using the (6×6) matrix $\boldsymbol{X}$ generated from the $a_{ik}a_{jl}$ products of the directional cosines, in agreement with (1.1.1), and the summation and contraction rules. Lekhnitskii (1950) and Ting (1987, 1996) show coefficients of the $\boldsymbol{X}$ matrix (denoted by $\boldsymbol{K}$ in the latter)

$$\boldsymbol{X} = \begin{bmatrix} \mathbf{a}_1 & 2\mathbf{a}_2 \\ \mathbf{a}_3 & \mathbf{a}_4 \end{bmatrix} \tag{1.1.23}$$

where

$$\mathbf{a}_1 = \begin{bmatrix} a_{11}^2 & a_{12}^2 & a_{13}^2 \\ a_{21}^2 & a_{22}^2 & a_{23}^2 \\ a_{31}^2 & a_{32}^2 & a_{33}^2 \end{bmatrix} \tag{1.1.24}$$

$$\mathbf{a}_2 = \begin{bmatrix} a_{12}a_{13} & a_{13}a_{11} & a_{11}a_{12} \\ a_{22}a_{23} & a_{23}a_{21} & a_{21}a_{22} \\ a_{32}a_{33} & a_{33}a_{31} & a_{31}a_{32} \end{bmatrix} \quad \mathbf{a}_3 = \begin{bmatrix} a_{21}a_{31} & a_{22}a_{32} & a_{23}a_{33} \\ a_{31}a_{11} & a_{32}a_{12} & a_{33}a_{13} \\ a_{11}a_{21} & a_{12}a_{22} & a_{13}a_{23} \end{bmatrix} \tag{1.1.25}$$

$$\mathbf{a}_4 = \begin{bmatrix} a_{22}a_{33} + a_{23}a_{32} & a_{23}a_{31} + a_{21}a_{33} & a_{21}a_{32} + a_{22}a_{31} \\ a_{32}a_{13} + a_{33}a_{12} & a_{33}a_{11} + a_{31}a_{13} & a_{31}a_{12} + a_{32}a_{11} \\ a_{12}a_{23} + a_{13}a_{22} & a_{13}a_{21} + a_{11}a_{23} & a_{11}a_{22} + a_{12}a_{21} \end{bmatrix} \tag{1.1.26}$$

The $\boldsymbol{X}$ matrix is not orthogonal, however, its determinant $|\boldsymbol{X}| = \pm 1$.
The contracted stress and tensorial strain components then transform as

$$\boldsymbol{\sigma}' = \boldsymbol{X}\boldsymbol{\sigma} \quad \boldsymbol{\varepsilon}' = \boldsymbol{X}\boldsymbol{\varepsilon} \tag{1.1.27}$$

and the contracted tensorial stiffness and compliance matrices as

$$\boldsymbol{L}' = \boldsymbol{X}\,\boldsymbol{L}\,\boldsymbol{X}^{-1} \quad \boldsymbol{M}' = \boldsymbol{X}\,\boldsymbol{M}\,\boldsymbol{X}^{-1} \tag{1.1.28}$$

Transformation of the engineering strains according to (1.1.12), $\boldsymbol{\varepsilon}'_{EG} = \boldsymbol{\Theta}\boldsymbol{\varepsilon}'$, $\boldsymbol{\varepsilon}_{EG} = \boldsymbol{\Theta}\boldsymbol{\varepsilon}$, yields

$$\boldsymbol{\varepsilon}'_{EG} = \boldsymbol{\Theta}\boldsymbol{X}\boldsymbol{\Theta}^{-1}\,\boldsymbol{\varepsilon}_{EG} = \left(\boldsymbol{X}^{-1}\right)^{\mathrm{T}}\boldsymbol{\varepsilon}_{EG} \tag{1.1.29}$$

where the equality follows from rewriting (1.1.13), and from (1.1.23)

$$\boldsymbol{\Theta} = \begin{bmatrix} \mathbf{I} & \mathbf{0} \\ \mathbf{0} & 2\mathbf{I} \end{bmatrix} \quad (\boldsymbol{X}^{-1})^{\mathrm{T}} = \begin{bmatrix} \mathbf{a}_1 & \mathbf{a}_2 \\ 2\mathbf{a}_3 & \mathbf{a}_4 \end{bmatrix} \tag{1.1.30}$$

The engineering stiffness and compliance matrices then transform as

$$\boldsymbol{L}'_{EG} = \boldsymbol{X}\,\boldsymbol{L}_{EG}\boldsymbol{X}^{\mathrm{T}} \quad \boldsymbol{M}'_{EG} = \left(\boldsymbol{X}^{-1}\right)^{\mathrm{T}}\boldsymbol{M}_{EG}\boldsymbol{X}^{-1} \tag{1.1.31}$$

These transformations are useful, for example, in analysis of ellipsoidal inclusions and inhomogeneities. In their principal system, properties of the latter are described by certain (6×6) matrices; the stiffness $\boldsymbol{L}$ selected according to the material symmetry of the inhomogeneity in Sect. 2.2, and the matrix $\boldsymbol{P}$ derived from their shape and orientation in Sect. 4.6. A change in orientation of the ellipsoids requires transformation of anisotropic $\boldsymbol{L}$ and/or $\boldsymbol{P}$ to new coordinates.

A special form of this coordinate transformation, involving rotation about a single axis, finds frequent use in operations with the plane stress stiffness matrix of a composite ply in analysis of fibrous laminates. Selecting x_3 as the axis of rigid body rotation by an angle θ, measured counter-clockwise from $\theta = 0$ at $x_2 = 0$, with $m = \cos\theta$, $n = \sin\theta$, yields

$$\boldsymbol{X} = \begin{bmatrix} m^2 & n^2 & 0 & 0 & 0 & 2mn \\ n^2 & m^2 & 0 & 0 & 0 & -2mn \\ 0 & 0 & 1 & 0 & 0 & 0 \\ 0 & 0 & 0 & m & -n & 0 \\ 0 & 0 & 0 & n & m & 0 \\ -mn & mn & 0 & 0 & 0 & m^2 - n^2 \end{bmatrix} \tag{1.1.32}$$

$$\boldsymbol{X}^{-1}(m, n) = \boldsymbol{X}(m, -n) \tag{1.1.33}$$

Among the coordinate transformations defined by the matrix of directional cosines $a_{ij} = \cos\left(x'_i, x_j\right)$ is that which converts the current square matrix of stress, strain, stiffness or compliance into its diagonal form. That yields nonzero coefficients which are eigenvalues of the matrix. For each eigenvalue λ of a square matrix $\boldsymbol{A}$ there exists an eigenvector $\boldsymbol{x}$ aligned with one of the principal directions of the matrix. They follow from the nontrivial solution of

$$(\boldsymbol{A} - \lambda \boldsymbol{I})\,\boldsymbol{x} = 0 \Rightarrow |\boldsymbol{A} - \lambda \boldsymbol{I}| = 0 \tag{1.1.34}$$

Expansion of the determinant yields the characteristic equation for the n eigenvalues

$$\lambda^n - I_1\lambda^{n-1} + \cdots + (-1)^{n-1}\lambda I_{n-1} + (-1)^n I_n = 0 \tag{1.1.35}$$

where the coefficients $I_1, \ldots, I_n$ are functions of the coefficients of $\boldsymbol{A}$, invariant under any coordinate transformation. For example, the first and last invariants are

$$I_1 = \sum_{i=1}^{n} \lambda_i = \mathrm{tr}\boldsymbol{A} \quad I_n = \prod_{i=1}^{n} \lambda_i = |\boldsymbol{A}| \tag{1.1.36}$$

Each eigenvalue λ, a root of (1.1.35), is substituted into $(1.1.34)_1$ to yield one of the n unit vectors $\boldsymbol{x}$.

For example, a (3×3) matrix $\boldsymbol{A} = \boldsymbol{A}^{\mathrm{T}}$

$$\boldsymbol{A} = \begin{bmatrix} A_{11} & A_{12} & A_{13} \\ & A_{22} & A_{23} \\ & & A_{33} \end{bmatrix} \tag{1.1.37}$$

has three invariants

$$
\begin{aligned}
I_1 &= A_{11} + A_{22} + A_{33} = \lambda_1 + \lambda_2 + \lambda_3 \\
I_2 &= \begin{vmatrix} A_{11} & A_{12} \\ A_{12} & A_{22} \end{vmatrix} + \begin{vmatrix} A_{22} & A_{23} \\ A_{23} & A_{33} \end{vmatrix} + \begin{vmatrix} A_{11} & A_{13} \\ A_{13} & A_{33} \end{vmatrix} = \lambda_1\lambda_2 + \lambda_2\lambda_3 + \lambda_3\lambda_1 \\
I_3 &= |\boldsymbol{A}| = \lambda_1\lambda_2\lambda_3
\end{aligned} \tag{1.1.38}
$$

Eigenvalues are obtained by solving

$$\lambda^3 - I_1\lambda^2 + I_2\lambda - I_3 = 0 \tag{1.1.39}$$

The coordinate directions of each of the three unit vectors $\boldsymbol{x}$ that belongs to one of the three principal values $\lambda^{(p)}$ follow from (1.1.34), which can be simplified by resorting to the tensorial form A_{ij} of $\boldsymbol{A}$. For each $\lambda^{(p)}$ there are three equations for ν_i

$$\left(A_{ij} - \lambda^{(p)}\delta_{ij}\right)\nu_i = 0 \tag{1.1.40}$$

which are complemented by the connection $\nu_1^2 + \nu_2^2 + \nu_3^2 = 1$. The three components ν_i provide one row of the matrix of directional cosines $a_{ji} = \cos\left(x'_j,\ x_i\right)$ for each direction associated with one of the principal values $\lambda^{(p)}$. Evaluation of principal values of stress and strain tensors and of the principal directions is one of the frequent applications of the above procedure.

We note in passing that a coordinate transformation of strain or stress or other tensors of the second rank, which are represented by a (3×3) array ε_{ij} or matrix $\boldsymbol{\varepsilon}$, can be written as $\varepsilon'_{ij} = a_{ik}a_{jl}\varepsilon_{kl}$ or as $\boldsymbol{\varepsilon}' = \mathbf{a}\boldsymbol{\varepsilon}\mathbf{a}^{\mathrm{T}}$, where $\mathbf{a}$ is the matrix of directional cosines. When transcribed into the contracted tensorial or engineering matrix notation, the result is equivalent to that found using (1.1.27).

A much broader exposition of most result in this chapter can be found in several continuum mechanics textbooks, such as Fung (1965, 1994), Malvern (1969) or Spencer (1980).

A list of symbols frequently used in Chaps. 3, 4, 5, 6, 7 and 8 appear in Table 2.5 (see p. 34).

Chapter 2
Anisotropic Elastic Solids

Properties of composite materials and their constituents often depend on both position and direction in a fixed system of coordinates. In the terminology of solid mechanics, such materials are heterogeneous and anisotropic. This chapter is concerned with the directional dependence, defined by certain material symmetry elements, and reflected in eight distinct forms of the stiffness and compliance matrices of elastic solids. Such materials include, for example, reinforcing fibers, particles and their coatings, or fibrous composites and laminates represented on the macroscale by homogenized solids with *equivalent or effective elastic moduli*. Identification of the positions of zero-valued coefficients, and of any connections between nonzero coefficients in those matrices is of particular interest. Different classes of crystals exhibit a much larger range of symmetries, derived from spatial arrangement of their lattices. Broader expositions of these topics can be found in several books, such as Love (1944), Lekhnitskii (1950), Green and Atkins (1960), Nye (1957, 1985), Hearmon (1961), Ting (1996), and Cowin and Doty (2007).

2.1 Elastic Strain Energy Density

The elastic strain energy stored in a unit volume of a homogeneous elastic material that is subjected to a certain uniform local strain state $\boldsymbol{\varepsilon}^{(c)}$ is defined by a scalar quantity $\mathcal{W}(\boldsymbol{\varepsilon}^{(c)})$, the strain energy density. Any deformation leading to another strain state, that starts at and is then reversed to $\boldsymbol{\varepsilon}^{(c)}$, has no effect on the magnitude of $\mathcal{W}(\boldsymbol{\varepsilon}^{(c)})$, hence the energy density is independent of the deformation path followed to reach the current strain. The energy accumulated in the unit volume is

$$\mathcal{W} = \int_0^{\boldsymbol{\varepsilon}^{(c)}} \sigma_{ij} \mathrm{d}\varepsilon_{ij} = \int_0^{\boldsymbol{\varepsilon}^{(c)}} L_{ijkl}\varepsilon_{kl} \mathrm{d}\varepsilon_{ij} \tag{2.1.1}$$

G.J. Dvorak, *Micromechanics of Composite Materials*, Solid Mechanics and Its Applications 186, DOI 10.1007/978-94-007-4101-0_2,

This integral is path independent if the integrand is the total differential

$$\mathrm{d}\mathcal{W} = \frac{\partial \mathcal{W}}{\partial \varepsilon_{ij}} \mathrm{d}\varepsilon_{ij} = L_{ijkl}\varepsilon_{kl}\mathrm{d}\varepsilon_{ij} = \frac{1}{2}\mathrm{d}(L_{ijkl}\varepsilon_{kl}\varepsilon_{ij}) \tag{2.1.2}$$

where $\mathrm{d}(L_{ijkl}\varepsilon_{kl}\varepsilon_{ij}) = L_{ijkl}(\varepsilon_{kl}\mathrm{d}\varepsilon_{ij} + \varepsilon_{ij}\mathrm{d}\varepsilon_{kl})$. The second derivative must be independent of the order of differentiation, hence the integrand

$$\frac{\partial^2 \mathcal{W}}{\partial \varepsilon_{kl}\partial \varepsilon_{ij}} = \frac{\partial^2 \mathcal{W}}{\partial \varepsilon_{ij}\partial \varepsilon_{kl}} \Rightarrow L_{ijkl} = L_{klij} \tag{2.1.3}$$

as anticipated by (1.1.7).

The argument leading to (2.1.3) can also be utilized to show independence of the complementary energy on the stress path, and diagonal symmetry of the compliance matrix $M_{ijkl} = M_{klij}$. Following the contraction (1.1.8) to (6×6) matrices, both $L_{\alpha\beta}$ and $M_{\alpha\beta}(\alpha, \beta = 1, 2, \ldots 6)$ are real and diagonally symmetric, with at most 21 independent coefficients.

Integration of (2.1.2) provides

$$\left.\begin{aligned} 2\mathcal{W} &= L_{ijkl}\varepsilon_{ij}\varepsilon_{kl} = M_{ijkl}\sigma_{ij}\sigma_{kl} = \sigma_{ij}\varepsilon_{ij} > 0 \\ 2\mathcal{W} &= L_{\alpha\beta}\varepsilon_{\alpha}\varepsilon_{\beta} = M_{\alpha\beta}\sigma_{\alpha}\sigma_{\beta} = \varepsilon_{\beta}\sigma_{\beta} > 0 \end{aligned}\right\} \tag{2.1.4}$$

where $i, j, \ldots = 1, 2, 3, \alpha, \beta, \ldots = 1, 2, \ldots 6$. Moreover, $\varepsilon_{\alpha}, \varepsilon_{\beta}$ are the engineering strain components and the stiffness and compliance matrices $\boldsymbol{L}_{EG} \rightarrow L_{\alpha\beta}, \boldsymbol{M}_{EG} \rightarrow M_{\alpha\beta}$.

The strain energy density $\mathcal{W}$ is a positive definite quadratic form and both $L_{\alpha\beta}$ and $M_{\alpha\beta}$ are positive definite matrices, with real, positive eigenvalues. Decomposition of the stress and strain tensors according to (1.1.14), enables writing of the strain energy density as a sum of distortional and dilatational parts

$$\mathcal{W} = \frac{1}{2}\sigma_{ij}\varepsilon_{ij} = \frac{1}{2}\left(\frac{1}{3}\sigma_{kk}\delta_{ij} + s_{ij}\right)\left(\frac{1}{3}\varepsilon_{kk}\delta_{ij} + e_{ij}\right) = \frac{1}{6}\sigma_{kk}\varepsilon_{kk} + \frac{1}{2}s_{ij}e_{ij} \tag{2.1.5}$$

where $s_{ij}\delta_{ij} = e_{ij}\delta_{ij} = 0; \delta_{ij}\delta_{ij} = 3$. In the absence of a specific constitutive relation that evaluates the coefficients of $L_{\alpha\beta}$ or $M_{\alpha\beta}$, this form of $\mathcal{W}$ is valid for any material symmetry.

Transcription of the energy function into the contracted tensorial and engineering (*EG*) notations is facilitated by expanding the product $\sigma_{ij}\varepsilon_{ij}$ in (2.1.5)

$$2\mathcal{W} = \sigma_{ij}\varepsilon_{ij} = \sigma_{11}\varepsilon_{11} + \sigma_{22}\varepsilon_{22} + \sigma_{33}\varepsilon_{33} + 2\sigma_{12}\varepsilon_{12} + 2\sigma_{23}\varepsilon_{23} + 2\sigma_{31}\varepsilon_{31} \tag{2.1.6}$$

In the two notations, this result is provided by the products derived using (1.1.12)

$$\left.\begin{aligned} 2\mathcal{W} &= \varepsilon_{ij}\sigma_{ij} \rightarrow \boldsymbol{\varepsilon}^{\mathrm{T}}\boldsymbol{\Theta}\,\boldsymbol{\sigma} = \boldsymbol{\sigma}^{\mathrm{T}}\boldsymbol{\Theta}\,\boldsymbol{\varepsilon} = \boldsymbol{\varepsilon}_{EG}^{\mathrm{T}}\boldsymbol{\sigma} = \boldsymbol{\sigma}^{\mathrm{T}}\boldsymbol{\varepsilon}_{EG} \\ 2\mathcal{W} &= \boldsymbol{\sigma}^{\mathrm{T}}\boldsymbol{\varepsilon}_{EG} = \boldsymbol{\varepsilon}_{EG}^{\mathrm{T}}\boldsymbol{L}_{EG}\boldsymbol{\varepsilon}_{EG} = \boldsymbol{\varepsilon}^{\mathrm{T}}\boldsymbol{L}\boldsymbol{\varepsilon}_{EG} = \boldsymbol{\varepsilon}^{\mathrm{T}}\boldsymbol{L}\boldsymbol{\Theta}\,\boldsymbol{\varepsilon} \end{aligned}\right\} \tag{2.1.7}$$

This shows that the product $\boldsymbol{\varepsilon}_{EG}^{\mathrm{T}}\boldsymbol{L}_{EG}\boldsymbol{\varepsilon}_{EG}$ of engineering strain and stiffness matrices provides the correct magnitude of the strain energy, to be used in Chap. 5. However, the following invariants transcribe as

$$s_{ij}s_{ij} = s_{11}^2 + s_{22}^2 + s_{33}^2 + 2(s_{23}^2 + s_{31}^2 + s_{12}^2) \rightarrow \boldsymbol{s}^{\mathrm{T}}\boldsymbol{\Theta}\,\boldsymbol{s} \tag{2.1.8}$$

and

$$e_{ij}e_{ij} = e_{11}^2 + e_{22}^2 + e_{33}^2 + 2(e_{23}^2 + e_{31}^2 + e_{12}^2) \rightarrow \boldsymbol{e}^{\mathrm{T}}\boldsymbol{\Theta}\boldsymbol{e} = \boldsymbol{e}_{EG}^{\mathrm{T}}\boldsymbol{\Theta}^{-1}\boldsymbol{e}_{EG} \tag{2.1.9}$$

The results indicate that transcription of tensorial expressions to matrix form needs to be performed with care.

Apart from the diagonal symmetry derived in (2.1.3), the structure of the elastic stiffness and compliance matrices depends on material symmetry, defined by reflection or symmetry planes and axes of rotational symmetry in Sect. 2.2. For each material symmetry, the inequalities (2.1.4) impose certain restrictions or bounds on the values of stiffness and compliance coefficients. Ting (1996) indicates that these restrictions provide more stringent limitations on elastic constants than those which ensure that the differential equations governing elastostatic problems are completely elliptic. Within their particular limits, the elastic moduli may exhibit significant changes and assume extreme values, as discussed in Sect. 2.5. Nye (1985), among others, shows examples of directional dependence of elastic moduli of certain crystals.

The necessary and sufficient conditions for positive definiteness of stiffness and compliance matrices require that all principal minors of $L_{\alpha\beta}$ or $M_{\alpha\beta}$ be positive. The minors are determinants of the five principal submatrices, generated by deleting same numbered rows and columns; they include the determinants $\|L_{\alpha\beta}\|$ and $\|M_{\alpha\beta}\|$. This guarantees that all diagonal terms of $L_{\alpha\beta}$ or $M_{\alpha\beta}$, as well as all eigenvalues of these matrices are positive.

As a positive definite and symmetric quadratic form, the strain energy density can also be written as a polynomial in the strain components, arranged as strain invariants consistent with the groups of transformations describing a particular crystal class. A complete list of the invariants appears in Green and Atkins (1960). Several different invariants of the anisotropic elasticity tensor with respect to arbitrary orthogonal transformations are discussed, for example, by Spencer (1971), Ting (1987), Ahmad (2002) and Ting and He (2006).

Evaluation of the effect of material symmetry on the structure of the stiffness and compliance matrices is facilitated by reference to the expanded form (2.1.4)

of the strain energy density $\mathcal{W}(\varepsilon_{\alpha\beta})$. Recall from (2.1.7) that $2\mathcal{W} = \boldsymbol{\varepsilon}_{EG}^{\mathrm{T}} \boldsymbol{L}_{EG} \boldsymbol{\varepsilon}_{EG}$, hence the expanded form is written using engineering strains $\boldsymbol{\varepsilon}_{EG} \rightarrow \varepsilon_\alpha$ from (1.1.11) and $\boldsymbol{L}_{EG} \rightarrow L_{\alpha\beta}$

$$\left.\begin{aligned} \mathcal{W}\left(\varepsilon_{\alpha\beta}\right) = L_{11}\varepsilon_1^2/2 &+L_{12}\varepsilon_1\varepsilon_2 &+L_{13}\varepsilon_1\varepsilon_3 &+L_{14}\varepsilon_1\varepsilon_4 &+L_{15}\varepsilon_1\varepsilon_5 &+L_{16}\varepsilon_1\varepsilon_6 \\ &+L_{22}\varepsilon_2^2/2 &+L_{23}\varepsilon_2\varepsilon_3 &+L_{24}\varepsilon_2\varepsilon_4 &+L_{25}\varepsilon_2\varepsilon_5 &+L_{26}\varepsilon_2\varepsilon_6 \\ & &+L_{33}\varepsilon_3^2/2 &+L_{34}\varepsilon_3\varepsilon_4 &+L_{35}\varepsilon_3\varepsilon_5 &+L_{36}\varepsilon_3\varepsilon_6 \\ & & &+L_{44}\varepsilon_4^2/2 &+L_{45}\varepsilon_4\varepsilon_5 &+L_{46}\varepsilon_4\varepsilon_6 \\ & & & &+L_{55}\varepsilon_5^2/2 &+L_{56}\varepsilon_5\varepsilon_6 \\ & & & & &+L_{66}\varepsilon_6^2/2 \end{aligned}\right\} \tag{2.1.10}$$

Specific symmetry elements are introduced by certain coordinate transformations which are required to preserve invariance of $\mathcal{W}(\varepsilon_{\alpha\beta})$. A strain component that changes its sign as a result of the transformation may change the expanded form of $\mathcal{W}$. To prevent that, the stiffness coefficients appearing in the affected terms of $\mathcal{W}$ are made equal to zero. For example, if a particular coordinate transformation induces a sign change in the strain ε_5, from $+\varepsilon_5$ to $-\varepsilon_5$, then $L_{15} = L_{25} = L_{35} = L_{45} = L_{56} = 0$ in the stiffness matrix of the solid defined by this transformation. Additional reductions follow from connections established between nonzero coefficients. In this manner, accumulation of symmetry elements reduces the number of independent elastic moduli from the maximum of 21 to the minimum of 2, in isotropic solids. Of course, identical coefficient reductions apply to both $\boldsymbol{L}_{EG}$ and $\boldsymbol{L}$, and also to $\boldsymbol{M}_{EG}$ and $\boldsymbol{M}$.

2.2 Material Symmetries

2.2.1 Elements of Material Symmetry

Early studies of material symmetry were inspired by observed properties of crystals. Voigt (1910) identified 32 crystal classes, among *eight* basic symmetry groups of transformations that preserve a particular form of $\mathcal{W}$. A systematic classification of crystal symmetries and complete groups of transformations for each crystal class are described in Green and Atkins (1960), following the formalism developed by Smith and Rivlin (1958). For each crystal class, their results also include representations of W by polynomials, in terms of sets of strain component invariants which form a polynomial basis for each transformation group. The related stress invariants have been used in definitions of assumed yield or failure surfaces of anisotropic solids (Hill 1948; Mulhern et al. 1967, 1969; Spencer 1972; Tsai and Wu 1971). A systematic formulation of general principles, and of equilibrium, transport and optical properties of crystals can be found in Nye (1957, 1985).

More recent studies, initiated by Cowin and Mehrabadi (1987, 1989) show that the eight basic symmetries can be defined by the number of planes of symmetry that each one admits, without reliance on the groups of transformations or crystallography. These results also allow determination of material symmetry of materials with initially unknown microstructures. For a comprehensive review, see Cowin and Mehrabadi (1995), Cowin and Doty (2007). Chadwick et al. (2001) reconcile the symmetry groups and symmetry planes approaches and show their equivalence. Ting (1996, 2003) provides a concise exposition of the number and orientation of symmetry planes for each of the eight symmetries.

Here we make contact with a subset of these results, and emphasize symmetry elements that can be identified by inspection of the microstructure of composite materials and laminates. Each symmetry element will be defined by a specific form of the matrix a_{ij} of directional cosines in (2.2.1) below. Applying this a_{ij} matrix yields transformed strain components, some of which may change values of certain terms of the strain energy density function $\mathcal{W}$ displayed in (2.1.10). As already mentioned, invariance of $\mathcal{W}$ under each such transformation is preserved by letting the stiffness coefficients of $L_{\alpha\beta}$ be equal to zero, in the terms changed by the transformation. The strain energy density $\mathcal{W}$ corresponding to a particular combination of material symmetry elements is generated by application of successive transformations, one for each of the specified symmetry elements. We consider only the effect of symmetry on the stiffness and compliance matrices, or on fourth order tensors that relate two second order tensors. Tensors defining transport and other properties experience different material symmetry effects, described by (Nye 1957, 1985), and with specific applications later.

Coordinate transformations consistent with the Euclidean space are translations, rotations and reflections, described by

$$x_i' = x_i^0 + a_{ij}x_j \quad a_{ij} = \cos(x_i', x_j) \quad i, j = 1, 2, 3 \tag{2.2.1}$$

where $x_i^0 \in V$ is the translation vector, and the a_{ij} is an orthogonal matrix of directional cosines which describes the reflection and rotation parts of the transformation.

Material symmetry in the Euclidean space requires the strain energy density $\mathcal{W}$ in (2.1.10) to remain invariant under coordinate transformations of both strain and stress components, implied by reflection or symmetry planes and axes of rotational symmetry.

$$\mathcal{W}(\varepsilon'_{\alpha\beta}) = \mathcal{W}(\varepsilon_{\alpha\beta}) \quad \mathcal{W}(\sigma'_{\alpha\beta}) = \mathcal{W}(\sigma_{\alpha\beta}) \tag{2.2.2}$$

Translational invariance assures homogeneity, or the same symmetry everywhere in a given material volume; it has no effect on material symmetry itself.

Material symmetry elements include, as appropriate, the three coordinate planes and one or more planes of symmetry, or reflection planes aligned with the x_3-axis, each defined by a unit normal vector n_i that contains an angle θ with the

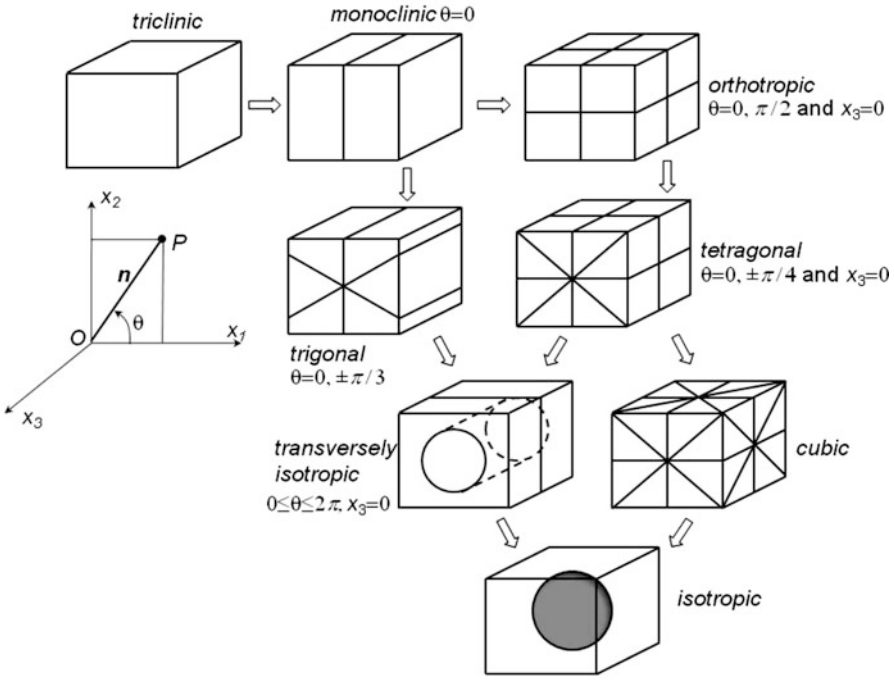

Fig. 2.1 Evolution of material symmetries by addition of planes and axes of symmetry

x_1- axis, measured counterclockwise, Fig. 2.1. Also, a vector m_j is defined in the plane itself. When such transformation is a reflection, the normal vector may reverse its direction, such that $a_{ij}n_j = -n_i$, while the $a_{ij}m_j = m_i$. The corresponding matrix of directional cosines is

$$a_{ij} = \delta_{ij} - 2n_i n_j \tag{2.2.3}$$

In particular, if the normal vector is $n_i = [\cos\theta, \sin\theta, 0]^{\mathrm{T}}$, $-\pi/2 < \theta \leqslant \pi/2$, then the reflection (2.2.3) is described by the transformation

$$a_{ij} = \begin{bmatrix} -\cos 2\theta & -\sin 2\theta & 0 \\ -\sin 2\theta & \cos 2\theta & 0 \\ 0 & 0 & 1 \end{bmatrix} \tag{2.2.4}$$

Also included among symmetry elements are axes of rotational symmetry, each defined by a unit axial vector and by the angle of rotation $\theta = 2\pi/n$, and called a n-th order or n-fold axis. For example, the transformation describing a rigid body rotation by an angle θ about the $x_3 -$ axis, measured counterclockwise from $\theta = 0$ at $x_2 = 0$ is

$$a_{ij} = \begin{bmatrix} \cos\theta & -\sin\theta & 0 \\ \sin\theta & \cos\theta & 0 \\ 0 & 0 & 1 \end{bmatrix} \tag{2.2.5}$$

Each of the eight material symmetries can be described by one or more reflection planes and/or axes of rotational symmetry.

In all anisotropic materials, both the strain energy and stiffness are invariant under *central inversion*, denoted by $\mathbf{C}$ and defined by selecting $a_{ij} = -\delta_{ij}$, as well as under identity or $\mathbf{I}_3$ transformation $a_{ij} = \delta_{ij}$. The identity $\mathbf{a}\mathbf{a}^{\mathrm{T}} = \mathbf{a}^{\mathrm{T}}\mathbf{a} = \mathbf{I}_3 \Rightarrow \mathbf{a}^{\mathrm{T}} = \mathbf{a}^{-1}$ shows that a material symmetry defined by an orthogonal (3×3) matrix $\mathbf{a}$ is also defined by $\mathbf{a}^{\mathrm{T}} = \mathbf{a}^{-1}$. The implication is that a material symmetric with respect to rotation by a certain angle θ remains symmetric when rotated by $-\theta$. Additional symmetry elements, such as glide planes, and n-fold screw and inversion axes are used in crystal physics (Nye 1957, 1985).

Figure 2.1, shows schematically the eight material symmetries, with their symmetry elements and interconnections, described in the following paragraphs. In the triclinic material at the upper left, there are no symmetry planes or axes, while in the isotropic material at the lower right, any plane and axis is an element of symmetry.

2.2.2 Triclinic Materials

No reflection planes or axes of rotational symmetry are prescribed to impose restrictions on the structure of the stiffness matrix, which remains fully populated by 21 independent coefficients $L_{\alpha\beta}$. Therefore, triclinic solids are symmetric only with respect central inversion $\mathbf{C}$, allowing for transformations $\mathbf{I}_3$ and $\mathbf{I}_3$, $\mathbf{C}$, which are shared by all material symmetries. In addition to the triclinic crystals, the fully populated matrices frequently appear in constitutive relations of elastic-plastic and other inelastic materials, where they may represent an instantaneous tangential or secant stiffness at a particular point of the deformation path. Cowin and Mehrabadi (1995, §10), indicate that a coordinate system can be selected such that three components of $L_{\alpha\beta}$ of the triclinic system become equal to zero, reducing the number of nonzero coefficients to 18.

2.2.3 Monoclinic Materials

A single plane of material symmetry is introduced, typically selected as one of the three coordinate planes. For example, reflection about the x_1x_2-plane at $x_3 = 0$ is described by

Table 2.1 Stiffness matrices of triclinic, monoclinic and orthotropic solids

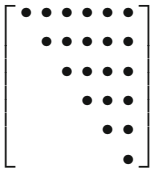	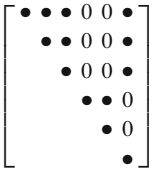	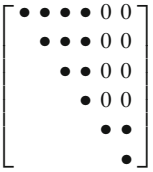	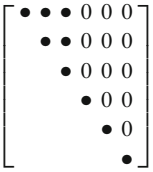
Triclinic	*Monoclinic (symm. plane $x_3 = 0$)*	*Monoclinic (symm. plane $x_1 = 0$)*	*(Orthotropic, Rhombic)*
$m = 21$	$m = 13$	$m = 13$	$m = 9$

$$a_{ij} = \cos\left(x'_i, x_j\right) = \begin{bmatrix} 1 & 0 & 0 \\ 0 & 1 & 0 \\ 0 & 0 & -1 \end{bmatrix} \tag{2.2.6}$$

which provides transformed strains ε'_α

$$\varepsilon'_1 = \varepsilon_1 \quad \varepsilon'_2 = \varepsilon_2 \quad \varepsilon'_3 = \varepsilon_3 \quad \varepsilon'_4 = -\varepsilon_4 \quad \varepsilon'_5 = -\varepsilon_5 \quad \varepsilon'_6 = \varepsilon_6 \tag{2.2.7}$$

Invariance of $\mathcal{W}$ in (2.1.10), with respect to the transformation (2.2.6), requires the terms affected by the above strain sign changes to vanish. That is enforced by setting

$$L_{14} = L_{15} = L_{24} = L_{25} = L_{34} = L_{35} = L_{46} = L_{56} = 0 \tag{2.2.8}$$

which reduces the number of stiffness coefficients from 21 to 13. The stiffness matrix for reflection about x_1x_2 plane appears in Table 2.1, where each bullet stands for a different stiffness coefficient.

When substituted into the matrix form of the constitutive relation (1.1.21), the nonzero coefficients in the upper right (3×3) partition, and the off-diagonal coefficients L_{45} or L_{56} in the lower right partition of these matrices cause coupling between normal strains and shear stresses, and between different shear strain and stress components. The letter m denotes the number of independent stiffness and compliance coefficients in the respective matrices.

Cowin and Mehrabadi (1995, §10) show that certain restricted rotations about the normal to the plane of symmetry provide further reduction of the non-zero coefficients from 13 to 12. If the x_2x_3−plane of symmetry is chosen at $x_1 = 0$, then permutation of subscripts in (2.2.8) yields the vanishing stiffness and compliance coefficients

$$L_{15} = L_{16} = L_{25} = L_{26} = L_{35} = L_{36} = L_{45} = L_{46} = 0 \tag{2.2.9}$$

Finally, for the x_1x_3-plane at $x_2 = 0$

$$L_{14} = L_{16} = L_{24} = L_{26} = L_{34} = L_{36} = L_{45} = L_{56} = 0 \tag{2.2.10}$$

Table 2.1 displays the stiffness matrices complying with (2.2.8) and (2.2.9).

Monoclinic symmetry applies, for example, to a homogenized unidirectional fibrous ply in the overall coordinate system of a laminated plate, when the fibers contain an arbitrary angle with the 0° direction of the laminate. Although the ply may have a higher, transversely isotropic symmetry in the local coordinates of the ply, in the overall system it has only reflective symmetry about any plane parallel to its mid-plane.

2.2.4 Orthotropic Materials

Together with rhombic and orthorombic crystals, orthotropic solids have three mutually perpendicular planes of reflective symmetry, with normals in the directions of the coordinate axes. These symmetry planes include those with $\theta = 0,\ \pi/2$ in Fig. 2.1.

Therefore, the form of $\mathcal{W}$ is found by superimposing (2.2.8) with reflections about the x_2x_3- and x_1x_3-planes, which are indicated in (2.2.9) and (2.2.10), respectively. It can be verified by inspection of (2.2.8), (2.2.9), (2.2.10) that using only two of the three symmetry planes yields the same zero-valued stiffness coefficients. However, the planes are not exchangeable, since material properties remain distinct in the three coordinate directions.

The number of independent moduli is reduced to a total of nine, with six on the main diagonal and $L_{12},\ L_{13},\ L_{23}$ in the upper left (3×3) partition; Table 2.1. No coupling terms remain in the upper or lower right partition. The compliance matrix has the same structure, with $M_{\alpha\beta}$ coefficients replacing the $L_{\alpha\beta}$. The zero-valued coefficients are

$$L_{\alpha 4} = L_{\alpha 5} = L_{\alpha 6} = 0 \quad \text{for } \alpha = 1, 2, 3 \quad \text{and} \quad L_{45} = L_{46} = L_{56} = 0 \tag{2.2.11}$$

Layered plane materials, such as composite laminates and plywood often exhibit orthotropic symmetry on the macroscale, in terms of effective or overall properties derived by homogenization of the material volume. However, on the more refined scale that recognizes individual layers or plies, these materials do not satisfy, in the direction normal to the interfaces, the translational invariance condition (2.2.1) that embodies the homogeneity requirement.

Table 2.2 Stiffness matrices of trigonal and tetragonal solids

$$\begin{bmatrix} L_{11} & L_{12} & L_{13} & L_{14} & 0 & 0 \\ & L_{11} & L_{13} & -L_{14} & 0 & 0 \\ & & L_{33} & 0 & 0 & 0 \\ & & & L_{44} & 0 & 0 \\ & & & & L_{44} & L_{14} \\ & & & & & (L_{11}-L_{12})/2 \end{bmatrix} \qquad \begin{bmatrix} L_{11} & L_{12} & L_{13} & 0 & 0 & 0 \\ & L_{11} & L_{13} & 0 & 0 & 0 \\ & & L_{33} & 0 & 0 & 0 \\ & & & L_{44} & 0 & 0 \\ & & & & L_{44} & 0 \\ & & & & & L_{66} \end{bmatrix}$$

Trigonal, axis rot.symm: x_3 $m=6$ | *Tetragonal, axis rot. symm: x_3* $m=6$

2.2.5 Trigonal and Tetragonal Materials

In contrast to the orthotropic symmetry, these materials are defined by prescribing certain equivalent planes of elastic symmetry, that require retention of material properties after exchange of the equivalent symmetry planes. Such exchange may be accomplished by rotation about a fixed axis of symmetry. For example, a rigid body rotation by an angle θ about the x_3-axis, measured ccw from $\theta = 0$ at $x_2 = 0$ as indicated by (2.2.5).

A trigonal material admits rigid body rotation about a 3-fold axis x_3, such that $\mathcal{W}$ in (2.1.10) remains invariant at $\theta = 0, \pm\pi/3$. This defines three equivalent planes, all aligned with x_3 and separated by 60° angles. The x_1x_2-plane is not a reflection plane. The principal diagonal of the stiffness matrix has only three independent coefficients, but coupling coefficients $L_{14} = -L_{24} = L_{56}$ are still present (Table 2.2).

$$\left.\begin{aligned} L_{11} = L_{22} \quad L_{44} = L_{55} \quad 2L_{66} = (L_{11}-L_{12}) \\ L_{13} = L_{23} \quad L_{14} = -L_{24} = L_{56} \\ L_{\alpha 5} = L_{\alpha 6} = 0 \ \text{ for } \alpha = 1,\ 2,\ 3,\ 4 \end{aligned}\right\} \tag{2.2.12}$$

A tetragonal material, has the x_1x_2-plane of reflection, and it admits a rigid body rotation about a 4-fold axis x_3, with invariance of $\mathcal{W}$ preserved at $\theta = 0, \pm\pi/4, \pi/2$. Therefore, the planes aligned with x_3 are separated by 45° angles, and they are equivalent or exchangeable planes of symmetry. To keep the strain energy (2.1.10) invariant under the transformations indicated by these symmetries, the following stiffness coefficients are connected or set equal to zero

$$\left.\begin{aligned} L_{11} = L_{22} \quad L_{44} = L_{55} \quad L_{13} = L_{23} \\ L_{\alpha 4} = L_{\alpha 5} = L_{\alpha 6} = 0 \ \text{ for } \alpha = 1,\ 2,\ 3 \quad L_{45} = L_{46} = L_{56} = 0 \end{aligned}\right\} \tag{2.2.13}$$

Both trigonal and tetragonal materials have $m = 6$ nonzero stiffness or compliance coefficients, which are not identically positioned or related.

2.2.6 *Transversely Isotropic or Hexagonal Materials*

These materials have two symmetry elements, one plane that may be selected as the x_1x_2-plane in Fig. 2.1, and perpendicular to that plane, an axis or rotational symmetry x_3 about any angle θ. In the x_1x_2-plane of symmetry, the material is isotropic, with properties independent of direction, so that all planes containing the x_3-axis are also planes of symmetry.

The matrix of directional cosines that describes rotation around x_3 by an angle θ, measured counter-clockwise from x_1 to x_1', is shown by (2.2.5). The strains $\varepsilon'_{ij} = a_{ik}a_{jl}\varepsilon_{kl}$ are

$$\left.\begin{aligned}
\varepsilon'_{11} &= \varepsilon_{11}\cos^2\theta + \varepsilon_{22}\sin^2\theta - 2\varepsilon_{12}\sin\theta\cos\theta \\
\varepsilon'_{22} &= \varepsilon_{11}\sin^2\theta + \varepsilon_{22}\cos^2\theta + 2\varepsilon_{12}\sin\theta\cos\theta \quad \varepsilon'_{33} = \varepsilon_{33} \\
\varepsilon'_{13} &= \varepsilon_{13}\cos\theta - \varepsilon_{23}\sin\theta \quad \varepsilon'_{23} = \varepsilon_{13}\sin\theta + \varepsilon_{23}\cos\theta \\
\varepsilon'_{12} &= (\varepsilon_{11} - \varepsilon_{22})\sin\theta\cos\theta - \varepsilon_{12}\left(\sin^2\theta - \cos^2\theta\right)
\end{aligned}\right\} \tag{2.2.14}$$

It can be verified that the following five strain invariants associated with transverse isotropy about $x_3 = 0$ are independent of the transformation (2.2.5). The strain energy $\mathcal{W}$ can be written as a polynomial in these invariants

$$\left.\begin{aligned}
&\varepsilon'_{33} = \varepsilon_{33} \quad \varepsilon'_{11} + \varepsilon'_{22} = \varepsilon_{11} + \varepsilon_{22} \\
&\varepsilon'_{11}\varepsilon'_{22} - \left(\varepsilon'_{12}\right)^2 = \varepsilon_{11}\varepsilon_{22} - \varepsilon_{12}^2 \\
&\left(\varepsilon'_{13}\right)^2 + \left(\varepsilon'_{23}\right)^2 = \varepsilon_{13}^2 + \varepsilon_{23}^2 \quad \left|\varepsilon'_{ij}\right| = \left|\varepsilon_{ij}\right|
\end{aligned}\right\} \tag{2.2.15}$$

Coefficients of the stiffness or compliance matrix are connected as those of the trigonal system in (2.2.12), but by introduction of the x_1x_2-plane of symmetry, they are further reduced to $L_{14} = L_{15} = L_{56} = 0$. That leaves five independent constants and zero coupling terms, as also shown in Table 2.3. Moreover, the constants need to satisfy (2.1.4) which requires the strain energy to be a positive definite quadratic form. This yields the connections (Nye 1985)

$$\left.\begin{aligned}
&L_{11} = L_{22} > |L_{12}| \quad L_{44} = L_{55} > 0 \quad 2L_{66} = (L_{11} - L_{12}) \\
&L_{13} = L_{23} \quad L_{14} = L_{15} = L_{56} = 0 \quad (L_{11} + L_{12})L_{33} > 2L_{13}^2 \\
&\qquad L_{\alpha 5} = L_{\alpha 6} = 0 \quad \text{for } \alpha = 1, 2, 3, 4
\end{aligned}\right\} \tag{2.2.16}$$

The same results follow for hexagonal or higher symmetry, when $\theta = \pi/n$ and $n \geqslant 3$.

Table 2.3 Stiffness matrices of transversely isotropic solids

$$\begin{bmatrix} L_{11} & L_{12} & L_{13} & 0 & 0 & 0 \\ & L_{11} & L_{13} & 0 & 0 & 0 \\ & & L_{33} & 0 & 0 & 0 \\ & & & L_{44} & 0 & 0 \\ & & & & L_{44} & 0 \\ & & & & & (L_{11}-L_{12})/2 \end{bmatrix} \qquad \begin{bmatrix} L_{11} & L_{12} & L_{12} & 0 & 0 & 0 \\ & L_{22} & L_{23} & 0 & 0 & 0 \\ & & L_{22} & 0 & 0 & 0 \\ & & & (L_{22}-L_{23})/2 & 0 & 0 \\ & & & & L_{55} & 0 \\ & & & & & L_{55} \end{bmatrix}$$

Axis of rotational symmetry: x_3 $m=5$ — *Axis of rotational symmetry*: x_1 $m=5$

Materials reinforced by fibers aligned in a single direction and randomly distributed in the transverse plane are regarded as transversely isotropic. A more extensive description of this symmetry, in notations commonly applied to unidirectional composites, appears in Sect. 2.3.

2.2.7 Cubic Materials

Nine planes of elastic symmetry are prescribed, arranged in sets of three and derived from the tetragonal symmetry. Three of the nine planes are perpendicular to the coordinate axes, and are interchangeable. Six planes have normals that contain an angle $\pi/4$ with the coordinate axes. Only three independent constants remain, and they must satisfy (2.1.4). This yields the following connections (Nye 1985)

$$\left.\begin{array}{ll} L_{11} = L_{22} = L_{33} > |L_{12}| & L_{12} = L_{13} = L_{23} \\ L_{44} = L_{55} = L_{66} > 0 & L_{11} + 2L_{12} > 0 \end{array}\right\} \tag{2.2.17}$$

The remaining 12 coefficients are all equal to zero. Many metals and ceramics crystallize in either tetragonal, or face or body-centered cubic system.

Analytical studies often prefer to employ the bulk modulus κ and two shear moduli μ and μ' which Zener (1948) identifies by means of the connections (Walpole 1981, 1985a)

$$\kappa = \frac{1}{3}(L_{11} + 2L_{12}) \quad \mu = \frac{1}{2}(L_{11} - L_{12}) \quad \mu' = L_{44} \tag{2.2.18}$$

In fact, μ and $\mu'$are two extreme shear moduli that bound every other shear modulus of the crystal. In an isotropic solid, they coincide as the unique shear modulus. The extent to which their ratio μ'/μ differs from unity is a measure of anisotropy. In general, μ' is larger than μ in most actual cubic crystals. All three moduli κ, μ and μ' are necessarily positive in accordance with the positive definiteness of the strain energy in (2.1.4).

The nonzero coefficients of the compliance matrix in engineering notation can be written as

$$\left.\begin{aligned} M_{11} = M_{22} = M_{33} = \frac{1}{9\kappa} + \frac{1}{3\mu} \quad M_{12} = M_{13} = M_{23} = \frac{1}{9\kappa} - \frac{1}{6\mu} \\ M_{44} = M_{55} = M_{66} = \frac{1}{\mu'} \end{aligned}\right\} \tag{2.2.19}$$

2.2.8 Isotropic Materials

At least three perpendicular axes of rotational symmetry about any angle are available. Any plane is a plane of symmetry, and invariance of the strain energy $\mathcal{W}$ is preserved under any orthogonal transformation of the coordinates. In addition to the connections (2.2.17), the shear moduli are equal, which reduces the number of independent moduli from three to two.

$$\left.\begin{aligned} &L_{11} = L_{22} = L_{33} \quad L_{12} = L_{13} = L_{23} \quad L_{44} = L_{55} = L_{66} = \frac{1}{2}(L_{11} - L_{12}) \\ &M_{11} = M_{22} = M_{33} \quad M_{12} = M_{13} = M_{23} \quad M_{44} = M_{55} = M_{66} = 2(M_{11} - M_{12}) \end{aligned}\right\} \tag{2.2.20}$$

The stiffness matrix of isotropic solids in the engineering notation is

$$\boldsymbol{L}_{EG} = \frac{E}{(1+\nu)(1-2\nu)} \begin{bmatrix} 1-\nu & \nu & \nu & 0 & 0 & 0 \\ & 1-\nu & \nu & 0 & 0 & 0 \\ & & 1-\nu & 0 & 0 & 0 \\ & & & (1-2\nu)/2 & 0 & 0 \\ & & & & (1-2\nu)/2 & 0 \\ & & & & & (1-2\nu)/2 \end{bmatrix} \tag{2.2.21}$$

The contracted tensorial stiffness matrix $\boldsymbol{L}$ in (1.1.22), written with bulk modulus K, shear modulus G has the nonzero coefficients

$$\left.\begin{aligned} L_{11} &= L_{22} = L_{33} = (3K + 4G)/3 \\ L_{12} &= L_{13} = L_{23} = L_{21} = L_{31} = L_{32} = (3K - 2G)/3 \\ L_{44} &= L_{55} = L_{66} = 2G \end{aligned}\right\} \tag{2.2.22}$$

The matrix $\boldsymbol{L}_{EG}$ is usually written using the Lamé constants λ, μ, with $L_{11} = \lambda + 2\mu$, $L_{12} = \lambda$ and $L_{44} = \mu$, repeated as indicated above. Relations between these

and the Young's modulus E, bulk modulus K, shear modulus G, and the Poisson's ratio ν are

$$\left.\begin{aligned} \lambda = \frac{E\nu}{(1+\nu)(1-2\nu)} = K - \frac{2}{3}G \quad E = \frac{9KG}{3K+G} \\ \mu = G = \frac{E}{2(1+\nu)} \quad K = \frac{E}{3(1-2\nu)} \end{aligned}\right\} \tag{2.2.22a}$$

Both $\boldsymbol{L}_{EG}$ and $\boldsymbol{L}$ appear in the constitutive relation $\sigma_\alpha = L_{\alpha\beta}\varepsilon_\beta, (\alpha, \beta = 1, 2, \ldots 6)$ where the stress and engineering or tensorial strain vectors are defined by (1.1.9)–(1.1.11). The compliance matrix has a similar structure, with $\boldsymbol{M}_{EG}$ written as

$$\left.\begin{aligned} M_{11} = M_{22} = M_{33} = 1/E \quad M_{12} = M_{13} = M_{23} = -\nu/E \\ M_{44} = M_{55} = M_{66} = 1/G = 1/\mu \end{aligned}\right\} \tag{2.2.23}$$

In the contracted tensorial component $\boldsymbol{M}$ matrix, $M_{44} = M_{55} = M_{66} = 1/2G = 1/2\mu$.

For isotropic solids with elastic moduli K and G, the strain energy function (2.1.5) is evaluated using $\sigma_{kk} = 3K\varepsilon_{kk}, s_{ij} = 2Ge_{ij}$. The result is

$$2\mathcal{W} = \frac{1}{9K}(\sigma_{kk})^2 + \frac{1}{G}J_2 = K(\varepsilon_{kk})^2 + 2Ge_{ij}e_{ij} \tag{2.2.24}$$

where $J_2 = s_{ij}s_{ij}/2$ is the second invariant of the stress deviator tensor. Since each of the two terms has to be positive definite, the moduli must satisfy $G > 0, K > 0$. This also implies that

$$E = \frac{9KG}{3K+G} \Rightarrow E > 0 \quad \nu = \frac{3K-2G}{2(3K+G)} \Rightarrow -1 < \nu < \frac{1}{2} \tag{2.2.25}$$

In materials regarded as rigid, all moduli become infinite. The Poisson's ratio approaches the low limit $\nu \to -1$ for $G \to \infty$ and finite K. The high limit $\nu \to 0.5$ is observed in incompressible materials, where $K \to \infty$ and G remains bounded. For example, $\nu \approx 0.45 - 0.49$ in soft rubbers and biological tissues, 0.33 in aluminum, 0.29 in steel, 0.1–0.4 or negative in certain polymer foams and nearly zero in cork (Lakes 1987).

Isotropic material symmetry applies to metals, ceramics and certain polymers, at scales exceeding the typical grain size by at least one order of magnitude, where translational invariance in (2.2.1) can be accepted. Applications at more refined scales are justified by lack of data or simplicity of modeling.

Different definitions of material symmetry and isotropy in particular have been developed for materials with cellular and other heterogeneous microstructures.

For example, Christensen (1987) shows that only six axes of five-fold symmetry associated with the pentagonal dodecahedron and the icosahedron are sufficient for isotropy of cellular and low density materials which transmit load by axial deformation of micro-struts arranged in a space network. The corresponding fiber composite is isotropic if the fibers take at least the six specific directions in three-dimensional space. Budiansky and Kimmel (1987) present a different derivation of isotropy for the macroscopic moduli of lung tissue modeled by a pin-jointed truss, again in the shape of the regular pentagonal dodecahedron.

2.2.9 *Decomposition of Isotropic Tensors and Matrices*

As shown in (1.1.16), the isotropic fourth-order identity tensor is a sum of two fourth rank tensors, $I_{ijkl} = J_{ijkl} + K_{ijkl}$. Inner products of these tensors show that they are isotropic and idempotent

$$\left.\begin{aligned} J_{ijkl}J_{klmn} &= \frac{1}{9}\delta_{ij}\delta_{kl}\delta_{kl}\delta_{mn} = \frac{1}{3}\delta_{ij}\delta_{mn} = J_{ijmn} \\ K_{ijkl}K_{klmn} &= I_{ijkl}K_{klmn} - J_{ijkl}(I_{klmn} - J_{klmn}) = K_{ijmn} \\ J_{ijkl}K_{klmn} &= J_{ijkl}(I_{klmn} - J_{klmn}) = 0 \end{aligned}\right\} \tag{2.2.26}$$

Moreover, since $\delta_{kl}\delta_{kl} = 3$, $J_{ijij} = 1$, $K_{ijij} = 5$, $J_{iijj} = 3$, $K_{iijj} = 0$.

These properties simplify evaluation of inner products of isotropic fourth rank tensors, such as stiffness and compliance tensors of isotropic solids, which both depend on at most two elastic moduli. The inner product then is

$$\left.\begin{aligned} U_{ijkl} &= u_1 J_{ijkl} + u_2 K_{ijkl} \quad V_{ijkl} = v_1 J_{ijkl} + v_2 K_{ijkl} \\ U_{ijkl}V_{lkmn} &= u_1 v_1 J_{ijmn} + u_2 v_2 K_{ijmn} \\ U^{-1}_{ijkl} &= \frac{1}{u_1} J_{ijkl} + \frac{1}{u_2} K_{ijkl} \quad U_{ijkl}U^{-1}_{lkpq} = I_{ijpq} \end{aligned}\right\} \tag{2.2.27}$$

where $u_s, v_s, s = 1, 2$, are positive scalars. It can be verified that the (6×6) matrices representing the tensors in the contracted tensorial notation also exhibit the above properties

$$\left.\begin{aligned} &\boldsymbol{J} = \boldsymbol{J}\boldsymbol{J} = \boldsymbol{J}^{\mathrm{T}} \quad \boldsymbol{K} = \boldsymbol{K}\boldsymbol{K} = \boldsymbol{K}^{\mathrm{T}} \quad \boldsymbol{K}\boldsymbol{J} = \boldsymbol{J}\boldsymbol{K} = \boldsymbol{0} \quad \boldsymbol{J} + \boldsymbol{K} = \boldsymbol{I} \\ &\boldsymbol{U} = u_1\boldsymbol{J} + u_2\boldsymbol{K} \quad \boldsymbol{U}^{-1} = \frac{1}{u_1}\boldsymbol{J} + \frac{1}{u_2}\boldsymbol{K} \quad \boldsymbol{U}\boldsymbol{U}^{-1} = \boldsymbol{I} \end{aligned}\right\} \tag{2.2.28}$$

Application to the stiffness matrices (2.2.21) and (2.2.22), written in the contracted tensorial notation ($\mu \rightarrow 2G$ in $L_{44},\ L_{55},\ L_{66}$), with the bulk and shear moduli K and G, yields

$$\boldsymbol{L} = 3K\boldsymbol{J} + 2G\boldsymbol{K} \quad \boldsymbol{M} = \frac{1}{3K}\boldsymbol{J} + \frac{1}{2G}\boldsymbol{K} \quad \boldsymbol{LM} = \boldsymbol{I} \tag{2.2.29}$$

where the matrices $\boldsymbol{J}$ and $\boldsymbol{K}$ were evaluated in (1.1.19). The coefficients L_{ij} appear in (2.2.22). The multiplication table (2.2.28) can be used to show that substitution of the above stiffness $\boldsymbol{L}$ and of both $\boldsymbol{\sigma}$ and $\boldsymbol{\varepsilon}$ from (1.1.18) into $\boldsymbol{\sigma} = \boldsymbol{L}\,\boldsymbol{\varepsilon}$ in (1.1.21), yields the elastic constitutive relation in the form $\boldsymbol{J\sigma} = 3K\boldsymbol{J\varepsilon}$ and $\boldsymbol{K\sigma} = 2G\boldsymbol{K\varepsilon}$, or $\sigma_{kk} = 3K\varepsilon_{kk}$ and $s_{ij} = 2Ge_{ij}$.

Walpole (1981, 1984) and Baerheim (1993) provide similar 'spectral' decompositions, and multiplication tables analogous to (2.2.28), for anisotropic tensors. However, their relative complexity limits widespread applications.

2.2.10 *Orientation Average of a Fourth-Order Tensor*

An isotropic fourth order tensor can also be created as an average of an anisotropic tensor H_{ijkl}, taken over all orientations. Under any orthogonal transformation (1.1.1) of H_{ijkl}, there are only two linear invariants, H_{ijij} and H_{iijj} (Ting 1987, 1996). If H_{ijkl} is represented by a (6×6) matrix $\boldsymbol{H}$, not necessarily symmetric and written in tensorial component notation, then the invariants are

$$\left.\begin{aligned} &H_{ijij} \rightarrow h_1 + h_3 \quad H_{iijj} \rightarrow h_1 + h_2 \\ &h_1 = (H_{11} + H_{22} + H_{33}) \quad h_3 = (H_{44} + H_{55} + H_{66}) \\ &h_2 = (H_{12} + H_{13} + H_{21} + H_{23} + H_{31} + H_{32}) \end{aligned}\right\} \tag{2.2.30}$$

With reference to the 'spectral' decomposition (2.2.29), the orientation average of $\{\boldsymbol{H}\}$ has the form (Kröner 1958)

$$\{\boldsymbol{H}\} = a\boldsymbol{J} + b\boldsymbol{K} \quad \{\boldsymbol{H}\}^{-1} = \frac{1}{a}\boldsymbol{J} + \frac{1}{b}\boldsymbol{K} \tag{2.2.31}$$

The scalars $a,\ b$ are

$$a = \frac{1}{3}H_{iijj} \quad b = \frac{1}{5}\left(H_{ijij} - a\right) \tag{2.2.32}$$

Evaluation of the nonzero coefficients of the (6×6) matrix $\{H_{\alpha\beta}\} = \{H_{\alpha\beta}\}^{\mathrm{T}}$ shows that

$$\left.\begin{aligned}\{H\}_{11} = \{H\}_{22} = \{H\}_{33} &= \frac{1}{15}(3h_1 + h_2 + 2h_3)\\ \{H\}_{12} = \{H\}_{13} = \{H\}_{23} &= \frac{1}{15}(h_1 + 2h_2 - h_3)\\ \{H\}_{44} = \{H\}_{55} = \{H\}_{66} &= \frac{1}{15}(2h_1 - h_2 + 3h_3)\end{aligned}\right\} \tag{2.2.33}$$

As an exercise, one may verify that these relations yield (2.2.31) for any $\boldsymbol{H} = a\boldsymbol{J} + b\boldsymbol{K}$. Orientation averages of anisotropic tensors are useful in modeling of polycrystals and composites consisting of randomly orientated grains or constituents.

2.3 Transversely Isotropic Composite Materials

2.3.1 Engineering and Hill's Moduli

Experimental measurements of elastic moduli of fibrous plies are usually performed on thin plies in the x_1x_2-plane, or on thin-walled cylindrical tubes with fibers aligned along the longitudinal x_1-axis. Details of such experiments appear, for example, in Herakovich (1998), and Daniel and Ishai (2006). Table 2.4 describes definitions of the engineering moduli, in terms of the strains measured in thin plies, under loading by a single stress component that needs to be applied for their experimental determination. Fibers are assumed aligned along the longitudinal x_1-axis. Transverse isotropy about x_1 and diagonal symmetry of M_{ij} also yield

$$E_{22} = E_{33} \qquad G_{23} = \frac{E_{22}}{2(1+\nu_{23})} \qquad \frac{\nu_{21}}{E_{22}} = \frac{\nu_{12}}{E_{11}} \qquad \nu_{23} = \nu_{32} \tag{2.3.1}$$

Note that transverse shear modulus $G_{23} = m$ depends on Poisson's ratio ν_{23}, derived from the out-of-plane strain ε_{33} caused by the stress σ_{22}. Values of the shear modulus are seldom included in ply property data, since reliable measurement of ε_{33} requires very large specimen thicknesses relative to those of a typical ply (0.13–0.23 mm).

Table 2.4 Evaluation of engineering moduli of fibrous plies

Applied	Measured	Calculated
σ_{11}	$\varepsilon_{11}, \varepsilon_{22} = \varepsilon_{33}$	$E_{11} = \sigma_{11}/\varepsilon_{11}, \nu_{12} = -\varepsilon_{22}/\varepsilon_{11} = \nu_{13}$
σ_{22}	$\varepsilon_{11}, \varepsilon_{22}, \varepsilon_{33}$	$E_{22} = \sigma_{22}/\varepsilon_{22}, \nu_{21} = -\varepsilon_{11}/\varepsilon_{22}, \nu_{23} = -\varepsilon_{33}/\varepsilon_{22}$
σ_{12}	ε_{12}^{EG}	$G_{12} = \sigma_{12}/(2\varepsilon_{12}^{EG})$

The engineering compliance matrix M_{ij} and the constitutive relation of a ply material are, for $x_A \equiv x_1$

$$\begin{bmatrix} \varepsilon_{11} \\ \varepsilon_{22} \\ \varepsilon_{33} \\ 2\varepsilon_{23} \\ 2\varepsilon_{31} \\ 2\varepsilon_{12} \end{bmatrix} = \begin{bmatrix} 1/E_{11} & -\nu_{21}/E_{22} & -\nu_{21}/E_{22} & 0 & 0 & 0 \\ -\nu_{12}/E_{11} & 1/E_{22} & -\nu_{32}/E_{22} & 0 & 0 & 0 \\ -\nu_{12}/E_{11} & -\nu_{23}/E_{22} & 1/E_{22} & 0 & 0 & 0 \\ 0 & 0 & 0 & 1/G_{23} & 0 & 0 \\ 0 & 0 & 0 & 0 & 1/G_{12} & 0 \\ 0 & 0 & 0 & 0 & 0 & 1/G_{12} \end{bmatrix} \begin{bmatrix} \sigma_{11} \\ \sigma_{22} \\ \sigma_{33} \\ \sigma_{23} \\ \sigma_{31} \\ \sigma_{12} \end{bmatrix} \tag{2.3.2}$$

The stiffness matrix of transversely isotropic solids is simplified by defining the coefficients of L_{ij} by Hill's (1964) moduli $k, l, n, m, p,$ written here for consistency with (2.3.2) with the axis of rotational symmetry $x_A \equiv x_1$, to yield

$$\begin{bmatrix} \sigma_{11} \\ \sigma_{22} \\ \sigma_{33} \\ \sigma_{23} \\ \sigma_{31} \\ \sigma_{12} \end{bmatrix} = \begin{bmatrix} n & l & l & 0 & 0 & 0 \\ l & k+m & k-m & 0 & 0 & 0 \\ l & k-m & k+m & 0 & 0 & 0 \\ 0 & 0 & 0 & m & 0 & 0 \\ 0 & 0 & 0 & 0 & p & 0 \\ 0 & 0 & 0 & 0 & 0 & p \end{bmatrix} \begin{bmatrix} \varepsilon_{11} \\ \varepsilon_{22} \\ \varepsilon_{33} \\ 2\varepsilon_{23} \\ 2\varepsilon_{31} \\ 2\varepsilon_{12} \end{bmatrix} \tag{2.3.3}$$

where

$$\left.\begin{aligned} k = [2(1-\nu_{23})/E_{22} - 4\nu_{12}^2/E_{11}]^{-1} \quad l = 2k\nu_{12} \\ n = E_{11} + 4k\nu_{12}^2 = E_{11} + l^2/k \quad m = G_{23} \quad p = G_{21} \end{aligned}\right\} \tag{2.3.4}$$

$$\left.\begin{aligned} E_{11} = n - l^2/k \quad \nu_{12} = l/2k \quad \nu_{21} = E_{22}\nu_{12}/E_{11} \\ E_{22} = E_{33} = \frac{4m(kn-l^2)}{n(k+m)-l^2} \quad \nu_{23} = \nu_{32} = \frac{n(k-m)-l^2}{n(k+m)-l^2} \end{aligned}\right\} \tag{2.3.5}$$

Here, k is the transverse bulk modulus, or plane strain bulk modulus for lateral dilatation without axial extension, n is related to uniaxial straining in the x_1-direction, and l is the associated cross modulus. The m and p are the transverse and longitudinal shear moduli.

It is worth mentioning that in the micromechanical literature originating in the United Kingdom, the fibers are often aligned with the $x_A \equiv x_3$ direction. That notation was frequently used in papers by Hill, Laws, Walpole and Willis, cited later. On the other hand, $x_A \equiv x_1$ is prevalent in papers on fibrous laminates.

Of course, change of coordinates has no effect on the physical definitions of the Hill's moduli, but it changes the position of first and third rows and columns in the

M_{ij} and L_{ij} matrices, and it needs to be carefully monitored to prevent errors in applications.

Moreover, (2.3.2) and (2.3.3) are often written in the contracted tensorial notation, where the multipliers 2 are transferred from the shear strain components to the shear moduli in the compliance and stiffness matrices, such that values of the stress components are not affected. This is illustrated in (2.3.11) and (2.3.13) below.

For isotropic solids, Hill's moduli appearing in the stiffness matrix (2.3.3) are expressed in bulk and shear moduli K and G and by Poisson's ratio ν, according to

$$\left.\begin{array}{lll} k+m=n=\dfrac{2G(1-\nu)}{1-2\nu} & k-m=l=\dfrac{2G\nu}{1-2\nu} & m=p=G \\ k=K+G/3 & l=K-2G/3 & n=K+4G/3 \end{array}\right\} \tag{2.3.6}$$

If Lamé constants λ and μ in (2.2.22a) are preferred, their connections to Hill's moduli are

$$k+m=n=\lambda+2\mu \quad k-m=l=\lambda \quad m=p=\mu \tag{2.3.7}$$

It is often advantageous to separate the axisymmetric from the shear strain and stress components, and write the elastic constitutive relations (2.3.3) of transversely isotropic solids, for $x_A \equiv x_1$, as

$$\left.\begin{array}{c} \begin{bmatrix} \sigma_{11} \\ (\sigma_{22}+\sigma_{33})/2 \end{bmatrix} = \begin{bmatrix} n & l \\ l & k \end{bmatrix} \begin{bmatrix} \varepsilon_{11} \\ (\varepsilon_{22}+\varepsilon_{33}) \end{bmatrix} \\ (\sigma_{22}-\sigma_{33}) = 2m(\varepsilon_{22}-\varepsilon_{33}) \\ \sigma_{23}=2m\varepsilon_{23} \quad \sigma_{31}=2p\varepsilon_{31} \quad \sigma_{12}=2p\varepsilon_{12} \\ \begin{bmatrix} \varepsilon_{11} \\ (\varepsilon_{22}+\varepsilon_{33}) \end{bmatrix} = \dfrac{1}{(kn-l^2)} \begin{bmatrix} k & -l \\ -l & n \end{bmatrix} \begin{bmatrix} \sigma_{11} \\ (\sigma_{22}+\sigma_{33})/2 \end{bmatrix} \end{array}\right\} \tag{2.3.8}$$

Of course, elastic properties of actual fibrous plies may not conform exactly to the widely used assumption of transverse isotropy, because the fibers may not be uniformly distributed in the transverse plane. For example, plies reinforced by aramid, carbon or glass fiber tows, containing thousands of very thin ($\sim$10 μm) filaments, are often subdivided into fiber and matrix-rich regions. Also, certain metal and ceramic matrix plies are reinforced by monolayers of relatively thick ($\sim$150 μm) boron or silicon carbide fibers. Such plies may have an orthotropic symmetry on the macroscale. Evaluation of the nine engineering moduli of orthotropic solids would expand Table 2.4 and require six applied stress components. However, since the constants are usually measured in plane stress applied to thin ply layers, experimental results are limited to those appearing in the table, and deviations from transverse isotropy are neglected. Transversely isotropic material symmetry is also adopted for properties of some cylindrically anisotropic fibers and of homogenized layered solids, such as surface coatings and thin films.

As shown in Sect. 3.9, the microstructure of aligned fiber materials allows derivation of universal connections involving the overall moduli, and known phase moduli and volume fractions. In transversely isotropic fiber systems, the number of independent overall moduli is thereby reduced from five to three, the two shear moduli m and p, and one of the moduli k, l, n, such as k. However, it is often convenient to use all five moduli in derivations.

2.3.2 Walpole's Notation

Using again the $x_A \equiv x_3$ convention, Walpole (1969) writes the relation $\boldsymbol{u} = \boldsymbol{A}\boldsymbol{w}$ between any symmetric second order tensors $\boldsymbol{u}, \boldsymbol{w}$, and a fourth-order tensor $\boldsymbol{A}$, all expressed in the contracted tensorial notation, in the expanded form by Hill (1964)

$$\left.\begin{array}{c} \begin{bmatrix} (u_{11}+u_{22})/2 \\ u_{33} \end{bmatrix} = \begin{bmatrix} \alpha & \beta_1 \\ \beta_2 & \gamma \end{bmatrix} \begin{bmatrix} (w_{11}+w_{22}) \\ w_{33} \end{bmatrix} \\ (u_{11}-u_{22}) = 2\delta(w_{11}-w_{22}) \\ u_{12} = 2\delta w_{12} \quad u_{23} = 2\varepsilon w_{23} \quad u_{31} = 2\varepsilon w_{31} \end{array}\right\} \tag{2.3.9}$$

For $\beta_1 = \beta_2 = \beta$, the $A_{ijkl} = A_{klij}$ is diagonally symmetric and transversely isotropic with respect to $x_A \equiv x_3$. It is positive definite if and only if $\alpha > 0, \delta > 0, \varepsilon > 0$, and $(\alpha\gamma - \beta^2) > 0$. In a symbolic form consistent with the contracted tensorial notation

$$\boldsymbol{A} = (2\alpha,\ \beta,\ \gamma,\ 2\delta,\ 2\varepsilon) \tag{2.3.10}$$

Equations 2.3.9 can then be replaced by

$$\begin{bmatrix} u_{11} \\ u_{22} \\ u_{33} \\ u_{23} \\ u_{13} \\ u_{12} \end{bmatrix} = \begin{bmatrix} (\alpha+\delta) & (\alpha-\delta) & \beta & 0 & 0 & 0 \\ (\alpha-\delta) & (\alpha+\delta) & \beta & 0 & 0 & 0 \\ \beta & \beta & \gamma & 0 & 0 & 0 \\ 0 & 0 & 0 & 2\varepsilon & 0 & 0 \\ 0 & 0 & 0 & 0 & 2\varepsilon & 0 \\ 0 & 0 & 0 & 0 & 0 & 2\delta \end{bmatrix} \begin{bmatrix} w_{11} \\ w_{22} \\ w_{33} \\ w_{23} \\ w_{13} \\ w_{12} \end{bmatrix} \tag{2.3.11}$$

The inverse $\boldsymbol{w} = \boldsymbol{A}^{-1}\boldsymbol{u}$ is written as

$$\boldsymbol{A}^{-1} = (\delta/(2\rho), -\beta/(2\rho), \alpha/\rho, 1/(2\delta), 1/(2\varepsilon)) \tag{2.3.12}$$

where $\rho = \alpha\gamma - \beta^2$. In matrix form, $\boldsymbol{w} = \boldsymbol{A}^{-1}\boldsymbol{u}$ is

$$\begin{bmatrix} w_{11} \\ w_{22} \\ w_{33} \\ w_{23} \\ w_{13} \\ w_{12} \end{bmatrix} = \begin{bmatrix} (\gamma/\rho + 1/\delta)/4 & (\gamma/\rho - 1/\delta)/4 & -\beta/2\rho & 0 & 0 & 0 \\ (\gamma/\rho - 1/\delta)/4 & (\gamma/\rho + 1/\delta)/4 & -\beta/2\rho & 0 & 0 & 0 \\ -\beta/2\rho & -\beta/2\rho & \alpha/\rho & 0 & 0 & 0 \\ 0 & 0 & 0 & 1/(2\varepsilon) & 0 & 0 \\ 0 & 0 & 0 & 0 & 1/(2\varepsilon) & 0 \\ 0 & 0 & 0 & 0 & 0 & 1/(2\delta) \end{bmatrix} \begin{bmatrix} u_{11} \\ u_{22} \\ u_{33} \\ u_{23} \\ u_{13} \\ u_{12} \end{bmatrix} \tag{2.3.13}$$

Walpole's notation is often used to describe different diagonally symmetric and transversely isotropic tensors in the micromechanics literature. Notice that the symbolic forms (2.3.10) and (2.3.12) are not affected by the choice of direction of the axis x_A of rotational symmetry; however, appropriate exchanges of rows and columns are required in the matrices (2.3.11) and (2.3.13). Moreover, notice that in the u_{ij} and w_{ij} in (2.3.9) are usually regarded as coefficients of the stress and strain tensors, hence the tensorial shear strain components in (2.3.11) and (2.3.13) are $\varepsilon_{23} = w_{23}$, etc., in contrast to their engineering form $2\varepsilon_{23} = w_{23}$, etc.

The engineering and contracted tensorial matrix notations invite the connections

$$\left.\begin{aligned} &\boldsymbol{\sigma} = \boldsymbol{L}\boldsymbol{\varepsilon} = \boldsymbol{L}_{EG}\boldsymbol{\varepsilon}_{EG} \quad \boldsymbol{L}_{EG} = \boldsymbol{L}\boldsymbol{\Theta}^{-1} = \boldsymbol{\Theta}^{-1}\boldsymbol{L} \\ &\boldsymbol{\varepsilon} = \boldsymbol{\Theta}^{-1}\boldsymbol{\varepsilon}_{EG} = \boldsymbol{M}\boldsymbol{\sigma} = \boldsymbol{\Theta}^{-1}\boldsymbol{M}_{EG}\boldsymbol{\sigma} \quad \boldsymbol{M}_{EG} = \boldsymbol{\Theta}\boldsymbol{M} = \boldsymbol{M}\boldsymbol{\Theta} \end{aligned}\right\} \qquad [1.1.22]$$

where the diagonal matrix $\boldsymbol{\Theta} = \text{diag}(1, 1, 1, 2, 2, 2)$. However, to preserve diagonal symmetry of the stiffness or compliance matrices $\boldsymbol{L}, \boldsymbol{M}$, these connections apply only to orthotropic, tetragonal, transversely isotropic, cubic and isotropic solids, all free of coupling between normal and shear strains and stresses.

Examples of application of Walpole's notation include stiffness and compliance matrices of transversely isotropic solids, written in the symbolic form consistent with the contracted tensorial notation and the $x_A \equiv x_3$ convention as

$$\boldsymbol{L} = (2k,\ l,\ n,\ 2m,\ 2p) \quad \boldsymbol{M} = (n/(2kE), -l/(2kE), 1/E, 1/2m, 1/2p) \tag{2.3.14}$$

For $x_A \equiv x_1$, the corresponding $\boldsymbol{L}$ and $\boldsymbol{M}$ matrices in the engineering notation are given by (2.3.3) and (2.3.2), where $kE = kE_{11} = kn - l^2$. Of course, (2.3.14) could be converted to engineering notation by changing $2m,\ 2p$ to $m,\ p$. For cubic material symmetry of §2.2.7, the stiffness and compliance can be written as

$$\boldsymbol{L} = (3\kappa,\ 2\mu,\ 2\mu') \quad \boldsymbol{M} = [1/(3\kappa),\ 1/(2\mu),\ 1/(2\mu')] \tag{2.3.15}$$

in terms of Zener's moduli (2.2.18). For isotropic stiffness and compliance tensors, the original Hill's (1965a) notation is, as in (2.2.29)

$$\boldsymbol{L} = (3K, 2G) \quad \boldsymbol{M} = (1/(3K), 1/(2G)) \tag{2.3.16}$$

Forms similar to $\boldsymbol{M}$ are also be used to define other tensors that have the dimension of a compliance, such as the $\boldsymbol{P}$ tensor in Sect. 4.6.

2.4 Cylindrically Orthotropic Materials

This is a separate symmetry class, characterized by distinct elastic moduli which are constant along each of the radial, tangential or hoop, and axial or longitudinal directions of cylindrical coordinates $r,\ \theta,\ z$. An orthogonal transformation from the Cartesian to the cylindrical system of coordinates is described by

$$\{r\ ,\ \theta,\ z\}_i^{\mathrm{T}} = a_{ij}x_j \tag{2.4.1}$$

where the a_{ij} is given in (2.2.5). Invariance is preserved only under translation in the z-direction and under a rotation by θ. Nine stiffness coefficients describe this type of symmetry. The constitutive relation uses the stiffness matrix $\boldsymbol{C}$, and is typically written as

$$\begin{bmatrix} \sigma_{rr} \\ \sigma_{\phi\phi} \\ \sigma_{zz} \\ \sigma_{\phi z} \\ \sigma_{zr} \\ \sigma_{r\phi} \end{bmatrix} = \begin{bmatrix} C_{rr} & C_{r\phi} & C_{rz} & 0 & 0 & 0 \\ & C_{\phi\phi} & C_{\phi z} & 0 & 0 & 0 \\ & & C_{zz} & 0 & 0 & 0 \\ & & & G_{\phi z} & 0 & 0 \\ & sym. & & & G_{zr} & 0 \\ & & & & & G_{r\phi} \end{bmatrix} \begin{bmatrix} \varepsilon_{rr} \\ \varepsilon_{\phi\phi} \\ \varepsilon_{zz} \\ 2\varepsilon_{\phi z} \\ 2\varepsilon_{zr} \\ 2\varepsilon_{r\phi} \end{bmatrix} \tag{2.4.2}$$

Radially or circumferentially orthotropic materials satisfy $C_{rr} > C_{\phi\phi}$ or $C_{rr} < C_{\phi\phi}$, respectively. Note that a transformation inverse to (2.4.1) renders the stiffness coefficients dependent on the angle θ, and thus on position in the Cartesian coordinate system.

Cylindrical orthotropic symmetry applies to fiber coatings or laminated composite cylinders, and also to anisotropic fibers where reliable experimental data are typically available only for the C_{zz} coefficient. Therefore, such fibers are often assumed to be only transversely isotropic, so that their properties can be extracted by micromechanical methods from those measured on matrix-based composites. The number of independent coefficients is then reduced from nine to five, using the following connections with Hill's moduli, written here for the $x_3 \equiv z$-axis of rotational symmetry

$$\left.\begin{array}{c} C_{rr} = C_{\phi\phi} = k + m \quad C_{r\phi} = k - m \quad C_{rz} = C_{\phi z} = l \quad C_{zz} = n \\ C_{rr} - C_{r\phi} = 2G_{r\phi} \quad G_{r\phi} = m \quad G_{\phi z} = G_{zr} = p \end{array}\right\} \tag{2.4.3}$$

2.5 Young's Modulus, Shear Modulus and Poisson's Ratio

Restrictions imposed on the elastic constants by positive definiteness of the strain energy function allow directional dependence of elastic moduli of anisotropic solids and thus invite search for directions that correspond to extremal values of engineering constants of practical interest, such as Young's modulus, shear modulus, and Poisson's ratio. As pointed out by Hayes and Shuvalov (1998), Sirotin and Shakol'skaya (1982) had derived the following expressions of the three moduli of any anisotropic elastic solid, as functions of compliance coefficients and spatial directions. In particular, the Young's modulus $E(\boldsymbol{n})$, defined as the ratio of the normal stress to normal strain, both acting in the direction of a certain unit vector $\boldsymbol{n}$, is given by

$$E(\boldsymbol{n}) = 1/(M_{ijkl} n_i n_j n_k n_l) \tag{2.5.1}$$

Explicit expressions and graphs of $E(\boldsymbol{n})$ for materials of different symmetry classes can be found in Backus (1970) and Nye (1957, 1985). The shear modulus $G(\boldsymbol{m}, \boldsymbol{n})$ is defined as the ratio of the shear stress to the shear strain on a square element whose two sides are described by two orthogonal unit normal vectors $\boldsymbol{m}$ and $\boldsymbol{n}$, such that $\boldsymbol{n} \cdot \boldsymbol{n} = \boldsymbol{m} \cdot \boldsymbol{m} = 1$ and $\boldsymbol{m} \cdot \boldsymbol{n} = 0$.

$$G(\boldsymbol{m}, \boldsymbol{n}) = G(\boldsymbol{n}, \boldsymbol{m}) = 1/(4 M_{ijkl} n_i m_j n_k m_l) \tag{2.5.2}$$

The Poisson's ratio $\nu(\boldsymbol{m}, \boldsymbol{n})$ is defined as the negative transverse strain along $\boldsymbol{m}$, divided by the axial strain in the direction of stretching force along the direction $\boldsymbol{n}$.

$$\nu(\boldsymbol{m}, \boldsymbol{n}) = -M_{ijkl} m_i m_j n_k n_l \,/\, (M_{pqrs} n_p n_q n_r n_s) \tag{2.5.3}$$

Ting (2005a) studied the maximum, minimum and saddle points of Young's modulus for a general anisotropic elastic material. He also shows that certain orthotropic and hexagonal materials can have a Young's modulus that is independent of the direction $\boldsymbol{n}$ (Ting 2005b). Srinivasan and Nigam (1969) derived certain invariant elastic moduli for crystals. Hayes and Shuvalov (1998) derived connections between extreme values of the three moduli of cubic materials, which had been identified by Turley and Sines (1971). Li (1976) presented a method for calculating Young's modulus, shear modulus and Poisson's ratio for hexagonal materials.

It turns out that (2.5.3) imposes no limits on the extreme values of Poisson's ratio in all anisotropic materials, where it may reach an arbitrarily large positive or negative value for certain directions of the above vectors (Boulanger and Hayes 1998; Ting 2004; Ting and Chen 2005; Ting and Barnett 2005). This admits existence and suggests design of auxetic materials with negative Poison's ratios (Lakes 1993; Zheng and Chen 2001; Baughman et al. 1998). They expand when stretched, which may enhance their shear moduli, indentation resistance and fracture toughness (Lakes 1987, 2000). With few exceptions, they do not exist in nature.

Table 2.5 Selected Symbols

Ω_0	Volume of the comparison medium surrounding $\Omega_r \ll \Omega_0$
Ω_r	Volume of homogeneous inclusion or inhomogeneity
Ω	Total volume $\Omega = \Omega_0 + \Omega_r$
$\partial\Omega$	Surface of volume Ω
$\partial\Omega_r$	Interface between Ω_r and Ω_0
$V, V_r, c_r = V_r/V$	Total and inhomogeneity volumes, and phase volume fraction in a composite aggregate
∂V_r	Interface between inhomogeneity $\boldsymbol{L}_r$ in V_r and matrix $\boldsymbol{L}_1$
$\boldsymbol{L}_0, \boldsymbol{M}_0$	Stiffness and compliance of a comparison medium in Ω_0
$\boldsymbol{L}_1, \boldsymbol{M}_1$	Stiffness and compliance of the matrix phase
$\boldsymbol{L}_r, \boldsymbol{M}_r$	Stiffness and compliance of an inhomogeneity in Ω_r or V_r
$\boldsymbol{L}, \boldsymbol{M}$	Overall stiffness and compliance of a composite aggregate
$\boldsymbol{\varepsilon}^0_\Omega, \boldsymbol{\varepsilon}^0$	Uniform overall strain applied to Ω or V
$\boldsymbol{\mu}_0, \boldsymbol{\mu}_r$	Uniform eigenstrain applied in Ω_0, and Ω_r or V_r
$\bar{\boldsymbol{\sigma}}_\Omega, \ \bar{\boldsymbol{\sigma}}$	Overall stress caused in Ω or V by the load set $\{\boldsymbol{\varepsilon}^0, \boldsymbol{\mu}_r, \boldsymbol{\mu}_0\}$
$\bar{\boldsymbol{\lambda}}$	Overall eigenstress caused in Ω and V by the load set $\{\boldsymbol{\varepsilon}^0, \boldsymbol{\mu}_r, \boldsymbol{\mu}_0\}$
$\boldsymbol{\sigma}^0_\Omega, \boldsymbol{\sigma}^0$	Uniform overall stress applied to Ω or V
$\boldsymbol{\lambda}_0, \boldsymbol{\lambda}_r$	Uniform eigenstress applied in Ω_0 and Ω_r or V_r
$\bar{\boldsymbol{\varepsilon}}_\Omega, \bar{\boldsymbol{\varepsilon}}$	Overall strain caused by load set $\{\boldsymbol{\sigma}^0, \boldsymbol{\lambda}_r, \boldsymbol{\lambda}^0\}$ in Ω or V
$\bar{\boldsymbol{\mu}}$	Overall eigenstrain caused by load set $\{\boldsymbol{\sigma}^0, \boldsymbol{\lambda}_r, \boldsymbol{\lambda}^0\}$
$\boldsymbol{\varepsilon}_r, \bar{\boldsymbol{\varepsilon}}_r$	Uniform and average local strain in Ω_r or V_r
$\boldsymbol{\sigma}_r, \bar{\boldsymbol{\sigma}}_r$	Uniform and average local stress in Ω_r or V_r
$\boldsymbol{\mu}_r^{eq}, \boldsymbol{\lambda}_r^{eq}$	Uniform equivalent eigenstrain and eigenstress in Ω_r or V_r
$\boldsymbol{\mu}_r^{dq}, \ \boldsymbol{\lambda}_r^{dq}$	Uniform damage-equivalent eigenstrain and eigenstress in Ω_r or V_r
$\boldsymbol{T}_r, \boldsymbol{R}_{rr}, \boldsymbol{R}_{r0}$	Partial strain and eigenstrain concentration factors
$\boldsymbol{W}_r, \boldsymbol{N}_{rr}, \boldsymbol{N}_{r0}$	Partial stress and eigenstress concentration factors

However, they can be realized by certain symmetric laminates with $(\pm\theta)_S$ layups, Sect. 10.7, or by homogenization of specific microstructures. For example, Almgren (1985) designed structures, in two or three dimensions consisting of rods, hinges, and springs that have a negative Poisson's ratio. Foam materials with negative Poisson's ratio have also been developed (Lakes 1987). Evans et al. (1991) used molecular modeling techniques to design a molecular network with a negative Poisson's ratio (see also Guo and Wheeler 2006). Some potential applications of auxetic materials can be found in review articles by Evans (1991) and Lakes (1993).

A list of symbols frequently used in the chapters that follow appears in Table 2.5.

Chapter 3
Elementary Concepts and Tools

This chapter provides a brief introduction to micromechanics. Following an overview of several descriptors of microstructural geometry is an outline of the procedures that predict overall response of a heterogeneous aggregate in terms of phase volume averages of local strain or stress fields. Applied loads include uniform overall strain or stress and a piecewise uniform distribution of eigenstrains or transformation strains in the phases. Derivations of theorems, formulae and connections that will frequently be used in subsequent chapters are presented in Sects. 3.7, 3.8 and 3.9. A summary of the overall and local response estimates appears in the concluding Sect. 3.10. Many symbols used in this and following chapters are summarized in Table 2.5.

3.1 Aggregates and Constituent Phases

Heterogeneous materials, such as fibrous or particulate composites and polycrystals, are modeled as aggregates of *homogeneous phases* that occupy simply or multiply connected parts V_r ($r = 1, 2, \ldots n$) of the total volume V. In a selected overall system of Cartesian coordinates defined in V, each phase in a volume V_r has certain constant physical properties, such as elastic moduli, coefficients of thermal expansion, thermal and electrical conductivity, and dielectric constant. Aligned or misaligned fibers, particles, matrices, coatings, interphases, or polycrystal grains are examples of constituent phases. Any of the eight material symmetries described in Chap. 2 may be exhibited by and assigned to a constituent phase.

A matrix-based composite reinforced by aligned isotropic or transversely isotropic fibers is a typical two-phase system, since all fibers have identical stiffness coefficients in the selected overall coordinate system. Any composite consisting of a homogeneous matrix and dispersed isotropic particles, aligned or misaligned short or long fibers, is also a two-phase system. However, if the reinforcements are anisotropic and misaligned or randomly orientated, then each particle or fiber

G.J. Dvorak, *Micromechanics of Composite Materials*, Solid Mechanics and Its Applications 186, DOI 10.1007/978-94-007-4101-0_3,

represents a distinct phase of a multiphase composite. Accordingly, polycrystals are multiphase systems, with each anisotropic grain or a set of similarly aligned grains representing a separate phase.

Composite materials and laminates often tolerate presence of distributed damage in the form of imperfect interface bonds, matrix cracks and fiber breaks. Such defects may be regarded as additional phases with modified or vanishing property values. However, perfect interface bonds and absence of damage are assumed to prevail in the materials described this chapter.

3.2 Heterogeneous Microstructures

Heterogeneity of the microstructure of composite materials is a function of the size scale used to solve a particular problem. Many different scales can be employed, depending on the typical absolute size of the constituents of interest, which may range from the nanoscale at 10^{-9} m, to the microscale at 10^{-6} m, to the mesoscale at 10^{-3} m, and finally to the macroscale. Both local and overall properties and interactions between the phases depend on phase geometry and phase material properties expressed at each scale. As an example, consider a laminated plate or shell made of fiber-reinforced plies, which have a polymer matrix that has been modified by an addition of nano-sized ceramic particles. Modeling of such system should start at the nanoscale, by first considering interactions of the particle surface layers with adjacent polymer chains that may result in chain alignment along particle surfaces. Such interface layers can be regarded as graded interphases with certain effective properties. Then, the mixture consisting of particles, interphases and bulk matrix is homogenized to provide estimates of effective properties of the modified matrix. Another homogenization is then performed at the microscale, where the modified matrix is reinforced by a certain volume fraction of aligned fibers. This yields effective properties of a macroscopic composite element, a fibrous ply. Finally, the plies are laid up in a certain orientation and stacking sequence, and bonded together to form a laminated plate or shell, with properties derived from those of the homogenized plies. Connections between local deformation and stress fields at all scales, established in the multiscale homogenization sequence, are then used to estimate local fields caused at the different scales by applied loads, and the expected response and load bearing capacity of the composite structure.

Transitions from local material properties to those of a homogenized mixture can be examined in the context of statistical geometry of random heterogeneous media, as described by Beran (1968), and more recently by Torquato (2002), who presents an authoritative and extensive overview of the subject.

3.2.1 Simple Descriptors

As in standard material characterization, a collection, or an ensemble, of material samples of similar shape and volume is considered. The ensemble volume $V >> \Omega$, where Ω is the volume of a single sample. Each sample contains the same nominal volume V_r of each constituent phase $r = 1, 2, \ldots n$, or a constant phase volume fraction $c_r = V_r/V$, such that $\Sigma c_r = 1$. Phase subvolumes of matrices, individual particles or fibers, are denoted by $\boldsymbol{v}_r$. In each sample, they are assumed to be of similar size and distributed at random.

A heterogeneous microstructure can be represented by a realization of a specific random process. In the infinite-volume limit, it is possible to invoke the *ergodic hypothesis*, which postulates that the result of averaging over all realizations of the ensemble is equal to the result of averaging over one realization of very large volume, for $\Omega \to V \to \infty$. A single Cartesian coordinate system $\boldsymbol{x} = (x_1, x_2, x_3)^{\mathrm{T}}$ is attached to each sample of the ensemble with the same fixed origin and orientation. Although all samples have identical external appearance in the $\boldsymbol{x}$-coordinates, any given point $\boldsymbol{x} \in \Omega$ selected in the same position in all samples, can reside in a different phase subvolume $\boldsymbol{v}_r$. The actual phase r hosting point $\boldsymbol{x}$ is conveniently identified by the value of the indicator or characteristic function of phase r, defined for each subvolume $\boldsymbol{v}_r$ as

$$I_r(\boldsymbol{x}) = \begin{cases} 1 & \text{if } \boldsymbol{x} \in \boldsymbol{v}_r \\ 0 & \text{otherwise} \end{cases} \tag{3.2.1}$$

such that $\sum \boldsymbol{I}_r = 1$.

In two-phase systems, preferred in what follows, the indicator function is a random variable with two possible values at a fixed point $\boldsymbol{x}$. The probability of finding a given phase r at any point $\boldsymbol{x} \in \Omega$ is

$$\boldsymbol{P}\{\boldsymbol{I}_r(\boldsymbol{x}) = 1\} = 1 - \boldsymbol{P}\{\boldsymbol{I}_r(\boldsymbol{x}) = 0\} \tag{3.2.2}$$

For all realizations of the ensemble, the expectation, or an ensemble average of $\boldsymbol{I}_r(\boldsymbol{x})$, is denoted by the *one-point probability function* of phase r

$$S_1^r(\boldsymbol{x}) \equiv \langle \boldsymbol{I}_r(\boldsymbol{x}) \rangle = \boldsymbol{P}\{\boldsymbol{I}_r(\boldsymbol{x}) = 1\} \tag{3.2.3}$$

For a function $\Phi(\boldsymbol{x}) \equiv \Phi[\boldsymbol{I}_r(\boldsymbol{x})]$ describing certain properties of a microstructure in one realization of a very large material volume, or equivalently in all realizations of the ensemble, the expectation or average $\overline{\Phi}$ is identified with the ensemble average $\langle \Phi \rangle$ indicated by the angular brackets

$$\langle \Phi \rangle \equiv \overline{\Phi} = \lim_{V \to \infty} \frac{1}{V} \int_V \Phi(\boldsymbol{x}) \mathrm{d}V \tag{3.2.4}$$

The volume fraction c_r of a phase r in a statistically homogeneous medium is defined by the one-point probability function (3.2.3) as

$$c_r = S_1^r(\boldsymbol{x}_1) = \langle \boldsymbol{I}_r(\boldsymbol{x}_1) \rangle = V_r / V \tag{3.2.5}$$

where $V_r = q_r \boldsymbol{v}_r$ is the total volume, comprised of q_r phase subvolumes $\boldsymbol{v}_r$, in the total volume V of the ensemble.

A more intuitive definition of the phase volume fraction is the *number density* η_r which counts the number of *r-th* phase subvolumes $\boldsymbol{v}_r$ in the total volume V. For subvolumes of similar size and shape, η_r is related to the dimensionless density c_r as follows

$$\eta_r = \lim_{q_r,\, V \to \infty} q_r / V \qquad c_r = \eta_r \boldsymbol{v}_r \tag{3.2.6}$$

The probability of finding a selected phase $r = 1, 2$ at two or more points $\boldsymbol{x}_i$, $i = 1, 2, \ldots N$, in volume Ω is equal to the expectation of the product, denoted by an N-point probability function for phase r

$$S_N^{(r)}(\boldsymbol{x}_1, \boldsymbol{x}_2, \ldots \boldsymbol{x}_N) = \left\langle \prod_{i=1}^{N} \boldsymbol{I}_r(\boldsymbol{x}_i) \right\rangle = \boldsymbol{P}\left\{ \boldsymbol{I}_r(\boldsymbol{x}_1) = 1, \boldsymbol{I}_r(\boldsymbol{x}_2) = 1, \ldots \boldsymbol{I}_r(\boldsymbol{x}_N) \right\} = 1 \tag{3.2.7}$$

Specific evaluations of these functions are difficult to obtain, and have thus been limited mostly to $S_2^{(r)}$ for up to three-dimensional two-phase systems with circular or spherical shapes of the second phase. However, the hierarchy of the N-point probability functions provides a conceptual basis for several definitions of important properties of composites microstructures.

3.2.2 Statistical Homogeneity and Material Symmetry

Statistical homogeneity of a heterogeneous medium relies on the ergodic hypothesis, defined by translational invariance of the N-point probability functions. This implies that $S_N^r(\boldsymbol{x}_i) \equiv S_N^r(\boldsymbol{x}_i + \boldsymbol{y})$, where $\boldsymbol{y}$ is a translation vector, and $\boldsymbol{x}_i + \boldsymbol{y}$ are well within Ω. Therefore, each member of the said hierarchy of S_N^r depends only on the relative position of any particular set of points $\boldsymbol{x}_i$, and is independent of the position of the origin of spatial coordinates in Ω. The relative position of any pair of the points $\boldsymbol{x}_i$ is written as $\boldsymbol{x}_{pq} = \boldsymbol{x}_p - \boldsymbol{x}_q$. It then follows that a heterogeneous aggregate is statistically homogeneous if and only if

$$S_N^r(\boldsymbol{x}_1, \boldsymbol{x}_2, \ldots \boldsymbol{x}_N) = S_N^r(\boldsymbol{x}_{pq}) \quad p \neq q = 1, 2, \ldots N \tag{3.2.8}$$

Statistical isotropy is another independent property of the microstructural geometry, defined in a Cartesian system by directional invariance of S_N^r, under coordinate transformations $x_i = a_{ij} x_j$ where a_{ij} is a matrix of directional cosines. Combined with the translational invariance of statistical homogeneity, statistical isotropy makes the S_N^r functions dependent only on the distance $x_{pq} = |\boldsymbol{x}_{pq}| = x_{qp}$ between pairs of points $\boldsymbol{x}_i$. Specific forms of S_N^r for $N = 2,\ 3$ are written as

$$S_2^r(\boldsymbol{x}_1, \boldsymbol{x}_2) = S_2^r(x_{12}) \qquad S_3^r(\boldsymbol{x}_1, \boldsymbol{x}_2, \boldsymbol{x}_3) = S_3^r(x_{12}, x_{23}, x_{31}) \tag{3.2.9}$$

Higher-order probability functions cannot be derived from lower order functions, except in systems with equal phase volume fractions $c_1 = c_2 = 0.5$, exhibiting phase-inversion symmetry. However, asymptotic values of S_3^r can be found for the following permutations of the distances $x_{12},\ x_{23}$ and x_{31} (Torquato 2002)

$$\left.\begin{aligned} &\lim_{x_{12}\to 0,\ x_{13}\to 0} S_3^r(x_{12}, x_{13}, x_{23}) = c_r && \lim_{x_{23}\to 0} S_3^r(x_{12}, x_{13}, x_{23}) = S_2^r(x_{12}) \\ &\lim_{x_{12}\ \text{fixed},\ x_{13}\to\infty} S_3^r(x_{12}, x_{13}, x_{23}) = c_r S_2^r(x_{12}) && \lim_{\text{all } x_{pq}\to\infty} S_3^r(x_{12}, x_{13}, x_{23}) = c_r^3 \end{aligned}\right\} \tag{3.2.10}$$

Statistical anisotropy is defined in a Cartesian system by invariance under the group of transformations that characterize one of the particular material symmetries described in Chap. 2. It often coexists with statistical homogeneity, for example, in solids made by stacking repetitive parallel layer pairs or sequences of different phase materials. Such layered materials are statistically homogeneous and transversely isotropic on the macroscale. By assigning different translational and/or orientation-dependent properties to the S_N^r functions, one can define statistically inhomogeneous and/or anisotropic aggregates that are representative, for example, of graded composites with phase densities varying in one or more directions.

3.2.3 Specific Surface

This is another useful descriptor of the microstructure, defined by

$$s(\boldsymbol{v}_r) = \eta_r(\partial \boldsymbol{v}_r) = c_r(\partial \boldsymbol{v}_r)/\boldsymbol{v}_r \tag{3.2.11}$$

It is the ratio of surface area $\partial \boldsymbol{v}_r$ to subvolume $\boldsymbol{v}_r$ of phase r, adjusted by the volume fraction c_r to the total area of all surfaces $\partial \boldsymbol{v}_r$ of the subvolumes $\boldsymbol{v}_r$, in a unit volume of the aggregate. In other words, it is the total area of all interfaces in a unit volume of a heterogeneous aggregate. In two-phase systems where c_2 is the volume fraction of the second phase, the specific surface is

$$\left.\begin{aligned} \mathbf{s}(\boldsymbol{v}_2) &= 2c_2/R \text{ for cylindrical fibers of radius } R \text{ and unit length} \\ \mathbf{s}(\boldsymbol{v}_2) &= 3c_2/R \text{ for spherical particles of radius } R \\ \mathbf{s}(\boldsymbol{v}_2) &= 2c_2A/At = 2c_2/t \text{ for platelets of area } A \text{ and thickness } t \end{aligned}\right\} \quad (3.2.12)$$

As an example, let us derive the specific surface or interfaces area in a 1 cm^3 volume of a matrix-based composite, reinforced by a volume fraction c_f of aligned S-glass, E-glass or P100 graphite fibers. Those fibers have nearly circular cross sections, with $R_f \approx 5\times10^{-6}$ m. A single fiber that is 1 cm long occupies the subvolume $\boldsymbol{v}_f = \pi\, 0.25\times10^{-6}\,cm^3$ and has the surface area $\partial\boldsymbol{v}_f = \pi\, 0.1\times10^{-2}\,cm^2$. There are $(4c_f/\pi)\times10^6$ fibers in 1 cm^3 of total volume. The specific surface or interface area of a fiber volume fraction $0 < c_f < 1$ is then $\mathbf{s}(\boldsymbol{v}_f)=c_f\times0.4\,m^2/1\,cm^3 = 2c_f/R_f$. On the other hand, in fiber composites reinforced by boron or SiC fibers, where $R \doteq 70\times10^{-6}$ m, there are $\boldsymbol{v}_f = \pi\, 49\times10^{-6}\,cm^3$, $\partial\boldsymbol{v}_f = \pi\, 140\times10^{-4}\,cm^2$, and the specific surface area of the fibers is $\mathbf{s}(\boldsymbol{v}_f) = c_f \times 0.0285\,m^2/1\,cm^3$, or only 7.13% of the surface area of the 10 μm diameter fibers.

Among common objects, books with sheet thickness of 1×10^{-4} m have a relatively small page surface area of 0.02 m^2, or 200 cm^2, in a 1 cm^3 of volume, of similar order as the $\mathbf{s}(\boldsymbol{v}_f)$ of boron or SiC fiber composite. However, the specific interface area assumes a significant magnitude in nanocomposites reinforced by platelets with $t = 10^{-9}$ to 10^{-8} m, or by spherical particles with $R = 10^{-8}$ to 10^{-6} m. For example, the area of interface contributed by each percentage point ($c_2 = 0.01$) of spherical particles with radius $R = 10$ nm turns out to be equal to 3 m^2 in each 1 cm^3 of material volume. In the same 1 cm^3 of material volume, each volume percent of flat platelets of thickness $t = 10^{-9}$ or 10^{-8} m creates the interfacial area equal to 20 or 2 m^2. If the particles or platelets are coated, e.g., by layers of aligned polymer chains and are present in higher concentrations, the coatings may occupy a significant fraction of the total volume. In fact, the entire 1 cm^3 volume could be filled with the single volume percent of above flat platelets if the coating thickness approached 0.5×10^{-7} m or 0.5×10^{-6} m, respectively. Large interphase regimes have been found in certain polymer nanocomposites reinforced by small loadings (1 wt.% or less) of nanotubes or graphitic nanofillers, as discussed in Sect. 9.3 (Ramanathan et al. 2005, 2008).

3.2.4 Two-Point Probability Function

For a phase r in a statistically homogeneous medium the two-point probability is the autocorrelation function of $\boldsymbol{I}_r$

$$S_2^r(\boldsymbol{x}_1,\ \boldsymbol{x}_2) = \langle \boldsymbol{I}_r(\boldsymbol{x}_1)\boldsymbol{I}_r(\boldsymbol{x}_2)\rangle = S_2^r(\boldsymbol{\rho}) \quad (3.2.13)$$

where $\boldsymbol{\rho} = \boldsymbol{x}_2 - \boldsymbol{x}_1$ reflects the translational invariance with respect to a specified direction. For example, in a statistically isotropic medium, the two-point function can be generated by randomly placing a line segment of length $\rho \equiv |\boldsymbol{\rho}|$ and counting the fraction of times the end points, but not necessarily the entire length of the segment, are found in volume $\boldsymbol{v}_r$ of phase r. Somewhat similar is Buffon's (1777) problem of placing a needle at random in a plane covered by straight, parallel lines a unit distance apart, or on a grid of such lines, and counting the probability of the needle crossing the lines (Clark 1933; Kendal and Moran 1962).

The two-point probability function indicates the relative position of individual subvolumes of the phases, which can be used to estimate different aspects of their distribution and interaction. As suggested by (3.2.10), third or higher order probability functions would follow by replacing the line segment by a triangle or by polygons. For small and very large distances and in the absence of long-range correlations

$$\lim_{\rho \to 0} S_2^r(\rho) \to c_r \qquad \lim_{\rho \to \infty} S_2^r(\rho) = c_r^2 \tag{3.2.14}$$

For small values of ρ, the $S_2^{(1)}(\rho)$ for the matrix ($r = 1$) of a two-phase, three-dimensional isotropic medium can be approximated by (Debye et al. 1957)

$$S_2^{(1)}(\rho) = c_1 - \frac{\boldsymbol{s}(\boldsymbol{v}_2)}{4}\rho + O(\rho^2) \tag{3.2.15}$$

The first derivative of this function at $\rho \to 0$ is thus equal to minus one-quarter of the specific surface area. Berryman (1987) generalized this result for anisotropic porous media by showing that the angular average of the anisotropic two-point spatial correlation function has the same relationship to the specific surface.

Figure 3.1, derived from Torquato's (2002), Table 5.1, illustrates this behavior, by showing the autocovariance $S_2^{(1)}(\rho) - c_1^2$ of matrix $r = 1$ containing an isotropic distribution of hard spheres of diameter D at three volume fractions c_2, computed from the Verlet (1972) correction to the Percus and Yevick (1958) approximation.

Higher order terms in (3.2.13) were evaluated by Torquato and Stell (1985) and Lu and Torquato (1990) for matrix-based aggregates containing either two or three-dimensional distributions of both penetrable and impenetrable hard discs or spheres of diameter D. Their results cover the entire range of volume fractions and extend to large ρ/D ratios. They show a rapid decrease of the difference $S_2^{(1)}(\rho) - c_1^2$ with increasing c_2, from its maximum $c_1 - c_1^2 = c_1 c_2$, which is the variance of the characteristic function (3.2.1) of either phase at $\rho/D = 0$, to zero at $\rho/D \approx 1.5 \div 2$. Small oscillations caused by volume exclusion effects are observed at higher ρ/D ratios, and are more evident at higher c_2. This indicates absence of significant interactions between phase subvolumes that are about two diameters apart.

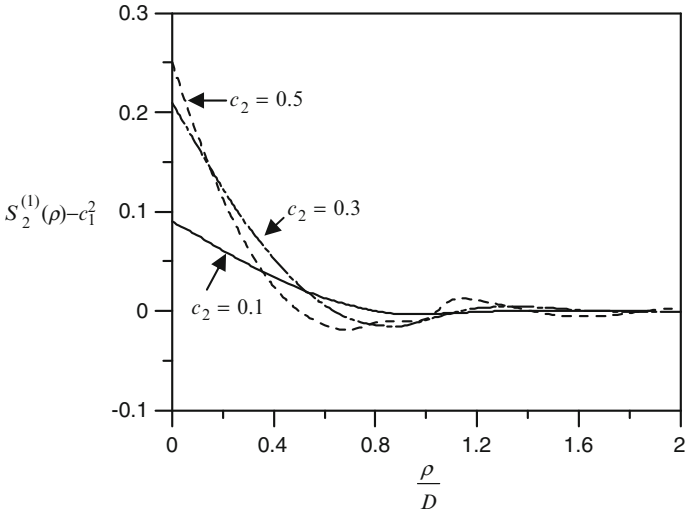

Fig. 3.1 Autocovariance of isotropic distribution of hard spheres of diameter D, density c_2

3.3 Representative Volume

3.3.1 Size Requirements

Design of composite structures relies, in part, on evaluation of *overall or effective properties* of the heterogeneous composite material, such as elastic moduli, coefficients of thermal expansion, or conductivity, which are then attributed to an equivalent homogeneous solid. On an appropriate material size scale, these effective properties can be measured experimentally, or estimated by theoretical models. In the latter, material constants are determined from local fields in a certain representative volume element, or RVE, of a statistically homogeneous material, which is subjected to macroscopically homogeneous boundary conditions applied to its surface.

For example, as shown in Chaps. 6 and 7, application of surface displacements or tractions derived from a uniform state of strain or stress leads to evaluation of bounds and estimates overall stiffness or compliance. A distribution of phase eigenstrains, such as thermal or transformation strains, which is statistically homogeneous and invariant under the group of transformations that define overall material symmetry, generates a macroscopically uniform eigenstrain in a traction-free representative volume of a heterogeneous solid. In the case of thermal strains caused in the phases by a uniform change in temperature, the overall strain can be related to effective thermal expansion coefficients. Conversely, a macroscopically uniform eigenstress is generated by the said distribution of phase eigenstrains if the representative volume is constrained by zero surface displacements.

To assure independence of the results on specific boundary conditions and on absolute size of the constituents, the representative volume should be of sufficient size to represent the typical microstructure, such that the resulting estimates of material constants are valid for any larger volume (Hill 1963a).

In the absence of a specific definition of the 'sufficient size', the representative volume is essentially a convenient theoretical concept, indicating an interior material volume removed from applied surface loads, and containing many microconstituents, such as particles or fibers, voids or microcracks, or crystalline grains.

However, recent estimates of the necessary rather than sufficient size of the RVE, suggest that a relatively small size should be adequate. In particular, Drugan and Willis (1996) found that the representative volume of a three-dimensional aggregate of identical spheres, based on the Percus and Yevick (1958) and Wertheim (1963) hard-sphere radial distribution function, need not be larger than twice the reinforcement diameter. This result applies to an estimate of the overall moduli that admits a 5% maximum error, and it holds for an entire range of sphere concentrations and stiffness magnitudes, including spherical voids. Notice that this outcome is anticipated by Fig. 3.1, which shows that the two-point probability function remains essentially constant for $\rho/D > 2$.

Additional confirmation of the above estimate of necessary RVE size was provided by Gusev's (1997) numerical evaluations of elastic moduli of periodic unit cell models of several Monte-Carlo realizations of two-phase composites reinforced by a random distribution of identical spherical particles. For a statistically isotropic mixture, the computed overall Young's and shear moduli of unit cells containing 8, 27 or 64 spheres at fixed concentrations were found to be within 3% and 7% of their average value. The periodic boundary conditions applied to the unit cells simulated a small uniform overall strain. As shown by Huet (1990) and Hazanov and Huet (1994) the results represent an upper bound on the elastic moduli, whereas application of a uniform traction field would produce a lower bound. Similar results were reached by Ostoja-Starzewski (1998). Therefore, careful evaluation of sufficient representative volume size is indicated for unit cell models of a given microstructure. This was pursued in detail by Pecullan et al. (1999) on two-dimensional finite element models composites consisting of square domains filled with $1 \leq n \leq (6 \times 6)$ unit cells of three different geometries; two designed to approximate the upper and lower bounds on bulk moduli, and one generating a composite with a negative Poisson's ratio. Their results show very small error associated with replacing the smallest scale regions by an equivalent homogeneous medium when $n \approx 3$.

Minimum representative volume requirements for unit cell models of perfectly bonded cubic polycrystals were examined by several numerical experiments. Ren and Zheng (2002, 2004) approximated the polycrystal by a square, plane stress model of increasing size, and concluded that the effective shear and Young's moduli can be approximated with less than 5% error by a representative volume size of 16 or less times the grain size. They also indicate a linear dependence of the required size on the crystal anisotropy. That effect was also observed by Nygårds (2003) who used a discrete version of the Voronoi algorithm to partition a finite

element mesh into grains. He suggests a rough approximation of the number of grains needed in a representative volume, in the form $N_{rep} \approx 0.03(A_Z - 1)/err^2$, where $A_Z = 2L_{44}/(L_{11} - L_{12})$ is Zener's (1948) measure of anisotropy of cubic crystals (2.2.18), and *err* is an acceptable error. Elvin (1996) simulated response of polycrystalline ice under compression and found that at least 230 grains were needed for the aggregate to exhibit homogenized elastic behavior.

A useful conclusion that can be drawn from such studies is that effective elastic moduli estimated by different homogenization methods in large representative volumes provide a close approximation of effective moduli of material volumes of finite size, containing 10–30 inhomogeneities in matrix-based systems, or few hundred grains in a polycrystal. This has implications for hierarchical modeling of multiscale and gradient microstructures, and for formulation of non-local constitutive equations for elastic composites (Drugan 2000).

3.3.2 Local Volume Fraction Fluctuations

As long as RVE size is accepted to be 'sufficiently large', the phase volume fractions are constants defined by (3.2.5). However, both their overall and local magnitudes may depend on a number of factors related to manufacturing and processing of a particular material, or to a position in a sample. For example, most polymer matrix fibrous composites are reinforced by fiber tows containing thousands of individual filaments with diameters of 5–20 μm. Therefore, the fiber volume fraction in a 0.125 mm thick ply may approach full saturation in the impregnated volume of each tow, and remain low in the matrix-rich regions separating the tows. Changes in matrix volume during consolidation and curing may affect the overall concentration. Even in systems consisting of apparently periodic monolayers of carefully laid 150–200 μm fibers, a series of micrographs of the microstructure may reveal differences of several percent from the 'nominal' volume fraction provided by the fabricator. Since the volume fraction magnitude may have a significant influence on certain overall properties, a reliable evaluation of actual distribution and volume fraction of the phases should be made in any comparison of experimental results with theoretical predictions.

In a representative or any material volume, the phase volume fraction may fluctuate as a function of position and of the ratio $V_O/\boldsymbol{v}_r$, which compares the size of a selected observation window V_O to that of typical subvolume $\boldsymbol{v}_r$ of a phase *r*. For statistically homogeneous and isotropic distributions of impenetrable and penetrable disks and spheres in a continuous matrix, Lu and Torquato (1990) and Quintanilla and Torquato (1997), had introduced a measure of local volume fraction fluctuations. In particular, they define the *coarseness C* as scaled standard deviation σ of the local volume fraction function, a random variable $c_r(\boldsymbol{x})$

$$C = \frac{\sigma}{c_r} = \frac{\left(\langle c_r^2 \rangle - c_r^2\right)^{1/2}}{c_r} \tag{3.3.1}$$

For an infinitely large observation window $V_O \to \infty$, the expected value $c_r(\boldsymbol{x}) \to c_r$. At the other extreme, for $V_O \to 0$, the $c_r(\boldsymbol{x}) \to \boldsymbol{I}_r(\boldsymbol{x})$, the phase indicator function (3.2.1). In two-phase media, the variance $\langle \boldsymbol{I}_2^2 \rangle - \langle \boldsymbol{I}_2 \rangle^2 = c_2 - c_2^2$, hence

$$C = (c_2/c_1)^{1/2} \text{ for } V_O \to 0 \qquad C = 0 \text{ for } V_O \to \infty \tag{3.3.2}$$

In observation windows of intermediate size, suggested for example by the Drugan and Willis (1996) estimate of $V_O/\boldsymbol{v}_r \geqslant 8$ as sufficient size of the representative volume for evaluation of elastic moduli of a matrix-based composite reinforced by a random distribution of spheres, one can utilize the asymptotic formula

$$C = \frac{1}{c_1\sqrt{V_O}} \left[\int_{\rho<\ell} [S_2^{(1)}(\rho) - c_1^2] \rho^{d-1} \mathrm{d}\rho \right]^{1/2} \tag{3.3.3}$$

where the spatial dimension $d = 2$ or 3 for disks or spheres. The correlation length ℓ can be taken as $(\ell/D)^3 \approx V_O/\boldsymbol{v}_r \geqslant 8$, where D is the diameter of circular disks or spheres of the second phase $r = 2$. Quintanilla and Torquato (1997) show that the volume fraction distribution can often be approximated by the normal distribution in the observation window, as

$$c_2(x) = \frac{1}{\sqrt{2\pi\sigma^2}} \exp\left(-[(x - c_2)/\sigma]^2/2\right) \tag{3.3.4}$$

where c_2 represents the mean value and $\sigma = c_2 C$ is the standard deviation (3.3.1).

Computed values of coarseness, scaled to $C(V_O/\boldsymbol{v}_2)^{1/2}$ appear to approach their long-range values at $V_O/\boldsymbol{v}_r \geqslant 8$, and at much smaller ratios for $c_2 = 0.2$. Lu and Torquato (1990) found these values for impenetrable spheres as

$$\left.\begin{aligned} C(V_O/\boldsymbol{v}_2)^{1/2} &\approx 0.25 \Rightarrow \sigma \approx 0.0177 \text{ at } c_2 = 0.2 \\ C(V_O/\boldsymbol{v}_2)^{1/2} &\approx 0.15 \Rightarrow \sigma = 0.0318 \text{ at } c_2 = 0.6 \end{aligned}\right\} \tag{3.3.5}$$

Together with (3.3.4), that indicates that fairly large deviations from the mean value may be found in small material volumes. Of course, this spread rapidly tightens at larger ratios of $V_O/\boldsymbol{v}_r$.

Another source of nonuniform phase distribution in material volumes is the development of clusters of particle or fiber reinforcements. This is expected at high volume fractions, according to different estimates of the upper limit $c_2 \leq c_{cp}$ of random closed packing. For example, the upper packing limit $c_{cp} = \pi/\sqrt{18} = 0.7405$ applies to monodisperse hard spheres in a face-centered cubic lattice. Somewhat lower limit $c_{cp} \approx 0.68$ is suggested for this material by the Monte Carlo simulations of Tobochnik and Chapin (1988), and by the 'drop and roll' algorithm

used by Visscher and Bolstrelli (1972), which yields $c_{cp} \approx 0.60$. However, isolated particle or fiber clusters can develop even at very low concentrations, for example, in nano-scale composite materials with large specific surface.

3.4 Stress and Strain Field Averages

Geometry of the microstructure of composite materials is usually specified only in terms of the shape, size, orientation and volume fractions of the phases. Therefore, actual local strain and stress fields can be found only in few selected models of well defined microstructures. However, estimates of phase volume averages of the local fields are within reach of several approximate methods. Of interest in this section are connections between the applied uniform overall fields and the resulting local fields and their averages.

A representative volume V of a heterogeneous solid, enclosed by surface ∂V, is loaded according to one of the two homogeneous boundary conditions described below, which apply a uniform overall stress or strain.

(*a*) Self-equilibrating surface tractions $t_i(\boldsymbol{x}) = \sigma_{ij}(\boldsymbol{x})n_j(\boldsymbol{x})$, derived from a certain overall stress field $\sigma_{ij}(\boldsymbol{x})$ are prescribed at all surface points $\boldsymbol{x} \in \partial V$ with the outside normal $n_j(\boldsymbol{x})$. The range of subscripts is $i, j = 1, 2, 3$, and $\boldsymbol{x}$ is a position coordinate. Interior stress field is continuous but not necessarily uniform, and it satisfies the equations of equilibrium $\sigma_{ij,j} = 0$ and the prescribed boundary conditions.

Volume average of the stress field in V is provided by the divergence theorem

$$\int_{\partial V} \sigma_{ik} n_k x_j \mathrm{d}S = \int_V \frac{\partial}{\partial x_k}(\sigma_{ik} x_j)\mathrm{d}V = \int_V [\sigma_{ik,k} x_j + \sigma_{ik} x_{j,k}]\mathrm{d}V = \int_V \sigma_{ij}(\boldsymbol{x})\mathrm{d}V \tag{3.4.1}$$

where $x_{j,k} = \delta_{jk}$ is the Kronecker delta. With reference to the Cauchy formula $t_i = \sigma_{ij} n_j$, the first integral is rewritten in a symmetric form and scaled by V. This yields the definition of the overall stress, which is the volume average $\bar{\sigma}_{ij}$ of the local stress field in V, generated by the prescribed surface tractions. With reference to (3.2.4)

$$\langle \sigma_{ij}(\boldsymbol{x}) \rangle \equiv \bar{\sigma}_{ij} = \frac{1}{V}\int_V \sigma_{ij}(\boldsymbol{x})\mathrm{d}V = \frac{1}{2V}\int_{\partial V} (t_i x_j + t_j x_i)\mathrm{d}S \tag{3.4.2}$$

Suppose now that the volume V is subdivided into n subvolumes V_r ($r = 1, 2 \ldots n$), perfectly bonded at their interfaces, such that $\Sigma_r V_r = V$. The subvolumes are typically selected to coincide with those of individual phases or parts of subdivided phases of the aggregate, so that each subvolume is filled by a homogeneous phase material. Nominal volume fractions are defined by (3.2.5) as $c_r = V_r/V$, so

that $\Sigma_r c_r = 1$. Traction continuity prevails at subvolume boundaries, hence the subvolume stress average $\bar{\sigma}_{ij}^r$ follows from (3.4.2), with the integrals taken over each V_r. The $\bar{\sigma}_{ij}$, $\bar{\sigma}_{ij}^r$ and $\sigma_{ij}(\boldsymbol{x})$ are represented either by diagonally symmetric (3×3) matrices, or by (6×1) vectors of the stress components written in the contracted notation (1.1.9) and denoted by $\bar{\boldsymbol{\sigma}}$, $\bar{\boldsymbol{\sigma}}_r$ and $\boldsymbol{\sigma}(\boldsymbol{x})$.

Stress averages in subvolumes V_r are then related to the overall average over V in (3.4.2) as

$$\langle \boldsymbol{\sigma} \rangle \equiv \bar{\boldsymbol{\sigma}} = \frac{1}{V} \int_V \boldsymbol{\sigma}(\boldsymbol{x}) \mathrm{d}V = \frac{1}{V} \sum_{r=1}^{n} \int_{V_r} \boldsymbol{\sigma}(\boldsymbol{x}) \mathrm{d}V = \sum_{r=1}^{n} c_r \bar{\boldsymbol{\sigma}}_r \tag{3.4.3}$$

Similar volume and subvolume averages and partitioning follow for any spatially variable and integrable quantity $\Phi(\boldsymbol{x})$ in V; see (3.2.4). Since traction continuity is preserved at surfaces of cracks or voids, and also at imperfectly bonded interfaces, the above average holds even in the presence of such imperfections.

(*b*) Surface displacements described by a continuous function of coordinates $u_i(\boldsymbol{x})$ are prescribed at all points $\boldsymbol{x} \in \partial V$, such that they cause only small strains, and do not generate any rigid body translation or rotation of V. These displacements are related to the resulting strain and rotation field inside V through a volume integral of the strain gradient $u_{i,j}(\boldsymbol{x})$, obtained from the displacement field $u_i(\boldsymbol{x})$, $\boldsymbol{x} \in V$.

$$u_{i,j} = \frac{1}{2}[(u_{i,j} + u_{j,i}) + (u_{i,j} - u_{j,i})] = \varepsilon_{ij} + \omega_{ij} \tag{3.4.4}$$

Integrating this over V and scaling by V provides volume averages of strain and rotation. However, the latter is zero when disallowed by the prescribed surface displacements. Application of the Gauss theorem then connects the average strain to the surface displacements as

$$\langle \varepsilon_{ij} \rangle \equiv \bar{\varepsilon}_{ij} = \frac{1}{V} \int_V \varepsilon_{ij} \mathrm{d}V = \frac{1}{2V} \int_{\partial V} (u_i n_j + u_j n_i) \mathrm{d}S \tag{3.4.5}$$

where n_j is the outside normal to ∂V. However, in the presence of damage, the second integral must also be taken over all interior free surfaces of cracks and voids, to account for displacement jumps at imperfectly bonded interfaces. Local deformations caused by such imperfections contribute to the overall strain.

Subdividing V into perfectly bonded subvolumes with preserved displacement continuity at the interfaces allows decomposition of $\bar{\varepsilon}_{ij}$ into a sum of subvolume strain averages. In both contracted tensorial and engineering matrix notations, the strain averages are

$$\langle \boldsymbol{\varepsilon} \rangle \equiv \bar{\boldsymbol{\varepsilon}} = \frac{1}{V} \int_V \boldsymbol{\varepsilon}(\boldsymbol{x}) \mathrm{d}V = \frac{1}{V} \sum_{r=1}^{n} \int_{V_r} \boldsymbol{\varepsilon}(\boldsymbol{x}) \mathrm{d}V = \sum_{r=1}^{n} c_r \bar{\boldsymbol{\varepsilon}}_r \tag{3.4.6}$$

Constitutive relations of each homogeneous phase residing in subvolumes V_r now follow by writing (1.1.21) with (6×6) phase stiffness and compliance matrices, expressed together with the strain vectors in either the contracted tensorial or engineering notations.

$$\boldsymbol{\sigma}_r(\boldsymbol{x}) = \boldsymbol{L}_r \boldsymbol{\varepsilon}_r(\boldsymbol{x}) \quad \boldsymbol{\varepsilon}_r(\boldsymbol{x}) = \boldsymbol{M}_r \boldsymbol{\sigma}_r(\boldsymbol{x}) \tag{3.4.7}$$

These relations between local stress and strain fields also apply to their volume averages (3.4.3) and (3.4.6), and can be written as

$$\bar{\boldsymbol{\sigma}} = \sum_{r=1}^{n} c_r \boldsymbol{\sigma}_r = \sum_{r=1}^{n} c_r \boldsymbol{L}_r \boldsymbol{\varepsilon}_r \quad \bar{\boldsymbol{\varepsilon}} = \sum_{r=1}^{n} c_r \boldsymbol{\varepsilon}_r = \sum_{r=1}^{n} c_r \boldsymbol{M}_r \boldsymbol{\sigma}_r \tag{3.4.8}$$

If the volume V is a representative volume of a heterogeneous solid, then stress and strain averages of local fields in V are connected by certain *effective or overall properties* of the homogenized volume V. As in the above paragraphs (*b*) and (*a*), suppose that the RVE is subjected to prescribed displacements causing a uniform overall strain $\boldsymbol{\varepsilon}^0$, or to prescribed tractions causing a uniform overall stress $\boldsymbol{\sigma}^0$. Overall constitutive relations of the homogenized aggregate in V then are

$$\bar{\boldsymbol{\sigma}} = \boldsymbol{L}\boldsymbol{\varepsilon}^0 \quad \bar{\boldsymbol{\varepsilon}} = \boldsymbol{M}\boldsymbol{\sigma}^0 \tag{3.4.9}$$

where $\boldsymbol{L}$ and $\boldsymbol{M}$ denote effective or overall stiffness and compliance matrices, and $\bar{\boldsymbol{\sigma}}, \bar{\boldsymbol{\varepsilon}}$ are overall volume averages of local stresses and strains caused by the prescribed $\boldsymbol{\varepsilon}^0$ or $\boldsymbol{\sigma}^0$, under the distinct boundary conditions. In later chapters, the top bars on $\bar{\boldsymbol{\sigma}}$ and $\bar{\boldsymbol{\varepsilon}}$ are used only when required for clarity. Otherwise, overall averages are denoted only by $\boldsymbol{\sigma}$ or $\boldsymbol{\varepsilon}$, and phase averages by $\boldsymbol{\sigma}_r$ and $\boldsymbol{\varepsilon}_r$.

Notice that the angular brackets $\langle\ \rangle$ designating the ensemble or overall average have been replaced by the top bar. This notation will be extended to averages taken over the relevant overall, or local volume designated by a subscript, and retained as needed in what follows.

3.5 Overall Properties and Local Fields

3.5.1 Mechanical Influence Functions and Concentration Factors

When a representative volume V of a heterogeneous medium is loaded by either surface tractions or displacements that are derived from uniform overall stress or strain fields, the variable local fields in material subvolumes V_r can be described in terms of certain influence functions of spatial coordinates. In a similar manner, volume averages of the local fields in V_r are related to the applied overall fields

by constant concentration factor tensors (Hill 1963a). The present discussion is concerned with definitions and certain properties of theses quantities. Their evaluation in specific composite systems is described in Chaps. 6 and 7.

First, consider a volume V subjected to displacements $u_i(\boldsymbol{x})$, prescribed at all surface points $\boldsymbol{x} \in \partial V$ as linear functions of coordinates, $u_i(\boldsymbol{x}) = \varepsilon^0_{ij} x_j$. The superscript $(^0)$ indicates that ε^0_{ij} is a prescribed overall strain, derived from the applied, linearly varying surface displacements. In a homogeneous or homogenized volume V, such displacements would create a uniform strain field $\varepsilon^0_{ij} = (u_{i,j} + u_{j,i})$, hence ε^0_{ij} is also equal to the volume average (3.4.6) of the strain field in V.

Actual strain fields generated by application of ε^0_{ij} in any given subvolume V_r of the heterogeneous volume V are not uniform. Since ε^0_{ij} is a constant tensor, the said fields can be expressed as functions of the position coordinate $\boldsymbol{x} \in V_r$ in either subscript or matrix notation as

$$\varepsilon^r_{ij}(\boldsymbol{x}) = A^r_{ijkl}(\boldsymbol{x})\varepsilon^0_{kl} \quad \boldsymbol{\varepsilon}_r(\boldsymbol{x}) = \boldsymbol{A}_r(\boldsymbol{x})\boldsymbol{\varepsilon}^0 \tag{3.5.1}$$

Recall that in the latter equation, both strain tensors are represented in either the contracted tensorial notation (1.1.10) or the engineering matrix notation (1.1.11) by (6×1) vectors, implying that the influence functions $\boldsymbol{A}_r(\boldsymbol{x})$ are dimensionless (6×6) matrices, which are not affected by the selected notation.

In a numerical analysis of a subdivided unit cell, each k-th column $\boldsymbol{a}^k_r(\boldsymbol{x})$ of the matrix $\boldsymbol{A}_r(\boldsymbol{x})$ is equal to the local strain vector $\boldsymbol{a}^k_r(\boldsymbol{x}) = \boldsymbol{A}_r(\boldsymbol{x})\,\boldsymbol{i}_k$ generated at point $\boldsymbol{x}$ by application of the overall strain $\boldsymbol{\varepsilon}^0_k = \boldsymbol{i}_k$, where $\boldsymbol{i}_k$ is the k-th column of the (6×6) identity matrix $\boldsymbol{I}$.

Mechanical strain concentration factor tensors or matrices are volume averages of the influence functions (3.5.1), taken over each subvolume V_r.

$$\bar{\boldsymbol{\varepsilon}}_r = \frac{1}{V_r}\int_{V_r} \boldsymbol{\varepsilon}(\boldsymbol{x})\,\mathrm{d}V = \frac{1}{V_r}\int_{V_r} \boldsymbol{A}_r(\boldsymbol{x})\boldsymbol{\varepsilon}^0 \mathrm{d}V = \boldsymbol{A}_r\,\boldsymbol{\varepsilon}^0 \tag{3.5.2}$$

Next, the volume V is loaded by surface tractions $t^0_i(\boldsymbol{x}) = \sigma^0_{ij}\, n_j(\boldsymbol{x})$, derived from a uniform overall stress field σ^0_{ij}, where the superscript $(^0)$ denotes a prescribed overall stress. The variable local stresses in each subvolume V_r are expressed through influence functions of position coordinates $\boldsymbol{x} \in V_r$

$$\sigma^r_{ij}(\boldsymbol{x}) = B^r_{ijkl}(\boldsymbol{x})\sigma^0_{kl} \qquad \boldsymbol{\sigma}_r(\boldsymbol{x}) = \boldsymbol{B}_r(\boldsymbol{x})\boldsymbol{\sigma}^0 \tag{3.5.3}$$

where the $\boldsymbol{\sigma}_r(\boldsymbol{x})$ are written in the contracted notation as (6×1) vectors, and the stress influence function tensors $\boldsymbol{B}_r(\boldsymbol{x})$ as (6×6) matrices. Columns $\boldsymbol{b}^k_r(\boldsymbol{x}) = \boldsymbol{B}_r(\boldsymbol{x})\,\boldsymbol{i}_k$ of the latter are again generated, in turn, by application of the applied stress component $\boldsymbol{\sigma}^0_k = \boldsymbol{i}_k$ of unit magnitude.

Volume averaging of local field over V_r provides the mechanical stress concentration factor tensors $\boldsymbol{B}_r$ as

$$\bar{\boldsymbol{\sigma}}_r = \frac{1}{V_r}\int \boldsymbol{\sigma}_r(\boldsymbol{x})\mathrm{d}V = \frac{1}{V_r}\int_{V_r} \boldsymbol{B}_r(\boldsymbol{x})\boldsymbol{\sigma}^0\mathrm{d}V = \boldsymbol{B}_r\boldsymbol{\sigma}^0 \tag{3.5.4}$$

Evaluation of the mechanical concentration factors $\boldsymbol{A}_r$ and $\boldsymbol{B}_r$ seldom relies on integration of the influence functions, which may not be easily found. Instead, they are replaced by estimates which follow from one of several analytical methods described in Chaps. 6 and 7.

It should be emphasized that the above $\bar{\boldsymbol{\varepsilon}}_r$ and $\bar{\boldsymbol{\sigma}}_r$ are the strain and stress averages of the respective phase fields in the total phase volume V_r, which includes all subvolumes $\boldsymbol{v}_r$ of the phase r in the representative volume V. Of course, in each randomly distributed phase subvolume $\boldsymbol{v}_r$, local fields and their average magnitudes may deviate from the above averages of phase fields, taken over all subvolumes of each phase.

The strain and stress concentration factors provide average phase fields under two distinct boundary conditions described with (3.4.5) and (3.4.2), which must be respected in evaluations of the local fields. However, they have certain common properties. In particular, (3.4.8) indicates that

$$\sum_{r=1}^{n} c_r\bar{\boldsymbol{\varepsilon}}_r = \bar{\boldsymbol{\varepsilon}} \quad \sum_{r=1}^{n} c_r\bar{\boldsymbol{\sigma}}_r = \bar{\boldsymbol{\sigma}} \quad r = 1, 2, \ldots n \tag{3.5.5}$$

where the overall averages are equal to the respective prescribed quantities. Therefore, the subvolume weighed sums of the transformation factors are

$$\sum_{r=1}^{n} c_r\boldsymbol{A}_r = \boldsymbol{I} \quad \sum_{r=1}^{n} c_r\boldsymbol{B}_r = \boldsymbol{I} \quad r = 1, 2, \ldots n \tag{3.5.6}$$

where $\boldsymbol{I}$ is the (6×6) identity matrix. This shows that only $n-1$ strain or stress concentration factors need to be evaluated for the phase volumes, and that the averages of local fields are related. In the particular case of two-phase systems, volume averages of strain or stress in the phases are closely related, while the actual local fields can be very different. The $\boldsymbol{A}_r$ and $\boldsymbol{B}_r$ matrices may not be diagonally symmetric.

3.5.2 Overall Stiffness and Compliance

Estimated or actual mechanical concentration factor tensors are often used in evaluation of overall stiffness and compliance of a representative volume of a heterogeneous medium. In particular, the overall stress and strain averages follow from equations (3.4.8) and (3.5.2), (3.5.4) as

$$\bar{\boldsymbol{\sigma}} = \sum_{r=1}^{n} c_r\boldsymbol{L}_r\bar{\boldsymbol{\varepsilon}}_r = \sum_{r=1}^{n} c_r\boldsymbol{L}_r\boldsymbol{A}_r\boldsymbol{\varepsilon}^0 \quad \bar{\boldsymbol{\varepsilon}} = \sum_{r=1}^{n} c_r\boldsymbol{M}_r\bar{\boldsymbol{\sigma}}_r = \sum_{r=1}^{n} c_r\boldsymbol{M}_r\boldsymbol{B}_r\boldsymbol{\sigma}^0 \tag{3.5.7}$$

Therefore, overall stiffness and compliance in (3.4.9) can be found from

$$\boldsymbol{L} = \sum_{r=1}^{n} c_r \boldsymbol{L}_r \boldsymbol{A}_r \quad \boldsymbol{M} = \sum_{r=1}^{n} c_r \boldsymbol{M}_r \boldsymbol{B}_r \tag{3.5.8}$$

By this sequence, suggested by Hill (1963a), derivation of overall properties and of strain and stress field averages in individual phase subvolumes of a representative volume is reduced to evaluation of the mechanical concentration factor tensors. Accuracy of the results depends on that of the concentration factors. Introduction of the concentration factors was a simplifying departure from the previously used equivalent inclusion method described in Sect. 4.2. The original derivation shown here had been reproduced by several writers, in different notations of their choice.

It should be emphasized that both phase and overall stiffness and compliance matrices of a representative volume of a statistically homogeneous medium must satisfy the *consistency conditions*

$$\boldsymbol{L}_r \boldsymbol{M}_r = \boldsymbol{I} \quad \boldsymbol{L}\boldsymbol{M} = \boldsymbol{I} \tag{3.5.9}$$

Moreover, they must comply with one of the eight material symmetries described in Chap. 2, which require that both $\boldsymbol{L} = \boldsymbol{L}^{\mathrm{T}}$ and $\boldsymbol{M} = \boldsymbol{M}^{\mathrm{T}}$ are *diagonally symmetric and positive definite*. Finally, no admissible prediction of overall stiffness and compliance may be in conflict with established bounds on such properties.

These requirements have to be satisfied by all admissible homogenization procedures that estimate overall stiffness $\boldsymbol{L}$ and compliance $\boldsymbol{M}$ in terms of phase geometry and properties. Unfortunately, that has not been fully appreciated by all developers or users of available material models. As shown in Chap. 7, even well-established methods may fail to provide admissible predictions, for example, by violating variational bounds on overall moduli, or certain restrictions on shape and alignment of the constituents, which guarantee diagonal symmetry.

Mechanical stress and strain concentration factors are connected by writing the local strain (3.5.2) as

$$\bar{\boldsymbol{\varepsilon}}_r = \boldsymbol{A}_r \boldsymbol{\varepsilon}^0 = \boldsymbol{A}_r \boldsymbol{M} \bar{\boldsymbol{\sigma}} = \boldsymbol{M}_r \bar{\boldsymbol{\sigma}}_r = \boldsymbol{M}_r \boldsymbol{B}_r \boldsymbol{\sigma}^0 \tag{3.5.10}$$

In finding local stress averages $\bar{\boldsymbol{\sigma}}_r$ in a representative volume, the overall average $\bar{\boldsymbol{\sigma}}$ of local stresses is regarded as equal to the prescribed overall stress, $\bar{\boldsymbol{\sigma}} = \boldsymbol{\sigma}^0$. Therefore, the strain and stress concentration factors are connected by

$$\boldsymbol{A}_r \boldsymbol{M} = \boldsymbol{M}_r \boldsymbol{B}_r \quad \boldsymbol{B}_r \boldsymbol{L} = \boldsymbol{L}_r \boldsymbol{A}_r \tag{3.5.11}$$

In two-phase composite aggregates, with phases $r = \alpha,\ \beta$, overall stiffness and compliance (3.5.8) can be written with regard to (3.5.6) as

$$\boldsymbol{L} = \boldsymbol{L}_\alpha + c_\beta (\boldsymbol{L}_\beta - \boldsymbol{L}_\alpha) \boldsymbol{A}_\beta \quad \boldsymbol{M} = \boldsymbol{M}_\alpha + c_\beta (\boldsymbol{M}_\beta - \boldsymbol{M}_\alpha) \boldsymbol{B}_\beta \tag{3.5.12}$$

For example, if $\boldsymbol{L}_\alpha = \boldsymbol{L}_1$, the stiffness of the matrix phase, then the second term in the first formula indicates the contribution of the reinforcement $r = \beta$ to overall stiffness. In particular, $\boldsymbol{L} - \boldsymbol{L}_\alpha = (\boldsymbol{L}_\beta - \boldsymbol{L}_\alpha)(\boldsymbol{I} - c_\alpha \boldsymbol{A}_\alpha)$, hence overall stiffness is elevated by an addition of the reinforcement when $\boldsymbol{L}_\beta - \boldsymbol{L}_\alpha$ is positive definite. Conversely, if the $r = \beta$ phase is more compliant in certain directions than the matrix, or if it contains cavities, then the overall stiffness is reduced. In any event, according to (3.5.6), only one concentration factor of a single phase, usually the reinforcing phase, is sufficient for determination of field averages in the other, matrix phase.

As written, the above connections hold in both contracted tensorial and engineering matrix notations, providing that $\boldsymbol{\varepsilon}_r$, $\boldsymbol{L}_r$, and $\boldsymbol{M}_r$ are all written in the same selected notation. Then, $\boldsymbol{A}_r$ and $\boldsymbol{B}_r$ are not affected by the chosen notation.

Connections (3.5.12) can be utilized in estimating mechanical concentration factors $\boldsymbol{A}_r, \boldsymbol{B}_r$ of either phase $r = \alpha, \beta$, in terms of an experimentally evaluated overall stiffness $\boldsymbol{L}$ or compliance $\boldsymbol{M}$ and known phase stiffnesses and volume fractions $c_\alpha + c_\beta = 1$. The results hold for any statistically homogeneous distribution of the phases, and provide strain and stress field averages over total phase volumes, regardless of phase shape and alignment.

$$\left.\begin{array}{ll} c_\alpha \boldsymbol{A}_\alpha = (\boldsymbol{L}_\alpha - \boldsymbol{L}_\beta)^{-1}(\boldsymbol{L} - \boldsymbol{L}_\beta) & c_\beta \boldsymbol{A}_\beta = -(\boldsymbol{L}_\alpha - \boldsymbol{L}_\beta)^{-1}(\boldsymbol{L} - \boldsymbol{L}_\alpha) \\ c_\alpha \boldsymbol{B}_\alpha = (\boldsymbol{M}_\alpha - \boldsymbol{M}_\beta)^{-1}(\boldsymbol{M} - \boldsymbol{M}_\beta) & c_\beta \boldsymbol{B}_\beta = -(\boldsymbol{M}_\alpha - \boldsymbol{M}_\beta)^{-1}(\boldsymbol{M} - \boldsymbol{M}_\alpha) \end{array}\right\} \tag{3.5.13}$$

Of course, actual local fields may exhibit deviations from the averages, taken over all phase volumes. However, as long as the reinforcements have low to medium volume fractions, and similar shapes that can be modeled by spheres, ellipsoids, and oblate or prolate spheroids, such as circular fibers, the Eshelby solution described in Sects. 4.1 and 4.2 indicates that their local fields are approximately uniform under application of a uniform overall strain or stress. Under such circumstances, and absent interface decohesion, (3.5.13) should provide good estimates of local fields for comparison with nominal strength or failure strain values of the reinforcements and of their interfaces with the surrounding matrix. In contrast, local fields in the matrix may develop sharp gradients in the vicinity of interfaces.

3.6 Phase Transformations

3.6.1 Eigenstrains and Eigenstresses

Eigenstrains or transformation strains represent a large group of deformations that are not caused by mechanical loads, exist in their absence, and are generated by different physical sources. A uniform eigenstrain applied in any traction-free

volume of a homogeneous or heterogeneous solid causes uniform, stress-free deformation. When this uniform eigenstrain is applied to a fully constrained material volume at zero surface displacements, the deformation is constrained by a layer of surface tractions that generate a strain-free stress, called an eigenstress or transformation stress. In a homogeneous solid, this eigenstress is also uniform. In a heterogeneous solid, the definition of a representative volume in Sect. 3.3 is expanded by stipulating that any statistically uniform distribution of phase eigenstrains generates a macroscopically uniform overall deformation of this volume under zero surface tractions, or a macroscopically uniform overall stress under zero surface displacements.

Transformation fields can be broadly divided into physically based and equivalent eigenstrains. *Physically based eigenstrains* are frequently introduced during fabrication of composites, laminates and polycrystals, and in service. One category of the physically based eigenstrains consists of known functions of thermal changes, moisture concentration or other processes assumed independent of mechanical loads. They are more easily evaluated than those in the second category, such as inelastic strains or certain phase transformations, which depend on past loading or deformation history of a particular material volume. Due to their stress-dependent evolution history, the latter are not always regarded as 'true' eigenstrains (Zaoui and Masson 1998). In the context of incremental deformation, the change of inelastic strains may indeed be stress-dependent during each loading step. However, when a particular loading step has been completed, the total current strain of a material point can be decomposed into an elastic part and a strain that would survive an instantaneous unloading to zero local stress. This latter part is the current eigenstrain, regardless of its past or recent evolution history (Rice 1970). Contributions of physically based eigenstrains to the total local strain and stress fields can be significant, possibly causing interfacial decohesion or matrix cracking and other modes of damage.

Equivalent eigenstrains, discussed in some detail in Chap. 4 are fictitious, in the sense that they have no direct physical origin. They are often introduced to simulate the effect of local material property changes on local fields and on overall response under applied mechanical and transformation loads. For example, the equivalent inclusion method discussed in Sect. 4.2 uses an equivalent eigenstrain induced in a homogeneous inclusion, to reproduce the effect of an identical inhomogeneity on local fields caused by overall loads. A damage-equivalent eigenstrains may be used to approximate the effect of interfacial decohesion or cavity formation on overall response; Sect. 4.3.4. In contrast to their physically based counterparts, equivalent eigenstrains depend on the magnitude of currently applied mechanical loads. They may also depend on physically based eigenstrains, for example, in applications of the equivalent inclusion method to problems involving physically based eigenstrains (Mura 1987, §25). Equivalent eigenstrains vanish in the absence of their loading sources.

In what follows, both types of transformation fields are regarded as internally applied loads, separate from external mechanical loads. To emphasize this difference, the eigenstrain fields will be denoted herein by the symbol $\boldsymbol{\mu}(\boldsymbol{x})$, and the related

eigenstress fields by $\boldsymbol{\lambda}(\boldsymbol{x})$. When needed, equivalent eigenstrains will be denoted by topical superscripts, such as $\boldsymbol{\mu}^{eq}$, and $\boldsymbol{\mu}^{dq}$ for damage-equivalent eigenstrains. Of course, the $\boldsymbol{\mu}(\boldsymbol{x})$ are strain vectors written in either tensorial component or engineering matrix notation, and $\boldsymbol{\lambda}(\boldsymbol{x})$ are stress vectors, similar to those described in (1.1.9), (1.1.10) and (1.1.11).

In both homogeneous and heterogeneous solids, a distribution of eigenstrains gives rise to stress and strain fields, often called *residual fields*, that remain in the material or structure after complete mechanical unloading. The total residual strain fields are compatible, and the residual stress fields are self-equilibrated; however, the transformation (eigenstrain and eigenstress) fields themselves need not satisfy such requirements. This suggests that total residual fields are superpositions of the transformation fields with certain elastic fields which restore and guarantee compatibility and equilibrium.

The distinction between the total residual, elastic and eigenstrain fields can be illustrated by imagining a heterogeneous medium, such as a polycrystal or composite, decomposed, without local rotations, into separate homogeneous but anisotropic grains or phase subvolumes. Each of these can be differently transformed, e.g., by application of a uniform temperature change. Such dissimilar phase volume and shape changes create an incompatible, stress-free deformation field in the subvolumes. Reassembly of the perfectly bonded material thus requires application of surface tractions to the transformed subvolumes, to restore displacement and traction continuity at the interfaces. These tractions generate the elastic parts of residual fields, and possibly additional eigenstrains if the deformation does not remain elastic. Such residual fields are superimposed with those caused in each phase or structure by any applied mechanical loads.

Presence of phase transformations expands the elastic constitutive relations (1.1.21) to

$$\left.\begin{aligned} \boldsymbol{\sigma}_r(\boldsymbol{x}) &= \boldsymbol{L}_r\boldsymbol{\varepsilon}_r(\boldsymbol{x}) + \boldsymbol{\lambda}_r(\boldsymbol{x}) & \qquad \boldsymbol{\varepsilon}_r(\boldsymbol{x}) &= \boldsymbol{M}_r\boldsymbol{\sigma}_r(\boldsymbol{x}) + \boldsymbol{\mu}_r(\boldsymbol{x}) \\ \boldsymbol{\lambda}_r(\boldsymbol{x}) &= -\boldsymbol{L}_r\boldsymbol{\mu}_r(\boldsymbol{x}) & \qquad \boldsymbol{\mu}_r(\boldsymbol{x}) &= -\boldsymbol{M}_r\boldsymbol{\lambda}_r(\boldsymbol{x}) \\ \boldsymbol{\sigma}_r(\boldsymbol{x}) &= \boldsymbol{L}_r[\boldsymbol{\varepsilon}_r(\boldsymbol{x}) - \boldsymbol{\mu}_r(\boldsymbol{x})] & \qquad \boldsymbol{\varepsilon}_r(\boldsymbol{x}) &= \boldsymbol{M}_r[\boldsymbol{\sigma}_r(\boldsymbol{x}) - \boldsymbol{\lambda}_r(\boldsymbol{x})] \end{aligned}\right\} \tag{3.6.1}$$

where the $\boldsymbol{L}_r$ and $\boldsymbol{M}_r = \boldsymbol{L}_r^{-1}$ are phase stiffness and compliance, and $\boldsymbol{\mu}_r(\boldsymbol{x})$ is a local value at $\boldsymbol{x}$ of a distributed eigenstrain field; the $\boldsymbol{\lambda}_r(\boldsymbol{x})$ is the related eigenstress, generated by $\boldsymbol{\mu}_r(\boldsymbol{x})$ while $\boldsymbol{\varepsilon}_r(\boldsymbol{x}) = \boldsymbol{0}$. For consistency of the constitutive relations, both strain and eigenstrain vectors and the stiffness and compliance matrices in (3.6.1) need to be written either in the contracted tensorial or in engineering matrix notations.

Notice that the adopted sign convention anticipates a positive isotropic eigenstrain to cause local compressive or negative eigenstress, and vice versa. This convention is not uniformly used in the literature, which may invite sign errors.

Both $\boldsymbol{\mu}(\boldsymbol{x})$ and $\boldsymbol{\lambda}(\boldsymbol{x})$ fields are defined by certain continuous functions belonging to class C^2 in each open region V_r, that may represent a part or an entire volume

of a homogeneous phase r. To illustrate the effect on stress equilibrium, we rewrite $(3.6.1)_1$ as

$$\sigma_{ij}(\boldsymbol{x}) = L_{ijkl}\varepsilon_{kl}(\boldsymbol{x}) + \lambda_{ij}(\boldsymbol{x}) = \tilde{\sigma}_{ij}(\boldsymbol{x}) + \lambda_{ij}(\boldsymbol{x}) \quad (i, j = 1, 2, 3) \tag{3.6.2}$$

and require that the stress field satisfies for all $\boldsymbol{x} \in V_r$ and on the surface ∂V_r of V_r

$$\tilde{\sigma}_{ij,j} + F_i + \lambda_{ij,j} = 0 \text{ in } V_r \qquad (\tilde{\sigma}_{ij} + \lambda_{ij})n_j = t_i \text{ on } \partial V_r \tag{3.6.3}$$

As in (3.4.2), the boundary tractions generate the average total stress $\tilde{\sigma}_{ij}$ in V_r. This shows that equilibrium can be satisfied if the eigenstress field modifies body forces and surface tractions as

$$\tilde{F}_i = F_i + \lambda_{ij,j} \text{ and } \tilde{t}_i = t_i - \lambda_{ij}n_j \tag{3.6.4}$$

The implication is that displacements caused in V_r by application of the transformation field $\mu_{ij}(\boldsymbol{x}) = -M_{ijkl}\lambda_{kl}(\boldsymbol{x})$ are equal to those generated by application of body forces $\lambda_{ij,j}(\boldsymbol{x})$ at $\boldsymbol{x} \in V_r$ and by surface tractions $-\lambda_{ij}(\boldsymbol{x})n_j$ at $\boldsymbol{x} \in \partial V_r$. Equations (3.6.4) also show that the leading terms on the right hand sides in (3.6.1) are caused, in part, by application of external loads, by internal residual fields generated by body forces $\lambda_{ij,j}(\boldsymbol{x})$ at $\boldsymbol{x} \in V_r$, and by surface tractions $-\lambda_{ij}(\boldsymbol{x})n_j$ at $\boldsymbol{x} \in \partial V_r$.

3.6.2 *Local Transformation Fields*

A distribution of phase transformations in a heterogeneous aggregate generates both local and overall deformations and stresses. In particular, the total local strain $\boldsymbol{\varepsilon}_r(\boldsymbol{x})$ in $(3.6.1)_2$ is the sum of elastic strain $\boldsymbol{M}_r\boldsymbol{\sigma}_r(\boldsymbol{x})$ and local eigenstrain $\boldsymbol{\mu}_r(\boldsymbol{x})$. The elastic strain is caused, in part, by an applied overall mechanical strain $\boldsymbol{\varepsilon}^0$, and by residual fields generated by an eigenstrain distribution in the entire volume.

A convenient representation of the total local strain and stress fields in a volume V of a heterogeneous medium can be obtained by replacing any variable transformation field by a piecewise uniform distributions $\boldsymbol{\mu}_r$ in phase or subdivided phase volumes $V_r, r = 1, 2, \ldots n$. The form

$$\boldsymbol{\varepsilon}_r(\boldsymbol{x}) = \boldsymbol{A}_r(\boldsymbol{x})\boldsymbol{\varepsilon}^0 + \sum_{s=1}^{n} \boldsymbol{D}_{rs}(\boldsymbol{x})\boldsymbol{\mu}_s \quad \boldsymbol{\sigma}_r(\boldsymbol{x}) = \boldsymbol{B}_r(\boldsymbol{x})\boldsymbol{\sigma}^0 + \sum_{s=1}^{n} \boldsymbol{F}_{rs}(\boldsymbol{x})\boldsymbol{\lambda}_s \tag{3.6.5}$$

expands (3.5.1) and (3.5.3) by including both mechanical loads and phase transformations (Dvorak 1990). Overall strain $\boldsymbol{\varepsilon}^0$ is again uniform, applied by prescribed displacement at the surface ∂V, and $\boldsymbol{A}_r(\boldsymbol{x})$ is the mechanical strain influence function. Overall stress $\boldsymbol{\sigma}^0$ is generated by surface tractions prescribed on ∂V, and

$\boldsymbol{B}_r(\boldsymbol{x})$ is the mechanical stress influence function. The $\boldsymbol{D}_{rs}(\boldsymbol{x})$ and $\boldsymbol{F}_{rs}(\boldsymbol{x})$ are transformation strain and stress influence function tensors that evaluate residual strain or stress fields caused in subvolumes V_r by the locally uniform transformations $\boldsymbol{\mu}_s$ or $\boldsymbol{\lambda}_s$ applied in another (or the same) subvolumes V_s, under $\boldsymbol{\varepsilon}^0 = \boldsymbol{0}$ or $\boldsymbol{\sigma}^0 = \boldsymbol{0}$, respectively. Included are the self-induced terms $\boldsymbol{D}_{rr}(\boldsymbol{x})$ and $\boldsymbol{F}_{rr}(\boldsymbol{x})$ that reflect contributions to total local fields in V_r by uniform local transformation fields $\boldsymbol{\mu}_r$ and $\boldsymbol{\lambda}_r$, respectively.

Numerical evaluation of the transformation influence functions in (3.6.5) can be carried out for any selected phase geometry in a representative volume of a heterogeneous material, at different levels of refinement, from the coarse distribution in phase subvolumes, to that afforded by a finite element subdivision of a unit cell. In the latter, the influence functions or concentration factors can be established between each pair of elements as follows. Overall boundary conditions apply zero overall strain $\boldsymbol{\varepsilon}^0 = \boldsymbol{0}$ (or stress $\boldsymbol{\sigma}^0 = \boldsymbol{0}$). Then, unit-valued components of phase eigenstrains $\boldsymbol{\mu}_s^k = \boldsymbol{i}_k$ (or eigenstress $\boldsymbol{\lambda}_s^k = \boldsymbol{i}_k$) are applied in turn in all elements V_s, including V_r. The $\boldsymbol{i}_k$ is the k-th column of the (6×6) identity matrix $\boldsymbol{I}$. The k-th column $\boldsymbol{D}_{rs}^k(\boldsymbol{x}) = \boldsymbol{D}_{rs}(\boldsymbol{x})\,\boldsymbol{i}_k$ (or $\boldsymbol{F}_{rs}^k(\boldsymbol{x}) = \boldsymbol{F}_{rs}(\boldsymbol{x})\,\boldsymbol{i}_k$) is the local strain or stress generated in V_r by $\boldsymbol{i}_k$. Volume averaging described in (3.5.2) and (3.5.4) then provides transformation strain and stress concentration factors $\boldsymbol{D}_{rs}$ and $\boldsymbol{F}_{rs}$ that evaluate the eigenstrain contributions to strain and stress averages $\bar{\boldsymbol{\varepsilon}}_r$ of $\boldsymbol{\varepsilon}_r(\boldsymbol{x})$ and $\bar{\boldsymbol{\sigma}}_r$ of $\boldsymbol{\sigma}_r(\boldsymbol{x})$ in V_r, respectively. A detailed derivation is presented in Sect. 12.1.3.

The influence functions and concentration factors are (6×6) matrices with dimensionless coefficients. Of course, the strain and eigenstrain vectors, stiffness and compliance matrices must all be written in either contracted tensorial or engineering matrix notations. However, the concentration and transformation tensors and matrices do not depend on the selected notation.

In two-phase material systems, the transformation influence functions can be derived in terms of the mechanical influence functions, by creating a uniform strain field. In particular, suppose the RVE of a two-phase composite systems, $r = \alpha,\ \beta$, is loaded only by two independent, uniform phase eigenstrains $\boldsymbol{\mu}_r \in V_r$, and by an as yet unknown, auxiliary overall strain $\hat{\boldsymbol{\varepsilon}}$, which is also uniform. Let us now separate the phases and apply to each one an auxiliary uniform overall stress $\hat{\boldsymbol{\sigma}}$ such that $\hat{\boldsymbol{\varepsilon}}$ becomes the local strain in both phases

$$\left.\begin{aligned} \hat{\boldsymbol{\sigma}} &= \boldsymbol{L}_\alpha(\hat{\boldsymbol{\varepsilon}} - \boldsymbol{\mu}_\alpha) = \boldsymbol{L}_\beta(\hat{\boldsymbol{\varepsilon}} - \boldsymbol{\mu}_\beta) \\ \hat{\boldsymbol{\varepsilon}} &= (\boldsymbol{L}_\alpha - \boldsymbol{L}_\beta)^{-1}(\boldsymbol{L}_\alpha\boldsymbol{\mu}_\alpha - \boldsymbol{L}_\beta\boldsymbol{\mu}_\beta) \end{aligned}\right\} \tag{3.6.6}$$

Since both the stress and strain are now uniform and of the same magnitude in all phases, the aggregate can be reassembled, providing that the overall stress $\hat{\boldsymbol{\sigma}}$ or strain $\hat{\boldsymbol{\varepsilon}}$ are applied at the outer surface ∂V. Traction and displacement continuity conditions are satisfied at all interfaces. Finally, the auxiliary overall strain $\hat{\boldsymbol{\varepsilon}}$ is removed, and the original overall strain reapplied. The phase strain $(3.6.5)_1$ then is

$$\boldsymbol{\varepsilon}_r(\boldsymbol{x}) = [\boldsymbol{I} - \boldsymbol{A}_r(\boldsymbol{x})]\hat{\boldsymbol{\varepsilon}} + \boldsymbol{A}_r(\boldsymbol{x})\boldsymbol{\varepsilon}^0 \quad r = \alpha, \beta \tag{3.6.7}$$

Since the two applied phase eigenstrains are independent, substitution for $\hat{\boldsymbol{\varepsilon}}$ from (3.6.6) and comparison of the resulting strain with $(3.6.5)_1$ yields the following connections between mechanical and eigenstrain influence functions, which hold for any micro-geometry of a representative volume of two-phase aggregates

$$\left.\begin{aligned} \boldsymbol{D}_{r\alpha}(\boldsymbol{x}) &= (\boldsymbol{I} - \boldsymbol{A}_r(\boldsymbol{x}))(\boldsymbol{L}_\alpha - \boldsymbol{L}_\beta)^{-1}\boldsymbol{L}_\alpha \\ \boldsymbol{D}_{r\beta}(\boldsymbol{x}) &= -(\boldsymbol{I} - \boldsymbol{A}_r(\boldsymbol{x}))(\boldsymbol{L}_\alpha - \boldsymbol{L}_\beta)^{-1}\boldsymbol{L}_\beta \end{aligned}\right\} \tag{3.6.8}$$

An analogous procedure yields the eigenstress influence functions $(3.6.5)_2$. The separated phases are subjected to auxiliary tractions that generate a uniform stress $\hat{\boldsymbol{\sigma}}$, and to eigenstrains $\boldsymbol{\mu}_r$, or eigenstresses $\boldsymbol{\lambda}_r = -\boldsymbol{L}_r\boldsymbol{\mu}_r$. Uniform phase strain and stress then are

$$\left.\begin{aligned} \hat{\boldsymbol{\varepsilon}} &= \boldsymbol{M}_\alpha\hat{\boldsymbol{\sigma}} + \boldsymbol{\mu}_\alpha = \boldsymbol{M}_\beta\hat{\boldsymbol{\sigma}} + \boldsymbol{\mu}_\beta \\ \hat{\boldsymbol{\sigma}} &= -(\boldsymbol{M}_\alpha - \boldsymbol{M}_\beta)^{-1}(\boldsymbol{\mu}_\alpha - \boldsymbol{\mu}_\beta) \end{aligned}\right\} \tag{3.6.9}$$

By removing the auxiliary stress $\hat{\boldsymbol{\sigma}}$ and reinstating $\boldsymbol{\sigma}^0$

$$\boldsymbol{\sigma}_r(\boldsymbol{x}) = \boldsymbol{B}_r(\boldsymbol{x})\boldsymbol{\sigma}^0 + [\boldsymbol{I} - \boldsymbol{B}_r(\boldsymbol{x})]\hat{\boldsymbol{\sigma}} \qquad r = \alpha, \beta \tag{3.6.10}$$

After substitution for $\hat{\boldsymbol{\sigma}}$ one recovers the eigenstress influence functions

$$\left.\begin{aligned} \boldsymbol{F}_{r\alpha}(\boldsymbol{x}) &= (\boldsymbol{I} - \boldsymbol{B}_r(\boldsymbol{x}))(\boldsymbol{M}_\alpha - \boldsymbol{M}_\beta)^{-1}\boldsymbol{M}_\alpha \\ \boldsymbol{F}_{r\beta}(\boldsymbol{x}) &= -(\boldsymbol{I} - \boldsymbol{B}_r(\boldsymbol{x}))(\boldsymbol{M}_\alpha - \boldsymbol{M}_\beta)^{-1}\boldsymbol{M}_\beta \end{aligned}\right\} \tag{3.6.11}$$

The transformation concentration factors $\boldsymbol{D}_{rs}$ and $\boldsymbol{F}_{rs}$ follow from replacement of the mechanical influence functions by the concentration factors $\boldsymbol{A}_r$ and $\boldsymbol{B}_r$ in (3.6.8) and (3.6.11).

The point-wise connections between mechanical and transformation influence functions can be established only in two-phase systems. In multiphase systems, similar connections exist only between the respective field averages or concentration factors, for example, when the reinforcements or all phases are modeled by ellipsoids, Sect. 8.2.2. In two-phase systems, the equality $(\boldsymbol{L}_\alpha - \boldsymbol{L}_\beta)^{-1}\boldsymbol{L}_\alpha = -\boldsymbol{M}_\beta(\boldsymbol{M}_\alpha - \boldsymbol{M}_\beta)^{-1}$ helps in showing that the uniform fields (3.6.6) and (3.6.9) are identical. They represent the only exact elasticity solution for local fields in any two-phase solid or structure that has an arbitrary microgeometry. However, the unloading steps leading to (3.6.8) and (3.6.11) involve mechanical influence functions or concentration factors that are defined and estimated in a representative volume. In Sect. 8.2.4, we show that the influence functions and concentration factors satisfy the following connections

$$\boldsymbol{D}_{r\alpha}(\boldsymbol{x}) + \boldsymbol{D}_{r\beta}(\boldsymbol{x}) = (\boldsymbol{I} - \boldsymbol{A}_r(\boldsymbol{x})) \qquad \boldsymbol{F}_{r\alpha}(\boldsymbol{x}) + \boldsymbol{F}_{r\beta}(\boldsymbol{x}) = (\boldsymbol{I} - \boldsymbol{B}_r(\boldsymbol{x})) \tag{3.6.12}$$

$$\boldsymbol{D}_{r\alpha}(\boldsymbol{x})\boldsymbol{M}_{\alpha} + \boldsymbol{D}_{r\beta}(\boldsymbol{x})\boldsymbol{M}_{\beta} = \boldsymbol{0} \qquad \boldsymbol{F}_{r\alpha}(\boldsymbol{x})\boldsymbol{L}_{\alpha} + \boldsymbol{F}_{r\beta}(\boldsymbol{x})\boldsymbol{L}_{\beta} = \boldsymbol{0} \tag{3.6.13}$$

$$c_{\alpha}\boldsymbol{D}_{\alpha\beta}\boldsymbol{M}_{\beta} = c_{\beta}\boldsymbol{M}_{\alpha}\boldsymbol{D}_{\beta\alpha}^{\mathrm{T}} \qquad c_{\alpha}\boldsymbol{F}_{\alpha\beta}\boldsymbol{L}_{\beta} = c_{\beta}\boldsymbol{L}_{\alpha}\boldsymbol{F}_{\beta\alpha}^{\mathrm{T}} \tag{3.6.14}$$

In multiphase systems, similar connections are obtained only between the mechanical and transformation concentration factors, in the context of a selected homogenization method. In both two and multiphase systems, local transformation field averages depend only on mechanical concentration factors and on phase stiffnesses or compliances (Dvorak and Benveniste 1992a, b).

3.6.3 Overall Response

A distribution of local phase transformations in a representative volume expands the overall constitutive relations (3.4.9) of a heterogeneous aggregate to

$$\left.\begin{aligned} \bar{\boldsymbol{\sigma}} &= \boldsymbol{L}\boldsymbol{\varepsilon}^{0} + \bar{\boldsymbol{\lambda}} & \bar{\boldsymbol{\varepsilon}} &= \boldsymbol{M}\boldsymbol{\sigma}^{0} + \bar{\boldsymbol{\mu}} \\ \bar{\boldsymbol{\lambda}} &= -\boldsymbol{L}\bar{\boldsymbol{\mu}} & \bar{\boldsymbol{\mu}} &= -\boldsymbol{M}\bar{\boldsymbol{\lambda}} \end{aligned}\right\} \tag{3.6.15}$$

where the $\bar{\boldsymbol{\lambda}}$ is the overall eigenstress under overall prescribed strain $\boldsymbol{\varepsilon}^{0}$, and $\bar{\boldsymbol{\mu}}$ is the overall eigenstrain that is superimposed with mechanical strain caused by $\boldsymbol{\sigma}^{0}$.

In both two and multi-phase systems, the overall eigenstrain and eigenstress follow from the Levin formula derived in Sect. 3.8. However, in two-phase materials, magnitudes of both $\bar{\boldsymbol{\lambda}}$ and $\bar{\boldsymbol{\mu}}$ can be readily derived using (3.6.6) and (3.6.9). Suppose that two distinct, uniform phase eigenstrains $\boldsymbol{\mu}_{r} = -\boldsymbol{M}_{r}\boldsymbol{\lambda}_{r}$, $r = \alpha,\ \beta$, are applied in a representative volume V of an aggregate constrained by zero-valued displacements at the outer surface ∂V. The overall uniform eigenstress caused by these eigenstrains follows by superposition of the auxiliary uniform stress $\hat{\boldsymbol{\sigma}}$ in (3.6.6) with the overall stress caused by removal of the auxiliary uniform strain $\hat{\boldsymbol{\varepsilon}}$

$$\bar{\boldsymbol{\lambda}} = \hat{\boldsymbol{\sigma}} - \boldsymbol{L}\hat{\boldsymbol{\varepsilon}} = (\boldsymbol{L}_{\alpha} - \boldsymbol{L})\hat{\boldsymbol{\varepsilon}} + \boldsymbol{\lambda}_{\alpha} = (\boldsymbol{L} - \boldsymbol{L}_{\alpha})(\boldsymbol{L}_{\alpha} - \boldsymbol{L}_{\beta})^{-1}(\boldsymbol{\lambda}_{\alpha} - \boldsymbol{\lambda}_{\beta}) + \boldsymbol{\lambda}_{\alpha} \tag{3.6.16}$$

$$\bar{\boldsymbol{\lambda}} = (\boldsymbol{L} - \boldsymbol{L}_{\beta})(\boldsymbol{L}_{\alpha} - \boldsymbol{L}_{\beta})^{-1}\boldsymbol{\lambda}_{\alpha} - (\boldsymbol{L} - \boldsymbol{L}_{\alpha})(\boldsymbol{L}_{\alpha} - \boldsymbol{L}_{\beta})^{-1}\boldsymbol{\lambda}_{\beta} \tag{3.6.17}$$

The overall uniform eigenstrain caused by such transformations in a traction free representative volume V follows by complete unloading from the auxiliary overall stress $\hat{\boldsymbol{\sigma}}$ in (3.6.9) to zero.

$$\bar{\boldsymbol{\mu}} = \hat{\boldsymbol{\varepsilon}} - \boldsymbol{M}\hat{\boldsymbol{\sigma}} = (\boldsymbol{M}_\alpha - \boldsymbol{M})\hat{\boldsymbol{\sigma}} + \boldsymbol{\mu}_\alpha = (\boldsymbol{M} - \boldsymbol{M}_\alpha)(\boldsymbol{M}_\alpha - \boldsymbol{M}_\beta)^{-1}(\boldsymbol{\mu}_\alpha - \boldsymbol{\mu}_\beta) + \boldsymbol{\mu}_\alpha \tag{3.6.18}$$

$$\bar{\boldsymbol{\mu}} = (\boldsymbol{M} - \boldsymbol{M}_\beta)(\boldsymbol{M}_\alpha - \boldsymbol{M}_\beta)^{-1}\boldsymbol{\mu}_\alpha - (\boldsymbol{M} - \boldsymbol{M}_\alpha)(\boldsymbol{M}_\alpha - \boldsymbol{M}_\beta)^{-1}\boldsymbol{\mu}_\beta \tag{3.6.19}$$

It should be noted that both $\bar{\boldsymbol{\lambda}}$ and $\bar{\boldsymbol{\mu}}$ depend on volume fractions $c_\alpha + c_\beta = 1$, and on mechanical concentration factors of the phases, through the overall stiffness $\boldsymbol{L}$ and compliance $\boldsymbol{M}$, as indicated by (3.5.8). Of course, if $\boldsymbol{L}$ or $\boldsymbol{M}$ are known from an experiment, then only phase properties and the local transformations are needed for determination of the overall response (Benveniste and Dvorak 1989).

3.7 Work, Energy and Reciprocal Theorems

3.7.1 Clapeyron and Virtual Work Theorems

A certain volume V of a heterogeneous solid is loaded by a combination of constant, piecewise continuous surface tractions t_i and displacements u_i, applied at respective parts of the surface $\partial V = \partial V_t + \partial V_u$. Moreover, a distribution of body forces $F_i(\boldsymbol{x})$ may be prescribed at $\boldsymbol{x} \in V$. The actual interior stress and strain fields caused in V by the applied loads are not known. Instead, certain interior fields are selected such that they comply with the following admissibility conditions. A statically admissible stress field $\sigma_{ij}(\boldsymbol{x})$ is continuous and has continuous partial derivatives with respect to the $\boldsymbol{x}-$coordinates, up to and including order 2, or is of class C^2. It satisfies equilibrium equations $\sigma_{ij,j} + F_i = 0$ at all interior points $\boldsymbol{x} \in V$, as well as traction boundary conditions $\sigma_{ij} n_j = t_i$ prescribed on ∂V_t. Applied body forces $F_i(\boldsymbol{x})$ are continuous functions of class C^1. An interior strain field $\varepsilon_{ij} = (u_{i,j} + u_{j,i})/2$ is derived from a kinematically admissible field of continuous displacements $u_i(\boldsymbol{x})$, of class C^3, that satisfy the displacement boundary conditions $u_i = u_i^0$ on ∂V_u.

Work generated by constant surface tractions and body forces applied in V, on surface and interior displacements is

$$\left.\begin{aligned} &\int_{\partial V} t_i u_i \mathrm{d}S + \int_V F_i u_i \mathrm{d}V = \int_{\partial V} \sigma_{ij} n_j u_i \mathrm{d}S + \int_V F_i u_i \mathrm{d}V \\ &= \int_V [\frac{\partial}{\partial x_j}(\sigma_{ij} u_i) + F_i u_i]\mathrm{d}V = \int_V [\sigma_{ij}\frac{\partial u_i}{\partial x_j} + u_i(\frac{\partial \sigma_{ij}}{\partial x_j} + F_i)]\mathrm{d}V \\ &= \int_V \sigma_{ij}(\varepsilon_{ij} + \omega_{ij})\mathrm{d}V = \int_V \sigma_{ij}\varepsilon_{ij}\mathrm{d}V = 2\mathcal{W} \end{aligned}\right\} \tag{3.7.1}$$

This is ***Clapeyron's theorem***, which states that the work of constant tractions and body forces on kinematically admissible displacements is equal to twice the strain energy $\mathcal{W}$ stored in V when the body is in equilibrium state. Moreover, transcription of the product $\sigma_{ij}\varepsilon_{ij} \rightarrow \boldsymbol{\varepsilon}_{EG}^{\mathrm{T}}\boldsymbol{L}_{EG}\boldsymbol{\varepsilon}_{EG}$ derived in (2.1.7) implies use of the engineering matrix notation in numerical evaluations of the results derived in this section.

Proof of the theorem relies only on the stated admissibility conditions and on the divergence theorem relating the respective volume and surface integrals. *The two admissible fields may, but do not need to be connected by a constitutive relation*. For example, each may have been found for different elastic and/or inelastic phases residing in the original subvolumes of V. In the latter case, the work terms are entirely fictitious. However, in an elastic solid, the strain energy is

$$\mathcal{W} = \int_V \mathcal{W}(\varepsilon_{ij})\mathrm{d}V = \frac{1}{2}\int_V L_{ijkl}\varepsilon_{ij}\varepsilon_{kl}\mathrm{d}V = \frac{1}{2}\int_V \sigma_{ij}\varepsilon_{ij}\mathrm{d}V \tag{3.7.2}$$

where $\mathcal{W}(\varepsilon_{ij})$, a positive definite quadratic form of the strain components, is the strain energy density in V. Expanded form of $\mathcal{W}$ is shown in (2.1.10).

Next, suppose that a distribution of transformation strains $\mu_{ij} = \mu_{ji}$ of class C^1 is also prescribed in phase subvolumes V_r comprising V. The class C^1 requirement may necessitate additional subdivisions of V. The displacement field $u_i(\boldsymbol{x})$ remains of class C^3, and assumes prescribed values $u_i = u_i^0$ on ∂V_u. As described in Sect. 3.6, surface tractions and body forces are now superimposed with eigenstress fields $\lambda_{ij} = -L_{ijkl}\mu_{kl}$, and are then replaced by the modified quantities (3.6.2), (3.6.3), (3.6.4), which must satisfy the above stated continuity conditions in V and on ∂V.

$$\tilde{\sigma}_{ij} = \sigma_{ij} - \lambda_{ij} \qquad \tilde{F}_i = F_i + \lambda_{ij,j} \qquad \tilde{t}_i = t_i - \lambda_{ij}n_j \tag{3.7.3}$$

Use of these in the first two terms of (3.7.1) yields the expression

$$\int_{\partial V}(t_i - \lambda_{ij}n_j)u_i\mathrm{d}S + \int_V (F_i + \lambda_{ij,j})u_i\mathrm{d}V \tag{3.7.4}$$

Application of *per partes* integration to the last term, together with the divergence theorem, and the connections $u_{i,j} = \varepsilon_{ij} + \omega_{ij}$, $\lambda_{ij} = \lambda_{ji}$, $\omega_{ij} = -\omega_{ji}$, provides

$$\int_V \lambda_{ij,j}u_i\mathrm{d}V = -\int_V \lambda_{ij}\varepsilon_{ij}\mathrm{d}V + \int_{\partial V}\lambda_{ij}u_in_j\mathrm{d}S \tag{3.7.5}$$

In the presence of the eigenstrain fields, and in superposition with separately admissible total stress and strain fields, (3.7.1) reads

$$\int_{\partial V} t_iu_i\mathrm{d}S + \int_V F_iu_i\mathrm{d}V - \int_V \lambda_{ij}\varepsilon_{ij}\mathrm{d}V = \int_V (\sigma_{ij} - \lambda_{ij})\varepsilon_{ij}\mathrm{d}V \tag{3.7.6}$$

Existence of the integrals needs to be verified for each applied eigenstress field. Equation (3.7.6) is equivalent to the Clapeyron theorem (3.7.1), with the stress now derived from the elastic strain, $\sigma_{ij} = L_{ijkl}(\varepsilon_{kl} - \mu_{kl})$.

The virtual work theorem evaluates the work performed by any kinematically admissible virtual displacements δu_i in the material volume, that satisfy homogeneous boundary conditions $\delta u_i = 0$, consistent with the prescribed displacements $u_i = u_i^0$ on ∂V_u, on an admissible stress field that *remains constant* along the virtual deformation path. Again, the two admissible fields need not be related by a constitutive relation. The derivation leading to (3.7.1) is reconstructed with virtual terms, providing the virtual work equation

$$\int_{\partial V_t} t_i \delta u_i \mathrm{d}S + \int_V F_i \delta u_i \mathrm{d}V = \int_V \sigma_{ij} \delta \varepsilon_{ij} \mathrm{d}V \tag{3.7.7}$$

where the first integral is taken only over ∂V_t because $\delta u_i = 0$ on ∂V_u.

Since the admissible fields need not be connected by any specific constitutive relations, and the integrals evaluate only a virtual energy change, the virtual work equation can be used in numerous applications, with any pair of possibly unrelated admissible fields. This is illustrated by derivation of the Levin formula in Sect. 3.8. In the presence of an eigenstress field, the virtual work equation becomes, in analogy to (3.7.6)

$$\int_{\partial V_t} t_i \delta u_i \mathrm{d}S + \int_V F_i \delta u_i \mathrm{d}V - \int_V \lambda_{ij} \delta \varepsilon_{ij} \mathrm{d}V = \int_V (\sigma_{ij} - \lambda_{ij}) \delta \varepsilon_{ij} \mathrm{d}V \tag{3.7.8}$$

3.7.2 *Minimum Potential and Complementary Energy Theorems*

As in the derivation of the virtual work equation (3.7.7), actual displacements u_i of *an elastic body in equilibrium* are superimposed with a kinematically admissible virtual displacement field δu_i, while applied body forces and surface tractions remain constant. The strain field thus changes to $\varepsilon'_{ij} = \varepsilon_{ij} + \delta \varepsilon_{ij}$. First variation of the strain energy is defined as

$$\delta \mathcal{W} = \int_V [\mathcal{W}(\varepsilon_{ij} + \delta \varepsilon_{ij}) - \mathcal{W}(\varepsilon_{ij})] \mathrm{d}V \tag{3.7.9}$$

Expansion of the first integrand in a Taylor series yields

$$\mathcal{W}(\varepsilon_{ij} + \delta \varepsilon_{ij}) = \mathcal{W}(\varepsilon_{ij}) + \frac{\partial \mathcal{W}(\varepsilon_{ij})}{\partial \varepsilon_{ij}} \delta \varepsilon_{ij} + \frac{1}{2} \frac{\partial^2 \mathcal{W}(\varepsilon_{ij})}{\partial \varepsilon_{ij} \partial \varepsilon_{kl}} \delta \varepsilon_{ij} \delta \varepsilon_{kl} + \ldots \tag{3.7.10}$$

The second term is equal to the derivative of the quadratic form in (3.7.2)

$$\frac{\partial \mathcal{W}(\varepsilon_{ij})}{\partial \varepsilon_{ij}} \delta\varepsilon_{ij} = \sigma_{ij}\,\delta\varepsilon_{ij} \tag{3.7.11}$$

and its integral follows from the virtual work equation as

$$\int_V \sigma_{ij}\,\delta\varepsilon_{ij}\,\mathrm{d}V = \int_V F_i\,\delta u_i\,\mathrm{d}V + \int_{\partial V} t_i\,\delta u_i\,\mathrm{d}S \qquad [3.7.7]$$

In (3.7.11), with reference to (2.1.2), there is $\partial \mathcal{W}/\partial\varepsilon_{ij} = \sigma_{ij}$ for $i = j$, and $\partial \mathcal{W}/\partial\varepsilon_{ij} = 2\sigma_{ij}$ for $i \neq j$. The third term in (3.7.10) is equal to strain energy density $\mathcal{W}(\delta\varepsilon_{ij})$ of virtual displacements, and is therefore positive. The first two terms in the expansion yield the first variation of strain energy

$$\delta\mathcal{W} = \int_V F_i\,\delta u_i\,\mathrm{d}V + \int_{\partial V} t_i\,\delta u_i\,\mathrm{d}S \tag{3.7.12}$$

Since applied body forces and surface tractions remain constant during application of virtual displacements, this can be written as

$$\delta\mathcal{W} - \delta\int_V F_i u_i\,\mathrm{d}V - \delta\int_{\partial V} t_i u_i\,\mathrm{d}S = \delta\left[\mathcal{W} - \int_V F_i u_i\,\mathrm{d}V - \int_{\partial V} t_i u_i\,\mathrm{d}S\right] = \delta\mathcal{V} = 0 \tag{3.7.13}$$

where

$$\mathcal{W} = \frac{1}{2}\int_V \sigma_{ij}\,\varepsilon_{ij}\,\mathrm{d}V - \int_V F_i u_i\,\mathrm{d}V - \int_{\partial V} t_i u_i\,\mathrm{d}S \tag{3.7.14}$$

defines the potential energy of an elastic body under constant tractions and body forces. The surface integrals in the last two equations are taken only over that part of the surface where tractions are prescribed. The second variation of $\mathcal{V}$ is positive, hence (3.7.13) defines the minimum of potential energy in $\mathcal{V}$.

The minimum potential energy theorem states that when potential energy of an elastic body has a minimum $\delta\mathcal{V} = 0$, the displacement field is that of actual equilibrium state and it satisfies boundary conditions prescribed at ∂V_u.

Next, write the strain energy (3.7.2) of an elastic body in equilibrium as a function of the stress field

$$\mathcal{W} = \int_V \mathcal{W}(\sigma_{ij})\mathrm{d}V = \frac{1}{2}\int_V M_{ijkl}\sigma_{ij}\sigma_{kl}\mathrm{d}V = \frac{1}{2}\int_V \varepsilon_{ij}\sigma_{ij}\,\mathrm{d}V \tag{3.7.15}$$

and define the first variation of $\mathcal{W}$ as

$$\delta\mathcal{W} = \int_V [\mathcal{W}(\sigma_{ij} + \delta\sigma_{ij}) - \mathcal{W}(\sigma_{ij})]\mathrm{d}V \tag{3.7.16}$$

where the field $(\sigma_{ij} + \delta\sigma_{ij})$ is a self-equilibrated stress field, with $(\delta\sigma_{ij})_{,j} = 0$ in V. It also satisfies traction boundary conditions by letting $\delta\sigma_{ij} n_j = 0$ on ∂V_t, while $\delta\sigma_{ij} n_j$ are arbitrary at ∂V_u. The first integrand is again expanded into a Taylor series, where we retain only the first two terms. Together with above properties of $\delta\sigma_{ij}$, this yields first variation of the quadratic form (3.7.15)

$$\left.\begin{aligned} \delta\mathcal{W} &= \int_V \varepsilon_{ij}\delta\sigma_{ij}\mathrm{d}V = \frac{1}{2}\int_V (u_{i,j} + u_{j,i})\delta\sigma_{ij}\mathrm{d}V = \int_V (u_i\delta\sigma_{ij})_{,j}\mathrm{d}V \\ &= \int_{\partial V} u_i\delta\sigma_{ij}n_j\mathrm{d}S \end{aligned}\right\} \tag{3.7.17}$$

Virtual surface tractions $\delta t_i = \delta\sigma_{ij}n_j$ vanish where actual surface traction are prescribed, hence they are applied only at the ∂V_u part of ∂V, where surface displacements are prescribed, to keep the virtual stress field in equilibrium. Since displacements remain constant, (3.7.17) can be recast as

$$\delta\left[\mathcal{W} - \int_{\partial V_u} u_i t_i \mathrm{d}S\right] = \delta\mathcal{V}^* = 0 \tag{3.7.18}$$

The complementary energy of an elastic body in equilibrium is the functional

$$\mathcal{V}^* = \frac{1}{2}\int_V \varepsilon_{ij}\sigma_{ij}\mathrm{d}V - \int_{\partial V_u} u_i t_i \mathrm{d}S \tag{3.7.19}$$

Theorem of minimum complementary energy follows from the condition $\delta\mathcal{V}^* = 0$ indicated by (3.7.18). It states that $\mathcal{V}^*$ reaches an absolute minimum when the stress field is that of equilibrium state and it satisfies traction boundary conditions prescribed at ∂V_t. This result is attributed to Castigliano. The above derivation of both theorems has followed that by Brdička (1959).

Of particular interest in subsequent derivation of energy bounds on overall stiffness and compliance in Sect. 6.1, are applications of these theorems to a representative volume V, loaded on ∂V by displacements corresponding to a uniform overall strain $\boldsymbol{\varepsilon}^0$, or by tractions creating an overall uniform stress $\boldsymbol{\sigma}^0$ (Hill 1963b). For the first boundary value problem, where a uniform overall strain $\boldsymbol{\varepsilon}^0$ is prescribed, the potential and complementary energies are

$$\left.\begin{aligned} \mathcal{V}^{(a)} \leq \mathcal{V} = \mathcal{W} &= \frac{1}{2}\int_V L_{ijkl}\varepsilon_{ij}\varepsilon_{kl}\mathrm{d}V \\ (\mathcal{V}^*)^{(a)} \geqslant \mathcal{V}^* &= \frac{1}{2}\int_V (2\varepsilon^0_{ij} - M_{ijkl}\sigma_{kl})\sigma_{ij}\mathrm{d}V \end{aligned}\right\} \tag{3.7.20}$$

The actual potential energy $\mathcal{V}^{(a)}$, equal to strain energy $\mathcal{W}^{(a)}$, is generated by the actual but unknown local strain and stress fields in the heterogeneous aggregate in V. It is smaller than the potential energy $\mathcal{V}$ generated there by any admissible local fields. Under the same overall strain $\boldsymbol{\varepsilon}^0$, the complementary energy (3.7.19) is larger than that derived from any admissible local fields.

For the second boundary value problem, where a uniform overall stress $\boldsymbol{\sigma}^0$ is applied, the energy inequalities are

$$\mathcal{V}^{(a)} \geqslant \mathcal{V} = \frac{1}{2}\int_V (2\sigma^0_{ij} - L_{ijkl}\varepsilon_{kl})\varepsilon_{ij}\mathrm{d}V \quad (\mathcal{V}^*)^{(a)} \leq \mathcal{V}^* = \frac{1}{2}\int_V M_{ijkl}\sigma_{ij}\sigma_{kl}\mathrm{d}V \tag{3.7.21}$$

Energy changes induced by superposition of external loads with phase eigenstrains are described in Chap. 5.

3.7.3 The Reciprocal Theorem

This theorem applies to linear elastic solids or structures, kept in equilibrium by prescribed displacements on a part ∂V_u of their surface, and in turn, by one of two independent systems of body forces and surface tractions distributed in V and on ∂V_t. The two systems are denoted here by $F_i^{(1)}$, $t_i^{(1)}$ and $F_i^{(2)}$, $t_i^{(2)}$. Each system is applied separately to the same solid or structure, generating interior displacements $u_i^{(1)}$, $u_i^{(2)}$, while the prescribed surface displacements are kept constant. The reciprocal theorem states that the work of force system $F_i^{(1)}$, $t_i^{(1)}$ on displacements $u_i^{(2)}$ caused by force system $F_i^{(2)}$, $t_i^{(2)}$ is equal to the work of forces $F_i^{(2)}$, $t_i^{(2)}$ on displacements $u_i^{(1)}$ caused by system $F_i^{(1)}$, $t_i^{(1)}$. This result is due to Betti (1872) and Rayleigh (1873). Sokolnikoff (1956, p. 392) writes the reciprocal theorem as

$$\int_{\partial V} t_i^{(1)}u_i^{(2)}\mathrm{d}S + \int_V F_i^{(1)}u_i^{(2)}\mathrm{d}V = \int_{\partial V} t_i^{(2)}u_i^{(1)}\mathrm{d}S + \int_V F_i^{(2)}u_i^{(1)}\mathrm{d}V \tag{3.7.22}$$

If a distribution of eigenstrains is also present in the elastic solid, the surface tractions and body forces are superimposed with eigenstress fields $\lambda_i^{(1)}$ and $\lambda_i^{(2)}$, which can be replaced in (3.7.22) by modified quantities in (3.7.3). Repetition of the

sequence in (3.7.1) and rearrangement of terms provides final form of the reciprocal theorem in the presence of eigenstress fields as

$$\left.\begin{aligned}\int_{\partial V} t_i^{(1)} u_i^{(2)} \mathrm{d}S + \int_V F_i^{(1)} u_i^{(2)} \mathrm{d}V - \int_V \lambda_{ij}^{(1)} \varepsilon_{ij}^{(2)} \mathrm{d}V \\ = \int_{\partial V} t_i^{(2)} u_i^{(1)} \mathrm{d}S + \int_V F_i^{(2)} u_i^{(1)} \mathrm{d}V - \int_V \lambda_{ij}^{(2)} \varepsilon_{ij}^{(1)} \mathrm{d}V\end{aligned}\right\} \tag{3.7.23}$$

The reciprocal theorem can also be written for local stress and strain fields. Referring to the last integral in (3.7.6)

$$\int_V (\sigma_{ij}^{(1)} - \lambda_{ij}^{(1)}) \varepsilon_{ij}^{(2)} \mathrm{d}V = \int_V (\sigma_{ij}^{(2)} - \lambda_{ij}^{(2)}) \varepsilon_{ij}^{(1)} \mathrm{d}V \tag{3.7.24}$$

Since the eigenstress field need not be continuous, existence of the above integrals needs to be verified in each application (Dvorak and Benveniste 1992).

Together with virtual work, the reciprocal theorem has found numerous applications. However, in contrast to the broader applicability of the former, it can be used only for elastic solids. Both theorems are now applied to solving the same particular problem.

3.8 The Levin Formula and the Hill Lemma

Consider first a specified distribution of local eigenstrains $\boldsymbol{\mu}_r(\boldsymbol{x})$, with related local eigenstresses $\boldsymbol{\lambda}_r(\boldsymbol{x}) = -\boldsymbol{L}_r \boldsymbol{\mu}_r(\boldsymbol{x})$, in the phases $r = 1, 2, \ldots n$ of a certain representative volume V of a heterogeneous medium, where both body forces and surface tractions vanish, $F_i(\boldsymbol{x}) = 0$, $t_i = 0$. Since the eigenstrain distribution is applied in the interior of a representative volume, it must generate, by the expanded definition of the RVE in Sect. 3.3, a uniform overall eigenstrain. This overall eigenstrain is now derived using, in turn, the virtual work and the reciprocal theorem.

The Levin formula (1967) describes the effect of a uniform change in temperature $\Delta\theta$ on the overall thermal strain of a representative volume of a multiphase heterogeneous solid. The eigenstrains are represented here by thermal strains, specified in each phase r as $\mu_{ij}^r = m_{ij}^r \Delta\theta$. The m_{ij} is the thermal strain vector of linear coefficients of thermal expansion, shown in the contracted tensorial notation in Table 8.1. Overall eigenstrain is sought as $\bar{\mu}_{ij} = \bar{m}_{ij} \Delta\theta$, where $\bar{m}_{ij}$ denotes the overall or macroscopic thermal strain vector of the heterogeneous aggregate. In many references, thermal strain tensors are denoted by α_{ij} and $\bar{\alpha}_{ij}$.

Levin's choice of admissible fields for this problem offers a good illustration of the utility of the virtual work theorem. A total of four admissible fields are

used in two virtual work equations. The first pair of overall and local admissible fields is selected as that caused by a uniform overall stress at zero temperature change. Denoted by a single prime, overall and local stresses and strains derived from $(3.4.7)_2$ and (3.5.4) are

$$\bar{\sigma}'_{ij} = \sigma^0_{ij} \quad \bar{\varepsilon}'_{ij} = M_{ijkl}\sigma^0_{kl} \quad (\sigma^r_{ij}(\boldsymbol{x}))' = B^r_{ijkl}(\boldsymbol{x})\sigma^0_{kl} \quad (\varepsilon^r_{ij}(\boldsymbol{x}))' = M^r_{ijkl}(\sigma^r_{ij}(\boldsymbol{x}))' \tag{3.8.1}$$

Top bars denote overall averages.

The second pair of admissible fields is generated only by a uniform change in temperature $\Delta\theta$, at zero overall stress. Overall and local stresses and strains are

$$\bar{\sigma}''_{ij} = 0 \quad \bar{\varepsilon}''_{ij} = \bar{m}_{ij}\,\Delta\theta \quad (\varepsilon^r_{ij}(\boldsymbol{x}))'' = M^r_{ijkl}(\sigma^r_{kl}(\boldsymbol{x}))'' + m^r_{ij}\,\Delta\theta \tag{3.8.2}$$

The first virtual work equation employs statically admissible stresses of the double primed second pair, and kinematically admissible strains of the first pair, yielding

$$\left.\begin{aligned} &\int_V (\sigma^r_{ij}(\boldsymbol{x}))''(\varepsilon^r_{ij}(\boldsymbol{x}))'\mathrm{d}V = \bar{\sigma}''_{ij}\bar{\varepsilon}'_{ij}\,V = 0 \\ &\Rightarrow \int_V (\sigma^r_{ij}(\boldsymbol{x}))'' M^r_{ijkl}(\sigma^r_{kl}(\boldsymbol{x}))'\mathrm{d}V = \int_V (\sigma^r_{kl}(\boldsymbol{x}))'' M^r_{klij}(\sigma^r_{ij}(\boldsymbol{x}))'\mathrm{d}V = 0 \end{aligned}\right\} \tag{3.8.3}$$

The second virtual work equation combines the two remaining admissible fields in

$$\int_V (\sigma^r_{ij}(\boldsymbol{x}))'(\varepsilon^r_{ij}(\boldsymbol{x}))''\mathrm{d}V = \bar{\sigma}'_{ij}\bar{\varepsilon}''_{ij}\,V \tag{3.8.4}$$

The primed local stress field is given by $(3.8.1)_3$ and $(\varepsilon^r_{ij}(\boldsymbol{x}))''$ by $(3.8.2)_3$. However, if the elastic field is written as $(\sigma^r_{ij}(\boldsymbol{x}))' = B^r_{ijkl}(\boldsymbol{x})\sigma^0_{kl} \neq 0$, $(3.8.3)_4$ renders the integral of $M^r_{ijkl}(\sigma^r_{kl}(\boldsymbol{x}))''$ equal to zero. Therefore, (3.8.4) assumes the form

$$\sigma^0_{kl}\int_V B^r_{ijkl}(\boldsymbol{x})\,m^r_{ij}\,\Delta\theta\,\mathrm{d}V = \sigma^0_{ij}\int_V B^r_{klij}(\boldsymbol{x})\,m^r_{kl}\,\Delta\theta\,\mathrm{d}V = \sigma^0_{ij}\,\bar{m}_{ij}\,\Delta\theta\,V \tag{3.8.5}$$

After rearrangement, the Levin formula provides the overall thermal strain vector

$$\bar{m}_{ij} = \frac{1}{V}\int_V (B^r_{ijkl}(\boldsymbol{x}))^{\mathrm{T}}\,m^r_{kl}\,\mathrm{d}V \quad \text{or} \quad \bar{\boldsymbol{m}} = \frac{1}{V}\int_V \boldsymbol{B}^{\mathrm{T}}_r(\boldsymbol{x})\,\boldsymbol{m}_r\,\mathrm{d}V \tag{3.8.6}$$

It is probably obvious that the derivation is not limited to thermal strains and that it can be generalized to a distribution of any number of other small eigenstrains distributed in V. That result is sometimes called the generalized Levin formula.

This generalized form also follows from, and illustrates here the use of, the elastic reciprocal theorem (Benveniste and Dvorak 1992). The heterogeneous aggregate in representative volume V is assumed to be free of external tractions, and is loaded only by small eigenstrains $\boldsymbol{\mu}(\boldsymbol{x})$, distributed in V such that the overall eigenstrain, denoted here by $\bar{\boldsymbol{\mu}}$, is uniform on the macroscale.

To find $\bar{\boldsymbol{\mu}}$, let us select two sets of force and displacement fields. One is represented by local eigenstresses $\lambda^r_{ij}(\boldsymbol{x}) = (\lambda^r_{ij})^{(1)}(\boldsymbol{x})$, with corresponding displacements $\bar{u}^{(1)}_i(\boldsymbol{x})$ and zero tractions on ∂V. The other is caused in V by certain auxiliary surface tractions $t^{(2)}_i(\boldsymbol{x}) \in \partial V$, which create a uniform overall stress $\bar{\sigma}^{(2)}_{ij} = t^{(2)}_i n_j$ and local stresses $(\sigma^r_{ij}(\boldsymbol{x}))^{(2)} = B^r_{ijkl}(\boldsymbol{x})\bar{\sigma}^{(2)}_{kl} = L^r_{ijkl}(\varepsilon^r_{kl}(\boldsymbol{x}))^{(2)}$ and strains $(\varepsilon^r_{ij}(\boldsymbol{x}))^{(2)} = M^r_{ijrs}(\sigma^r_{rs}(\boldsymbol{x}))^{(2)}$ in V. The reciprocal theorem then states that

$$-\int_V \lambda^{(1)}_{ij}\varepsilon^{(2)}_{ij}\mathrm{d}V = \int_{\partial V} t^{(2)}_i \bar{u}^{(1)}_i \mathrm{d}S \tag{3.8.7}$$

The integrands are rewritten as

$$\left.\begin{aligned} &\lambda^{(1)}_{ij}\varepsilon^{(2)}_{ij} = \lambda^{(1)}_{ij} M^r_{ijkl} B^r_{klqr}\bar{\sigma}^{(2)}_{qr} = \lambda^{(1)}_{qr} M^r_{qrkl} B^r_{klij}\bar{\sigma}^{(2)}_{ij} \\ &\int_{\partial V} t^{(2)}_i \bar{u}^{(1)}_i \mathrm{d}S = \bar{\sigma}^{(2)}_{ij}\frac{1}{2}\int_{\partial V}\left(\bar{u}^{(1)}_i n_j + \bar{u}^{(1)}_j n_i\right)\mathrm{d}S = \bar{\sigma}^{(2)}_{ij}\bar{\mu}^{(1)}_{ij}V \end{aligned}\right\} \tag{3.8.8}$$

where $\bar{\mu}^{(1)}_{ij}$ is the overall eigenstrain. Noting that $M^r_{klqr}(\lambda^r_{qr})^{(1)}(\boldsymbol{x}) = -(\mu^r_{kl})^{(1)}(\boldsymbol{x})$, one can solve the last two equations for the overall averaged eigenstrain as

$$\bar{\mu}_{ij} = \frac{1}{V}\int_V (B^r_{ijkl}(\boldsymbol{x}))^{\mathrm{T}}\mu_{kl}(\boldsymbol{x})\mathrm{d}V \quad \text{or} \quad \bar{\boldsymbol{\mu}} = \frac{1}{V}\int_V \boldsymbol{B}^{\mathrm{T}}_r(\boldsymbol{x})\boldsymbol{\mu}_r(\boldsymbol{x})\mathrm{d}V \tag{3.8.9}$$

In a traction-free volume, this eigenstrain is equal to the overall strain. In contrast, if the volume V is prevented from overall deformation by prescribing $u_i = 0$ on the surface ∂V, then an analogous derivation provides the overall eigenstress at $\bar{\boldsymbol{\varepsilon}} = \mathbf{0}$.

$$\bar{\lambda}_{ij} = \frac{1}{V}\int_V (A^r_{ijkl}(\boldsymbol{x}))^{\mathrm{T}}\lambda_{kl}(\boldsymbol{x})\mathrm{d}V \quad \text{or} \quad \bar{\boldsymbol{\lambda}} = \frac{1}{V}\int_V \boldsymbol{A}^{\mathrm{T}}_r(\boldsymbol{x})\boldsymbol{\lambda}_r(\boldsymbol{x})\mathrm{d}V \tag{3.8.10}$$

A similar application of the reciprocal theorem was described by Rice (1970).

In the terminology of Eshelby (1961), the eigenstress (3.8.10) is generated by application of surface displacements on ∂V that cause an overall *image strain* $\bar{\boldsymbol{\varepsilon}}^{im}$ such that $\bar{\boldsymbol{\varepsilon}} = \bar{\boldsymbol{\mu}} - \bar{\boldsymbol{\varepsilon}}^{im} = \mathbf{0}$, as required by the boundary conditions. An image stress is defined in an analogous manner under overall tractions.

For a piecewise uniform distribution of eigenstrains $\boldsymbol{\mu}_r(\boldsymbol{x}) = \boldsymbol{\mu}_r$ in the phases, the influence functions are integrated according to (3.5.2) and (3.5.4), and the above integrals are replaced with

$$\bar{\boldsymbol{\lambda}} = \sum_{r=1}^{n} c_r \boldsymbol{A}_r^{\mathrm{T}} \boldsymbol{\lambda}_r \quad \bar{\boldsymbol{\mu}} = \sum_{r=1}^{n} c_r \boldsymbol{B}_r^{\mathrm{T}} \boldsymbol{\mu}_r \tag{3.8.11}$$

Of course, this also applies to the thermal strains. Referring to $(3.8.1)_{2,3}$ and $(3.6.1)_3$, we rewrite the first form as

$$\bar{\boldsymbol{\lambda}} = -\sum_{r=1}^{n} c_r \boldsymbol{A}_r^{\mathrm{T}} \boldsymbol{L}_r \boldsymbol{\mu}_r = -\boldsymbol{L} \sum_{r=1}^{n} c_r \boldsymbol{B}_r^{\mathrm{T}} \boldsymbol{\mu}_r \tag{3.8.12}$$

and by comparison with $(3.8.11)_2$ prove that $\bar{\boldsymbol{\lambda}} = -\boldsymbol{L}\bar{\boldsymbol{\mu}}$, $\bar{\boldsymbol{\mu}} = -\boldsymbol{M}\bar{\boldsymbol{\lambda}}$, as stipulated in (3.6.15).

Equations (3.8.9), (3.8.10) and (3.8.11) are equivalent forms of the Levin formula that defines overall averages of local transformation fields, in a representative volume of a heterogeneous aggregate. Only in homogeneous materials, where $\boldsymbol{A}_r = \boldsymbol{I}$, $\boldsymbol{B}_r = \boldsymbol{I}$, are the overall transformation strains equal to sums of their local volume averages, as in (3.4.3) and (3.4.6).

It is important to recognize the differences in averaging of elastic, transformation, and total strains. Standard averaging of local elastic strains $(3.6.1)_2$ over the volume V yields

$$\frac{1}{V}\int_V \boldsymbol{M}_r \boldsymbol{\sigma}_r(\boldsymbol{x})\mathrm{d}V = \frac{1}{V}\int_V [\boldsymbol{\varepsilon}_r(\boldsymbol{x}) - \boldsymbol{\mu}_r(\boldsymbol{x})]\mathrm{d}V = \bar{\boldsymbol{\varepsilon}} - \frac{1}{V}\int_V \boldsymbol{\mu}_r(\boldsymbol{x})\mathrm{d}V \tag{3.8.13}$$

However, according to (3.8.9), the overall eigenstrain that represents the volume average of the local transformation strains is

$$\bar{\boldsymbol{\mu}} = \frac{1}{V}\int_V \boldsymbol{B}_r^{\mathrm{T}}(\boldsymbol{x})\boldsymbol{\mu}_r(\boldsymbol{x})\mathrm{d}V \neq \frac{1}{V}\int_V \boldsymbol{\mu}_r(\boldsymbol{x})\mathrm{d}V \tag{3.8.14}$$

Therefore, the average over V of elastic strains in $(3.6.1)_2$ is not equal to the actual overall elastic strain

$$\frac{1}{V}\int_V \boldsymbol{M}_r \boldsymbol{\sigma}_r(\boldsymbol{x})\mathrm{d}V \neq (\bar{\boldsymbol{\varepsilon}} - \bar{\boldsymbol{\mu}}) = \boldsymbol{M}\boldsymbol{\sigma}^0 \tag{3.8.15}$$

except, of course, in the absence of transformation strains, when elastic and total strains coincide and the last relation is replaced by (3.5.7) with (3.5.8).

The distinct eigenstrain averaging in heterogeneous and homogeneous materials has not been uniformly recognized in the micromechanics literature, even long

after the Levin (1967) paper, leading to numerous unnoticed violations of (3.8.10) and (3.8.11), especially in certain papers on inelastic behavior of composite materials.

The first introduction of Levin's result outside the former USSR was apparently made by Rosen and Hashin (1970), in the original context of overall thermal expansion of composite materials. In application to two-phase systems, they utilize (3.5.6) to replace the mechanical concentration factor tensors by local and overall moduli, local CTEs and volume fractions. In two-phase systems, $r = \alpha,\ \beta$, one can indeed write (3.8.11) as

$$\bar{\boldsymbol{\lambda}} = c_\alpha \boldsymbol{A}_\alpha^{\mathrm{T}} \boldsymbol{\lambda}_\alpha + c_\beta \boldsymbol{A}_\beta^{\mathrm{T}} \boldsymbol{\lambda}_\beta \quad \bar{\boldsymbol{\mu}} = c_\alpha \boldsymbol{B}_\alpha^{\mathrm{T}} \boldsymbol{\mu}_\alpha + c_\beta \boldsymbol{B}_\beta^{\mathrm{T}} \boldsymbol{\mu}_\beta \tag{3.8.16}$$

and employ (3.5.13) to arrive at the results already known from uniform fields

$$\bar{\boldsymbol{\lambda}} = (\boldsymbol{L} - \boldsymbol{L}_\beta)(\boldsymbol{L}_\alpha - \boldsymbol{L}_\beta)^{-1} \boldsymbol{\lambda}_\alpha - (\boldsymbol{L} - \boldsymbol{L}_\alpha)(\boldsymbol{L}_\alpha - \boldsymbol{L}_\beta)^{-1} \boldsymbol{\lambda}_\beta \tag{3.6.17}$$

and

$$\bar{\boldsymbol{\mu}} = (\boldsymbol{M} - \boldsymbol{M}_\beta)(\boldsymbol{M}_\alpha - \boldsymbol{M}_\beta)^{-1} \boldsymbol{\mu}_\alpha - (\boldsymbol{M} - \boldsymbol{M}_\alpha)(\boldsymbol{M}_\alpha - \boldsymbol{M}_\beta)^{-1} \boldsymbol{\mu}_\beta \tag{3.6.19}$$

which Rosen and Hashin (1970) write as

$$\left.\begin{aligned} \bar{\boldsymbol{\lambda}} &= \boldsymbol{\lambda}_\alpha + (\boldsymbol{L} - \boldsymbol{L}_\alpha)(\boldsymbol{L}_\alpha - \boldsymbol{L}_\beta)^{-1}(\boldsymbol{\lambda}_\alpha - \boldsymbol{\lambda}_\beta) \\ \bar{\boldsymbol{\mu}} &= \boldsymbol{\mu}_\alpha + (\boldsymbol{M} - \boldsymbol{M}_\alpha)(\boldsymbol{M}_\alpha - \boldsymbol{M}_\beta)^{-1}(\boldsymbol{\mu}_\alpha - \boldsymbol{\mu}_\beta) \end{aligned}\right\} \tag{3.8.17}$$

Such elimination cannot be carried out for more than two phases, but that has no effect on Levin's key results (3.8.6) and (3.8.9), (3.8.10) and (3.8.11), which provide similar relations for multiphase aggregates, albeit dependent on the elastic local fields, or mechanical concentration factors. The latter are reproduced by Rosen and Hashin (1970) in their §2, which confirms (3.8.6) for multiphase systems. However, in opening their §3, they state: "The direct method of Levin cannot be applied to composites of three or more constituents as discussed earlier." This statement is evidently limited to the "direct" method (3.8.17).

As shown in (3.5.6), the overall compliance of two-phase aggregates depends on at least one concentration factor. Therefore, if the compliance is estimated, rather than measured in an experiment, there is no difference in accuracy of Levin's formula when applied to binary or multiphase systems. Moreover, since shape-independent two-phase results (3.8.17) follow from the uniform field method, the correct conclusion is:

Levin's formula is indispensable only in applications to multiphase aggregates, while the uniform field method yields equivalent results for two-phase systems. This argument is further supported by the analysis of thermal eigenstrain fields presented in Chap. 8.

The Hill lemma (1963a, 1967, 1971, 2000), originally derived for elastic and elastic-plastic heterogeneous aggregates, relates overall and internal work involving

inelastic strains. These are replaced here by a distribution $\boldsymbol{\mu}_r(\boldsymbol{x})$ of eigenstrains in the representative volume V, which is loaded by a uniform overall stress $\boldsymbol{\sigma}^0$. Total local and overall strains are given by $(3.6.1)_2$ and $(3.6.15)_2$, respectively, as

$$\boldsymbol{\varepsilon}_r(\boldsymbol{x}) = \boldsymbol{M}_r\boldsymbol{\sigma}_r(\boldsymbol{x}) + \boldsymbol{\mu}_r(\boldsymbol{x}) \quad \bar{\boldsymbol{\varepsilon}} = \boldsymbol{M}\boldsymbol{\sigma}^0 + \bar{\boldsymbol{\mu}} \tag{3.8.18}$$

These strains satisfy (3.4.6) and represent a compatible, kinematically admissible set. Similarly, local and overall stresses satisfy (3.4.3), with $\bar{\boldsymbol{\sigma}} = \boldsymbol{\sigma}^0$ and both are parts of the same equilibrium set. The virtual work theorem then guarantees equality of work terms

$$\bar{\boldsymbol{\sigma}}^{\mathrm{T}}\bar{\boldsymbol{\varepsilon}} = \frac{1}{V}\int_V [\boldsymbol{\sigma}_r(\boldsymbol{x})]^{\mathrm{T}}\boldsymbol{\varepsilon}_r(\boldsymbol{x})\mathrm{d}V = \overline{\boldsymbol{\sigma}_r{}^{\mathrm{T}}\boldsymbol{\varepsilon}_r} \tag{3.8.19}$$

This equality is the Hill lemma. Note that it holds for any volume, but only if either or both the overall stress or strain are uniform. For example, the strain $\bar{\boldsymbol{\varepsilon}}$ may represent the average (3.4.6) of any compatible field $\boldsymbol{\varepsilon}(\boldsymbol{x})$, but the field $\boldsymbol{\sigma}(\boldsymbol{x}) - \bar{\boldsymbol{\sigma}}$ must be free of surface tractions on ∂V, doing no net work on the strain. Recall from (2.1.7) that the engineering matrix notation (1.1.11) should be used in evaluation of (3.8.19).

3.9 Universal Connections for Elastic Moduli of Fibrous Composites

As pointed out in Sect. 2.3.1, the number of independent overall elastic moduli of two-phase aligned fiber composites can be reduced below that implied by their overall material symmetry, by certain universal connections, involving phase moduli and volume fractions. In transversely isotropic systems of Sect. 2.3, with a plane of symmetry that is perpendicular to the fiber direction, and an axis of rotation parallel to the fibers, the number of independent moduli is reduced from five to three. In monoclinic systems of Sect. 2.2.3, which have only a single plane of symmetry perpendicular to the fiber direction, the number of independent moduli is reduced from 13 to 9. Another strategy for evaluation of independent moduli of transversely isotropic aggregates of cubic crystals was outlined by Walpole (1985b). These connections have to be respected in prescribing values of independent phase and overall moduli in solutions of elastic and elastic-inelastic problems, to assure consistency of material constants.

More extensive connections exist between physical constants of piezoelectric fibrous composites, as shown by Benveniste and Dvorak (1992a). Those provide substantial reductions in the number of independent overall or effective elastic moduli, as well as of dielectric and piezoelectric constants and related influence functions. Chen and Zheng (2000) established additional results for different properties of the phases.

3.9.1 Hill's Universal Connections for Transversely Isotropic Composites

A large representative volume of this composite material consists of a homogeneous matrix ($r = \alpha$) and a statistically homogeneous distribution of aligned cylindrical fibers ($r = \beta$) of arbitrary cross sections. Phase volume fractions $c_\alpha + c_\beta = 1$. Both phases and the composite itself are transversely isotropic in a fixed Cartesian coordinate system, with $x_A \equiv x_1$ axis of rotational symmetry. Their elastic moduli related to axisymmetric loading and deformation are denoted by $k_r,\ l_r,\ n_r$ and $k,\ l,\ n$, defined in Sect. 2.3.1. The relevant part of the constitutive relation (2.3.8) is rewritten here as

$$\left.\begin{array}{ll} \sigma_A = \sigma_{11} = n\varepsilon_A + l\varepsilon_T & \sigma_T = (\sigma_{22} + \sigma_{33})/2 = l\varepsilon_A + k\varepsilon_T \\ \varepsilon_A = \varepsilon_{11} & \varepsilon_T = (\varepsilon_{22} + \varepsilon_{33}) \end{array}\right\} \tag{3.9.1}$$

Perfect bonds are assumed to exist at the interfaces, which are all aligned with $x_A \equiv x_1$, hence both phases and the composite experience identical uniform normal strain in the longitudinal direction.

Phase and overall stress and strain averages are related by (3.4.3) and (3.4.6).

$$\left.\begin{array}{ll} \varepsilon_A^{(1)} = \varepsilon_A^{(2)} = \varepsilon_A & c_\alpha \varepsilon_T^{(\alpha)} + c_\beta \varepsilon_T^{(\beta)} = \varepsilon_T \\ c_\alpha \sigma_A^{(\alpha)} + c_\beta \sigma_A^{(\beta)} = \sigma_A & c_\alpha \sigma_T^{(\alpha)} + c_\beta \sigma_T^{(\beta)} = \sigma_T \end{array}\right\} \tag{3.9.2}$$

After substitution from the constitutive relations (3.9.1), the equations for σ_A and σ_T, are written in terms of phase and overall strain averages

$$\left.\begin{array}{l} \sigma_A = c_\alpha(n_\alpha \varepsilon_A + l_\alpha \varepsilon_T^{(\alpha)}) + c_\beta(n_\beta \varepsilon_A + l_\beta \varepsilon_T^{(\beta)}) = n\varepsilon_A + l(c_\alpha \varepsilon_T^{(\alpha)} + c_\beta \varepsilon_T^{(\beta)}) \\ \sigma_T = c_\alpha(l_\alpha \varepsilon_A + k_\alpha \varepsilon_T^{(\alpha)}) + c_\beta(l_\beta \varepsilon_A + k_\beta \varepsilon_T^{(\beta)}) = l\varepsilon_A + k(c_\alpha \varepsilon_T^{(\alpha)} + c_\beta \varepsilon_T^{(\beta)}) \end{array}\right\} \tag{3.9.3}$$

Since both equations are derived from local and overall constitutive relations for the same material system, they are similar and the coefficients multiplying each strain component must be proportional. For example, for $\varepsilon_T^{(\alpha)}$, the ratio is $(k - k_\alpha)/(l - l_\alpha)$, and similar ratios are readily found for $\varepsilon_T^{(\beta)}$ and ε_A. Equalities of the ratios provide Hill's (1964) universal connections between phase and overall moduli of two-phase fiber systems

$$\frac{k - k_\alpha}{l - l_\alpha} = \frac{k - k_\beta}{l - l_\beta} = \frac{l - c_\alpha l_\alpha - c_\beta l_\beta}{n - c_\alpha n_\alpha - c_\beta n_\beta} = \frac{k_\alpha - k_\beta}{l_\alpha - l_\beta} \tag{3.9.4}$$

Those can be used to find overall $l,\ n$, in terms of overall modulus k, and known phase moduli and volume fractions. The number of independent elastic moduli of a

two-phase fiber system is thus reduced from five to three, usually taken as the plane strain bulk modulus k and transverse and longitudinal shear moduli m and p. Of course, the latter are not related by the universal connections.

3.9.2 *Universal Connections for Monoclinic Systems Based on Uniform Fields*

Equations 3.6.6 show how application of certain auxiliary overall stress or strain vectors can create a single uniform strain and stress field everywhere in a material made of two perfectly bonded phases of any material symmetry and shape, which have been transformed by different uniform eigenstrains. However, any number of different uniform strain fields can also be created in a *fibrous two-phase solid*, with uniformly transformed phases, by application of axisymmetric overall tractions that generate a piecewise uniform stress fields (Dvorak 1983, 1986, 1990; Benveniste and Dvorak 1989). The uniform strain field that can be created in the absence of phase transformations is examined next.

The fibrous composite material considered consists again of two homogeneous elastic phases $r = \alpha,\ \beta$, perfectly bonded along cylindrical interfaces generated by lines parallel to the x_1-axis. Phase cross sections can be arbitrary, but isotropy and, unless otherwise noted, statistical homogeneity of the aggregate in the transverse x_2x_3- plane are not required, hence the total volume V need not be representative. Matrix-based composites reinforced by aligned fibers, ribbons or other cylindrical shapes, as well as certain lamellar and layered materials, are examples of such systems. Present derivation focuses on systems made of isotropic or transversely isotropic phases with the x_1- axis of rotational symmetry, although similar results could be found for certain other material symmetries of the phases. Phase transverse isotropy and alignment guarantee existence of one plane of overall symmetry, the x_2x_3-plane, together with at least monoclinic overall material symmetry, and only eight zero stiffness coefficients shown in Table 2.1. The present derivation applies to materials which are free of phase eigenstrains. The more general case which includes application of uniform phase eigenstrains is described in Chap. 8.

The composite material is loaded by uniform auxiliary axisymmetric stress components, denoted by $\hat{\sigma}_A$ and $\hat{\sigma}_T$, that are supposed to generate a uniform strain field at all interior points.

$$\hat{\boldsymbol{\varepsilon}}_\alpha(\boldsymbol{x}) = \hat{\boldsymbol{\varepsilon}}_\beta(\boldsymbol{x}) = \hat{\hat{\boldsymbol{\varepsilon}}} \tag{3.9.5}$$

where $\hat{\hat{\boldsymbol{\varepsilon}}}$ denotes an as yet unknown overall strain. Since all interfaces are parallel to the x_1- axis, traction continuity at the interfaces can be satisfied by the following uniform auxiliary phase stress fields.

$$\left.\begin{array}{ll} \hat{\sigma}_1^{\alpha} \neq \hat{\sigma}_1^{\beta} & \hat{\sigma}_1 = c_\alpha \hat{\sigma}_1^{\alpha} + c_\beta \hat{\sigma}_1^{\beta} \\ \hat{\sigma}_j = \hat{\sigma}_j^{\alpha} = \hat{\sigma}_j^{\beta} & \text{for} \quad j = 2, 3, \ldots 6 \end{array}\right\} \tag{3.9.6}$$

According to (3.9.5), differences between individual phase strain components must vanish. Substitution of (3.9.6) into phase constitutive relations $\hat{\boldsymbol{\varepsilon}}_r = \boldsymbol{M}_r \hat{\boldsymbol{\sigma}}_r$, and the requirement $\hat{\boldsymbol{\varepsilon}}_\alpha - \hat{\boldsymbol{\varepsilon}}_\beta = \mathbf{0}$, provide

$$M_{i1}^{\alpha} \hat{\sigma}_1^{\alpha} - M_{i1}^{\beta} \hat{\sigma}_1^{\beta} + \sum_{j=2}^{6} (M_{ij}^{\alpha} - M_{ij}^{\beta}) \hat{\sigma}_j = 0 \tag{3.9.7}$$

where $i = 1, 2, \ldots 6$. This is a system of six equations for the seven unknown phase stresses in (3.9.6). Therefore, the solution depends on a free parameter, enabling many different solutions. All are independent of the transverse geometry of the fibrous microstructure and phase volume fractions, hence they represent a class of exact elasticity solutions for two-phase fibrous solids and columnar structures.

The uniform overall auxiliary stress $\hat{\boldsymbol{\sigma}}^0$, and its components $\hat{\sigma}_A$ and $\hat{\sigma}_T$ that are expected to generate the uniform strain field (3.9.5), are related to phase stresses by

$$\left.\begin{array}{ll} \hat{\boldsymbol{\sigma}}^0 = [\hat{\sigma}_A, \ \hat{\sigma}_T, \ \hat{\sigma}_T, \ 0, \ 0, \ 0]^{\mathrm{T}} & \\ \hat{\sigma}_A = \hat{\sigma}_1 = c_\alpha \hat{\sigma}_1^{\alpha} + c_\beta \hat{\sigma}_1^{\beta} & \hat{\sigma}_T = \hat{\sigma}_2 = \hat{\sigma}_3 \end{array}\right\} \tag{3.9.8}$$

The $\hat{\sigma}_T$ is selected as the free parameter in the solution of (3.9.8), which then yields the normal longitudinal and transverse stress in the two transversely isotropic phases

$$\hat{\sigma}_1^r = q(l_r \Delta l - n_r \Delta k) \hat{\sigma}_T \quad \hat{\sigma}_2^r = \hat{\sigma}_3^r = \hat{\sigma}_T \quad r = \alpha, \beta \tag{3.9.9}$$

where $q^{-1} = (l_\alpha k_\beta - k_\alpha l_\beta) = 2k_\alpha k_\beta (\nu_L^{\alpha} - \nu_L^{\beta}) \neq 0$, and $\Delta\eta = \eta_\alpha - \eta_\beta$ for any quantity η_r. The $\nu_L^r = \nu_{12}^r$ in (2.3.5) are phase longitudinal Poisson's ratios. A different solution, for $(\nu_L^{\alpha} - \nu_L^{\beta}) = 0$, appears in *op. cit.*

The uniform strain field $\hat{\hat{\boldsymbol{\varepsilon}}}$ that is caused in the entire volume V by the auxiliary overall stress $\hat{\boldsymbol{\sigma}}^0$ can be found by substituting the stresses into phase constitutive relations

$$\hat{\varepsilon}_1 = -q \, \Delta k \hat{\sigma}_T \quad \hat{\varepsilon}_2 = \hat{\varepsilon}_3 = (q/2) \Delta l \hat{\sigma}_T \tag{3.9.10}$$

The overall stress that supports the uniform field is applied along the proportional path

$$\hat{\sigma}_A / \hat{\sigma}_T = q[(c_\alpha l_\alpha + c_\beta l_\beta) \Delta l - (c_\alpha n_\alpha + c_\beta n_\beta) \Delta k] \tag{3.9.11}$$

Overall strain components are related by

$$\hat{\varepsilon}_1/\hat{\varepsilon}_2 = \hat{\varepsilon}_1/\hat{\varepsilon}_3 = -2\Delta k/\Delta l \tag{3.9.12}$$

Since no overall moduli have been employed in Eqs. (3.9.9), (3.9.10), (3.9.11), (3.9.12), those results hold for any volume of fibrous or bonded columnar material.

Next, recall that a representative volume of a monoclinic fibrous system with the x_2x_3 − plane of material symmetry has 13 nonzero stiffness coefficients among the maximum 21 of the triclinic system, with

$$L_{15} = L_{16} = L_{25} = L_{26} = L_{35} = L_{36} = L_{45} = L_{46} = 0 \qquad [2.2.9]$$

Overall constitutive relation of the aggregate, which is now loaded by the uniform stress $\hat{\boldsymbol{\sigma}}^0$ in (3.9.8) and undergoes uniform deformation $\hat{\hat{\boldsymbol{\varepsilon}}}$ in its entire volume, is

$$\hat{\boldsymbol{\sigma}}^0 - \boldsymbol{L}\hat{\hat{\boldsymbol{\varepsilon}}} = \boldsymbol{0} \tag{3.9.13}$$

where, according to (3.9.10), $\hat{\hat{\boldsymbol{\varepsilon}}} = q\,\hat{\sigma}_T[-\Delta k,\ \Delta l/2,\ \Delta l/2,\ 0,\ 0,\ 0]^{\mathrm{T}}$. This yields four equations relating phase and overall moduli

$$\left.\begin{aligned} &L_{11}\Delta k - (L_{12}+L_{13})\Delta l/2 + \hat{\sigma}_A/(q\hat{\sigma}_T) = 0\\ &L_{12}\Delta k - (L_{22}+L_{23})\Delta l/2 + q^{-1} = 0\\ &L_{13}\Delta k - (L_{23}+L_{33})\Delta l/2 + q^{-1} = 0\\ &L_{14}\Delta k - (L_{24}+L_{34})\Delta l/2 = 0 \end{aligned}\right\} \tag{3.9.14}$$

with $\hat{\sigma}_A/\hat{\sigma}_T$ from (3.9.11), and with $q^{-1} = (l_\alpha k_\beta - k_\alpha l_\beta) = 2k_\alpha k_\beta(\nu_L^\alpha - \nu_L^\beta) \neq 0$ and $\Delta\eta = \eta_\alpha - \eta_\beta$ for $\eta_r = k_r,\ l_r,\ n_r, r = \alpha,\ \beta$.

For composites exhibiting overall transverse isotropy

$$L_{11} = n \qquad L_{12} = L_{13} = l \qquad (L_{22} + L_{23}) = 2k \tag{3.9.15}$$

Equations (3.9.13) and (2.3.8) yield

$$\hat{\sigma}_A = n\,\hat{\varepsilon}_1 + 2l\,\hat{\varepsilon}_2 \quad \hat{\sigma}_T = l\,\hat{\varepsilon}_1 + 2k\,\hat{\varepsilon}_2 \tag{3.9.16}$$

for the uniform auxiliary stresses and strains, that are now known functions of phase moduli and volume fractions. After substitution of the auxiliary fields and some algebra, Eq. (3.9.16) yield Hill's (1964) universal connections (3.9.4) between phase and overall moduli.

Following a procedure somewhat similar to that leading to (3.9.14), one can also derive six connections between phase moduli and certain coefficients of the mechanical concentration factors $\boldsymbol{A}_r$ or $\boldsymbol{B}_r$ (Dvorak 1990, §6).

3.10 Constitutive Relations and Local Fields in Heterogeneous Aggregates

This section presents a summary of some frequently used results derived in this chapter. A macroscopic representative volume V of a multiphase material is considered, consisting of $r, s = 1, 2, \ldots n$ perfectly bonded phases, or phase subvolumes V_r, with known stiffnesses $\boldsymbol{L}_r$ or compliances $\boldsymbol{M}_r = \boldsymbol{L}_r^{-1}$ and volume fractions $c_r = V_r / V$. Each phase may exhibit any of the eight material symmetries described in Sect. 2.2. Two homogeneous boundary conditions can be specified for the representative volume V, providing either a state of uniform overall strain $\boldsymbol{\varepsilon}^0$, or stress $\boldsymbol{\sigma}^0$. Moreover, a distribution of eigenstrains $\boldsymbol{\mu}_r$ or eigenstresses $\boldsymbol{\lambda}_r = -\boldsymbol{L}_r \boldsymbol{\mu}_r$, piecewise uniform in phase subvolumes V_r, is prescribed in V.

These combined mechanical and transformation loads are represented by two dimensionally consistent load sets $\{\boldsymbol{\varepsilon}^0, \boldsymbol{\mu}_r\}$ or $\{\boldsymbol{\sigma}^0, \boldsymbol{\lambda}_r\}$, which generate overall responses $\bar{\boldsymbol{\sigma}} = \boldsymbol{L}\boldsymbol{\varepsilon}^0 + \bar{\boldsymbol{\lambda}}$ or $\bar{\boldsymbol{\varepsilon}} = \boldsymbol{M}\boldsymbol{\sigma}^0 + \bar{\boldsymbol{\mu}}$, respectively.

The goal is to find expressions for evaluation of local fields in the phases and of the overall stiffness or compliance, and of the overall eigenstress or eigenstrain. The sequence of steps leading to these results is different under the two load sets which represent either displacement or traction conditions applied at the outer boundary ∂V of the representative volume V.

3.10.1 Overall Strain $\boldsymbol{\varepsilon}^0$ and Phase Eigenstrains $\boldsymbol{\mu}_r$ are Prescribed

Local strain and stress fields in subvolumes or phases V_r are sought using (3.6.1) and $(3.6.5)_1$, in the form

$$\boldsymbol{\varepsilon}_r(\boldsymbol{x}) = \boldsymbol{A}_r(\boldsymbol{x})\boldsymbol{\varepsilon}^0 + \sum_{s=1}^{n} \boldsymbol{D}_{rs}(\boldsymbol{x})\boldsymbol{\mu}_s \quad \boldsymbol{\sigma}_r(\boldsymbol{x}) = \boldsymbol{L}_r(\boldsymbol{\varepsilon}_r(\boldsymbol{x}) - \boldsymbol{\mu}_r) \tag{3.10.1}$$

For two-phase composite materials, with phases denoted by $r, s = \alpha, \beta$, the transformation strain influence functions are

$$\left.\begin{aligned} \boldsymbol{D}_{r\alpha}(\boldsymbol{x}) &= (\boldsymbol{I} - \boldsymbol{A}_r(\boldsymbol{x}))(\boldsymbol{L}_\alpha - \boldsymbol{L}_\beta)^{-1}\boldsymbol{L}_\alpha \\ \boldsymbol{D}_{r\beta}(\boldsymbol{x}) &= -(\boldsymbol{I} - \boldsymbol{A}_r(\boldsymbol{x}))(\boldsymbol{L}_\alpha - \boldsymbol{L}_\beta)^{-1}\boldsymbol{L}_\beta \end{aligned}\right\} \tag{3.6.8}$$

where $\boldsymbol{A}_r(\boldsymbol{x})$ are mechanical strain influence functions. Related transformation and mechanical strain concentration factors follow by replacing $\boldsymbol{A}_r(\boldsymbol{x})$ by its volume average over V_r

$$\boldsymbol{A}_r = \frac{1}{V_r}\int_{V_r} \boldsymbol{A}(\boldsymbol{x})\mathrm{d}V \quad \boldsymbol{D}_{rs} = \frac{1}{V_r}\int_{V_r} \boldsymbol{D}_{rs}(\boldsymbol{x})\mathrm{d}V \tag{3.10.2}$$

Overall stress imposed on the representative volume by application of an overall strain $\boldsymbol{\varepsilon}^0$ and eigenstrains $\boldsymbol{\mu}_r$ is described by (3.6.15) and (3.8.12) as

$$\bar{\boldsymbol{\sigma}} = \boldsymbol{L}\boldsymbol{\varepsilon}^0 + \bar{\boldsymbol{\lambda}} \qquad \bar{\boldsymbol{\lambda}} = \sum_{r=1}^{n} c_r \boldsymbol{A}_r^{\mathrm{T}}\boldsymbol{\lambda}_r = -\sum_{r=1}^{n} c_r \boldsymbol{A}_r^{\mathrm{T}}\boldsymbol{L}_r\boldsymbol{\mu}_r \tag{3.10.3}$$

where $\bar{\boldsymbol{\lambda}}$ is the overall uniform eigenstress contributed solely by local eigenstrains. Effective or overall stiffness and compliance of the composite material in the representative volume V are

$$\boldsymbol{L} = \sum_{r=1}^{n} c_r \boldsymbol{L}_r \boldsymbol{A}_r \quad \boldsymbol{M} = \boldsymbol{L}^{-1} \tag{3.5.8}$$

The actual overall material symmetry of the representative volume may depend on shape, spatial distribution and material symmetry of the phases. In the above expression, it is encoded in the products $\boldsymbol{L}_r\boldsymbol{A}_r$, which depend only on material symmetry and geometry of the phases or subvolumes V_r, but may not represent the effect of their spatial distribution. This is explained further in Chaps. 6 and 7.

3.10.2 *Overall Stress $\boldsymbol{\sigma}^0$ and Phase Eigenstresses $\boldsymbol{\lambda}_r$ are Prescribed*

The eigenstresses $\boldsymbol{\lambda}_r$ are preferred here as assigned quantities, but if desired, they can be exchanged for eigenstrains $\boldsymbol{\mu}_r = -\boldsymbol{M}_r\boldsymbol{\lambda}_r$. Local stress and strain fields in subvolumes or phases V_r are found from $(3.6.5)_2$ and (3.6.1) as

$$\boldsymbol{\sigma}_r(\boldsymbol{x}) = \boldsymbol{B}_r(\boldsymbol{x})\boldsymbol{\sigma}^0 + \sum_{s=1}^{n} \boldsymbol{F}_{rs}(\boldsymbol{x})\boldsymbol{\lambda}_s \quad \boldsymbol{\varepsilon}_r(\boldsymbol{x}) = \boldsymbol{M}_r[\boldsymbol{\sigma}_r(\boldsymbol{x}) - \boldsymbol{\lambda}_r] \tag{3.10.4}$$

For two-phase composite materials, with phases denoted as $r, s = \alpha, \beta$, the transformation stress influence functions are

$$\begin{aligned} \boldsymbol{F}_{r\alpha}(\boldsymbol{x}) &= (\boldsymbol{I} - \boldsymbol{B}_r(\boldsymbol{x}))(\boldsymbol{M}_\alpha - \boldsymbol{M}_\beta)^{-1}\boldsymbol{M}_\alpha \\ \boldsymbol{F}_{r\beta}(\boldsymbol{x}) &= -(\boldsymbol{I} - \boldsymbol{B}_r(\boldsymbol{x}))(\boldsymbol{M}_\alpha - \boldsymbol{M}_\beta)^{-1}\boldsymbol{M}_\beta \end{aligned} \tag{3.6.11}$$

where the $\boldsymbol{B}_r(\boldsymbol{x})$ are mechanical stress influence functions.

Related mechanical and transformation stress concentration factors are the volume averages over V_r

$$\boldsymbol{B}_r = \frac{1}{V_r}\int_{V_r} \boldsymbol{B}_r(\boldsymbol{x})\,\mathrm{d}V \quad \boldsymbol{F}_{rs} = \frac{1}{V_r}\int_{V_r} \boldsymbol{F}_{rs}(\boldsymbol{x})\,\mathrm{d}V \tag{3.10.5}$$

Replacement of the influence functions in (3.10.4) by the concentration factors provides an equation for evaluation of phase stress averages $\boldsymbol{\sigma}_r$.

Overall deformation of the representative volume caused by an overall stress $\boldsymbol{\sigma}^0$ and eigenstrains $\boldsymbol{\mu}_r$ is macroscopically uniform and described by (3.6.15), (3.8.9) and (3.8.11) as

$$\bar{\boldsymbol{\varepsilon}} = \boldsymbol{M}\boldsymbol{\sigma}^0 + \bar{\boldsymbol{\mu}} \qquad \bar{\boldsymbol{\mu}} = \frac{1}{V}\int_V \boldsymbol{B}_r^{\mathrm{T}}(\boldsymbol{x})\,\boldsymbol{\mu}_r \mathrm{d}V = -\sum_{r=1}^{n} c_r \boldsymbol{B}_r^{\mathrm{T}}\boldsymbol{M}_r\boldsymbol{\lambda}_r \tag{3.10.6}$$

where $\bar{\boldsymbol{\mu}}$ is the overall uniform eigenstrain generated only by the local eigenstrains. Effective or overall compliance of the composite material in the representative volume V is

$$\boldsymbol{M} = \sum_{r=1}^{n} c_r \boldsymbol{M}_r \boldsymbol{B}_r \tag{3.5.8}$$

Material symmetry of the aggregate depends on that of the products $\boldsymbol{M}_r\boldsymbol{B}_r$, which may or may not agree with that implied by spatial distribution of the phases.

Connections (3.5.6), (3.5.9) and (3.5.11) are independent of prescribed loads, valid under both overall strain or stress

$$\sum_{r=1}^{n} c_r \boldsymbol{A}_r = \boldsymbol{I} \quad \sum_{r=1}^{n} c_r \boldsymbol{B}_r = \boldsymbol{I} \quad r = 1, 2, \ldots n. \tag{3.5.6}$$

$$\boldsymbol{L}\boldsymbol{M} = \boldsymbol{I} \quad \boldsymbol{A}_r\boldsymbol{M} = \boldsymbol{M}_r\boldsymbol{B}_r \quad \boldsymbol{B}_r\boldsymbol{L} = \boldsymbol{L}_r\boldsymbol{A}_r \tag{3.10.7}$$

Independent of overall loads are also connections (3.6.12), (3.6.13), (3.6.14) that apply to mechanical and transformation concentration factors and influence functions.

These results illustrate the remarkable simplicity of generally valid connections between local fields and overall response generated by one of the two homogeneous boundary conditions and local eigenstrains. In addition to the known elastic moduli of the phases, $n - 1$ concentrations factors are needed in a system containing n phases, hence a single concentration factor is sufficient in analysis of the commonly used two-phase systems. The concentration factors depend on overall and phase elastic moduli and on the shape of the phases or reinforcements. Together with overall moduli, they are estimated by certain bounding and averaging methods, described in Chaps. 6 and 7.

Chapter 4
Inclusions, Inhomogeneities and Cavities

Overall mechanical properties and local strain and stress field averages, caused in individual phases of heterogeneous solids by remotely applied uniform strain or stress, are often derived from estimates of local fields in ellipsoidal homogeneous inclusions and inhomogeneities, bonded to a large volume of a surrounding matrix or 'comparison medium'. The attraction of this approach lies in the relative simplicity of evaluation of the local fields, and in the adaptability of ellipsoidal shapes, such as prolate or oblate ellipsoids, spheroids, cylinders, spheres, penny-shaped discs or slits, to represent either short or long fibers, particles, voids and cracks of different shapes. Transition from local fields in a single inhomogeneity to those in interacting inhomogeneities comprising composite aggregates and polycrystals is accomplished, in part, by assigning certain properties to the comparison medium, as shown in Chaps. 6 and 7.

In Sects. 4.1, 4.2, and 4.3 we discuss evaluation of local fields in the interior of volume Ω_r of an isolated or solitary ellipsoidal inhomogeneity of stiffness $\boldsymbol{L}_r$, surrounded by a large volume $\Omega_0 \gg \Omega_r$ of a homogeneous comparison medium of stiffness $\boldsymbol{L}_0$, in the total volume $\Omega = \Omega_r + \Omega_0$. Loads are applied on the surface $\partial\Omega$ as linearly varying displacements or as self-equilibrating tractions that generate an overall uniform strain $\boldsymbol{\varepsilon}^0_\Omega$ or stress $\boldsymbol{\sigma}^0_\Omega$. Moreover, uniform transformations strains or eigenstrains described in Sect. 3.6.1 are applied both in the interior and exterior of the inhomogeneity.

Solutions of ellipsoidal inclusion and inhomogeneity problems are derived in terms of certain concentration factor tensors which connect local field averages to either mechanical loads or to transformation strains. They are shown to depend only on the stiffnesses $\boldsymbol{L}_r$, $\boldsymbol{L}_0$, and on Hill's tensor $\boldsymbol{P} = \boldsymbol{S}\boldsymbol{L}_0^{-1} = \boldsymbol{P}^{\mathrm{T}}$, where $\boldsymbol{S}$ is the Eshelby tensor for a particular shape of the transformed ellipsoidal inclusion in $\boldsymbol{L}_0$. Once the $\boldsymbol{L}_r$, $\boldsymbol{L}_0$ and $\boldsymbol{P}$ matrices have been assembled, solutions of inclusion and inhomogeneity problems follow from simple closed-form expressions. In Sect. 4.4, these results are applied to multiphase composites with very low reinforcement density, where inhomogeneities $\boldsymbol{L}_r$ interact only with the matrix $\boldsymbol{L}_1$, but not with each other. Derivation of the elastic Green's function and of the Eshelby tensor,

G.J. Dvorak, *Micromechanics of Composite Materials*, Solid Mechanics and Its Applications 186, DOI 10.1007/978-94-007-4101-0_4,

and of exterior fields averaged over certain ellipsoidal volumes surrounding Ω_r is deferred to Sect. 4.5. It is followed by a collection of $\boldsymbol{P}$ matrices for typical ellipsoidal inclusion and crack shapes in isotropic and transversely isotropic solids, which should be useful in applications. The closing Sect. 4.7 contains a short summary of procedures useful in numerical evaluations.

4.1 Homogeneous Ellipsoidal Inclusions: The Eshelby Solution

4.1.1 A Transformed Homogeneous Inclusion

A large volume Ω of a homogeneous and possibly anisotropic solid $\boldsymbol{L}_0$ is considered, free of surface tractions or constraints on its surface $\partial\Omega$. *A transformed homogeneous inclusion* is an ellipsoidal subvolume $\Omega_r \ll \Omega$, subjected to a uniform transformation strain or eigenstrain $\boldsymbol{\mu}_r = \left[\mu_1^r, \mu_2^r, \mu_3^r, \mu_4^r, \mu_5^r, \mu_6^r\right]^{\mathrm{T}}$. As in (1.1.10) or (1.1.11), the shear components are written either in contracted tensorial ($\mu_4^r = \mu_{32}^r, \dots$), or in engineering matrix ($\mu_4^r = 2\mu_{32}^r, \dots$) notations. Originally denoted by $\boldsymbol{e}^{\mathrm{T}}$ (Eshelby 1957, 1961), and by other authors by $\boldsymbol{\varepsilon}^*$ (e.g., Mura 1987), the transformation strain and stress vectors are denoted here by the kernel letters $\boldsymbol{\mu}$ and $\boldsymbol{\lambda}$, to emphasize that they are distinct from other deformations, and when physically motivated, independent of applied mechanical loads; Sect. 3.6.

If the transformed inclusion Ω_r were separated from its surroundings and left free of surface tractions, then its total strain would be equal to the stress-free transformation strain $\boldsymbol{\mu}_r$. Conversely, if the separated inclusion is prevented from deforming by a layer of body force, then the interior strain-free stress or eigenstress is $\boldsymbol{\lambda}_r = -\boldsymbol{L}_0\boldsymbol{\mu}_r$. However, the surface $\partial\Omega_r$ is a perfectly bonded interface that does not accommodate any cracks, overlaps or body forces. Therefore, to reconnect the transformed inclusion along $\partial\Omega_r$, the body force layer must be removed by superposition with an equal and opposite layer applied at the surface of the cavity containing the inclusion. This superposition adjusts the strain and stress fields outside and inside Ω_r to the constraint imposed by the surrounding elastic medium $\boldsymbol{L}_0$. Since $\Omega_r \ll \Omega$, the transformation $\boldsymbol{\mu}_r$ causes only local disturbances of stresses and displacements, which become negligible at exterior points far removed from Ω_r. Early solutions specific to different inclusion, inhomogeneity and cavity geometries were reviewed by Sternberg (1958).

In his classic paper, John D. Eshelby (1957) presented a new perspective on solution of inclusion and inhomogeneity problems, by showing that the strain and stress in a uniformly transformed homogeneous inclusion of ellipsoidal shape in $\boldsymbol{L}_0$ has the form

$$\left.\begin{aligned} \varepsilon_{ij}^r = S_{ijkl}\mu_{kl}^r \quad \sigma_{ij}^r = L_{ijkl}^0(\varepsilon_{kl}^r - \mu_{kl}^r) = -L_{ijkl}^0(I_{klpq} - S_{klpq})\mu_{pq}^r \\ \boldsymbol{\varepsilon}_r = \boldsymbol{S}\boldsymbol{\mu}_r \quad \boldsymbol{\sigma}_r = \boldsymbol{L}_0(\boldsymbol{\varepsilon}_r - \boldsymbol{\mu}_r) = -\boldsymbol{L}_0(\boldsymbol{I} - \boldsymbol{S})\boldsymbol{\mu}_r \end{aligned}\right\} \tag{4.1.1}$$

where the Eshelby tensor $\boldsymbol{S}$, stiffness $\boldsymbol{L}_0$, and strains $\boldsymbol{\varepsilon}_r$, $\boldsymbol{\mu}_r$ and stresses $\boldsymbol{\sigma}_r$ are represented by (6×6) matrices and (6×1) vectors, respectively, in either the contracted tensorial or engineering notation of Sect. 1.

The important feature of the solution is that in both isotropic and anisotropic solids, as long as $\boldsymbol{\mu}_r$ is uniform and Ω_r is of ellipsoidal shape, *the strain* $\boldsymbol{\varepsilon}_r$ *and stress* $\boldsymbol{\sigma}_r$ *are both spatially uniform in the interior of* Ω_r, but not necessarily coaxial with $\boldsymbol{\mu}_r$ (Eshelby 1957, 1961; Willis 1964; Kinoshita and Mura 1971). Therefore, coefficients of $\boldsymbol{S}$ are dimensionless constants that depend on elastic moduli $\boldsymbol{L}_0$, and on aspect ratios of the ellipsoid Ω_r. The fourth order Eshelby tensor exhibits symmetries $S_{ijkl} = S_{jikl} = S_{ijlk}$, but it is not necessarily symmetric under exchange of the first and second pairs; in general, $S_{ijkl} \neq S_{klij}$. The (6×6) matrix $\boldsymbol{S}$ may not be diagonally symmetric; it also becomes singular for certain extreme aspect ratios of the ellipsoid, encountered, for example, in modeling of fibers or cracks. However, a related symmetric tensor $\boldsymbol{P} = \boldsymbol{S}\boldsymbol{L}_0^{-1} = \boldsymbol{P}^{\mathrm{T}}$ is more convenient in most applications (Hill 1965a). Frequently used forms of $\boldsymbol{P}$ for selected ellipsoidal shapes and cracks are summarized in Sect. 4.6.

4.1.2 Local Fields in Ellipsoidal Inclusions

To illustrate the utility of (4.1.1), we now find local fields caused in homogeneous inclusions by a uniform overall stress or strain and by piecewise uniform transformation strains. By suitably adjusting the magnitude of $\boldsymbol{\mu}_r$, we then show in Sect. 4.2 how to generate in a homogeneous medium $\boldsymbol{L}_0$ strain and stress fields equal to those caused by uniform overall strain or stress in an ellipsoidal inhomogeneity $\boldsymbol{L}_r$ or cavity in Ω_r.

External tractions and displacements causing the uniform overall fields are similar to those described in Sect. 3.4. First, tractions that create a uniform overall stress $\boldsymbol{\sigma}_\Omega^0$ are applied at the outer boundary $\partial\Omega$, together with two independent eigenstrains, $\boldsymbol{\mu}_r \in \Omega_r$ and $\boldsymbol{\mu}_0 \in \Omega_0$, in the total volume $\Omega = \Omega_0 + \Omega_r$. Since both Ω and Ω_0 are very large relative to Ω_r, $\boldsymbol{\mu}_r$ has no effect on the magnitude of the overall strain, which is uniform and equal to $\bar{\boldsymbol{\varepsilon}}_\Omega = \boldsymbol{M}_0\boldsymbol{\sigma}_\Omega^0 + \boldsymbol{\mu}_0$. Local fields inside Ω_r are obtained by first applying $\boldsymbol{\sigma}_\Omega^0$ and $\boldsymbol{\mu}_0$ in both Ω_0 and Ω_r. This is followed by application of the eigenstrain $\boldsymbol{\mu}_r - \boldsymbol{\mu}_0$ inside Ω_r, while the exterior surface $\partial\Omega$ is traction-free. According to (4.1.1), the latter application generates in Ω_r the strain $\boldsymbol{S}(\boldsymbol{\mu}_r - \boldsymbol{\mu}_0)$ and stress $-\boldsymbol{L}_0(\boldsymbol{I} - \boldsymbol{S})(\boldsymbol{\mu}_r - \boldsymbol{\mu}_0)$. After superposition, the total uniform fields caused in the homogeneous inclusion Ω_r by the load set $\{\boldsymbol{\sigma}_\Omega^0, \boldsymbol{\mu}_r, \boldsymbol{\mu}_0\}$ are

$$\left.\begin{aligned} \boldsymbol{\varepsilon}_r &= \boldsymbol{M}_0\boldsymbol{\sigma}_\Omega^0 + \boldsymbol{\mu}_0 + \boldsymbol{S}(\boldsymbol{\mu}_r - \boldsymbol{\mu}_0) = \boldsymbol{M}_0\boldsymbol{\sigma}_r + \boldsymbol{\mu}_r \\ \boldsymbol{\sigma}_r &= \boldsymbol{\sigma}_\Omega^0 - \boldsymbol{L}_0(\boldsymbol{I} - \boldsymbol{S})(\boldsymbol{\mu}_r - \boldsymbol{\mu}_0) = \boldsymbol{L}_0(\boldsymbol{\varepsilon}_r - \boldsymbol{\mu}_r) \end{aligned}\right\} \tag{4.1.2}$$

Parts of the above fields that remain after removal of the overall stress, at $\boldsymbol{\sigma}_\Omega^0 = 0$, are the residual fields caused in Ω_r by the two eigenstrains.

Next, consider the load set $\{\boldsymbol{\varepsilon}^0_\Omega, \boldsymbol{\mu}_r, \boldsymbol{\mu}_0\}$, where $\boldsymbol{\varepsilon}^0_\Omega$ is the overall strain and the local eigenstrains are still present in their respective subvolumes. Application of a uniform, stress-free strain $\boldsymbol{\mu}_0$ everywhere in Ω, together with local eigenstrain $\boldsymbol{\mu}_r - \boldsymbol{\mu}_0$ in Ω_r, generates in Ω_r the partial local strain $\boldsymbol{\mu}_0 + \boldsymbol{S}(\boldsymbol{\mu}_r - \boldsymbol{\mu}_0)$ and stress $-\boldsymbol{L}_0(\boldsymbol{I} - \boldsymbol{S})(\boldsymbol{\mu}_r - \boldsymbol{\mu}_0)$. Then, an additional uniform strain of magnitude $\boldsymbol{\varepsilon}^0_\Omega - \boldsymbol{\mu}_0$ is applied as a mechanical strain to Ω, causing the uniform overall stress $\boldsymbol{L}_0\left(\boldsymbol{\varepsilon}^0_\Omega - \boldsymbol{\mu}_0\right)$. Superposition provides the total fields generated in Ω_r by the load set $\{\boldsymbol{\varepsilon}^0_\Omega, \boldsymbol{\mu}_r, \boldsymbol{\mu}_0\}$

$$\left.\begin{aligned} \boldsymbol{\sigma}_r &= \boldsymbol{L}_0[\boldsymbol{\varepsilon}^0_\Omega - \boldsymbol{\mu}_r + \boldsymbol{S}(\boldsymbol{\mu}_r - \boldsymbol{\mu}_0)] = \boldsymbol{L}_0(\boldsymbol{\varepsilon}_r - \boldsymbol{\mu}_r) \\ \boldsymbol{\varepsilon}_r &= \boldsymbol{\varepsilon}^0_\Omega + \boldsymbol{S}(\boldsymbol{\mu}_r - \boldsymbol{\mu}_0) = \boldsymbol{M}_0\boldsymbol{\sigma}_r + \boldsymbol{\mu}_r \end{aligned}\right\} \tag{4.1.3}$$

Note that the respective local fields in (4.1.2) and (4.1.3) are identical when the overall fields are related by $\boldsymbol{\sigma}^0_\Omega = \bar{\boldsymbol{\sigma}}_\Omega = \boldsymbol{L}_0\left(\bar{\boldsymbol{\varepsilon}}_\Omega - \boldsymbol{\mu}_0\right), \boldsymbol{\varepsilon}^0_\Omega = \bar{\boldsymbol{\varepsilon}}_\Omega$, at the exterior surface points, where the displacement field $u_i\left(x_j\right) = \varepsilon^0_{ij}x_j$ is a linear function of coordinates. In most circumstances, interaction with surroundings ceases at distances greater than one order of magnitude of the largest 'diameter' of the inclusion.

Of course, the strain and stress fields created by $\boldsymbol{\mu}_r \in \Omega_r$ are not uniform at exterior points surrounding Ω_r. They can be found, for example, by solving for an ellipsoidal cavity Ω_r loaded on its wall by tractions derived from the known interior stress field (Tanaka and Mura 1982). Eshelby (1957, 1961) and Mura (1987) present exterior field solutions for several common ellipsoidal inclusion shapes and material symmetries. A simple estimate of the average strain in an ellipsoidal domain surrounding Ω_r is offered by the Tanaka-Mori theorem in Sect. 4.5.4.

Analytical evaluations of the $\boldsymbol{S}$ tensors for ellipsoidal shapes are available for some orthotropic solids and for those of higher material symmetries. Mura (1987) presents a rich collection of Eshelby tensors and local field solutions for homogenous inclusions in both isotropic and anisotropic solids transformed by different distributions of eigenstrains, for inclusions interacting with a free boundary of a half-space (Kouris and Mura 1989), and for pairs of interacting inclusions (Moschovidis and Mura 1975). Additional solutions appear in two reviews (Mura 1988; Hirose, et al. 1996). These results open the way toward evaluations of both interior and exterior fields of inclusions and inhomogeneities subjected to non-uniform overall strains, or located in close proximity of other inhomogeneities as they often are in actual composite materials. Ju and Zhang (1998), among others, have utilized solutions for directly interacting inhomogeneities in finding estimates of overall moduli of certain composite systems. Numerical procedures are needed for evaluation of the $\boldsymbol{S}$ tensor in anisotropic solids of lesser symmetry (Ghahremani 1977; Gavazzi and Lagoudas 1990). They are useful, for example, in solving inclusion problems in elastic-plastic or damaged materials, where the surrounding medium has an incrementally evolving material symmetry. Ting and Lee (1997) discuss related analytical methods.

Asaro and Barnett (1975) analyzed local fields caused by transformation strains defined by a polynomial of degree M in the position coordinates x_i. They proved a theorem showing that application of such variable stress-free transformation strain inside homogeneous ellipsoidal inclusions in any anisotropic elastic solid generates strain and stress fields that are also polynomial in degree M in the position coordinates inside the inclusion. The elastic strain and rotation tensors inside the inclusion can be expressed in terms of simple surface integrals over a unit sphere, which are amenable to numerical computations. Local fields in inclusions subjected to variable eigenstrains, or to inhomogeneous boundary conditions, are useful in certain applications; for example, in analysis of functionally graded composites (Zuiker and Dvorak 1994).

Until recently, several attempts to prove that uniform interior fields can be generated in transformed homogeneous inclusions of other than ellipsoidal shape have not succeeded, as shown by Rodin (1996), Nozaki and Taya (1997), Lubarda and Markenscoff (1998), Markenscoff (1998) and Kawashita and Nozaki (2001). However, Liu et al. (2006) and Liu (2009) had established existence of certain multiply connected, periodic and non-ellipsoidal inclusions which undergo approximately uniform elastic deformation in response to application of a uniform eigenstrain. They found a number of such shapes and configurations using the finite element method.

4.2 Ellipsoidal Inhomogeneities: The Equivalent Inclusion Method

Here we consider again a very large volume Ω, consisting of subvolumes $\Omega = \Omega_0 + \Omega_r$. However, the homogeneous comparison medium $\boldsymbol{L}_0$ is now present only in Ω_0, while Ω_r contains an ellipsoidal inhomogeneity of different stiffness $\boldsymbol{L}_r$. Any of the eight material symmetries described in Chap. 2 can be admitted to represent $\boldsymbol{L}_0$ or $\boldsymbol{L}_r$. A uniform overall strain $\boldsymbol{\varepsilon}^0_\Omega$, or stress $\boldsymbol{\sigma}^0_\Omega$, are applied by surface displacements or surface tractions prescribed on $\partial\Omega$. No eigenstrains are present.

Elastic constitutive relations of the inhomogeneity are

$$\boldsymbol{\varepsilon}_r = \boldsymbol{M}_r\boldsymbol{\sigma}_r \quad \boldsymbol{\sigma}_r = \boldsymbol{L}_r\boldsymbol{\varepsilon}_r \tag{4.2.1}$$

The effect of the inhomogeneity on overall response of Ω becomes negligible at a large distance from Ω_r, hence the overall uniform fields are related by the elastic constitutive equations for a homogeneous solid $\boldsymbol{L}_0$

$$\boldsymbol{\sigma}_\Omega = \boldsymbol{L}_0\boldsymbol{\varepsilon}^0_\Omega \quad \boldsymbol{\varepsilon}_\Omega = \boldsymbol{M}_0\boldsymbol{\sigma}^0_\Omega \tag{4.2.2}$$

These applied fields are now rewritten as $\boldsymbol{\sigma}_\Omega = \boldsymbol{L}_0\boldsymbol{\varepsilon}_\Omega$ and $\boldsymbol{\varepsilon}_\Omega = \boldsymbol{M}_0\boldsymbol{\sigma}_\Omega$, with the superscript $(^0)$ temporarily suspended. Both local and overall stiffness and compliance matrices satisfy $\boldsymbol{L}_r\boldsymbol{M}_r = \boldsymbol{I}$ and $\boldsymbol{L}_0\boldsymbol{M}_0 = \boldsymbol{I}$.

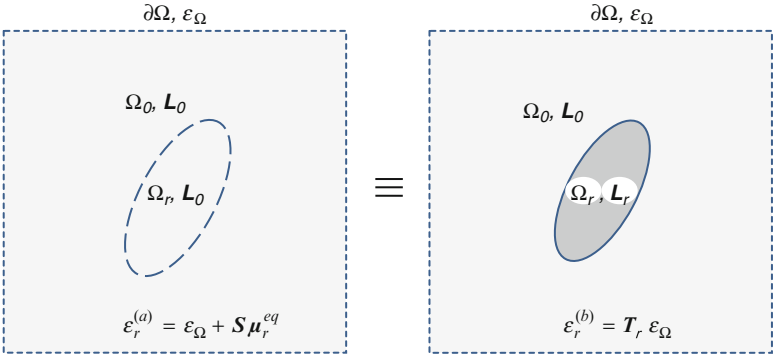

Fig. 4.1 The equivalent inclusion method evaluates the equivalent eigenstrain $\boldsymbol{\mu}_r^{eq}$ that makes the local strain $\boldsymbol{\varepsilon}_r^{(a)}$ in the homogeneous inclusion equal to the strain $\boldsymbol{\varepsilon}_r^{(b)}$ in the inhomogeneity

Local fields caused inside and outside an inhomogeneity by each of the overall strain or stress are derived using the equivalent inclusion method, which compares solutions of two problems for the same geometry of Ω and Ω_r, under either displacement or traction boundary conditions on the surface $\partial\Omega$. The former case is illustrated in Fig. 4.1 (Eshelby 1957, 1961).

(*a*) The volume Ω of a homogeneous solid $\boldsymbol{L}_0$ is subjected to an overall uniform strain $\boldsymbol{\varepsilon}_\Omega$ or stress $\boldsymbol{\sigma}_\Omega$, and to a uniform equivalent eigenstrain $\boldsymbol{\mu}_r^{eq}$ of as yet unknown magnitude, applied inside an ellipsoidal homogeneous inclusion Ω_r. Since $\boldsymbol{\mu}_0 = \boldsymbol{0}$, the strain and stress in Ω_r follow from (4.1.3), or from (4.1.2), as

$$\left.\begin{aligned} \boldsymbol{\sigma}_r^{(a)} &= \boldsymbol{L}_0\left[\boldsymbol{\varepsilon}_\Omega - (\boldsymbol{I}-\boldsymbol{S})\,\boldsymbol{\mu}_r^{eq}\right] = \boldsymbol{L}_0\left(\boldsymbol{\varepsilon}_r^{(a)} - \boldsymbol{\mu}_r^{eq}\right) \quad \boldsymbol{\varepsilon}_r^{(a)} = \boldsymbol{\varepsilon}_\Omega + \boldsymbol{S}\,\boldsymbol{\mu}_r^{eq} \\ \boldsymbol{\varepsilon}_r^{(a)} &= \boldsymbol{M}_0\boldsymbol{\sigma}_\Omega + \boldsymbol{S}\,\boldsymbol{\mu}_r^{eq} = \boldsymbol{M}_0\boldsymbol{\sigma}_r + \boldsymbol{\mu}_r^{eq} \quad \boldsymbol{\sigma}_r^{(a)} = \boldsymbol{\sigma}_\Omega - \boldsymbol{L}_0\,(\boldsymbol{I}-\boldsymbol{S})\,\boldsymbol{\mu}_r^{eq} \end{aligned}\right\} \tag{4.2.3}$$

(*b*) A similar problem for the same geometry is posed for an inhomogeneity of stiffness $\boldsymbol{L}_r$ that has now replaced the homogenous inclusion inside Ω_r. The volume Ω is subjected to the same remotely applied strain $\boldsymbol{\varepsilon}_\Omega$ or stress $\boldsymbol{\sigma}_\Omega$, but no transformation strain is applied in the inhomogeneity. The respective local fields are determined below by finding a specific value of $\boldsymbol{\mu}_r^{eq}$, such that it generates in the homogeneous inclusion the stress and strain present in the inhomogeneity. Local fields inside the inhomogeneity are also uniform. Therefore, the constant overall and local stress and strain tensors of rank two can be related by constant tensors of rank four, represented by (6×6) matrices $\boldsymbol{T}_r$ and $\boldsymbol{W}_r$, with constant, dimensionless coefficients. Under the two distinct boundary conditions, which apply overall strain $\boldsymbol{\varepsilon}_\Omega$ or overall stress $\boldsymbol{\sigma}_\Omega$, the respective local fields are

$$\left.\begin{aligned} \boldsymbol{\varepsilon}_r^{(b)} &= \boldsymbol{T}_r\boldsymbol{\varepsilon}_\Omega = \boldsymbol{T}_r\boldsymbol{M}_0\boldsymbol{\sigma}_\Omega \quad \boldsymbol{\sigma}_r^{(b)} = \boldsymbol{L}_r\boldsymbol{\varepsilon}_r^{(b)} \\ \boldsymbol{\sigma}_r^{(b)} &= \boldsymbol{W}_r\boldsymbol{\sigma}_\Omega = \boldsymbol{W}_r\boldsymbol{L}_0\boldsymbol{\varepsilon}_\Omega \quad \boldsymbol{\varepsilon}_r^{(b)} = \boldsymbol{M}_r\boldsymbol{\sigma}_r^{(b)} \end{aligned}\right\} \tag{4.2.4}$$

The $\boldsymbol{T}_r$ and $\boldsymbol{W}_r$ are the partial mechanical strain and stress concentration factors of the inhomogeneity. They are similar to the $\boldsymbol{A}_r$ and $\boldsymbol{B}_r$ concentration factors described in Sect. 3.5, but they apply only to fields in a single inhomogeneity that resides in a large volume of a surrounding medium $\boldsymbol{L}_0$, whereas the $\boldsymbol{A}_r$ and $\boldsymbol{B}_r$ refer to field averages in many, usually interacting inhomogeneities in a representative material volume. As long as the strain and stiffness coefficients are both written in either contracted tensorial and engineering notations, the concentration factors are not affected by the chosen notation.

Equations (4.2.4) yield two relations connecting the partial strain and stress concentration factors

$$\boldsymbol{W}_r\boldsymbol{L}_0 = \boldsymbol{L}_r\boldsymbol{T}_r \quad \boldsymbol{M}_r\boldsymbol{W}_r = \boldsymbol{T}_r\boldsymbol{M}_0 \tag{4.2.5}$$

Evaluation of $\boldsymbol{T}_r$ and $\boldsymbol{W}_r$ by the equivalent inclusion method requires the equivalent eigenstrain $\boldsymbol{\mu}_r^{eq}$ in (4.2.3) to reach values that generate local stress and strain fields in the homogeneous inclusion equal to those caused in the inhomogeneity $\boldsymbol{L}_r$, while both configurations are subjected to the same uniform overall strain $\boldsymbol{\varepsilon}_\Omega$ or stress $\boldsymbol{\sigma}_\Omega$. To that end, the corresponding terms in (4.2.3) and (4.2.4) must satisfy

$$\boldsymbol{\varepsilon}_r^{(a)} = \boldsymbol{\varepsilon}_r^{(b)} \quad \boldsymbol{\sigma}_r^{(a)} = \boldsymbol{\sigma}_r^{(b)} \tag{4.2.6}$$

These equalities yield partial concentration factors and associated equivalent eigenstrains, written now in the original notation for prescribed overall fields $\boldsymbol{\varepsilon}_\Omega^0$ and $\boldsymbol{\sigma}_\Omega^0$

$$\boldsymbol{T}_r = \left[\boldsymbol{I} + \boldsymbol{S}\boldsymbol{L}_0^{-1}(\boldsymbol{L}_r - \boldsymbol{L}_0)\right]^{-1} \quad \boldsymbol{\mu}_r^{eq} = -\boldsymbol{L}_0^{-1}(\boldsymbol{L}_r - \boldsymbol{L}_0)\boldsymbol{T}_r\boldsymbol{\varepsilon}_\Omega^0 \tag{4.2.7}$$

$$\boldsymbol{W}_r = [\boldsymbol{I} + \boldsymbol{L}_0(\boldsymbol{I} - \boldsymbol{S})(\boldsymbol{M}_r - \boldsymbol{M}_0)]^{-1} \quad \boldsymbol{\mu}_r^{eq} = (\boldsymbol{I} - \boldsymbol{S})^{-1}\boldsymbol{M}_0(\boldsymbol{I} - \boldsymbol{W}_r)\boldsymbol{\sigma}_\Omega^0 \tag{4.2.8}$$

More convenient forms of the partial concentration factors are obtained using Hill's (1965a) tensors $\boldsymbol{P}$ or $\boldsymbol{Q}$. Those are defined by

$$\left.\begin{aligned} \boldsymbol{P} = \boldsymbol{S}\boldsymbol{L}_0^{-1} = (\boldsymbol{L}^* + \boldsymbol{L}_0)^{-1} = \boldsymbol{P}^{\mathrm{T}} \quad \boldsymbol{Q} = \boldsymbol{L}_0(\boldsymbol{I} - \boldsymbol{P}\boldsymbol{L}_0) = (\boldsymbol{M}^* + \boldsymbol{M}_0)^{-1} = \boldsymbol{Q}^{\mathrm{T}} \\ \boldsymbol{P}\boldsymbol{L}_0 + \boldsymbol{M}_0\boldsymbol{Q} = \boldsymbol{I} \end{aligned}\right\} \tag{4.2.9}$$

In contrast to the Eshelby tensor, these tensors are symmetric under exchange of the first and second pair of indexes, hence the (6×6) matrices that represent them in contracted tensorial or engineering matrix notation are diagonally symmetric.

The $\boldsymbol{L}^*$ and $\boldsymbol{M}^*$ matrices represent Hill's (1965a) *constraint tensors*, defining the stiffness and compliance of an ellipsoidal cavity. In particular, the Eshelby

solution guarantees that application to the cavity wall $\partial\Omega_r$ of surface tractions, corresponding to a uniform stress field $\boldsymbol{\sigma}^*$, generates a uniform strain $\boldsymbol{\varepsilon}^*$, derived from resulting surface displacements of the cavity wall according to (3.4.5). If surface displacements derived from a uniform strain $\boldsymbol{\varepsilon}^*$ were applied to the cavity wall $\partial\Omega_r$, then the resulting tractions would create a uniform stress field $\boldsymbol{\sigma}^*$ in a homogeneous solid**.** This implies the connections

$$\boldsymbol{\sigma}^* = -\boldsymbol{L}^*\boldsymbol{\varepsilon}^* \quad \boldsymbol{\varepsilon}^* = -\boldsymbol{M}^*\boldsymbol{\sigma}^* \tag{4.2.10}$$

where the sign convention anticipates expansion of the cavity by hydrostatic pressure and vice versa. The constraint tensors are symmetric under exchange of the first and second pair of subscripts, hence the corresponding (6×6) matrices satisfy $\boldsymbol{L}^* = (\boldsymbol{L}^*)^{\mathrm{T}}$ and $\boldsymbol{M}^* = (\boldsymbol{M}^*)^{\mathrm{T}}$, $\boldsymbol{L}^*\boldsymbol{M}^* = \boldsymbol{I}$. Both depend only on the elastic moduli of the surrounding medium $\boldsymbol{L}_0$ and on cavity shape. For example, for a spherical cavity in an isotropic medium $\boldsymbol{L}_0$, the constitutive relation is (Walpole 1981)

$$\left.\begin{aligned} \boldsymbol{L}^* &= 3K^*\boldsymbol{J} + 2G^*\boldsymbol{K} \quad \boldsymbol{M}^* = (1/3K^*)\boldsymbol{J} + (1/2G^*)\boldsymbol{K} \\ K^* &= 4G_0/3 \quad G^* = \frac{3}{2}\left(\frac{1}{G_0} + \frac{10}{9K_0 + 8G_0}\right)^{-1} \end{aligned}\right\} \tag{4.2.11}$$

where the projectors $\boldsymbol{J} + \boldsymbol{K} = \boldsymbol{I}$ are defined in Sect. 2.2.9, and K_0, G_0 are elastic moduli of the surrounding medium $\boldsymbol{L}_0$. A more general form of (4.2.10) appears in (4.3.27).

The $\boldsymbol{P}$ and $\boldsymbol{Q}$ matrices render the Eshelby problem solution (4.1.1) for a transformed homogeneous inclusion in the simple form

$$\left.\begin{aligned} \boldsymbol{\varepsilon}_r = \boldsymbol{S}\boldsymbol{\mu}_r = -\boldsymbol{P}\boldsymbol{\lambda}_r \quad \boldsymbol{\sigma}_r = -\boldsymbol{L}_0(\boldsymbol{I} - \boldsymbol{S})\boldsymbol{\mu}_r = -\boldsymbol{Q}\boldsymbol{\mu}_r \\ \boldsymbol{\lambda}_r = -\boldsymbol{L}_0\boldsymbol{\mu}_r \quad \boldsymbol{\mu}_r = -\boldsymbol{M}_0\boldsymbol{\lambda}_r \end{aligned}\right\} \tag{4.2.12}$$

Partial concentration factors $\boldsymbol{T}_r$, $\boldsymbol{W}_r$ in (4.2.7) and (4.2.8) then relate local strain $\boldsymbol{\varepsilon}_r$ and stress $\boldsymbol{\sigma}_r$ in an ellipsoidal inhomogeneity of stiffness $\boldsymbol{L}_r$ to the respective applied overall fields

$$\left.\begin{aligned} \boldsymbol{\varepsilon}_r &= \boldsymbol{T}_r\boldsymbol{\varepsilon}_\Omega^0 = [\boldsymbol{I} + \boldsymbol{P}(\boldsymbol{L}_r - \boldsymbol{L}_0)]^{-1}\boldsymbol{\varepsilon}_\Omega^0 \quad \boldsymbol{\sigma}_r = \boldsymbol{L}_r\boldsymbol{\varepsilon}_r \\ \boldsymbol{\sigma}_r &= \boldsymbol{W}_r\boldsymbol{\sigma}_\Omega^0 = [\boldsymbol{I} + \boldsymbol{Q}(\boldsymbol{M}_r - \boldsymbol{M}_0)]^{-1}\boldsymbol{\sigma}_\Omega^0 \quad \boldsymbol{\varepsilon}_r = \boldsymbol{M}_r\boldsymbol{\sigma}_r \end{aligned}\right\} \tag{4.2.13}$$

Other convenient forms of the partial strain and stress concentration factor tensors follow from the definitions of $\boldsymbol{P}$ and $\boldsymbol{Q}$ as

$$\left.\begin{aligned} \boldsymbol{T}_r{}^{-1} &= \boldsymbol{I} + \boldsymbol{P}(\boldsymbol{L}_r - \boldsymbol{L}_0) = (\boldsymbol{L}^* + \boldsymbol{L}_0)^{-1}(\boldsymbol{L}^* + \boldsymbol{L}_r) = \boldsymbol{P}(\boldsymbol{L}^* + \boldsymbol{L}_r) \\ \boldsymbol{W}_r{}^{-1} &= \boldsymbol{I} + \boldsymbol{Q}(\boldsymbol{M}_r - \boldsymbol{M}_0) = (\boldsymbol{M}^* + \boldsymbol{M}_0)^{-1}(\boldsymbol{M}^* + \boldsymbol{M}_r) = \boldsymbol{Q}(\boldsymbol{M}^* + \boldsymbol{M}_r) \end{aligned}\right\} \tag{4.2.14}$$

Although neither $\boldsymbol{T}_r$ nor $\boldsymbol{W}_r$ need to be diagonally symmetric, it can be shown that

$$\left.\begin{aligned} \boldsymbol{T}_r\boldsymbol{P} = \boldsymbol{P}\boldsymbol{T}_r^{\mathrm{T}} \quad \boldsymbol{W}_r\boldsymbol{Q} = \boldsymbol{Q}\boldsymbol{W}_r^{\mathrm{T}} \\ \boldsymbol{T}_r(\boldsymbol{L}_r - \boldsymbol{L}_0) = (\boldsymbol{L}_r - \boldsymbol{L}_0)\boldsymbol{T}_r^{\mathrm{T}} \quad \boldsymbol{W}_r(\boldsymbol{M}_r - \boldsymbol{M}_0) = (\boldsymbol{M}_r - \boldsymbol{M}_0)\boldsymbol{W}_r^{\mathrm{T}} \end{aligned}\right\} \tag{4.2.15}$$

In summary, since both $\boldsymbol{L}_0$, $\boldsymbol{L}_r$ and $\boldsymbol{M}_0$, $\boldsymbol{M}_r$ are known, evaluation of the partial concentration factors is reduced to finding the tensors $\boldsymbol{P}$ or $\boldsymbol{Q}$ for the specific ellipsoidal shape of the inhomogeneity. Both depend only on the stiffness $\boldsymbol{L}_0$ and on the shape of Ω_r, but not on $\boldsymbol{L}_r$. *Therefore, a* $\boldsymbol{P}$ *tensor found for a particular inclusion shape in a material symmetry of* $\boldsymbol{L}_0$ *provides a concentration factor for an inhomogeneity of any local stiffness* $\boldsymbol{L}_r$*, embedded in* $\boldsymbol{L}_0$. Coefficients of $\boldsymbol{P}$ tensors for typical ellipsoidal shapes appear in Sect. 4.6 below.

Traction-free cavities of ellipsoidal shape can be regarded as inhomogeneities with zero stiffness. Average strain caused by displacements of the cavity wall is found from (4.2.13) at $\boldsymbol{L}_r = \boldsymbol{0}$. In a large volume of a comparison medium or 'matrix' $\boldsymbol{L}_0$ that is loaded by a uniform overall strain $\boldsymbol{\varepsilon}_\Omega^0$ or stress $\boldsymbol{\sigma}_\Omega^0 = \boldsymbol{L}_0\boldsymbol{\varepsilon}_\Omega^0$, the cavity strain average is

$$\boldsymbol{\varepsilon}_r = (\boldsymbol{I} - \boldsymbol{P}\boldsymbol{L}_0)^{-1}\boldsymbol{\varepsilon}_\Omega^0 = (\boldsymbol{I} - \boldsymbol{S})^{-1}\boldsymbol{M}_0\boldsymbol{\sigma}_\Omega^0 = \boldsymbol{Q}^{-1}\boldsymbol{L}_0\boldsymbol{\varepsilon}_\Omega^0 = \boldsymbol{Q}^{-1}\boldsymbol{\sigma}_\Omega^0 \tag{4.2.16}$$

4.3 Transformed Inhomogeneities

4.3.1 Method of Uniform Fields

Here we show how to find local fields caused in an inhomogeneity by application of physically based uniform transformation strains or eigenstrains $\boldsymbol{\mu}_0 \in \Omega_0$ and $\boldsymbol{\mu}_r \in \Omega_r$, or eigenstresses $\boldsymbol{\lambda}_0 = -\boldsymbol{L}_0\boldsymbol{\mu}_0$ and $\boldsymbol{\lambda}_r = -\boldsymbol{L}_r\boldsymbol{\mu}_r$, both superimposed with overall fields $\boldsymbol{\varepsilon}_\Omega^0$ or $\boldsymbol{\sigma}_\Omega^0$. Regardless of their specific physical origin, both eigenstrains are regarded as independent applied loads. Their presence is reflected in phase constitutive relations (4.2.1) and (4.2.2) as

$$\left.\begin{aligned} \boldsymbol{\sigma}_r(\boldsymbol{x}) = \boldsymbol{L}_r[\boldsymbol{\varepsilon}_r(\boldsymbol{x}) - \boldsymbol{\mu}_r] = \boldsymbol{L}_r\boldsymbol{\varepsilon}_r(\boldsymbol{x}) + \boldsymbol{\lambda}_r \quad \boldsymbol{\varepsilon}_r(\boldsymbol{x}) = \boldsymbol{M}_r\boldsymbol{\sigma}_r(\boldsymbol{x}) + \boldsymbol{\mu}_r \quad \text{for } \boldsymbol{x} \in \Omega_r \\ \boldsymbol{\sigma}_0(\boldsymbol{x}) = \boldsymbol{L}_0[\boldsymbol{\varepsilon}_0(\boldsymbol{x}) - \boldsymbol{\mu}_0] = \boldsymbol{L}_0\boldsymbol{\varepsilon}_0(\boldsymbol{x}) + \boldsymbol{\lambda}_0 \quad \boldsymbol{\varepsilon}_0(\boldsymbol{x}) = \boldsymbol{M}_0\boldsymbol{\sigma}_0(\boldsymbol{x}) + \boldsymbol{\mu}_0 \quad \text{for } \boldsymbol{x} \in \Omega_0 \end{aligned}\right\} \tag{4.3.1}$$

Since local fields caused by each of the two applied load sets $\{\boldsymbol{\varepsilon}_\Omega^0, \boldsymbol{\mu}_r, \boldsymbol{\mu}_0\}$ and $\{\boldsymbol{\sigma}_\Omega^0, \boldsymbol{\lambda}_r, \boldsymbol{\lambda}_0\}$ are uniform inside an ellipsoidal inhomogeneity $\boldsymbol{L}_r$ in Ω_r, they can be sought as a superposition of the contributions

$$\boldsymbol{\varepsilon}_r = \boldsymbol{T}_r\boldsymbol{\varepsilon}_\Omega^0 + \boldsymbol{R}_{rr}\boldsymbol{\mu}_r + \boldsymbol{R}_{r0}\boldsymbol{\mu}_0 \qquad \boldsymbol{\sigma}_r = \boldsymbol{L}_r(\boldsymbol{\varepsilon}_r - \boldsymbol{\mu}_r) \tag{4.3.2}$$

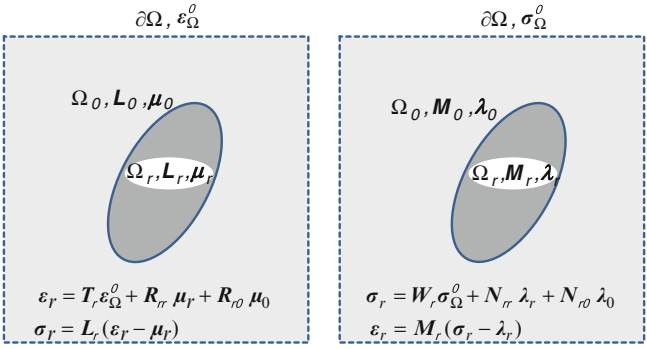

Fig. 4.2 Local strain and stress fields caused in an inhomogeneity $\boldsymbol{L}_r$ by the distinct load sets $\{\boldsymbol{\varepsilon}^0_\Omega, \boldsymbol{\mu}_r, \boldsymbol{\mu}_0\}$ and $\{\boldsymbol{\sigma}^0_\Omega, \boldsymbol{\lambda}_r, \boldsymbol{\lambda}_0\}$

or

$$\boldsymbol{\sigma}_r = \boldsymbol{W}_r \boldsymbol{\sigma}^0_\Omega + \boldsymbol{N}_{rr}\boldsymbol{\lambda}_r + \boldsymbol{N}_{r0}\boldsymbol{\lambda}_0 \quad \boldsymbol{\varepsilon}_r = \boldsymbol{M}_r(\boldsymbol{\sigma}_r - \boldsymbol{\lambda}_r) \tag{4.3.3}$$

where the $\boldsymbol{R}_{r\beta}$ and $\boldsymbol{N}_{r\beta}$, $(\beta = r, 0)$ are (6×6) partial transformation concentration factor matrices that represent tensors of rank four, with constant coefficients which depend on elastic moduli of both $\boldsymbol{L}_0$ and $\boldsymbol{L}_r$. They define contributions to the local strain or stress fields in Ω_r by the prescribed phase eigenstrains or eigenstresses, under zero overall strain $\boldsymbol{\varepsilon}^0_\Omega$, or stress $\boldsymbol{\sigma}^0_\Omega$, respectively, as indicated in Fig. 4.2.

Each of the two load sets contains dimensionally consistent terms, hence the concentration factor coefficients are dimensionless.

Assuming that at least one of the mechanical concentration factors $\boldsymbol{T}_r$ or $\boldsymbol{W}_r$ is known, the transformation concentration factors $\boldsymbol{R}_{r\beta}$ and $\boldsymbol{N}_{r\beta}$ can be found by creating in the entire two-phase volume certain auxiliary uniform strain and stress fields (Dvorak 1990). The two phases are separated, transformed by uniform phase eigenstrains $\boldsymbol{\mu}_r$ and $\boldsymbol{\mu}_0$, and loaded by as yet unknown surface tractions derived from the same auxiliary uniform stress $\hat{\boldsymbol{\sigma}}$. Of course, we wish to select $\hat{\boldsymbol{\sigma}}$ such as to create the same uniform strain $\hat{\boldsymbol{\varepsilon}} = \boldsymbol{\varepsilon}_r(\boldsymbol{x})$ in both phases, so that they can later be reconnected.

As in (3.6.6), this selection is made by solving

$$\hat{\boldsymbol{\sigma}} = \boldsymbol{L}_r(\hat{\boldsymbol{\varepsilon}} - \boldsymbol{\mu}_r) = \boldsymbol{L}_0(\hat{\boldsymbol{\varepsilon}} - \boldsymbol{\mu}_0) \quad \hat{\boldsymbol{\varepsilon}} = \boldsymbol{M}_r(\hat{\boldsymbol{\sigma}} - \boldsymbol{\lambda}_r) = \boldsymbol{M}_0(\hat{\boldsymbol{\sigma}} - \boldsymbol{\lambda}_0) \tag{4.3.4}$$

for the auxiliary uniform strain and stress, in the form

$$\hat{\boldsymbol{\varepsilon}} = -(\boldsymbol{L}_r - \boldsymbol{L}_0)^{-1}(\boldsymbol{\lambda}_r - \boldsymbol{\lambda}_0) \quad \hat{\boldsymbol{\sigma}} = -(\boldsymbol{M}_r - \boldsymbol{M}_0)^{-1}(\boldsymbol{\mu}_r - \boldsymbol{\mu}_0) \tag{4.3.5}$$

Now that both stresses and strains in the two phases are uniform and of the same respective magnitude, the phases can be reconnected, while the fields $\hat{\boldsymbol{\varepsilon}}$ or $\hat{\boldsymbol{\sigma}}$ are maintained by application of corresponding displacements or tractions at the surface $\partial\Omega$ of Ω.

Finally, the overall strain or stress applied to the restored aggregate are reduced from the auxiliary to the actual magnitudes of interest. Complete unloading to zero from the respective overall uniform fields (4.3.3) provides

$$\boldsymbol{\varepsilon}_r = (\boldsymbol{I} - \boldsymbol{T}_r)\hat{\boldsymbol{\varepsilon}} \quad \boldsymbol{\sigma}_r = (\boldsymbol{I} - \boldsymbol{W}_r)\hat{\boldsymbol{\sigma}} \tag{4.3.6}$$

Since the two eigenstrains are independent, implementing these unloading steps and comparing the resulting local fields with those in (4.3.2) or (4.3.3), at either $\boldsymbol{\varepsilon}_\Omega^0 = \boldsymbol{0}$ or $\boldsymbol{\sigma}_\Omega^0 = \boldsymbol{0}$, yields the following connections between the mechanical and transformation concentration factors

$$\left.\begin{aligned} \boldsymbol{R}_{rr} &= (\boldsymbol{I} - \boldsymbol{T}_r)(\boldsymbol{L}_r - \boldsymbol{L}_0)^{-1}\boldsymbol{L}_r = \boldsymbol{T}_r\boldsymbol{P}\boldsymbol{L}_r \\ \boldsymbol{R}_{r0} &= -(\boldsymbol{I} - \boldsymbol{T}_r)(\boldsymbol{L}_r - \boldsymbol{L}_0)^{-1}\boldsymbol{L}_0 = -\boldsymbol{T}_r\boldsymbol{P}\boldsymbol{L}_0 \end{aligned}\right\} \tag{4.3.7}$$

and

$$\left.\begin{aligned} \boldsymbol{N}_{rr} &= (\boldsymbol{I} - \boldsymbol{W}_r)(\boldsymbol{M}_r - \boldsymbol{M}_0)^{-1}\boldsymbol{M}_r = \boldsymbol{W}_r\boldsymbol{Q}\boldsymbol{M}_r \\ \boldsymbol{N}_{r0} &= -(\boldsymbol{I} - \boldsymbol{W}_r)(\boldsymbol{M}_r - \boldsymbol{M}_0)^{-1}\boldsymbol{M}_0 = -\boldsymbol{W}_r\boldsymbol{Q}\boldsymbol{M}_0 \end{aligned}\right\} \tag{4.3.8}$$

where $\boldsymbol{T}_r + \boldsymbol{R}_{rr} + \boldsymbol{R}_{r0} = \boldsymbol{I}$ and $\boldsymbol{W}_r + \boldsymbol{N}_{rr} + \boldsymbol{N}_{r0} = \boldsymbol{I}$. The (6×6) matrices $\boldsymbol{R}_{rr}$, $\boldsymbol{R}_{r0}$ and $\boldsymbol{N}_{rr}$, $\boldsymbol{N}_{r0}$ need not be diagonally symmetric, but it can be verified that

$$\boldsymbol{R}_{rr}\boldsymbol{M}_r = \boldsymbol{M}_r\boldsymbol{R}_{rr}^{\mathrm{T}} \qquad \boldsymbol{N}_{rr}\boldsymbol{L}_r = \boldsymbol{L}_r\boldsymbol{N}_{rr}^{\mathrm{T}} \tag{4.3.9}$$

In a homogeneous medium, for $\boldsymbol{L}_r \to \boldsymbol{L}_0$, the $\boldsymbol{T}_r \to \boldsymbol{I}$ and $\boldsymbol{R}_{rr} \to \boldsymbol{P}\boldsymbol{L}_0 = \boldsymbol{S}$, the Eshelby tensor.

After appropriate substitutions and exchanges $\boldsymbol{\lambda}_r = -\boldsymbol{L}_r\boldsymbol{\mu}_r$ and $\boldsymbol{\lambda}_0 = -\boldsymbol{L}_0\boldsymbol{\mu}_0$ of the transformation terms for brevity, local fields caused in the inhomogeneity $\boldsymbol{L}_r$ by the two load sets are

$$\boldsymbol{\varepsilon}_r = \boldsymbol{T}_r[\boldsymbol{\varepsilon}_\Omega^0 - \boldsymbol{P}(\boldsymbol{\lambda}_r - \boldsymbol{\lambda}_0)] \quad \boldsymbol{\sigma}_r = \boldsymbol{L}_r\boldsymbol{T}_r\boldsymbol{\varepsilon}_\Omega^0 + \boldsymbol{\lambda}_r - \boldsymbol{L}_r\boldsymbol{T}_r\boldsymbol{P}(\boldsymbol{\lambda}_r - \boldsymbol{\lambda}_0)$$
$$\text{for } \{\boldsymbol{\varepsilon}_\Omega^0, \boldsymbol{\mu}_r, \boldsymbol{\mu}_0\} \tag{4.3.10}$$

$$\boldsymbol{\sigma}_r = \boldsymbol{W}_r\left[\boldsymbol{\sigma}_\Omega^0 - \boldsymbol{Q}(\boldsymbol{\mu}_r - \boldsymbol{\mu}_0)\right] \quad \boldsymbol{\varepsilon}_r = \boldsymbol{M}_r\boldsymbol{W}_r\boldsymbol{\sigma}_\Omega^0 + \boldsymbol{\mu}_r - \boldsymbol{M}_r\boldsymbol{W}_r\boldsymbol{Q}(\boldsymbol{\mu}_r - \boldsymbol{\mu}_0)$$
$$\text{for } \left\{\boldsymbol{\sigma}_\Omega^0, \boldsymbol{\lambda}_r, \boldsymbol{\lambda}_0\right\} \tag{4.3.11}$$

Notice that uniform fields (4.3.4) and (4.3.5) can be created for any shape of the inhomogeneity. If the mechanical influence functions in the inhomogeneity are known, so that $\boldsymbol{\varepsilon}_r(\boldsymbol{x}) = \boldsymbol{T}_r(\boldsymbol{x})\boldsymbol{\varepsilon}_\Omega^0 = \boldsymbol{M}_r\boldsymbol{\sigma}_r(\boldsymbol{x})$, or $\boldsymbol{\sigma}_r(\boldsymbol{x}) = \boldsymbol{W}_r(\boldsymbol{x})\boldsymbol{\sigma}_\Omega^0 = \boldsymbol{L}_r\boldsymbol{\varepsilon}_r(\boldsymbol{x})$, and are used in the unloading (4.3.6), then (4.3.7) and (4.3.8) can be augmented to provide the transformation influence functions $\boldsymbol{R}_{r\beta}(\boldsymbol{x})$ and $\boldsymbol{N}_{r\beta}(\boldsymbol{x})$, $(\beta = r, 0)$.

Exterior fields surrounding an inhomogeneity $\boldsymbol{L}_r$, can be described in a similar manner, providing that the mechanical influence functions are known

$$\boldsymbol{\varepsilon}_0(\boldsymbol{x}) = \boldsymbol{T}_0(\boldsymbol{x})\boldsymbol{\varepsilon}^0_\Omega = \boldsymbol{M}_0\boldsymbol{\sigma}_0(\boldsymbol{x}) \quad \boldsymbol{\sigma}_0(\boldsymbol{x}) = \boldsymbol{W}_0(\boldsymbol{x})\boldsymbol{\sigma}^0_\Omega = \boldsymbol{L}_0\boldsymbol{\varepsilon}_0(\boldsymbol{x}) \tag{4.3.12}$$

Unloading from the auxiliary uniform fields (4.3.4) or (4.3.5) yields the exterior fields in the form

$$\boldsymbol{\varepsilon}_0(\boldsymbol{x}) = [\boldsymbol{I} - \boldsymbol{T}_0(\boldsymbol{x})]\,\hat{\boldsymbol{\varepsilon}} \qquad \boldsymbol{\sigma}_0(\boldsymbol{x}) = [\boldsymbol{I} - \boldsymbol{W}_0(\boldsymbol{x})]\,\hat{\boldsymbol{\sigma}} \tag{4.3.13}$$

The transformation influence functions for the exterior fields in Ω_0 are

$$\boldsymbol{R}_{0r} = (\boldsymbol{I} - \boldsymbol{T}_0(\boldsymbol{x}))(\boldsymbol{L}_r - \boldsymbol{L}_0)^{-1}\boldsymbol{L}_r \quad \boldsymbol{R}_{00} = -(\boldsymbol{I} - \boldsymbol{T}_0(\boldsymbol{x}))(\boldsymbol{L}_r - \boldsymbol{L}_0)^{-1}\boldsymbol{L}_0 \tag{4.3.14}$$

$$\boldsymbol{N}_{0r} = (\boldsymbol{I} - \boldsymbol{W}_0(\boldsymbol{x}))(\boldsymbol{M}_r - \boldsymbol{M}_0)^{-1}\boldsymbol{M}_r \quad \boldsymbol{N}_{00} = -(\boldsymbol{I} - \boldsymbol{W}_0(\boldsymbol{x}))(\boldsymbol{M}_r - \boldsymbol{M}_0)^{-1}\boldsymbol{M}_0 \tag{4.3.15}$$

The exterior fields are

$$\left.\begin{aligned} \boldsymbol{\varepsilon}_0(\boldsymbol{x}) &= \boldsymbol{T}_0(\boldsymbol{x})\boldsymbol{\varepsilon}^0_\Omega + \boldsymbol{R}_{0r}(\boldsymbol{x})\boldsymbol{\mu}_r + \boldsymbol{R}_{00}(\boldsymbol{x})\boldsymbol{\mu}_0 \\ \boldsymbol{\sigma}_0(\boldsymbol{x}) &= \boldsymbol{L}_0\,[\boldsymbol{\varepsilon}_0(\boldsymbol{x}) - \boldsymbol{\mu}_0] \quad \text{for } \{\boldsymbol{\varepsilon}^0_\Omega, \boldsymbol{\mu}_r, \boldsymbol{\mu}_0\} \end{aligned}\right\} \tag{4.3.16}$$

$$\left.\begin{aligned} \boldsymbol{\sigma}_0(\boldsymbol{x}) &= \boldsymbol{W}_0(\boldsymbol{x})\boldsymbol{\sigma}^0_\Omega + \boldsymbol{N}_{0r}(\boldsymbol{x})\boldsymbol{\lambda}_r + \boldsymbol{N}_{00}(\boldsymbol{x})\boldsymbol{\lambda}_0 \\ \boldsymbol{\varepsilon}_0(\boldsymbol{x}) &= \boldsymbol{M}_0\boldsymbol{\sigma}_0(\boldsymbol{x}) + \boldsymbol{\mu}_0 \quad \text{for } \{\boldsymbol{\sigma}^0_\Omega, \boldsymbol{\lambda}_r, \boldsymbol{\lambda}_0\} \end{aligned}\right\} \tag{4.3.17}$$

4.3.2 The Equivalent Inclusion Method

For completeness, the above results are now rederived using the equivalent inclusion method outlined in Sect. 4.2. In this context, Eshelby (1961) and Mura (1987) describe a transformed inhomogeneity as an 'inhomogeneous inclusion'. Two systems of identical geometry, deformed by the same uniform overall strain $\boldsymbol{\varepsilon}^0_\Omega$, are considered. One is a homogeneous solid $\boldsymbol{L}_0$ containing a homogeneous inclusion Ω_r, where we apply uniform eigenstrains $\boldsymbol{\mu}_r + \boldsymbol{\mu}^{eq}_r$, together with a uniform eigenstrain $\boldsymbol{\mu}_0$ in Ω_0. The other system contains an inhomogeneity $\boldsymbol{L}_r$ in Ω_r, perfectly bonded to a large surrounding volume Ω_0 of material $\boldsymbol{L}_0$. The goal is to find the equivalent eigenstrain $\boldsymbol{\mu}^{eq}_r$ such that its superposition with $\boldsymbol{\mu}_r$ generates in both Ω_r and Ω_0 of the homogeneous system the same strain and stress fields that the applied load set $\{\boldsymbol{\varepsilon}^0_\Omega, \boldsymbol{\mu}_r, \boldsymbol{\mu}_0\}$ causes in the second two-phase system with an inhomogeneity.

According to (4.1.3), the stress and strain in the homogeneous inclusion now are

$$\left.\begin{aligned}\boldsymbol{\sigma}_r^{(a)} &= \boldsymbol{L}_0[\boldsymbol{\varepsilon}_\Omega^0 - (\boldsymbol{I}-\boldsymbol{S})(\boldsymbol{\mu}_r + \boldsymbol{\mu}_r^{eq}) - \boldsymbol{S}\boldsymbol{\mu}_0] = \boldsymbol{L}_0(\boldsymbol{\varepsilon}_r^{(a)} - \boldsymbol{\mu}_r - \boldsymbol{\mu}_r^{eq})\\ \boldsymbol{\varepsilon}_r^{(a)} &= \boldsymbol{\varepsilon}_\Omega^0 + \boldsymbol{S}(\boldsymbol{\mu}_r + \boldsymbol{\mu}_r^{eq} - \boldsymbol{\mu}_0) = \boldsymbol{M}_0\boldsymbol{\sigma}_r^{(a)} + \boldsymbol{\mu}_r + \boldsymbol{\mu}_r^{eq}\end{aligned}\right\} \tag{4.3.18}$$

Local fields in the inhomogeneity $\boldsymbol{L}_r$ are again sought in the form

$$\boldsymbol{\varepsilon}_r^{(b)} = \boldsymbol{T}_r\boldsymbol{\varepsilon}_\Omega^0 + \boldsymbol{R}_{rr}\boldsymbol{\mu}_r + \boldsymbol{R}_{r0}\boldsymbol{\mu}_0 \quad \boldsymbol{\sigma}_r^{(b)} = \boldsymbol{L}_r(\boldsymbol{\varepsilon}_r^{(b)} - \boldsymbol{\mu}_r) \tag{4.3.2}$$

The equivalent inclusion method requires the corresponding pairs to satisfy

$$\boldsymbol{\varepsilon}_r^{(a)} = \boldsymbol{\varepsilon}_r^{(b)} \quad \boldsymbol{\sigma}_r^{(a)} = \boldsymbol{\sigma}_r^{(b)} \tag{4.2.6}$$

Derivation of $\boldsymbol{R}_{rr}$ and $\boldsymbol{R}_{r0}$ by this method follows the steps leading to $\boldsymbol{T}_r$ in (4.2.7), and it yields the results already recorded in (4.3.7). Using the two equations (4.2.6) in turn, the equivalent eigenstrain is found as

$$\left.\begin{aligned}\boldsymbol{S}\boldsymbol{\mu}_r^{eq} &= -(\boldsymbol{I}-\boldsymbol{T}_r)\boldsymbol{\varepsilon}_\Omega^0 + (\boldsymbol{R}_{rr}-\boldsymbol{S})\boldsymbol{\mu}_r + (\boldsymbol{R}_{r0}+\boldsymbol{S})\boldsymbol{\mu}_0\\ &= -\boldsymbol{P}(\boldsymbol{L}_r - \boldsymbol{L}_0)[\boldsymbol{T}_r\boldsymbol{\varepsilon}_\Omega^0 + (\boldsymbol{R}_{rr}-\boldsymbol{I})\boldsymbol{\mu}_r + \boldsymbol{R}_{r0}\boldsymbol{\mu}_0]\end{aligned}\right\} \tag{4.3.19}$$

The equality can be verified as an exercise. The result now includes contributions by each of the three independently applied loads $\boldsymbol{\varepsilon}_\Omega^0, \boldsymbol{\mu}_r, \boldsymbol{\mu}_0$.

Next, let us apply to Ω a uniform overall stress $\boldsymbol{\sigma}_\Omega^0$, together with uniform eigenstrains $\boldsymbol{\mu}_r + \boldsymbol{\mu}_r^{eq}$ in Ω_r, and a uniform eigenstrain $\boldsymbol{\mu}_0$ in Ω_0. The equivalent eigenstrain $\boldsymbol{\mu}_r^{eq}$ in Ω_r is now different from that in (4.3.19). The connection $\boldsymbol{\lambda}_r^{eq} = -\boldsymbol{L}_r\boldsymbol{\mu}_r^{eq}$ introduces an equivalent eigenstress. Using (4.1.2), we write local fields in the homogeneous inclusion as

$$\left.\begin{aligned}\boldsymbol{\varepsilon}_r^{(a)} &= \boldsymbol{M}_0\boldsymbol{\sigma}_\Omega^0 + \boldsymbol{\mu}_0 + \boldsymbol{S}(\boldsymbol{\mu}_r + \boldsymbol{\mu}_r^{eq} - \boldsymbol{\mu}_0) = \boldsymbol{M}_0\boldsymbol{\sigma}_r + \boldsymbol{\mu}_r + \boldsymbol{\mu}_r^{eq}\\ \boldsymbol{\sigma}_r^{(a)} &= \boldsymbol{\sigma}_\Omega^0 - \boldsymbol{L}_0(\boldsymbol{I}-\boldsymbol{S})(\boldsymbol{\mu}_r + \boldsymbol{\mu}_r^{eq} - \boldsymbol{\mu}_0) = \boldsymbol{L}_0(\boldsymbol{\varepsilon}_r - \boldsymbol{\mu}_r - \boldsymbol{\mu}_r^{eq})\end{aligned}\right\} \tag{4.3.20}$$

Local stress caused by the applied loads in the inhomogeneity $\boldsymbol{L}_r$ is written as in (4.3.3)

$$\boldsymbol{\sigma}_r^{(b)} = \boldsymbol{W}_r\boldsymbol{\sigma}_\Omega^0 + \boldsymbol{N}_{rr}\boldsymbol{\lambda}_r + \boldsymbol{N}_{r0}\boldsymbol{\lambda}_0 \quad \boldsymbol{\varepsilon}_r^{(b)} = \boldsymbol{M}_r\boldsymbol{\sigma}_r^{(b)} + \boldsymbol{\mu}_r \tag{4.3.21}$$

Referring again to the equality (4.2.6), one can recover the results $(4.2.8)_1$ and the equivalent eigenstrain

$$\boldsymbol{Q}\boldsymbol{\mu}_r^{eq} = (\boldsymbol{I}-\boldsymbol{W}_r)[\boldsymbol{\sigma}_\Omega^0 - \boldsymbol{Q}(\boldsymbol{\mu}_r - \boldsymbol{\mu}_0)] \tag{4.3.22}$$

If the load sets $\{\boldsymbol{\varepsilon}^0_\Omega, \boldsymbol{\mu}_r, \boldsymbol{\mu}_0\}$ or $\{\boldsymbol{\sigma}^0_\Omega, \boldsymbol{\lambda}_r, \boldsymbol{\lambda}_0\}$ are applied in superposition with the equivalent eigenstrains (4.3.19) or (4.3.22) within an ellipsoidal homogeneous inclusion $\boldsymbol{L}_0$ in Ω_r, then they reproduce there the local strain and stress fields that are generated by these load sets in a perfectly bonded inhomogeneity $\boldsymbol{L}_r$ residing in Ω_r. Therefore, both the interior and exterior total fields in $\Omega = \Omega_0 + \Omega_r$ are made equal by addition of the equivalent eigenstrains to the loads acting on the homogeneous medium $\boldsymbol{L}_0$ in Ω.

The equivalent inclusion method is applicable only to ellipsoidal inhomogeneities, whereas the uniform field method can be used to analyze inhomogeneities of any shape, providing that the $\boldsymbol{T}_r(\boldsymbol{x})$ or $\boldsymbol{W}_r(\boldsymbol{x})$ and $\boldsymbol{T}_0(\boldsymbol{x})$ or $\boldsymbol{W}_0(\boldsymbol{x})$, or their respective volume averages are known. The latter method is more transparent, because it does not rely on the equivalent eigenstrain, which may also depend on the applied, physically motivated eigenstrains. However, both methods are limited to problems involving uniform overall fields and piecewise uniform transformation strains in the phases.

4.3.3 Contrasting Mechanical and Transformation Strains

It is important to keep in mind that mechanical and transformation strains have a different effect on overall and local fields inside and in the exterior of an inclusion or inhomogeneity. As an example, consider two separate loading states applied to a large volume V of the material $\boldsymbol{L}_0$ in Ω_0 that contains a traction-free cavity in Ω_r. One involves applications of a uniform overall strain $\boldsymbol{\varepsilon}^0_\Omega$. In the other loading state, the volume V is traction-free, and transformed by a uniform eigenstrain $\boldsymbol{\mu}_0$.

The strains $\boldsymbol{\varepsilon}^0_\Omega$ and $\boldsymbol{\mu}_0$ are of the same magnitude $\boldsymbol{\eta}$. In both cases, the same uniform deformation prevails at points far removed from Ω_r. However, their respective contributions to the stress field in Ω_0, and to the local deformation of the cavity in Ω_r are very different. Around the cavity, the mechanical strain $\boldsymbol{\varepsilon}^0_\Omega = \boldsymbol{\eta}$ creates concentrated fields that depend on cavity shape. In contrast, application of the eigenstrain $\boldsymbol{\mu}_0 = \boldsymbol{\eta}$ to the same solid generates only a uniform stress-free strain, independent of cavity shape or position, everywhere in the solid.

Another illustration is provided by embedding an ellipsoidal inhomogeneity $\boldsymbol{L}_r$ in subvolume Ω_r of a large volume Ω_0 of a homogeneous solid $\boldsymbol{L}_0$. An overall strain $\boldsymbol{\varepsilon}^0_\Omega = \boldsymbol{\eta}$ is applied together with the eigenstrain $\boldsymbol{\mu}_0 = \boldsymbol{\eta}$ in Ω_0 only; $\boldsymbol{\mu}_r = \boldsymbol{0}$ in Ω_r. The outer surface $\partial\Omega_0$ is now traction-free, hence the average stress in Ω_0 is $\bar{\boldsymbol{\sigma}}_0 = \boldsymbol{0}$. However, local stress in the inhomogeneity $\boldsymbol{L}_r$ in Ω_r follows from (4.3.2) as

$$\boldsymbol{\sigma}_r = \boldsymbol{L}_r\boldsymbol{\varepsilon}_r = \boldsymbol{L}_r(\boldsymbol{T}_r\boldsymbol{\varepsilon}^0_\Omega + \boldsymbol{R}_{r0}\boldsymbol{\mu}_0) = \boldsymbol{L}_r(\boldsymbol{T}_r + \boldsymbol{R}_{r0})\boldsymbol{\eta} = \boldsymbol{L}_r\boldsymbol{T}_r(\boldsymbol{I} - \boldsymbol{S})\boldsymbol{\eta} \tag{4.3.23}$$

This indicates that an equivalent eigenstrain applied to the exterior of an inhomogeneity, for example, to simulate stress reduction caused there by damage or inelastic deformation, generates nonvanishing local fields inside and nearby the inhomogeneity.

To reduce this local stress also to zero, an auxiliary eigenstrain $\boldsymbol{\mu}_r^{aux}$ needs to be applied inside Ω_r, such that

$$\boldsymbol{\sigma}_r = \boldsymbol{L}_r(\boldsymbol{\varepsilon}_r - \boldsymbol{\mu}_r^{aux}) = \boldsymbol{L}_r\left[\boldsymbol{T}_r\boldsymbol{\eta} - (\boldsymbol{I} - \boldsymbol{R}_{rr})\boldsymbol{\mu}_r^{aux} + \boldsymbol{R}_{r0}\boldsymbol{\eta}\right] = \boldsymbol{0} \tag{4.3.24}$$

Of course, this yields $\boldsymbol{\mu}_r^{aux} = \boldsymbol{\eta}$, and it confirms that a uniform eigenstrain does not generate a stress field in a traction-free heterogeneous medium. A more direct way to show this is to apply $\boldsymbol{\varepsilon}_\Omega^0 = \boldsymbol{\mu}_r = \boldsymbol{\mu}_0 = \boldsymbol{\eta}$ and recall from (4.3.7) that $\boldsymbol{T}_r + \boldsymbol{R}_{rr} + \boldsymbol{R}_{r0} = \boldsymbol{I}$. Then, the local stress is $\boldsymbol{\sigma}_r = \boldsymbol{L}_r(\boldsymbol{\varepsilon}_r - \boldsymbol{\eta}) = \boldsymbol{L}_r(\boldsymbol{I}\boldsymbol{\eta} - \boldsymbol{\eta}) = \boldsymbol{0}$.

4.3.4 *Imperfectly Bonded Inhomogeneities and Cavities*

So far, we have assumed that the inhomogeneity is perfectly bonded along its interface $\partial\Omega_r$ with the surrounding 'matrix' $\boldsymbol{L}_0$. Of course, other than perfect bonds are often present, due for example, to the presence of elastic or inelastic coatings, or to partial or complete interface separation. The original single interface is now replaced by two surfaces, the cavity wall $\partial\Omega_c$, and the surface $\partial\Omega_r$ surrounding the partially or completely debonded material inside the cavity. Traction continuity is always preserved. However, displacement jumps may open between pairs of points originally in contact, but now separated at the two sides of an imperfect interface. Stress and strain averages taken over the volume of the matrix cavity Ω_c still follow from the displacements and tractions present at the cavity wall, as in (3.4.2) and (3.4.5), but they may no longer be connected by an effective stiffness of the material inside Ω_r. In fact, as shown in Chap. 6, inhomogeneities surrounded by coatings or imperfect interface bonds may not exhibit a unique effective stiffness.

Elastic fields of imperfectly bonded or coated inhomogeneities need to be evaluated separately, with regard to the type of bond or coating and a particular physical mechanism of the decohesion process. Some of those are described in Chap. 9. However, each such solution must comply with certain connections between local strain and stress averages, which are then reflected in evaluation of the overall field averages and stiffness matrices of the damaged material. Those connections are derived here in terms of the surface displacements and tractions at the 'loaded cavity' wall.

Traction continuity along the interface guarantees that stress averages $\bar{\boldsymbol{\sigma}}_r^c = \bar{\boldsymbol{\sigma}}_r^d$, derived from tractions along the cavity wall or the surface of the inhomogeneity, respectively. Interpenetrations are excluded, hence the displacement jumps cause some or all components of the average strain $\bar{\boldsymbol{\varepsilon}}_r^d$ inside an imperfectly bonded inhomogeneity to be smaller than those of the average $\bar{\boldsymbol{\varepsilon}}_r^c$ in the surrounding loaded cavity. Both follow from (3.4.5). This average strain difference can be eliminated by applying to the debonded inhomogeneity a uniform *damage-equivalent eigenstrain* $\boldsymbol{\mu}_r^{dq} = \bar{\boldsymbol{\varepsilon}}_r^c - \bar{\boldsymbol{\varepsilon}}_r^d$, which corresponds to the volume average of the strain derived from the displacement jumps at the imperfect interface. The average strain $\bar{\boldsymbol{\varepsilon}}_r^c$ can be generated in the surrounding matrix cavity by applying $\boldsymbol{\mu}_r^{dq}$ to a perfectly bonded

inhomogeneity. Of course, a perfect bond at all points of the interface may not be reinstated by this application, which cancels only the averages of displacement jump components along the interface (Dvorak and Zhang 2001).

We now proceed to derive a general connection between any pair of field averages $\bar{\boldsymbol{\varepsilon}}_r^c$, $\bar{\boldsymbol{\sigma}}_r^c$ inside the cavity. This task is rather simple when there is complete interfacial separation, which creates a traction free cavity with $\bar{\boldsymbol{\sigma}}_r^c = \mathbf{0}$ and $\bar{\boldsymbol{\varepsilon}}_r^c \neq \mathbf{0}$. The latter can be reproduced in a perfectly bonded inhomogeneity by application of a uniform damage equivalent eigenstrain $\boldsymbol{\mu}_r^{dq} = \boldsymbol{\varepsilon}_r^c$, which yields zero stress average inside Ω_c, as in Sect. 4.4.3.

For the load set $\{\varepsilon_\Omega^0, \boldsymbol{\mu}_r, \boldsymbol{\mu}_0\}$, the strain and stress averages $\boldsymbol{\varepsilon}_r$ and $\boldsymbol{\sigma}_r$ in a perfectly bonded inhomogeneity are given by (4.3.2). By applying an additional uniform eigenstrain $\boldsymbol{\mu}_r^{dq}$ in the inhomogeneity, the local fields in Ω_r remain uniform and become

$$\bar{\boldsymbol{\sigma}}_r^c = \boldsymbol{L}_r(\bar{\boldsymbol{\varepsilon}}_r^c - \boldsymbol{\mu}_r - \boldsymbol{\mu}_r^{dq}) \qquad \bar{\boldsymbol{\varepsilon}}_r^c = \boldsymbol{T}_r\boldsymbol{\varepsilon}_\Omega^0 + \boldsymbol{R}_{rr}(\boldsymbol{\mu}_r + \boldsymbol{\mu}_r^{dq}) + \boldsymbol{R}_{r0}\boldsymbol{\mu}_0 \quad (4.3.25)$$

where $\boldsymbol{\mu}_0$ is the uniform eigenstrain applied in the exterior Ω_0 of Ω_r, and $\boldsymbol{\varepsilon}_\Omega^0$ is the overall strain, both uniform and applied to the large surrounding volume Ω_0 of a comparison medium $\boldsymbol{L}_0$. The eigenstrain concentration factors $\boldsymbol{R}_{rr} = \boldsymbol{T}_r\boldsymbol{P}\boldsymbol{L}_r$ and $\boldsymbol{R}_{r0} = -\boldsymbol{T}_r\boldsymbol{P}\boldsymbol{L}_0$ appear in (4.3.7).

The damage-equivalent eigenstrain is equal to the difference

$$\boldsymbol{\mu}_r^{dq} = \bar{\boldsymbol{\varepsilon}}_r^c - \boldsymbol{M}_r\bar{\boldsymbol{\sigma}}_r^c - \boldsymbol{\mu}_r \quad (4.3.26)$$

where $\bar{\boldsymbol{\sigma}}_r^c$ is average stress derived from the tractions at the imperfect interface. The $\boldsymbol{\mu}_r^{dq}$ is now added to the original load set as $\{\boldsymbol{\varepsilon}_\Omega^0, \boldsymbol{\mu}_r + \boldsymbol{\mu}_r^{dq}, \boldsymbol{\mu}_0\}$ acting on the undamaged composite system.

Since $\boldsymbol{I} - \boldsymbol{R}_{rr} = \boldsymbol{T}_r(\boldsymbol{I} - \boldsymbol{S})$ and $\boldsymbol{M}^* = [(\boldsymbol{I} - \boldsymbol{S})^{-1} - \boldsymbol{I}]\boldsymbol{M}_0 = (\boldsymbol{I} - \boldsymbol{S})^{-1}\boldsymbol{S}\boldsymbol{M}_0$ in (4.3.7) and (4.2.9), the field averages inside the loaded ellipsoidal cavity are connected by

$$\left.\begin{aligned}\bar{\boldsymbol{\varepsilon}}_r^c &= (\boldsymbol{I} - \boldsymbol{S})^{-1}(\boldsymbol{\varepsilon}_\Omega^0 - \boldsymbol{S}\boldsymbol{\mu}_0) - \boldsymbol{M}^*\bar{\boldsymbol{\sigma}}_r^c \\ &= (\boldsymbol{I} - \boldsymbol{S})^{-1}[\boldsymbol{\varepsilon}_\Omega^0 - \boldsymbol{S}(\boldsymbol{\mu}_0 + \boldsymbol{M}_0\bar{\boldsymbol{\sigma}}_r^c)]\end{aligned}\right\} \quad (4.3.27)$$

This extends Hill's constitutive relation (4.2.10) of a uniformly deformed ellipsoidal cavity loaded by interface tractions in equilibrium with $\bar{\boldsymbol{\sigma}}_r^c$, by including the effect of remotely applied uniform overall strain $\boldsymbol{\varepsilon}_\Omega^0$ and uniform matrix eigenstrain $\boldsymbol{\mu}_0$. Notice that both $\bar{\boldsymbol{\varepsilon}}_r^c$ and $\boldsymbol{\mu}_r^{dq}$ depend on $\boldsymbol{L}_r$ only if $\bar{\boldsymbol{\sigma}}_r^c = \bar{\boldsymbol{\sigma}}_r^d = \boldsymbol{L}_r\bar{\boldsymbol{\varepsilon}}_r^d \neq \mathbf{0}$. Otherwise, $\boldsymbol{\mu}_r^{dq}$ is a stress-free strain, independent of $\boldsymbol{L}_r$, that adjusts the local strain to $\bar{\boldsymbol{\varepsilon}}_r^c$.

As one might expect, if $\bar{\boldsymbol{\varepsilon}}_r^c$ is connected to $\bar{\boldsymbol{\sigma}}_r^c = \boldsymbol{L}_r^d\bar{\boldsymbol{\varepsilon}}_r^c$ by a certain damage-induced stiffness $\boldsymbol{L}_r^d$, then (4.3.27) can be reduced to $\bar{\boldsymbol{\varepsilon}}_r^c = \boldsymbol{T}_r{}^d\boldsymbol{\varepsilon}_\Omega^0$ where the $\boldsymbol{T}_r{}^d$ follows from (4.2.12) with $\boldsymbol{L}_r \to \boldsymbol{L}_r^d$. Of course, even if it exists at a particular instant of interface decohesion, the $\boldsymbol{L}_r^d$ may not be easily computed. In contrast,

evaluation of the average damage-equivalent eigenstrain $\boldsymbol{\mu}_r^{dq} = \bar{\boldsymbol{\varepsilon}}_r^c - \bar{\boldsymbol{\varepsilon}}_r^d$ requires only integration of displacement jumps along the imperfect interface, according to (3.4.5). In this manner, the contribution of displacement jumps at imperfect interfaces to both cavity and overall strains in composite aggregates can be easily evaluated, the latter using the Levin formula $(3.8.11)_2$, where $\boldsymbol{B}_r$ or $\boldsymbol{W}_r$ are taken for a perfectly bonded inhomogeneity.

Notice that the $\boldsymbol{\mu}_r^{eq}$ in the equivalent inclusion method in Sects. 4.2 and 4.3.2 is introduced in a homogeneous solid to simulate an inhomogeneity, while the present damage-equivalent eigenstrain is applied to a perfectly bonded heterogeneous system.

For *cavities or voids*, the results show that in the absence of interface tractions, at $\bar{\boldsymbol{\sigma}}_r^c \to \boldsymbol{0}$, the $\boldsymbol{\mu}_r^{dq}$ transforms a perfectly bonded inhomogeneity $\boldsymbol{L}_r$ such that its average strain $\bar{\boldsymbol{\varepsilon}}_r = \bar{\boldsymbol{\varepsilon}}_r^c$, the traction-free cavity strain. The same result follows if an ellipsoidal cavity in Ω_r is regarded as an inhomogeneity with vanishing stiffness, at $\boldsymbol{L}_r \to \boldsymbol{0}, \boldsymbol{T}_r \to (\boldsymbol{I} - \boldsymbol{P}\boldsymbol{L}_0)^{-1}$, at $\boldsymbol{R}_{rr} \to \boldsymbol{0}, \boldsymbol{R}_{r0} \to -(\boldsymbol{I} - \boldsymbol{S})^{-1}\boldsymbol{S}$ in (4.2.13), (4.3.7), so that the average cavity strain agrees with (4.3.27)

$$\bar{\boldsymbol{\varepsilon}}_r^c = (\boldsymbol{I} - \boldsymbol{S})^{-1}(\boldsymbol{\varepsilon}_\Omega^0 - \boldsymbol{S}\boldsymbol{\mu}_0) \qquad \bar{\boldsymbol{\sigma}}_r^c = \boldsymbol{0} \tag{4.3.28}$$

Next, *for the load set* $\{\boldsymbol{\sigma}_\Omega^0, \boldsymbol{\lambda}_r, \boldsymbol{\lambda}_0\}$ we write the field averages in the imperfectly bonded inhomogeneity $\boldsymbol{L}_r$ in terms of a damage-equivalent eigenstress $\boldsymbol{\lambda}_r^{dq} = -\boldsymbol{L}_r\boldsymbol{\mu}_r^{dq}$.

$$\bar{\boldsymbol{\varepsilon}}_r^c = \boldsymbol{M}_r(\bar{\boldsymbol{\sigma}}_r^c - \boldsymbol{\lambda}_r - \boldsymbol{\lambda}_r^{dq}) \quad \bar{\boldsymbol{\sigma}}_r^c = \boldsymbol{W}_r\boldsymbol{\sigma}_\Omega^0 + \boldsymbol{N}_{rr}(\boldsymbol{\lambda}_r + \boldsymbol{\lambda}_r^{dq}) + \boldsymbol{N}_{r0}\boldsymbol{\lambda}_0 \tag{4.3.29}$$

where $\boldsymbol{N}_{rr} = \boldsymbol{W}_r\boldsymbol{Q}\boldsymbol{M}_r, \boldsymbol{N}_{r0} = -\boldsymbol{W}_r\boldsymbol{Q}\boldsymbol{M}_0$ from (4.3.8). The $\boldsymbol{Q}$ and $\boldsymbol{W}_r$ matrices are given by (4.2.9) and (4.2.13). Since $\boldsymbol{\mu}_0 = -\boldsymbol{M}_0\boldsymbol{\lambda}_0$, (4.3.29) provides

$$\boldsymbol{M}_r(\boldsymbol{\lambda}_r + \boldsymbol{\lambda}_r^{dq}) = -(\boldsymbol{I} - \boldsymbol{S})^{-1}\boldsymbol{M}_0\boldsymbol{\sigma}_\Omega^0 + \boldsymbol{M}_0\boldsymbol{\lambda}_0 + (\boldsymbol{M}^* + \boldsymbol{M}_r)\bar{\boldsymbol{\sigma}}_r^c \tag{4.3.30}$$

and

$$\left.\begin{aligned}\bar{\boldsymbol{\varepsilon}}_r^c &= (\boldsymbol{I} - \boldsymbol{S})^{-1}\boldsymbol{M}_0\boldsymbol{\sigma}_\Omega^0 - \boldsymbol{M}_0\boldsymbol{\lambda}_0 - \boldsymbol{M}^*\bar{\boldsymbol{\sigma}}_r^c \\ &= (\boldsymbol{I} - \boldsymbol{S})^{-1}[\boldsymbol{M}_0\boldsymbol{\sigma}_\Omega^0 - \boldsymbol{S}\boldsymbol{M}_0\bar{\boldsymbol{\sigma}}_r^c] - \boldsymbol{M}_0\boldsymbol{\lambda}_0\end{aligned}\right\} \tag{4.3.31}$$

In a large volume $\Omega \gg \Omega_r$, a small transformed inhomogeneity or cavity has a negligible effect on the overall strain. Therefore, both (4.3.27) and (4.3.31) predict the same cavity strain under the distinct overall mechanical loads. In a *traction-free cavity*, $\bar{\boldsymbol{\sigma}}_r^c \to \boldsymbol{0}$

$$\bar{\boldsymbol{\varepsilon}}_r^c = (\boldsymbol{I} - \boldsymbol{S})^{-1}\boldsymbol{M}_0\boldsymbol{\sigma}_\Omega^0 - \boldsymbol{M}_0\boldsymbol{\lambda}_0 \qquad \bar{\boldsymbol{\sigma}}_r^c = \boldsymbol{0} \tag{4.3.32}$$

which agrees with (4.3.28).

4.4 Dilute Approximation of Overall Properties and Local Fields

The results for a single inhomogeneity $\boldsymbol{L}_r$ can be utilized to estimate overall properties of a representative volume V of a statistically homogeneous composite aggregate containing a very low concentration of inhomogeneities and/or cavities, not exceeding about 5%. The 'matrix' or comparison medium $\boldsymbol{L}_0$ is now replaced by the actual matrix phase $r = 1$ with stiffness $\boldsymbol{L}_1$. The inhomogeneities or reinforcements are phases $r = 2,\ 3,\ \ldots\ n$, having stiffnesses $\boldsymbol{L}_r$ and volume fractions c_r, which satisfy

$$c_1 = 1 - \sum\nolimits_{r=2}^{n} c_r \quad \sum\nolimits_{r=2}^{n} c_r = \sum\nolimits_{r=2}^{n} V_r / V \ll 1 \tag{4.4.1}$$

In the dilute approximation, each inhomogeneity interacts only with the matrix, but not with other inhomogeneities. However, the average strain $\Sigma_{s=1}^{n}(c_s \boldsymbol{\varepsilon}_s) = \boldsymbol{\varepsilon}^0$ or stress $\Sigma_{s=1}^{n}(c_s \boldsymbol{W}_s) = \boldsymbol{\sigma}^0$ in the entire volume are not necessarily equal to their matrix averages, hence $\Sigma_{s=1}^{n}(c_s \boldsymbol{T}_s) = \Sigma_{s=1}^{n}(c_s \boldsymbol{W}_s) \equiv \boldsymbol{I}$, and the actual magnitude of $\boldsymbol{T}_1$ or $\boldsymbol{W}_1$ follows from this identity. In fact, $\boldsymbol{T}_1 = \boldsymbol{I}$ only when all inhomogeneities $r \geq 2$ are rigid, and $\boldsymbol{W}_1 = \boldsymbol{I}$ when all $r \geq 2$ are traction-free cavities, voids or cracks. That is illustrated by the examples in Sect. 4.4.4.

The advantage of this method is that each inhomogeneity may have a different ellipsoidal shape and alignment, which indicate the corresponding forms of the tensors $\boldsymbol{P}_r = (\boldsymbol{L}_r^* + \boldsymbol{L}_1)^{-1}$ and $\boldsymbol{Q}_r = (\boldsymbol{M}_r^* + \boldsymbol{M}_1)^{-1}$ in (4.2.9), all evaluated in the matrix $\boldsymbol{L}_1$ for each shape, $r = 2,\ 3,\ \ldots\ n$. That is demonstrated by (4.4.6).

4.4.1 Overall Strain $\boldsymbol{\varepsilon}^0$ and Phase Eigenstrains $\boldsymbol{\mu}_1,\ \boldsymbol{\mu}_r$ Are Prescribed

Overall properties are obtained using the procedure described in Sect. 3.5. Suppose that the composite aggregate is loaded by the load set $\{\boldsymbol{\varepsilon}^0, \boldsymbol{\mu}_1, \boldsymbol{\mu}_r\}$, where the overall strain $\boldsymbol{\varepsilon}^0$ and the phase eigenstrains are all uniform. Local field averages for $r \geq 2$ are written by referring to (4.3.2), where we retain the concentration factors $\boldsymbol{T}_r$, $\boldsymbol{R}_{rr}$ and change the $\boldsymbol{R}_{r0}$ to $\boldsymbol{R}_{r1} = -\boldsymbol{T}_r \boldsymbol{P}_r \boldsymbol{L}_1$, and let $\boldsymbol{P}_r = \boldsymbol{S}_r \boldsymbol{L}_1^{-1}$. The phase fields are

$$\left.\begin{aligned} \boldsymbol{\varepsilon}_1 = \tfrac{1}{c_1}\left[\boldsymbol{\varepsilon}^0 - \sum_{r=2}^{n} c_r \boldsymbol{\varepsilon}_r\right] \quad \boldsymbol{\sigma}_1 = \boldsymbol{L}_1(\boldsymbol{\varepsilon}_1 - \boldsymbol{\mu}_1) \\ \boldsymbol{\varepsilon}_r = \boldsymbol{T}_r \boldsymbol{\varepsilon}^0 + \boldsymbol{R}_{r1}\boldsymbol{\mu}_1 + \boldsymbol{R}_{rr}\boldsymbol{\mu}_r \quad \boldsymbol{\sigma}_r = \boldsymbol{L}_r(\boldsymbol{\varepsilon}_r - \boldsymbol{\mu}_r) = \boldsymbol{L}_r \boldsymbol{\varepsilon}_r + \boldsymbol{\lambda}_r \quad r \geq 2 \end{aligned}\right\} \tag{4.4.2}$$

where $\boldsymbol{\lambda}_r = -\boldsymbol{L}_r\boldsymbol{\mu}_r$, and

$$\boldsymbol{T}_1 = \frac{1}{c_1}\left[\boldsymbol{I} - \sum_{r=2}^{n} c_r\boldsymbol{T}_r\right] \quad \boldsymbol{T}_r = [\boldsymbol{I} + \boldsymbol{P}_r(\boldsymbol{L}_r - \boldsymbol{L}_1)]^{-1} \tag{4.4.3}$$

$$\boldsymbol{R}_{r1} = -\boldsymbol{T}_r\boldsymbol{P}_r\boldsymbol{L}_1 \quad \boldsymbol{R}_{rr} = \boldsymbol{T}_r\boldsymbol{P}_r\boldsymbol{L}_r \tag{4.4.4}$$

Notice that the local strain average (4.4.2) in any inhomogeneity $\boldsymbol{L}_r$ depends only on the phase and matrix stiffness, and is thus independent of the volume fractions and stiffness of the other inhomogeneities that may be present in the dilutely reinforced composite. This agrees with the initial assumption that each inhomogeneity interacts only with the matrix but not with other inhomogeneities. The concentration factors satisfy $\boldsymbol{T}_r + \boldsymbol{R}_{r1} + \boldsymbol{R}_{rr} = \boldsymbol{I}$, hence the aggregate undergoes uniform deformation when the strains $\boldsymbol{\varepsilon}^0$, $\boldsymbol{\mu}_1$, $\boldsymbol{\mu}_r$ are of the same magnitude.

Overall stress caused by the applied overall strain and by the phase eigenstrains can be obtained as in (3.10.3), with $\boldsymbol{A}_r \to \boldsymbol{T}_r$

$$\sum_{s=1}^{n} c_s\boldsymbol{\sigma}_s = \bar{\boldsymbol{\sigma}} = \boldsymbol{L}\boldsymbol{\varepsilon}^0 + \bar{\boldsymbol{\lambda}} \quad \bar{\boldsymbol{\lambda}} = -\sum_{s=1}^{n} c_s\boldsymbol{T}_s^{\mathrm{T}}\boldsymbol{L}_s\boldsymbol{\mu}_s \tag{4.4.5}$$

where $\bar{\boldsymbol{\lambda}} = -\boldsymbol{L}\,\bar{\boldsymbol{\mu}}$ is the overall eigenstress (3.8.12), and $\bar{\boldsymbol{\mu}}$ is the overall eigenstrain. Overall stiffness of the aggregate follows from (3.5.8), (4.4.1) and (4.4.3) as

$$\left.\begin{aligned} \boldsymbol{L} &= c_1\boldsymbol{L}_1\boldsymbol{T}_1 + \sum_{r=2}^{n} c_r\boldsymbol{L}_r\boldsymbol{T}_r = \boldsymbol{L}_1\left(\boldsymbol{I} - \sum_{r=2}^{n} c_r\boldsymbol{T}_r\right) + \sum_{r=2}^{n} c_r\boldsymbol{L}_r\boldsymbol{T}_r \\ &= \boldsymbol{L}_1 + \sum_{r=2}^{n} c_r(\boldsymbol{L}_r - \boldsymbol{L}_1)\boldsymbol{T}_r = \boldsymbol{L}_1 + \sum_{r=2}^{n} c_r[\boldsymbol{P}_r + (\boldsymbol{L}_r - \boldsymbol{L}_1)^{-1}]^{-1} = \boldsymbol{L}^{\mathrm{T}} \end{aligned}\right\} \tag{4.4.6}$$

4.4.2 *Overall Stress $\boldsymbol{\sigma}^0$ and Phase Eigenstresses $\boldsymbol{\lambda}_1$, $\boldsymbol{\lambda}_r$ Are Prescribed*

Under the load set $\{\boldsymbol{\sigma}^0, \boldsymbol{\lambda}_1, \boldsymbol{\lambda}_r\}$, the stress field averages in the matrix $\boldsymbol{L}_1$ and inhomogeneities $\boldsymbol{L}_r$, $r = 2, .3...n$ are

$$\left.\begin{aligned} \boldsymbol{\sigma}_1 &= \frac{1}{c_1}\left[\boldsymbol{\sigma}^0 - \sum_{r=2}^{n} c_r\boldsymbol{\sigma}_r\right] \quad \boldsymbol{\varepsilon}_1 = \boldsymbol{M}_1(\boldsymbol{\sigma}_1 - \boldsymbol{\lambda}_1) \\ \boldsymbol{\sigma}_r &= \boldsymbol{W}_r\boldsymbol{\sigma}^0 + \boldsymbol{N}_{r1}\boldsymbol{\lambda}_1 + \boldsymbol{N}_{rr}\boldsymbol{\lambda}_r \quad \boldsymbol{\varepsilon}_r = \boldsymbol{M}_r(\boldsymbol{\sigma}_r - \boldsymbol{\lambda}_r) = \boldsymbol{M}_r\boldsymbol{\sigma}_r + \boldsymbol{\mu}_r \end{aligned}\right\} \tag{4.4.7}$$

where $\boldsymbol{\mu}_r = -\boldsymbol{M}_r\boldsymbol{\lambda}_r$, $\boldsymbol{W}_r + \boldsymbol{N}_{r1} + \boldsymbol{N}_{rr} = \boldsymbol{I}$ and

$$\boldsymbol{W}_1 = \frac{1}{c_1}\left[\boldsymbol{I} - \sum_{r=2}^{n} c_r \boldsymbol{W}_r\right] \quad \boldsymbol{W}_r = [\boldsymbol{I} + \boldsymbol{Q}_r(\boldsymbol{M}_r - \boldsymbol{M}_1)]^{-1} \tag{4.4.8}$$

$$\boldsymbol{N}_{r1} = -\boldsymbol{W}_r\boldsymbol{Q}_r\boldsymbol{M}_1 \quad \boldsymbol{N}_{rr} = \boldsymbol{W}_r\boldsymbol{Q}_r\boldsymbol{M}_r \tag{4.4.9}$$

Again, the strain average in each inhomogeneity $r \geq 2$ depends only on $\boldsymbol{Q}$ and on the compliances $\boldsymbol{M}_r$ and $\boldsymbol{M}_1$; it is not influenced by the presence of other inhomogeneities $s \neq r$.

Overall strain caused by the loads $\boldsymbol{\sigma}^0$, $\boldsymbol{\mu}_1$, $\boldsymbol{\mu}_r$ is found using (3.10.6), as

$$\sum_{s=1}^{n} c_s\boldsymbol{\varepsilon}_s = \bar{\boldsymbol{\varepsilon}} = \boldsymbol{M}\boldsymbol{\sigma}^0 + \bar{\boldsymbol{\mu}} = \boldsymbol{M}\boldsymbol{\sigma}^0 + \sum_{s=1}^{n} c_s\boldsymbol{W}_s{}^{\mathrm{T}}\boldsymbol{\mu}_s \tag{4.4.10}$$

The overall compliance is

$$\left.\begin{aligned} \boldsymbol{M} &= c_1\boldsymbol{M}_1\boldsymbol{W}_1 + \sum_{r=2}^{n} c_r\boldsymbol{M}_r\boldsymbol{W}_r = \boldsymbol{M}_1 + \sum_{r=2}^{n} c_r(\boldsymbol{M}_r - \boldsymbol{M}_1)\boldsymbol{W}_r \\ &= \boldsymbol{M}_1 + \sum_{r=2}^{n} c_r[\boldsymbol{Q}_r + (\boldsymbol{M}_r - \boldsymbol{M}_1)^{-1}]^{-1} = \boldsymbol{M}^{\mathrm{T}} \end{aligned}\right\} \tag{4.4.11}$$

Identities $\Sigma_{s=1}^{n}(c_s\boldsymbol{T}_s) = \Sigma_{s=1}^{n}(c_s\boldsymbol{W}_s) = \boldsymbol{I}$, and connections (4.2.5) with $\boldsymbol{L}_0 = \boldsymbol{L}_1$, show that the overall properties are consistent

$$\begin{aligned} \boldsymbol{M} &= \sum_{s=1}^{n} c_s\boldsymbol{M}_s\boldsymbol{W}_s\left(\sum_{s=1}^{n} c_s\boldsymbol{W}_s\right)^{-1} \\ &= \sum_{s=1}^{n} c_s\boldsymbol{T}_s\boldsymbol{M}_1\left(\sum_{s=1}^{n} c_s\boldsymbol{L}_s\boldsymbol{T}_s\boldsymbol{M}_1\right)^{-1} = \left(\sum_{s=1}^{n} c_s\boldsymbol{L}_s\boldsymbol{T}_s\right)^{-1} = \boldsymbol{L}^{-1} \end{aligned} \tag{4.4.12}$$

Moreover, definitions of local field averages in $(4.4.2)_3$ and $(4.4.7)_3$ suggest that

$$\left.\begin{aligned} \boldsymbol{\varepsilon}_r &= \boldsymbol{T}_r\boldsymbol{\varepsilon}^0 = \boldsymbol{T}_r\boldsymbol{M}\boldsymbol{\sigma}^0 = \boldsymbol{M}_r\boldsymbol{\sigma}_r = \boldsymbol{M}_r\boldsymbol{W}_r\boldsymbol{\sigma}^0 \Rightarrow \boldsymbol{T}_r\boldsymbol{M} = \boldsymbol{M}_r\boldsymbol{W}_r \\ \boldsymbol{\sigma}_r &= \boldsymbol{W}_r\boldsymbol{\sigma}^0 = \boldsymbol{W}_r\boldsymbol{L}\boldsymbol{\varepsilon}^0 = \boldsymbol{L}_r\boldsymbol{\varepsilon}_r = \boldsymbol{L}_r\boldsymbol{T}_r\boldsymbol{\varepsilon}^0 \Rightarrow \boldsymbol{W}_r\boldsymbol{L} = \boldsymbol{L}_r\boldsymbol{T}_r \end{aligned}\right\} \tag{4.4.13}$$

Application of these connections in Levin formula for the overall transformation fields in (4.4.5) and (4.4.10) shows that those fields are also consistent.

$$\bar{\boldsymbol{\lambda}} = \sum_{r=1}^{n} c_r\boldsymbol{T}_r{}^{\mathrm{T}}\boldsymbol{\lambda}_r = -\sum_{r=1}^{n} c_r\boldsymbol{T}_r{}^{\mathrm{T}}\boldsymbol{L}_r\boldsymbol{\mu}_r = -\sum_{r=1}^{n} c_r\boldsymbol{L}\boldsymbol{W}_r{}^{\mathrm{T}}\boldsymbol{\mu}_r = -\boldsymbol{L}\bar{\boldsymbol{\mu}} \tag{4.4.14}$$

Equations (4.4.6) and (4.4.11) provide reliable estimates of overall properties of matrix-based composite aggregates which have added phases in very low concentrations.

4.4.3 *Debonded Inhomogeneities Creating Traction-Free Cavities*

Consider again an aggregate with dilute reinforcements $\boldsymbol{L}_r$ in matrix $\boldsymbol{L}_1$. A certain volume fraction c_d of originally bonded inhomogeneities $\boldsymbol{L}_2$ now undergoes complete decohesion from the matrix. That changes the overall compliance $\boldsymbol{M} \to \boldsymbol{M}_d$, which is evaluated next by two procedures. One adjusts the compliance by assigning vanishing stiffness to the volume fraction c_d of cavities. The second procedure simulates presence of these cavities by inducing a damage equivalent eigenstrain in the volume fraction c_d of inhomogeneities $\boldsymbol{L}_2$, while the aggregate remains perfectly bonded, as explained in Sect. 4.3.4. For simplicity, all inhomogeneities $\boldsymbol{L}_2$ are assumed to have the same shape and alignment, described by a single matrix $\boldsymbol{Q}$.

In preparation for the first procedure, notice that for any $\boldsymbol{L}_r \to \boldsymbol{0}$, the term $(\boldsymbol{M}_r - \boldsymbol{M}_1)\boldsymbol{W}_r = [(\boldsymbol{M}_r - \boldsymbol{M}_1)^{-1} + \boldsymbol{Q}]^{-1} \to \boldsymbol{Q}^{-1}$. Then, the presence of c_d cavities changes the overall compliance (4.4.11) to its damage-modified form

$$\left.\begin{aligned} \boldsymbol{M}_d &= \boldsymbol{M}_1 + (c_2 - c_d)(\boldsymbol{M}_2 - \boldsymbol{M}_1)\boldsymbol{W}_2 + c_d \boldsymbol{Q}^{-1} \\ &= \boldsymbol{M}_1 + c_2(\boldsymbol{M}_2 - \boldsymbol{M}_1)\boldsymbol{W}_2 + c_d[\boldsymbol{Q}^{-1} - (\boldsymbol{M}_2 - \boldsymbol{M}_1)\boldsymbol{W}_2] \\ &= \boldsymbol{M} + c_d \boldsymbol{Q}^{-1}[\boldsymbol{W}_2{}^{-1} - \boldsymbol{Q}(\boldsymbol{M}_2 - \boldsymbol{M}_1)]\boldsymbol{W}_2 \\ &= \boldsymbol{M} + c_d \boldsymbol{Q}^{-1}\boldsymbol{W}_2 \end{aligned}\right\} \tag{4.4.15}$$

where $\boldsymbol{W}_2$ follows from (4.4.8). The overall strain caused by application of the uniform overall stress $\boldsymbol{\sigma}^0$ is

$$\bar{\boldsymbol{\varepsilon}}_d = \boldsymbol{M}_d \boldsymbol{\sigma}^0 = (\boldsymbol{M} + c_d \boldsymbol{Q}^{-1}\boldsymbol{W}_2)\boldsymbol{\sigma}^0. \tag{4.4.16}$$

In the second procedure, the entire aggregate remains perfectly bonded. The traction free cavities are simulated by introducing in the volume fraction $c_d \leq c_2$ of inhomogeneities $\boldsymbol{L}_2$ a damage-equivalent eigenstrain $\boldsymbol{\mu}_2^{dq} = -\boldsymbol{M}_2 \boldsymbol{\lambda}_2^{dq}$ derived from (4.3.30), with $\boldsymbol{\lambda}_0 = \boldsymbol{0}$, $\bar{\boldsymbol{\sigma}}_2^d = \boldsymbol{0}$, $\boldsymbol{\sigma}_\Omega = \boldsymbol{\sigma}^0$ and $\boldsymbol{M}_0 = \boldsymbol{M}_1$.

$$\boldsymbol{\mu}_2^{dq} = (\boldsymbol{I} - \boldsymbol{S})^{-1}\boldsymbol{M}_1\boldsymbol{\sigma}^0 = \boldsymbol{Q}^{-1}\boldsymbol{\sigma}^0 \tag{4.4.17}$$

The overall damage-equivalent eigenstrain follows from Levin's formula as

$$\bar{\boldsymbol{\mu}}^{dq} = c_d \boldsymbol{W}_2{}^{\mathrm{T}} \boldsymbol{\mu}_2^{dq} = c_d \boldsymbol{W}_2{}^{\mathrm{T}} \boldsymbol{Q}^{-1}\boldsymbol{\sigma}^0 = c_d \boldsymbol{Q}^{-1}\boldsymbol{W}_2\boldsymbol{\sigma}^0 \tag{4.4.18}$$

with $\boldsymbol{W}_2{}^{\mathrm{T}}\boldsymbol{Q}^{-1} = \boldsymbol{Q}^{-1}\boldsymbol{W}_2$ from (4.2.15). The overall strain caused by the applied stress $\boldsymbol{\sigma}^0$ and by $\bar{\boldsymbol{\mu}}_r^{dq}$ is

$$\left.\begin{aligned}\bar{\boldsymbol{\varepsilon}}_d &= \boldsymbol{M}\boldsymbol{\sigma}^0 + \bar{\boldsymbol{\mu}}_r^{dq} = \boldsymbol{M}\boldsymbol{\sigma}^0 + c_d\,\boldsymbol{Q}^{-1}\boldsymbol{W}_2\boldsymbol{\sigma}^0 \\ &= (\boldsymbol{M} + c_d\,\boldsymbol{Q}^{-1}\boldsymbol{W}_2)\boldsymbol{\sigma}^0 = \boldsymbol{M}_d\boldsymbol{\sigma}^0\end{aligned}\right\} \tag{4.4.19}$$

This shows that the damage equivalent eigenstrain generates the same change in the overall strain as does the damage-modified overall compliance $\boldsymbol{M}_d$ in (4.4.15). Moreover, since $\boldsymbol{W}_2 = [\boldsymbol{I} + \boldsymbol{Q}(\boldsymbol{M}_2 + \boldsymbol{M}_1)]^{-1}$ there is $\boldsymbol{M}_d = \boldsymbol{M}_d^{\mathrm{T}}$ (4.4.17).

It should be emphasized that the damage-equivalent eigenstrain should be used if and only if the overall strain change is caused by complete decohesion, from a perfect bond to cavities. The technique may also be used during partial decohesion, but only if the interface integral of the displacement jumps and tractions is evaluated by a finite element or by another independent method, and then converted into a damage equivalent eigenstrain using (3.4.5).

4.4.4 *Applications to Particulate Suspensions and Porous Media*

One of the earliest applications of the dilute approximation is the Einstein's formula, for the effective viscosity of a *dilute suspension* of rigid particles, $r = 2$, with volume fraction $c_2 \ll 1$, in an incompressible viscous fluid $r = 1$ (Einstein 1905). To arrive at the result, let us first solve a more general problem: Derive the stiffness, compliance and local fields in a dilute mixture of elastic particles with known stiffness $\boldsymbol{L}_2$ in a matrix $\boldsymbol{L}_1$. Suppose that the mixture is subjected to a uniform overall strain $\boldsymbol{\varepsilon}^0$ and, to illustrate applications of the results found in Sect. 4.4.1, to a uniform change in temperature $\Delta\theta$, which causes the thermal eigenstrains $\boldsymbol{\mu}_1 = \boldsymbol{m}_1\Delta\theta$ in the matrix and $\boldsymbol{\mu}_2 = \boldsymbol{m}_2\Delta\theta$ in the particles. Thermal strain vectors of the isotropic phases are $\boldsymbol{m}_r = [\alpha^{(r)}, \alpha^{(r)}, \alpha^{(r)}, 0, 0, 0]^{\mathrm{T}}$ for $r = 1, 2$, where $\alpha^{(r)}$ is the linear coefficient of thermal expansion.

Overall stiffness and compliance of the suspension can be written using (4.4.6), and (2.2.29), in terms of the as yet unknown overall moduli G and K, and the projection matrices $\boldsymbol{J}$ and $\boldsymbol{K}$ in Sect. 2.2.9 and (1.1.19).

$$\boldsymbol{L} = \boldsymbol{L}_1 + c_2(\boldsymbol{L}_2 - \boldsymbol{L}_1)\boldsymbol{T}_2 = 3K\boldsymbol{J} + 2G\boldsymbol{K} \quad \boldsymbol{M} = \frac{1}{3K}\boldsymbol{J} + \frac{1}{2G}\boldsymbol{K} \tag{4.4.20}$$

where phase volume fractions $c_1 + c_2 = 1$, $c_2 \ll 1$. Constitutive relations of the phases are

$$\boldsymbol{L}_r = 3K_r\boldsymbol{J} + 2G_r\boldsymbol{K} \qquad \boldsymbol{L}_r^{-1} = \boldsymbol{M}_r = \frac{1}{3K_r}\boldsymbol{J} + \frac{1}{2G_r}\boldsymbol{K} \tag{4.4.21}$$

and K_r and G_r are known phase moduli. The strain concentration factor (4.4.3) of the inhomogeneities is $\boldsymbol{T}_2 = [\boldsymbol{I} + \boldsymbol{P}(\boldsymbol{L}_2 - \boldsymbol{L}_1)]^{-1}$, where the $\boldsymbol{P}$ matrix for a spherical inclusion is assembled using the constraint tensors (4.2.11) in (4.2.9). Coefficients $P_{\alpha\beta}$, written in the contracted tensorial notation, are

$$\left.\begin{aligned} \boldsymbol{P} &= \frac{1}{3K_1 + 4G_1}\boldsymbol{J} + \frac{3(K_1 + 2G_1)}{5G_1(3K_1 + 4G_1)}\boldsymbol{K} \\ \boldsymbol{P}^{-1} &= (3K_1 + 4G_1)\boldsymbol{J} + \frac{5G_1(3K_1 + 4G_1)}{3(K_1 + 2G_1)}\boldsymbol{K} \end{aligned}\right\} \tag{4.4.22}$$

The result also appears later in (4.6.3). The strain concentration factors can now be written in an expanded form

$$\left.\begin{aligned} &\boldsymbol{T}_1 = \frac{1}{c_1}[\boldsymbol{I} - c_2\boldsymbol{T}_2] \\ &\boldsymbol{T}_2 = [\boldsymbol{I} + \boldsymbol{P}(\boldsymbol{L}_2 - \boldsymbol{L}_1)]^{-1} = \left[1 + \frac{3\Delta K}{3K_1 + 4G_1}\right]^{-1}\boldsymbol{J} + \left[1 + \frac{6\Delta G(K_1 + 2G_1)}{5G_1(3K_1 + 4G_1)}\right]^{-1}\boldsymbol{K} \end{aligned}\right\} \tag{4.4.23}$$

where

$$\boldsymbol{L}_2 - \boldsymbol{L}_1 = 3(K_2 - K_1)\boldsymbol{J} + 2(G_2 - G_1)\boldsymbol{K} = 3\Delta K\boldsymbol{J} + 2\Delta G\boldsymbol{K} \tag{4.4.24}$$

Overall stiffness of the particulate mixture follows from (4.4.20)

$$\left.\begin{aligned} &\boldsymbol{L} = \boldsymbol{L}_1 + c_2(\boldsymbol{L}_2 - \boldsymbol{L}_1)\boldsymbol{T}_2 = \boldsymbol{L}_1 + c_2\Big[\boldsymbol{P} + (\boldsymbol{L}_2 - \boldsymbol{L}_1)^{-1}\Big]^{-1} \\ &= 3\left\{K_1 + c_2\Delta K\frac{3K_1 + 4G_1}{3K_2 + 4G_1}\right\}\boldsymbol{J} + 2\left\{G_1 + c_2\Delta G\left[1 + \frac{6\Delta G(K_1 + 2G_1)}{5G_1(3K_1 + 4G_1)}\right]^{-1}\right\}\boldsymbol{K} \end{aligned}\right\} \tag{4.4.25}$$

The terms in curly brackets are the overall bulk and shear moduli, obtained as a sum of the separate contributions of the matrix and particle moduli. Notice that the contribution of the particles to the overall moduli is introduced only through the ΔK and ΔG from (4.4.23).

Total strain fields caused in the two phases by the mechanical overall strain $\boldsymbol{\varepsilon}^0$ and temperature change $\Delta\theta$ follow from (4.4.2) and (4.3.10) as

$$\left.\begin{aligned} &\boldsymbol{\varepsilon}_1 = \frac{1}{c_1}\left[\boldsymbol{\varepsilon}^0 - c_2\boldsymbol{\varepsilon}_2\right] \quad \boldsymbol{\sigma}_1 = \boldsymbol{L}_1(\boldsymbol{\varepsilon}_1 - \boldsymbol{m}_1\Delta\theta) \\ &\boldsymbol{\varepsilon}_2 = \boldsymbol{T}_2\boldsymbol{\varepsilon}^0 + (\boldsymbol{R}_{21}\boldsymbol{m}_1 + \boldsymbol{R}_{22}\boldsymbol{m}_2)\Delta\theta = \boldsymbol{T}_2[\boldsymbol{\varepsilon}^0 - \boldsymbol{P}(\boldsymbol{L}_1\boldsymbol{m}_1 - \boldsymbol{L}_2\boldsymbol{m}_2)\Delta\theta] \\ &\boldsymbol{\sigma}_2 = \boldsymbol{L}_2(\boldsymbol{\varepsilon}_2 - \boldsymbol{m}_2\Delta\theta) \end{aligned}\right\} \tag{4.4.26}$$

The eigenstrain concentration factors were derived in (4.4.4) as

$$\boldsymbol{R}_{21} = -\boldsymbol{T}_2\boldsymbol{P}\boldsymbol{L}_1 \quad \boldsymbol{R}_{22} = \boldsymbol{T}_2\boldsymbol{P}\boldsymbol{L}_2 \tag{4.4.27}$$

and they can be constructed from (4.4.22, 4.4.23), by multiplication of the relevant coefficients of the $\boldsymbol{J}$ and $\boldsymbol{K}$ matrices. Numerical evaluation of phase strains is simplified by recalling that both thermal strains are isotropic, which suggests that $\boldsymbol{K}\boldsymbol{m}_r\Delta\theta = \boldsymbol{0}$. Therefore, only the coefficient of $\boldsymbol{J}$ in (4.4.26) will appear in evaluation of the phase strains, which is left for an exercise. Overall eigenstress is found from (4.4.5)

$$\bar{\boldsymbol{\lambda}} = -\boldsymbol{L}\boldsymbol{m}\Delta\theta = -(c_1\boldsymbol{T}_1{}^{\mathrm{T}}\boldsymbol{L}_1\boldsymbol{m}_1 + c_2\boldsymbol{T}_2{}^{\mathrm{T}}\boldsymbol{L}_2\boldsymbol{m}_2)\Delta\theta \tag{4.4.28}$$

where for spherical inhomogeneities $\boldsymbol{T}_r{}^{\mathrm{T}} = \boldsymbol{T}_r$ according to (4.4.24). The overall thermal strain vector is $\boldsymbol{m} = [\alpha, \alpha, \alpha, 0, 0, 0]^{\mathrm{T}}$, where α is the overall linear coefficient of thermal expansion. Overall stress caused by application of $\boldsymbol{\varepsilon}^0$ and $\Delta\theta$ is $\bar{\boldsymbol{\sigma}} = \boldsymbol{L}\boldsymbol{\varepsilon}^0 + \bar{\boldsymbol{\lambda}}$, where the overall stiffness is derived in (4.4.25).

Einstein's (1905) formula estimates the effective viscosity of a suspension of rigid particles in a viscous, incompressible fluid. An analogous elasticity solution is obtained by replacing the fluid viscosity coefficient with the matrix shear modulus G_1, and by letting $K_1 \to \infty$. Moduli of the rigid particles are unbounded, $G_2 \to \infty$, $K_2 \to \infty$. Since both phases are incompressible, there is no overall volume change and the overall bulk modulus is also unbounded, $K \to \infty$, and the Poisson's ratio $\nu \to 0.5$. The multiplier of $\boldsymbol{J}$ in (4.4.25), equal to $3K_r$, becomes unbounded. However, the overall shear modulus G is finite. By letting $\Delta G \to \infty$ in the multiplier of $\boldsymbol{K}$ in (4.4.25) and then taking the limit of the remainder at $K_1 \to \infty$, we find that

$$2G = 2G_1 + \lim_{K_1\to\infty}\left[c_2\frac{5G_1(3K_1+4G_1)}{3(K_1+2G_1)}\right] = 2G_1\left[1+\frac{5}{2}c_2\right] \tag{4.4.29}$$

which is analogous to the Einstein's formula for effective viscosity the suspension. Overall Young's modulus $E = 3G$.

Another application of (4.4.23, 4.4.24, 4.4.25, 4.4.26, 4.4.27, 4.4.28) is to a *porous medium,* a matrix which contains a small volume fraction of spherical cavities $r = 2$. If the cavities are traction-free, then $\Delta K \to -K_1$ and $\Delta G \to -G_1$ in (4.4.24), and the overall stiffness assumes the form that reveals their weakening effect.

$$\boldsymbol{L} = 3K_1\left[1 - c_2\frac{3K_1+4G_1}{4G_1}\right]\boldsymbol{J} + 2G_1\left[1 - c_2\frac{5(3K_1+4G_1)}{9K_1+8G_1}\right]\boldsymbol{K} \tag{4.4.30}$$

When the matrix is incompressible, the overall bulk modulus is also unbounded, while the shear modulus follows from (4.4.30), as the limit of the second term at $K_1 \to \infty$. The resulting overall shear modulus of the porous solid is

$2G = 2G_1(1 - 5c_2/3)$. Comparison with (4.4.29) shows that the cavities have a lesser effect on stiffness than do rigid particles. However, the difference between 5/2 and 5/3 is small.

Of interest in applications to geomechanics is evaluation of the bulk modulus of a *undrained porous medium*, saturated by a fluid that has elastic moduli $K_f > 0$, $G_2 = 0$, and is under pressure $p = -\sigma_{kk}^{(2)}/3$. The porosity of rocks and condensed soils is usually very small, hence the skeleton may be modeled by a dilute concentration of cavities, where the pressure is uniformly applied to all cavity and exterior surfaces. Under such circumstances, the fluid (f) filling a cavity can be regarded as an inhomogeneity with the stiffness $\boldsymbol{L}_f = 3K_f\boldsymbol{J}$. The G_1, K_1 are moduli of the solid 'matrix'. According to (4.4.20), the bulk modulus is (1/3) of the multiplier of the $\boldsymbol{J}$ matrix, in the decomposed form of the overall stiffness $\boldsymbol{L}$.

The bulk moduli of the undrained and drained or dry porous medium then follow from (4.4.25) with $K_2 = K_f$, and from (4.4.30) as

$$K_U = K_1 + c_2\frac{3K_1 + 4G_1}{3K_f + 4G_1}(K_f - K_1) \quad K_D = K_1\left[1 - c_2\frac{3K_1 + 4G_1}{4G_1}\right] \tag{4.4.31}$$

More convenient notation employs strain concentration factors T_2^D and T_2^U of the cavities under drained and undrained conditions

$$K_U = K_1 + c_2T_2^U(K_f - K_1) \quad K_D = K_1(1 - c_2T_2^D) = K_1(1 - \beta) \tag{4.4.32}$$

where $\beta = 1 - K_D/K_1 = c_2T_2^D$ is the Biot (1941) coefficient. The concentration factors of the cavities ($r = 2$) and the matrix or skeleton ($r = 1$), in the drained and undrained states are

$$T_2^D = \beta/c_2 \quad T_2^U = \frac{T_2^D}{1 + (T_2^D - 1)K_f/K_1} = \frac{\beta/c_2}{1 + (\beta/c_2 - 1)K_f/K_1} \tag{4.4.33}$$

and

$$T_1^D = \frac{1 - \beta}{1 - c_2} = \frac{K_D}{(1 - c_2)K_1} \quad T_1^U = \frac{1 - c_2T_2^U}{1 - c_2} \tag{4.4.34}$$

Equations (4.4.31) can be solved to eliminate G_1 and yield

$$K_U - K_D = c_2T_U(K_f - K_1) + K_1\beta = \frac{\beta(K_f - K_1)}{1 + (\beta/c_2 - 1)K_f/K_1} + \beta K_1 \tag{4.4.35}$$

which is the Gassman relation between the undrained and drained bulk moduli of the porous medium.

Under overall isotropic strain $\varepsilon^0_{kk}/3$, applied to the saturated porous medium, the overall isotropic stress is $\sigma_{kk} = 3K_U\varepsilon^0_{kk}$. It is also a sum of the stress $3K_D\varepsilon^0_{kk}$ caused in the dry skeleton by the applied overall strain, and by the overall effect of the pressure applied in the cavities. The latter can be regarded as an eigenstress $\lambda^{(2)}_{kk} = -3p$. The corresponding overall eigenstress follows from the Levin formula as $\bar{\lambda}_{kk} = -3c_2 pT_2^D = -3\beta p$. Therefore, the overall stress caused by application the overall strain $\varepsilon^0_{kk}/3$ and fluid pressure p is

$$\bar{\sigma}_{kk}/3 = (K_D\varepsilon^0_{kk} - \beta p) = K_U\varepsilon^0_{kk} \tag{4.4.36}$$

This is in agreement with the result of Rice and Cleary (1976). Application of a temperature change $\Delta\theta$ would cause a dilatation of the skeleton, and an addition to the overall eigenstress. The result can be derived as an exercise, from (4.4.28), by converting the overall eigenstrain to a corresponding eigenstress and adding that to $\boldsymbol{J}\bar{\boldsymbol{\sigma}} = \bar{\sigma}_{kk}/3$.

Notice that the simple model of a dilute suspension of particles or cavities provides generally valid results (4.4.29), (4.4.35) and (4.4.36), which were first found using different lines of reasoning. Applications of eigenstrains to more complex material response were developed by Suvorov and Selvadurai (2010).

4.5 Green's Function and Eshelby's Tensor in Elastic Solids

4.5.1 Introduction

The Green's function for an elastically anisotropic solid provides a fundamental solution to various problems of mechanics and mathematical physics. For an exposition of the mathematical background the reader is referred to one of the many mathematical texts (Roach 1982; Arfken and Weber 1995). Here we consider only linearly elastic solids which are unbounded in extent, homogeneous and everywhere in equilibrium. The elastostatic Green's function is defined as the displacement field at a point $\boldsymbol{x}$, due to a point force applied at a different point $\boldsymbol{x}'$. For example, in an isotropic solid, the displacement at $\boldsymbol{x}$ caused by a force P_j concentrated at $\boldsymbol{x}'$ is given by the generalized solution of Kelvin's problem (Eshelby 1957; Mura 1987, p. 63)

$$u_i = G_{ij}(\boldsymbol{x} - \boldsymbol{x'})P_j = \frac{P_j}{16\pi\mu(1-\nu)R}\left[(3-4\nu)\delta_{ij} + \frac{(x_i - x'_i)(x_j - x'_j)}{R^2}\right] \tag{4.5.1}$$

where $R = [(x_i - x'_i)(x_i - x'_i)]^{1/2}$. It can be verified that tractions generated by this displacement field on any closed surface surrounding $\boldsymbol{x}'$ have the resultant P_j.

The Green's function has an exact analytic expression only in the case of isotropy or transverse isotropy (Lifshitz and Rozenzweig 1947; Kröner 1953; Willis 1964; Mura and Kinoshita 1971; Pan and Chou 1976; Withers 1989). Many different

procedures have been proposed to derive the Green's function. These include the eigenfunction expansion method (Mura 1987), Fredholm's technique (1900), the Fourier transform method (Synge 1957; Barnett 1972), the Radon transform (Bacon, et al. 1979), and related procedures which involve the solutions of the roots of sextic equations (Ting and Lee 1997; Lee 2002).

The ellipsoidal inclusion or inhomogeneity problem is one of the few solvable three-dimensional elasticity problems. As pointed out in Sect. 4.1, pioneering investigation of the subject is due to Eshelby (1957), who employed the Green's function method and solved the problem of an ellipsoidal inclusion analytically. This result has found a wide range of applications in micromechanics and material physics communities. A detailed exposition of the topic in the uncoupled mechanical context can be found in monographs by Mura (1987) and Nemat-Nasser and Hori (1999), and in the review papers (Willis 1981; Walpole 1981; Mura 1988).

4.5.2 Green's Function and Its First Derivative

We first recall from Sect. 2.1 that the constitutive relation for linearly elastic materials can be written as $\sigma_{ij} = L_{ijkl}\varepsilon_{kl}$ where σ_{ij} is the stress tensor, ε_{kl} is the strain tensor and L_{ijkl} is the tensor of elastic moduli, which satisfies the symmetry relations $L_{ijkl} = L_{jikl} = L_{ijlk} = L_{klij}$. Therefore, the (6×6) matrix $\boldsymbol{L}=\boldsymbol{L}^{\mathrm{T}}$ has at most 21 independent components. If $u_i(\boldsymbol{x})$ denotes the displacement vector, the strain and rotation tensors are given by

$$\varepsilon_{ij} = \frac{1}{2}(u_{i,j} + u_{j,i}) \quad \omega_{ij} = \frac{1}{2}(u_{i,j} - u_{j,i}) \tag{4.5.2}$$

In the absence of body forces, the stress field $\sigma_{ij}(\boldsymbol{x})$ should satisfy the equilibrium equation $\nabla \cdot \sigma = \sigma_{ij,j} = 0$. Substituting from (4.5.2) into $\sigma_{ij} = L_{ijkl}\varepsilon_{kl}$ yields the Navier's equation $L_{ijkl}u_{k,lj} = 0$.

To express this equation in terms of the displacement defined by the Green's function as $u_k = G_{kp}(\boldsymbol{x}-\boldsymbol{x}')P_p$, we define a unit body force $\delta_{ip}\delta(\boldsymbol{x}-\boldsymbol{x}')$ and arrive at the governing equation for the Green's function for a linearly elastic material with arbitrary anisotropy in the form

$$L_{ijkl}\frac{\partial^2 G_{kp}(\boldsymbol{x}-\boldsymbol{x}')}{\partial x_j\,\partial x_l} + \delta_{ip}\delta(\boldsymbol{x}-\boldsymbol{x}') = 0 \tag{4.5.3}$$

where δ_{ij} is the Kronecker delta and $\delta(\boldsymbol{x}-\boldsymbol{x}')$ is the Dirac delta function. Specifically, the Green's tensor $G_{kp}(\boldsymbol{x},\boldsymbol{x}')$ is defined as a field which gives the displacement component u_k at $\boldsymbol{x}$, in response to a x_p component of a unit point force applied at $\boldsymbol{x}'$. The Green's tensor is translationally invariant, centrosymmetric and satisfies the relations (Bacon et al. 1979)

$$G_{ij}(\boldsymbol{x},\boldsymbol{x}') = G_{ij}(\boldsymbol{x}-\boldsymbol{x}') = G_{ij}(\boldsymbol{x}'-\boldsymbol{x}) = G_{ji}(\boldsymbol{x}-\boldsymbol{x}') \tag{4.5.4}$$

For convenience, Green's function will be written as a (3×3) matrix form $\boldsymbol{G}$. We will employ the Fourier transform method to derive the Green's function and its first derivative for generally anisotropic solids. The quantities of the first derivative of Green's function are related to the strain fields (and correspondingly the stresses) due to a point force source, and can also be linked to solutions of point defects and loops (Willis 1970). The derivation procedure follows the approach of Barnett (1972), in which the solution is expressed as a line integral over a unit circle. To start, we let $\boldsymbol{x}'$ be the origin and apply the Fourier transform to (4.5.3). The Green's function in the transformed domain is defined by

$$\hat{\boldsymbol{G}}(\boldsymbol{\xi}) = \frac{1}{8\pi^3}\int_R \boldsymbol{G}(\boldsymbol{x})\exp(i\boldsymbol{\xi}\cdot\boldsymbol{x})\mathrm{d}V(\boldsymbol{\xi}) \tag{4.5.5}$$

The integration domain R denotes the infinite space. Thus, (4.5.3) becomes

$$L_{ijkl}\xi_j\xi_l\hat{G}_{kp} = \delta_{ip} \tag{4.5.6}$$

The components of $\hat{G}_{ij}$ can be obtained by solving the algebraic equation

$$\hat{G}_{ij}(\xi) = k_{ij}^{-1} \tag{4.5.7}$$

where the tensor k_{ij} is defined by

$$k_{ij} = L_{ijkl}\xi_k\xi_l \tag{4.5.8}$$

and $k_{ij}k_{jk}^{-1} = \delta_{ik}$. It should be noted the $\hat{\boldsymbol{G}}(\boldsymbol{\xi})$ are even in $\boldsymbol{\xi}$ and are homogeneous function of degree -2 in $|\boldsymbol{\xi}|$.

By employing the Fourier inversion formula, the Green's functions $\boldsymbol{G}$ is derived in the form

$$\left.\begin{aligned}\boldsymbol{G}(\boldsymbol{x}) =& \frac{1}{(2\pi)^3}\int \hat{\boldsymbol{G}}(\boldsymbol{\xi})\exp(-i\boldsymbol{\xi}\cdot\boldsymbol{x})\mathrm{d}V(\boldsymbol{\xi}) = \frac{1}{(2\pi)^3}\int \hat{\boldsymbol{G}}(\boldsymbol{\xi})\cos(\boldsymbol{\xi}\cdot\boldsymbol{x})\mathrm{d}V(\boldsymbol{\xi})\\ =& \frac{1}{(2\pi)^3}\lim_{r\to\infty}\int_{\partial\Theta}\hat{\boldsymbol{G}}(\bar{\boldsymbol{\xi}})\frac{\sin\left(r\bar{\boldsymbol{\xi}}\cdot\boldsymbol{x}\right)}{\bar{\boldsymbol{\xi}}\cdot\boldsymbol{x}}\mathrm{d}S\left(\bar{\boldsymbol{\xi}}\right)\end{aligned}\right\} \tag{4.5.9}$$

where $\bar{\boldsymbol{\xi}} = \boldsymbol{\xi}/|\boldsymbol{\xi}| = \boldsymbol{\xi}/r$, $|\boldsymbol{\xi}| \equiv r$; $dV(\xi) = r^2 drdS\left(\bar{\boldsymbol{\xi}}\right)$, and $\partial\Theta$ denotes the surface of a unit sphere Θ. Since (Synge 1957)

$$\lim_{r\to\infty}\frac{1}{\pi}\frac{\sin\left(r\bar{\boldsymbol{\xi}}\cdot\boldsymbol{x}\right)}{\bar{\boldsymbol{\xi}}\cdot\boldsymbol{x}} = \delta\left(\bar{\boldsymbol{\xi}}\cdot\boldsymbol{x}\right) \tag{4.5.10}$$

the Green's tensors $\boldsymbol{G}$ for a point source at $\boldsymbol{x}'$ can be represented in terms of a line integral (Laws 1977)

$$\left.\begin{aligned} G_{ij}(\boldsymbol{x}-\boldsymbol{x}') &= \frac{1}{8\pi^2}\int_{\partial\Theta}\hat{G}_{ij}(\bar{\boldsymbol{\xi}})\delta(\bar{\boldsymbol{\xi}}\cdot(\boldsymbol{x}-\boldsymbol{x}'))\mathrm{d}S(\bar{\boldsymbol{\xi}}) \\ &= \frac{1}{8\pi^2\,|\boldsymbol{x}-\boldsymbol{x}'|}\oint_{\mathrm{C}}\hat{G}_{ij}(\bar{\boldsymbol{\xi}})\mathrm{d}s \end{aligned}\right\} \tag{4.5.11}$$

where ds is element of arc, and the contour C is taken around the unit circle which has its center at $\boldsymbol{x}'$ and lies in the plane perpendicular to $\boldsymbol{x}-\boldsymbol{x}'$. The expression of the Green's function involves a contour integration around a unit circle. The original derivation of (4.5.11) dates back to earlier references, see for instance, Lifshitz and Rozenzweig (1947) and Synge (1957).

For isotropic solids, the integrand $\hat{\boldsymbol{G}}$ can be obtained and the Green's function can be exactly integrated, to yield another form

$$G_{ij}\left(\boldsymbol{x}-\boldsymbol{x}'\right) = \frac{1}{4\pi\mu}\frac{\delta_{ij}}{|\boldsymbol{x}-\boldsymbol{x}'|} - \frac{1}{16\pi\mu\,(1-\nu)}\frac{\partial^2}{\partial x_i\,\partial x_j}\,|\boldsymbol{x}-\boldsymbol{x}'| \tag{4.5.12}$$

where μ is the shear modulus and ν is Poisson's ratio. Analytical investigations of Green's functions for anisotropic materials can also be found in the works by Willis (1965), Indenbom and Orlov (1968), Ting (1996, 2000), Ting and Lee (1997), Lee (2002), Suvorov and Dvorak (2002), and the references cited therein. For general anisotropic materials, closed form solutions of the integral (4.5.11) are unlikely to be found. However, it is not difficult to evaluate the integral by numerical integration procedures.

To perform numerical integrations, define $\boldsymbol{x}-\boldsymbol{x}' = \boldsymbol{t}\,|\boldsymbol{x}-\boldsymbol{x}'|$ where $\boldsymbol{t}$ is a unit vector, expressed in the spherical coordinates as $[\sin\phi\cos\theta,\ \sin\phi\sin\theta,\ \cos\phi]^{\mathrm{T}}$ The vector $\bar{\boldsymbol{\xi}}$ in (4.5.9) can be parameterized by (Barnett 1972)

$$\bar{\xi}_s = a_s\cos\beta + b_s\sin\beta \quad s = 1,2,3 \tag{4.5.13}$$

where

$$\left.\begin{array}{lll} a_1 = \sin\theta & a_2 = -\cos\theta & a_3 = 0 \\ b_1 = \cos\phi\cos\theta & b_2 = \cos\phi\sin\theta & b_3 = -\sin\phi \end{array}\right\} \tag{4.5.14}$$

and in reference to (4.5.11), $ds = d\beta$. The integral (4.5.11) can be programmed for numerical evaluation in a straightforward manner because the integrands are all well-behaved functions. For example, one can carry out the integrations using Gaussian quadrature formula (e.g., Press et al. 1989)

$$\boldsymbol{G}(\boldsymbol{x}-\boldsymbol{x}') \approx \frac{1}{8\pi^2\,|\boldsymbol{x}-\boldsymbol{x}'|}\sum_{p=1}^{N} w_p\hat{\boldsymbol{G}}(\beta_p) \tag{4.5.15}$$

where β_p are the integration points in the interval $(0, 2\pi)$ and w_p are the Gaussian weights. This numerical scheme, valid for arbitrary anisotropy of the solid, turns out to be very accurate and efficient. Further, the numerical result will pass smoothly into the isotropic limit which can be checked with the known exact Kelvin's solutions for isotropic solids. A further observation of (4.5.11) indicates that $G_{ij} = G_{ji}$ and that the Green's functions $\boldsymbol{G}$ follow the decomposition

$$\boldsymbol{G}(\boldsymbol{x} - \boldsymbol{x'}) = |\boldsymbol{x} - \boldsymbol{x'}|^{-1} \boldsymbol{g}(\boldsymbol{l}) \quad l_i = (x_i - x_i')/|\boldsymbol{x} - \boldsymbol{x'}| \tag{4.5.16}$$

where $\boldsymbol{g}$ are even functions of $\boldsymbol{l}$ only. Therefore, $\boldsymbol{G}(\boldsymbol{x},\boldsymbol{x'}) = \boldsymbol{G}(\boldsymbol{x'},\boldsymbol{x})$, as in (4.5.4).

To find the first derivative of $\boldsymbol{G}(\boldsymbol{x})$, differentiate (4.5.11) with respect to x_s

$$G_{ij,s}(\boldsymbol{x} - \boldsymbol{x'}) = \frac{1}{8\pi^2} \int_{\partial\Theta} \hat{\boldsymbol{G}}_{ij}(\bar{\boldsymbol{\xi}}) \bar{\xi}_s \delta'(\bar{\boldsymbol{\xi}} \cdot (\boldsymbol{x} - \boldsymbol{x'})) \mathrm{d}S(\bar{\boldsymbol{\xi}}) \tag{4.5.17}$$

From the definition of the delta function and its derivative and by change of variables (Barnett 1972), this can be further recast in the form

$$G_{ij,s}(\boldsymbol{x} - \boldsymbol{x'}) = \frac{1}{8\pi^2 |\boldsymbol{x} - \boldsymbol{x'}|^2} \oint_C \left[-t_s \hat{G}_{ij}(\bar{\boldsymbol{\xi}}) + \bar{\xi}_s F_{ij}(\bar{\boldsymbol{\xi}}) \right] \mathrm{d}s \tag{4.5.18}$$

where $\boldsymbol{t}$ is a unit vector along $\boldsymbol{x} - \boldsymbol{x'}$, and $F_{ij} = L_{pqrs} \hat{G}_{ip} \hat{G}_{rj} \rho_{sq}$, with $\rho_{ij} = \bar{\xi}_i t_j + \bar{\xi}_j t_i$.

A different parametrization of the unit sphere was adopted by Ghahremani (1977) and Gavazzi and Lagoudas (1990). A line integral expression for the second derivative of the Green function was also provided by Barnett (1972). Willis (1975) reformulated Barnett's derivation and obtained a general result for all derivatives. Similar expressions for the Green's tensors and their derivatives for piezoelectric solids can be found in Chen (1993a, b) and Chen and Lin (1993).

4.5.3 The Inclusion Problem

Consider an unbounded space Ω containing an ellipsoidal region Ω_r which has the same material property as the surrounding matrix, but undergoes certain prescribed transformation strain $\mu_{kl}^r(\boldsymbol{x})$ inside. The constitutive relation can be written in the form

$$\sigma_{ij} = L_{ijkl}\left(\varepsilon_{kl} - w(\boldsymbol{x})\mu_{kl}^r\right) \quad w(\boldsymbol{x}) = \begin{cases} 1 & \boldsymbol{x} \in \Omega_r \\ 0 & \text{otherwise} \end{cases} \tag{4.5.19}$$

Substituting this into the equilibrium equation $\sigma_{ij,j} = 0$ and employing the Green's function, the displacement field caused by the transformation field in the inclusion is

$$u_m(\boldsymbol{x}) = -\int_{\Omega} G_{mi}(\boldsymbol{x}-\boldsymbol{x}')\frac{\partial}{\partial x'_j}\{w(\boldsymbol{x}')[L_{ijkl}\mu^r_{kl}(\boldsymbol{x}')]\}\mathrm{d}\boldsymbol{x}' \tag{4.5.20}$$

Performing integration by parts with respect to $\boldsymbol{x}'$ and noting that $\partial/\partial x'_i = -\partial/\partial x_i$, we can show that the strain field in the solid can be expressed as

$$\varepsilon_{mn}(\boldsymbol{x}) = -\int_{\Omega_r} \Gamma_{mnij}(\boldsymbol{x}-\boldsymbol{x}')\lambda^r_{ij}(\boldsymbol{x}')\mathrm{d}\boldsymbol{x}' \tag{4.5.21}$$

where the eigenstress $\lambda^r_{ij}(\boldsymbol{x}') = -L_{ijkl}\mu^r_{kl}(\boldsymbol{x}')$, and

$$\Gamma_{mnij}(\boldsymbol{x}-\boldsymbol{x}') = -\frac{1}{2}\left[G_{mi,nj}(\boldsymbol{x}-\boldsymbol{x}') + G_{ni,mj}(\boldsymbol{x}-\boldsymbol{x}')\right] \tag{4.5.22}$$

Notice that since $\lambda_{ij}(\boldsymbol{x}') = \lambda_{ji}(\boldsymbol{x}')$, the operator Γ is also equivalent to

$$\left.\begin{aligned}\Gamma_{mnij}(\boldsymbol{x}-\boldsymbol{x}') = -\frac{1}{4}\big[&G_{mi,nj}(\boldsymbol{x}-\boldsymbol{x}') + G_{mj,ni}(\boldsymbol{x}-\boldsymbol{x}')\\ &+G_{ni,mj}(\boldsymbol{x}-\boldsymbol{x}')+G_{nj,mi}(\boldsymbol{x}-\boldsymbol{x}')\big]\end{aligned}\right\} \tag{4.5.23}$$

If the transformation field is uniform inside the inclusion, then (4.5.21) reduces to the form

$$\varepsilon_{mn}(\boldsymbol{x}) = -P_{mnij}(\boldsymbol{x})\,\lambda^r_{ij} \tag{4.5.24}$$

where

$$P_{mnij}(\boldsymbol{x}) = -\frac{1}{2}\int_{\Omega_r}[G_{mi.nj}(\boldsymbol{x}-\boldsymbol{x}') + G_{ni,mj}(\boldsymbol{x}-\boldsymbol{x}')]\mathrm{d}\boldsymbol{x}' \tag{4.5.25}$$

Equivalently, the elastic strain field can be written in terms of the uniform transformation field as

$$\varepsilon_{mn}(\boldsymbol{x}) = S_{mnkl}(\boldsymbol{x})\mu^r_{kl} \tag{4.5.26}$$

where

$$S_{mnkl}(\boldsymbol{x}) = -\frac{1}{2}\int_{\Omega_r}\left\{L_{ijkl}\left[G_{mi,nj}(\boldsymbol{x}-\boldsymbol{x}') + G_{ni,mj}(\boldsymbol{x}-\boldsymbol{x}')\right]\right\}\mathrm{d}\boldsymbol{x}' = P_{mnij}L_{ijkl} \tag{4.5.27}$$

If $\boldsymbol{x} \in \Omega_r$, and the inclusion Ω_r is ellipsoidal in shape, then this equation gives the Eshelby tensor $\boldsymbol{S}$, and (4.5.25) the $\boldsymbol{P}$ tensor (4.2.9). The derivatives in (4.5.25)

can also be written as

$$\left.\begin{aligned}\int_{\Omega_r} \frac{\partial^2 G_{mi}(\boldsymbol{x}-\boldsymbol{x}')}{\partial x_n \partial x_j}\mathrm{d}\boldsymbol{x}' &= \frac{1}{8\pi^2}\int_{\Omega_r}\frac{\partial^2}{\partial x_n \partial x_j}\int_{\partial\Theta}\hat{G}_{mi}\left(\bar{\boldsymbol{\xi}}\right)\delta\left(\left(\boldsymbol{x}-\boldsymbol{x}'\right)\cdot\bar{\boldsymbol{\xi}}\right)\mathrm{d}S\left(\bar{\boldsymbol{\xi}}\right)\mathrm{d}V\left(\boldsymbol{x}'\right)\\ &= \frac{1}{8\pi^2}\int_{\Omega_r}\frac{\partial^2}{\partial x_n \partial x_j}\int_{\partial\Theta}\hat{G}_{mi}\left(\bar{\boldsymbol{\xi}}\right)\psi\left(\boldsymbol{x},\bar{\boldsymbol{\xi}}\right)\mathrm{d}S\left(\bar{\boldsymbol{\xi}}\right)\end{aligned}\right\} \tag{4.5.28}$$

where

$$\psi\left(\boldsymbol{x},\bar{\boldsymbol{\xi}}\right)=\int_{\Omega_r}\delta\left[\left(\boldsymbol{x}-\boldsymbol{x}'\right)\cdot\bar{\boldsymbol{\xi}}\right]\mathrm{d}V\left(\boldsymbol{x}'\right) \tag{4.5.29}$$

The $\psi\left(\boldsymbol{x},\bar{\boldsymbol{\xi}}\right)$ is the area of the section Ω_r cut off by the plane through $\boldsymbol{x}$ and perpendicular to $\bar{\boldsymbol{\xi}}$. If the inclusion is an ellipsoid, one can integrate this analytically. For example, if the ellipsoid is characterized by $\alpha_{ij}x_i'x_j'=1$, it was shown by Laws (1977) that for $\boldsymbol{x}\in\Omega_r$

$$\psi\left(\boldsymbol{x},\bar{\boldsymbol{\xi}}\right)=\frac{\pi}{t^3\sqrt{\alpha}}\left\{t^2-\left(\boldsymbol{x}\cdot\bar{\boldsymbol{\xi}}\right)^2\right\} \tag{4.5.30}$$

where $t^2=\alpha_{ij}^{-1}\bar{\xi}_i\bar{\xi}_j$ and $\alpha=\det\alpha_{ij}$. From (4.5.25, 4.5.26, 4.5.27, 4.5.28, 4.5.29, 4.5.30) we now have

$$P_{mnij}=\frac{1}{2\pi\sqrt{\alpha}}\int_{\partial\Theta}\frac{1}{t^3}\left[\hat{G}_{mi}\left(\bar{\boldsymbol{\xi}}\right)\bar{\xi}_n\bar{\xi}_j+\hat{G}_{ni}\left(\bar{\boldsymbol{\xi}}\right)\bar{\xi}_m\bar{\xi}_j\right]\mathrm{d}S\left(\bar{\boldsymbol{\xi}}\right) \tag{4.5.31}$$

It is seen that $\boldsymbol{P}$ does not depend on $\boldsymbol{x}$ for $\boldsymbol{x}\in\Omega_r$. If the ellipsoid is coaxial with the coordinates, and a_1, a_2, a_3 are its semi-axes, then the strain and rotation fields inside the inclusion can be expressed as

$$\left.\begin{aligned}\varepsilon_{ij} &= -\left[\frac{a_1a_2a_3}{4\pi}\int_{\partial\Theta}\frac{1}{t^3}P_{ijkl}(\bar{\xi})\mathrm{d}S(\bar{\xi})\right]\lambda_{kl}\\ \omega_{ij} &= -\left[\frac{a_1a_2a_3}{4\pi}\int_{\partial\Theta}\frac{1}{t^3}R_{ijkl}(\bar{\xi})\mathrm{d}S(\bar{\xi})\right]\lambda_{kl}\end{aligned}\right\} \tag{4.5.32}$$

where $P_{ijkl}(\bar{\xi})$, $R_{ijkl}(\bar{\xi})$, and t are given by

$$\left.\begin{aligned} P_{ijkl}(\bar{\xi}) &= \frac{1}{4}\left[k_{ik}^{-1}\bar{\xi}_j\bar{\xi}_l + k_{il}^{-1}\bar{\xi}_k\bar{\xi}_j + k_{jk}^{-1}\bar{\xi}_i\bar{\xi}_l + k_{jl}^{-1}\bar{\xi}_i\bar{\xi}_k\right] \\ R_{ijkl}(\bar{\xi}) &= \frac{1}{4}\left[k_{ik}^{-1}\bar{\xi}_j\bar{\xi}_l - k_{jk}^{-1}\bar{\xi}_i\bar{\xi}_l + k_{il}^{-1}\bar{\xi}_k\bar{\xi}_j - k_{jl}^{-1}\bar{\xi}_i\bar{\xi}_k\right] \\ t &= \left(a_1^2\bar{\xi}_1^2 + a_2^2\bar{\xi}_2^2 + a_3^2\bar{\xi}_3^2\right)^{\frac{1}{2}} \end{aligned}\right\} \tag{4.5.33}$$

Forms equivalent to (4.5.25) can also be expressed as (Chen 1993b)

$$\left.\begin{aligned} P_{ijkl} &= \frac{1}{4\pi a_1 a_2 a_3}\int_{\partial\Omega_r}\frac{x_r n_r}{4}\left(k_{ik}n_j n_l + k_{il}n_j n_k + k_{jk}n_i n_l + k_{jl}n_i n_k\right)\mathrm{d}S \\ R_{ijkl} &= \frac{1}{4\pi a_1 a_2 a_3}\int_{\partial\Omega_r}\frac{x_r n_r}{4}\left(k_{ik}n_j n_l - k_{il}n_j n_k + k_{jk}n_i n_l - k_{jl}n_i n_k\right)\mathrm{d}S \end{aligned}\right\} \tag{4.5.34}$$

where $\boldsymbol{n}$ is the unit normal of the ellipsoidal surface $\partial\Omega_r$ and $k_{ij} = c_{ij}^{-1}$ with $c_{ik} = L_{ijkl}n_j n_l$.

Except for some typical ellipsoidal shapes of the inclusion in materials with certain elastic symmetry, closed form expressions for the $\boldsymbol{P}$ tensor or the Eshelby tensor $\boldsymbol{S}$ cannot be found analytically. However, to evaluate the $\boldsymbol{P}$ tensor for arbitrary anisotropy of the medium, and for any shape of the inclusion, one can carry out the integrations numerically in terms of Gaussian quadratures. In order to do this, the integrals in (4.5.32) are first parameterized on the surface of a unit sphere following a coordinate transformation described by Mura (1987). For example, the tensor P_{ijkl} in (4.5.25) can be written as

$$P_{ijkl} = \frac{1}{16\pi}\int_{-1}^{1} d\zeta_3 \int_0^{2\pi}\left(k_{ik}\bar{\xi}_j\bar{\xi}_l + k_{il}\bar{\xi}_j\bar{\xi}_k + k_{jk}\bar{\xi}_i\bar{\xi}_l + k_{jl}\bar{\xi}_i\bar{\xi}_k\right)\mathrm{d}\omega \tag{4.5.35}$$

where

$$\left.\begin{aligned} k_{ik} &= k_{ik}\left(\bar{\xi}\right) \quad \bar{\xi}_i = \zeta_i/a_i \ \text{(no sum on } i\text{)} \\ \zeta_1 &= \left(1-\zeta_3^2\right)^{\frac{1}{2}}\cos\omega \quad \zeta_2 = \left(1-\zeta_3^2\right)^{\frac{1}{2}}\sin\omega \end{aligned}\right\} \tag{4.5.36}$$

The double integral can be computed using the Gaussian quadrature formula (Chen 1993a)

$$P_{ijkl} = \frac{1}{16\pi}\sum_{p=1}^{M}\sum_{q=1}^{N}\left[\left(k_{ik}\bar{\xi}_j\bar{\xi}_l + k_{il}\bar{\xi}_j\bar{\xi}_k + k_{jk}\bar{\xi}_i\bar{\xi}_l + k_{jl}\bar{\xi}_i\bar{\xi}_k\right)w_{pq}\left(\omega_q, \zeta_{3p}\right)\right] \tag{4.5.37}$$

where $\bar{\xi}_i = \bar{\xi}_i\left(\omega_q, \zeta_{3p}\right)$, M and N refer to the Gaussian points used for the integrations over ζ_3 and ω, respectively, and w_{pq} are the Gaussian weights. The selection of the integration points M and N depends on the aspect ratio of the ellipsoidal inclusion, material constants, and the desired accuracy. Similar expressions can also be written for the $\boldsymbol{R}$ tensor.

4.5.4 The Tanaka-Mori Theorem for Exterior Fields

This is a very useful theorem that provides an estimate of the average strain caused in the exterior of a homogeneous inclusion Ω_r by a uniform eigenstrain μ^r_{kl} applied in the interior of this inclusion (Tanaka and Mori 1972). The double inhomogeneity model described in Sect. 7.4 is based on this theorem. Recall from (4.5.26) and (4.5.27) that the total strain field caused by μ^r_{kl} in a large volume Ω is

$$\varepsilon_{mn}(\boldsymbol{x}) = -\frac{1}{2}\mu^r_{kl}\int\limits_{\Omega_r}\left\{L_{ijkl}\left[G_{mi,nj}\left(\boldsymbol{x}-\boldsymbol{x}'\right)+G_{ni,mj}\left(\boldsymbol{x}-\boldsymbol{x}'\right)\right]\right\}\mathrm{d}\boldsymbol{x}' \tag{4.5.38}$$

If the inclusion Ω_r has an ellipsoidal shape, then the integral is constant for $\boldsymbol{x} \in \Omega_r$. The stress field associated with this strain field is $\sigma_{mn}(\boldsymbol{x}) = L_{mnpq}[\varepsilon_{pq}(\boldsymbol{x}) - \mu_{pq}]$, with $\mu_{pq} = 0$ for $\boldsymbol{x} \notin \Omega_r$.

Next, suppose that two other domains Ω_1 and Ω_2 surrounding Ω_r are defined such that $\Omega_r \subseteq \Omega_1 \subset \Omega_2$. Their shape, size and position can be selected as desired. Let us now find the integral of $\boldsymbol{\varepsilon}(\boldsymbol{x})$ in $\Omega_2 - \Omega_1$.

$$\int\limits_{\Omega_2-\Omega_1}\varepsilon_{mn}(\boldsymbol{x})\mathrm{d}\boldsymbol{x} = -\frac{1}{2}\int\limits_{\Omega_2-\Omega_1}\mathrm{d}\boldsymbol{x}\left\{\int\limits_{\Omega_r}\mu^r_{kl}\left\{L_{ijkl}\left[G_{mi,nj}\left(\boldsymbol{x}-\boldsymbol{x}'\right)+G_{ni,mj}\left(\boldsymbol{x}-\boldsymbol{x}'\right)\right]\right\}\mathrm{d}\boldsymbol{x}'\right\} \tag{4.5.39}$$

Since the integrand has no singularity in $\Omega_2 - \Omega_1$, the order of integration with respect to $\boldsymbol{x}$ and $\boldsymbol{x}'$ can be interchanged, and

$$\int\limits_{\Omega_2-\Omega_1}\varepsilon_{mn}(\boldsymbol{x})\mathrm{d}\boldsymbol{x} = -\frac{1}{2}\int\limits_{\Omega_r}\mathrm{d}\boldsymbol{x}'\left\{\int\limits_{\Omega_2-\Omega_1}\mu^r_{kl}\left\{L_{ijkl}\left[G_{mi,nj}\left(\boldsymbol{x}-\boldsymbol{x}'\right)+G_{ni,mj}\left(\boldsymbol{x}-\boldsymbol{x}'\right)\right]\right\}\mathrm{d}\boldsymbol{x}\right\} \tag{4.5.40}$$

The integral on the right hand side is actually equal to the strain generated at $\boldsymbol{x}' \in \Omega_r$ by the uniform eigenstrain μ^r_{kl} applied in the interior of $\Omega_2 - \Omega_1$.

If both Ω_2 and Ω_1 are ellipsoids, then (4.5.27) provides the integrand in the form

$$\left.\begin{aligned} &-\frac{1}{2}\int\limits_{\Omega_2-\Omega_1}\mu_{kl}^r\left\{L_{ijkl}\left[G_{mi,nj}\left(\boldsymbol{x}-\boldsymbol{x}'\right)+G_{ni,mj}\left(\boldsymbol{x}-\boldsymbol{x}'\right)\right]\right\}\mathrm{d}\boldsymbol{x}\\ &=\left[S_{mnkl}(\Omega_2)-S_{mnkl}(\Omega_1)\right]\mu_{kl}^r. \end{aligned}\right\} \tag{4.5.41}$$

Since both $S_{mnkl}(\Omega_2)$ and $S_{mnkl}(\Omega_1)$ are constant tensors, their difference is a constant tensor in Ω_r. Substituting (4.5.41) into (4.5.40) and completing the integration over Ω_r

$$\frac{1}{\Omega_r}\int\limits_{\Omega_2-\Omega_1}\varepsilon_{mn}(\boldsymbol{x})\mathrm{d}\boldsymbol{x}=\left[S_{mnkl}(\Omega_2)-S_{mnkl}(\Omega_1)\right]\mu_{kl}^r \tag{4.5.42}$$

Finally, from (3.5.2), the average strain caused inside the volume $\Omega_2-\Omega_1$ by the eigenstrain $\mu_{kl}^r\in\Omega_r\subseteq\Omega_1\subset\Omega_2$ follows from the last equation as

$$\bar{\varepsilon}_{mn}^{(\Omega_2-\Omega_1)}=\frac{1}{\Omega_2-\Omega_1}\int\limits_{\Omega_2-\Omega_1}\varepsilon_{mn}(\boldsymbol{x})\mathrm{d}\boldsymbol{x}=\frac{\Omega_r}{\Omega_2-\Omega_1}\left[S_{mnkl}(\Omega_2)-S_{mnkl}(\Omega_1)\right]\mu_{kl}^r \tag{4.5.43}$$

In Ω_r

$$\bar{\varepsilon}_{mn}^r=\frac{1}{\Omega_r}\int\limits_{\Omega_r}\varepsilon_{mn}(\boldsymbol{x})\mathrm{d}\boldsymbol{x}=S_{mnkl}(\Omega_r)\mu_{kl}^r \tag{4.5.44}$$

It is also of interest to determine the average local strains in a double inclusion in a homogeneous medium $\boldsymbol{L}_0$, consisting of two ellipsoidal volumes Ω_1 and Ω_2 such that $\Omega_r\equiv\Omega_1\subset\Omega_2$; Fig. 4.3. The volume surrounding Ω_r is denoted by $\Omega_g=\Omega_2-\Omega_r$. Two distinct uniform eigenstrains are applied, denoted by μ_{kl}^g in the entire volume Ω_2, and by $\mu_{kl}^r-\mu_{kl}^g$ inside Ω_r. Of course, this is equivalent to simultaneously applying μ_{kl}^g in Ω_g and μ_{kl}^r in Ω_r. The strain average created in Ω_g by μ_{kl}^g, applied alone in the entire Ω_2, is equal to $S_{mnkl}(\Omega_2)\mu_{kl}^g$, while the contribution of μ_{kl}^r is suggested by (4.5.43). Superimposition of the two fields yields the average strain in the surrounding Ω_g as

$$\bar{\varepsilon}_{mn}^g=S_{mnkl}(\Omega_2)\mu_{kl}^g+\frac{\Omega_r}{\Omega_2-\Omega_r}\left[S_{mnkl}(\Omega_2)-S_{mnkl}(\Omega_r)\right]\left(\mu_{kl}^r-\mu_{kl}^g\right) \tag{4.5.45}$$

while in Ω_r

$$\bar{\varepsilon}_{mn}^r=S_{mnkl}(\Omega_2)\mu_{kl}^g+S_{mnkl}(\Omega_r)(\mu_{kl}^r-\mu_{kl}^g) \tag{4.5.46}$$

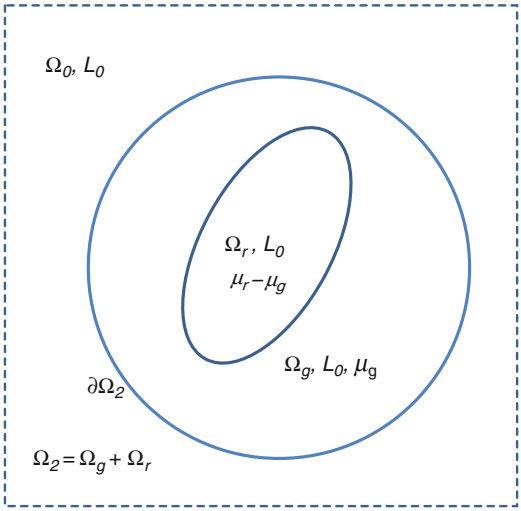

Fig. 4.3 Geometry of the double inclusion

The results (4.5.43) and (4.5.44) hold for any ellipsoidal shape and position of $\Omega_r \subseteq \Omega_1 \subset \Omega_2$. However, if both $\Omega_1 \subset \Omega_2$ and $\Omega_r \subset \Omega_1$ have the same shape and alignment and only different size, then they also share the same Eshelby tensor. For example, one can select a particular ellipsoidal shape for all $\Omega_r \equiv \Omega_1 \subset \Omega_2$, and conclude that the total strain average caused by $\mu^r_{kl} \in \Omega_r$ inside $\Omega_g = \Omega_2 - \Omega_r$ is equal to zero.

Another interesting result that follows from the theorem extends the Eshelby solution to strain and eigenstrain averages. Indeed, the average eigenstrain in the volume Ω_2 in the homogeneous medium $\boldsymbol{L}_0$ is given by the Levin formula (3.8.11) as $\mu^{(2)}_{kl} = f\mu^r_{kl} + (1-f)\mu^g_{kl}$; $f = \Omega_r/\Omega_2$, since all $\boldsymbol{B}_r = \boldsymbol{I}$. Then, (4.5.45) and (4.5.46) yield the average strain in Ω_2

$$\bar{\varepsilon}^{(2)}_{mn} = [f\bar{\varepsilon}^r_{mn} + (1-f)\bar{\varepsilon}^g_{mn}] = S^{(2)}_{mnkl}\mu^{(2)}_{kl} \tag{4.5.47}$$

In a similar way, it can be shown that the above mean field theorem also holds for the rotation tensor $\boldsymbol{\omega}$. Extension of the Tanaka and Mori (1972) result to non-uniform transformation fields in the inclusion was described by Hori and Nemat-Nasser (1993).

4.5.5 Shape-Independent Relations

Milgrom and Shtrikman (1992) derived the following exact relations between the coefficients of the Eshelby's tensor for all geometric shapes of inclusions, which

reduce the number of unknown coefficients. Recall from (4.5.26) that the strain caused in the inclusion Ω_r by a uniform transformation strain μ^r_{kl} applied inside Ω_r is

$$\varepsilon_{mn}(\boldsymbol{x}) = S_{mnkl}(\boldsymbol{x})\mu^r_{kl} \qquad [4.5.26]$$

where $S_{mnkl}(\boldsymbol{x})$ was expressed in (4.5.27). Notice that there are no restrictions on the location of the point $\boldsymbol{x}$, or on the geometric shape of the inclusion. Using the definition (4.5.3) of Green's functions and taking the *ip* trace there, Milgrom and Shtrikman (1992) show, with reference to (4.2.9), that

$$M_{ijkl}Q_{ijkl} = I_{ijij} - S_{ijij} = 3 \qquad (4.5.48)$$

where M_{ijkl} denotes the compliance of the comparison medium, where both Q_{ijkl} and S_{ijij} are evaluated. Since $I_{ijkl} = (\delta_{ik}\delta_{jl} + \delta_{il}\delta_{jk})/2$ and $I_{ijij} = (\delta_{ii}\delta_{jj} + \delta_{ij}\delta_{ij})/2 = 6$, there is

$$S_{ijij} = 3 \quad \text{for } \boldsymbol{x} \in \Omega_r \qquad (4.5.49)$$

and zero outside the inclusion.

Dually, a corresponding dimensionless tensor relates the applied transformation stress $\boldsymbol{\lambda}_{kl}$ applied in Ω_r to the resulting stress field in (4.5.19) as

$$\sigma_{mn}(\boldsymbol{x}) = [w(\boldsymbol{x})I_{mnkl} - S_{mnkl}(\boldsymbol{x})]^{\mathrm{T}}\lambda_{kl} = T^*_{mnkl}(\boldsymbol{x})\lambda_{kl} \qquad (4.5.50)$$

This can be verified, with $\boldsymbol{SM} = \boldsymbol{P}$ in (4.2.9), and with (4.5.19) and (4.5.26), that $\boldsymbol{\sigma} = \boldsymbol{L}(\boldsymbol{\varepsilon} - w\boldsymbol{\mu}_r) = \boldsymbol{L}(\boldsymbol{S} - w\boldsymbol{I})\boldsymbol{\mu}_r = (w\boldsymbol{I} - \boldsymbol{S})^{\mathrm{T}}\boldsymbol{\lambda}_r$, where $\boldsymbol{\lambda}_r = -\boldsymbol{L}\boldsymbol{\mu}_r$. The tensor $\boldsymbol{T}^* = (\boldsymbol{I} - \boldsymbol{S})^{\mathrm{T}}$ is not related to the $\boldsymbol{T}_r$ in Sect. 4.2; it can be written as

$$\begin{aligned} T^*_{mnkl} &= [w(\boldsymbol{x})I_{mnkl} - S_{mnkl}(\boldsymbol{x})]^{\mathrm{T}} \\ &= \frac{1}{2}\left[\int_{\Omega_r} L_{ijkl}\left(G_{mi,nj} + G_{ni,mj}\right) d\boldsymbol{x}' + (\delta_{mk}\delta_{nl} + \delta_{ml}\delta_{nk})\, w(\boldsymbol{x})\right]^{\mathrm{T}} \end{aligned} \qquad (4.5.51)$$

In an analogous manner, one can show that

$$T^*_{ijij} = 3 \quad \text{for } \boldsymbol{x} \in \Omega_r \qquad (4.5.52)$$

and zero outside Ω_r.

A remarkable feature is that these are pointwise relations valid for the entire domain without regard to the geometric shape of the inclusion, or to the elastic symmetry of the medium. For inclusions of ellipsoidal in shape, Hill (1965a, Eq. (20)) derived an equivalent to (4.5.51) using a different approach.

4.6 Coefficients of P Matrices for Selected Ellipsoidal Shapes

4.6.1 Sources and Notation

Evaluations of the field averages in the phases, and of the total and interaction energies caused by the various applied loads, both require numerical values of the coefficients of the matrices representing the partial strain or stress concentration factors $\boldsymbol{T}_r$ or $\boldsymbol{W}_r$ for specific inclusion or inhomogeneity shapes. They are also needed in evaluation of actual mechanical concentration factors described in Sect. 3.5.1. As suggested by (4.2.13), (4.2.14) the concentration factors are functions of the phase elastic moduli and of the Hill's tensors $\boldsymbol{P}$, that reflect the effect of shape, and depend only on the stiffness of the solid surrounding the inhomogeneity.

Derivation of these tensors is outlined in (4.5.31–4.5.37). Several different integration procedures are given in detail in the original papers by Hill (1965a), Walpole (1969, 1977, 1981), Willis (1980, 1981), and Laws (1977, 1985). Suvorov and Dvorak (2002), derived expression for the rate $\dot{\boldsymbol{P}}$ of the Hill's tensor in anisotropic solids which experience prescribed rates of change in the coefficients of their stiffness matrices. Such changes may be caused, for example, by temperature or moisture content variations, or by phase transformations. Masson (2008) used the Cauchy theory of residues to derive new expressions for $\boldsymbol{P}$ tensors in general anisotropic solids. An extensive derivation and collection of the $\boldsymbol{S} = \boldsymbol{P}\boldsymbol{L}_0$ tensors appears in Mura's (1987) monograph, among others.

Additional results can be found in Kröner (1958), who evaluated the Eshelby tensor $\boldsymbol{S}$ for a spheroid in an isotropic material. Willis (1980) presents coefficients of $\boldsymbol{P}$ for a flat disc, with semi-axes $(a,\ a,\ \varepsilon a)$, $\varepsilon \ll 1$ in an isotropic solid, to first order in ε, and also for a thin cylinder with semi-axes $(\varepsilon l,\ \varepsilon l,\ l)$, $\varepsilon \ll 1$, to second order in ε. Laws (1985) derived the $\boldsymbol{P}$ tensor to first order in ε for a penny-shaped crack in a transversely isotropic material. Withers (1989) derived the Eshelby tensor $\boldsymbol{S}$ for oblate and prolate spheroids in a transversely isotropic solid. For spheroids in an isotropic solid, the $\boldsymbol{P}$ tensor is given by Ponte-Castaneda and Willis (1995). Derivations of the $\boldsymbol{S}$ and $\boldsymbol{P}$ tensors in piezoelectric solids can be found, for example, in Benveniste (1992), Chen (1994), Deeg (1980), Dunn and Taya (1993), Dunn (1994), Huang and Yu (1994), Kuhn et al. (2002), Michelitsch and Levin (2000) and Mikata (2000).

Here we present a collection of results that should be useful in finding the concentration factors for many typical shapes of ellipsoidal inhomogeneities and cracks in both isotropic and transversely isotropic solids. The contracted tensorial and Walpole's notations of Sects. 1 and 2.3.2 are used. Inclusion shape is given by

$$(x_1/a_1)^2 + (x_2/a_2)^2 + (x_3/a_3)^2 = 1 \tag{4.6.1}$$

where the coordinate system is aligned with the principal axes of the ellipsoid, and is also used for stiffness or compliance of the host medium. Of course, except in

isotropic media, ellipsoids that are not aligned with the principal directions may perceive the host medium as highly anisotropic. Even in an isotropic medium, the $\boldsymbol{P}$ tensor of a misaligned ellipsoid has to be transformed to the overall coordinate system of the representative volume. The (6×6) matrix form is transformed using the $\boldsymbol{X}$ matrix, as described in Sect. 1.

Recall from (4.1.1) that the strain in a homogeneous ellipsoidal inclusion Ω_r which is transformed by uniform eigenstrain $\boldsymbol{\mu}_r$ is also uniform and given by $\boldsymbol{\varepsilon}_r = \boldsymbol{S}\boldsymbol{\mu}_r$. Definitions (4.2.9) of the tensors $\boldsymbol{P}$ and $\boldsymbol{Q}$ suggest that the local fields inside the transformed homogeneous inclusion are related by (4.2.12), or by

$$\boldsymbol{\varepsilon}_r = \boldsymbol{M}_0\boldsymbol{\sigma}_r + \boldsymbol{\mu}_r = -\boldsymbol{P}\boldsymbol{\lambda}_r \quad \boldsymbol{\sigma}_r = \boldsymbol{L}_0\boldsymbol{\varepsilon}_r + \boldsymbol{\lambda}_r = -\boldsymbol{Q}\boldsymbol{\mu}_r \tag{4.6.2}$$

where $\boldsymbol{\lambda}_r = -\boldsymbol{L}_0\boldsymbol{\mu}_r$ is the eigenstress that would be caused by $\boldsymbol{\mu}_r$ in a fully constrained volume Ω_r. Therefore, the $\boldsymbol{P}$ has the dimension of compliance. Transcription of a (9×9) matrix P_{ijkl} to the (6×6) matrix $P_{\alpha\beta}$, written in the contracted tensorial notation, should follow the rules for subscripts in (1.1.8). However, when $\boldsymbol{\varepsilon}_r \rightarrow \boldsymbol{\varepsilon}_r^{EG} = \boldsymbol{\Theta}\,\boldsymbol{\varepsilon}_r$ in the engineering matrix notation (1.1.12), then $P_{\alpha\beta} = P_{ijkl}$ for $\alpha, \beta \leq 3$, but $P_{\alpha\beta} = 2P_{ijkl}$ for either α or $\beta \leq 3$, and $P_{\alpha\beta} = 4P_{ijkl}$ for both $\alpha, \beta > 3$.

4.6.2 A Spherical Inclusion in an Isotropic Solid

This shape is defined by letting $a_1 = a_2 = a_3$ in (4.6.1). The result is written in the tensorial component notation (2.2.29) as

$$\boldsymbol{P} = \frac{1}{3K_0 + 4G_0}\boldsymbol{J} + \frac{3(K_0 + 2G_0)}{5G_0(3K_0 + 4G_0)}\boldsymbol{K} \tag{4.6.3}$$

where $\boldsymbol{J}$ and $\boldsymbol{K}$ are the projection tensors defined in (1.1.19). The related Hill's constraint tensors $\boldsymbol{L}^*, \boldsymbol{M}^*$ for a spherical cavity are shown in (4.2.11). In terms of the Lamé constants (2.3.7), $\lambda_0 = K_0 - 2G_0/3$, $\mu_0 = G_0$, The nonzero components of the $\boldsymbol{P} = \boldsymbol{P}^{\mathrm{T}}$ tensor are

$$\left.\begin{aligned} P_{11} = P_{22} = P_{33} &= \frac{6K_0 + 17G_0}{15G_0(3K_0 + 4G_0)} \\ P_{12} = P_{13} = P_{23} &= \frac{-(3K_0 + G_0)}{15G_0(3K_0 + 4G_0)} \\ P_{44} = P_{55} = P_{66} &= \frac{3(K_0 + 2G_0)}{5G_0(3K_0 + 4G_0)} \end{aligned}\right\} \tag{4.6.4}$$

4.6.3 An Elliptical Cylinder in a Transversely Isotropic Solid

The elliptical cylinder shape is obtained by letting $a_3 \to \infty$ in (4.6.1), as

$$x_1^2/a_1^2 + x_2^2/a_2^2 \le 1 \quad \rho = a_1/a_2 \tag{4.6.5}$$

Both the cylinder axis and the axis of material rotational symmetry are aligned with the x_3-direction. For $\rho \neq 1$, the $\boldsymbol{P}$ tensor it is represented by a (6×6) matrix with the following nonzero coefficients derived by Suvorov and Dvorak (2002) for $x_A \equiv x_3$

$$\left.\begin{aligned} P_{11} &= \frac{\rho(L^0_{22}+L^0_{66})+2L^0_{66}}{2L^0_{22}L^0_{66}(1+\rho)^2} & P_{12} &= -\frac{\rho(L^0_{66}-L^0_{22})}{2L^0_{22}L^0_{66}(1+\rho)^2} \\ P_{22} &= \frac{\rho[L^0_{22}+L^0_{66}(1+2\rho)]}{2L^0_{22}L^0_{66}(1+\rho)^2} & P_{44} &= \frac{\rho}{L^0_{44}(1+\rho)} \\ P_{66} &= \frac{L^0_{22}(1+\rho^2)+2\rho L^0_{66}}{L^0_{22}L^0_{66}(1+\rho)^2} & P_{55} &= \frac{1}{L^0_{44}(1+\rho)} \end{aligned}\right\} \tag{4.6.6}$$

This result holds in contracted tensorial notation when $L^0_{44} = L^0_{55} = 2p_0, L^0_{66} = 2m_0$, and in the engineering matrix notation when $L^0_{44} = L^0_{55} = p_0, L^0_{66} = m_0$. Results for an elliptic cylinder in an orthotropic solid were also derived in *op. cit.* The L^0_{ij} can be found in terms of Hill's moduli (2.3.3), after exchanges of the first and third rows and columns to conform with the present $x_A \equiv x_3$ convention. For a circular cylinder, the $\boldsymbol{P}$ matrix in Walpole's notation appears in (4.6.11).

4.6.4 A Slit Crack and Flat Disc in an Orthotropic Solid

Laws (1977) obtained the $\boldsymbol{P}$ tensor for an inclusion in the shape of a flat ribbon or slit crack in an orthotropic material. The slit is located in the principal x_1x_3-plane, aligned with x_3-axis, and x_2 is the normal to crack plane; $x_A \equiv x_3$. The non-zero coefficients of (6×6) $\boldsymbol{P}$ matrix in the limit $\varepsilon = a_2/a_1 \to 0$, correct to the order $\mathrm{O}(\varepsilon)$, are

$$\left.\begin{aligned} P_{11} &= \varepsilon\frac{L_{22}+L_{66}(\alpha\beta)^{1/2}}{L_{11}L_{66}(\alpha^{1/2}+\beta^{1/2})} & P_{12} &= -\varepsilon\frac{L_{12}+L_{66}}{L_{11}L_{66}(\alpha\beta)^{1/2}(\alpha^{1/2}+\beta^{1/2})} \\ P_{22} &= \frac{1}{L_{22}}+\varepsilon\frac{L_{22}-L_{66}[\alpha+\beta+(\alpha\beta)^{1/2}]}{L_{22}L_{66}(\alpha\beta)^{1/2}(\alpha^{1/2}+\beta^{1/2})} & P_{44} &= \frac{1}{L_{44}}-\varepsilon\frac{(L_{55})^{1/2}}{(L_{44})^{3/2}} \\ P_{55} &= \varepsilon\frac{1}{(L_{44}L_{55})^{1/2}} & P_{66} &= \frac{1}{L_{66}}-\varepsilon\frac{2(L_{11}L_{22}-L_{12}^2)}{L_{11}L_{66}^2(\alpha\beta)^{1/2}(\alpha^{1/2}+\beta^{1/2})} \end{aligned}\right\} \tag{4.6.7}$$

where L_{ij} denote the stiffness coefficients of the comparison medium in contracted tensorial notation. The $\alpha,\ \beta$ are roots of

$$L_{11}L_{66}x^2 - (L_{11}L_{22} - L_{12}^2 - 2L_{12}L_{66})x + L_{22}L_{66} = 0 \tag{4.6.8}$$

Chen (1994) found the $\boldsymbol{P}$ and related tensors for a slit-like inclusion in an orthorombic piezoelectric solid.

A flat disc resides in a transversely isotropic medium with principal material directions x_i, on the x_2x_3 − plane with normal $x_A = x_1$, which coincides with one of the principal directions. The shape is defined as

$$x_2^2/a_2^2 + x_3^2/a_3^2 \le 1 \tag{4.6.9}$$

The non-zero components of $\boldsymbol{P}$ are

$$P_{33} = 1/L_{33}^0 \quad P_{44} = 1/L_{44}^0 \quad P_{55} = 1/L_{55}^0 \tag{4.6.10}$$

According to (2.3.3), $L_{33}^0 = n_0, L_{44}^0 = L_{55}^0 = 2p_0$, in the contracted tensorial notation. The $\boldsymbol{P}$ matrix for a penny-shaped crack, taken as a spheroid $(a,\ a,\ \varepsilon a)$, with $\varepsilon \ll 1$ and also for a fiber of large length a, $(\varepsilon a, \varepsilon a, a)$, in an isotropic medium, both correct to the order $\mathrm{O}(\varepsilon)$, was evaluated by Willis (1980).

4.6.5 Spheroids in an Isotropic Solid

Ponte-Castaneda and Willis (1995) found the $\boldsymbol{P}$ matrix for an oblate or prolate spheroidal inclusion in an isotropic medium. This matrix is transversely isotropic, and in the Walpole's notation (2.3.14), it is written as

$$\boldsymbol{P} = (2k_P, l_P, n_P, 2m_P, 2p_P) \tag{4.6.11}$$

The coefficients are not actual Hill's moduli, they only indicate the structure of $\boldsymbol{P}$ when they replace their counterparts in the stiffness matrix written in terms of those moduli.

The spheroid surface may be generated by rotation of the ellipse (4.6.5) about the $x_A = x_1$−axis, as in Fig. 7.5. The results apply to both oblate ($\rho = a_1/a_2 < 1$) and prolate ($\rho > 1$) spheroids, providing that the parameter

$$\left.\begin{aligned} h &= \frac{\rho[\arccos(\rho) - \rho(1-\rho^2)^{1/2}]}{(1-\rho^2)^{1/2}} \quad \text{for } \rho < 1 \\ h &= \frac{\rho[\rho(\rho^2-1)^{1/2} - \operatorname{arccosh}(\rho)]}{(\rho^2-1)^{3/2}} \quad \text{for } \rho > 1 \end{aligned}\right\} \tag{4.6.12}$$

The coefficients of $\boldsymbol{P}$ in (4.6.11) are

$$\left.\begin{aligned} k_P &= \frac{[7h-2(1+2h)\rho^2]G_0+3[h-2(1-h)\rho^2]K_0}{8(1-\rho^2)(4G_0+3K_0)G_0} \\ l_P &= \frac{[2(1-h)\rho^2-h](G_0+3K_0)}{4(1-\rho^2)(4G_0+3K_0)G_0} \\ n_P &= \frac{[6-5h-8(1-h)\rho^2]G_0+3[h-2(1-h)\rho^2]K_0}{2(1-\rho^2)(4G_0+3K_0)G_0} \\ m_P &= \frac{[15h-2(1+6h)\rho^2]G_0+3(3h-2\rho^2)K_0}{16(1-\rho^2)(4G_0+3K_0)G_0} \\ p_P &= \frac{2(4-3h-2\rho^2)G_0+3[2-3h+(2-3h)\rho^2]K_0}{8(1-\rho^2)(4G_0+3K_0)G_0} \end{aligned}\right\} \tag{4.6.13}$$

The K_0 and G_0 are elastic moduli of the isotropic comparison medium that contains the inclusion. Since $\boldsymbol{L}_0$ is isotropic, the results depend only on the aspect ratio of the spheroids, not on the choice of the x_A axis.

4.7 Summary of Principal Results

Results derived in this chapter can be used to evaluate local volume averages of strain and stress fields in either a homogeneous inclusion $\boldsymbol{L}_0$, an inhomogeneity $\boldsymbol{L}_r$, or a cavity or crack that occupies a volume Ω_r, in an infinitely extended volume $\Omega = \Omega_0 + \Omega_r$ filled with a homogeneous, possibly anisotropic solid of stiffness $\boldsymbol{L}_0$. Overall averages of these fields at dilute concentrations appear in Sect. 4.4. Phase elastic moduli which provide coefficients of the (6×6) matrices $\boldsymbol{L}_0$ and $\boldsymbol{L}_r$ are assumed to be known. Homogeneous boundary conditions are prescribed on the surface $\partial\Omega$ that apply either displacements creating a uniform overall strain $\boldsymbol{\varepsilon}^0_\Omega$, or tractions generating uniform overall stress $\boldsymbol{\sigma}^0_\Omega$ at the remote exterior points of Ω_r. Moreover, applied independently of mechanical loads, are uniform phase eigenstrains or transformation strains $\boldsymbol{\mu}_r$ and $\boldsymbol{\mu}_0$, in Ω_r and Ω_0, respectively. Related eigenstresses or transformation stresses are $\boldsymbol{\lambda}_r = -\boldsymbol{L}_r\boldsymbol{\mu}_r$ in Ω_r and $\boldsymbol{\lambda}_0 = -\boldsymbol{L}_0\boldsymbol{\mu}_0$ in Ω_0. These terms define two distinct, dimensionally consistent load sets $\{\boldsymbol{\varepsilon}^0_\Omega, \boldsymbol{\mu}_r, \boldsymbol{\mu}_0\}$ and $\{\boldsymbol{\sigma}^0_\Omega, \boldsymbol{\lambda}_r, \boldsymbol{\lambda}_0\}$.

Local fields, caused by either one of the two load sets in inclusions, inhomogeneities and cavities of ellipsoidal shape, are uniform. Actual shapes of these entities are approximated by selected ellipsoids. Then, coefficients of the $\boldsymbol{P}$ matrices in Sect. 4.6 are assembled for selected shapes, using elastic moduli of the surrounding phase $\boldsymbol{L}_0$. All results of interest for the load set $\{\boldsymbol{\varepsilon}^0_\Omega, \boldsymbol{\mu}_r, \boldsymbol{\mu}_0\}$ follow in terms of the known load set components, the three matrices $\boldsymbol{L}_0$, $\boldsymbol{L}_r$ and $\boldsymbol{P}$, and the volume fraction $c_r \ll 1$ for dilute approximations of local and overall

fields. For the load set $\{\boldsymbol{\sigma}^0_\Omega, \boldsymbol{\lambda}_r, \boldsymbol{\lambda}_0\}$, the results are obtained with the matrices $\boldsymbol{M}_0 = \boldsymbol{L}_0^{-1}, \boldsymbol{M}_r = \boldsymbol{L}_r^{-1}$ and $\boldsymbol{Q} = \boldsymbol{L}_0(\boldsymbol{I} - \boldsymbol{P}\boldsymbol{L}_0)$. Relevant parts of previously derived relations are denoted by their equation numbers in [•] brackets.

4.7.1 Homogeneous Ellipsoidal Inclusions

Strain and stress fields in a *homogeneous ellipsoidal inclusion* $\boldsymbol{L}_0$ in Ω_r are uniform, and for the load set $\{\boldsymbol{\varepsilon}^0_\Omega, \boldsymbol{\mu}_r, \boldsymbol{\mu}_0\}$ they are

$$\left.\begin{aligned} \boldsymbol{\sigma}_r &= \boldsymbol{L}_0[\boldsymbol{\varepsilon}^0_\Omega - \boldsymbol{\mu}_r + \boldsymbol{S}(\boldsymbol{\mu}_r - \boldsymbol{\mu}_0)] = \boldsymbol{L}_0(\boldsymbol{\varepsilon}_r - \boldsymbol{\mu}_r) \\ \boldsymbol{\varepsilon}_r &= \boldsymbol{\varepsilon}^0_\Omega + \boldsymbol{S}(\boldsymbol{\mu}_r - \boldsymbol{\mu}_0) = \boldsymbol{M}_0\boldsymbol{\sigma}_r + \boldsymbol{\mu}_r \end{aligned}\right\} \quad [4.1.3]$$

For the load set $\{\boldsymbol{\sigma}^0_\Omega, \boldsymbol{\lambda}_r, \boldsymbol{\lambda}_0\}$

$$\left.\begin{aligned} \boldsymbol{\varepsilon}_r &= \boldsymbol{M}_0\boldsymbol{\sigma}^0_\Omega + \boldsymbol{\mu}_0 + \boldsymbol{S}(\boldsymbol{\mu}_r - \boldsymbol{\mu}_0) = \boldsymbol{M}_0\boldsymbol{\sigma}_r + \boldsymbol{\mu}_r \\ \boldsymbol{\sigma}_r &= \boldsymbol{\sigma}^0_\Omega - \boldsymbol{L}_0(\boldsymbol{I} - \boldsymbol{S})(\boldsymbol{\mu}_r - \boldsymbol{\mu}_0) = \boldsymbol{L}_0(\boldsymbol{\varepsilon}_r - \boldsymbol{\mu}_r) \end{aligned}\right\} \quad [4.1.2]$$

where $\boldsymbol{S}$ is the Eshelby tensor for a selected ellipsoidal shape of Ω_r.

4.7.2 Inhomogeneities and Cavities of Ellipsoidal Shape

For the load set $\{\boldsymbol{\varepsilon}^0_\Omega, \boldsymbol{\mu}_r, \boldsymbol{\mu}_0\}$, the strain and stress fields in an inhomogeneity $\boldsymbol{L}_r$ are

$$\boldsymbol{\varepsilon}_r = \boldsymbol{T}_r\boldsymbol{\varepsilon}^0_\Omega + \boldsymbol{R}_{rr}\boldsymbol{\mu}_r + \boldsymbol{R}_{r0}\boldsymbol{\mu}_0 \quad \boldsymbol{\sigma}_r = \boldsymbol{L}_r(\boldsymbol{\varepsilon}_r - \boldsymbol{\mu}_r) \quad [4.3.2]$$

where

$$\boldsymbol{T}_r = [\boldsymbol{I} + \boldsymbol{P}(\boldsymbol{L}_r - \boldsymbol{L}_0)]^{-1} \quad [4.2.14]$$

and

$$\boldsymbol{R}_{rr} = \boldsymbol{T}_r\boldsymbol{P}\boldsymbol{L}_r \quad \boldsymbol{R}_{r0} = -\boldsymbol{T}_r\boldsymbol{P}\boldsymbol{L}_0 \quad [4.3.7]$$

The $\boldsymbol{P}$ tensor is related to the Eshelby tensor $\boldsymbol{S}$ by

$$\left.\begin{aligned} \boldsymbol{P} = \boldsymbol{S}\boldsymbol{L}_0^{-1} = (\boldsymbol{L}^* + \boldsymbol{L}_0)^{-1} = \boldsymbol{P}^{\mathrm{T}} \quad \boldsymbol{Q} = \boldsymbol{L}_0(\boldsymbol{I} - \boldsymbol{P}\boldsymbol{L}_0) = (\boldsymbol{M}^* + \boldsymbol{M}_0)^{-1} = \boldsymbol{Q}^{\mathrm{T}} \\ \boldsymbol{P}\boldsymbol{L}_0 + \boldsymbol{M}_0\boldsymbol{Q} = \boldsymbol{I} \end{aligned}\right\} \quad [4.2.9]$$

and $\boldsymbol{L}^*, \boldsymbol{M}^*$ are Hill's constraint tensors describing stiffness and compliance of an ellipsoidal cavity (4.2.10).

A traction-free cavity is regarded as an inhomogeneity with vanishing stiffness $\boldsymbol{L}_r \to \boldsymbol{0}$, hence $\boldsymbol{T}_r \to (\boldsymbol{I}-\boldsymbol{S})^{-1}$, $\boldsymbol{R}_{rr} \to \boldsymbol{0}$, $\boldsymbol{R}_{r0} = -(\boldsymbol{I}-\boldsymbol{S})^{-1}\boldsymbol{S}$. However, if the cavity wall is loaded by surface tractions that generate an average stress $\bar{\boldsymbol{\sigma}}_r^c$, then the cavity strain average is

$$\left.\begin{aligned}\bar{\boldsymbol{\varepsilon}}_r^c &= (\boldsymbol{I}-\boldsymbol{S})^{-1}(\boldsymbol{\varepsilon}_\Omega^0 - \boldsymbol{S}\boldsymbol{\mu}_0) - \boldsymbol{M}^*\bar{\boldsymbol{\sigma}}_r^c \\ &= (\boldsymbol{I}-\boldsymbol{S})^{-1}[\boldsymbol{\varepsilon}_\Omega^0 - \boldsymbol{S}(\boldsymbol{\mu}_0 + \boldsymbol{M}_0\bar{\boldsymbol{\sigma}}_r^c)]\end{aligned}\right\} \qquad [4.3.27]$$

For the load set $\{\boldsymbol{\sigma}_\Omega^0, \boldsymbol{\lambda}_r, \boldsymbol{\lambda}_0\}$ the stress and strain fields in an inhomogeneity L_r are

$$\boldsymbol{\sigma}_r = \boldsymbol{W}_r\boldsymbol{\sigma}_\Omega^0 + \boldsymbol{N}_{rr}\boldsymbol{\lambda}_r + \boldsymbol{N}_{r0}\boldsymbol{\lambda}_0 \quad \boldsymbol{\varepsilon}_r = \boldsymbol{M}_r\boldsymbol{\sigma}_r + \boldsymbol{\mu}_r \qquad [4.3.3]$$

where

$$\boldsymbol{W}_r = [\boldsymbol{I} + \boldsymbol{Q}(\boldsymbol{M}_r - \boldsymbol{M}_0)]^{-1} \qquad [4.2.13]$$

and

$$\boldsymbol{N}_{rr} = \boldsymbol{W}_r\boldsymbol{Q}\boldsymbol{M}_r \quad \boldsymbol{N}_{r0} = -\boldsymbol{W}_r\boldsymbol{Q}\boldsymbol{M}_0 \qquad [4.3.8]$$

The mechanical partial concentration factors $\boldsymbol{T}_r, \boldsymbol{W}_r$ need not be diagonally symmetric, however

$$\left.\begin{aligned}\boldsymbol{T}_r\boldsymbol{P} = \boldsymbol{P}\boldsymbol{T}_r^{\mathrm{T}} \quad \boldsymbol{W}_r\boldsymbol{Q} = \boldsymbol{Q}\boldsymbol{W}_r^{\mathrm{T}} \\ \boldsymbol{T}_r(\boldsymbol{L}_r - \boldsymbol{L}_0) = (\boldsymbol{L}_r - \boldsymbol{L}_0)\boldsymbol{T}_r^{\mathrm{T}} \quad \boldsymbol{W}_r(\boldsymbol{M}_r - \boldsymbol{M}_0) = (\boldsymbol{M}_r - \boldsymbol{M}_0)\boldsymbol{W}_r^{\mathrm{T}}\end{aligned}\right\} \qquad [4.2.15]$$

The (6×6) matrices $\boldsymbol{R}_{rr}$, $\boldsymbol{R}_{r0}$ and $\boldsymbol{N}_{rr}$, $\boldsymbol{N}_{r0}$ need not be diagonally symmetric, but it can be verified that

$$\boldsymbol{R}_{rr}\boldsymbol{M}_r = \boldsymbol{M}_r\boldsymbol{R}_{rr}^T \quad \boldsymbol{N}_{rr}\boldsymbol{L}_r = \boldsymbol{L}_r\boldsymbol{N}_{rr}^T \qquad [4.3.9]$$

Useful connections are

$$\left.\begin{aligned}\boldsymbol{T}_r + \boldsymbol{R}_{rr} + \boldsymbol{R}_{r0} = \boldsymbol{I} \quad \boldsymbol{W}_r + \boldsymbol{N}_{rr} + \boldsymbol{N}_{r0} = \boldsymbol{I} \\ \boldsymbol{W}_r\boldsymbol{L}_0 = \boldsymbol{L}_r\boldsymbol{T}_r \quad \boldsymbol{M}_r\boldsymbol{W}_r = \boldsymbol{T}_r\boldsymbol{M}_0\end{aligned}\right\} \qquad [4.2.5]$$

A cavity that is loaded by surface tractions, in equilibrium with uniform stress $\bar{\boldsymbol{\sigma}}_r^c$ on its wall, and subjected to the eigenstress $\boldsymbol{\lambda}_0$ in its exterior and to a remotely applied uniform stress $\boldsymbol{\sigma}^0$, undergoes the average strain

$$\boldsymbol{M}^*\bar{\boldsymbol{\sigma}}_r^c = (\boldsymbol{I}-\boldsymbol{S})^{-1}\boldsymbol{M}_0\boldsymbol{\sigma}_\Omega^0 - \boldsymbol{M}_0\boldsymbol{\lambda}_0 - \bar{\boldsymbol{\varepsilon}}_r^c \qquad [4.3.31]$$

In a traction-free cavity, $\bar{\boldsymbol{\sigma}}_r^c = \mathbf{0}$. Since $\boldsymbol{\sigma}_\Omega^0 = \boldsymbol{L}_0(\boldsymbol{\varepsilon}_\Omega^0 - \boldsymbol{\mu}_0)$, [4.3.31] and [4.3.27] yield the same cavity strain. Partially debonded inhomogeneities are discussed in Sect. 4.4.3.

4.7.3 Multiphase Aggregate with Dilute Reinforcements $\boldsymbol{L}_r$ in Matrix $\boldsymbol{L}_1$

Volume fractions of phases $r = 1,\ 2,\ \ldots n$ are defined by

$$c_1 = 1 - \sum_{r=2}^{n} c_r \quad \sum_{r=2}^{n} c_r = \sum_{r=2}^{n} V_r / V \ll 1 \qquad [4.4.1]$$

The reinforcements $r = 2,\ \ldots n$ interact only with the matrix $r = 1$, but not with each other.

For the load set $\{\boldsymbol{\varepsilon}^0,\ \boldsymbol{\mu}_r,\ \boldsymbol{\mu}_1\}$, where $\boldsymbol{\mu}_1$ is a uniform eigenstrain applied in the matrix $r = 1$, the phase field averages are

$$\left.\begin{aligned} c_1\boldsymbol{\varepsilon}_1 &= \boldsymbol{\varepsilon}^0 - \sum_{s=2}^{n} c_s\boldsymbol{\varepsilon}_s \quad \boldsymbol{\sigma}_1 = \boldsymbol{L}_1(\boldsymbol{\varepsilon}_1 - \boldsymbol{\mu}_1) \\ \boldsymbol{\varepsilon}_r &= \boldsymbol{T}_r\boldsymbol{\varepsilon}^0 + \boldsymbol{R}_{r1}\boldsymbol{\mu}_1 + \boldsymbol{R}_{rr}\boldsymbol{\mu}_r \quad \boldsymbol{\sigma}_r = \boldsymbol{L}_r(\boldsymbol{\varepsilon}_r - \boldsymbol{\mu}_r) = \boldsymbol{L}_r\boldsymbol{\varepsilon}_r + \boldsymbol{\lambda}_r \end{aligned}\right\} \qquad [4.4.2]$$

Overall stress caused by the applied overall strain and by phase eigenstrains is obtained from the Levin formula as

$$\sum_{s=1}^{N} c_s\boldsymbol{\sigma}_s = \bar{\boldsymbol{\sigma}} = \boldsymbol{L}\boldsymbol{\varepsilon}_\Omega^0 + \bar{\boldsymbol{\lambda}} = \boldsymbol{L}\boldsymbol{\varepsilon}_\Omega^0 + \sum_{s=1}^{N} c_r\boldsymbol{T}_r^{\mathrm{T}}\boldsymbol{\lambda}_r \qquad [4.4.5]$$

where $\bar{\boldsymbol{\lambda}} = -\boldsymbol{L}\bar{\boldsymbol{\mu}}$ is the overall eigenstress at $\boldsymbol{\varepsilon}^0 = \mathbf{0}$, and $\boldsymbol{\lambda}_r = -\boldsymbol{L}_r\boldsymbol{\mu}_r$ at $\boldsymbol{\varepsilon}_r = \mathbf{0}$.

Overall stiffness of the dilutely reinforced aggregate is

$$\left.\begin{aligned} \boldsymbol{L} &= c_1\boldsymbol{L}_1\boldsymbol{T}_1 + \sum_{r=2}^{N} c_r\boldsymbol{L}_r\boldsymbol{T}_r = \boldsymbol{L}_1 + \sum_{r=2}^{N} c_r(\boldsymbol{L}_r - \boldsymbol{L}_1)\boldsymbol{T}_r \\ &= \boldsymbol{L}_1 + \sum_{r=2}^{N} c_r[\boldsymbol{P}_r + (\boldsymbol{L}_r - \boldsymbol{L}_1)^{-1}]^{-1} = \boldsymbol{L}^{\mathrm{T}} \end{aligned}\right\} \qquad [4.4.6]$$

Strain and eigenstrain concentration factors $\boldsymbol{T}_r, \boldsymbol{R}_{rr}, \boldsymbol{R}_{r1}$ follow from [4.2.13] and [4.3.7] above, with $\boldsymbol{L}_0 = \boldsymbol{L}_1$.

For the load set $\{\boldsymbol{\sigma}^0, \boldsymbol{\lambda}_r, \boldsymbol{\lambda}_1\}$, field averages in the phases are

$$\left.\begin{aligned} \boldsymbol{\sigma}_1 &= \frac{1}{c_1}\left[\boldsymbol{\sigma}^0 - \sum_{s=2}^{n} c_s \boldsymbol{\sigma}_s\right] \quad \boldsymbol{\varepsilon}_1 = \boldsymbol{M}_1(\boldsymbol{\sigma}_1 - \boldsymbol{\lambda}_1) \\ \boldsymbol{\sigma}_r &= \boldsymbol{W}_r \boldsymbol{\sigma}^0 + \boldsymbol{N}_{r1}\boldsymbol{\lambda}_1 + \boldsymbol{N}_{rr}\boldsymbol{\lambda}_r \quad \boldsymbol{\varepsilon}_r = \boldsymbol{M}_r(\boldsymbol{\sigma}_r - \boldsymbol{\lambda}_r) = \boldsymbol{M}_r\boldsymbol{\sigma}_r + \boldsymbol{\mu}_r \end{aligned}\right\} \quad [4.4.7]$$

where $\boldsymbol{\mu}_r = -\boldsymbol{M}_r\boldsymbol{\lambda}_r$ and $\boldsymbol{W}_r, \boldsymbol{N}_{rr}, \boldsymbol{N}_{r1}$ appear in (4.2.13) and (4.3.8).

Overall strain caused by the load set $\{\boldsymbol{\sigma}^0, \boldsymbol{\lambda}_r, \boldsymbol{\lambda}_1\}$, with $\boldsymbol{\mu}_r = -\boldsymbol{M}_r\boldsymbol{\lambda}_r$, $\boldsymbol{\mu}_1 = -\boldsymbol{M}_1\boldsymbol{\lambda}_1$, is

$$\sum_{s=1}^{N} c_s \boldsymbol{\varepsilon}_s = \bar{\boldsymbol{\varepsilon}} = \boldsymbol{M}\boldsymbol{\sigma}^0 + \bar{\boldsymbol{\mu}} = \boldsymbol{M}\boldsymbol{\sigma}^0 + \sum_{r=2}^{N} c_r \boldsymbol{W}_r{}^{\mathrm{T}}\boldsymbol{\mu}_r \quad [4.4.10]$$

Overall compliance of the aggregate is

$$\boldsymbol{M} = c_1\boldsymbol{M}_1\boldsymbol{W}_1 + \sum_{r=2}^{N} c_r \boldsymbol{M}_r\boldsymbol{W}_r = \boldsymbol{M}_1 + \sum_{r=2}^{N} c_r(\boldsymbol{M}_r - \boldsymbol{M}_1)\boldsymbol{W}_r = \boldsymbol{M}^{\mathrm{T}} \quad [4.4.11]$$

As shown in (4.4.12), the overall compliance of a dilutely reinforced solid is $\boldsymbol{M} = \boldsymbol{L}^{-1}$.

Chapter 5
Energies of Inhomogeneities, Dilute Reinforcements and Cracks

As in the previous chapter, we consider homogeneous inclusions and inhomogeneities in subvolumes Ω_r of an infinitely extended homogeneous volume Ω_0 of a comparison medium or 'matrix' of stiffness $\boldsymbol{L}_0$; the total volume $\Omega = \Omega_0 + \Omega_r$. In Sects. 5.1.4 and in 5.2 and 5.3, we examine composite aggregates with dilute reinforcement, which may consist of many distinct inhomogeneities $\boldsymbol{L}_r$ in a matrix $\boldsymbol{L}_1$, as described in Sect. 4.4. Systems containing cracks are discussed in Sect. 5.4. Loads applied to both single and multiple inhomogeneity systems include displacement or traction fields acting at a remote boundary to generate uniform overall strain or stress, and piecewise uniform, physically based eigenstrains in both matrix and inhomogeneities. Those include thermal and moisture-induced strains, phase transformations, and inelastic strains. Low loading rates causing only small strains are assumed.

When applied separately to a homogeneous material, each of these loads generates a certain amount of potential energy $\mathcal{V}$ defined in Sect. 3.7. When applied together to a heterogeneous material, they generate the total potential energy, which is equal to the sum of the energies caused by the applied loads and of the potential energy generated by interactions between individual load components and/or inhomogeneities. Different interaction energies are derived for selected combinations of applied loads and material configurations. The results are useful in several applications, e.g., in estimating the energy released by interfacial decohesion of inhomogeneities from the surrounding matrix, or energy changes associated with phase transformations.

Many aspects of this subject were examined by Eshelby (1956, 1957, 1961) and Mura (1987), who were using the equivalent inclusion method of Sect. 4.3.2 to simulate local fields in inhomogeneities. The present treatment describes local field averages by the partial mechanical and transformation concentration factors found in Sects 4.2 and 4.3, and it covers a much broader range of problems.

G.J. Dvorak, *Micromechanics of Composite Materials*, Solid Mechanics and Its Applications 186, DOI 10.1007/978-94-007-4101-0_5,

Since equivalent eigenstrains are no longer needed, the role of physically based eigenstrains in the energy balance becomes more transparent. Eshelby's results are recovered as special cases, and Mura's often appear along the way to a more explicit form.

Energy terms evaluated in the different systems include the strain energy $\mathcal{W}$ generated by surface displacements causing uniform overall strains $\boldsymbol{\varepsilon}^0_\Omega$ or $\boldsymbol{\varepsilon}^0$, and by a distribution of uniform phase or subvolume eigenstrains $\boldsymbol{\mu}_r$. The potential energy $\mathcal{V}$ is generated by surface tractions causing uniform overall stresses $\boldsymbol{\sigma}^0_\Omega$ or $\boldsymbol{\sigma}^0$, and by a distribution of uniform phase or subvolume eigenstresses $\boldsymbol{\lambda}_r = -\boldsymbol{L}_r\boldsymbol{\mu}_r$.

As pointed out by Eshelby, in the context of thermodynamics, the strain energy is the Helmholtz free energy of a selected volume V of the aggregate, $\mathcal{F} = \mathcal{W} - \theta_0\mathcal{S}$, where the product of absolute temperature and entropy $\theta_0\mathcal{S} = 0$ at isothermal conditions. The potential energy $\mathcal{V}$ is the Gibbs free energy $\mathcal{G} = \mathcal{V} - \theta_0\mathcal{S}$ under such conditions. To preserve these conditions, material properties are assumed to be independent of temperature changes.

5.1 Energy Changes Caused by Mechanical Loads

5.1.1 Uniform Overall Strain Is Applied

To introduce the subject, consider a solitary inhomogeneity $\boldsymbol{L}_r$ of arbitrarily shaped subvolume Ω_r, perfectly bonded along the interface $\partial\Omega_r$ to the volume $\Omega_0 = \Omega - \Omega_r$ of a comparison medium $\boldsymbol{L}_0$. A uniform overall strain $\boldsymbol{\varepsilon}^0_\Omega = \bar{\boldsymbol{\varepsilon}}_\Omega$ is applied, but no phase eigenstrains are present. Volume average of the equilibrium stress fields in the phases is

$$\left.\begin{aligned}\bar{\boldsymbol{\sigma}}_\Omega &= \frac{1}{\Omega}\int_\Omega \boldsymbol{\sigma}(\boldsymbol{x})\mathrm{d}V = \frac{1}{\Omega}\left[\int_{\Omega_0}\boldsymbol{L}_0\boldsymbol{\varepsilon}(\boldsymbol{x})\mathrm{d}V + \int_{\Omega_r}\boldsymbol{L}_r\boldsymbol{\varepsilon}(\boldsymbol{x})\mathrm{d}V\right]\\ &= \frac{1}{\Omega}\left[\int_\Omega \boldsymbol{L}_0\boldsymbol{\varepsilon}(\boldsymbol{x})\mathrm{d}V + \int_{\Omega_r}(\boldsymbol{L}_r - \boldsymbol{L}_0)\boldsymbol{\varepsilon}(\boldsymbol{x})\mathrm{d}V\right]\end{aligned}\right\} \tag{5.1.1}$$

The second integral is now written in terms of the partial strain influence function $\boldsymbol{T}_r(\boldsymbol{x})$, which for ellipsoidal inhomogeneities reduces to the concentration factor $\boldsymbol{T}_r$ in (4.2.13).

$$\frac{1}{\Omega}\int_{\Omega_r}(\boldsymbol{L}_r - \boldsymbol{L}_0)\boldsymbol{\varepsilon}(\boldsymbol{x})\mathrm{d}V = \frac{1}{\Omega}\int_{\Omega_r}(\boldsymbol{L}_r - \boldsymbol{L}_0)\boldsymbol{T}_r(\boldsymbol{x})\boldsymbol{\varepsilon}^0_\Omega\mathrm{d}V = \frac{\Omega_r}{\Omega}(\boldsymbol{L}_r - \boldsymbol{L}_0)\boldsymbol{T}_r\boldsymbol{\varepsilon}^0_\Omega \tag{5.1.2}$$

The elastic strain energy $\mathcal{W}$ of the strained volume $\Omega = \Omega_0 + \Omega_r$ is found by utilizing the statically admissible stress averages (5.1.1) and (5.1.2) in the virtual work equation

$$\mathcal{W} = \frac{1}{2}\int_{\Omega} [\boldsymbol{\sigma}(\boldsymbol{x})]^{\mathrm{T}}\boldsymbol{\varepsilon}(\boldsymbol{x})\mathrm{d}V = \frac{1}{2}\bar{\boldsymbol{\sigma}}_{\Omega}^{\mathrm{T}}\boldsymbol{\varepsilon}_{\Omega}^{0}\Omega \tag{5.1.3}$$

where the applied uniform strain $\boldsymbol{\varepsilon}_{\Omega}^{0}$ and the local field $\boldsymbol{\varepsilon}(\boldsymbol{x})$ are selected as the kinematically admissible set. After substitution from (5.1.1) and (5.1.2), the total strain energy is decomposed into $\mathcal{W} = \mathcal{W}_0 + \mathcal{W}_I$

$$\left.\begin{aligned} \mathcal{W}_0 &= \frac{1}{2}(\boldsymbol{\varepsilon}_{\Omega}^{0})^{\mathrm{T}}\boldsymbol{L}_0\boldsymbol{\varepsilon}_{\Omega}^{0}\Omega \\ \mathcal{W}_I &= \frac{1}{2}(\boldsymbol{\varepsilon}_{\Omega}^{0})^{\mathrm{T}}(\boldsymbol{L}_r - \boldsymbol{L}_0)\boldsymbol{T}_r\boldsymbol{\varepsilon}_{\Omega}^{0}\Omega_r = \frac{1}{2}(\boldsymbol{\varepsilon}_{\Omega}^{0})^{\mathrm{T}}(\boldsymbol{W}_r\boldsymbol{L}_0 - \boldsymbol{L}_0\boldsymbol{T}_r)\boldsymbol{\varepsilon}_{\Omega}^{0}\Omega_r \end{aligned}\right\} \tag{5.1.4}$$

where $\boldsymbol{L}_r\boldsymbol{T}_r = \boldsymbol{W}_r\boldsymbol{L}_0$. $\mathcal{W}_0$ is the energy of the homogeneous comparison medium under $\boldsymbol{\varepsilon}_{\Omega}^{0}$, and $\mathcal{W}_I$ is the *interaction energy* between the inhomogeneity $\boldsymbol{L}_r$ and the prescribed overall strain $\boldsymbol{\varepsilon}_{\Omega}^{0}$. In subscript notation, for an inhomogeneity of any shape for which the integrals exist

$$\mathcal{W}_I = \frac{1}{2}\int_{\Omega_r} (\varepsilon_{ij})_{\Omega}^{0}[W_{ijkl}^{r}(\boldsymbol{x})L_{klmn}^{0} - L_{ijkl}^{0}T_{klmn}^{r}(\boldsymbol{x})](\varepsilon_{mn})_{\Omega}^{0}\mathrm{d}V \tag{5.1.5}$$

It is often convenient to write $\mathcal{W}_I$ as a surface integral over the interface $\partial\Omega_r$. Actual interface traction and displacement vectors, caused on the 'matrix' side $\partial\Omega_r^{+}$ of the interface by the applied overall strain $\boldsymbol{\varepsilon}_{\Omega}^{0}$ are defined by

$$t_i = \sigma_{ij}n_j \quad \text{and} \quad u_i = \varepsilon_{ij}x_j \quad x_i \in \partial\Omega_r^{+} \tag{5.1.6}$$

We also define the displacement and traction vectors

$$u_i^{0} \quad \text{and} \quad \tilde{t}_i^{\Omega} = \tilde{\sigma}_{ij}^{\Omega}n_j = L_{ijkl}^{0}(\varepsilon_{kl})_{\Omega}^{0}n_j \tag{5.1.7}$$

that would be generated on this interface $\partial\Omega_r^{+}$, drawn in a homogeneous volume Ω, by the overall strain $(\varepsilon_{ij})_{\Omega}^{0} = u_{i,j}^{0}$ applied at $\partial\Omega$. Substituting these vectors into (5.1.5) provides the interaction energy between the overall strain and the inhomogeneity $\boldsymbol{L}_r$, evaluated as an integral over the surface $\partial\Omega_r$, following the sequence shown in (3.7.1)

$$\mathcal{W}_I = \frac{1}{2}\int_{\Omega_r} [(\varepsilon_{ij})_{\Omega}^{0}\sigma_{ij}(\boldsymbol{x}) - \varepsilon_{ij}(\boldsymbol{x})\tilde{\sigma}_{ij}^{\Omega}]\mathrm{d}V = \frac{1}{2}\int_{\partial\Omega_r} (t_i u_i^{0} - \tilde{t}_i^{\Omega}u_i)\mathrm{d}S \tag{5.1.8}$$

This result is a form of the *Eshelby (1956) formula*, indicating that at a given overall strain, the interaction energy is generated by the work of the tractions and displacements at the interface of the inhomogeneity on those acting there in a homogeneous medium, respectively. As shown later, this result also applies to interface tractions and displacements associated with an imperfect interface, where the local field averages comply with (4.3.27). Moreover, this result applies to interaction between the applied strain $\boldsymbol{\varepsilon}^0_\Omega$ and a traction-free cavity in Ω_r; in that particular case, $\boldsymbol{L}_r = \boldsymbol{0}$, $\boldsymbol{W}_r = \boldsymbol{0}$ in (5.1.4) and (5.1.5), causing $t_i = 0$ in (5.1.8).

5.1.2 Uniform Overall Stress Is Applied

Next, the above material $\boldsymbol{L}_0 \in \Omega_0$ containing a perfectly bonded inhomogeneity $\boldsymbol{L}_r \in \Omega_r$ of arbitrary shape is loaded by a uniform overall stress $\boldsymbol{\sigma}^0_\Omega$ applied at a remote external boundary $\partial\Omega$ by surface tractions $t^0_i = (\sigma_{ij})^0_\Omega n_j$. The resulting overall strain is $u_{i,j} = \bar{\varepsilon}^\Omega_{ij}$. Evaluation of the potential energy V of the aggregate and applied loads utilizes the Clapeyron theorem (3.7.1) and virtual work of the equilibrium stress state on the phase strain averages. The result is

$$\mathcal{V} = \frac{1}{2}\int_\Omega \sigma_{ij}\varepsilon_{ij}\mathrm{d}V - \int_{\partial\Omega} t_i u_i \mathrm{d}S = -\frac{1}{2}\int_\Omega \sigma_{ij}\varepsilon_{ij}\mathrm{d}V = -\frac{1}{2}(\sigma_{ij})^0_\Omega \bar{\varepsilon}^\Omega_{ij}\Omega \tag{5.1.9}$$

A procedure similar to (5.1.1), (5.1.2), (5.1.3), (5.1.4), provides the strain averages and the total potential energy as $\mathcal{V} = \mathcal{V}_0 + \mathcal{V}_I$, where

$$\left.\begin{aligned} \mathcal{V}_0 &= -\frac{1}{2}(\boldsymbol{\sigma}^0_\Omega)^{\mathrm{T}}\boldsymbol{M}_0\boldsymbol{\sigma}^0_\Omega\Omega \\ \mathcal{V}_I &= -\frac{1}{2}(\boldsymbol{\sigma}^0_\Omega)^{\mathrm{T}}(\boldsymbol{M}_r - \boldsymbol{M}_0)\boldsymbol{W}_r\boldsymbol{\sigma}^0_\Omega\Omega_r = \frac{1}{2}(\boldsymbol{\sigma}^0_\Omega)^{\mathrm{T}}(\boldsymbol{M}_0\boldsymbol{W}_r - \boldsymbol{T}_r\boldsymbol{M}_0)\boldsymbol{\sigma}^0_\Omega\Omega_r \end{aligned}\right\} \tag{5.1.10}$$

The $\boldsymbol{W}_r$, given by (4.2.13), is the r-phase volume average of the partial stress influence function $\boldsymbol{W}_r(\boldsymbol{x})$, and $\boldsymbol{T}_r\boldsymbol{M}_0 = \boldsymbol{M}_r\boldsymbol{W}_r$.

$\mathcal{V}_I = \mathcal{V} - \mathcal{V}_0$ is the interaction energy between the prescribed stress $\boldsymbol{\sigma}^0_\Omega$ and the inhomogeneity $\boldsymbol{L}_r$. A surface integral form is obtained in analogy with the sequence (5.1.5), (5.1.6), (5.1.7), (5.1.8), as the original form of the Eshelby (1956) formula

$$\mathcal{V}_I = \frac{1}{2}\int_{\partial\Omega_r} (t_i\tilde{u}^\Omega_i - t^0_i u_i)\mathrm{d}S \tag{5.1.11}$$

where t_i, u_i denote actual traction and displacement vectors on $\partial\Omega_r^+$, the 'matrix' or cavity side of the interface, analogous to those in (5.1.6). On the other hand, tractions and displacements

$$t_i^0 = (\sigma_{ij})_\Omega^0 n_j \quad \text{and} \quad \tilde{u}_{i,j}^\Omega = \tilde{\varepsilon}_{ij}^\Omega = L_{ijkl}^0 (\sigma_{kl})_\Omega^0 \tag{5.1.12}$$

would be caused on $\partial\Omega_r^+$ if the applied overall stress was applied to a homogeneous medium $\boldsymbol{M}_0$.

For a solitary inhomogeneity that has no effect on the magnitude of overall stiffness $\boldsymbol{L}_0$, the overall stress and strain are related by $\bar{\boldsymbol{\sigma}}_\Omega = \boldsymbol{L}_0 \bar{\boldsymbol{\varepsilon}}_\Omega$. Substituting this into $(5.1.10)_3$ shows that the interaction energies (5.1.8) and (5.1.11) are identical, not affected by the changed boundary conditions. However, $\mathcal{W}_0$ and $\mathcal{V}_0$ have opposite signs. Notice that these forms of the interaction energy between overall mechanical loads $\boldsymbol{\varepsilon}_\Omega^0$ or $\boldsymbol{\sigma}_\Omega^0$ and an inhomogeneity $\boldsymbol{L}_r$ involve only surface tractions and displacements acting at $\partial\Omega_r$, assuming perfect contact. Imperfect contact may involve additional work of the surface tractions on displacement jumps.

Since the energy $\mathcal{W}_0$ in a homogeneous medium $\boldsymbol{L}_0$, derived in $(5.1.4)_1$, is independent of $\boldsymbol{L}_r$, any changes in $\boldsymbol{L}_r$ are reflected only in the interaction energy. If the inhomogeneity has a 'higher' stiffness than the comparison medium, or more precisely, if the matrix $\boldsymbol{L}_r - \boldsymbol{L}_0$ is positive semi-definite, then $\boldsymbol{M}_r - \boldsymbol{M}_0$ is negative semi-definite and the interaction energy is positive. On the other hand, an inhomogeneity with 'lower' stiffness than the medium $\boldsymbol{L}_0$ reduces the total potential energy. Therefore, in the former case, the interaction energy is available for a phase transformation or interface separation that reduces the effective stiffness of the material inside Ω_r.

Eshelby (1961) decomposed the total energy that may favor formation of a new inhomogeneity or precipitate into four parts,

$$\mathcal{V}_{tot} = \mathcal{V}_0 + \mathcal{V}_A + \mathcal{V}_{inc} + \mathcal{V}_I \tag{5.1.13}$$

where $\mathcal{V}_0 + \mathcal{V}_A$ represent energy of the loading mechanism and the potential energy caused by external loads, both evaluated in the absence of the precipitate. $\mathcal{V}_{inc}$ is the increase in potential energy cased by introduction of the precipitate at zero overall stress, and $\mathcal{V}_I$ is the interaction energy. Choosing the overall stress to make the Gibbs free energy of formation of the inhomogeneity $\Delta\mathcal{V}_{tot} = \mathcal{V}_{inc} + \mathcal{V}_I < 0$ favors spontaneous precipitate formation.

5.1.3 *Energy Based Evaluation of Overall Stiffness and Compliance of Dilute Mixtures*

We recall from Sect. 4.4 that local fields in a composite material with very low or dilute reinforcement density can be approximated by those in a single

inhomogeneity $\boldsymbol{L}_r$. In a two-phase system, $r = 1, 2$, $c_2 = 1 - c_1 \ll 1$. The stiffness and compliance $\boldsymbol{L}_1$, $\boldsymbol{M}_1$ of the actual matrix now replaces the $\boldsymbol{L}_0$, $\boldsymbol{M}_0$ of the comparison medium and, as indicated in (4.4.2) and (4.4.3), the overall applied strain $\boldsymbol{\varepsilon}^0$ is substituted for $\boldsymbol{\varepsilon}^0_\Omega$ in evaluation of local strain field averages. Subject to these modifications, (5.1.1) and (5.1.2) can be readily applied to dilute mixtures. In particular, rewriting the first integral in (5.1.1) as

$$\frac{1}{V}\int_V \boldsymbol{\sigma}(\boldsymbol{x})\mathrm{d}V = \bar{\boldsymbol{\sigma}} = \boldsymbol{L}\boldsymbol{\varepsilon}^0 \tag{5.1.14}$$

and letting $\boldsymbol{L}_0 \to \boldsymbol{L}_1$ in (5.1.2), (5.1.3), (5.1.4), or $\boldsymbol{M}_0 \to \boldsymbol{M}_1$ in (5.1.9), (5.1.10), yields

$$\boldsymbol{L} = \boldsymbol{L}_1 + c_r(\boldsymbol{L}_r - \boldsymbol{L}_1)\boldsymbol{T}_r \qquad \boldsymbol{M} = \boldsymbol{M}_1 + c_r(\boldsymbol{M}_r - \boldsymbol{M}_1)\boldsymbol{W}_r \tag{5.1.15}$$

For two-phase systems, these results coincide with those derived in (4.4.6) and (4.4.12) from strain and stress field averages. They also extend to multiphase systems, where contributions of all reinforcement volume fractions to matrix stiffness or compliance are added. Therefore, both energy-based and averaging methods give the same estimate of overall moduli.

5.1.4 *Energy Released by Complete Decohesion of a Part of Dilute Reinforcement*

The result of interest here is the change in total energy $\Delta\mathcal{W} = \mathcal{W}_d - \mathcal{W}$ per unit volume V of the aggregate, caused by complete decohesion of a certain volume fraction $c_d = V_d/V$ of identical inhomogeneities $\boldsymbol{L}_2$ from the matrix $\boldsymbol{L}_1$, while the composite is loaded by a fixed *uniform overall strain* $\boldsymbol{\varepsilon}^0$, and the walls of the new cavities remain traction free. $\mathcal{W}_d$ is the energy after decohesion, equal to that generated in the damaged system by applying $\boldsymbol{\varepsilon}^0$ from an initially traction-free state. The dilute approximation of overall stiffness and compliance, and the effect of cavitation on those quantities are described in Sect. 4.4. We recall that the volume fraction of reinforcements and cavities is $1 - c_1 \ll 1$.

Total energy of the undamaged aggregate is denoted by $\mathcal{W} = \mathcal{W}_1 + \mathcal{W}_I$, and $\mathcal{W}_d = \mathcal{W}_1 + \mathcal{W}_I^d$ is the total energy after decohesion. As shown in $(5.1.4)_1$, the strain energy of the homogeneous matrix is equal to $2\mathcal{W}_1 = (\boldsymbol{\varepsilon}^0)^{\mathrm{T}}\boldsymbol{L}_1\boldsymbol{\varepsilon}^0\, V$, and it is not affected by decohesion. Therefore, $\Delta\mathcal{W} = \mathcal{W}_d - \mathcal{W} = \mathcal{W}_I^d - \mathcal{W}_I$ is equal to the difference in interaction energies between the applied strain and the cavities and inhomogeneities.

Interaction energy follows from the Eshelby formula in the form similar to $(5.1.4)_2$. First, each inhomogeneity is perfectly bonded to the matrix $\boldsymbol{L}_1$, and its strain concentration factor is taken as equal to that of a solitary inhomogeneity.

The interaction energy between the volume fraction $c_2 = V_2/V = 1 - c_1$ of inhomogeneities and the applied strain $\boldsymbol{\varepsilon}^0$ is

$$\frac{1}{V}\mathcal{W}_I = \frac{1}{2}c_2(\boldsymbol{\varepsilon}^0)^{\mathrm{T}}(\boldsymbol{L}_2 - \boldsymbol{L}_1)\boldsymbol{T}_2\boldsymbol{\varepsilon}^0 \tag{5.1.16}$$

where $\boldsymbol{T}_2 = [\boldsymbol{I} + \boldsymbol{P}(\boldsymbol{L}_2 - \boldsymbol{L}_1)]^{-1}$ is the strain concentration factor of the bonded inhomogeneities derived in Sect. 4.2.

Next, a certain volume fraction c_d of the inhomogeneities undergoes complete decohesion from the matrix, so that the still bonded inhomogeneities are left in the volume fraction $c_2 - c_d$. Complete decohesion of an inhomogeneity can be accounted for by replacing its original stiffness $\boldsymbol{L}_2$ by $\boldsymbol{L}_d \to \boldsymbol{0}$. From (4.2.13), the partial strain concentration factor of a cavity is $\boldsymbol{T}_d = (\boldsymbol{I} - \boldsymbol{P}\boldsymbol{L}_1)^{-1} = (\boldsymbol{I} - \boldsymbol{S})^{-1}$, where $\boldsymbol{S} = \boldsymbol{P}\boldsymbol{L}_1$ is the Eshelby tensor for the selected cavity shape, evaluated in the matrix $\boldsymbol{L}_1$. The total interaction energy between the bonded inhomogeneities plus cavities and the applied strain follows from (5.1.16) as

$$\frac{1}{V}\mathcal{W}_I^d = \frac{(c_2 - c_d)}{2}(\boldsymbol{\varepsilon}^0)^{\mathrm{T}}(\boldsymbol{L}_2 - \boldsymbol{L}_1)\boldsymbol{T}_2\boldsymbol{\varepsilon}^0 - \frac{c_d}{2}(\boldsymbol{\varepsilon}^0)^{\mathrm{T}}\boldsymbol{L}_1\boldsymbol{T}_c\boldsymbol{\varepsilon}^0 \tag{5.1.17}$$

The change $\Delta\mathcal{W} = \mathcal{W}_I^d - \mathcal{W}_I$ in the total strain energy per unit volume V of the aggregate, caused by complete decohesion of a certain volume fraction c_d of the inhomogeneities is

$$\frac{\Delta\mathcal{W}}{V} = \frac{1}{V}(\mathcal{W}_I^d - \mathcal{W}_I) = -\frac{c_d}{2}(\boldsymbol{\varepsilon}^0)^{\mathrm{T}}[\boldsymbol{L}_2\boldsymbol{T}_2 - \boldsymbol{L}_1(\boldsymbol{T}_d - \boldsymbol{T}_2)]\boldsymbol{\varepsilon}^0 \tag{5.1.18}$$

Since the difference $(\boldsymbol{T}_d - \boldsymbol{T}_2)$ should be positive semi-definite for open cavities, the $\Delta\mathcal{W}$ represents a decrease in the total strain energy, equal to that released by decohesion.

Notice that even for $c_d \to c_2$, the $\Delta\mathcal{W}$ retains a contribution by $\boldsymbol{L}_2$ and $\boldsymbol{T}_2$, as a reminder of the fact that this energy was released from an originally bonded aggregate. It is therefore different from the total energy of a porous medium, consisting of a volume fraction c_c of cavities in a homogeneous matrix $\boldsymbol{L}_1$

$$\frac{1}{V}\mathcal{W}_p = \frac{1}{2}(\boldsymbol{\varepsilon}^0)^{\mathrm{T}}\boldsymbol{L}_1[\boldsymbol{I} - c_c(\boldsymbol{I} - \boldsymbol{S})^{-1}]\,\boldsymbol{\varepsilon}^0 \tag{5.1.19}$$

where the last term follows from $\boldsymbol{T}_c = (\boldsymbol{I} - \boldsymbol{P}\boldsymbol{L}_1)^{-1} = (\boldsymbol{I} - \boldsymbol{S})^{-1}$.

As indicated in Sect. 5.1.3, overall stiffness of the damaged aggregate can be derived from its total strain energy. With reference to (5.1.17)

$$\boldsymbol{L}_d = \boldsymbol{L}_1 + (c_2 - c_d)(\boldsymbol{L}_2 - \boldsymbol{L}_1)\boldsymbol{T}_2 - c_d\boldsymbol{L}_1\boldsymbol{T}_d \tag{5.1.20}$$

which, with the above value of $\boldsymbol{T}_d$, agrees with (4.4.6).

Under a constant, uniform overall stress $\boldsymbol{\sigma}^0$, we now find the change in the potential energy $\Delta\mathcal{V}$ in an aggregate that experiences complete decohesion of a certain volume fraction c_d of inhomogeneities. As indicated by (5.1.9) the total potential energy of a certain volume V of an undamaged composite material loaded by $\boldsymbol{\sigma}^0$ is $2\mathcal{V} = -(\boldsymbol{\sigma}^0)^{\mathrm{T}}\bar{\boldsymbol{\varepsilon}}\,V$, where $\bar{\boldsymbol{\varepsilon}}$ is the average overall strain caused by application of $\boldsymbol{\sigma}^0$. The $\Delta\mathcal{V} = \mathcal{V}_d - \mathcal{V}$ must reflect changes in potential energies of both material volume and applied loads. According to (5.1.9), these changes depend on the difference $\Delta\bar{\boldsymbol{\varepsilon}} = \bar{\boldsymbol{\varepsilon}}_d - \bar{\boldsymbol{\varepsilon}}$ between the overall strain averages after and before decohesion at constant $\boldsymbol{\sigma}^0$; $2\Delta\mathcal{V} = -(\boldsymbol{\sigma}^0)^{\mathrm{T}}\Delta\boldsymbol{\varepsilon}^0\,V$.

As shown in (4.4.10), (4.4.11), overall deformation of the undamaged two-phase aggregate, loaded only by $\boldsymbol{\sigma}^0$, is

$$\bar{\boldsymbol{\varepsilon}} = \boldsymbol{M}\boldsymbol{\sigma}^0 = [\boldsymbol{M}_1 + c_2(\boldsymbol{M}_2 - \boldsymbol{M}_1)\boldsymbol{W}_2]\boldsymbol{\sigma}^0 \tag{5.1.21}$$

where $\boldsymbol{W}_2 = [\boldsymbol{I} + \boldsymbol{Q}(\boldsymbol{M}_2 - \boldsymbol{M}_1)]^{-1}$, $(\boldsymbol{M}_2 - \boldsymbol{M}_1)\boldsymbol{W}_2 = [(\boldsymbol{M}_2 - \boldsymbol{M}_1)^{-1} + \boldsymbol{Q}]^{-1}$, $\boldsymbol{Q} = \boldsymbol{L}_1(\boldsymbol{I} - \boldsymbol{S})$. Since $(\boldsymbol{M}_2 - \boldsymbol{M}_1)^{-1} \to \boldsymbol{0}$ in the volume fraction c_c of the debonded inhomogeneities, the above overall strain in the damaged aggregate changes to

$$\bar{\boldsymbol{\varepsilon}}_d = \boldsymbol{M}_d\boldsymbol{\sigma}^0 = [\boldsymbol{M}_1 + (c_2 - c_d)(\boldsymbol{M}_2 - \boldsymbol{M}_1)\boldsymbol{W}_2 + c_d\,\boldsymbol{Q}^{-1}]\boldsymbol{\sigma}^0 \tag{4.4.15}$$

Therefore, the change in overall strain caused by complete decohesion of c_d of inhomogeneities is

$$\Delta\bar{\boldsymbol{\varepsilon}} = \bar{\boldsymbol{\varepsilon}}_d - \bar{\boldsymbol{\varepsilon}} = c_d[-(\boldsymbol{M}_2 - \boldsymbol{M}_1)\boldsymbol{W}_2 + \boldsymbol{Q}^{-1}]\boldsymbol{\sigma}^0 \tag{5.1.22}$$

and

$$\frac{\Delta\mathcal{V}}{V} = -\frac{1}{2}(\boldsymbol{\sigma}^0)^{\mathrm{T}}\Delta\boldsymbol{\varepsilon}^0 = -\frac{1}{2}(\boldsymbol{\sigma}^0)^{\mathrm{T}}c_c[-(\boldsymbol{M}_2 - \boldsymbol{M}_1)\boldsymbol{W}_2 + \boldsymbol{Q}^{-1}]\boldsymbol{\sigma}^0 \tag{5.1.23}$$

Comparison of the magnitudes of $\Delta\mathcal{W}$ and $\Delta\mathcal{V}$ is left as an exercise. Notice that the latter includes the contribution of work of applied surface tractions or overall stress $\boldsymbol{\sigma}^0$ on damage-induced overall strain.

The average energy released over the surface of a single inhomogeneity can be obtained by dividing $\Delta\mathcal{W}/V$ or $\Delta\mathcal{V}/V$ by the specific surface $\boldsymbol{s}(\boldsymbol{v}_r) = \eta_r\partial\boldsymbol{v}_r$, defined in (3.2.11) as a product of the number density η_r with the interface area of each inhomogeneity. As discussed in Sect. 3.2.3, the specific surface area increases in inverse proportion to the 'diameter' of each inhomogeneity. Therefore, the energy released and the likelihood of decohesion are reduced with decreasing particle size or fiber 'diameter', and it may become very small for nanosized inhomogeneities.

If interface decohesion is identified as the dominant damage mechanism in a particular material, then its extent or volume fraction c_d can be estimated by comparing measured changes in effective stiffness or compliance of the material with the above estimates.

5.2 Energy Changes Caused by Uniform Phase Eigenstrains

Here we consider a system consisting of a homogeneous matrix $\boldsymbol{L}_1$ containing perfectly bonded inhomogeneities $\boldsymbol{L}_r$ in dilute concentration. The shape of each ellipsoidal inhomogeneity is defined by the tensor $\boldsymbol{S}_r = \boldsymbol{P}_r\boldsymbol{L}_1$. Recall that the inhomogeneities interact only with the matrix. First, let the external boundary ∂V of the total volume $V = V_1 + \Sigma_{r=2}^{n} V_r$ remain traction free, while uniform, *physically based eigenstrains* are applied as $\boldsymbol{\mu}_r$ in each V_r and $\boldsymbol{\mu}_1$ in V_1. In the absence of mechanical loads, local stresses are equal to residual stresses $\boldsymbol{\sigma}(\boldsymbol{x}) = \boldsymbol{\sigma}_\mu(\boldsymbol{x})$ which have zero overall average, $\bar{\boldsymbol{\sigma}}_\mu = \boldsymbol{0}$. Overall strain is equal to the eigenstrain derived from the Levin formula in Sect. 3.8, or from

$$\bar{\boldsymbol{\varepsilon}} = \bar{\boldsymbol{\mu}} = \boldsymbol{\mu}_1 + \sum_{r=2}^{n} c_r \boldsymbol{W}_r{}^{\mathrm{T}}(\boldsymbol{\mu}_r - \boldsymbol{\mu}_1) \qquad [4.4.10]$$

Potential energy of the system is generated only by interaction between applied phase eigenstrains and the residual stress field. This interaction energy is the scalar product of the elastic strain field with the residual stress field.

$$\left.\begin{aligned} \mathcal{V}_I &= \frac{1}{2}\int_V [\boldsymbol{\varepsilon}(\boldsymbol{x}) - \boldsymbol{\mu}_r - \boldsymbol{\mu}_1]^{\mathrm{T}}\boldsymbol{\sigma}_\mu(\boldsymbol{x})\mathrm{d}V = -\frac{1}{2}\int_V (\boldsymbol{\mu}_r + \boldsymbol{\mu}_1)^{\mathrm{T}}\boldsymbol{\sigma}_\mu(\boldsymbol{x})\mathrm{d}V \\ &= -\frac{1}{2}\int_V \boldsymbol{\mu}_1^{\mathrm{T}}\boldsymbol{\sigma}_\mu(\boldsymbol{x})\mathrm{d}V - \frac{1}{2}\int_{V_r} (\boldsymbol{\mu}_r - \boldsymbol{\mu}_1)^{\mathrm{T}}\boldsymbol{\sigma}_\mu(\boldsymbol{x})\mathrm{d}V = -\frac{1}{2}\sum_{r=2}^{n} (\boldsymbol{\mu}_r - \boldsymbol{\mu}_1)^{\mathrm{T}}\boldsymbol{\sigma}_r^\mu V_r \end{aligned}\right\} \qquad (5.2.1)$$

Since $\bar{\boldsymbol{\sigma}}_\mu = \boldsymbol{0}$, and $\bar{\boldsymbol{\varepsilon}}$ is also uniform on ∂V, virtual work renders volume integrals over V, of both $\boldsymbol{\varepsilon}^{\mathrm{T}}(\boldsymbol{x})\boldsymbol{\sigma}_\mu(\boldsymbol{x})$ and $\boldsymbol{\mu}_1^{\mathrm{T}}\boldsymbol{\sigma}_\mu(\boldsymbol{x})$, equal to zero. The $\boldsymbol{\sigma}_r^\mu$ denotes the residual stress caused in either homogeneous inclusion or inhomogeneities in subvolumes V_r, by the eigenstrains $\boldsymbol{\mu}_r \in V_r$ and $\boldsymbol{\mu}_1 \in (V - V_r)$ under zero overall stress. It has a constant value in subvolumes of ellipsoidal shape in V_r. In a transformed homogeneous inclusion, the Eshelby solution $(4.1.2)_2$ yields the local residual stress

$$\boldsymbol{\sigma}_r^\mu = -\boldsymbol{L}_1(\boldsymbol{I} - \boldsymbol{S}_r)(\boldsymbol{\mu}_r - \boldsymbol{\mu}_1) = -\boldsymbol{Q}_r(\boldsymbol{\mu}_r - \boldsymbol{\mu}_1) \qquad (5.2.2)$$

that evaluates (5.2.1) as

$$\left.\begin{aligned} \mathcal{V}_I &= \frac{1}{2}\sum_{r=2}^{n} (\boldsymbol{\mu}_r - \boldsymbol{\mu}_1)^{\mathrm{T}}\boldsymbol{Q}_r(\boldsymbol{\mu}_r - \boldsymbol{\mu}_1)V_r \\ \text{or as} \qquad \mathcal{V}_I &= \frac{1}{2}\sum_{r=2}^{n} Q_{ijpq}^r \left(\mu_{pq}^r - \mu_{pq}^{(1)}\right)\left(\mu_{ij}^r - \mu_{ij}^{(1)}\right) V_r \end{aligned}\right\} \qquad (5.2.3)$$

Residual stress in an inhomogeneity $\boldsymbol{L}_r$ follows from (4.3.3), (4.3.8) or (4.3.11), as

$$\boldsymbol{\sigma}_r^{\mu} = -\boldsymbol{N}_{rr}\boldsymbol{L}_r\boldsymbol{\mu}_r - \boldsymbol{N}_{r1}\boldsymbol{L}_1\boldsymbol{\mu}_1 = -\boldsymbol{W}_r\boldsymbol{Q}(\boldsymbol{\mu}_r - \boldsymbol{\mu}_1) \tag{5.2.4}$$

Since $\boldsymbol{W}_r\boldsymbol{Q} = \boldsymbol{Q}\boldsymbol{W}_r{}^{\mathrm{T}}$ in (4.2.15), the energy (5.2.1) of a transformed inhomogeneity $\boldsymbol{L}_r$ in a traction-free 'matrix' $\boldsymbol{L}_1$ is

$$\mathcal{V}_I = \frac{1}{2}(\boldsymbol{\mu}_r - \boldsymbol{\mu}_1)^{\mathrm{T}}\boldsymbol{W}_r\boldsymbol{Q}(\boldsymbol{\mu}_r - \boldsymbol{\mu}_1)V_r \tag{5.2.5}$$

For $\boldsymbol{L}_r \to \boldsymbol{L}_1$ and $\boldsymbol{W}_r \to \boldsymbol{I}$, one recovers (5.2.3). Application of a uniform eigenstrain $\boldsymbol{\mu}_r = \boldsymbol{\mu}_1$ in the entire traction-free heterogeneous volume is a stress-free transformation involving no mechanical work. Notice that no mechanical work can be contributed by equivalent eigenstrains that depend on mechanical loads, because they are equal to zero in their absence.

Next, the same system is now constrained at its outer boundary ∂V, such that the overall strain $\boldsymbol{\varepsilon}^0 = \boldsymbol{0}$, while uniform phase eigenstrains $\boldsymbol{\mu}_1$, $\boldsymbol{\mu}_r = -\boldsymbol{M}_r\boldsymbol{\lambda}_r$ are applied in the matrix $r = 1$ and dilute reinforcements $r = 2, 3, \ldots n$. Overall stress is equal to the overall eigenstress (4.4.5), evaluated by the Levin formula as

$$\bar{\boldsymbol{\sigma}} = \bar{\boldsymbol{\sigma}}_{\mu} = \bar{\boldsymbol{\lambda}} = \boldsymbol{\lambda}_1 + \sum_{r=2}^{n} c_r\boldsymbol{T}_r{}^{\mathrm{T}}(\boldsymbol{\lambda}_r - \boldsymbol{\lambda}_1) \tag{5.2.6}$$

Potential energy of the system is generated by interaction between the phase eigenstrains and the residual stress field, or between the eigenstrains and inhomogeneities. This interaction energy is written as in (5.2.1), as a scalar product of the elastic strain field with the residual stress field

$$\left.\begin{aligned} \mathcal{W}_I &= \frac{1}{2}\int_V [\boldsymbol{\varepsilon}(\boldsymbol{x}) - \boldsymbol{\mu}_r - \boldsymbol{\mu}_1]^{\mathrm{T}}\boldsymbol{\sigma}_{\mu}(\boldsymbol{x})\mathrm{d}V = -\frac{1}{2}\int_V (\boldsymbol{\mu}_r + \boldsymbol{\mu}_1)^{\mathrm{T}}\boldsymbol{\sigma}_{\mu}(\boldsymbol{x})\mathrm{d}V \\ &= -\frac{1}{2}\boldsymbol{\mu}_1^{\mathrm{T}}\bar{\boldsymbol{\lambda}}\,V - \frac{1}{2}\sum_{r=2}^{n}(\boldsymbol{\mu}_r - \boldsymbol{\mu}_1)^{\mathrm{T}}\boldsymbol{\sigma}_r^{\mu}V_r \end{aligned}\right\} \tag{5.2.7}$$

Under $\boldsymbol{\varepsilon}^0 = \boldsymbol{0}$ and uniform $\bar{\boldsymbol{\sigma}}_{\mu}$ on ∂V, virtual work renders the volume integral of $\boldsymbol{\varepsilon}^{\mathrm{T}}(\boldsymbol{x})\boldsymbol{\sigma}_{\mu}(\boldsymbol{x})$ equal to zero. Residual stress $\boldsymbol{\sigma}_r^{\mu}$ is caused in V_r by the eigenstrains $\boldsymbol{\mu}_r \in V_r$ and $\boldsymbol{\mu}_1 \in (V - V_r)$ under zero overall strain. Inside a homogeneous inclusion, it is given by the Eshelby solution $(4.1.3)_1$, with $\boldsymbol{S}_r = \boldsymbol{P}_r\boldsymbol{L}_1$

$$\boldsymbol{\sigma}_r^{\mu} = \boldsymbol{L}_1[\boldsymbol{S}_r(\boldsymbol{\mu}_r - \boldsymbol{\mu}_1) - \boldsymbol{\mu}_r] \tag{5.2.8}$$

In an inhomogeneity $\boldsymbol{L}_r$, according to (4.4.2) at $\boldsymbol{\varepsilon}^0 = \boldsymbol{0}$

$$\boldsymbol{\sigma}_r^{\mu} = \boldsymbol{L}_r[\boldsymbol{R}_{r1}\boldsymbol{\mu}_1 + (\boldsymbol{R}_{rr} - \boldsymbol{I})\boldsymbol{\mu}_r] = \boldsymbol{L}_r[\boldsymbol{T}_r\boldsymbol{P}_r(\boldsymbol{L}_r\boldsymbol{\mu}_r - \boldsymbol{L}_1\boldsymbol{\mu}_1) - \boldsymbol{\mu}_r] \quad (5.2.9)$$

Substitution of these residual stress averages into (5.2.7) yields the interaction energy of the transformed volume V under zero overall strain.

The above results can be used, for example, to estimate energy and local stress changes caused by a spontaneous transformation of homogeneous inclusions or inhomogeneities, or by a uniform change in temperature of a traction-free or constrained aggregate. In the former case, the aggregate may be traction-free at a certain fabrication and/or processing temperature θ_0, where $\mathcal{W}_I \to 0$. Subsequent changes in temperature $\Delta\theta = \theta - \theta_0$ should elevate the interaction energy regardless of the relative magnitude of the thermal eigenstrains. Of course, since $\Delta\theta < 0$ during cooling to ambient temperature, both thermal eigenstrains are usually $\mu_i^{\eta} \leqslant 0$. Local stress (5.2.4) is also equal to zero at θ_0, but its isotropic component should be positive during cooling $(m_i^r - m_i^{(1)})\Delta\theta \leqslant 0$, i.e., when the reinforcement phase has 'higher' coefficients of thermal expansion. The resulting tensile tractions along the interface may encourage interface decohesion between matrix and reinforcement. On the other hand, if the matrix $\boldsymbol{L}_1$ contracts more than the reinforcement during cooling, the increasing compression along their mutual interface may support growth of radial matrix cracks. Either type of cracking should reduce the local thermal stress, and thus release some or all of the accumulated interaction energy.

5.3 Energy Changes Caused by Mechanical Loads and Phase Eigenstrains

5.3.1 The Load Set $\{\boldsymbol{\varepsilon}^0,\ \boldsymbol{\mu}_1,\ \boldsymbol{\mu}_r\}$

Here we consider again the dilutely reinforced material system of Sect. 5.2, now loaded not only by the uniform, physically motivated phase eigenstrains $\boldsymbol{\mu}_r$ in V_r, $r > 1$, and $\boldsymbol{\mu}_1$ in V_1, but also by a uniform overall strain $\boldsymbol{\varepsilon}^0$ caused by displacements applied at the external boundary ∂V of the total volume $V = V_1 + \Sigma_{r=2}^{n} V_r$. The two loading states are independent and the total stress and strain fields they generate in V are superpositions of the mechanical fields $\boldsymbol{\sigma}_\rho(\boldsymbol{x})$ and $\boldsymbol{\varepsilon}_\rho(\boldsymbol{x})$ caused by the applied overall strain, with the residual fields $\boldsymbol{\sigma}_\mu(\boldsymbol{x})$ and $\boldsymbol{\varepsilon}_\mu(\boldsymbol{x})$ generated by the two eigenstrains at zero overall strain

$$\boldsymbol{\sigma}(\boldsymbol{x}) = \boldsymbol{\sigma}_\rho(\boldsymbol{x}) + \boldsymbol{\sigma}_\mu(\boldsymbol{x}) \quad \boldsymbol{\varepsilon}(\boldsymbol{x}) = \boldsymbol{\varepsilon}_\rho(\boldsymbol{x}) + \boldsymbol{\varepsilon}_\mu(\boldsymbol{x}) \quad (5.3.1)$$

Both stress fields are in equilibrium, and each total strain field is compatible. For brevity, the fields in (5.3.1) will be denoted only by their kernel letters, as $\boldsymbol{\sigma}$, $\boldsymbol{\varepsilon}$; $\boldsymbol{\sigma}_\rho$, $\boldsymbol{\varepsilon}_\rho$; $\boldsymbol{\sigma}_\mu$, $\boldsymbol{\varepsilon}_\mu$.

Under a prescribed deformation path, the total residual strain $\boldsymbol{\varepsilon}_\mu$ does not contribute to the overall strain average $\bar{\boldsymbol{\varepsilon}} = \boldsymbol{\varepsilon}^0$ in V, hence $\bar{\boldsymbol{\varepsilon}}_\mu = \mathbf{0}$. This implies that the residual deformation is constrained by the overall eigenstress $\bar{\boldsymbol{\sigma}}_\mu = \bar{\boldsymbol{\lambda}} = -\boldsymbol{L}\bar{\boldsymbol{\mu}}$. Both two-phase and multiphase systems can be considered; their overall response is indicated by (4.4.5), as

$$\bar{\boldsymbol{\sigma}} = \boldsymbol{L}(\boldsymbol{\varepsilon}^0 - \bar{\boldsymbol{\mu}}) = \bar{\boldsymbol{\sigma}}_\rho + \bar{\boldsymbol{\lambda}} \qquad \bar{\boldsymbol{\lambda}} = \boldsymbol{\lambda}_1 + \sum_{r=2}^{n} c_r \boldsymbol{T}_r^{\mathrm{T}}(\boldsymbol{\lambda}_r - \boldsymbol{\lambda}_1) \tag{5.3.2}$$

where $\bar{\boldsymbol{\sigma}}_\rho = \boldsymbol{L}\boldsymbol{\varepsilon}^0$, and the overall eigenstress $\bar{\boldsymbol{\sigma}}_\mu = \bar{\boldsymbol{\lambda}} = -\boldsymbol{L}\bar{\boldsymbol{\mu}}$ follows from the Levin formula (3.8.11) with $\boldsymbol{A}_r \to \boldsymbol{T}_r$, $c_r \ll 1$, $\boldsymbol{L}$ from (4.4.6) and $c_r = V_r/V$.

Potential energy is equal to a work integral of the stress field on elastic strains

$$\mathcal{W} = \frac{1}{2}\int_V (\boldsymbol{\varepsilon}_\rho + \boldsymbol{\varepsilon}_\mu^e)^{\mathrm{T}}(\boldsymbol{\sigma}_\rho + \boldsymbol{\sigma}_\mu)\mathrm{d}V \tag{5.3.3}$$

Elastic parts of the mechanical and residual strain fields in V_1 and V_r are

$$\boldsymbol{\varepsilon}_\rho = \boldsymbol{M}_\eta\boldsymbol{\sigma}_\rho \qquad \boldsymbol{\varepsilon}_\mu^e = \boldsymbol{\varepsilon}_\mu - \boldsymbol{\mu}_\eta = \boldsymbol{M}_\eta\boldsymbol{\sigma}_\mu \qquad \eta = 1,\ r \tag{5.3.4}$$

Therefore, work integrals of the scalar products of the mechanical and residual fields in (5.3.3) satisfy

$$\int_V (\boldsymbol{\varepsilon}_\rho)^{\mathrm{T}}\boldsymbol{\sigma}_\mu \mathrm{d}V = \int_V (\boldsymbol{\sigma}_\rho)^{\mathrm{T}}\boldsymbol{\varepsilon}_\mu^e \mathrm{d}V = \int_V (\boldsymbol{\varepsilon}_\mu^e)^{\mathrm{T}}(\boldsymbol{\sigma}_\rho)\mathrm{d}V \tag{5.3.5}$$

This reduces (5.3.3) to

$$\mathcal{W} = \frac{1}{2}\int_V [(\boldsymbol{\varepsilon}_\rho)^{\mathrm{T}}\boldsymbol{\sigma}_\rho + (\boldsymbol{\varepsilon}_\mu^e + 2\boldsymbol{\varepsilon}_\rho)^{\mathrm{T}}\boldsymbol{\sigma}_\mu]\mathrm{d}V \tag{5.3.6}$$

Evaluation of total energy is facilitated by observing that $u_i^\mu = 0$ on ∂V, and that $\sigma_{ij,j}^\mu = 0$ in V. The integral of the scalar product of the residual stresses and total strains thus becomes

$$\int_V \sigma_{ij}^\mu \varepsilon_{ij}^\mu \mathrm{d}V = \int_V \sigma_{ij}^\mu u_{i,j}^\mu \mathrm{d}V = \int_{\partial V} \sigma_{ij}^\mu u_i^\mu n_j \mathrm{d}S - \int_V \sigma_{ij,j}^\mu u_i^\mu \mathrm{d}V = 0 \tag{5.3.7}$$

Since $\boldsymbol{\varepsilon}_\mu^e(\boldsymbol{x}) = \boldsymbol{\varepsilon}_\mu(\boldsymbol{x}) - \boldsymbol{\mu}(\boldsymbol{x})$, this result reduces the integrand $\boldsymbol{\varepsilon}_\mu^e\boldsymbol{\sigma}_\mu$ in (5.3.6) to $-\boldsymbol{\mu}^{\mathrm{T}}(\boldsymbol{x})\boldsymbol{\sigma}_\mu(\boldsymbol{x})$. The eigenstrains are applied as $\boldsymbol{\mu}_1$ in $V - V_r$ and $\boldsymbol{\mu}_r$ in subvolumes

V_r, and residual stress averages which they generate in those subvolumes are found under $\boldsymbol{\varepsilon}^0 = \boldsymbol{0}$. In particular, residual stress caused by $\boldsymbol{\mu}_r$ in ellipsoidal subvolumes V_r is piecewise uniform and found using (4.4.2), (4.4.3), (4.4.4), as

$$\boldsymbol{\sigma}_r^{\mu} = \boldsymbol{L}_r[\boldsymbol{R}_{r1}\boldsymbol{\mu}_1 + (\boldsymbol{R}_{rr} - \boldsymbol{I})\boldsymbol{\mu}_r] = \boldsymbol{L}_r[\boldsymbol{T}_r\boldsymbol{P}_r(\boldsymbol{L}_r\boldsymbol{\mu}_r - \boldsymbol{L}_1\boldsymbol{\mu}_1) - \boldsymbol{\mu}_r] \qquad [5.2.9]$$

Residual stress in V_1 is not uniform, but according to (4.4.5), its volume average is equal to

$$\bar{\boldsymbol{\sigma}}_1^{\mu} = \frac{1}{c_1}\left(\bar{\boldsymbol{\lambda}} - \sum_{r=2}^{n} c_r\boldsymbol{\sigma}_r^{\mu}\right) \qquad (5.3.8)$$

Total energy in (5.3.6) is now decomposed into $\mathcal{W} = \mathcal{W}_0 + \mathcal{W}_{\mu} + \mathcal{W}_I$, where each term is evaluated using virtual work

$$\mathcal{W}_0 = \frac{1}{2}\int_V (\boldsymbol{\varepsilon}_{\rho})^{\mathrm{T}}\boldsymbol{\sigma}_{\rho}\mathrm{d}V = \frac{1}{2}(\boldsymbol{\varepsilon}^0)^{\mathrm{T}}\bar{\boldsymbol{\sigma}}_{\rho}\,V = \frac{1}{2}(\boldsymbol{\varepsilon}^0)^{\mathrm{T}}\boldsymbol{L}\boldsymbol{\varepsilon}^0\,V \qquad (5.3.9)$$

$$\left.\begin{aligned}\mathcal{W}_{\mu} &= \frac{1}{2}\int_V (\boldsymbol{\varepsilon}_{\mu}^{e})^{\mathrm{T}}\boldsymbol{\sigma}_{\mu}\mathrm{d}V = -\frac{1}{2}\int_V \boldsymbol{\mu}^{\mathrm{T}}\boldsymbol{\sigma}_{\mu}\,\mathrm{d}V \\ &= -\frac{1}{2}\left[\frac{1}{c_1}\boldsymbol{\mu}_1^{\mathrm{T}}\left(\bar{\boldsymbol{\lambda}} - \sum_{r=2}^{n} c_r\boldsymbol{\sigma}_r^{\mu}\right)V_1 + \sum_{r=2}^{n}(\boldsymbol{\mu}_r)^{\mathrm{T}}\boldsymbol{\sigma}_r^{\mu}V_r\right] \\ &= -\frac{1}{2}\left[\boldsymbol{\mu}_1^{\mathrm{T}}\bar{\boldsymbol{\lambda}} + \sum_{r=2}^{n} c_r(\boldsymbol{\mu}_r - \boldsymbol{\mu}_1)^{\mathrm{T}}\boldsymbol{\sigma}_r^{\mu}\right]V\end{aligned}\right\} \qquad (5.3.10)$$

$$\mathcal{W}_I = \int_V (\boldsymbol{\varepsilon}_{\rho})^{\mathrm{T}}\boldsymbol{\sigma}_{\mu}\mathrm{d}V = (\boldsymbol{\varepsilon}^0)^{\mathrm{T}}\bar{\boldsymbol{\lambda}}\,V \qquad (5.3.11)$$

and where $\boldsymbol{L}$ is given by (4.4.6).

Of course, the present energies $\mathcal{W}_0$ and $\mathcal{W}_I$ are different from those introduced in (5.1.4) and (5.2.1). In particular, $\mathcal{W}_0$ is again generated by overall strain $\boldsymbol{\varepsilon}^0$, applied to the inhomogeneous aggregate. It is thus equal to the total energy $\mathcal{W}$ in (5.1.3), which includes the interaction energy (5.1.5) between applied overall strain and inhomogeneities.

$\mathcal{W}_{\mu}$ is the work of applied eigenstrains on the residual stress field. Notice that the result is similar to (5.2.7), where $\boldsymbol{\mu}_1$ was applied in V and $(\boldsymbol{\mu}_r - \boldsymbol{\mu}_1)$ in V_r. Therefore, it is equal to interaction energy between applied eigenstrains and constituent phases, under zero overall strain.

$\mathcal{W}_I$ represents here the interaction energy between mechanical and transformation fields. Notice that it does not directly include interactions of the loads with

inhomogeneities, reflected in (5.1.4) or (5.1.10) and already included here in $\mathcal{W}_0$ and $\mathcal{W}_\mu$. For $\boldsymbol{\mu}_r \to \boldsymbol{0}$, $\boldsymbol{\mu}_1 \to \boldsymbol{0}$, one recovers the total energy (5.1.3).

As shown by (5.3.11), $\mathcal{W}_I$ is evaluated as the work of an applied uniform overall strain $\boldsymbol{\varepsilon}^0$ on overall volume average of residual stress, or eigenstress $\bar{\boldsymbol{\lambda}}$, caused by constant phase eigenstrains. Also, it is equal to the work that the elastic part $\bar{\boldsymbol{\sigma}}_\rho = \boldsymbol{L}\boldsymbol{\varepsilon}^0$ of the overall stress would have to perform on overall eigenstrain $\bar{\boldsymbol{\mu}} = -\boldsymbol{M}\,\bar{\boldsymbol{\lambda}}$, to restore overall strain to $\bar{\boldsymbol{\varepsilon}} = \boldsymbol{\varepsilon}^0$. Equation 5.3.11 can be recast into

$$\mathcal{W}_I = \sum_{r=1}^{n} (\boldsymbol{T}_r \boldsymbol{\varepsilon}^0)^{\mathrm{T}} \boldsymbol{\lambda}_r \, V_r = \sum_{r=1}^{n} (\boldsymbol{\varepsilon}_r^\rho)^{\mathrm{T}} \boldsymbol{\lambda}_r V_r = -\sum_{r=1}^{n} (\boldsymbol{\sigma}_r^\rho)^{\mathrm{T}} \boldsymbol{\mu}_r V_r \tag{5.3.12}$$

where $\boldsymbol{\varepsilon}_r^\rho$, $\boldsymbol{\sigma}_r^\rho$ denote mechanical parts of the local fields in (5.3.1). Therefore, $\mathcal{W}_I$ can also be interpreted as the work of local stresses caused by mechanical loading on applied local eigenstrains.

5.3.2 The Load Set $\{\boldsymbol{\sigma}^0,\ \boldsymbol{\lambda}_r,\ \boldsymbol{\lambda}_1\}$

When the title loads are applied to a composite aggregate with dilute reinforcement, $c_r \ll 1$, mechanical strain fields $\boldsymbol{\varepsilon}_\rho(\boldsymbol{x})$ generated by overall stress $\boldsymbol{\sigma}^0$ are superimposed with the residual fields $\boldsymbol{\varepsilon}_\mu(\boldsymbol{x})$ caused by eigenstrains $\boldsymbol{\mu}_r$ in V_r and $\boldsymbol{\mu}_1$ in V_1 under zero overall stress. Similar superposition applies to the stress fields. Total fields are

$$\boldsymbol{\sigma}(\boldsymbol{x}) = \boldsymbol{\sigma}_\rho(\boldsymbol{x}) + \boldsymbol{\sigma}_\mu(\boldsymbol{x}) \quad \boldsymbol{\varepsilon}(\boldsymbol{x}) = \boldsymbol{\varepsilon}_\rho(\boldsymbol{x}) + \boldsymbol{\varepsilon}_\mu(\boldsymbol{x}) \tag{5.3.13}$$

They satisfy equilibrium and compatibility conditions. Overall eigenstrain or residual strain $\bar{\boldsymbol{\mu}}$ is derived from (3.8.9) where $\boldsymbol{B}_r \to \boldsymbol{W}_r$. Overall constitutive relation is

$$\bar{\boldsymbol{\varepsilon}} = \boldsymbol{M}\boldsymbol{\sigma}^0 + \bar{\boldsymbol{\mu}} \qquad \bar{\boldsymbol{\mu}} = \boldsymbol{\mu}_1 + \sum_{r=2}^{n} c_r \boldsymbol{W}_r{}^{\mathrm{T}} (\boldsymbol{\mu}_r - \boldsymbol{\mu}_1) \tag{5.3.14}$$

Total potential energy of a large volume V subjected to the load set $\{\boldsymbol{\sigma}^0,\ \boldsymbol{\mu}_r,\ \boldsymbol{\mu}_1\}$ or $\{\boldsymbol{\sigma}^0,\ \boldsymbol{\lambda}_r,\ \boldsymbol{\lambda}_1\}$, is a sum of the strain energy and of the potential energy of surface tractions. The former is a scalar product of the superimposed stresses and elastic parts of strains in (5.3.13)

$$\mathcal{V} = \frac{1}{2} \int_V (\boldsymbol{\varepsilon}_\rho + \boldsymbol{\varepsilon}_\mu^e)^{\mathrm{T}} (\boldsymbol{\sigma}_\rho + \boldsymbol{\sigma}_\mu) \mathrm{d}V - \int_{\partial V} (\boldsymbol{u}_\rho + \boldsymbol{u}_\mu)^{\mathrm{T}} \boldsymbol{t}^0 \mathrm{d}S \tag{5.3.15}$$

where the surface displacements $\boldsymbol{u}_\rho$, $\boldsymbol{u}_\mu$ are generated on ∂V by $\boldsymbol{\varepsilon}_\rho$, $\boldsymbol{\varepsilon}_\mu$. Recall now that

$$\boldsymbol{\varepsilon}_\rho = \boldsymbol{M}_\eta \boldsymbol{\sigma}_\rho \quad \boldsymbol{\varepsilon}^e_\mu = \boldsymbol{\varepsilon}_\mu - \boldsymbol{\mu}_\eta = \boldsymbol{M}_\eta \boldsymbol{\sigma}_\mu \quad \eta = 1, r \qquad [5.3.4]$$

However, $\bar{\sigma}^\mu_{ij} = 0$, hence the residual traction on ∂V is now $t^\mu_i = \sigma^\mu_{ij} n_j = 0$ and

$$\int_V (\boldsymbol{\varepsilon}_\rho)^{\mathrm{T}} \boldsymbol{\sigma}_\mu \, \mathrm{d}V = \int_V (\boldsymbol{\sigma}_\rho)^{\mathrm{T}} \boldsymbol{\varepsilon}^e_\mu \, \mathrm{d}V = (\bar{\boldsymbol{\varepsilon}}_\rho)^{\mathrm{T}} \bar{\boldsymbol{\sigma}}_\mu \, V = 0 \qquad (5.3.16)$$

where $\bar{\boldsymbol{\varepsilon}}_\rho = \boldsymbol{M}\boldsymbol{\sigma}^0$ is the mechanical part of the overall strain. This is the Colonnetti theorem (Mura 1987).

The integral of $\varepsilon^\mu_{ij} \bar{\sigma}^\mu_{ij}$ over V, evaluated in (5.3.7), is again equal to zero and $\boldsymbol{\varepsilon}^e_\mu(\boldsymbol{x}) = -\boldsymbol{\mu}(\boldsymbol{x})$. This eliminates the interaction term in the strain energy integral in (5.3.15) and leaves there the sum of the work of mechanical stresses on conjugate strains, and of the eigenstrains on residual stress field under zero overall stress. In particular

$$\frac{1}{2}\int_V (\boldsymbol{\varepsilon}_\rho + \boldsymbol{\varepsilon}^e_\mu)^{\mathrm{T}} (\boldsymbol{\sigma}_\rho + \boldsymbol{\sigma}_\mu) \mathrm{d}V = \frac{1}{2}\int_V [\bar{\boldsymbol{\varepsilon}}^{\mathrm{T}}_\rho \boldsymbol{\sigma}^0 - (\boldsymbol{\mu}_r + \boldsymbol{\mu}_1)^{\mathrm{T}} \boldsymbol{\sigma}_\mu] \mathrm{d}V \qquad (5.3.17)$$

Turning our attention to the potential energy of applied loads in (5.3.15), we recall that $t^0_i = \sigma^0_{ij} n_j$, $\sigma^0_{ij,j} = 0$ and find

$$\left.\begin{aligned} -\int_{\partial V} (u^\rho_i + u^\mu_i) \sigma^0_{ij} n_j \, \mathrm{d}S &= -\int_V [(u^\rho_{i,j} + u^\mu_{i,j}) \sigma^0_{ij} + (u^\rho_i + u^\mu_i) \sigma^0_{ij,j}] \mathrm{d}V \\ &= -\int_V (\varepsilon^\rho_{ij} + \varepsilon^\mu_{ij}) \sigma^0_{ij} \mathrm{d}V \end{aligned}\right\} \qquad (5.3.18)$$

Total potential energy is now written as the sum $\mathcal{V} = \mathcal{V}_0 + \mathcal{V}_\mu + \mathcal{V}_I$, where

$$\mathcal{V}_0 = -\frac{1}{2}\bar{\boldsymbol{\varepsilon}}^{\mathrm{T}}_\rho \boldsymbol{\sigma}^0 V = -\frac{1}{2}(\boldsymbol{\sigma}^0)^{\mathrm{T}} \boldsymbol{M} \boldsymbol{\sigma}^0 V \qquad \mathcal{V}_\mu = -\frac{1}{2}\int_{V_r} (\boldsymbol{\mu}_r - \boldsymbol{\mu}_1)^{\mathrm{T}} \boldsymbol{\sigma}_\mu \mathrm{d}V \qquad (5.3.19)$$

$$\mathcal{V}_I = -\bar{\boldsymbol{\mu}}^{\mathrm{T}} \boldsymbol{\sigma}^0 V = -\left[\boldsymbol{\mu}^{\mathrm{T}}_1 + \sum_{r=2}^{n} c_r (\boldsymbol{\mu}_r - \boldsymbol{\mu}_1)^{\mathrm{T}} \boldsymbol{W}_r\right] \boldsymbol{\sigma}^0 V \qquad (5.3.20)$$

with the overall eigenstrain $\bar{\boldsymbol{\mu}} \equiv \bar{\boldsymbol{\varepsilon}}_\mu$ from (5.3.14).

If the overall strain $\bar{\boldsymbol{\varepsilon}} = \boldsymbol{\varepsilon}^0$ in (5.3.10) is related to the overall stress $\bar{\boldsymbol{\sigma}} = \boldsymbol{\sigma}^0$ in (5.3.19) by $\bar{\boldsymbol{\sigma}} = \boldsymbol{L}\bar{\boldsymbol{\varepsilon}}$, then $\mathcal{V}_0 = -\mathcal{W}_0$. The energy $\mathcal{V}_\mu$ of the residual fields in Ω_r under zero overall stress has already been evaluated as the interaction energy for a homogeneous inclusion in (5.2.3), and for an inhomogeneity in (5.2.5). For an ellipsoidal inhomogeneity, residual part of local stress in $\mathcal{V}_\mu$ is obtained from (4.3.11) at $\boldsymbol{\sigma}^0_\Omega \to \boldsymbol{0}$. Therefore, in the absence of phase transformations, the present results coincide with those found in Sect. 5.1, and in the absence of mechanical loads with those found in Sect. 5.2. In both cases, the present $\mathcal{V}_I$ would be zero.

Interaction energy $\mathcal{V}_I$ is equal to the work of constant overall surface tractions $t_i^0 = \sigma_{ij}^0 n_j$ on surface displacements $\bar{u}_i^\mu = \bar{\varepsilon}_{ij}^\mu x_j$, generated on ∂V by the applied eigenstrains, as first observed by Eshelby (1957, 1961). Interaction energies $\mathcal{V}_I = \mathcal{W}_I$ if $\bar{\boldsymbol{\sigma}} = \boldsymbol{L}\bar{\boldsymbol{\varepsilon}}$. If eigenstrains are prescribed only in V_r and $\boldsymbol{\mu}_1 = \boldsymbol{0}$, then the interaction energy can be found as

$$\mathcal{V}_I = -\sum_{r=2}^{n} \boldsymbol{\mu}_r^{\mathrm{T}} \boldsymbol{W}_r \boldsymbol{\sigma}^0 V_r = -\sum_{r=2}^{n} \boldsymbol{\mu}_r^{\mathrm{T}} \boldsymbol{\sigma}_r^\rho V_r = \sum_{r=2}^{n} \boldsymbol{\lambda}_r^{\mathrm{T}} \boldsymbol{\varepsilon}_r^\rho V_r \tag{5.3.21}$$

For $\boldsymbol{L}_r \to \boldsymbol{L}_0$, this result coincides with Eshelby's (1961, Eq. 2.43) for a transformed homogeneous inclusion; $\boldsymbol{\sigma}_r^\rho$ and $\boldsymbol{\varepsilon}_r^\rho$ are defined in (5.3.1).

5.4 Energy Changes Caused by Cracks

It is well known that composite materials may contain distributed systems of cracks introduced by either monotonic or cyclic loads, by changes in temperature or moisture content, or by phase transformations. Matrix cracks are preferred in a well designed system, where they should bypass the fibers or other reinforcements, and thus not substantially impair their load carrying capacity. Analysis of such systems relies on established micromechanical methods, where cracks are represented by oblate or flat cavities. Theoretical predictions, as well as experiments show reduction of certain elastic moduli. Those should be measured during small unloading steps, which keep cracks stationary and still open. Of course, shape, size and density of cracks causing observed moduli changes are internal variables, hence their state and evolution under applied loads are not generally known. However, they can be estimated with some confidence in fibrous laminates, which exhibit well-documented transverse cracking in the matrix, on planes aligned with the fiber direction and normal to the plane of individual plies, as well as isolated fiber breaks. Those can represented by aligned slit or penny-shaped cracks discussed next. Extensive analysis of many crack problems can be found in Hutchinson and Suo (1992), Kachanov (1992) and Nemat-Nasser and Hori (1999).

5.4.1 Aligned Slit Cracks in an Orthotropic Solid

A volume V of a 'matrix' material $\boldsymbol{L}_1$ contains a dilute distribution of aligned slit cracks with the cross section in the principal x_1x_2-plane, and with x_3 normal to the crack plane. A schematic drawing of the crack is shown later in Fig. 10.17. The crack width is $|x_1| < 2a_1$. Taken as a limit of an infinitely long elliptic cylinder V_r, each crack is described by

$$x_1^2/a_1^2 + x_2^2/a_2^2 < 1 \qquad |x_3| < \infty \qquad \varepsilon = a_2/a_1 \to 0 \tag{5.4.1}$$

Such cracks, also called transverse cracks, are observed in laminated plates and shells, where they span the thickness of a ply and propagate as tunneling cracks on planes aligned with the fiber direction. In that case, $\boldsymbol{L}_1$ is replaced by the ply stiffness $\boldsymbol{L}$. Crack volume fraction c_c is defined here by the number η of ellipsoidal cylindrical voids or cracks per unit area in the x_1x_2-plane, per unit length $|x_3| = 1$, as

$$c_c = \pi a_1 a_2 \eta = \pi a_1^2 \eta \varepsilon = \frac{1}{4}\pi \bar{\beta} \varepsilon \tag{5.4.2}$$

where $\bar{\beta} = 4\eta a_1^2$ denotes the crack density parameter (Laws et al. 1983). Thus $\bar{\beta}$ is equal to the average number of cracks of width $2a_1$ in a square with side $2a_1$. For example, if all cracks were arranged in a single column or ply of thickness $2a_1$, then at $\bar{\beta} = 1$ their average distance would be ply thickness $2a_1$, and it would become infinite at $\bar{\beta} = 0$. At dilute concentration of cracks, $\bar{\beta} \ll 1$.

First, a uniform overall stress $\boldsymbol{\sigma}^0$ is applied at the surface ∂V of V, such that all cracks remain open and traction-free. The traction field remains continuous, hence averages of stress and strain in the matrix are $\bar{\boldsymbol{\sigma}}_1 = \boldsymbol{\sigma}^0$, $\bar{\boldsymbol{\varepsilon}}_1 = \boldsymbol{M}_1\boldsymbol{\sigma}^0$. However, displacement jumps or crack opening displacements make a separate contribution to overall deformation of the volume V. Average strain caused in a cavity V_r by displacements of its wall follows from (4.3.32) as

$$\boldsymbol{\varepsilon}_r = (\boldsymbol{I} - \boldsymbol{S})^{-1}\boldsymbol{M}_1\boldsymbol{\sigma}^0 = \boldsymbol{Q}^{-1}\boldsymbol{\sigma}^0 \tag{5.4.3}$$

where $\boldsymbol{Q} = \boldsymbol{L}_1(\boldsymbol{I} - \boldsymbol{P}\boldsymbol{L}_1)$, is defined in (4.2.9). The dilute approximation implies that each cavity or crack interacts only with the 'matrix' and not with other cavities or cracks. Therefore, the overall strain caused in V by an applied stress $\boldsymbol{\sigma}^0$ follows from (4.4.10) and (4.4.11) as

$$\bar{\boldsymbol{\varepsilon}} = (\boldsymbol{M}_1 + c_r\boldsymbol{Q}^{-1})\boldsymbol{\sigma}^0 \tag{5.4.4}$$

The $\boldsymbol{P}$ matrix for slit cracks, correct to order ε, is given by (4.6.7) with (4.6.8). By examining the product $\boldsymbol{P}\boldsymbol{L}_1$ at $\varepsilon \to 0$, one finds that $\boldsymbol{Q}^{-1}$ becomes singular. However, the tensor

$$\boldsymbol{\Lambda} = \lim_{\varepsilon \to 0} \varepsilon \boldsymbol{Q}^{-1} \tag{5.4.5}$$

remains finite. In particular, using his form of $\boldsymbol{P}$ in (4.6.7), Laws (1977) evaluated nonzero coefficients of $\boldsymbol{\Lambda}$ as

$$\left.\begin{aligned} \Lambda_{22} &= \frac{L_{11}(\alpha^{1/2}+\beta^{1/2})}{L_{11}L_{22}-L_{12}^2} \qquad \Lambda_{44} = \frac{1}{(L_{44}L_{55})^{1/2}} \\ \Lambda_{66} &= \frac{(L_{11}L_{22})^{1/2}(\alpha^{1/2}+\beta^{1/2})}{L_{11}L_{22}-L_{12}^2} \end{aligned}\right\} \tag{5.4.6}$$

where α, β are roots of

$$L_{11}L_{66}x^2 - (L_{11}L_{22} - L_{12}^2 - 2L_{12}L_{66})x + L_{22}L_{66} = 0 \qquad [4.6.8]$$

The overall strain in (5.4.4) is now expressed in terms of the compliance of the damaged medium

$$\bar{\boldsymbol{\varepsilon}} = [\boldsymbol{M}_1 + \pi a_1^2 \eta \boldsymbol{\Lambda}]\boldsymbol{\sigma}^0 \tag{5.4.7}$$

Potential energy $\mathcal{V} = \mathcal{V}_0 + \mathcal{V}_I$ of the crack and 'matrix' system of volume V of unit length $|x_3| = 1$, or thickness of the ply, follows from (5.1.9) to (5.1.11) as

$$\mathcal{V}_0 = -\frac{1}{2}(\boldsymbol{\sigma}^0)^{\mathrm{T}}\boldsymbol{M}_1\boldsymbol{\sigma}^0 V \quad \mathcal{V}_I = -\frac{1}{2}\pi a_1^2 \eta (\boldsymbol{\sigma}^0)^{\mathrm{T}}\boldsymbol{\Lambda}\boldsymbol{\sigma}^0 V \tag{5.4.8}$$

Substituting for Λ_{ij} from (5.4.6) finally yields

$$\mathcal{V}_I = \frac{1}{2}\pi a_1^2 \eta [\Lambda_{22}(\sigma_2^0)^2 + \Lambda_{44}(\sigma_4^0)^2 + \Lambda_{66}(\sigma_6^0)^2]\, V \tag{5.4.9}$$

This form shows contributions of individual crack modes, by the opening Mode I under the overall stress component σ_2^0, and by the shear Modes II and III under $\sigma_4^0 = \sigma_{23}^0$ and $\sigma_6^0 = \sigma_{12}^0$, respectively. Since $\boldsymbol{\Lambda}$ depends only on stiffness coefficients of the matrix, and not on the absolute size of the cracks, these results can be extended to a finite concentration of aligned slit cracks.

The interaction energy $\mathcal{V}_I$ between an applied overall stress and cracks is equal to the energy released by the crack system. It is also equal to the work of the applied stress on crack-induced contribution to the overall strain.

Next, under a uniform overall strain $\boldsymbol{\varepsilon}^0$ applied to the matrix $\boldsymbol{L}_1$ containing a dilute distribution of aligned ellipsoidal cylindrical cavities (5.4.1), the average overall stress is again equal to matrix stress average $\bar{\boldsymbol{\sigma}} = \boldsymbol{\sigma}_1$. Strain average in each cavity is found as in (5.4.3), $\boldsymbol{\varepsilon}_c = (\boldsymbol{I} - \boldsymbol{S})^{-1}\boldsymbol{\varepsilon}^0 = \boldsymbol{Q}^{-1}\boldsymbol{L}_1\boldsymbol{\varepsilon}^0$. Applied overall strain is $\boldsymbol{\varepsilon}^0 = \boldsymbol{M}_1\bar{\boldsymbol{\sigma}} + c_c\boldsymbol{\varepsilon}_c$, hence

$$\bar{\boldsymbol{\sigma}} = \boldsymbol{L}_1(\boldsymbol{I} - c_c\, \boldsymbol{Q}^{-1}\boldsymbol{L}_1)\, \boldsymbol{\varepsilon}^0 \tag{5.4.10}$$

Taking again the limit (5.4.5) in the transition from elliptic cylinders to cracks provides

$$\bar{\boldsymbol{\sigma}} = \boldsymbol{L}_1(\boldsymbol{I} - \pi a_1^2 \eta \boldsymbol{\Lambda} \boldsymbol{L}_1)\boldsymbol{\varepsilon}^0 \tag{5.4.11}$$

Total potential energy $\mathcal{W} = \mathcal{W}_0 + \mathcal{W}_I$ of the volume V then follows from (5.1.4) as

$$\mathcal{W}_0 = \frac{1}{2}(\boldsymbol{\varepsilon}^0)^{\mathrm{T}} \boldsymbol{L}_1 \boldsymbol{\varepsilon}^0 V \quad \mathcal{W}_I = -\frac{1}{2}\pi a_1^2 \eta (\boldsymbol{\varepsilon}^0)^{\mathrm{T}} \boldsymbol{L}_1 \boldsymbol{\Lambda}\, \boldsymbol{L}_1 \boldsymbol{\varepsilon}^0 V \tag{5.4.12}$$

Interaction energies $\mathcal{W}_I$ and $\mathcal{V}_I$ are identical under the different boundary conditions. However, $\mathcal{W}_0$ and $\mathcal{V}_0$ change signs.

For a solid $\boldsymbol{L}_1$ containing a dilute distribution of open aligned slit cracks, these results provide overall compliance (5.4.7), overall stiffness (5.4.11), and total energy $\mathcal{W}_I$ and $\mathcal{V}_I$ released by the cracks, per unit crack length $|x_3| = 1$ in (5.4.1).

5.4.2 *Aligned Penny-Shaped Cracks in a Transversely Isotropic Solid*

Such cracks are modeled as a limiting shape

$$x_1^2 + x_2^2 = a^2 \quad x_3 \to 0 \tag{5.4.13}$$

of an oblate spheroid $(x_1/a)^2 + (x_2/a)^2 + (x_3/b)^2 = 1$, for $\varepsilon = b/a \to 0$, with normals aligned in x_3-direction. The number of cracks per unit volume is denoted by η, and their volume fraction is

$$c_c = \frac{4}{3}\pi a^3 \eta \varepsilon = \frac{\pi}{6}\alpha\varepsilon \tag{5.4.14}$$

where $\alpha = 8\eta a^3$ is the crack density parameter. For $\alpha = 1$, there is one crack of diameter $2a$ in a cube of side $2a$ (Laws and Dvorak 1987). A different density measure had been used by Budiansky and O'Connell (1976) for randomly distributed elliptical cracks.

Suppose that a large volume V of material L_{ij} containing a dilute density of cracks is loaded by a uniform overall stress $\boldsymbol{\sigma}^0$. Average strain caused by opening displacement of a single crack follows from (4.3.32) in the form

$$\boldsymbol{\varepsilon}_c = (\boldsymbol{I} - \boldsymbol{S})^{-1} \boldsymbol{M}_1 \boldsymbol{\sigma}^0 = \boldsymbol{Q}^{-1} \boldsymbol{\sigma}^0 \tag{5.4.3}$$

As shown by Laws (1985), $\boldsymbol{Q}^{-1}$ is again singular, but the tensor $\boldsymbol{\Lambda} = \lim_{\varepsilon \to 0} \varepsilon \boldsymbol{Q}^{-1}$ remains finite. In present coordinates, one first solves the equation

$$L_{33}L_{44}x^2 - (L_{11}L_{33} - 2L_{13}L_{44} - L_{13}^2)x + L_{11}L_{44} = 0 \tag{5.4.15}$$

and then substitutes the roots $\gamma_1,\ \gamma_2$ into the following nonzero coefficients of $\mathbf{\Lambda}$

$$\left.\begin{aligned}\Lambda_{33} &= \frac{2(L_{11}L_{33})^{1/2}(\gamma_1^{1/2}+\gamma_2^{1/2})}{\pi(L_{11}L_{33}-L_{13}^2)}\\ \Lambda_{55} = \Lambda_{66} &= [4L_{33}(\gamma_1^{1/2}+\gamma_2^{1/2})]\\ &\times\left[\pi\{L_{11}L_{33}-L_{13}^2+L_{33}(\gamma_1^{1/2}+\gamma_2^{1/2})[(L_{11}-L_{12})L_{44}/2]^{1/2}\}\right]^{-1}\end{aligned}\right\} \tag{5.4.16}$$

Total potential energy $\mathcal{V}=\mathcal{V}_0+\mathcal{V}_I$ is obtained from (5.1.9) to (5.1.11) with

$$\mathcal{V}_0=-\frac{1}{2}(\boldsymbol{\sigma}^0)^{\mathrm{T}}\boldsymbol{M}_1\boldsymbol{\sigma}^0V \quad \mathcal{V}_I=-\frac{2}{3}\pi a^3\eta(\boldsymbol{\sigma}^0)^{\mathrm{T}}\mathbf{\Lambda}\boldsymbol{\sigma}^0V \tag{5.4.17}$$

After substitution for Λ_{ij} from (5.4.16), the interaction energy is

$$\mathcal{V}_I=-\frac{2}{3}\pi a^3\eta\left\{\Lambda_{33}(\sigma_{33}^0)^2+\Lambda_{44}\left[(\sigma_{13}^0)^2+(\sigma_{23}^0)^2\right]\right\}V \tag{5.4.18}$$

where the individual contributions correspond to opening Mode I and to the two shear modes. The strain energy under overall applied strain and related results can be obtained by following similar derivations in Sect. 5.4.1.

Chapter 6
Evaluations and Bounds on Elastic Moduli of Heterogeneous Materials

This chapter is concerned with composites and polycrystals, consisting of two or more distinct phases that have known stiffnesses $\boldsymbol{L}_r$ defined in the fixed overall coordinate system of a representative volume V. Phase volume fractions c_r, $\Sigma_{r=1}^{n} c_r = 1$, are no longer small, hence evaluation of both overall properties and local fields must reflect *interactions between individual phase volumes.* Spatial distribution of the phases in V is statistically homogeneous, as described in Sect. 3.2.2, and perfect bonding is assumed at all interfaces. Of interest are derivations of upper and lower bounds on the overall stiffness $\boldsymbol{L} = \boldsymbol{L}^{\mathrm{T}}$ and compliance $\boldsymbol{M} = \boldsymbol{L}^{-1}$ of the aggregate, and of estimates of phase volume averages of strain and stress fields, caused in the heterogeneous system by application of uniform overall strain $\boldsymbol{\varepsilon}^0$ or stress $\boldsymbol{\sigma}^0$. Those are sought in terms of known volume fractions, elastic moduli, shape and alignment of the constituent phases, Sects. 6.1 and 6.2.

Three approaches to these goals will be described here. The average field approximations of phase interactions, or AFA is based on solitary inhomogeneity solutions of Chap. 4, modified for applications to many interacting inhomogeneities. One form of the average field approximation yields Hashin-Shtrikman (H-S) variational bounds on overall stiffness and compliance, presented for particulate mixtures and aligned fiber composites in Sect. 6.3. Other AFA methods bracketed by these bounds are described in Chap. 7.

The second group of methods includes the Hashin (1962, 1972, 1979) and Hashin and Rosen (1964) composite sphere and cylinder assemblage (CSA/CCA) bounds. Identical composite elements of the same phase volume fraction and variable diameter fill in a random manner the entire volume V. Exact elastic fields are found for a single element subjected to traction or displacement boundary conditions that impose uniform overall stress or strain. The minimum energy theorems (3.7.20)–(3.7.21) then provide another set of variational bounds, yielding four results after role exchange of the phases. Best bounds are selected as the closest among the CSA/CCA and/or H-S bounds, the lowest upper and highest lower bound. Periodic fiber microstructures, such as the PHA model described in Chap. 12, exhibit long-range order. The upper and lower bounds on their elastic moduli are often closer,

G.J. Dvorak, *Micromechanics of Composite Materials*, Solid Mechanics and Its Applications 186, DOI 10.1007/978-94-007-4101-0_6,

albeit somewhat lower than the CCA bounds (Accorsi and Nemat-Nasser 1986; Teply and Dvorak 1988; Nemat-Nasser and Hori 1995, 1999; Nemat-Nasser et al. 1982).

In the third group is the generalized self-consistent method, or GSCM in Sect. 6.5, developed by Christensen and Lo (1979) and Christensen (1990). Overall shear moduli predictions are found by constructing exact elasticity solution of a three-phase system, consisting of a cylindrical or spherical two-phase element, similar to CSA/CCA, embedded in the effective medium. The interaction energy (5.1.11) between the element and effective medium is required to be equal to zero. The GSCM estimates of overall moduli are often closely bracketed by the CSA or CCA bounds for the same geometries, hence both provide more rigorous, usually best available and accurate evaluations of overall moduli.

Subject to certain restrictions, the Hashin-Shtrikman bounds can be found for multiphase materials. However the CSA/CCA bounds and the GSCM estimates are limited to two-phase systems.

6.1 Elementary Energy Bounds

The least restrictive but historically significant bounds, derived by Voigt (1889) and Reuss (1929), offer an illustration of the utility of the potential and complementary energy theorems of Sect. 3.7 in estimating overall stiffness or compliance of a heterogeneous aggregate. Derivation of the Voigt bound adopts the uniform applied overall strain field as the local strain field in all phases, or grains in a polycrystal. This field is kinematically admissible, since it satisfies the prescribed displacement boundary conditions, and is compatible in a representative volume V. Then, according to (3.5.2), $\boldsymbol{\varepsilon}_r = \boldsymbol{\varepsilon}^0$, $\boldsymbol{A}_r = \boldsymbol{I}$, and the actual magnitude $\mathcal{V}^{(a)}$ of the potential energy $(3.7.20)_1$ of the RVE, and its approximation derived with the admissible strain field, must satisfy the inequality

$$2\mathcal{V}^{(a)} = \int_V (\boldsymbol{\varepsilon}^0)^{\mathrm{T}} \boldsymbol{L} \boldsymbol{\varepsilon}^0 \mathrm{d}V \leq \sum_{r=1}^{n} \int_{V_r} (\boldsymbol{\varepsilon}^0)^{\mathrm{T}} \boldsymbol{L}_r \boldsymbol{\varepsilon}^0 \mathrm{d}V = \int_V (\boldsymbol{\varepsilon}^0)^{\mathrm{T}} \boldsymbol{L}_{\mathrm{V}} \boldsymbol{\varepsilon}^0 \mathrm{d}V \qquad (6.1.1)$$

where $\boldsymbol{L}$ is the actual but unknown overall stiffness. This suggests that the Voigt estimate of overall stiffness is $\boldsymbol{L}_{\mathrm{V}} = \sum_{r=1}^{n} c_r \boldsymbol{L}_r$, and that $(\boldsymbol{L}_{\mathrm{V}} - \boldsymbol{L})$ is positive semi-definite.

The Reuss bound is based on the assumption that the equilibrium stress field in the phases is uniform and equal to the overall stress applied to the RVE; or that all $\boldsymbol{\sigma}_r = \boldsymbol{\sigma}^0$, and $\boldsymbol{B}_r = \boldsymbol{I}$ in (3.5.4). That field is evidently statically admissible. The actual complementary energy $(\mathcal{V}^*)^{(a)}$ of the material in the representative volume and its approximation follow from $(3.7.21)_2$, and they must comply with

$$2(\mathcal{V}^*)^{(a)} = \int_V (\boldsymbol{\sigma}^0)^{\mathrm{T}} \boldsymbol{M} \boldsymbol{\sigma}^0 \mathrm{d}V \leq \sum_{r=1}^{n} \int_{V_r} (\boldsymbol{\sigma}^0)^{\mathrm{T}} \boldsymbol{M}_r \boldsymbol{\sigma}^0 \mathrm{d}V = \int_V (\boldsymbol{\sigma}^0)^{\mathrm{T}} \boldsymbol{M}_{\mathrm{R}} \boldsymbol{\sigma}^0 \mathrm{d}V \tag{6.1.2}$$

This shows that the Reuss estimate of overall compliance is $\boldsymbol{M}_{\mathrm{R}} = \sum_{r=1}^{n} c_r \boldsymbol{M}_r$, and that $(\boldsymbol{M}_{\mathrm{R}} - \boldsymbol{M})$ is positive semi-definite.

In summary, if one defines $\boldsymbol{M}_{\mathrm{V}} = \boldsymbol{L}_{\mathrm{V}}^{-1}$ and $\boldsymbol{L}_{\mathrm{R}} = \boldsymbol{M}_{\mathrm{R}}^{-1}$, then $\boldsymbol{L}_{\mathrm{V}}$ and $\boldsymbol{L}_{\mathrm{R}}$ are the upper and lower bounds on the actual stiffness $\boldsymbol{L}$, while $\boldsymbol{M}_{\mathrm{R}}$ and $\boldsymbol{M}_{\mathrm{V}}$ are the upper and lower bounds of the actual compliance $\boldsymbol{M} = \boldsymbol{L}^{-1}$ of the heterogeneous system in the representative volume V. Similar energy bounds with somewhat improved local fields were derived by Paul (1960).

Of course, the Voigt and Reuss bounds depend only on the phase moduli and volume fractions, without reference to the geometry of the microstructure. For example, for a macroscopically isotropic composite, according to (2.2.29), the Voigt and Reuss bounds on the effective bulk and shear elastic moduli are

$$\left.\begin{aligned} K_{\mathrm{V}} &= \sum_{r=1}^{n} c_r K_r & G_{\mathrm{V}} &= \sum_{r=1}^{n} c_r G_r \\ K_{\mathrm{R}}^{-1} &= \sum_{r=1}^{n} c_r K_r^{-1} & G_{\mathrm{R}}^{-1} &= \sum_{r=1}^{n} c_r G_r^{-1} \end{aligned}\right\} \tag{6.1.3}$$

For a two-phase system, Hill (1963a) shows that the difference between the bounds is

$$K_{\mathrm{V}} - K_{\mathrm{R}} = (K_1 - K_2)^2 (K_1/c_1 + K_2/c_2)^{-1} > 0 \tag{6.1.4}$$

which indicates that they are close only for small contrast between phase moduli, but quite inadequate otherwise. Without information about the shape or spatial distribution of the phases, these bounds are at best limited to isotropic polycrystals.

6.2 Hashin-Shtrikman and Walpole Bounds on Overall Elastic Moduli

In several seminal papers appearing in the early 1960s, Hashin and Shtrikman (1962a, b, 1963) formulated a novel variational principle that lead to much tighter bounds on overall elastic moduli of multiphase heterogeneous materials, written in terms of phase properties and information about the geometry of the microstructure. Hill (1963b) connected the H-S variational principle to standard extremum theorems (3.7.20), (3.7.21), which were then utilized by Walpole (1966) in a more complete derivation of the bounding theorems, described below.

As pointed out earlier, another set of CCA/CSA assemblage bounds for two-phase systems, reinforced by particles or by aligned fibers, was developed by Hashin (1962) and Hashin and Rosen (1964). Hashin (1964, 1965, 1967, 1972, 1979) surveys both approaches, which had established a rigorous foundation and inspiration for many later developments that comprise contemporary micromechanics.

6.2.1 *Overall Strain $\boldsymbol{\varepsilon}^0$ is Prescribed*

A representative volume V of a multiphase material is considered , consisting of perfectly bonded subvolumes V_r of phases $\boldsymbol{L}_r$ that are present in certain volume fractions c_r, such that $\sum_r c_r = 1$. Traction and displacement continuity prevails at all interfaces. Application of a uniform overall strain $\boldsymbol{\varepsilon}^0$ creates in V a compatible local strain field $\boldsymbol{\varepsilon}(\boldsymbol{x}) = \boldsymbol{A}(\boldsymbol{x})\boldsymbol{\varepsilon}^0$ in the phases, together with local stresses $\boldsymbol{\sigma}(\boldsymbol{x}) = \boldsymbol{L}_r\boldsymbol{\varepsilon}(\boldsymbol{x})$ in equilibrium. The $\boldsymbol{A}(\boldsymbol{x})$ is a certain mechanical strain influence function determined later. In parallel, the actual strain field $\boldsymbol{\varepsilon}(\boldsymbol{x})$ is recreated in an identical volume V of a homogeneous comparison medium $\boldsymbol{L}_0$ by applying there an equivalent eigenstrain field $\boldsymbol{\mu}(\boldsymbol{x})$, such that $\boldsymbol{\varepsilon}(\boldsymbol{x})$ has the applied magnitude $\boldsymbol{\varepsilon}^0$ at the surface ∂V. The original stress $\boldsymbol{\sigma}(\boldsymbol{x})$ is restored by the eigenstress field $\boldsymbol{\lambda}(\boldsymbol{x}) = -\boldsymbol{L}_0\boldsymbol{\mu}(\boldsymbol{x})$. In the present context, the $\boldsymbol{\lambda}(\boldsymbol{x})$ is usually regarded as a polarization stress, in analogy to polarization vector in electrostatics (Kröner 1958). The stress and transformation fields are, from (3.6.1)

$$\left.\begin{aligned} \boldsymbol{\sigma}(\boldsymbol{x}) = \boldsymbol{L}_r\boldsymbol{\varepsilon}(\boldsymbol{x}) = \boldsymbol{L}_0\boldsymbol{\varepsilon}(\boldsymbol{x}) + \boldsymbol{\lambda}(\boldsymbol{x}) \\ \boldsymbol{\lambda}(\boldsymbol{x}) = (\boldsymbol{L}_r - \boldsymbol{L}_0)\boldsymbol{\varepsilon}(\boldsymbol{x}) \qquad \boldsymbol{\mu}(\boldsymbol{x}) = -\boldsymbol{L}_0^{-1}(\boldsymbol{L}_r - \boldsymbol{L}_0)\boldsymbol{\varepsilon}(\boldsymbol{x}) \end{aligned}\right\} \tag{6.2.1}$$

The stiffness $\boldsymbol{L}_0$ of the comparison medium is now related to known stiffnesses $\boldsymbol{L}_r$ of the constituent phases (Walpole 1966). To this end, the local fields are selected as phase volume averages $\bar{\boldsymbol{\varepsilon}}_r = \boldsymbol{\varepsilon}(\boldsymbol{x}) - \boldsymbol{\varepsilon}'_r(\boldsymbol{x}) = \boldsymbol{A}_r\boldsymbol{\varepsilon}^0$ that satisfy $\sum_{r=1}^n c_r\bar{\boldsymbol{\varepsilon}}_r = \boldsymbol{\varepsilon}^0$. The concentration factors $\boldsymbol{A}_r$ were introduced in (3.5.2). In the present context, they represent an average of an actual or as yet unspecified elastic field in the phase. The eigenstress field $\boldsymbol{\lambda}(\boldsymbol{x})$ in $\boldsymbol{L}_0$ is replaced in the same way by a piecewise uniform distribution $\boldsymbol{\lambda}_r = (\boldsymbol{L}_r - \boldsymbol{L}_0)\bar{\boldsymbol{\varepsilon}}_r$ in phase subvolumes. Local stress field $(6.2.1)_1$ becomes

$$\boldsymbol{\sigma}^*(\boldsymbol{x}) = \boldsymbol{L}_0\boldsymbol{\varepsilon}(\boldsymbol{x}) + (\boldsymbol{L}_r - \boldsymbol{L}_0)\bar{\boldsymbol{\varepsilon}}_r = \boldsymbol{L}_r\boldsymbol{A}_r\boldsymbol{\varepsilon}^0 + \boldsymbol{L}_0\boldsymbol{\varepsilon}'_r(\boldsymbol{x}) \tag{6.2.2}$$

where $\boldsymbol{\sigma}^*(\boldsymbol{x})$ and $\boldsymbol{\varepsilon}(\boldsymbol{x})$ are in equilibrium and derived from continuous displacements, respectively. Since $\bar{\boldsymbol{\varepsilon}}_r(\boldsymbol{x}) = \bar{\boldsymbol{\varepsilon}}_r$, the deviation $\boldsymbol{\varepsilon}'_r(\boldsymbol{x}) = \boldsymbol{\varepsilon}_r(\boldsymbol{x}) - \bar{\boldsymbol{\varepsilon}}_r$ has the average $\bar{\boldsymbol{\varepsilon}}'_r = \boldsymbol{0}$ in each phase volume V_r. The fields $\boldsymbol{\sigma}^*(\boldsymbol{x})$ and $\boldsymbol{\varepsilon}(\boldsymbol{x})$ have volume averages $\bar{\boldsymbol{\sigma}}^* = \boldsymbol{L}\boldsymbol{\varepsilon}^0$ and $\bar{\boldsymbol{\varepsilon}} = \boldsymbol{\varepsilon}^0$ over the total volume V, and $\boldsymbol{\varepsilon}^0$ is uniform on ∂V. This suggests the virtual work equality

$$\int_V \left(\boldsymbol{\varepsilon}^0 - \boldsymbol{\varepsilon}(\boldsymbol{x})\right)^{\mathrm{T}} \boldsymbol{\sigma}^*(\boldsymbol{x}) \mathrm{d}V = 0 \tag{6.2.3}$$

The minimum potential energy theorem provides *an upper bound* on the actual potential energy $\mathcal{V}^{(a)}$, generated in the aggregate by the applied overall strain $\boldsymbol{\varepsilon}^0$. According to $(3.7.20)_1$, the actual potential energy $\mathcal{V}^{(a)}$ and its approximation must satisfy the inequality

$$2\mathcal{V}^{(a)} = \int_V (\boldsymbol{\varepsilon}^0)^{\mathrm{T}} \boldsymbol{L}^{(a)} \boldsymbol{\varepsilon}^0 \mathrm{d}V \le \sum_{r=1}^{n} \int_{V_r} \boldsymbol{\varepsilon}^{\mathrm{T}}(\boldsymbol{x}) \boldsymbol{L}_r \boldsymbol{\varepsilon}(\boldsymbol{x}) \mathrm{d}V \tag{6.2.4}$$

where the first integral represents the potential energy of a homogenized medium that has the actual but as yet unknown effective stiffness $\boldsymbol{L}^{(a)}$ as the heterogeneous aggregate in V. The second integral evaluates the potential energy generated by the strain fields $\boldsymbol{\varepsilon}_r(\boldsymbol{x}) = \bar{\boldsymbol{\varepsilon}}_r + \boldsymbol{\varepsilon'}_r(\boldsymbol{x})$.

A more compact form of the last integral in (6.2.4) can be found by adding (6.2.3)

$$2\mathcal{V}^{(a)} \le \sum_{r=1}^{n} \int_{V_r} \boldsymbol{\varepsilon}^{\mathrm{T}}(\boldsymbol{x})\, \boldsymbol{L}_r \boldsymbol{\varepsilon}(\boldsymbol{x})\, \mathrm{d}V + \int_V \left(\boldsymbol{\varepsilon}^0 - \boldsymbol{\varepsilon}(\boldsymbol{x})\right)^{\mathrm{T}} [\boldsymbol{L}_r \boldsymbol{A}_r \boldsymbol{\varepsilon}^0 + \boldsymbol{L}_0 \boldsymbol{\varepsilon'}_r(\boldsymbol{x})] \mathrm{d}V \tag{6.2.5}$$

This can simplified by noticing that $\boldsymbol{L}_r \boldsymbol{A}_r \boldsymbol{\varepsilon}^0 = \boldsymbol{L}_r \bar{\boldsymbol{\varepsilon}}_r = \boldsymbol{L}_r [\boldsymbol{\varepsilon}(\boldsymbol{x}) - \boldsymbol{\varepsilon'}_r(\boldsymbol{x})]$ and that

$$\int_{V_r} \left(\boldsymbol{\varepsilon}^0\right)^{\mathrm{T}} \boldsymbol{L}_0 \boldsymbol{\varepsilon'}_r(\boldsymbol{x}) \mathrm{d}V = 0 \qquad \int_{V_r} (\bar{\boldsymbol{\varepsilon}}_r)^{\mathrm{T}} [(\boldsymbol{L}_0 - \boldsymbol{L}_r) \boldsymbol{\varepsilon'}_r(\boldsymbol{x})] \mathrm{d}V = 0 \tag{6.2.6}$$

Then

$$\left.\begin{aligned} 2\mathcal{V}^{(a)} &\le \sum_{r=1}^{n} \left(\boldsymbol{\varepsilon}^0\right)^{\mathrm{T}} \boldsymbol{L}_r \boldsymbol{A}_r \boldsymbol{\varepsilon}^0 V_r + \sum_{r=1}^{n} \int_{V_r} \boldsymbol{\varepsilon}^{\mathrm{T}}(\boldsymbol{x})\, \boldsymbol{L}_r \boldsymbol{\varepsilon}(\boldsymbol{x})\, \mathrm{d}V \\ &\quad - \sum_{r=1}^{n} \int_{V_r} \boldsymbol{\varepsilon}^{\mathrm{T}}(\boldsymbol{x}) \left[\boldsymbol{L}_r \left(\boldsymbol{\varepsilon}(\boldsymbol{x}) - \boldsymbol{\varepsilon'}_r(\boldsymbol{x})\right) + \boldsymbol{L}_0 \boldsymbol{\varepsilon'}_r(\boldsymbol{x})\right] \mathrm{d}V \\ 2\mathcal{V}^{(a)} &\le \sum_{r=1}^{n} \left(\boldsymbol{\varepsilon}^0\right)^{\mathrm{T}} \boldsymbol{L}_r \boldsymbol{A}_r \boldsymbol{\varepsilon}^0 V_r - \sum_{r=1}^{n} \int_{V_r} (\boldsymbol{\varepsilon}(\boldsymbol{x}))^{\mathrm{T}} [(\boldsymbol{L}_0 - \boldsymbol{L}_r) \boldsymbol{\varepsilon'}_r(\boldsymbol{x})] \mathrm{d}V \\ &\le \sum_{r=1}^{n} \left(\boldsymbol{\varepsilon}^0\right)^{\mathrm{T}} \boldsymbol{L}_r \boldsymbol{A}_r \boldsymbol{\varepsilon}^0 V_r - \sum_{r=1}^{n} \int_{V_r} \left(\bar{\boldsymbol{\varepsilon}}_r + \boldsymbol{\varepsilon'}_r(\boldsymbol{x})\right)^{\mathrm{T}} [(\boldsymbol{L}_0 - \boldsymbol{L}_r) \boldsymbol{\varepsilon'}_r(\boldsymbol{x})] \mathrm{d}V \end{aligned}\right\} \tag{6.2.7}$$

This renders the potential energy inequality (6.2.4) in the form

$$\left.\begin{aligned} 2\mathcal{V}^a = (\boldsymbol{\varepsilon}^0)^{\mathrm{T}}\boldsymbol{L}^{(a)}\boldsymbol{\varepsilon}^0 V \le \sum_{r=1}^{n} (\boldsymbol{\varepsilon}^0)^{\mathrm{T}}\boldsymbol{L}_r\boldsymbol{A}_r\boldsymbol{\varepsilon}^0 V_r \\ - \sum_{r=1}^{n} \int_{V_r} \big(\boldsymbol{\varepsilon}'_r(\boldsymbol{x})\big)^{\mathrm{T}}(\boldsymbol{L}_0 - \boldsymbol{L}_r)\boldsymbol{\varepsilon}'_r(\boldsymbol{x})\,\mathrm{d}V \end{aligned}\right\} \tag{6.2.8}$$

At a given value of $\boldsymbol{\varepsilon}^0$, the inequality compares the actual stiffness $\boldsymbol{L}^{(a)}$ of the composite aggregate with its *upper bound approximation* $\boldsymbol{L}^{(+)}$, derived from local fields denoted now by $\bar{\boldsymbol{\varepsilon}}_r = \boldsymbol{A}_r^{(+)}\boldsymbol{\varepsilon}^0$.

$$\boldsymbol{L}^{(a)} = \frac{1}{V}\sum_{r=1}^{n} \int_{V_r} \boldsymbol{L}_r\boldsymbol{A}_r^{(a)}(\boldsymbol{x})\mathrm{d}V \qquad \boldsymbol{L}^{(+)} = \sum\nolimits_{r=1}^{n} c_r\boldsymbol{L}_r\boldsymbol{A}_r^{(+)} \tag{6.2.9}$$

For the total energy of the approximate fields to reach a minimum value, the last term in (6.2.8) must be positive, hence $(\boldsymbol{L}_0 - \boldsymbol{L}_r)$ has to be positive semi-definite, where we denote the required $\boldsymbol{L}_0 = \boldsymbol{L}_0^{(+)}$. The final form of the energy bound is

$$(\boldsymbol{\varepsilon}^0)^{\mathrm{T}}(\boldsymbol{L}^{(+)} - \boldsymbol{L}^{(a)})\boldsymbol{\varepsilon}^0 V \ge \sum_{r=1}^{n} \int_{V_r} \big(\boldsymbol{\varepsilon}'_r(\boldsymbol{x})\big)^{\mathrm{T}}(\boldsymbol{L}_0^{(+)} - \boldsymbol{L}_r)\boldsymbol{\varepsilon}'_r(\boldsymbol{x})\,\mathrm{d}V \tag{6.2.10}$$

suggesting that if $(\boldsymbol{L}_0^{(+)} - \boldsymbol{L}_r)$ is positive semi-definite for all r, then so is $(\boldsymbol{L}^{(+)} - \boldsymbol{L}^{(a)})$.

A lower bound $\boldsymbol{L}^{(-)}$ on the actual effective stiffness $\boldsymbol{L}^{(a)}$ of the heterogeneous aggregate follows from the minimum complementary energy theorem. The actual complementary energy $(\mathcal{V}^*)^{(a)}$, generated by the overall applied strain $\boldsymbol{\varepsilon}^0$ in both the aggregate and the equivalent homogenized material in V, must be smaller than that obtained from the approximate local fields (6.2.2). In the present application, $(3.7.20)_2$ provides the inequality

$$2(\mathcal{V}^*)^{(a)} \ge \sum_{r=1}^{n} \int_{V_r} (\boldsymbol{\sigma}^*)^{\mathrm{T}}(2\boldsymbol{\varepsilon}^0 - \boldsymbol{M}_r\boldsymbol{\sigma}^*)\mathrm{d}V \tag{6.2.11}$$

where spatial variability of $\boldsymbol{\sigma}^*$ is no longer emphasized.

Subtract now (6.2.3) from the right hand side of (6.2.11) and retrace the derivation of (6.2.10) to find

$$2(\mathcal{V}^*)^{(a)} \ge \sum_{r=1}^{n} (\boldsymbol{\varepsilon}^0)^{\mathrm{T}}\boldsymbol{L}_r\boldsymbol{A}_r\boldsymbol{\varepsilon}^0 V_r + \sum_{r=1}^{n} (\boldsymbol{\varepsilon}'_r)^{\mathrm{T}}\boldsymbol{L}_0(\boldsymbol{M}_0 - \boldsymbol{M}_r)\boldsymbol{L}_0\boldsymbol{\varepsilon}'_r\mathrm{d}V_r \tag{6.2.12}$$

The actual magnitude $(\mathcal{V}^*)^{(a)}$ of the complementary energy follows from (6.2.11), after replacement of the approximate $\boldsymbol{\sigma}^*$ by the actual but unknown stress field $\boldsymbol{\sigma}^{(a)}(\boldsymbol{x}) = \boldsymbol{L}_r\boldsymbol{\varepsilon}^{(a)}(\boldsymbol{x}) = \boldsymbol{L}_r\boldsymbol{A}_r^{(a)}(\boldsymbol{x})\boldsymbol{\varepsilon}^0$ that is caused in the aggregate by the applied $\boldsymbol{\varepsilon}^0$. The $\boldsymbol{A}_r^{(a)}(\boldsymbol{x})$ is the mechanical strain influence function (3.5.1).

$$2(\mathcal{V}^*)^{(a)} = \sum_{r=1}^{n}\int_{V_r}[\boldsymbol{A}_r^{(a)}(\boldsymbol{x})\boldsymbol{\varepsilon}^0]^{\mathrm{T}}\boldsymbol{L}_r[2\boldsymbol{\varepsilon}^0 - \boldsymbol{A}_r^{(a)}(\boldsymbol{x})\boldsymbol{\varepsilon}^0]\mathrm{d}V = \boldsymbol{\varepsilon}^0\boldsymbol{L}^{(a)}\boldsymbol{\varepsilon}^0 \tag{6.2.13}$$

The actual overall stiffness of the aggregate, and its lower bound in (6.2.12) are denoted by

$$\boldsymbol{L}^{(a)} = \frac{1}{V}\sum_{r=1}^{n}\int_{V_r}\boldsymbol{L}_r\boldsymbol{A}_r^{(a)}(\boldsymbol{x})\mathrm{d}V \quad \boldsymbol{L}^{(-)} = \frac{1}{V}\sum_{r=1}^{n}\boldsymbol{L}_r\boldsymbol{A}_r^{(-)}V_r \tag{6.2.14}$$

This changes the inequality (6.2.12) to

$$\left.\begin{aligned} 2(\mathcal{V}^*)^{(a)} &\geq \sum_{r=1}^{n}(\boldsymbol{\varepsilon}^0)^{\mathrm{T}}\boldsymbol{L}_r\boldsymbol{A}_r^{(-)}\boldsymbol{\varepsilon}^0V_r + \sum_{r=1}^{n}(\boldsymbol{\varepsilon}'_r)^{\mathrm{T}}\boldsymbol{L}_0(\boldsymbol{M}_0 - \boldsymbol{M}_r)\boldsymbol{L}_0\boldsymbol{\varepsilon}'_r\mathrm{d}V_r \\ (\boldsymbol{\varepsilon}^0)^{\mathrm{T}}(\boldsymbol{L}^{(-)} - \boldsymbol{L}^{(a)})\boldsymbol{\varepsilon}^0V &\leq -\sum_{r=1}^{n}(\boldsymbol{\varepsilon}'_r)^{\mathrm{T}}\boldsymbol{L}_0(\boldsymbol{M}_0 - \boldsymbol{M}_r)\boldsymbol{L}_0\boldsymbol{\varepsilon}'_r\mathrm{d}V_r \end{aligned}\right\} \tag{6.2.15}$$

For a lower bound on $\boldsymbol{L}^{(a)}$, the difference $(\boldsymbol{L}^{(-)} - \boldsymbol{L}^{(a)})$ should be negative semi-definite and $(\boldsymbol{M}_0 - \boldsymbol{M}_r)$ positive semi-definite. The $(\boldsymbol{M}_0 - \boldsymbol{M}_r)$ and $(\boldsymbol{L}_r - \boldsymbol{L}_0)$ are both either positive semi-definite or negative semi-definite, depending on the choice of $\boldsymbol{L}_0$. Therefore, $\boldsymbol{L}_0^{(-)}$ must be selected such that $(\boldsymbol{L}_0^{(-)} - \boldsymbol{L}_r)$ is negative semi-definite.

Inequalities (6.2.10) and (6.2.15) provide the theorems (Hashin and Shtrikman 1962a, b; Walpole 1966)

$$\left.\begin{aligned} &\textit{If in all subvolumes } V_r, (\boldsymbol{L}_0^{(+)} - \boldsymbol{L}_r) \textit{ is positive semi} - \textit{definite}, \\ &\quad \textit{then so is } (\boldsymbol{L}^{(+)} - \boldsymbol{L}^{(a)}) \\ &\textit{If in all subvolumes } V_r, \ (\boldsymbol{L}_0^{(-)} - \boldsymbol{L}_r) \textit{ is negative semi} - \textit{definite}, \\ &\quad \textit{then so is } (\boldsymbol{L}^{(-)} - \boldsymbol{L}^{(a)}) \end{aligned}\right\} \tag{6.2.16}$$

The $\boldsymbol{L}^{(+)}$ or $\boldsymbol{L}^{(-)}$ are upper or lower bounds on the actual effective stiffness $\boldsymbol{L}^{(a)}$ of the heterogeneous aggregate. The $\boldsymbol{L}_0^{(+)}$ or $\boldsymbol{L}_0^{(-)}$ are constructed using all available moduli of individual phases to satisfy the indicated inequalities. In positive

semi-definite matrices, all eigenvalues and the determinants of principal minors are positive or zero. In an isotropic aggregate, both $(G_0^{(+)} - G_r)$ and $(K_0^{(+)} - K_r)$ must be positive, negative or zero, according to the bounding theorems. In transversely isotropic solids, similar requirements apply to all moduli $k,\ m,\ p,\ E_{11} = E_A = (n - l^2/k)$ and to the expression $(k - l^2/n)$ in the $(\boldsymbol{L}_0^{(+)} - \boldsymbol{L}_r)$ and the $(\boldsymbol{L}_0^{(-)} - \boldsymbol{L}_r)$ forms. At very high contrast, $\boldsymbol{L}_0^{(+)} \to \infty,\ \boldsymbol{L}_0^{(-)} = \boldsymbol{L}_1$, when at least one phase is rigid, only the lower bound is finite, and $\boldsymbol{L}^{(+)} \to \infty$. For porous media, where $\boldsymbol{L}_0^{(+)} \to \boldsymbol{L}_1,\ \boldsymbol{L}_0^{(-)} = \boldsymbol{0}$, only the upper bound is positive and $\boldsymbol{L}^{(-)} = \boldsymbol{0}$.

6.2.2 *Overall Stress $\boldsymbol{\sigma}^0$ is Prescribed*

Next, energy bounds on the effective overall compliance $\boldsymbol{M}^{(a)}$ of the heterogeneous aggregate are derived using the minimum potential and complementary energy theorems, following the procedure in Sect. 6.2.1. The representative volume V is now loaded by surface tractions that create a uniform overall stress $\boldsymbol{\sigma}^0$, and an equilibrium local stress field $\boldsymbol{\sigma}(\boldsymbol{x})$ with a compatible strain field $\boldsymbol{\varepsilon}(\boldsymbol{x}) = \boldsymbol{M}_r\boldsymbol{\sigma}(\boldsymbol{x})$ in the phases $r = 1, 2, \ldots n$. The heterogeneous material in volume V is again replaced by a homogeneous comparison medium $\boldsymbol{L}_0$. The stress $\boldsymbol{\sigma}(\boldsymbol{x})$ is generated in $\boldsymbol{L}_0$ by an applied eigenstrain field $\boldsymbol{\mu}(\boldsymbol{x})$, such that it assumes the applied magnitude $\boldsymbol{\sigma}^0$ at the surface ∂V. The strain field in $\boldsymbol{L}_0$ then is

$$\boldsymbol{\varepsilon}(\boldsymbol{x}) = \boldsymbol{M}_0\boldsymbol{\sigma}(\boldsymbol{x}) + \boldsymbol{\mu}(\boldsymbol{x}) = \boldsymbol{M}_r\boldsymbol{\sigma}(\boldsymbol{x}) \ \Rightarrow \ \boldsymbol{\mu}(\boldsymbol{x}) = (\boldsymbol{M}_r - \boldsymbol{M}_0)\boldsymbol{\sigma}(\boldsymbol{x}) \quad (6.2.17)$$

An approximation of $\boldsymbol{\mu}(\boldsymbol{x})$ is introduced in the form $\boldsymbol{\mu}_r = (\boldsymbol{M}_r - \boldsymbol{M}_0)\bar{\boldsymbol{\sigma}}_r$, where $\bar{\boldsymbol{\sigma}}_r = \boldsymbol{B}_r\boldsymbol{\sigma}^0,\ \sum_{r=1}^{n} c_r\bar{\boldsymbol{\sigma}}_r = \boldsymbol{\sigma}^0$, and the strain (6.2.17) is replaced by

$$\boldsymbol{\varepsilon}^*(\boldsymbol{x}) = \boldsymbol{M}_0\boldsymbol{\sigma}(\boldsymbol{x}) + (\boldsymbol{M}_r - \boldsymbol{M}_0)\bar{\boldsymbol{\sigma}}_r = \boldsymbol{M}_r\boldsymbol{B}_r\boldsymbol{\sigma}^0 + \boldsymbol{M}_0\boldsymbol{\sigma}'_r(\boldsymbol{x}) \quad (6.2.18)$$

The difference $\boldsymbol{\sigma}'_r(\boldsymbol{x}) = \boldsymbol{\sigma}(\boldsymbol{x}) - \bar{\boldsymbol{\sigma}}_r$ has a zero volume average in each phase r, hence $\bar{\boldsymbol{\sigma}}'_r = \boldsymbol{0}$. Overall strain derived from phase averages of $\boldsymbol{\varepsilon}^*(\boldsymbol{x})$ in a representative volume is uniform. Equilibrium and compatibility conditions are met by the approximate stress and strain fields, which also satisfy the virtual work equality

$$\int_V \left(\boldsymbol{\sigma}^0 - \boldsymbol{\sigma}(\boldsymbol{x})\right)^{\mathrm{T}}\boldsymbol{\varepsilon}^*(\boldsymbol{x})\,\mathrm{d}V = 0 \quad (6.2.19)$$

The minimum complementary energy theorem provides an upper bound on the actual complementary energy $(\mathcal{V}^*)^{(a)}$ generated in the aggregate by the applied overall stress, and also on the effective compliance $\boldsymbol{M}^{(a)}$. According to (3.7.21)

$$2(\mathcal{V}^*)^{(a)} = \int_V (\boldsymbol{\sigma}^0)^{\mathrm{T}} \boldsymbol{M}^{(a)} \boldsymbol{\sigma}^0 \mathrm{d}V \leq \sum_{r=1}^{n} \int_{V_r} \boldsymbol{\sigma}^{\mathrm{T}} \boldsymbol{M}_r \boldsymbol{\sigma} \, \mathrm{d}V \tag{6.2.20}$$

Equation (6.2.19) is now added to the right hand side, and a derivation similar to that in (6.2.6), (6.2.7), (6.2.8) yields the upper bound $\boldsymbol{M}^{(+)} = \sum c_r \boldsymbol{M}_r \boldsymbol{B}_r^{(+)}$ on the overall compliance

$$(\boldsymbol{\sigma}^0)^{\mathrm{T}} (\boldsymbol{M}^{(+)} - \boldsymbol{M}^{(a)}) \boldsymbol{\sigma}^0 V \geq \sum_{r=1}^{n} \int_{V_r} (\boldsymbol{\sigma'}_r)^{\mathrm{T}} (\boldsymbol{M}_0 - \boldsymbol{M}_r) \boldsymbol{\sigma'}_r \mathrm{d}V \tag{6.2.21}$$

This shows that if $(\boldsymbol{M}_0 - \boldsymbol{M}_r)$ is positive semi-definite for all r, then so is $(\boldsymbol{M}^{(+)} - \boldsymbol{M}^{(a)})$.

Finally, a lower bound on $\boldsymbol{M}^{(a)}$ follows from the minimum potential energy theorem. Taking $(\mathcal{V})^{(a)}$ from $(3.7.21)_2$

$$2(\mathcal{V})^{(a)} = (\boldsymbol{\sigma}^0)^{\mathrm{T}} \boldsymbol{M}^{(a)} \boldsymbol{\sigma}^0 V \geq \sum_{r=1}^{n} \int_{V_r} (2\boldsymbol{\sigma}^0 - \boldsymbol{L}_r \boldsymbol{\varepsilon}^*)^{\mathrm{T}} \boldsymbol{\varepsilon}^* \mathrm{d}V \tag{6.2.22}$$

then subtracting (6.2.19) from the right hand side, and following the procedure leading to (6.2.13), yields the lower bound on the overall compliance, $\boldsymbol{M}^{(-)} = \sum c_r \boldsymbol{M}_r \boldsymbol{B}_r^{(-)}$

$$(\boldsymbol{\sigma}^0)^{\mathrm{T}} (\boldsymbol{M}^{(a)} - \boldsymbol{M}^{(-)}) \boldsymbol{\sigma}^0 V \geq \sum_{r=1}^{n} (\boldsymbol{\sigma'}_r)^{\mathrm{T}} \boldsymbol{M}_0 (\boldsymbol{L}_0 - \boldsymbol{L}_r) \boldsymbol{M}_0 \boldsymbol{\sigma'}_r \mathrm{d}V_r \tag{6.2.23}$$

Since $(\boldsymbol{L}_0 - \boldsymbol{L}_r)$ and $(\boldsymbol{M}_r - \boldsymbol{M}_0)$ are both either positive definite or negative definite, depending on the choice of $\boldsymbol{L}_0$, (6.2.21) and (6.2.23) suggest the theorems (Walpole 1966)

$$\left.\begin{array}{l} \textit{If in all subvolumes } V_r, (\boldsymbol{M}_0^{(+)} - \boldsymbol{M}_r) \textit{ is positive semi} - \textit{definite}, \\ \quad \textit{then so is } (\boldsymbol{M}^{(+)} - \boldsymbol{M}^{(a)}) \\ \textit{If in all subvolumes } V_r, \ (\boldsymbol{M}_0^{(-)} - \boldsymbol{M}_r) \textit{ is negative semi} - \textit{definite}, \\ \quad \textit{then so is } (\boldsymbol{M}^{(-)} - \boldsymbol{M}^{(a)}) \end{array}\right\} \tag{6.2.24}$$

The $\boldsymbol{M}^{(+)}$ or $\boldsymbol{M}^{(-)}$ are the upper or lower bounds on the actual effective compliance $\boldsymbol{M}^{(a)}$ of the heterogeneous aggregate. Selection of $\boldsymbol{M}_0^{(+)}$ or $\boldsymbol{M}_0^{(-)}$ is analogous to that described after (6.2.16). So are their magnitudes in systems with high contrast between moduli.

6.3 Evaluation of H-S Bounds for Ellipsoidal Inhomogeneities

Original derivation of the local field averages in individual phases by Hashin and Shtrikman (1962b, 1963b) relied on probability distribution functions of the type described in Sect. 3.2. In a more recent formulation, Willis (1977) found stiffness and conductivity bounds for a microstructural geometry represented by the two-point probability function, using the Hashin-Shtrikman (1962a, 1963) variational principle. Weng (1992) evaluated the corresponding $\boldsymbol{P}$ tensor in an ellipsoidal inhomogeneity, and confirmed that $\boldsymbol{P} = \boldsymbol{S}\boldsymbol{L}_0{}^{-1}$, as anticipated in (4.2.9). For ellipsoidal inhomogeneities, the H-S and Willis bounds can be made to coincide with the above results. Therefore, the AFA-type H-S bounds are often referred to as two-point bounds, and the Voigt-Reuss bounds as one-point bounds, because they depend only on $S_1^r(\boldsymbol{x}) = c_r$. More elaborate and often tighter three point and multipoint bounds, found for certain particulate and fibrous systems, are described by Milton (1985, 2002) and Torquato (2002), together with selected microstructures by which some bounds may be realized. The methods used in their derivation and evaluation are often entirely different from those exposed herein, and therefore beyond the present scope.

6.3.1 *Local Field and Overall Elastic Moduli of Multiphase Systems*

The stress and strain fields inside a solitary ellipsoidal inhomogeneity embedded in a large volume Ω of a comparison medium $\boldsymbol{L}_0$ were derived in Sect. 4.2. Those offer a simple analytical evaluation of the H-S bounds. Under a uniform strain $\boldsymbol{\varepsilon}_\Omega^0$ or stress $\boldsymbol{\sigma}_\Omega^0$ applied to Ω, these fields are both uniform and are given by $\boldsymbol{\varepsilon}_r = \boldsymbol{T}_r\boldsymbol{\varepsilon}_\Omega^0$ or $\boldsymbol{\sigma}_r = \boldsymbol{W}_r\boldsymbol{\sigma}_\Omega^0$, where

$$\left.\begin{aligned} \boldsymbol{T}_r{}^{-1} &= \boldsymbol{I} + \boldsymbol{P}(\boldsymbol{L}_r - \boldsymbol{L}_0) = (\boldsymbol{L}^* + \boldsymbol{L}_0)^{-1}(\boldsymbol{L}^* + \boldsymbol{L}_r) = \boldsymbol{P}(\boldsymbol{L}^* + \boldsymbol{L}_r) \\ \boldsymbol{W}_r{}^{-1} &= \boldsymbol{I} + \boldsymbol{Q}(\boldsymbol{M}_r - \boldsymbol{M}_0) = (\boldsymbol{M}^* + \boldsymbol{M}_0)^{-1}(\boldsymbol{M}^* + \boldsymbol{M}_r) = \boldsymbol{Q}(\boldsymbol{M}^* + \boldsymbol{M}_r) \end{aligned}\right\} \quad [4.2.14]$$

and

$$\left.\begin{aligned} \boldsymbol{P} = \boldsymbol{S}\boldsymbol{L}_0^{-1} = (\boldsymbol{L}^* + \boldsymbol{L}_0)^{-1} = \boldsymbol{P}^{\mathrm{T}} \quad \boldsymbol{Q} = \boldsymbol{L}_0(\boldsymbol{I} - \boldsymbol{P}\boldsymbol{L}_0) = (\boldsymbol{M}^* + \boldsymbol{M}_0)^{-1} = \boldsymbol{Q}^{\mathrm{T}} \\ \boldsymbol{P}\boldsymbol{L}_0 + \boldsymbol{M}_0\boldsymbol{Q} = \mathbf{I} \end{aligned}\right\} \quad [4.2.9]$$

where the matrix $\boldsymbol{S}$ represents the Eshelby tensor for the selected ellipsoidal shape of the inhomogeneities, in the contracted notation of Sect. 1 and Sect. 4.1.1. The constraint matrices $\boldsymbol{M}^* = (\boldsymbol{L}^*)^{-1}$ in (4.2.10) represent the compliance and stiffness tensors of the cavity in $\boldsymbol{L}_0$, containing the inhomogeneity.

To find overall averages of the approximate stress and strain fields in the interacting inhomogeneities at finite concentrations c_r, we recall from (3.4.8) that the sum of their local volume averages in V must be equal to the applied overall magnitudes of $\boldsymbol{\varepsilon}^0$ or $\boldsymbol{\sigma}^0$ on ∂V. Therefore, the $\boldsymbol{\varepsilon}^0_\Omega$ or $\boldsymbol{\sigma}^0_\Omega$ are connected to $\boldsymbol{\varepsilon}^0$or $\boldsymbol{\sigma}^0$ by (Walpole 1966)

$$\left.\begin{aligned} \sum\nolimits_{r=1}^{n} c_r \boldsymbol{\varepsilon}_r = \sum\nolimits_{r=1}^{n} c_r \boldsymbol{T}_r \boldsymbol{\varepsilon}^0_\Omega = \boldsymbol{\varepsilon}^0 \;\Rightarrow\; \boldsymbol{\varepsilon}^0_\Omega = \Big(\sum\nolimits_{r=1}^{n} c_r \boldsymbol{T}_r\Big)^{-1} \boldsymbol{\varepsilon}^0 \\ \sum\nolimits_{r=1}^{n} c_r \boldsymbol{\sigma}_r = \sum\nolimits_{r=1}^{n} c_r \boldsymbol{W}_r \boldsymbol{\sigma}^0_\Omega = \boldsymbol{\sigma}^0 \;\Rightarrow\; \boldsymbol{\sigma}^0_\Omega = \Big(\sum\nolimits_{r=1}^{n} c_r \boldsymbol{W}_r\Big)^{-1} \boldsymbol{\sigma}^0 \end{aligned}\right\} \tag{6.3.1}$$

The phase field averages $\boldsymbol{\varepsilon}_r$ and $\boldsymbol{\sigma}_r$ are approximated by

$$\left.\begin{aligned} \boldsymbol{\varepsilon}_r &= \boldsymbol{T}_r \Big(\sum\nolimits_{s=1}^{n} c_s \boldsymbol{T}_s\Big)^{-1} \boldsymbol{\varepsilon}^0 = \boldsymbol{A}_r \boldsymbol{\varepsilon}^0 \\ \boldsymbol{\sigma}_r &= \boldsymbol{W}_r \Big(\sum\nolimits_{s=1}^{n} c_s \boldsymbol{W}_s\Big)^{-1} \boldsymbol{\sigma}^0 = \boldsymbol{B}_r \boldsymbol{\sigma}^0 \end{aligned}\right\} \tag{6.3.2}$$

Notice that the local field averages $\boldsymbol{\sigma}_r$, $\boldsymbol{\varepsilon}_r$ remain unchanged, while the $\boldsymbol{\varepsilon}^0_\Omega$ or $\boldsymbol{\sigma}^0_\Omega$ are adjusted by the matrices $\big(\sum_{r=1}^{n} c_r \boldsymbol{T}_r\big)^{-1}$ and $\big(\sum_{r=1}^{n} c_r \boldsymbol{W}_r\big)^{-1}$. Therefore, the latter may be regarded as concentration factors for a uniformly deformed comparison medium $\boldsymbol{L}_0$, with regard to the homogenized aggregate $\boldsymbol{L}$ of the same volume. Both become identities when $\boldsymbol{L}_0 = \boldsymbol{L}$.

Two equivalent forms of the above mechanical concentration factors follow from (4.2.14), one where the shape of the inhomogeneities is described by the constraint matrices $\boldsymbol{L}^*$or $\boldsymbol{M}^*$, and another that relies in that regard on the $\boldsymbol{P} = (\boldsymbol{L}^* + \boldsymbol{L}_0)^{-1}$or $\boldsymbol{Q} = (\boldsymbol{M}^* + \boldsymbol{M}_0)^{-1}$, defined in (4.2.9). In both cases, the following definitions show that $\big(\sum_{r=1}^{n} c_r \boldsymbol{A}_r\big) = \big(\sum_{r=1}^{n} c_r \boldsymbol{B}_r\big) = \boldsymbol{I}$.

$$\left.\begin{aligned} \boldsymbol{A}_r &= [\boldsymbol{I} + \boldsymbol{P}(\boldsymbol{L}_r - \boldsymbol{L}_0)]^{-1} \left[\sum_{s=1}^{n} c_s [\boldsymbol{I} + \boldsymbol{P}(\boldsymbol{L}_s - \boldsymbol{L}_0)]^{-1}\right]^{-1} \\ &= (\boldsymbol{L}^* + \boldsymbol{L}_r)^{-1} \left[\sum_{s=1}^{n} c_s (\boldsymbol{L}^* + \boldsymbol{L}_s)^{-1}\right]^{-1} \end{aligned}\right\} \tag{6.3.3}$$

$$\left.\begin{aligned} \boldsymbol{B}_r &= [\boldsymbol{I} + \boldsymbol{Q}(\boldsymbol{M}_r - \boldsymbol{M}_0)]^{-1}\left[\sum_{s=1}^{n} c_s[\boldsymbol{I} + \boldsymbol{Q}(\boldsymbol{M}_s - \boldsymbol{M}_0)]^{-1}\right]^{-1} \\ &= (\boldsymbol{M}^* + \boldsymbol{M}_r)^{-1}\left[\sum_{s=1}^{n} c_s(\boldsymbol{M}^* + \boldsymbol{M}_s)^{-1}\right]^{-1} \end{aligned}\right\} \tag{6.3.4}$$

Overall stiffness and compliance matrices of the aggregate can then be written according to (3.5.8), in terms of these concentration factors.

$$\left.\begin{aligned} \boldsymbol{L} &= \sum_{r=1}^{n} c_r \boldsymbol{L}_r \boldsymbol{A}_r = \sum_{r=1}^{n} c_r \boldsymbol{L}_r [\boldsymbol{I} + \boldsymbol{P}(\boldsymbol{L}_r - \boldsymbol{L}_0)]^{-1}\left[\sum_{s=1}^{n} c_s[\boldsymbol{I} + \boldsymbol{P}(\boldsymbol{L}_s - \boldsymbol{L}_0)]^{-1}\right]^{-1} \\ &= \sum_{r=1}^{n} c_r(\boldsymbol{L}^* + \boldsymbol{L}_r)\boldsymbol{A}_r - \boldsymbol{L}^* = \left[\sum_{r=1}^{n} c_r(\boldsymbol{L}^* + \boldsymbol{L}_r)^{-1}\right]^{-1} - \boldsymbol{L}^* = \boldsymbol{L}^{\mathrm{T}} \end{aligned}\right\} \tag{6.3.5}$$

$$\left.\begin{aligned} \boldsymbol{M} &= \sum_{r=1}^{n} c_r \boldsymbol{M}_r \boldsymbol{B}_r = \sum_{r=1}^{n} c_r \boldsymbol{M}_r [\boldsymbol{I} + \boldsymbol{Q}(\boldsymbol{M}_r - \boldsymbol{M}_0)]^{-1}\left[\sum_{s=1}^{n} c_s[\boldsymbol{I} + \boldsymbol{Q}(\boldsymbol{M}_s - \boldsymbol{M}_0)]^{-1}\right]^{-1} \\ &= \sum_{r=1}^{n} c_r(\boldsymbol{M}^* + \boldsymbol{M}_r)\boldsymbol{B}_r - \boldsymbol{M}^* = \left[\sum_{r=1}^{n} c_r(\boldsymbol{M}^* + \boldsymbol{M}_r)^{-1}\right]^{-1} - \boldsymbol{M}^* = \boldsymbol{M}^{\mathrm{T}} \end{aligned}\right\} \tag{6.3.6}$$

since $\boldsymbol{L}^* = (\boldsymbol{L}^*)^{\mathrm{T}}$ and $\boldsymbol{M}^* = (\boldsymbol{M}^*)^{\mathrm{T}}$.

Notice that the comparison media that yield the H-S bounds, and other apparently acceptable choices of $\boldsymbol{L}_0$, $\boldsymbol{M}_0$ in (6.3.5) or (6.3.6), may not be readily identified with known materials. Instead, in agreement with the local field form used in (6.2.1), the concentration factors evaluated using such $\boldsymbol{L}_0$, $\boldsymbol{M}_0$ should be regarded as averages of elastic fields that may exist in phase subvolumes of any shape and alignment, represented by a distribution of similar ellipsoidal inhomogeneities. Only the self-consistent and Mori-Tanaka estimates in Sect. 7 specify the comparison media as $\boldsymbol{L}_0$ and $\boldsymbol{L}_1$, respectively.

Diagonal symmetry of the overall stiffness and compliance matrices and of the underlying fourth-order tensors requires identical $\boldsymbol{L}^*$ and $\boldsymbol{M}^* = (\boldsymbol{L}^*)^{-1}$, or $\boldsymbol{P}$, $\boldsymbol{Q}$ tensors for all $r = 1, 2, \ldots n$, implying the same ellipsoidal shape and alignment, but allowing for different size. Another form of the above stiffness and compliance estimates, often useful in matrix-based systems, can be derived from the above as

$$\left.\begin{aligned} &\sum_{r=1}^{n} c_r \boldsymbol{A}_r = \boldsymbol{I} \Rightarrow c_1 \boldsymbol{A}_1 = \boldsymbol{I} - \sum_{r=2}^{n} c_r \boldsymbol{A}_r \quad c_1 \boldsymbol{B}_1 = \boldsymbol{I} - \sum_{r=2}^{n} c_r \boldsymbol{B}_r \\ &\boldsymbol{L} = \boldsymbol{L}_1 + \sum_{r=2}^{n} c_r(\boldsymbol{L}_r - \boldsymbol{L}_1)\boldsymbol{A}_r \quad \boldsymbol{M} = \boldsymbol{M}_1 + \sum_{r=2}^{n} c_r(\boldsymbol{M}_r - \boldsymbol{M}_1)\boldsymbol{B}_r \end{aligned}\right\} \tag{6.3.7}$$

That separates the matrix phase and requires identical $\boldsymbol{L}^*$ and $\boldsymbol{M}^* = (\boldsymbol{L}^*)^{-1}$, or $\boldsymbol{P}$, $\boldsymbol{Q}$ tensors, only for the inhomogeneities $r = 2,\ 3,\ \ldots\ n$.

In composites reinforced by randomly orientated anisotropic inhomogeneities, such as discontinuous carbon fibers, the overall $\boldsymbol{L}$ in (6.3.5) is often represented by the orientation average $\{(\boldsymbol{L}^* + \boldsymbol{L}_r)^{-1}\}$, denoted by the curly brackets; c. f., Sect. 2.2.10. Systems containing inhomogeneities of different shape, orientation and spatial distribution may be analyzed using the double inclusion model in Sect. 7.4.

Consistency $\boldsymbol{LM} = \boldsymbol{I}$ of the results can be established when $\boldsymbol{L}^*\boldsymbol{M}^* = \boldsymbol{I}$ and $\boldsymbol{L}_r\boldsymbol{M}_r = \boldsymbol{I}$. The last terms in (6.3.5) and (6.3.6) provide the equalities

$$\left.\begin{aligned}(\boldsymbol{L} + \boldsymbol{L}^*)^{-1} &= \sum_{r=1}^{n} c_r(\boldsymbol{L}^* + \boldsymbol{L}_r)^{-1} = \sum_{r=1}^{n} c_r \boldsymbol{P}_r \\ (\boldsymbol{M} + \boldsymbol{M}^*)^{-1} &= \sum_{r=1}^{n} c_r(\boldsymbol{M}^* + \boldsymbol{M}_r)^{-1} = \sum_{r=1}^{n} c_r \boldsymbol{Q}_r\end{aligned}\right\} \tag{6.3.8}$$

where $\boldsymbol{P}_r$ and $\boldsymbol{Q}_r$ are introduced for convenience. Since $\boldsymbol{L}^*\boldsymbol{M}^* = \boldsymbol{I}$, one can show that

$$(\boldsymbol{P}_r{}^{-1} - \boldsymbol{L}_r)(\boldsymbol{Q}_r{}^{-1} - \boldsymbol{M}_r) = \boldsymbol{P}_r\boldsymbol{L}_r + \boldsymbol{M}_r\boldsymbol{Q}_r = \boldsymbol{I} \tag{6.3.9}$$

and that

$$\left.\begin{aligned}\sum_{r=1}^{n} c_r \boldsymbol{P}_r\boldsymbol{L}_r &= \sum_{r=1}^{n} c_r(\boldsymbol{L}^* + \boldsymbol{L}_r)^{-1}\boldsymbol{L}_r + \sum_{r=1}^{n} c_r(\boldsymbol{L}^* + \boldsymbol{L}_r)^{-1}\boldsymbol{L}^* \\ &\quad - \sum_{r=1}^{n} c_r(\boldsymbol{L}^* + \boldsymbol{L}_r)^{-1}\boldsymbol{L}^* \\ &= \boldsymbol{I} - \left(\sum_{r=1}^{n} c_r \boldsymbol{P}_r\right)\boldsymbol{L}^* = \boldsymbol{I} - (\boldsymbol{L}^* + \boldsymbol{L})^{-1}\boldsymbol{L}^*\end{aligned}\right\} \tag{6.3.10}$$

A similar derivation yields

$$\sum_{r=1}^{n} c_r \boldsymbol{M}_r\boldsymbol{Q}_r = \boldsymbol{I} - \boldsymbol{M}^*\sum_{r=1}^{n} c_r \boldsymbol{Q}_r = \boldsymbol{I} - \boldsymbol{M}^*(\boldsymbol{M} + \boldsymbol{M}^*) \tag{6.3.11}$$

Finally, from (6.3.9)

$$\left.\begin{aligned}&(\boldsymbol{L}^* + \boldsymbol{L})^{-1}\boldsymbol{L}^* + \boldsymbol{M}^*(\boldsymbol{M} + \boldsymbol{M}^*)^{-1} = \boldsymbol{I} \\ &\boldsymbol{L}^*(\boldsymbol{M} + \boldsymbol{M}^*) + (\boldsymbol{L}^* + \boldsymbol{L})\boldsymbol{M}^* = (\boldsymbol{L}^* + \boldsymbol{L})(\boldsymbol{M} + \boldsymbol{M}^*) \\ &\boldsymbol{LM} = \boldsymbol{L}^*\boldsymbol{M}^* = \boldsymbol{I}\end{aligned}\right\} \tag{6.3.12}$$

QED.

Proofs of diagonal symmetry and consistency of the overall stiffness and compliance derived in (6.3.5) and (6.3.6) represent two of the admissibility conditions for average field approximations of overall properties. The third condition connects the moduli of admissible comparison media to those of the phases, such that overall moduli are bracketed by the Hashin-Shtrikman bounds (6.2.16) or (6.2.24). Additional conditions may be imposed by tighter bounds in Sect. 6.4.

Any of the eight material symmetries discussed in Chap. 2, and defined in the same Cartesian coordinates, can represent the phase moduli in $\boldsymbol{L}_r$ or $\boldsymbol{M}_r$. Since the coefficients of $\boldsymbol{L}_0$ are related to those in $\boldsymbol{L}_r$, material symmetry of the comparison medium $\boldsymbol{L}_0$ may not be lower than that of the $\boldsymbol{L}_r$ which has the lowest material symmetry, or highest anisotropy. However, material symmetries of the predicted overall $\boldsymbol{L}$ or $\boldsymbol{M}$ are determined by the $(\boldsymbol{L}^* + \boldsymbol{L}_r) = \boldsymbol{P}_r$ matrices appearing in (6.3.5). Therefore, the predictions may or may not correspond to the actual material symmetry of a given heterogeneous aggregate, which depends, in part, on the spatial distribution of the constituent phases in the representative volume. If the overall material symmetry is known beforehand, it may be incorporated, to some extent, in the formulation of the double inclusion model in Sect. 7.4.

The relative effect of different reinforcement shapes has not been extensively investigated. Wu (1966) had shown that reinforcement by platelets has the greatest effect on overall moduli of two-phase systems estimated by the self-consistent method, at $\boldsymbol{L}_0 = \boldsymbol{L}$. Spherical and needle-like randomly orientated reinforcements appeared to have a lesser effect. Walpole (1980) found a range of values of the dielectric constant, estimated by the self-consistent and differential schemes, for inhomogeneities of any shape. Most of the specific results in the technical literature refer to spherical of aligned fiber reinforcements, which are of interest in many applications.

At higher volume fractions, interactions between adjacent inhomogeneities disturb the uniform local fields that may prevail there at low and medium concentrations. However, finite element solutions, obtained with the periodic hexagonal model of a two-phase fibrous system, e. g., by Teply and Dvorak (1988), indicate that the disturbances start to become significant only at high fiber volume fractions (50–60%), at least in systems with large contrast between fiber and matrix moduli, such as glass-epoxy. Therefore, local field averages derived using the mechanical concentration factors (6.3.3) and (6.3.4) should provide good approximations of field averages in individual ellipsoidal inhomogeneities, at low to moderate volume concentrations. Of course, these fields are never uniform in the matrix, hence matrix concentration factors deliver only volume averages, related to those in the inhomogeneities by the connections $\sum_{r=1}^{n} c_r \boldsymbol{A}_r = \boldsymbol{I}$, $\sum_{r=1}^{n} c_r \boldsymbol{B}_r = \boldsymbol{I}$ in (3.5.6).

In actual evaluations of the upper and lower bounds $\boldsymbol{L}^{(+)}$, $\boldsymbol{L}^{(-)}$ and $\boldsymbol{M}^{(+)}$, $\boldsymbol{M}^{(-)}$ on actual stiffness and compliance $\boldsymbol{L}^{(a)}$ and $M^{(a)}$ of a heterogeneous aggregate from (6.3.5) or (6.3.6), one first selects the coefficients of $\boldsymbol{L}_0$ or $\boldsymbol{M}_0 = \boldsymbol{L}_0^{-1}$ according to each of the theorems (6.2.16) or (6.2.24), and then proceeds to evaluate the $\boldsymbol{P}$ (or $\boldsymbol{Q}$) tensors shown in Sect. 4.6 for the selected shape of the inhomogeneities

in $\boldsymbol{L}_0$. Choosing any $\boldsymbol{L}_0$ [or $\boldsymbol{M}_0$], which renders both $(\boldsymbol{L}_0^{(+)} - \boldsymbol{L}_r)$ and $(\boldsymbol{L}_r - \boldsymbol{L}_0^{(-)})$ [or both $(\boldsymbol{M}_0^{(+)} - \boldsymbol{M}_r)$ and $(\boldsymbol{M}_r - \boldsymbol{M}_0^{(-)})$] positive semi-definite, yields an admissible estimate of overall $\boldsymbol{L}$ or $\boldsymbol{M}$, in the H-S sense. Exchanges of phase moduli produce different sets of upper and lower bounds on elastic moduli of a particular composite material. Most restrictive bounds are identified with the lowest of the upper bounds and highest of the lower bounds, without regard to the underlying method.

6.3.2 H-S Bounds on Overall Elastic Moduli of Multiphase Systems

The bounding theorems (6.2.16) or (6.2.24) and equations (6.3.5) or (6.3.6) imply that stiffness and compliance bounds for multiphase media can be written as

$$\left.\begin{aligned} \boldsymbol{L}^{(\pm)} &= \sum_{r=1}^{n} c_r \boldsymbol{L}_r \boldsymbol{A}_r = \sum_{r=1}^{n} c_r \boldsymbol{L}_r [\boldsymbol{I} - \boldsymbol{P}(\boldsymbol{L}_0^{(\pm)} - \boldsymbol{L}_r)]^{-1} \\ &\quad \times \left[\sum_{s=1}^{n} c_s [\boldsymbol{I} - \boldsymbol{P}(\boldsymbol{L}_0^{(\pm)} - \boldsymbol{L}_s)]^{-1} \right]^{-1} \\ \boldsymbol{M}^{(\pm)} &= \sum_{r=1}^{n} c_r \boldsymbol{M}_r \boldsymbol{B}_r = \sum_{r=1}^{n} c_r \boldsymbol{M}_r [\boldsymbol{I} - \boldsymbol{Q}(\boldsymbol{M}_0^{(\pm)} - \boldsymbol{M}_r)]^{-1} \\ &\quad \times \left[\sum_{s=1}^{n} c_s [\boldsymbol{I} - \boldsymbol{Q}(\boldsymbol{M}_0^{(\pm)} - \boldsymbol{M}_s)]^{-1} \right]^{-1} \end{aligned}\right\} \tag{6.3.13}$$

Notice that the coefficients of the $\boldsymbol{L}_0^{(\pm)}$ or $\boldsymbol{M}_0^{(\pm)}$ matrices defining the upper or lower bounds are compared to those in each $\boldsymbol{L}_r$ or $\boldsymbol{M}_r$ present in the system, not necessarily to those in a single one. For example, certain carbon fibers have low transverse but high longitudinal tension and shear moduli relative to those of an epoxy matrix, hence elastic moduli or coefficients $L^r_{\alpha\beta}$, $M^r_{\alpha\beta}$ of each phase appear in both $\boldsymbol{L}_0^{(+)}$ and $\boldsymbol{L}_0^{(-)}$. Of course, if one of the phases, such as the matrix $\boldsymbol{L}_1$ is relatively compliant, so that $(\boldsymbol{L}_r - \boldsymbol{L}_1)$ is positive semi-definite for all $r = 2, 3, \ldots n$, then $\boldsymbol{L}_0 = \boldsymbol{L}_1$ yields a lower bound.

Among specific results useful in applications are bounds on the overall bulk and shear moduli K and G of a statistically homogeneous and isotropic composite, consisting of any number of perfectly bonded isotropic and homogeneous phases $r = 1, 2, \ldots n$. Those were first derived by Hashin and Shtrikman (1963), and for spherical inhomogeneities with a wider selection of phase moduli by Walpole (1966), in the form

$$\left.\begin{aligned}\left[\sum_{r=1}^{n} c_r (K_L^* + K_r)^{-1}\right]^{-1} - K_L^* \le K \le \left[\sum_{r=1}^{n} c_r (K_U^* + K_r)^{-1}\right]^{-1} - K_U^* \\ \left[\sum_{r=1}^{n} c_r (G_L^* + G_r)^{-1}\right]^{-1} - G_L^* \le G \le \left[\sum_{r=1}^{n} c_r (G_U^* + G_r)^{-1}\right]^{-1} - G_U^*\end{aligned}\right\} \tag{6.3.14}$$

where

$$\left.\begin{aligned} K_L^* = 4G_L/3 \qquad & K_U^* = 4G_U/3 \\ G_L^* = \frac{3}{2}\left(\frac{1}{G_L} + \frac{10}{9K_L + 8G_L}\right)^{-1} \qquad & G_U^* = \frac{3}{2}\left(\frac{1}{G_U} + \frac{10}{9K_U + 8G_U}\right)^{-1}\end{aligned}\right\} \tag{6.3.15}$$

and the K_L, G_L or K_U, G_U are selected as the lowest and highest moduli among all phases, such that for any phase r, $K_L \le K_r \le K_U$ and $G_L \le G_r \le G_U$. For multiphase fiber or hybrid composites, bounds on k, m and p can be found in Hashin (1965) and Walpole (1969).

Hill (1963a) shows that the overall bulk and shear moduli increase [decrease] when at least one of the two moduli is raised [reduced] in one or both phases. More broadly, the overall strain energy of a heterogeneous elastic continuum subjected to a fixed overall strain is a monotonic function of the phase moduli.

6.3.3 H-S Bounds on Elastic Moduli of Two-Phase Systems

Overall stiffness of a two-phase, matrix based aggregate, $r = 1, 2$, in (6.3.7) is

$$\boldsymbol{L} = \boldsymbol{L}_1 + c_2(\boldsymbol{L}_2 - \boldsymbol{L}_1)\boldsymbol{A}_2 \tag{6.3.16}$$

where the coefficients of $\boldsymbol{L}_1$ depend on elastic moduli of the matrix. $\boldsymbol{L}_2$ is the elastic stiffness of the reinforcement phase $r = 2$. All reinforcement subvolumes have the same shape and alignment, described by a single tensor $\boldsymbol{P}$, evaluated using the elastic moduli of the selected comparison medium $\boldsymbol{L}_0$. From (6.3.3)

$$\left.\begin{aligned}\boldsymbol{A}_1{}^{-1} = c_1\boldsymbol{I} + c_2[\boldsymbol{I} + \boldsymbol{P}(\boldsymbol{L}_2 - \boldsymbol{L}_0)]^{-1}[\boldsymbol{I} + \boldsymbol{P}(\boldsymbol{L}_1 - \boldsymbol{L}_0)] \\ \boldsymbol{A}_2{}^{-1} = c_2\boldsymbol{I} + c_1[\boldsymbol{I} + \boldsymbol{P}(\boldsymbol{L}_1 - \boldsymbol{L}_0)]^{-1}[\boldsymbol{I} + \boldsymbol{P}(\boldsymbol{L}_2 - \boldsymbol{L}_0)]\end{aligned}\right\} \tag{6.3.17}$$

If the matrix is relatively compliant, such that $(\boldsymbol{L}_1 - \boldsymbol{L}_2)$ is negative semi-definite, then the comparison media for evaluation of the lower and upper bounds on

the actual overall stiffness $\boldsymbol{L}^{(a)}$ are selected as $\boldsymbol{L}_0^{(-)} = \boldsymbol{L}_1$, $\boldsymbol{L}_0^{(+)} = \boldsymbol{L}_2$. The corresponding pair of bounds is

$$\left.\begin{aligned}
\boldsymbol{L}^{(-)} &= \boldsymbol{L}_1 + c_2[(\boldsymbol{L}_2 - \boldsymbol{L}_1)^{-1} + c_1\boldsymbol{P}]^{-1} = (\boldsymbol{L}^{(-)})^{\mathrm{T}} \\
\boldsymbol{L}^{(+)} &= \boldsymbol{L}_1 + c_2(\boldsymbol{L}_2 - \boldsymbol{L}_1)\{c_2\boldsymbol{I} + c_1[\boldsymbol{I} - \boldsymbol{P}(\boldsymbol{L}_2 - \boldsymbol{L}_1)]^{-1}\} \\
&= \boldsymbol{L}_1 + c_2\Big[c_2(\boldsymbol{L}_2 - \boldsymbol{L}_1)^{-1} + c_1\{(\boldsymbol{L}_2 - \boldsymbol{L}_1)[\boldsymbol{I} - \boldsymbol{P}(\boldsymbol{L}_2 - \boldsymbol{L}_1)]\}^{-1}\Big]^{-1} \\
&= (\boldsymbol{L}^{(+)})^{\mathrm{T}}
\end{aligned}\right\} \tag{6.3.18}$$

When the reinforcement is very stiff, the selection $\boldsymbol{L}_0^{(-)} = \boldsymbol{L}_1$, $\boldsymbol{L}_0^{(+)} \to \infty$ provides the lower bound

$$\boldsymbol{L}^{(-)} = \boldsymbol{L}_1 + c_2(c_1\boldsymbol{P})^{-1} = (\boldsymbol{L}^{(-)})^{\mathrm{T}} \tag{6.3.19}$$

Next, for an aggregate with a relatively stiff matrix and compliant reinforcement, such that $(\boldsymbol{L}_1 - \boldsymbol{L}_2)$ is positive semi-definite, the upper and lower bounds on $\boldsymbol{L}^{(a)}$ are evaluated using $\boldsymbol{L}_0^{(-)} = \boldsymbol{L}_2$, $\boldsymbol{L}_0^{(+)} = \boldsymbol{L}_1$. The above bounds exchange their positions

$$\left.\begin{aligned}
\boldsymbol{L}^{(-)} = \boldsymbol{L}_1 + c_2\Big[c_2(\boldsymbol{L}_2 - \boldsymbol{L}_1)^{-1} + c_1\{(\boldsymbol{L}_2 - \boldsymbol{L}_1)[\boldsymbol{I} - \boldsymbol{P}(\boldsymbol{L}_2 - \boldsymbol{L}_1)]\}^{-1}\Big]^{-1} = (\boldsymbol{L}^{(-)})^{\mathrm{T}} \\
\boldsymbol{L}^{(+)} = \boldsymbol{L}_1 + c_2[(\boldsymbol{L}_2 - \boldsymbol{L}_1)^{-1} + c_1\boldsymbol{P}]^{-1} = (\boldsymbol{L}^{(+)})^{\mathrm{T}}
\end{aligned}\right\} \tag{6.3.20}$$

For a porous medium, the upper bound on overall stiffness is found by letting $\boldsymbol{L}_0 = \boldsymbol{L}_1$, $\boldsymbol{L}_2 \to \boldsymbol{0}$

$$\boldsymbol{L}^{(+)} = \boldsymbol{L}_1 + c_2(c_1\boldsymbol{P} - \boldsymbol{M}_1)^{-1} = (\boldsymbol{L}^{(+)})^{\mathrm{T}} \tag{6.3.21}$$

Bounds on the bulk and shear moduli of a statistically homogeneous two-phase composite, consisting of isotropic and perfectly bonded phases $r = 1, 2$, of any micro-geometry, were first derived by Hashin and Shtrikman (1963), for the 'well-ordered' phase moduli satisfying $(G_1 - G_2)(K_1 - K_2) \geq 0$. Walpole (1966) derived a more inclusive result, allowing for $(G_1 - G_2)(K_1 - K_2) \leq 0$. He also pointed out that the results coincide with those obtained from (6.3.16) with the $\boldsymbol{P}$ tensor evaluated for a spherical inclusion in an appropriate comparison medium.

The general form of the bounds on the bulk modulus is

$$\frac{c_1}{1 + c_2(K_1 - K_2)(K_2 + K_L^*)^{-1}} \leq \frac{K - K_2}{K_1 - K_2} \leq \frac{c_1}{1 + c_2(K_1 - K_2)(K_2 + K_U^*)^{-1}} \tag{6.3.22}$$

The shear modulus bounds are

$$\frac{c_1}{1+c_2(G_1-G_2)(G_2+G_L^*)^{-1}} \le \frac{G-G_2}{G_1-G_2} \le \frac{c_1}{1+c_2(G_1-G_2)(G_2+G_U^*)^{-1}} \tag{6.3.23}$$

The inequalities hold when $K_1 - K_2 > 0$ and $G_1 - G_2 > 0$, and need to be reversed when the signs change. For $(G_1 - G_2)(K_1 - K_2) \ge 0$, one selects $K_L^* = 4G_2/3 \le K_U^* = 4G_1/3$, and

$$G_L^* = \frac{3}{2}\left(\frac{1}{G_1} + \frac{10}{9K_1+8G_1}\right)^{-1} \quad G_U^* = \frac{3}{2}\left(\frac{1}{G_2} + \frac{10}{9K_2+8G_2}\right)^{-1} \tag{6.3.24}$$

However, in the 'not well-ordered' case, when $(K_1-K_2) < 0$ and $(G_1-G_2) > 0$, the above expressions are replaced by $K_L^* = 4G_2/3 \le K_U^* = 4G_1/3$ and

$$G_L^* = \frac{3}{2}\left(\frac{1}{G_2} + \frac{10}{9K_1+8G_2}\right)^{-1} \quad G_U^* = \frac{3}{2}\left(\frac{1}{G_1} + \frac{10}{9K_2+8G_1}\right)^{-1} \tag{6.3.25}$$

Notice that differences between the respective upper and lower bounds are limited to those between the star-marked quantities. The bulk modulus bounds can be reduced to the exact solution for a composite sphere subjected to surface tractions or displacements creating an overall isotropic stress or strain.

Of interest in applications are also the following simple formulae by Walpole (1985c), for bounds on overall moduli of two-phase isotropic composites. The selected comparison medium is also isotropic, with elastic moduli K_0, G_0. The result agrees again with (6.3.16) when $\boldsymbol{P}$ is evaluated for a spherical inclusion in $\boldsymbol{L}_0$.

$$\left.\begin{aligned} K &= c_1K_1 + c_2K_2 - c_1c_2(K_1-K_2)^2(c_1K_2 + c_2K_1 + 4G_0/3)^{-1} \\ G &= c_1G_1 + c_2G_2 - c_1c_2(G_1-G_2)^2(c_1G_2 + c_2G_1 + 3G^*/2)^{-1} \\ G^* &= [1/G_0 + 10/(9K_0+8G_0)]^{-1} \end{aligned}\right\} \tag{6.3.26}$$

It can be verified that the upper [lower] bound on K is obtained by selecting G_0 as the highest [lowest] phase G_r in the system. The upper [lower] bound on G follows by using the larger [smaller] of K_1, K_2, and also of G_1, G_2. Admissible estimates of K and G can be obtained using any other values of K_0, G_0 bracketed by these selections. For example, if both phase and overall K and G are known from experimental measurements on a particular material system with a known phase volume fraction, then (6.3.26) can be solved for the moduli K_0, G_0. This may prove useful in extrapolating measured values of overall moduli to the same system with different phase volume fractions.

Bounds on elastic moduli of two-phase aligned fiber composites with all interfaces aligned parallel to the longitudinal axis of rotational symmetry of the transversely isotropic aggregate, are presented together with the composite element assemblage bounds on transverse shear modulus in Sect. 6.4.1. They can also be found using the following expressions derived by Walpole (1985c). For a lower [upper] bound on overall moduli, the comparison medium moduli k_0, m_0 and p_0 are selected as the lowest [highest] values among the six phase moduli k_r, m_r and p_r of the two phases, $r = 1,\ 2$.

$$\left.\begin{aligned} k &= c_1k_1 + c_2k_2 - c_1c_2(k_1 - k_2)^2(c_1k_2 + c_2k_1 + m_0)^{-1} \\ m &= c_1m_1 + c_2m_2 - c_1c_2(m_1 - m_2)^2[c_1m_2 + c_2m_1 + m_0k_0/(k_0{+}2m_0)]^{-1} \\ p &= c_1p_1 + c_2p_2 - c_1c_2(p_1 - p_2)^2(c_1p_2 + c_2p_1 + p_0)^{-1} \end{aligned}\right\} \tag{6.3.27}$$

These bounds coincide with those derived from (6.3.16) with the $\boldsymbol{P}$ matrix (4.6.6) for a circular cylindrical inclusion ($\rho = 1$).

For small differences between phase moduli, the present bounds differ only by a third-order infinitesimal, in contrast to the second-order differential between the Voigt and Reuss bounds (6.1.4). Large contrast between the phase moduli may elevate the distance between the bounds, especially at intermediate volume concentrations. At very low or very high volume fractions, the upper and lower bounds converge toward the corresponding modulus of the dominant phase.

6.4 Composite Element Assemblage Bounds

The second method mentioned in the introduction uses exactly solvable microstructural elements and minimum energy theorems in evaluation of overall moduli of the entire representative volume. Hashin (1962, 1972) and Hashin and Rosen (1964) implemented this idea with the composite sphere (CSA) and composite cylinder assemblage (CCA) models, Fig. 6.1, that represent two-phase isotropic particulate mixtures or aligned fiber composites. In both elements, matrix stiffness is denoted by $\boldsymbol{L}_1$ and reinforcement stiffness by $\boldsymbol{L}_2$. All composite elements have the same prescribed phase volume fraction, but different diameters, including those which tend towards zero. Centers of composite spheres in the CSA may not be located in the plane of the drawing.

A single element is subjected to surface displacements or tractions which would generate uniform strain or stress fields in a homogeneous sphere or cylinder. The same boundary conditions are applied to the aggregate and to all elements. Therefore, the resulting fields are kinematically or statically admissible and similar in all elements comprising the entire volume. Bounds on individual moduli are obtained by direct substitution into the energy theorems in Sect. 3.8, of the exact local fields generated by the corresponding boundary conditions in a composite sphere

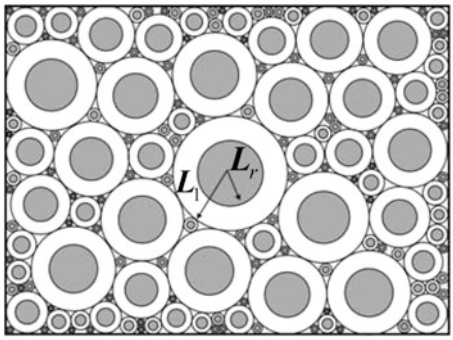

Fig. 6.1 Composite sphere (CSA) and composite cylinder (CCA) assemblage models

or cylinder element. Appropriate traction or displacement boundary conditions both yield identical overall elastic bulk moduli K of the CSA, and the axisymmetric k, l, n and longitudinal shear moduli p of the CCA. However, application of a uniform transverse shear stress or strain to either model yields distinct transverse shear moduli G and m, which are identified with the respective bounds.

Bounds on the shear modulus of the composite sphere element are rather complex functions of phase moduli; they can be found in Hashin (1962). Bounds on the transverse shear modulus of fiber composites are described next. As pointed out by Milton (2002), the assemblage models could be realized as actual composite materials, by replacing the smallest elements with a homogeneous or homogenized material, which would have only a small influence on the CSA/CCA overall moduli.

6.4.1 *Bounds on Elastic Moduli of Aligned Fiber Composites*

Original derivations of bounds on the five elastic moduli of a fiber composite made of two transversely isotropic phases were obtained by Hashin (1965, 1979), Hashin and Rosen (1964) and Hill (1964). Only three of the five overall moduli, denoted by k, m, p in (2.3.3), are independent in a fiber system, as shown by

$$\frac{k-k_1}{l-l_1}=\frac{k-k_2}{l-l_2}=\frac{l-c_1l_1-c_2l_2}{n-c_1n_1-c_2n_2}=\frac{k_1-k_2}{l_1-l_2} \qquad [3.9.4]$$

where $r = 1,\ 2$ denote the phases.

The three moduli in (3.9.4), associated with axisymmetric deformation of the aligned fiber composite, follow from an exact elastic solution for a single circular cylinder composite element shown in Fig. 6.1. An upper or lower H-S bound on k provides upper or lower bounds on the moduli l and n of the same system. Hill (1964) derived the bounds on k as

$$\frac{c_1k_1(k_2+m_1)+c_2k_2(k_1+m_1)}{c_1(k_2+m_1)+c_2(k_1+m_1)} \le k \le \frac{c_1k_1(k_2+m_2)+c_2k_2(k_1+m_2)}{c_1(k_2+m_2)+c_2(k_1+m_2)} \tag{6.4.1}$$

The phase moduli satisfy $m_1 \le m_2$. The shell has the shear modulus m_1 or m_2. The remaining moduli l and n are related to k by the universal connections.

According to (2.3.5), the longitudinal Young's modulus $E_A = E_{11} = n - l^2/k$ and the related Poisson's ratio $\nu_A = \nu_{12} = l/(2k)$, hence the upper and lower bounds on these two moduli are

$$\frac{c_1c_2}{c_1/k_2+c_2/k_1+1/m_1} \le \frac{E_A - c_1E_1 - c_2E_2}{4(\nu_1-\nu_2)^2} \le \frac{c_1c_2}{c_1/k_2+c_2/k_1+1/m_2} \tag{6.4.2}$$

and

$$\frac{c_1c_2}{c_1/k_2+c_2/k_1+1/m_2} \le \frac{\nu_A - c_1\nu_1 - c_2\nu_2}{(\nu_1-\nu_2)(1/k_2-1/k_1)} \le \frac{c_1c_2}{c_1/k_2+c_2/k_1+1/m_1} \tag{6.4.3}$$

where the E_i and ν_i, $i = 1, 2$, denote the $E_A^{(i)}$ and $\nu_A^{(i)}$ moduli of the phases, and $m_1 \le m_2$. Since the difference between the bounds on E_A is proportional to $(\nu_1-\nu_2)^2$, which is often very small, *this and only this modulus can be approximated by the 'rule of mixtures' expression* $E_A \doteq c_1E_1+c_2E_2 = E_1+c_2(E_2-E_1)$.

The longitudinal shear modulus p is the same for arbitrary geometry of the phases in the transverse plane and for the cylinder assemblage and hexagonal array models (Hashin 1965, 1979; Hashin and Rosen 1964). Assuming that $p_1 < p_2$, the results are

$$\frac{c_2}{1/(p_2-p_1)+c_1/(2p_1)} + p_1 \le p \le p_2 + \frac{c_1}{1/(p_1-p_2)+c_2/(2p_2)} \tag{6.4.4}$$

Each of the above upper [or lower] bounds represents an exact overall modulus of a composite cylinder element, or of a continuous composite cylinder assemblage, with the 'stiffer' phase placed in the shell (as $r = 1$) or fiber (as $r = 2$).

As already mentioned, a composite cylinder does not exhibit a unique transverse shear modulus. Therefore, derivation of *upper and lower bounds on the transverse shear modulus m* using the CCA model requires two different solutions. The upper bound is established by applying surface displacements, consistent with a state of uniform transverse shear strain, and by finding the overall shear stress average (3.4.2) from the resulting surface tractions. The lower bound requires application of surface tractions derived from a uniform transverse shear stress, which is then related to the average shear strain provided by (3.4.5) and the surface displacements. Both solutions are obtained under generalized plane strain that admits uniform normal strain and zero overall normal stress in the longitudinal direction. Spatial continuity of the CCA model guarantees that these solutions hold in the entire representative volume.

The CCA bounds were first derived by Hashin and Rosen (1964) and later expressed in closed form by Behrens (1971) and Hashin (1979). The closest bounds follow by combining the CCA bounds with any tighter H-S bounds.

For $m_2 > m_1,\ k_2 > k_1$

$$m \geq m^{(-)} = m_1 + \frac{c_2}{\dfrac{1}{(m_2 - m_1)} + \dfrac{c_1(k_1 + 2m_1)}{2m_1(k_1 + m_1)}} \tag{6.4.5}$$

$$m \leq m^{(+)} = m_1 \left[1 + \frac{c_2(1 + \beta_1)}{\rho - c_2[1 + 3c_1^2\beta_1^2(1 + c_2^3\alpha)^{-1}]} \right] \tag{6.4.6}$$

where

$$\left.\begin{array}{c} \alpha = (\beta_1 - \gamma\beta_2)/(1 + \gamma\beta_2) \qquad \gamma = m_2/m_1 \qquad \rho = (\gamma + \beta_1)/(\gamma - 1) \\ \beta_1 = k_1/(k_1 + 2m_1) \qquad \beta_2 = k_2/(k_2 + 2m_2) \end{array}\right\} \tag{6.4.7}$$

For $m_2 < m_1,\ k_2 < k_1$

$$m \geq m^{(-)} = m_1 \left[1 + \frac{c_2(1 + \beta_1)}{\rho - c_2[1 + 3c_1^2\beta_1^2(c_2^3\alpha - \beta_1)^{-1}]} \right] \tag{6.4.8}$$

$$m \leq m^{(+)} = m_1 + \frac{c_2}{\dfrac{1}{(m_2 - m_1)} + \dfrac{c_1(k_1 + 2m_1)}{2m_1(k_1 + m_1)}} \tag{6.4.9}$$

For arbitrary geometry of phase crossections, and for phase moduli arranged as $m_2 > m_1, k_2 > k_1$, the transverse shear modulus m is bracketed by

$$\frac{c_2}{\dfrac{1}{(m_2 - m_1)} + \dfrac{c_1(k_1 + 2m_1)}{2m_1(k_1 + m_1)}} + m_1 \leq m \leq m_2 + \frac{c_1}{\dfrac{1}{(m_1 - m_2)} + \dfrac{c_2(k_2 + 2m_2)}{2m_2(k_2 + m_2)}} \tag{6.4.10}$$

This upper bound is higher than that given by the CCA model, but the lower bound is also higher than that generated by the CCA model. Hashin (1979) indicates that composite cylinder assemblage models give a lower value of both $m^{(-)}$ and $m^{(+)}$ for $m_2 > m_1$ and $k_2 > k_1$. When these inequalities are reversed, the arbitrary phase geometry gives a lower $m^{(+)}$, but no conclusion is drawn for $m^{(-)}$.

The results can also be applied to porous media, for $k_1 \to 0,\ m_1 \to 0$, where they only offer an upper bound, and to solids with one very stiff or rigid phase, where only the lower bound has a finite magnitude. With the possible exception of the transverse shear modulus m, the bounds on all other moduli are the best possible in terms of phase volume fractions for any transverse geometry.

Bounds on the off-diagonal moduli in the stiffness matrix follow from (2.3.5), where one selects among all available bounds on k and m those that produce the highest upper bound and lowest lower bound on each off-diagonal coefficient. Of interest are bounds on the transverse Young's modulus $E_{22} = E_{33} = E_T$ and Poisson's ratio $\nu_{23} = \nu_{32} = \nu_T$ for a fibrous material of arbitrary phase geometry. Since an aligned fiber composite is transversely isotropic, these must be connected by (2.3.4). Upper and lower bounds on the remaining Hill's moduli n and l follow from the above bounds on k, E_A and ν_A, as

$$E_A^{(-)} + 4k^{(-)}(\nu_A^{(-)})^2 \le n \le E_A^{(+)} + 4k^{(+)}(\nu_A^{(+)})^2 \tag{6.4.11}$$

$$2k^{(-)}\nu_A^{(-)} \le l \le 2k^{(+)}\nu_A^{(+)} \tag{6.4.12}$$

Hashin (1979) gives bounds on the transverse Young's modulus as

$$E_T^{(\pm)} = \frac{4k^{(\pm)}m^{(\pm)}}{k^{(\pm)} + q^{(\pm)}m^{(\pm)}} \qquad q^{(\pm)} = 1 + 4k^{(\pm)}\nu_A^{(\mp)}/E_A^{(\pm)} \tag{6.4.13}$$

where $\nu_A = \nu_{12}$. The transverse Poisson's ratio follows from the standard formula for transverse isotropy, $\nu_T = \nu_{23} = \nu_{32} = (E_T/2m) - 1$. Using the upper or lower bound values of E_T and m may or may not yield higher or lower numerical values of ν_T.

The CCA and CSA models, in combination with the H-S bounds, often provide superior bounds on overall elastic moduli of composite materials reinforced by spherical particles and aligned circular cylindrical fibers, which are of interest in many applications. On the macroscale, the assemblages are statistically homogeneous and isotropic (CSA) or transversely isotropic (CCA), and they satisfy the original requirements that Hill (1963a) specified for a representative volume. They also satisfy the added requirements in the second paragraph of Sect. 3.3.1, because they exhibit a macroscopically uniform deformation in response to application of uniform phase eigenstrains. Local fields are not uniform, they follow from analytical formulas which may be found in Hashin (1962) and Hashin and Rosen (1964). However, averages of the local fields in the two phases, or mechanical concentration factors $\boldsymbol{A}_r$, $\boldsymbol{B}_r$ for the assemblage models can be found from (3.5.13).

6.4.2 Application to a Carbon/Copper Composite

This example presents evaluation procedures and magnitudes of the upper and lower bounds of overall moduli of an aligned fiber composite system P100S/Cu. That and similar systems with different reinforcement geometries are useful in applications requiring high electrical and thermal conductivity combined with high stiffness and strength. The P100S carbon fiber is regarded as transversely isotropic, with Hill's moduli defined in (2.4.3)

$$\left.\begin{aligned} E_{11}^f = 760.00 \text{ GPa},\ E_{22}^f = 7.85 \text{ GPa},\ \nu_{12}^f = 0.20 \\ G_{23}^f = m_f = 2.90 \text{ GPa},\ G_{12}^f = p_f = 20.00 \text{ GPa} \end{aligned}\right\} \tag{6.4.14}$$

According to (2.3.4), the remaining phase Hill's moduli are, in units of GPa

$$\left.\begin{aligned} k_f = 6.0784,\ l_f = 2.4314,\ n_f = 760.9725 \\ k_m = 154.3210,\ l_m = 108.0247,\ m_m = p_m = 46.2963,\ n_m = 200.6173 \end{aligned}\right\} \tag{6.4.15}$$

The copper matrix is isotropic, with elastic moduli $E_m = 125.00$ GPa, $\nu_m = 0.35$. The fiber and matrix moduli satisfy the inequalities

$$\left.\begin{aligned} k_m > k_f,\ \ l_m > l_f,\ \ m_m > m_f,\ \ n_m < n_f,\ \ p_m > p_f \\ E_{11}^m < E_{11}^f,\ \ k_f - l_f^2/n_m < k_m - l_m^2/n_f \end{aligned}\right\} \tag{6.4.16}$$

The inequalities indicate that the combined higher [or lower] phase moduli define the coefficients of the comparison media $\boldsymbol{L}_0^{(+)}$ [or $\boldsymbol{L}_0^{(-)}$] in (6.2.16), both transversely isotropic according to (2.3.3).

The upper or lower bounds on the three independent overall moduli k, m and p of the composite can be computed by different methods which yield identical outcomes in this case. First and most direct approach relies on (6.3.27), which provide the H-S upper or lower bounds on the three overall moduli with the larger or smaller comparison media moduli k_0, m_0 and p_0. That method is preferred in systems with mixed phase moduli magnitudes, which do not satisfy specified pairs of inequalities. The second choice relies on the CCA form (6.4.4) for $p^{(\pm)}$, and on the arbitrary transverse geometry forms (6.4.8–6.4.9) and (6.4.13) for $m^{(\pm)}$ and $E_T^{(\pm)}$, respectively. It turns out that the two choices give identical and very close bounds for m, p, with $m^{(-)}$ higher than $m_{CCA}^{(-)}$. These most restrictive bounds on $E_{22} = E_{33} = E_T$, $G_{23} = G_{32} = G_T = m$, and $G_{12} = G_{13} = p$ appear in Fig. 6.2 and Table 6.1.

6.5 The Generalized Self-consistent Method

Developed by Christensen and Lo (1979), and advanced by Christensen (1990), primarily for evaluation of transverse shear moduli of particulate or fiber reinforced two-phase composites, this material model incorporates the above assemblage models and the "self-consistency" assumption. The latter states that elastic moduli of the aggregate remain equal, to the first order, to those of the surrounding effective medium, when the dominant part of the disturbance between the embedded element and the effective medium is minimized.

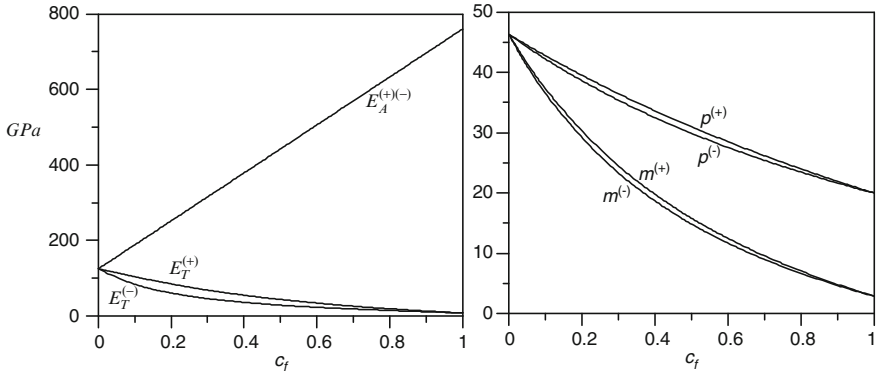

Fig. 6.2 Bounds on the Young's and shear moduli of a P100S/copper composite

Table 6.1 Upper and lower bounds on elastic moduli of a P100S/copper composite

c_f	$E_T{}^{(-)}$	$E_T{}^{(+)}$	$m^{(-)}$	$m^{(+)}$	$p^{(-)}$	$p^{(+)}$
0.0	125.0000	125.0000	46.2963	46.2963	46.2963	46.2963
0.1	84.0568	103.6553	36.4769	37.2713	42.2068	42.7637
0.3	46.1190	68.4543	23.2930	24.4604	35.3751	36.4499
0.5	28.7584	43.7345	14.8430	15.8034	29.8955	30.9721
0.7	18.5344	26.1629	8.9768	9.5620	25.4027	26.1745
0.9	11.1868	13.1524	4.6578	4.8488	21.6521	21.9378
1.0	7.8500	7.8500	2.9000	2.9000	20.0000	20.0000

As in the CCA and CSA models, the composite microstructure is modeled by a cylindrical or spherical composite element, that consists of a core with stiffness $\boldsymbol{L}_r$, surrounded by concentric matrix layer $\boldsymbol{L}_1$. Phase volume fractions in the composite element are those present in the actual system. However, in contrasts to the assemblage models, the composite element is now embedded in a homogeneous effective medium $\boldsymbol{L}$, as an inhomogeneity with zero interaction energy.

The interaction energy is found from the Eshelby formula (5.1.8) or (5.1.11). The integral is evaluated along the interface between the matrix layer and the surrounding effective medium, with tractions and displacements that follow from an exact elasticity solution for local fields in each of the three phases $\boldsymbol{L}_r$, $\boldsymbol{L}_1$ and $\boldsymbol{L}$, under uniform overall shear stress or conjugate shear strain applied to the large volume of surrounding effective medium, Fig. 6.3. In a composite reinforced by spherical inhomogeneities, this procedure reproduces the lower bound on the bulk modulus K of the composite sphere assemblage in (6.3.22). In an aligned fiber two-phase composite, it yields each of the four moduli k, E_A, ν_A, p predicted by the composite cylinder assemblage model, shown in Sect. 6.4.1. However, new estimates are obtained for the shear moduli G and m. Complete derivation is rich in algebraic detail, but the results have been rendered in relatively simple form summarized below.

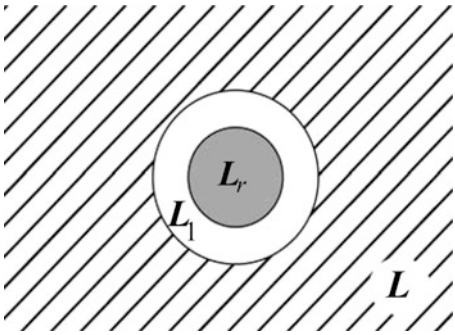

Fig. 6.3 Geometry of the generalized self-consistent model (GSCM) of Christensen and Lo (1979). Stiffnesses of inhomogeneity, matrix and effective medium are denoted by $\boldsymbol{L}_r, \boldsymbol{L}_1, \boldsymbol{L}$

6.5.1 Shear Modulus of a Two-Phase Particulate Composite

An isotropic composite has a matrix with moduli $G_m,\ \nu_m$, reinforced by a statistically homogeneous distribution of isotropic and polydisperse spherical inhomogeneities with moduli $G_i,\ \nu_i$ and volume fraction $c = (d_r/d_1)^3$, given by the ratio of the outer diameters of $\boldsymbol{L}_r$, and $\boldsymbol{L}_1$ in Fig. 6.3. The generalized self-consistent estimate of the overall shear modulus G of this composite is (Christensen and Lo 1979; Christensen 1990)

$$A(G/G_m)^2 + B(G/G_m) + C = 0 \tag{6.5.1}$$

where

$$\left.\begin{aligned} A = {} & 8(4-5\nu_m)\eta_1\eta_4 c^{10/3} - 2(63\eta_2\eta_4 + 2\eta_1\eta_3)c^{7/3} + 252\eta_2\eta_4 c^{5/3} \\ & - 50(7-12\nu_m+8\nu_m^2)\eta_2\eta_4 c + 4(7-10\nu_m)\eta_2\eta_3 \end{aligned}\right\} \tag{6.5.2}$$

$$\left.\begin{aligned} B = {} & -4(1-5\nu_m)\eta_1\eta_4 c^{10/3} + 4(63\eta_2\eta_4 + 2\eta_1\eta_3)c^{7/3} - 504\eta_2\eta_4 c^{5/3} \\ & + 150(3-\nu_m)\nu_m\eta_2\eta_4 c - 3(7-15\nu_m)\eta_2\eta_3 \end{aligned}\right\} \tag{6.5.3}$$

$$\left.\begin{aligned} C = {} & -4(7-5\nu_m)\eta_1\eta_4 c^{10/3} - 2(63\eta_2\eta_4 + 2\eta_1\eta_3)c^{7/3} + 252\eta_2\eta_4 c^{5/3} \\ & - 25(7-\nu_m^2)\eta_2\eta_4 c - (7+5\nu_m)\eta_2\eta_3 \end{aligned}\right\} \tag{6.5.4}$$

The η coefficients are given in corrected form by Christensen (1990) as

$$\left.\begin{aligned} \eta_1 &= (7+5\nu_i)(7-10\nu_m)\eta_4 + 105(\nu_i-\nu_m) \\ \eta_2 &= (7+5\nu_i)\eta_4 + 35(1-\nu_i) \\ \eta_3 &= (8-10\nu_m)\eta_4 + 15(1-\nu_m) \\ \eta_4 &= (G_i/G_m - 1) \end{aligned}\right\} \tag{6.5.5}$$

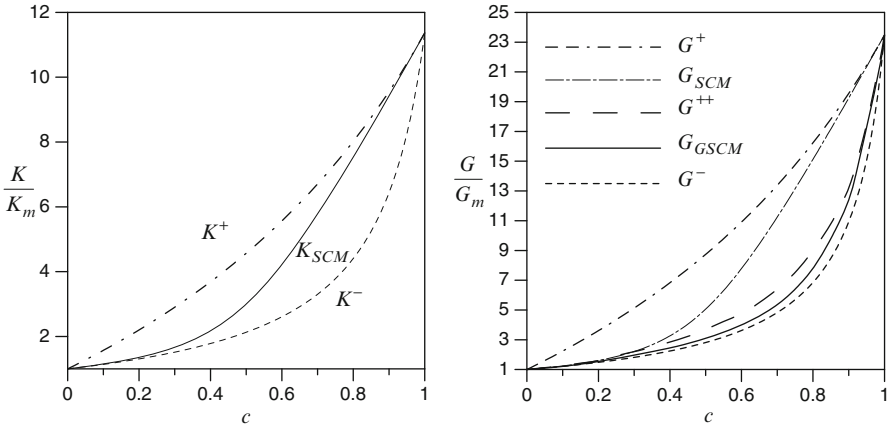

Fig. 6.4 Bounds and GSCM estimates of bulk and shear moduli of a S-glass spheres/epoxy composite, as functions of spheres volume fraction c. Glass moduli are $E_s = 87.0$ GPa, $\nu_s = 0.22$; epoxy moduli are $E_m = 4.1$ GPa, $\nu_m = 0.35$

For a dilute suspension, at a small volume fraction c, this result is reduced, using the binomial expansion of (6.5.1), to

$$\frac{G}{G_m} = 1 + \frac{15(1-\nu_m)\eta_4 c}{7 - 5\nu_m + 2(4-5\nu_m)(\eta_4+1)} + \mathrm{O}(c^2) \quad \text{for } c \to 0 \tag{6.5.6}$$

which agrees with Eshelby's (1957, p. 390) result. By letting $\eta_4 \to \infty$, $\nu_m = 0.5$, one recovers the Einstein formula (4.4.29). The corresponding overall bulk modulus K of the particulate composite is supplied by the lower bound in (6.3.22), assuming of course, that $G_1 = G_m < G_i = G_2$.

Figure 6.4 shows the bulk and shear moduli of a composite made of S-glass spherical particles in an epoxy matrix, estimated by both the generalized self-consistent method and by the Hashin-Shtrikman bounds. The $K^{(+)}, K^{(-)}$ and $G^{(+)}$, $G^{(-)}$ bounds were computed using (6.3.22–6.3.23). The much tighter $G^{(++)} < G^{(+)}$ upper bound was derived by Hashin (1962) from the CSA model. The K_{SCM} and G_{SCM} are standard self-consistent estimates evaluated from (6.3.26) with $K_0 = K$, $G_0 = G$, as explained in Sect. 7.1. The G/G_m figure illustrates a comparison of different bounding methods, and it shows that the GSCM prediction is bracketed by the tightest $G^{(++)}$ and $G^{(-)}$ bounds. The GSCM is generally close or coincides with the lower H-S bound on the shear modulus.

Figure 6.5 compares the results of different predictions with experimental results for the ratio μ/μ_m of effective to matrix shear viscosity of several particulate suspensions. The same analysis provides elastic shear moduli ratios. At very low concentration, dominated by polydisperse mixtures, the results are well approximated by the Einstein formula (4.4.29), and also by the differential scheme. However, at both low and very high, monodisperse concentrations, only the GSCM

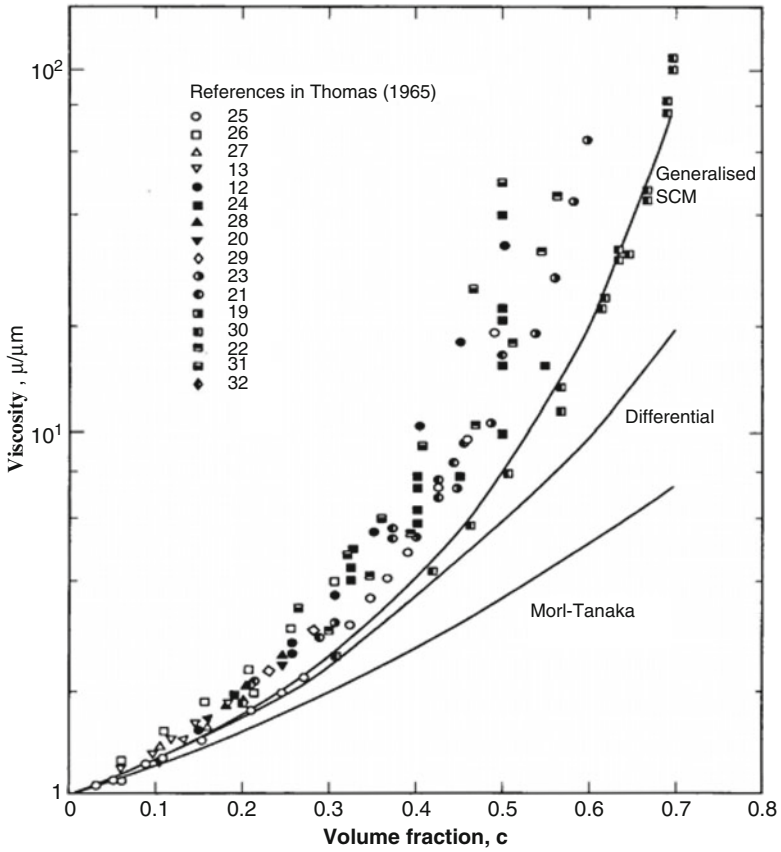

Fig. 6.5 Effective shear modulus/viscosity of polydisperse suspensions of particles in an incompressible matrix (Reprinted with permission from Christensen 1990)

provides the correct result, while the differential scheme and the Mori-Tanaka method, described in the next chapter, underestimate the measured viscosity. Table 6.2 presents numerical values of the moduli ratios. At very high volume fractions, the effective shear modulus and viscosity may become bounded by those of the particle phase. Christensen (1990) provides additional comparisons of GSCM and the Mori-Tanaka and differential schemes with experiments, confirming the agreement seen in Fig. 6.5.

In suspensions of *very stiff particles* in a relatively compliant matrix, the parameter $\eta_4 = (G_i/G_m - 1)$ in (6.5.2), (6.5.3), (6.5.4), (6.5.5) may become too large. Then, the said equations should be replaced by the following GSCM prediction of the overall shear moduli of a suspension of rigid spherical inhomogeneities in an elastic matrix with moduli $G_m,\ \nu_m$ (R. M. Christensen 2010, private communication).

Table 6.2 The overall to matrix shear moduli ratio predicted by the generalized self-consistent method and by the lower Hashin-Shtrikman bound

G/G_m	$\nu_m = 0.3333$		$\nu_m = 0.49999$	
c	*GSCM*	*HSLB*	*GSCM*	*HSLB*
0.1	1.237	1.233	1.290	1.278
0.3	1.980	1.900	2.500	2.071
0.5	3.476	3.100	8.098	3.500
0.7	7.141	5.900	78.807	6.833
0.9	25.64	19.90	4725.5	23.50
0.95	57.59	41.71	40666.9	48.49

$$A_R(G/G_m)^2 + 2B_R(G/G_m) + C_R = 0 \tag{6.5.7}$$

$$\left.\begin{aligned} A_R = {} & 8(4-5\nu_m)(7-10\nu_m)c^{10/3} - 50(7-12\nu_m+8\nu_m^2)c^{7/3} \\ & + 252c^{5/3} - 50(7-12\nu_m+8\nu_m^2)c + 8(4-5\nu_m)(7-10\nu_m) \end{aligned}\right\} \tag{6.5.8}$$

$$\left.\begin{aligned} B_R = {} & -2(1-5\nu_m)(7-10\nu_m)c^{10/3} + 50(7-12\nu_m+8\nu_m^2)c^{7/3} \\ & - 252c^{5/3} + 75\nu_m(3-\nu_m)c - 3(4-5\nu_m)(7-15\nu_m) \end{aligned}\right\} \tag{6.5.9}$$

$$\left.\begin{aligned} C_R = {} & -4(7-5\nu_m)(7-10\nu_m)c^{10/3} - 50(7-12\nu_m+8\nu_m^2)c^{7/3} \\ & + 252c^{5/3} - 25(7-\nu_m^2)c - 2(4-5\nu_m)(7+5\nu_m) \end{aligned}\right\} \tag{6.5.10}$$

At very high concentrations, which can be realized in suspensions of polydisperse spherical inhomogeneities, the shear moduli ratio of a composite reinforced by rigid inhomogeneities depends on the Poisson's ratio of the matrix. This ratio was estimated by Christensen (1990) and Christensen (2010) (private communication), as the leading term in an asymptotic expansion of (6.5.1), with coefficients corrected by Christensen et al. (1992). For $c \to 1$

$$\left.\begin{aligned} \frac{G}{G_m} &\to \frac{3}{(1-c)} \quad \text{for } \nu_m = 1/3 \\ \frac{G}{G_m} &\to \frac{27}{4(1-c)^3} \quad \text{for } \nu_m = 1/2 \end{aligned}\right\} \tag{6.5.11}$$

Under similar circumstances, for $c \to 1$, the H-S lower bound can be reduced to

$$\left.\begin{aligned} \frac{G}{G_m} &\to \frac{15}{7(1-c)} \quad \text{for } \nu_m = 1/3 \\ \frac{G}{G_m} &\to \frac{5}{2(1-c)} \quad \text{for } \nu_m = 1/2 \end{aligned}\right\} \tag{6.5.12}$$

At intermediate concentrations, $0 < c < 1$, the H-S lower bound yields

$$G/G_m = 1 + \frac{15(1-\nu_m)}{2(4-5\nu_m)}\left[\frac{c}{(1-c)}\right] \tag{6.5.13}$$

Table 6.2 shows that at increasing concentrations, the GSCM predicts much higher magnitudes of the shear modulus of particulate suspensions than does the H-S lower bound, in agreement with the experimental results in Fig. 6.5, where the lower H-S bound is equal to the Mori-Tanaka estimate. At high concentrations, the computed GSCM values are very sensitive to small differences in the matrix Poisson's ratio when $\nu_m \to 0.5$. For example, when $\nu_m = 0.4999$ instead of the value shown, the GSCM prediction changes to $G/G_m = 3689$ and $G/G_m = 19540$ at $c = 0.9$ and $c = 0.95$, respectively.

At the other end of property spectrum are low-density materials, often modeled by thin-walled cells. A comprehensive exposition of their properties can be found for polymer-based systems in Gibson and Ashby (1997) and for metal foams in Ashby et al. (2000). A hierarchy of microstructures for cellular and other low density materials was examined by Christensen (1995, 2003).

6.5.2 *Transverse Shear Modulus of a Two-Phase Aligned Fiber Composite*

Except for the overall m, both the GSCM and the H-S lower bounds on $k,\ E_A,\ \nu_A$ in (6.4.1), (6.4.2), (6.4.3) predict the same values of overall moduli of the transversely isotropic composite. The transverse shear modulus of a transversely isotropic fiber composite, consisting of isotropic phases with fiber and matrix elastic moduli $G_f,\ \nu_f$ and $G_m,\ \nu_m$, was derived by Christensen and Lo (1979) and Christensen (1990) as

$$A_F(m/G_m)^2 + B_F(m/G_m) + C_F = 0 \tag{6.5.14}$$

In the notation $\gamma = G_f/G_m,\ c = (a/b)^2,\ \eta_m = 3 - 4\nu_m$ and $\eta_f = 3 - 4\nu_f$, the constants are

$$\left.\begin{aligned} A_F = {} & 3(\gamma-1)(\gamma+\eta_f)c(1-c)^2 \\ & + [\gamma\eta_m + \eta_f\eta_m - (\gamma\eta_m - \eta_f)c^3][(\gamma-1)\eta_m c - (\gamma\eta_m + 1)] \end{aligned}\right\} \tag{6.5.15}$$

$$\left.\begin{aligned} B_F = {} & -6(\gamma-1)(\gamma+\eta_f)c(1-c)^2 \\ & + [\gamma\eta_m + (\gamma-1)c + 1][(\eta_m - 1)(\gamma+\eta_f) - 2(\gamma\eta_m - \eta_f)c^3] \\ & + (\gamma-1)(\eta_m+1)c[\gamma + \eta_f + (\gamma\eta_m - \eta_f)c^3] \end{aligned}\right\} \tag{6.5.16}$$

$$\left.\begin{aligned} C_F = {} & 3(\gamma-1)(\gamma+\eta_f)c(1-c)^2 \\ & + [1 + \gamma\eta_m + (\gamma-1)c][\gamma + \eta_f + (\gamma\eta_m - \eta_f)c^3] \end{aligned}\right\} \tag{6.5.17}$$

For dilute concentration, at $c << 1$, (6.5.14) yields

$$m/G_m = 1 + \frac{(G_f - G_m)(1+\eta_m)}{(G_f\eta_m + G_m)}c \quad \text{for } c \to 0 \tag{6.5.18}$$

At high concentrations of very stiff fibers, at $G_f/G_m >> 1$ and $\nu_f \to 0.5$, the above terms in (6.5.15), (6.5.16), (6.5.17), after canceling of common terms, become

$$\left.\begin{aligned} A_F &= 3c(1-c)^2 - \eta_m^2(1-c)(1-c^3) \\ B_F &= -3c(1-c)^2 + (c/2)(1+\eta_m)(1+\eta_m c^3) \\ &\quad - (1/2)(\eta_m + c)[1 - \eta_m(1-2c^3)] \\ C_F &= 3c(1-c)^2 + (\eta_m + c)(1+\eta_m c^3) \end{aligned}\right\} \tag{6.5.19}$$

The first term of an asymptotic expansion of (6.5.14) is

$$\frac{m}{G_m} \to \frac{1}{1-c}\left[\frac{3 - 4\nu_m + (33 - 96\nu_m + 64\nu_m^2)^{1/2}}{6(1-2\nu_m)}\right] \text{ for } c \to 1,\ \nu_m < 0.5 \tag{6.5.20}$$

and

$$\frac{m}{G_m} \to \frac{4}{(1-c)^3} \text{ for } c \to 1,\ \nu_m = 0.5 \tag{6.5.21}$$

In Fig. 6.6, the $m^{(-)}$ is the H-S lower bound, $m^{(+)}$ is the H-S upper bound both from (6.3.18) or (6.3.27), and $m^{(++)}$ is Hashin's upper bound (6.4.6). The m_{SCM} follows from (6.3.27) when $m_0 = m$ and $k_0 = k$, while m_{GSCM} is the solution of (6.5.14). E_A and E_T are Young's moduli in the longitudinal and transverse directions, evaluated from (6.4.2) and (2.3.5), respectively. In the latter, the H-S bounds on m and (6.4.1) bounds on k are used together with the universal connections (3.9.4) for evaluation of the modulus l. Table 6.3 shows a comparison of the above Hashin's bounds with the generalized self-consistent estimates. Christensen (1990, 1998) describes additional applications of this model to porous solids, to composites with extreme matrix properties, and to highly concentrated suspensions. He also compares the results with those predicted by the Mori-Tanaka method and by the differential scheme. The comparison shows superior agreement of the GSCM prediction with experiments. The GSCM estimates are apparently the best that can be obtained by analytical methods for the two geometries considered.

On the macroscale, the model is statistically homogeneous and isotropic or transversely isotropic, and it satisfies the original requirements that Hill (1963a) specified for a representative volume. However, as in the CSA and CCA models,

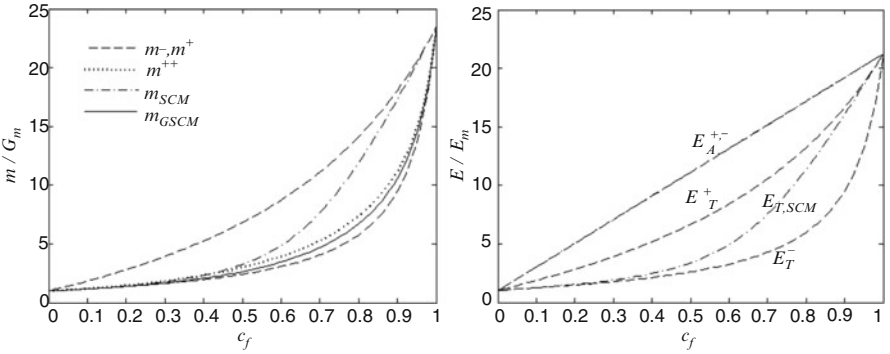

Fig. 6.6 Bounds, GSCM and self-consistent estimates of Young's and shear moduli of a S-glass fiber/epoxy composite. Glass moduli are $E_f = 87.0$ GPa, $\nu_f = 0.22$; epoxy moduli are $E_m = 4.1$ GPa, $\nu_m = 0.35$, $G_f/G_m = 23.46$

Table 6.3 Hashin's (1979) bounds on overall transverse shear modulus m of a fibrous S-glass/epoxy composite

$E_f = 87$ GPa,	$\nu_f = 0.22$,	$E_m = 4.1$ GPa,	$\nu_m = 0.35$
c_f	$m^{(-)}$	m_{GSCM}	$m^{(++)}$
0.1	1.772	1.774	1.800
0.3	2.477	2.577	2.761
0.5	3.674	4.014	4.542
0.7	6.158	7.132	7.981
0.9	14.41	16.06	16.97

the mechanical concentration factors $\boldsymbol{A}_r$, $\boldsymbol{B}_r$ are not explicitly available, but accessible from the original derivation, or more directly from (3.5.13). A different interpretation of GSCM which may simplify evaluation of these factors in two-phase systems was presented by Benveniste (2008).

An extension of the GSCM procedure, developed by Hervé and Zaoui (1995), derives elastic strain and stress fields in a n-layered transversely isotropic cylindrical inhomogeneity in a matrix, and implements the condition $W_I = 0$ for the interaction energy under remotely applied, overall uniform fields. Their results provide the four moduli k, E_A, ν_A, p of an assemblage of multi-layered composite cylinders, derived from the Hashin-Rosen model by a recursive algorithm, and a new estimate for the transverse shear modulus. Those may be useful in predicting effective properties of composites with multilayered fiber coatings.

Chapter 7
Estimates of Mechanical Properties of Composite Materials

Together with the methods described in the previous chapter, overall moduli and local field averages in the phases can be estimated by one of several approximate methods, which use different models of the microstructure. Among those described here are variants of the average field approximation, or AFA, which rely on strain or stress field averages in solitary ellipsoidal inhomogeneities, embedded in large volumes of different comparison media $\boldsymbol{L}_0$. Among the most widely used procedures are the self-consistent and Mori-Tanaka methods, and the differential scheme, described in Sects. 7.1, 7.2 and 7.3. Those are followed by several double inclusion or double inhomogeneity models in Sect. 7.4, and by illustrative comparison with finite element evaluations for functionally graded materials in Sect. 7.5.

Although the methods described here can also be applied to periodic composites, providing that their overall material symmetry is taken into account, this special and rather rare class of actual materials has been analyzed by methods not discussed herein, but revisited in Chap. 12. Extensive treatment and related references can be found in Babuska (1975), Suquet (1987), Nemat-Nasser and Hori (1999), and Walker (1993). Bensoussan et al. (1978) and Sanchez-Palencia (1980) survey basic theory of periodic homogenization problems.

All moduli estimates depend in different ways on the elastic moduli, volume fraction, shape and orientation of the phases. Spatial distribution of the phases is also reflected in certain estimates. However, absolute size of individual phases is not a factor in evaluation of overall moduli by the models. Of course, large differences in scale may cause interactions that distort the magnitudes of phase field averages in the small constituents. In such multi-scale systems, homogenization should proceed in sequence, at increasingly coarser scales, by first homogenizing the matrix and the finer scale inhomogeneities, before proceeding to the next scale. Hierarchical or multi-scale computational models had been described, for example, by Zohdi et al. (1996), Ghosh et al. (2001), Zohdi and Wriggers (2005) and Oskay and Fish (2007).

G.J. Dvorak, *Micromechanics of Composite Materials*, Solid Mechanics and Its Applications 186, DOI 10.1007/978-94-007-4101-0_7,

7.1 The Self-consistent Method (SCM)

The original idea of the method may be attributed to Einstein (1905). Evolution of the current form dates back to the work of Bruggeman (1935), who had used it to estimate dielectric, conductivity, and elastic constants of composite aggregates. That was followed by Hershey (1954), Kerner (1956), Kröner (1958), Hill (1965a) who applied the method to polycrystals, and by Budiansky (1965) and Hill (1965b, c) who applied it to composites. Laws (1973, 1974) extended the method to thermo-elastic problems, and Laws and McLaughlin (1978) used it to estimate creep compliances of linear visco-elastic solids. Other self-consistent estimates were found by Christensen and Waals (1972), Boucher (1974), Berryman (1980), and by Cleary et al. (1980), and by many other writers. Hill's version of the method is in current use; see also the reviews by Laws (1980), Walpole (1981, 1984), Willis (1981), and Nemat-Nasser and Hori (1999) for additional results and references.

7.1.1 Estimates of Overall Elastic Moduli

In the original version of this method, interaction between individual subvolumes of the phases is approximated by embedding each subvolume Ω_r of phase $\boldsymbol{L}_r$ as a solitary ellipsoidal inhomogeneity in a large volume Ω of $\boldsymbol{L}_0 \equiv \boldsymbol{L}$, that has the as yet unknown overall stiffness $\boldsymbol{L}$ of the aggregate. Overall uniform strain $\boldsymbol{\varepsilon}^0$ or stress $\boldsymbol{\sigma}^0$ is applied at the remote boundary $\partial\Omega$, Fig. 7.1. The mechanical strain and stress

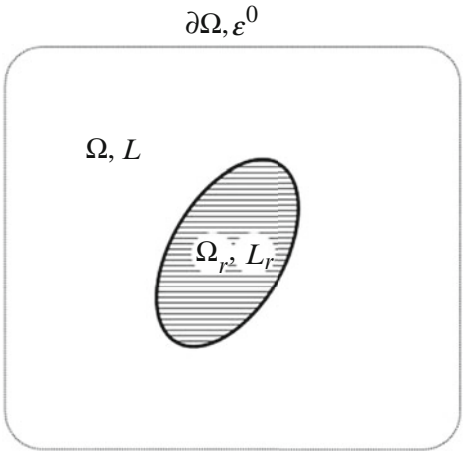

Fig. 7.1 The self-consistent model (SCM). Stiffness of the inhomogeneity and of the comparison medium are denoted by $\boldsymbol{L}_r$ and by $\boldsymbol{L}_0 = \boldsymbol{L}$

concentration factors of each phase $\boldsymbol{L}_r$ follow from the expressions for their partial counterparts in (4.2.14) as

$$\left.\begin{aligned} \boldsymbol{A}_r &= [\boldsymbol{I} + \boldsymbol{P}(\boldsymbol{L}_r - \boldsymbol{L})]^{-1} = (\boldsymbol{L}^* + \boldsymbol{L}_r)^{-1}(\boldsymbol{L}^* + \boldsymbol{L}) \\ \boldsymbol{B}_r &= [\boldsymbol{I} + \boldsymbol{Q}(\boldsymbol{M}_r - \boldsymbol{M})]^{-1} = (\boldsymbol{M}^* + \boldsymbol{M}_r)^{-1}(\boldsymbol{M}^* + \boldsymbol{M}) \end{aligned}\right\} \tag{7.1.1}$$

Substitution of the concentration factors (7.1.1) into the first right-hand terms of (6.3.5) yields the overall stiffness

$$\boldsymbol{L} = \sum_{r=1}^{n} c_r \boldsymbol{L}_r \boldsymbol{A}_r = \left[\sum_{r=1}^{n} c_r \boldsymbol{L}_r \left(\boldsymbol{L}^* + \boldsymbol{L}_r\right)^{-1}\right]\left(\boldsymbol{L}^* + \boldsymbol{L}\right) \tag{7.1.2}$$

Diagonal symmetry of $\boldsymbol{L}$ is established by expanding the first term

$$\left.\begin{aligned} &\sum_{r=1}^{n} c_r \boldsymbol{L}_r (\boldsymbol{L}^* + \boldsymbol{L}_r)^{-1} + \sum_{r=1}^{n} c_r \boldsymbol{L}^* (\boldsymbol{L}^* + \boldsymbol{L}_r)^{-1} - \sum_{r=1}^{n} c_r \boldsymbol{L}^* (\boldsymbol{L}^* + \boldsymbol{L}_r)^{-1} \\ &= \sum_{r=1}^{n} c_r (\boldsymbol{L}^* + \boldsymbol{L}_r)(\boldsymbol{L}^* + \boldsymbol{L}_r)^{-1} - \sum_{r=1}^{n} c_r \boldsymbol{L}^* (\boldsymbol{L}^* + \boldsymbol{L}_r)^{-1} \\ &= \mathbf{I} - \boldsymbol{L}^* \sum_{r=1}^{n} c_r (\boldsymbol{L}^* + \boldsymbol{L}_r)^{-1} \end{aligned}\right\} \tag{7.1.3}$$

and by

$$\left.\begin{aligned} \boldsymbol{L} &= \sum_{r=1}^{n} c_r \boldsymbol{L}_r \boldsymbol{A}_r = \left[\boldsymbol{I} - \boldsymbol{L}^* \sum_{r=1}^{n} c_r (\boldsymbol{L}^* + \boldsymbol{L}_r)^{-1}\right]\left(\boldsymbol{L}^* + \boldsymbol{L}\right) \\ \boldsymbol{L} &= \boldsymbol{L}^* + \boldsymbol{L} - \boldsymbol{L}^* \sum_{r=1}^{n} c_r \left(\boldsymbol{L}^* + \boldsymbol{L}_r\right)^{-1}\left(\boldsymbol{L}^* + \boldsymbol{L}\right) \\ \mathbf{0} &= \boldsymbol{L}^*\left[\boldsymbol{I} - \left(\sum_{r=1}^{n} c_r (\boldsymbol{L}^* + \boldsymbol{L}_r)^{-1}(\boldsymbol{L}^* + \boldsymbol{L})\right)\right] \\ \boldsymbol{L} &= \left[\sum_{r=1}^{n} c_r (\boldsymbol{L}^* + \boldsymbol{L}_r)^{-1}\right]^{-1} - \boldsymbol{L}^* = \boldsymbol{L}^{\mathrm{T}} \qquad \boldsymbol{L}^* \neq \mathbf{0} \end{aligned}\right\} \tag{7.1.4}$$

That also confirms that the self-consistent estimate of the overall stiffness $\boldsymbol{L}$ follows from the general estimate (6.3.5), when one selects $\boldsymbol{L}_0 = \boldsymbol{L}$, and evaluates

$\boldsymbol{P} = (\boldsymbol{L}^* + \boldsymbol{L})^{-1}$ using the coefficients of $\boldsymbol{L}$. A similar proof can be derived for the overall compliance. The inclusion problem solution (4.2.14) and (6.3.5), both with identical $\boldsymbol{P}$ matrix, provide the same result.

In each application of the self-consistent method, it is necessary to select or identify the overall material symmetry of $\boldsymbol{L} = \boldsymbol{L}^{\mathrm{T}}$ according to the dominant geometry of the microstructure. The as yet unknown coefficients of $\boldsymbol{L}$ are thereby identified and then used to construct the $\boldsymbol{P}$ or $\boldsymbol{Q}$ and $\boldsymbol{A}_r$ or $\boldsymbol{B}_r$, for substitution into (7.1.2) or (7.1.5). The resulting system of implicit algebraic equations is solved for the magnitudes of the coefficients of $\boldsymbol{L}$ or $\boldsymbol{M}$.

An iterative solution may start using initial values of the coefficients of $\boldsymbol{L}_0$ consistent with the bounding theorems (6.2.16), taken as one of the H-S bounds (6.3.13). The iteration then proceeds until $\boldsymbol{L}_0 \to \boldsymbol{L}$ or $\boldsymbol{M}_0 \to \boldsymbol{M}$, respectively. The resulting estimate of the overall moduli is evidently bracketed by the H-S bounds. That was demonstrated, for example, by Hill (1964) for fiber composites, and by Kröner et al. (1966) for isotropic aggregates of cubic crystals. In multiphase systems, the self-consistent estimate assigns each phase, even a matrix phase, the same shape and alignment, defined by the single $\boldsymbol{P}$ or $\boldsymbol{Q}$ matrix in (7.1.1).

In a two-phase system, $r = 1,\ 2$, where $c_1\boldsymbol{A}_1 = \boldsymbol{I} - c_2\boldsymbol{A}_2$, (7.1.2) is reduced to

$$\boldsymbol{L} = \boldsymbol{L}_1 + c_2\,(\boldsymbol{L}_2 - \boldsymbol{L}_1)\,\boldsymbol{A}_2 \qquad \boldsymbol{M} = \boldsymbol{M}_1 + c_2\,(\boldsymbol{M}_2 - \boldsymbol{M}_1)\,\boldsymbol{B}_2 \tag{7.1.5}$$

The $\boldsymbol{L}_1$ represents the stiffness of a matrix, and $\boldsymbol{A}_2$ is the concentration factor of the inhomogeneity. In matrix-based particulate or fibrous aggregates, the overall moduli do not change if the role of the two phases is reversed, as long as their volume fractions remain unchanged, because the model treats all phases 'on an equal footing' (Hill 1965c).

7.1.2 Elastic Moduli of Two-Phase Fiber Composites

For a fiber composite consisting of two phases $r = 1, 2$, both transversely isotropic about and aligned in the longitudinal direction, the self-consistent estimates of overall moduli were derived by Hill (1965b) from elasticity solutions of an extended composite cylinder element with a surrounding shell made of the effective medium. The composite is transversely isotropic, with the overall stiffness matrix in (2.3.3). The plane strain bulk modulus k is connected to the transverse shear modulus m by

$$\frac{1}{k+m} = \frac{c_1}{k_1+m} + \frac{c_2}{k_2+m} \tag{7.1.6}$$

where m is the positive root of the cubic

$$\frac{c_1 k_1}{k_1 + m} + \frac{c_2 k_2}{k_2 + m} = 2\left(\frac{c_1 m_2}{m_2 - m} + \frac{c_2 m_1}{m_1 - m}\right) \tag{7.1.7}$$

The longitudinal shear modulus p is the positive root of the quadratic

$$\frac{c_1 p}{p - p_2} + \frac{c_2 p}{p - p_1} = \frac{1}{2} \tag{7.1.8}$$

If the matrix $r = 1$ or both phases are isotropic, with moduli K_1 and G_1, then according to (2.3.6), the modulus $k_1 = K_1 + G_1/3$, and $m_1 = p_1 = G_1$. The overall modulus k and the phase moduli are then substituted into the universal connections

$$\frac{k - k_1}{l - l_1} = \frac{k - k_2}{l - l_2} = \frac{l - c_1 l_1 - c_2 l_2}{n - c_1 n_1 - c_2 n_2} = \frac{k_1 - k_2}{l_1 - l_2} \tag{3.9.4}$$

which yield the two remaining overall moduli n and l. It can be verified that the above results are bracketed by the Hashin-Shtrikman bounds in Sect. 6.3.3, but not necessarily by tighter bounds.

The overall moduli can be also evaluated by solving the Walpole's equations (6.3.27) for $k_0 \to k, m_0 \to m$ and $p_0 \to p$.

$$\left.\begin{aligned} k &= c_1 k_1 + c_2 k_2 - c_1 c_2 (k_1 - k_2)^2 (c_1 k_2 + c_2 k_1 + m_0)^{-1} \\ m &= c_1 m_1 + c_2 m_2 - c_1 c_2 (m_1 - m_2)^2 [c_1 m_2 + c_2 m_1 + m_0 k_0/(k_0 + 2m_0)]^{-1} \\ p &= c_1 p_1 + c_2 p_2 - c_1 c_2 (p_1 - p_2)^2 (c_1 p_2 + c_2 p_1 + p_0)^{-1} \end{aligned}\right\} \tag{6.3.27}$$

In contrast to the Hashin-Shtrikman bounds on overall $\boldsymbol{L}$ or $\boldsymbol{M}$, derived with comparison media of constant stiffness $\boldsymbol{L}_0^{(+)}$ or $\boldsymbol{L}_0^{(-)}$, the self-consistent method relies on variable $\boldsymbol{L}_0 = \boldsymbol{L}$, which depends on phase volume fractions. Therefore, the self-consistent estimates of moduli are not aligned with either bound, but approach the lower or upper bound at $c_f \to 0$ or $c_f \to 1$.

That is illustrated in Figs. 6.4 and 6.6 for a glass/epoxy fiber composite. The generalized self-consistent (GSCM) estimate of the transverse shear modulus shown in Fig. 6.6 is typically closer and aligned with the H-S lower bound, and with the Hashin and Rosen (1964) CCA upper bound $m^{(++)}$.

The above results may also be applied to two-phase systems reinforced with aligned discontinuous fibers that have sufficiently large length/diameter aspect ratio. For example, Laws and McLaughlin (1979) computed the overall compliances of a glass-polyester composites, where the fibers were modeled as aligned prolate spheroids. The fiber length effect receded entirely at aspect ratios exceeding 100

for any fiber concentration. Since the effect of fiber length depends also on the magnitude of phase moduli and volume fractions, their procedure has to be repeated in applications to any other system of interest. The role of phase moduli was illustrated by Russel (1973) in dilutely reinforced systems.

Self-consistent estimates of overall elastic moduli of composite materials reinforced by randomly oriented needle-like short fibers or by disk-shaped platelets were derived by Walpole (1969, eqns (60)-(61)). At a given volume fraction of reinforcement, platelets have a stronger effect in determining the overall bulk and shear moduli of the aggregate.

7.1.3 *Elastic Moduli of Two-Phase Particulate Composites*

Polycrystals, or matrix-based composites reinforced by a random or any other dispersion of spheres that provides for overall statistical isotropy are considered. The effective, or overall bulk and shear moduli G and K of such composites were found by Hill (1965c) as

$$\frac{c_1 K_1}{K_1 + 4G/3} + \frac{c_2 K_2}{K_2 + 4G/3} + 5\left(\frac{c_1 G_2}{G - G_2} + \frac{c_2 G_1}{G - G_1}\right) + 2 = 0 \qquad (7.1.9)$$

and

$$\frac{1}{K + 4G/3} = \frac{c_1}{K_1 + 4G/3} + \frac{c_2}{K_2 + 4G/3} \qquad (7.1.10)$$

The latter result gives an exact value of K for isotropic composites of arbitrary geometry when the phases have identical shear moduli (Hill 1963a). Since K depends on the shear modulus G, given by the quartic equation (7.1.9), the self-consistent method predicts only one independent modulus of an isotropic two-phase system. As an alternative, Walpole's (1985c) equations (6.3.26) can be iteratively solved for $K_0 \to K$ and $G_0 \to G$.

Figure 6.4 shows an example of a self-consistent prediction G_{SCM} of the shear modulus of a S-glass/epoxy particulate composite, that is bracketed by the H-S bounds G^+ and G^-. However, it violates the tighter Hashin bound G^{++}, which is respected by the generalized self-consistent estimate G_{GSCM}.

If the disperse phase is replaced by cavities, $K_2 = G_2 = 0$, and also when both phases are incompressible, $K_1, K_2 \to \infty$, then (7.1.9) has a positive root when and only when $c_2 < 0.5$, and $G = 0$ at $c_2 > 0.5$. That prediction is contradicted, for example, by properties of closed cell foams. Budiansky and O'Connell (1976) also derived an unexpected prediction, in applications of the self-consistent method to isotropic solids containing randomly oriented circular cracks of radius a and density N/V, the number of cracks per unit volume. Both

overall moduli reach zero at $\varepsilon = N\langle a^3\rangle/V \to 9/16$, which might estimate a critical crack density, albeit not confirmed by later estimates by the Mori-Tanaka and double inhomogeneity models, as shown in Sects. 7.2 and 7.4 below. However, such physically improbable outcomes do not arise in fiber composites weakened by aligned slit or penny-shaped cracks, where all moduli decrease gradually to either finite or zero values with increasing crack density (Laws et al. 1983; Laws and Dvorak 1987). Similar issues arise in other applications of the method, e.g., to dielectrics (Milton 2002). Therefore, the method should not be used when the phase moduli are of different order in magnitude, or when at least one of them assumes extreme or zero magnitude. Such situations may also be encountered when the method is applied to composites with elastic-plastic, viscous, and other inelastic matrices, which may have low instantaneous tangential stiffness.

7.1.4 Restrictions on Constituent Shape and Alignment

Equations 7.1.3 show that the method predicts a diagonally symmetric stiffness matrix $\boldsymbol{L} = \boldsymbol{L}^{\mathrm{T}}$ when applied to systems where each phase subvolume has the same shape and alignment described by a single $\boldsymbol{P}$ tensor. Applications of the self-consistent method to multi-phase composites that have more than one reinforcement phase shape or alignment, yield stiffness or compliance estimates that are not diagonally symmetric (Benveniste et al. 1991b). However, numerical experiments described, in part, in (7.1.15) and (7.1.16) below, indicate that different phase shapes and alignments may be admitted for the reinforcement phase $\boldsymbol{L}_2$ in a matrix-based two-phase system, $r = 1,\ 2$.

Concentration factors (7.1.1) for a two-phase system are

$$\boldsymbol{A}_2^s = [\boldsymbol{I} + \boldsymbol{P}_s(\boldsymbol{L}_2 - \boldsymbol{L})]^{-1} \quad \boldsymbol{B}_2^s = [\boldsymbol{I} + \boldsymbol{Q}_s(\boldsymbol{M}_2 - \boldsymbol{M})]^{-1} \tag{7.1.11}$$

where

$$\boldsymbol{P}_s = \left(\boldsymbol{L}_s^* + \boldsymbol{L}\right)^{-1} \quad \boldsymbol{Q}_s = \boldsymbol{L}\left(\boldsymbol{I} - \boldsymbol{P}_s\boldsymbol{L}\right) = \left(\boldsymbol{M}_s^* + \boldsymbol{M}\right)^{-1} \tag{7.1.12}$$

Each superscript $s = 2, \ldots n$, denotes a particular shape and/or alignment of an inhomogeneity $\boldsymbol{L}_2$. The $\boldsymbol{P}_s$ or $\boldsymbol{Q}_s$ in (7.1.11) depend only on the overall $\boldsymbol{L}$ or $\boldsymbol{M}$, and not directly on $\boldsymbol{L}_r$ or $\boldsymbol{M}_r$ of either phase.

Overall stiffness of such two-phase systems follows from (7.1.2) as

$$\boldsymbol{L} = \boldsymbol{L}_1 + \sum_{s=2}^{n} c_1^s\left(\boldsymbol{L}_2 - \boldsymbol{L}_1\right)\boldsymbol{A}_2^s = \boldsymbol{L}_1 + \left(\boldsymbol{L}_2 - \boldsymbol{L}_1\right)\sum_{s=2}^{n} c_2^s\boldsymbol{A}_2^s \tag{7.1.13}$$

where the phase volume fractions $c_1 + \Sigma c_2^s = 1$ and

$$\boldsymbol{A}_2^s = [\boldsymbol{I} + \boldsymbol{P}_s\left(\boldsymbol{L}_2 - \boldsymbol{L}\right)]^{-1} = \left(\boldsymbol{L}_s^* + \boldsymbol{L}_2\right)^{-1}\left(\boldsymbol{L}_s^* + \boldsymbol{L}\right) \tag{7.1.14}$$

As an example of the self-consistent moduli prediction for a two-phase composite with different reinforcement shapes, Benveniste et al. (1991b), selected a two-phase composite with a Ti_3Al matrix, reinforced by SiC fibers of circular crossection, and by SiC circular discs. Both the fiber axes and the normals to the disks planes are aligned with the x_3–axis of a Cartesian system. The phases are isotropic, and have the following elastic moduli

$$\left.\begin{aligned} \mathrm{Ti_3Al}: \quad & E_1 = 96.5\ \mathrm{GPa}, \quad G_1 = 37.1\ \mathrm{GPa} \\ \mathrm{SiC}: \quad & E_2 = 431.0\mathrm{GPa}, \quad G_2 = 172.0\ \mathrm{GPa} \end{aligned}\right\} \tag{7.1.15}$$

The self-consistent estimate (7.1.16) of the overall stiffness of this systems, was obtained as the ninth iteration of the solution of (7.1.13) and (7.1.14). It is expected that diagonal symmetry of the overall stiffness may also be found in other reinforcement shape combinations in two-phase systems. However replacement of the above elastic moduli of the circular discs by a third set of different moduli renders a stiffness estimate which is not diagonally symmetric. That can be verified as an exercise.

$$(\boldsymbol{L})_9 = \begin{bmatrix} 269.95 & 95.45 & 82.80 & 0 & 0 & 0 \\ & 269.95 & 82.80 & 0 & 0 & 0 \\ & & 249.24 & 0 & 0 & 0 \\ & & & 64.44 & 0 & 0 \\ & \textit{sym.} & & & 64.44 & \\ & & & & & 87.25 \end{bmatrix} \mathrm{GPa} \tag{7.1.16}$$

7.2 The Mori-Tanaka Method (M-T)

The presented form of this method was proposed by Benveniste (1987a), who interpreted a brief derivation by Mori and Tanaka (1973) of the average stress caused by transformed homogeneous inclusions in a large matrix volume. In the context of the procedures leading to the estimates of concentration factors in Sect. 6.3.1, their result suggests that the inclusion should embedded in a large volume of the matrix phase, and subjected to an average matrix stress. A different form of the method was suggested by Weng (1984). Numerous applications to many different problems have appeared in the literature. For example, composites with coated fibers were analyzed by Benveniste et al. (1989) and by Chen et al. (1990). Porous materials were treated by Zhao et al. (1989). Specific results for many typical composite systems were derived by Chen et al. (1992).

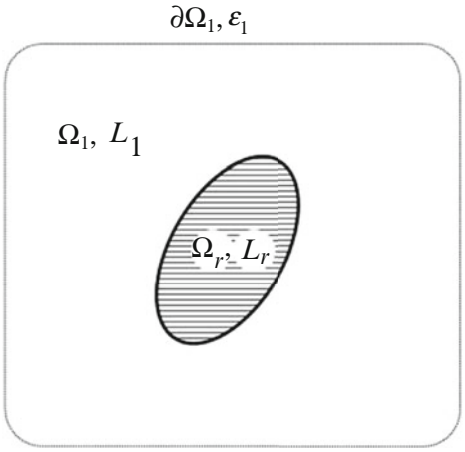

Fig. 7.2 The Mori-Tanaka (M-T) model. Stiffnesses of the inhomogeneity and matrix are denoted by $\boldsymbol{L}_r$ and by $\boldsymbol{L}_1 = \boldsymbol{L}_0$

7.2.1 *Elastic Moduli and Local Fields of Multiphase Composites*

This AFA method approximates interaction between phases in a matrix-based system by regarding each reinforcement $\boldsymbol{L}_r$ as a solitary inhomogeneity Ω_r embedded in a large volume Ω_1 of the matrix $\boldsymbol{L}_1$. The as yet unknown average strain $\boldsymbol{\varepsilon}_1$ or stress $\boldsymbol{\sigma}_1$ in the matrix phase are applied as a uniform strain or stress at a remote boundary $\partial\Omega_1$, Fig. 7.2.

The inclusion-based form of this method utilizes (4.2.14), for the average strain $\boldsymbol{\varepsilon}_r$ in a single inhomogeneity $\boldsymbol{L}_r$

$$\boldsymbol{\varepsilon}_r = \boldsymbol{T}_r \boldsymbol{\varepsilon}_1 \quad \boldsymbol{T}_r = [\boldsymbol{I} + \boldsymbol{P}\,(\boldsymbol{L}_r - \boldsymbol{L}_1)]^{-1} \tag{7.2.1}$$

where both the Eshelby tensor $\boldsymbol{S} = \boldsymbol{P}\boldsymbol{L}_1$ and the $\boldsymbol{P} = \left(\boldsymbol{L}^* + \boldsymbol{L}_1\right)^{-1}$ and $\boldsymbol{L}^*$ tensors in (4.2.9) are evaluated in $\boldsymbol{L}_1$.

When a *uniform overall strain* $\boldsymbol{\varepsilon}^0$ is applied to the representative volume of a composite material, the matrix average strain $\boldsymbol{\varepsilon}_1$ is found by referring to (3.5.5) which indicates that $\sum c_r \boldsymbol{\varepsilon}_r = (\sum c_r \boldsymbol{T}_r)\,\boldsymbol{\varepsilon}_1 = \boldsymbol{\varepsilon}^0$. Of course, $\boldsymbol{T}_1 \boldsymbol{\varepsilon}_1 = \boldsymbol{\varepsilon}_1$, since the partial strain concentration factor of the matrix, $\boldsymbol{T}_1 = \boldsymbol{I}$. Notice the difference from the dilute approximation result (4.4.3). Therefore, the local strain averages are

$$\boldsymbol{\varepsilon}_1 = \boldsymbol{A}_1 \boldsymbol{\varepsilon}^0 = \left[c_1 \boldsymbol{I} + \sum_{s=2}^{n} c_s \boldsymbol{T}_s\right]^{-1} \boldsymbol{\varepsilon}^0 \quad \boldsymbol{\varepsilon}_r = \boldsymbol{A}_r \boldsymbol{\varepsilon}^0 = \boldsymbol{T}_r \left[c_1 \boldsymbol{I} + \sum_{s=2}^{n} c_s \boldsymbol{T}_s\right]^{-1} \boldsymbol{\varepsilon}^0 \tag{7.2.2}$$

Overall stiffness of a multiphase system, $r = 1, 2, \ldots, n$, is then found as

$$\left.\begin{aligned} \boldsymbol{L} &= \sum_{r=1}^{n} c_r \boldsymbol{L}_r \boldsymbol{A}_r = \left[\sum_{r=1}^{n} c_r \boldsymbol{L}_r \boldsymbol{T}_r\right]\left[\sum_{s=1}^{n} c_s \boldsymbol{T}_s\right]^{-1} \\ &= \boldsymbol{L}_1 + \left[\sum_{r=2}^{n} c_r \left(\boldsymbol{L}_r - \boldsymbol{L}_1\right) \boldsymbol{T}_r\right]\left[\sum_{s=1}^{n} c_s \boldsymbol{T}_s\right]^{-1} \end{aligned}\right\} \tag{7.2.3}$$

After some algebra, this form can be converted to $(6.3.5)_2$, with both $\boldsymbol{L}^*$ and $\boldsymbol{P}$ evaluated in the matrix, $\boldsymbol{L}_0 = \boldsymbol{L}_1$ as shown in (7.2.29).

For a two-phase composite $r = 1,\ 2$, with matrix $\boldsymbol{L}_1$ of volume fraction c_1, and reinforcements $\boldsymbol{L}_2$, the corresponding expressions are

$$\left.\begin{aligned} \boldsymbol{A}_1 &= \left[c_1 \boldsymbol{I} + (1 - c_1)[\boldsymbol{I} + \boldsymbol{P}(\boldsymbol{L}_2 - \boldsymbol{L}_1)]^{-1}\right]^{-1} \\ \boldsymbol{A}_2 &= \left[(1 - c_1)\, \boldsymbol{I} + c_1 \boldsymbol{P}\, (\boldsymbol{L}_2 - \boldsymbol{L}_1)\right]^{-1} \end{aligned}\right\} \tag{7.2.4}$$

$$\boldsymbol{L} = \boldsymbol{L}_1 + (1 - c_1)\, (\boldsymbol{L}_2 - \boldsymbol{L}_1)\, [\boldsymbol{I} + c_1 \boldsymbol{P}\, (\boldsymbol{L}_2 - \boldsymbol{L}_1)]^{-1} \tag{7.2.5}$$

Equation (7.2.26) below shows a more general form of the two-phase composite stiffness, which admits different shapes and alignments, or different $\boldsymbol{P}$ tensors for the inhomogeneities of phase $\boldsymbol{L}_2$.

When the composite is subjected to a *uniform overall stress* $\boldsymbol{\sigma}^0$, the above sequence is modified. It starts with the estimate of the average stress in each phase embedded in a large matrix volume loaded by a uniform stress $\boldsymbol{\sigma}_1$

$$\boldsymbol{\sigma}_r = \boldsymbol{W}_r \boldsymbol{\sigma}_1 \quad \boldsymbol{W}_r = [\boldsymbol{I} + \boldsymbol{Q}\, (\boldsymbol{M}_r - \boldsymbol{M}_1)]^{-1} \tag{7.2.6}$$

where $\boldsymbol{Q} = \boldsymbol{L}_1 (\boldsymbol{I} - \boldsymbol{P}\boldsymbol{L}_1) = \left(\boldsymbol{M}^* + \boldsymbol{M}_1\right)^{-1}$ and again, $\boldsymbol{W}_1 = \boldsymbol{I}$. Since $(\sum c_r \boldsymbol{W}_r)\, \boldsymbol{\sigma}_1 = \boldsymbol{\sigma}^0$, the local stress average are

$$\boldsymbol{\sigma}_r = \boldsymbol{B}_r \boldsymbol{\sigma}^0 = \boldsymbol{W}_r \left[c_1 \boldsymbol{I} + \sum_{s=2}^{n} c_s \boldsymbol{W}_s\right]^{-1} \boldsymbol{\sigma}^0 \quad \sum_{s=1}^{n} c_s \boldsymbol{B}_s = \boldsymbol{I} \tag{7.2.7}$$

The overall compliance of the composite aggregate follows from (6.3.6) as

$$\left.\begin{aligned} \boldsymbol{M} &= \sum_{r=1}^{n} c_r \boldsymbol{M}_r \boldsymbol{B}_r = \left[\sum_{r=1}^{n} c_r \boldsymbol{M}_r \boldsymbol{W}_r\right]\left[\sum_{s=1}^{n} c_s \boldsymbol{W}_s\right]^{-1} \\ &= \boldsymbol{M}_1 + \left[\sum_{r=2}^{n} c_r \left(\boldsymbol{M}_r - \boldsymbol{M}_1\right) \boldsymbol{W}_r\right]\left[\sum_{s=1}^{n} c_s \boldsymbol{W}_s\right]^{-1} \end{aligned}\right\} \tag{7.2.8}$$

For two-phase systems with matrix $\boldsymbol{M}_1$ of volume fraction c_1

$$\boldsymbol{B}_1=\Big[c_1\boldsymbol{I}+(1-c_1)\,[\boldsymbol{I}+\boldsymbol{Q}\,(\boldsymbol{M}_2-\boldsymbol{M}_1)]^{-1}\Big]^{-1}\quad \boldsymbol{B}_2=[\boldsymbol{I}+c_1\boldsymbol{Q}\,(\boldsymbol{M}_2-\boldsymbol{M}_1)]^{-1} \tag{7.2.9}$$

$$\boldsymbol{M}=\boldsymbol{M}_1+(1-c_1)\,(\boldsymbol{M}_2-\boldsymbol{M}_1)\,[\boldsymbol{I}+c_1\boldsymbol{Q}\,(\boldsymbol{M}_2-\boldsymbol{M}_1)]^{-1} \tag{7.2.10}$$

If for all r, the difference $(\boldsymbol{L}_1-\boldsymbol{L}_r)$ is positive [or negative] semi-definite, then, according to the bounding theorems (6.2.16), the method delivers the upper [or lower] Hashin-Shtrikman bound on the overall $\boldsymbol{L}$. These and other connections with the bounds were examined by Norris (1989) and Weng (1990, 1992). In composites which display a large contrast between constituent moduli, the Mori-Tanaka method tends to underestimate [or overestimate], even at moderate concentrations, the actual overall elastic moduli, c. f., Fig. 6.5. However, in applications to two-phase media containing voids and/or cracks dispersed in a homogeneous matrix, the method delivers a Hashin-Shtrikman upper bound which, unlike the self-consistent estimate, approaches zero value only when so does the matrix volume fraction.

7.2.2 *Elastic Moduli of Fibrous, Particulate and Layered Composites*

For a *two-phase fiber composite*, with transversely isotropic fiber and matrix phases, where phase elastic moduli denoted by k_f, m_f and p_f and k_m, m_m and p_m, the Mori-Tanaka method estimates of the corresponding overall moduli are

$$k=\frac{c_f k_f(k_m+m_m)+c_m k_m(k_f+m_m)}{c_f(k_m+m_m)+c_m(k_f+m_m)} \tag{7.2.11}$$

$$m=\frac{m_f m_m(k_m+2m_m)+k_m m_m(c_f m_f+c_m m_m)}{k_m m_m+(k_m+2m_m)(c_f m_m+c_m m_f)} \tag{7.2.12}$$

$$p=\frac{2c_f p_f p_m+c_m(p_f p_m+p_m^2)}{2c_f p_m+c_m(p_f+p_m)} \tag{7.2.13}$$

The remaining two moduli follow from the universal connections (3.9.4) as

$$\left.\begin{aligned} l&=\frac{c_f l_f(k_m+m_m)+c_m l_m(k_f+m_m)}{c_f(k_m+m_m)+c_m(k_f+m_m)}\\ n-c_f n_f-c_m n_m&=(l-c_f l_f-c_m l_m)\frac{(l_f-l_m)}{(k_f-k_m)}\end{aligned}\right\} \tag{7.2.14}$$

The above axisymmetric moduli k, l, and n, coincide with those of a single composite cylinder that has a fiber core and matrix shell (Hill 1964), and also with those of an assemblage of such composite cylinders shown in Fig. 6.1. It can be verified that the same results are obtained from the Walpole's formulae (6.3.27) when the comparison medium moduli are selected there as equal to those of the matrix, i.e., $k_0 = k_m,\ m_0 = m_m,\ p_0 = p_m$. Estimates of overall elastic moduli of *multi-phase aligned fiber composites* can be found in Chen et al. (1992).

Figure 6.5 shows the M-T estimate of the overall transverse shear modulus m and the transverse Young's modulus E_T, for a glass fiber/epoxy composite. Since the difference between the fiber and matrix stiffness $\left(\boldsymbol{L}_f - \boldsymbol{L}_m\right)$ is positive definite and $\boldsymbol{L}_m = \boldsymbol{L}_1$ is the comparison medium in this case, the M-T estimates coincide with the H-S lower bounds $m^{(-)}$ and $E_T^{(-)}$.

For isotropic particulate composites with an isotropic matrix $r = 1$ containing isotropic spherical reinforcements $r = 2$, Benveniste (1987a) found the Mori-Tanaka method estimates of the bulk and shear moduli as

$$\left.\begin{aligned} \frac{K - K_1}{K_2 - K_1} &= \frac{c_2}{1 + c_1(K_2 - K_1)(K_1 + 4G_1/3)^{-1}} \\ \frac{G - G_1}{G_2 - G_1} &= \frac{c_2}{1 + c_1(G_2 - G_1)\left(G_1 + \dfrac{G_1(9K_1 + 8G_1)}{6(K_1 + 2G_1)}\right)^{-1}} \end{aligned}\right\} \tag{7.2.15}$$

When $G_1 < G_2,\ K_1 < K_2$, these expressions are equivalent to the Hashin-Shtrikman lower bounds and they also follow from Walpole's formulae (6.3.26) for $G_0 = G_1,\ K_0 = K_1$. The ratio G/G_1 found from (7.2.15) is also equal to G/G_m in (6.5.13). Upper bounds are obtained by exchanging the phase subscripts in (7.2.15).

In the P100/Cu composite, Fig. 6.2, the Mori-Tanaka estimates coincide with the upper bounds $k^{(+)}$, $m^{(+)}$ and $p^{(+)}$, and the lower bounds $n^{(-)}$ and $E_A^{(-)}$. In the S-glass/epoxy fiber composite considered in Fig. 6.4, the Mori Tanaka estimate of the overall shear modulus G_T coincides with the H-S lower bound $G^{(-)}$. In both illustrations, the method delivers a fairly accurate prediction of the relevant elastic modulus.

Another measure of accuracy of the method was presented by Christensen et al. (1992). They evaluated the percent error in the shear modulus of a particulate composite, compared to the generalized self-consistent estimate of Sect. 6.5, for different combinations of phase moduli and particle volume fractions. As expected, the error was magnified by large contrast between phase moduli, but it turned out to be less than 10% for $c_2 \leq 0.4$ at $\nu_1 = 1/2,\ \nu_2 = 1/3$, and $0.2 < G_2/G_1 < 10$. At higher particle concentrations, the Mori-Tanaka method tends to underestimate the effective shear modulus obtained from experiments and the generalized self-consistent method, as illustrated in Fig. 6.5.

Next, we consider a *multi-layer composite aggregate* consisting of platelets or flat discs $r = 2, 3, \ldots, n$, all bonded to a continuous matrix $r = 1$, and aligned such that

their normals are parallel to the x_1–axis. Since the in-plane size of the discs need not be limited, this composite is equivalent to flat multilayer plates or solids, without a distinct matrix, which appear in assorted technological applications, including layered coatings, soil and rock formations, and sediments. Each layer is regarded as transversely isotropic, with the x_1–axis of rotational symmetry normal to the layer plane. Transverse isotropy prevails on the overall scale, hence there are five independent overall elastic moduli (2.3.3), exhibiting the interrelations.

$$\left.\begin{aligned} m &= \sum_{r=1}^{n} c_r m_r \quad n^{-1} = \sum_{r=1}^{n} c_r (n_r)^{-1} \quad p^{-1} = \sum_{r=1}^{n} c_r (p_r)^{-1} \\ k &= l^2/n + \sum_{r=1}^{n} c_r (k_r - l_r^2/n_r) \quad l/n = \sum_{r=1}^{n} c_r l_r/n_r \end{aligned}\right\} \tag{7.2.16}$$

These results agree with the self-consistent estimates found by Laws (1974, eqns (42)–(46)) and also with those found by Postma (1955) for multilayered solids.

7.2.3 *Elastic Moduli of Solids Containing Randomly Oriented Reinforcements and Cracks*

Here we find an estimate of overall stiffness of a multi-phase and matrix-based composite, reinforced by randomly oriented but otherwise identical ellipsoidal inhomogeneities, such that the composite is isotropic on the macroscale. As already mentioned, this result can be found in terms of averages over all orientations in Sect. 2.2.10, of the orientation dependent terms in the overall stiffness (7.2.3). Those are, of course, the strain concentration factors (7.2.1) that depend on both $\boldsymbol{P}$ and $\boldsymbol{L}_r$. Using curly brackets for the averages, the desired overall stiffness is

$$\boldsymbol{L} = \boldsymbol{L}_1 + \left[\sum_{s=2}^{n} c_s \{(\boldsymbol{L}_s - \boldsymbol{L}_1)\, \boldsymbol{T}_s\}\right] \left[\sum_{s=1}^{n} c_s \{\boldsymbol{T}_s\}\right]^{-1} \tag{7.2.17}$$

Analytic derivations of the scalars in the orientation average $\{\boldsymbol{T}_s\}$, for different oblate and prolate spheroidal shapes, including spheres, needles, disks and penny-shaped cracks, were carried out by Kröner (1958), Wu (1966) and Berryman (1980), who also shows corrections to earlier solutions, and denotes $a = P$, $b = Q$. In numerical evaluation of the orientation averages, the nonzero coefficients of the (6×6) matrix $\{T_{\alpha\beta}\} = \{T_{\alpha\beta}\}^{\mathrm{T}}$ follow from (2.2.30) and (2.2.33) in terms of the coefficients of $T_{\alpha\beta}$.

Chen et al. (1992) found the orientation averages of the moduli (7.2.17), for matrix based composites consisting of an isotropic matrix $\boldsymbol{L}_1$, reinforced by

randomly oriented short fibers, distribution of which is isotropic on the macroscale. General forms of the averaged moduli are

$$\left.\begin{aligned} K &= K_1 + \frac{1}{3}\sum_{r=2}^{n} c_r\,(\delta_r - 3K_1\alpha_r)\left[c_1 + \sum_{r=2}^{n} c_r\alpha_r\right]^{-1} \\ G &= G_1 + \frac{1}{2}\sum_{r=2}^{n} c_r\,(\eta_r - 2G_1\beta_r)\left[c_1 + \sum_{r=2}^{n} c_r\beta_r\right]^{-1} \end{aligned}\right\} \tag{7.2.18}$$

where the parameters $\alpha_r, \beta_r, \delta_r, \eta_r$ depend on the moduli and geometry of the phases. K_1, G_1 are the bulk and shear moduli of the matrix, and each fiber orientation has a different stiffness $\boldsymbol{L}_r$. Berryman (1980) derived expressions for their evaluation for cracks and other shapes.

When the fibers are modeled by randomly distributed very long prolate spheroids, made of an isotropic material moduli with K_2 and G_2, the effective overall bulk and shear moduli K and G are

$$\left.\begin{aligned} K &= K_2 - c_1(K_2 - K_1)\left[1 - c_2\frac{3(K_2 - K_1)}{3(G_1 + K_2) + G_2}\right]^{-1} \\ G &= G_2 - c_1(G_2 - G_1) \\ &\quad\times\left[1 - \frac{(G_2 - G_1)}{5[3(G_1 + K_2) + G_2]} - \frac{2}{5}c_2(G_2 - G_1)\left(\frac{1}{(G_2 + \gamma_1)} + \frac{1}{(G_2 + G_1)}\right)\right]^{-1} \end{aligned}\right\} \tag{7.2.19}$$

For the isotropic matrix, $\gamma_1 = G_1(3K_1 + G_1)/(3K_1 + 7G_1)$.

Of interest in many applications are composites reinforced by relatively short, randomly distributed fibers which are transversely isotropic, such as carbon, with moduli k_r, l_r, m_r, n_r, and p_r in the local coordinates aligned with fiber axis. The fiber diameter is usually <20 μm, hence the fiber aspect ratio is very high. For such short fiber composite, the coefficients in (7.2.18) are

$$\left.\begin{aligned} \alpha_r &= \frac{3(K_1 + G_1) + k_r - l_r}{3(G_1 + k_r)} \qquad \beta_r = \frac{1}{5}\left[\frac{4G_1 + 2k_r + l_r}{3(G_1 + k_r)} + \frac{4G_1}{G_1 + p_r} + \frac{2(G_1 + \gamma_1)}{m_r + \gamma_1}\right] \\ \delta_r &= \frac{1}{3}\left[2l_r + n_r + \frac{(2k_r + l_r)(3K_1 + 2G_1 - l_r)}{G_1 + k_r}\right] \\ \eta_r &= \frac{1}{5} \\ &\quad\times\left[\frac{2}{3}(n_r - l_r) + \frac{8G_1m_r(3K_1 + 4G_1)}{(3K_1 + 7G_1)m_r + (3K_1 + G_1)G_1} + \frac{8G_1p_r}{G_1 + p_r} + \frac{(4G_1 + 2l_r)(k_r - l_r)}{3(G_1 + k_r)}\right] \end{aligned}\right\} \tag{7.2.20}$$

In addition to the above results, Chen et al. (1992) provide similar parameters for composites reinforced by randomly oriented, transversely isotropic platelets or disks of vanishing thickness. When the disks are isotropic, the overall bulk and shear moduli are

$$\left.\begin{aligned} K &= K_2 - c_1(K_2 - K_1)\left[1 - c_2\frac{3(K_2 - K_1)}{3K_2 + 4G_2}\right]^{-1} \\ G &= G_2 - c_1(G_2 - G_1)\left[1 - \frac{2}{5}c_2\left(\frac{2(G_2 - G_1)}{3K_2 + 4G_2} + \frac{G_2 - G_1}{G_2}\right)\right]^{-1} \end{aligned}\right\} \tag{7.2.21}$$

This M-T result is identical to that predicted by the self-consistent method (Walpole 1969, eqn. (61)). At a given concentration, the platelets yield higher overall moduli than do needles or short fibers, as first observed by Wu (1966). Another analysis of overall elastic moduli of randomly reinforced composites was developed by Christensen and Waals (1972).

The above results apply only to composites reinforced by a spatially random distribution of short fibers or other reinforcements. However, preferential fiber orientations can develop, for example, in systems produced by injection of liquid polymer and short fiber mixtures into final shape moulds. Actual distributions are not easily detected, but when they are, they can be related to overall material symmetry of the composite by certain orientation distribution functions (Ferrari and Johnson 1989). Actual material symmetry can be deduced, for example, from directionally dependent velocities of ultrasonic waves (Sayers 1992; Dunn and Ledbetter 2000).

The Mori-Tanaka method also predicts overall properties of solids containing a distribution of *cavities and cracks*. As long as the cavities are approximated by spherical inhomogeneities with vanishing stiffness, the overall moduli can be obtained by letting $G_2 = K_2 = 0$ in (7.2.15).

Using Berryman's (1980) results, Benveniste (1987a) found the moduli for a solid with randomly oriented penny-shaped cracks of radius a as

$$\frac{K}{K_1} = \left[1 + \frac{16\eta(1 - \nu_1^2)}{9(1 - 2\nu_1)}\right]^{-1} \qquad \frac{G}{G_1} = \left[1 + \frac{32\eta(1 - \nu_1)(5 - \nu_1)}{45(2 - \nu_1)}\right]^{-1} \tag{7.2.22}$$

where $\eta = Na^3/V$, and N/V is the number of cracks in a unit volume V. Both the 'matrix' and the cracked medium are isotropic, with elastic moduli K_1, G_1, ν_1 and K, G, respectively. In contrast to the self-consistent prediction of these moduli by Budiansky and O'Connell (1976), who found zero moduli at $(\varepsilon) = \eta \to 9/16$, the above expressions predict only a gradual decrease with growing η. At very low crack concentrations, for $\eta \ll 1$, there is agreement with the dilute estimate by Walsh (1965). Of course, crack configurations yielding vanishing elastic moduli can be constructed or imagined with different values of η, including those obtained

by the self-consistent method. However, as shown by (7.1.14), the method also predicts zero shear modulus of a matrix with 0.5 volume fraction of spherical cavities.

7.2.4 Restrictions on Constituent Shape and Alignment

In applications to multiphase systems, the diagonally symmetric Mori-Tanaka estimates of overall stiffness $\boldsymbol{L}=\boldsymbol{L}^{\mathrm{T}}$ and compliance $\boldsymbol{M}=\boldsymbol{M}^{\mathrm{T}}$ follow from (6.3.5) and (6.3.6), providing that all inhomogeneities have the same shape and alignment, described by a single $\boldsymbol{P}$ or $\boldsymbol{Q}$ tensor. Here we show that the said symmetry can also be established in applications of the method to two-phase composites, consisting of the matrix phase $\boldsymbol{L}_1$ and many perfectly bonded ellipsoidal inhomogeneities $s = 2,3,\ldots,n$ of phase $\boldsymbol{L}_2$, which may have different shape and/or alignment, described by $\boldsymbol{P}_s$ or $\boldsymbol{L}_s^*$. The proof was derived by Benveniste et al. (1991b).

According to (7.2.1), the local strain averages are $\boldsymbol{\varepsilon}_s = \boldsymbol{T}_s\boldsymbol{\varepsilon}_1 = [\boldsymbol{I}+\boldsymbol{P}_s(\boldsymbol{L}_2-\boldsymbol{L}_1)]^{-1}\boldsymbol{\varepsilon}_1$, where $\boldsymbol{\varepsilon}_1$ is the average strain in the matrix $r = 1$ and $s = 2,3,\ldots,n$, while $\boldsymbol{\varepsilon}_1 = \boldsymbol{T}_1\boldsymbol{\varepsilon}_1$ and $\boldsymbol{T}_1 = \boldsymbol{I}$. A more convenient form of the partial concentration factors $\boldsymbol{T}_s$ is now derived, by defining a new tensor $\boldsymbol{P}_1^s$.

$$\left.\begin{aligned} &\boldsymbol{P}_s(\boldsymbol{L}_2-\boldsymbol{L}_1)\boldsymbol{P}_1^s = \boldsymbol{P}_s-\boldsymbol{P}_1^s \Rightarrow (\boldsymbol{L}_2-\boldsymbol{L}_1) = \left(\boldsymbol{P}_1^s\right)^{-1}-(\boldsymbol{P}_s)^{-1} \\ &\boldsymbol{P}_s(\boldsymbol{L}_2-\boldsymbol{L}_1) = \boldsymbol{P}_s\left(\boldsymbol{P}_1^s\right)^{-1}-\boldsymbol{I} \quad \boldsymbol{P}_1^s(\boldsymbol{L}_2-\boldsymbol{L}_1) = \boldsymbol{I}-\boldsymbol{P}_1^s(\boldsymbol{P}_s)^{-1} \end{aligned}\right\} \tag{7.2.23}$$

Since $\boldsymbol{P}_s=\left(\boldsymbol{L}_s^*+\boldsymbol{L}_1\right)^{-1}=\boldsymbol{P}_s{}^{\mathrm{T}}$, this shows that $\boldsymbol{P}_1^s=[(\boldsymbol{L}_2-\boldsymbol{L}_1)+(\boldsymbol{P}_s)^{-1}]^{-1} = (\boldsymbol{P}_1^s)^{\mathrm{T}}$and also that $\boldsymbol{P}_1^s = \left(\boldsymbol{L}_s^*+\boldsymbol{L}_2\right)^{-1}$. The partial strain concentration factors can be written in a modified form

$$(\boldsymbol{T}_s)^{-1}=\boldsymbol{I}+\boldsymbol{P}_s(\boldsymbol{L}_2-\boldsymbol{L}_1)=\boldsymbol{P}_s\left(\boldsymbol{P}_1^s\right)^{-1} \Rightarrow \boldsymbol{T}_s=\boldsymbol{P}_1^s(\boldsymbol{P}_s)^{-1}=\boldsymbol{I}-\boldsymbol{P}_1^s(\boldsymbol{L}_2-\boldsymbol{L}_1) \tag{7.2.24}$$

The overall stiffness of a matrix-based two-phase system $\boldsymbol{L}_1$, $\boldsymbol{L}_2$, with subvolumes $s = 1,2,3,\ldots,n$ that have different shapes and alignment for $s \geq 2$, follows from (7.2.3) as

$$\left.\begin{aligned} \boldsymbol{L} &= \boldsymbol{L}_1+\sum_{s=2}^{n} c_s(\boldsymbol{L}_2-\boldsymbol{L}_1)\boldsymbol{A}_s \\ &= \boldsymbol{L}_1-(\boldsymbol{L}_2-\boldsymbol{L}_1)\left[c_1\boldsymbol{I}-\sum_{s=1}^{n} c_s\boldsymbol{T}_s\right]\left[\sum_{s=1}^{n} c_s\boldsymbol{T}_s\right]^{-1} \end{aligned}\right\} \tag{7.2.25}$$

Substitution of the modified $\boldsymbol{T}_s$ yields the overall stiffness in the following diagonally symmetric form, which is then adjusted using (7.2.23), to depend only on the $\boldsymbol{P}_s$ matrices that describe shape and alignment of different inhomogeneities $\boldsymbol{L}_2$.

$$\left.\begin{aligned}\boldsymbol{L} &= \boldsymbol{L}_2 - (\boldsymbol{L}_2 - \boldsymbol{L}_1)\, c_1 \left[\sum_{s=1}^{n} c_s \left[\boldsymbol{I} - \boldsymbol{P}_1^s (\boldsymbol{L}_2 - \boldsymbol{L}_1)\right]\right]^{-1} \\ &= \boldsymbol{L}_2 - c_1 \left[\sum_{s=1}^{n} c_s \left[(\boldsymbol{L}_2 - \boldsymbol{L}_1)^{-1} - \boldsymbol{P}_1^s\right]\right]^{-1} = \boldsymbol{L}^{\mathrm{T}} \\ &= \boldsymbol{L}_2 - c_1 \left[\sum_{s=1}^{n} c_s \left\{(\boldsymbol{L}_2 - \boldsymbol{L}_1)^{-1} - \left[(\boldsymbol{L}_2 - \boldsymbol{L}_1) + (\boldsymbol{P}_s)^{-1}\right]^{-1}\right\}\right]^{-1}\end{aligned}\right\} \tag{7.2.26}$$

Therefore, two-phase systems with arbitrary phase geometry are admissible in implementation of the Mori-Tanaka method, as they appear to be in the self-consistent method. In contrast, applications of either of the two procedures to multiphase systems require all inhomogeneities to have the same shape and alignment, or spatial distributions amenable to orientation averaging. As already indicated in the opening paragraph, the inhomogeneities need not be of the same size, but they should belong to the same size scale. The shape and alignment constraints are relaxed by the double-inclusion model *CB*, in Sect. 7.4.4 and Fig. 7.7.

In closing this section, we convert (7.2.3) to a diagonally symmetric form, valid for multiphase composite systems with the same shape and alignment of the reinforcement, given by one pair of $\boldsymbol{L}^*$ and $\boldsymbol{P} = \left(\boldsymbol{L}^* + \boldsymbol{L}_1\right)^{-1}$ tensors, both evaluated in the matrix $\boldsymbol{L}_1$. Recall from (7.2.1) that $\boldsymbol{T}_r = [\boldsymbol{I} + \boldsymbol{P}\,(\boldsymbol{L}_r - \boldsymbol{L}_1)]^{-1} = \left(\boldsymbol{L}^* + \boldsymbol{L}_r\right)^{-1}\left(\boldsymbol{L}^* + \boldsymbol{L}_1\right)$. Substitute this into (7.2.3), written as

$$\left.\begin{aligned}\boldsymbol{L} &= \sum_{r=1}^{n} c_r \boldsymbol{L}_r \boldsymbol{A}_r = \left[\sum_{r=1}^{n} c_r \boldsymbol{L}_r \boldsymbol{T}_r\right]\left[\sum_{r=1}^{n} c_r \boldsymbol{T}_r\right]^{-1} \\ &= \left[\sum_{r=1}^{n} c_r \boldsymbol{L}_r \left(\boldsymbol{L}^* + \boldsymbol{L}_r\right)^{-1}\right]\left[\sum_{r=1}^{n} c_r \left(\boldsymbol{L}^* + \boldsymbol{L}_r\right)^{-1}\right]^{-1}\end{aligned}\right\} \tag{7.2.27}$$

and use (7.1.3) to find

$$\sum_{r=1}^{n} c_r \boldsymbol{L}_r \left(\boldsymbol{L}^* + \boldsymbol{L}_r\right)^{-1} = \boldsymbol{I} - \boldsymbol{L}^* \sum_{r=1}^{n} c_r \left(\boldsymbol{L}^* + \boldsymbol{L}_r\right)^{-1} \tag{7.2.28}$$

Finally, take this into (7.2.27) to get the last equality in (6.3.5)

$$\boldsymbol{L} = \left[\sum_{r=1}^{n} c_r \left(\boldsymbol{L}^* + \boldsymbol{L}_r\right)^{-1}\right]^{-1} - \boldsymbol{L}^* = \boldsymbol{L}^{\mathrm{T}} \tag{7.2.29}$$

This confirms that the Mori-Tanaka method yields the stiffness predicted by (6.3.5), providing that both $\boldsymbol{L}^*$ and $\boldsymbol{P}$ are evaluated in the matrix, $\boldsymbol{L}_0 = \boldsymbol{L}_1$. Therefore, either the self-consistent or the Mori-Tanaka predictions of overall stiffness and compliance can be generated by solving inhomogeneity problems in Figs. 7.1 or 7.2, or by using (6.3.5) and (6.3.6), with $\boldsymbol{L}_0 = \boldsymbol{L}$ or $\boldsymbol{L}_0 = \boldsymbol{L}_1$ respectively. Both approaches require evaluation of the $\boldsymbol{P}$ tensor, but only in the matrix phase for the M-T method. Recall that (6.3.5) also yields the H-S bounds, as described in Sect. 6.3.2.

7.2.5 Derivation of Effective Phase Moduli

Experimentally determined overall moduli of a two-phase composite material, and those of one phase may be used to estimate the effective moduli of the other phase. For example, mechanical testing of thin fibers and filaments is limited to simple tension and torsion, which yield the longitudinal Young's modulus $\boldsymbol{E}_{11}$ and if the fiber is regarded as transversely isotropic according to (2.3.3), the longitudinal shear modulus p. The remaining elastic moduli of transversely isotropic fibers, such as carbon or graphite fibers, cannot be found by direct measurement. However, estimates of effective magnitudes of the unknown moduli can be derived from experimentally measured overall or macroscopic elastic moduli of two-phase aligned fiber composites reinforced by such fibers. Matrix moduli and phase volume fractions also need to be known. Composite test samples used in such tests should be fabricated in a manner that assures good fiber alignment and statistically homogeneous distribution of the fibers in the transverse plane, which may not be found in all standard fibrous plies. The same approach can yield effective moduli of reinforcements consisting of particles of irregular shape and varied composition.

Loading conditions that provide the overall moduli of fibrous systems are described in Table 2.4. The measured values are used to generate coefficients of the compliance and stiffness $\boldsymbol{M}$ and $\boldsymbol{L}$ in (2.3.2) and (2.3.3). Together with the known moduli of the composite matrix and the matrix volume fraction c_1, the overall elastic moduli k, m, and p included in the coefficients of $\boldsymbol{M}$ and $\boldsymbol{L}$ are substituted into expressions for self-consistent or Mori-Tanaka estimates of these moduli.

In particular, self-consistent estimates of the fiber moduli k_2, m_2, and p_2 can be found by solving in sequence equations (7.1.6), (7.1.7), (7.1.8). The remaining moduli n_2, l_2 then follow from the universal connections (3.9.4). Mori-Tanaka estimates of all five fiber moduli can be found by solving (7.2.11), (7.2.12), (7.2.13) for k_f, m_f, and p_f . For particulate composites, self-consistent estimates of effective reinforcement moduli, say, K_2 and G_2 follow from (7.1.9) and (7.1.10), and the

Mori-Tanaka estimates from (7.2.15). The pairs of equations in (7.2.19) or (7.2.21) may also be used to estimate 'effective' moduli of randomly oriented fiber or platelet reinforcements.

The same approach can be used for evaluation of effective moduli of a matrix, of interest in materials with large specific surface areas, which may promote realignment of polymer chains or other interfacial reactions leading to moduli changes. Again, elastic properties of the other phase, and of the aggregate need to be known together with phase volume fractions.

7.3 The Differential Scheme

This averaging method employs an incremental sequence of dilute approximations discussed in Sect. 4.4, to find the stiffness or compliance matrix of a composite made of two or more phases in non-dilute concentrations. In each increment, a homogeneous matrix or a 'backbone' medium $\boldsymbol{L}_0$ is enriched by inserting a dilute concentration of inhomogeneities of one or more distinct phases $\boldsymbol{L}_r$, $r = 1, 2, \ldots, n$, and the mixture is homogenized. This incremental homogenization continues until it reaches final phase concentrations. The choice of $\boldsymbol{L}_0$ and of the volume fraction increments Δc_r added in each step may yield different estimates of the final stiffness. However, the sequence of dilute approximations guarantees diagonal symmetry of the predicted overall stiffness and compliance for any combination of phase properties, shapes and alignments.

First proposed by Bruggeman (1935) and Roscoe (1952), and later expanded by Boucher (1974), the method was reviewed by Cleary et al. (1980). McLaughlin (1977) had shown that stiffness estimates for two-phase dispersion of spheres and fiber reinforced materials, generated by incremental additions to a unit matrix volume, lie between the Hashin-Shtrikman bounds. Callegari, et al. (1985), Norris (1985) and Norris et al. (1985) expanded the basic theory of the method and examined how such bounds can be realized by two-phase systems. Benveniste (1987b) suggested creating a two-phase dispersion by adding composite spheres, and had recovered the Hashin and Shtrikman (1962a, b) composite sphere assemblage results in the context of heat conduction. Applications of the differential scheme to materials containing distributions of cracks were explored by Hashin (1988).

Two procedures can be employed to reach an estimate of overall stiffness (Norris et al. 1985). In the *fixed volume process* or FVP, the initial 'backbone' material of stiffness $\boldsymbol{L}_0$ resides in a fixed representative volume V_0. Each addition of phase volumes $\Delta \mathrm{v}_1 + \Delta \mathrm{v}_2 + \cdots + \Delta \mathrm{v}_n = \Delta \mathrm{v}$ is preceded by removing from V_0 an equivalent volume $\Delta \mathrm{v}$ of the already homogenized material which always includes certain volume ratio of $\boldsymbol{L}_0$. After a current increment is homogenized, the phase volume fractions in the FVP procedure satisfy

$$\sum_{r=0}^{n} \mathrm{v}_r(t) = V_0 \quad \sum_{r=0}^{n} \Delta \mathrm{v}_r(t) = 0 \quad c_r(t) = \mathrm{v}_r(t)/V_0 \quad \sum_{r=0}^{n} c_r(t) = 1 \qquad (7.3.1)$$

This volume exchange process continues until all phase volume fractions reach their prescribed magnitudes in V_0. At the end point, some of the backbone material may be left as one of the actual phases, or it may be entirely replaced by the gradually added phases $r = 1, 2, \ldots n$. In any event, the final stiffness prediction depends on $\boldsymbol{L}_0$, and on the phase volume ratios added in each step.

Physically more plausible is the alternative *variable volume process* (VVP), which builds the same two or multiphase material $r = 1, 2, \ldots n$ by starting with volume v_1 of an actual phase $\boldsymbol{L}_1$, usually selected as the matrix material. Volume v_1 remains constant during homogenization. Dilute reinforcement volumes $\Delta \mathrm{v}_r, r \geq 2$, are added in certain ratios, until all phase volumes reach their prescribed final magnitudes $\mathrm{v}_1, \mathrm{v}_2, \ldots \mathrm{v}_n$. The mixture is homogenized after each such addition, hence the current total volume $V(t)$ increases from $V(0) = \mathrm{v}_1$ as a function of 'time' t, until it reaches the final volume $V = \Sigma_{r=1}^{n} \mathrm{v}_r$. Since all $r > 1$ phase volumes gradually increase, their volumes and volume fractions are

$$\mathrm{v}_1 + \sum_{r=2}^{n} \mathrm{v}_r(t) = V(t) \quad c_r(t) = \mathrm{v}_r(t)/V(t) \quad \sum_{r=2}^{n} c_r(t) = 1 - c_1(t) \tag{7.3.2}$$

where $c_1(t)$ decreases from 1 to its final magnitude.

Corresponding changes in the overall stiffness can be derived with reference to (4.4.6), where $\boldsymbol{L}_1$ is now replaced by the overall $\boldsymbol{L}(t)$ found in the previous step. The stiffness increment caused by addition of small reinforcement volumes in the VVP sequence is

$$\Delta \boldsymbol{L}(t) = \boldsymbol{L}\,(t + \Delta t) - \boldsymbol{L}(t) = \sum_{r=1}^{n} \frac{\Delta \mathrm{v}_r}{V(t)} \left[\boldsymbol{L}_r - \boldsymbol{L}(t)\right] \boldsymbol{T}_r(t) \tag{7.3.3}$$

where $\boldsymbol{T}_r(t) = \{\mathbf{I} + \boldsymbol{P}_r(t)\,[\boldsymbol{L}_r - \boldsymbol{L}(t)]\}^{-1}$ denote the partial strain concentration factors for each inhomogeneity added to the currently homogenized medium $\boldsymbol{L}(t)$. In each step, the $\boldsymbol{P}_r(t)$ needs to be updated as a function of $\boldsymbol{L}(t)$. This expression for $\Delta \boldsymbol{L}(t)$ provides a recursive formula for numerical evaluation of each next stiffness increment until the final overall stiffness $\boldsymbol{L}$ is reached at prescribed phase concentrations.

A differential equation for evaluation of $\boldsymbol{L}$ is obtained by letting $\Delta \mathrm{v}_r \to 0$ and $V(t) \gg \Delta V \to 0$. Then

$$\frac{\partial}{\partial t} \frac{\mathrm{v}_r}{V} = \dot{\mathrm{v}}_r / V - \mathrm{v}_r \dot{V} / V^2 \doteq \dot{\mathrm{v}}_r / V \tag{7.3.4}$$

The $\dot{\mathrm{v}}_r$ can be replaced by $\dot{c}_r$, with the substitution $\mathrm{v}_1 / V = c_1 = 1 - c$, where c follows from (7.3.2)

$$\frac{\mathrm{v}_r}{\mathrm{v}_1} = \frac{c_r}{c_1} \Rightarrow \frac{\dot{\mathrm{v}}_r}{\mathrm{v}_1} = \frac{\dot{c}_r}{(1-c)} + c_r \frac{\dot{c}}{(1-c)^2} = \frac{\dot{\mathrm{v}}_r}{V(1-c)} \tag{7.3.5}$$

Substitution into (7.3.3) yields the following system of coupled ordinary differential equations for evaluation of the overall stiffness

$$\dot{\boldsymbol{L}} = \sum_{r=1}^{n} (\boldsymbol{L}_r - \boldsymbol{L})\, \boldsymbol{T}_r \left(\dot{c}_r + c_r \frac{\dot{c}}{(1-c)} \right) \tag{7.3.6}$$

starting at $t = 0$ with the initial conditions $\boldsymbol{L}(0) = \boldsymbol{L}_1$ (Norris 1985). This equation also governs the removal-replacement or FVP procedure, where $\boldsymbol{L}(0) = \boldsymbol{L}_0$.

Specific applications require a selection of the initial 'backbone' medium $\boldsymbol{L}_0$, typically chosen as the actual matrix of the composite system, $\boldsymbol{L}_0 = \boldsymbol{L}_1$. Then, in a two-phase system $r = 1, 2$, where the reinforcements have stiffness $\boldsymbol{L}_2$ and are added by increments Δc_2, there is $c_r = c = c_2$ and (7.3.6) is reduced to

$$\frac{\mathrm{d}\boldsymbol{L}}{\mathrm{d}c_2} = \frac{1}{(1-c_2)} (\boldsymbol{L}_2 - \boldsymbol{L})\, \boldsymbol{T}_2 \tag{7.3.7}$$

Together with $\boldsymbol{T}_2 = \boldsymbol{T}_2(\boldsymbol{L})$, this is a coupled system of ordinary differential equations which can be integrated to yield the final stiffness. McLaughlin (1977) derived (7.3.7) as his equation (4), and had shown its solutions for both an isotropic dispersion of spheres and transversely isotropic dispersion of aligned and similar spheroids. In both cases, the predicted moduli lie between the corresponding Hashin-Shtrikman bounds. However, as shown by Christensen (1990), shear moduli estimates generated by the differential scheme can be very different from those predicted by the much more rigorous generalized self-consistent method, Fig. 6.5.

The matrix $\boldsymbol{L}_1$ can function both as a 'backbone' and one of the incrementally added phases. Norris (1985) shows that this enables a wider selection of the path followed in adding the phase increments. For example, each phase can be added by a separate sequence while the other phases remain constant or zero, and the order of these sequences can be varied within certain restrictions. This family of differential schemes can generate many different overall stiffness estimates of uncertain value, depending on the choice of the path. Of course, it seems reasonable to add in each step all reinforcement volumes in proportion to their final densities, as they might be added in actual fabrication. This happens in the variable volume of VVP process, which gradually reduces the matrix volume fraction from unity to its final magnitude. However both FVP and VVP are governed by (7.3.6).

Since each phase $r > 1$ is recognized only while being added to the mixture, the differential scheme does not offer a direct insight into phase interactions, as reflected by the mechanical strain and stress concentration factors. Only in two-phase systems $r = \alpha, \beta$, one can find estimates of concentration factor tensors $\boldsymbol{A}_r$, $\boldsymbol{B}_r$, in terms of the current or final overall stiffness $\boldsymbol{L}$ and phase stiffnesses $\boldsymbol{L}_\alpha$, $\boldsymbol{L}_\beta$, using (3.5.13). The main advantage of the differential scheme is its freedom from the restrictions on shape and alignment of the reinforcements, discussed in Sects. 7.1.4 and 7.2.4.

7.4 The Double Inclusion and Double Inhomogeneity Models

7.4.1 Field Averages in a Double Inhomogeneity

In this class of models of possibly multiphase composite materials, each inhomogeneity $\boldsymbol{L}_r$ resides in an ellipsoidal subvolume Ω_r, which is surrounded by a layer or coating of another material $\boldsymbol{L}_g$ in a volume $\Omega_g = \Omega_2 - \Omega_r$. All volumes Ω_2 are also ellipsoids, not necessarily coaxial with Ω_r. Each double inhomogeneity is then embedded in a large volume $\Omega_0 \supset \Omega_2 \supset \Omega_r$ of a comparison medium $\boldsymbol{L}_0$. A uniform overall strain $\boldsymbol{\varepsilon}^0$ is applied at the remote boundary $\partial\Omega_0$, Fig. 7.3. Several different predictions of overall stiffness of a composite aggregate can be derived using this model, based on distinct selections of the shapes and orientations of Ω_r and Ω_2, and of the stiffnesses $\boldsymbol{L}_r$, $\boldsymbol{L}_g$ and $\boldsymbol{L}_0$. The original form of the equivalent inclusion method was derived by Hori and Nemat-Nasser (1993), together with an extension to a configuration with multiple layers surrounding Ω_r, which can be useful, for example, in modeling of graded interphases.

All interfaces are assumed to be perfectly bonded, but boundary conditions at $\partial\Omega_2$ and $\partial\Omega_r$, and actual local fields in the phases, are not known. However, strain averages in Ω_r and Ω_g can be approximated by referring to the Tanaka-Mori (1972) theorem in Sect. 4.5.4, which describes those caused in the double inclusion in a homogeneous medium by uniform eigenstrains applied in Ω_r and Ω_g. A homogeneous double inclusion is created in $\boldsymbol{L}_0$, in parallel with the double inhomogeneity of the same geometry. The connection between the field averages in the double inclusion and inhomogeneity is established by a formal application of the equivalent inclusion method of Sect. 4.3.2, albeit to local fields that are not necessarily uniform.

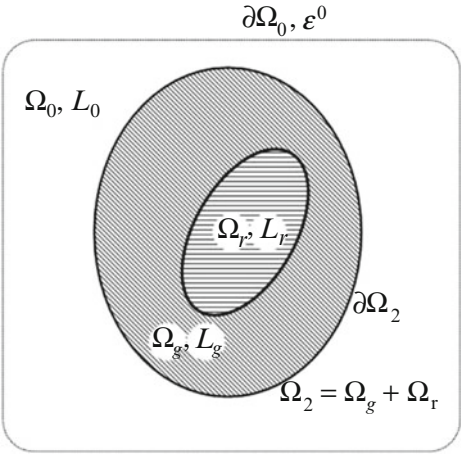

Fig. 7.3 Geometry of the double inclusion and the double inhomogeneity models

To evaluate effective stiffness of a double inhomogeneity, recall from Sect. 4.5.4 the derivation of average strains caused in a homogeneous double inclusion $\Omega_0 \supset \Omega_2 \supset \Omega_r$ by eigenstrains μ^g_{mn} and μ^r_{mn}, applied in the subvolumes $\Omega_g = \Omega_2 - \Omega_r$ and Ω_r, respectively, all in $\boldsymbol{L}_0$. In superposition with a uniform overall strain ε^0_{mn} applied at the remote boundary $\partial\Omega_0$, the total local strain averages, denoted by top bars are

$$\bar{\varepsilon}^g_{mn} = \varepsilon^0_{mn} + S_{mnkl}(\Omega_2)\mu^g_{kl} + \frac{\Omega_r}{\Omega_2 - \Omega_r}\left[S_{mnkl}(\Omega_2) - S_{mnkl}(\Omega_r)\right](\mu^r_{kl} - \mu^g_{kl}) \tag{4.5.45}$$

$$\bar{\varepsilon}^r_{mn} = \varepsilon^0_{mn} + S_{mnkl}(\Omega_2)\mu^g_{kl} + S_{mnkl}(\Omega_r)(\mu^r_{kl} - \mu^g_{kl}) \tag{4.5.46}$$

In the double inclusion model, the above eigenstrains are regarded as equivalent eigenstrains, applied in the respective volumes of the homogeneous comparison medium $\boldsymbol{L}_0$, to generate average local fields equal to those in the corresponding double inhomogeneity. The polarization fields (6.2.1) are now generated by two distinct local eigenstrains, in an admissible $\boldsymbol{L}_0$ restricted by (6.2.16).

Converting the second and fourth order tensors to contracted tensorial or engineering matrix notation, and writing them as (6×1) and (6×6) matrices, renders the above equations in the form

$$\bar{\boldsymbol{\varepsilon}}^{(a)}_g = \boldsymbol{\varepsilon}^0 + \boldsymbol{S}_2\boldsymbol{\mu}^{eq}_g + \gamma\,\Delta\boldsymbol{S}\left(\boldsymbol{\mu}^{eq}_r - \boldsymbol{\mu}^{eq}_g\right) \tag{7.4.1}$$

$$\bar{\boldsymbol{\varepsilon}}^{(a)}_r = \boldsymbol{\varepsilon}^0 + \boldsymbol{S}_2\boldsymbol{\mu}^{eq}_g + \boldsymbol{S}_r\left(\boldsymbol{\mu}^{eq}_r - \boldsymbol{\mu}^{eq}_g\right) \tag{7.4.2}$$

where $\gamma = \Omega_r/(\Omega_2 - \Omega_r)$, and $\Delta\boldsymbol{S} = \boldsymbol{S}_2 - \boldsymbol{S}_r$ is the difference between the Eshelby tensors of the ellipsoids Ω_2 and Ω_r in $\boldsymbol{L}_0$. The local stress averages are

$$\bar{\boldsymbol{\sigma}}^{(a)}_g = \boldsymbol{L}_0\left(\bar{\boldsymbol{\varepsilon}}^{(a)}_g - \boldsymbol{\mu}^{eq}_g\right) \qquad \bar{\boldsymbol{\sigma}}^{(a)}_r = \boldsymbol{L}_0\left(\bar{\boldsymbol{\varepsilon}}^{(a)}_r - \boldsymbol{\mu}^{eq}_r\right) \tag{7.4.3}$$

Average stresses caused inside the double inhomogeneity by the overall applied strain $\boldsymbol{\varepsilon}^0$ have the form

$$\bar{\boldsymbol{\sigma}}^{(b)}_g = \boldsymbol{L}_g\bar{\boldsymbol{\varepsilon}}^{(b)}_g \quad \bar{\boldsymbol{\sigma}}^{(b)}_r = \boldsymbol{L}_r\bar{\boldsymbol{\varepsilon}}^{(b)}_r \tag{7.4.4}$$

The equivalent eigenstrains, and the average strains and stresses in the double inhomogeneity follow from the equalities implied by the equivalent inclusion method, expressed in terms of the respective subvolume averages of local fields

$$\bar{\boldsymbol{\varepsilon}}^{(a)}_g = \bar{\boldsymbol{\varepsilon}}^{(b)}_g \quad \bar{\boldsymbol{\varepsilon}}^{(a)}_r = \bar{\boldsymbol{\varepsilon}}^{(b)}_r \quad \bar{\boldsymbol{\sigma}}^{(a)}_g = \bar{\boldsymbol{\sigma}}^{(b)}_g \quad \bar{\boldsymbol{\sigma}}^{(a)}_r = \bar{\boldsymbol{\sigma}}^{(b)}_r \tag{7.4.5}$$

Notice that in contrast to the fields employed in the original application of the method in Sect. 4.3.2, the current local fields may not be uniform. Consequences

appear in (7.4.17). Substitution into (7.4.3) for the strains $\bar{\boldsymbol{\varepsilon}}_g^{(a)}$ and $\bar{\boldsymbol{\varepsilon}}_r^{(a)}$ from (7.4.1) and (7.4.2) and implementation of (7.4.5) yields the equivalent eigenstrains

$$\boldsymbol{\mu}_g^{eq} = \boldsymbol{\Phi}_g \boldsymbol{\varepsilon}^0 \quad \boldsymbol{\mu}_r^{eq} = \boldsymbol{\Phi}_r \boldsymbol{\varepsilon}^0 \tag{7.4.6}$$

where

$$\boldsymbol{\Phi}_g = -\Big[\Delta \boldsymbol{S} + (\boldsymbol{S}_r + \boldsymbol{E}_r)(\boldsymbol{S}_r - \gamma\,\Delta \boldsymbol{S} + \boldsymbol{E}_r)^{-1}\left(\boldsymbol{S}_r - \gamma\,\Delta \boldsymbol{S} + \boldsymbol{E}_g\right)\Big]^{-1} \tag{7.4.7}$$

$$\boldsymbol{\Phi}_r = -\Big[(\boldsymbol{S}_r + \boldsymbol{E}_r) + \Delta \boldsymbol{S}\left(\boldsymbol{S}_r - \gamma\,\Delta \boldsymbol{S} + \boldsymbol{E}_g\right)^{-1}(\boldsymbol{S}_r - \gamma\,\Delta \boldsymbol{S} + \boldsymbol{E}_r)\Big]^{-1} \tag{7.4.8}$$

and $\boldsymbol{E}_g = \left(\boldsymbol{L}_g - \boldsymbol{L}_0\right)^{-1}\boldsymbol{L}_0$, $\boldsymbol{E}_r = (\boldsymbol{L}_r - \boldsymbol{L}_0)^{-1}\boldsymbol{L}_0$.

The equivalent eigenstrains (7.4.6) are now used in (7.4.1), (7.4.2), (7.4.3) to find the local strain and stress averages in the subvolumes Ω_r and Ω_g of the double inhomogeneity.

$$\left.\begin{aligned} \bar{\boldsymbol{\varepsilon}}_g &= \left[\boldsymbol{I} + \boldsymbol{S}_2\boldsymbol{\Phi}_g + \gamma\Delta \boldsymbol{S}\left(\boldsymbol{\Phi}_r - \boldsymbol{\Phi}_g\right)\right]\boldsymbol{\varepsilon}^0 \\ \bar{\boldsymbol{\sigma}}_g &= \boldsymbol{L}_0\left[\boldsymbol{I} - (\boldsymbol{I} - \boldsymbol{S}_2)\,\boldsymbol{\Phi}_g + \gamma\Delta \boldsymbol{S}\left(\boldsymbol{\Phi}_r - \boldsymbol{\Phi}_g\right)\right]\boldsymbol{\varepsilon}^0 \end{aligned}\right\} \tag{7.4.9}$$

$$\left.\begin{aligned} \bar{\boldsymbol{\varepsilon}}_r &= \boldsymbol{T}^{(r)}\boldsymbol{\varepsilon}^0 = \left(\boldsymbol{I} + \Delta \boldsymbol{S}\,\boldsymbol{\Phi}_g + \boldsymbol{S}_r\boldsymbol{\Phi}_r\right)\boldsymbol{\varepsilon}^0 \\ \bar{\boldsymbol{\sigma}}_r &= \boldsymbol{L}_0\left[\boldsymbol{I} + \Delta \boldsymbol{S}\,\boldsymbol{\Phi}_g - (\boldsymbol{I} - \boldsymbol{S}_r)\,\boldsymbol{\Phi}_r\right]\boldsymbol{\varepsilon}^0 \end{aligned}\right\} \tag{7.4.10}$$

Corresponding field averages over the entire volume $\Omega_2 = \Omega_r + \Omega_g$ can be found in analogy to (3.5.5) as

$$\bar{\boldsymbol{\varepsilon}}_2 = f_r\bar{\boldsymbol{\varepsilon}}_r + (1 - f_r)\bar{\boldsymbol{\varepsilon}}_g \qquad \bar{\boldsymbol{\sigma}}_2 = f_r\,\bar{\boldsymbol{\sigma}}_r + (1 - f_r)\,\bar{\boldsymbol{\sigma}}_g \tag{7.4.11}$$

or

$$\bar{\boldsymbol{\varepsilon}}_2 = (\boldsymbol{I} + \boldsymbol{S}_2\,\boldsymbol{\Phi}_2)\,\boldsymbol{\varepsilon}^0 = \boldsymbol{T}_2^{(r)}\boldsymbol{\varepsilon}^0 \qquad \bar{\boldsymbol{\sigma}}_2 = \boldsymbol{L}_0\left[\boldsymbol{I} - (\boldsymbol{I} - \boldsymbol{S}_2)\,\boldsymbol{\Phi}_2\right]\boldsymbol{\varepsilon}^0 \tag{7.4.12}$$

with

$$\boldsymbol{\Phi}_2 = f_r\,\boldsymbol{\Phi}_r + (1 - f_r)\,\boldsymbol{\Phi}_g \tag{7.4.13}$$

where $f_r = \Omega_r/\Omega_2 = \gamma(1 - f_r)$, $\gamma = \Omega_r/(\Omega_2 - \Omega_r)$. The partial strain concentration factors $\boldsymbol{T}^{(r)}$ and $\boldsymbol{T}_2^{(r)} = (\boldsymbol{I} + \boldsymbol{S}_2\boldsymbol{\Phi}_2)$ in (7.4.10) and (7.4.12) describe average strains in the single inhomogeneity $\boldsymbol{L}_r$ and double inhomogeneity $\boldsymbol{L}_2$, while both are present in a dilute concentration in the homogeneous medium $\boldsymbol{L}_0$ which is remotely loaded by the uniform strain $\boldsymbol{\varepsilon}^0$. The strain $\bar{\boldsymbol{\mu}}_2 = \boldsymbol{\Phi}_2\boldsymbol{\varepsilon}^0$ is now an average equivalent eigenstrain in the total volume Ω_2 of the double inclusion in a

homogeneous medium $\boldsymbol{L}_0$. Although the eigenstrains are only piecewise uniform in Ω_r and Ω_g, the Eshelby tensor $\boldsymbol{S}_2$ and the average equivalent eigenstrain $\bar{\boldsymbol{\mu}}_2$ provide the average strain $\bar{\boldsymbol{\varepsilon}}_2$ suggested by (4.5.47) and the Tanaka-Mori (1972) theorem.

Derivation of the overall stiffness of the double inhomogeneity is completed by relating the averages (7.4.12) by $\bar{\boldsymbol{\sigma}}_2 = \boldsymbol{L}_2^{(r)} \bar{\boldsymbol{\varepsilon}}_2$, where

$$\boldsymbol{L}_2^{(r)} = \boldsymbol{L}_0 \Big[\boldsymbol{I} - \boldsymbol{\Phi}_2 (\boldsymbol{I} + \boldsymbol{S}_2 \boldsymbol{\Phi}_2)^{-1} \Big] = \boldsymbol{L}_0 - \Big[(\boldsymbol{L}_0 \boldsymbol{\Phi}_2)^{-1} + \boldsymbol{P}_2 \Big]^{-1} \tag{7.4.14}$$

and $\boldsymbol{P}_2 = \boldsymbol{S}_2 \boldsymbol{L}_0^{-1} = \boldsymbol{P}_2^{\mathrm{T}}$. The superscript $(^{(r)})$ reminds that this tensor depends on both $\boldsymbol{S}_r$ and $\boldsymbol{L}_r$, which may be different within each subvolume Ω_2. Diagonal symmetry of $\boldsymbol{L}_2^{(r)}$ requires that $(\boldsymbol{L}_0 \boldsymbol{\Phi}_2) = (\boldsymbol{L}_0 \boldsymbol{\Phi}_2)^{\mathrm{T}}$.

Once the effective stiffness of the double inhomogeneity is known, it can be used in modeling of composite aggregates that contain an assemblage of different inclusion pairs, each within its own outer boundary $\partial\Omega_2$ defined by a single $\boldsymbol{S}_2$, and perfectly bonded to a common comparison medium $\boldsymbol{L}_0$. Such applications are described below. Hori and Nemat-Nasser (1993) give a proof of consistency $\boldsymbol{M}_2^{(r)} = (\boldsymbol{L}_2^{(r)})^{-1}$ of the (7.4.14) estimate and of many other features of the double inhomogeneity model.

7.4.2 *Double Inhomogeneity Microstructures*

The double inhomogeneity may not represent an element of the actual composite material, and the traction and displacement fields at the interface with the surrounding medium are not known. However, a double inhomogeneity with known effective stiffness $\boldsymbol{L}_2^{(r)}$ can be regarded as a single material inhomogeneity embedded in different concentrations in a large volume of a suitably selected medium $\boldsymbol{L}_0$, in the context of one of the average field or AFA approximations of overall stiffness of an aggregate. For example, the partial strain concentration factor $\boldsymbol{T}_2^{(r)}$ derived in (7.4.12) can be used in (6.3.2) to develop a corresponding $\boldsymbol{A}_2^{(r)}$ for substitution into the overall stiffness formula (6.3.5). Since the stiffness $\boldsymbol{L}_2^{(r)}$ depends on the shape and orientation of Ω_r selected for each inhomogeneity $\boldsymbol{L}_r$, and on the stiffness $\boldsymbol{L}_g$, a composite aggregate 'reinforced' by double inhomogeneities of different stiffnesses $\boldsymbol{L}_2^{(r)}$ is a multi-phase system. This implies that the enclosures Ω_2 need to have the same shape and alignment, described by $\boldsymbol{S}_2$, to satisfy the restrictions outlined in Sects. 7.1.3 and 7.2.4. Interpenetration or overlap of the Ω_2 subvolumes are excluded. Inhomogeneities in the interior of enclosures Ω_2 may have different shapes, orientations and material properties, subject to the requirement that $\boldsymbol{L}_2^{(r)} = (\boldsymbol{L}_2^{(r)})^{\mathrm{T}}$.

Different choices of $\boldsymbol{S}_2$ impose a spatial distribution on the subvolumes Ω_r of the inhomogeneities $\boldsymbol{L}_r$ in the entire volume of a composite material. For example,

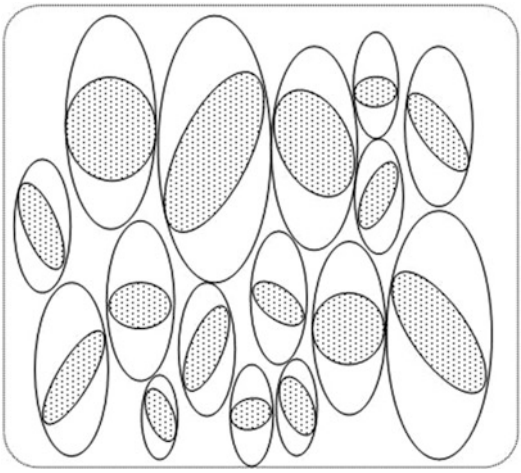

Fig. 7.4 Spheroidal inhomogeneities distributed with spheroidal spatial symmetry that promotes layered texture and isotropy in the transverse plane

in the composite sphere assemblage of Fig. 6.1, the outer surfaces of the shells surrounding the inhomogeneities impose a spherical distribution, with density $c_2 = \Omega_2/\Omega_0$, $0 < c_2 \leq 1$, where Ω_2 is the total volume of all double inhomogeneities in the representative volume Ω_0 of the composite. However, $c_2 \leq 1$ in general, depending on the selected range of sphere diameters. If all spheres are of the same size, then their volume fraction may not exceed the upper packing limit, $c_2 \leq c_{cp}$ which different methods cited in Sect. 3.3.2 estimate as $0.6 \leq c_{cp} \leq 0.7405$.

Spherical distributions with either variable or constant enclosure diameters are useful in modeling of two-phase or multiphase statistically isotropic aggregates, but they are not well suited for materials with statistically anisotropic distributions of reinforcements. Overall transverse isotropy, due to particle alignment or distribution in a layered texture, can be reproduced by prolate or oblate spheroidal enclosures, which promote such textures with either enhanced or reduced layer spacing, respectively. Figure 7.4 shows such arrangement, where possibly anisotropic spheroidal inhomogeneities $\boldsymbol{L}_r$ have many different shapes and orientations, and are distributed with spheroidal symmetry in the representative volume. Prolate spheroids with parallel symmetry planes depict all enclosures and some inhomogeneities in this idealized image. All spheroidal enclosures have identical aspect ratios and alignment.

Each transverse plane intersects the spheroidal enclosures in an assemblage of circles, hence isotropic distribution of reinforcements is assured in this plane of the aggregate. In a similar manner, aligned ellipsoidal enclosures may impose orthotropic overall symmetry, even on aggregates reinforced by particles which have

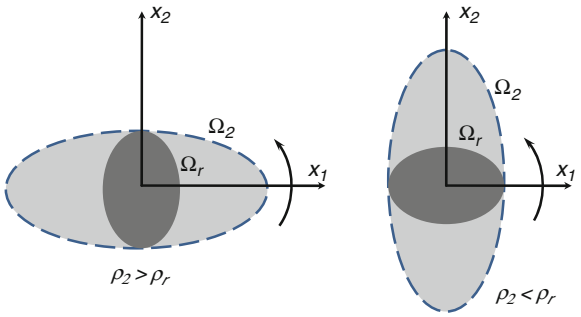

Fig. 7.5 Pairs of coaxial oblate and prolate spheroids

the same shape and random alignment. Overall transverse isotropy or orthotropy could also be imposed by aligned cylindrical enclosures containing ribbons of ellipsoidal crossections.

While the above mentioned choices of enclosure shapes allow modeling of different statistically isotropic or anisotropic aggregates, they also impose restrictions on the total volume fraction $c_r = \Omega_r/\Omega_0$ of inhomogeneities that can be accommodated by the double inclusion model. In particular,

$$c_r = \Omega_r/\Omega_0 = f_r c_2 = (\Omega_r/\Omega_2)(\Omega_2/\Omega_0) \tag{7.4.15}$$

where $f_r = \Omega_r/\Omega_2 < 1$ is the volume fraction of each inhomogeneity inside Ω_2, and $c_2 = \Omega_2/\Omega_0 \leq 1$ is the volume fraction occupied by the double inhomogeneities in a representative volume of the composite aggregate. While the magnitude of f_r may approach unity when Ω_2 and Ω_r are of similar orientation and size, for example, in coated reinforcements, the magnitude of c_r is often significantly reduced, even at $c_2 \to 1$, by a large difference in aspect ratios or orientations of Ω_2 and Ω_r.

Of course, actual dimensions or volume magnitudes of either Ω_r or Ω_2 can not be enforced in the double inhomogeneity model, or by other AFA models, since they all admit only volume fraction, shape and alignment information. The two volume fractions, the aspect ratios of the ellipsoids used in deriving the $\boldsymbol{P}_2$ and $\boldsymbol{P}_r$ tensors, and the orientations of these ellipsoids in the coordinates of the representative volume, are the only parameters that define the geometry of the microstructure.

The effect of aspect ratio differences on the respective volume fractions was illustrated by Ponte Castaneda and Willis (1995), who considered two double inhomogeneities, each formed by a pair of coaxial spheroids Ω_r and Ω_2, defined by (4.6.1), Fig. 7.5. Both Ω_r and Ω_2 share the $x_1 -$ axis of rotational symmetry. Individual aspect ratios are $\rho_r = a_1^{(r)}/a_2^{(r)}$ and $\rho_2 = a_1^{(2)}/a_2^{(2)}$, where the length is $|x_1| = a_1$ and the diameter $|x_2| = a_2 = |x_3| = a_3$. Volumes of the spheroids are $|\Omega_r| = (4\pi/3)a_1^{(r)}(a_2^{(r)})^2$, and $|\Omega_2| = (4\pi/3)a_1^{(2)}(a_2^{(2)})^2$, and their ratio is $f_r = |\Omega_r|/|\Omega_0|$.

First, let $\rho_2 > \rho_r$, and $a_2^{(r)} = a_2^{(2)}, a_1^{(r)} < a_1^{(2)}$, so that a 'flatter' Ω_r is enclosed by an 'elongated' Ω_2. Next, let $\rho_2 < \rho_r$, so that $a_1^{(r)} \le a_1^{(2)}$ and $a_2^{(r)} < a_2^{(2)}$; a 'flatter' Ω_2 surrounds and comes in contact with an 'elongated' Ω_r when $a_1^{(r)} = a_1^{(2)}$. This yields volume fraction limits

$$\left.\begin{aligned} f_r &= \left(\frac{\rho_r}{\rho_2}\right) \quad \rho_r|_{\min} = \rho_2 f_r \quad \rho_2|_{\max} = \rho_r / f_r \quad \text{for } \rho_2 > \rho_r \\ f_r &= \left(\frac{\rho_2}{\rho_r}\right)^2 \quad \rho_r|_{\max} = \rho_2 / \sqrt{f_r} \quad \rho_2|_{\min} = \rho_r \sqrt{f_r} \quad \text{for } \rho_2 < \rho_r \end{aligned}\right\} \tag{7.4.16}$$

Coefficients of $\boldsymbol{P}_2$ for oblate and prolate spheroids in a transversely isotropic solid can be derived from those of the related Eshelby tensor $\boldsymbol{S}$, which were determined by Withers (1989). A simpler form of $\boldsymbol{P}$, valid for spheroids in an isotropic solid, is given by Ponte Castaneda and Willis (1995), Sect. 4.6.5. Spherical enclosures surrounded by an isotropic matrix or an isotropic comparison medium are indicated in modeling of randomly orientated inhomogeneities or cracks. For the former, the corresponding $\boldsymbol{P}$ tensor appears in Sect. 4.6.2. Aligned penny-shaped or slit cracks can be enclosed by flat disks of ribbons, with $\boldsymbol{P}$ tensor described in Sects. 4.6.4 or 4.6.3. The effort involved in finding the required coefficients of the $\boldsymbol{P}$ tensors is reduced by selecting $\boldsymbol{L}_0 = \boldsymbol{L}_g = \boldsymbol{L}_1$, as suggested in (7.4.25) below. However, any differences in alignments of Ω_r call for transforming their coefficients into overall coordinates attached to the representative volume, as described in Chap. 1.

7.4.3 *Connections with the Self-consistent and Mori-Tanaka Estimates*

The double inhomogeneity model may assume several different forms, each determined by a particular choice of the $\boldsymbol{S}_2$ tensors, and the stiffnesses $\boldsymbol{L}_g$ and $\boldsymbol{L}_0$, which complement the $\boldsymbol{S}_r$ and $\boldsymbol{L}_r$ characterizing the actual inhomogeneity. One such form, for a two-phase system with aligned reinforcements of the same shape, postulates that $\boldsymbol{S}_2 = \boldsymbol{S}_r = \boldsymbol{S}$, or $\Delta\boldsymbol{S} = \boldsymbol{0}$, and it satisfies the diagonal symmetry requirement $\boldsymbol{L}_2^{(r)} = (\boldsymbol{L}_2^{(r)})^\mathrm{T}$ by selecting the external comparison medium $\boldsymbol{L}_0 = \boldsymbol{L}_0^\mathrm{T}$ to have the same stiffness $\boldsymbol{L}_0 = \boldsymbol{L}_2^{(r)}$. This implies that $\boldsymbol{T}_2^{(r)} = \boldsymbol{I}$, $\boldsymbol{\Phi}_2 = \boldsymbol{0}$, and that $\boldsymbol{\Phi}_g + \gamma\boldsymbol{\Phi}_r = \boldsymbol{0}$ in (7.4.13). The double inhomogeneity now behaves as a neutral inhomogeneity, however, the average strain in the inhomogeneity $\boldsymbol{L}_r$ in Ω_r follows from (7.4.10) as

$$\bar{\boldsymbol{\varepsilon}}_r = \left[\boldsymbol{I} + \frac{1}{1-f_r}\left(\boldsymbol{S}_r - f_r\boldsymbol{S}_2\right)\boldsymbol{\Phi}_r\right]\boldsymbol{\varepsilon}^0 = \boldsymbol{T}^{(r)}\boldsymbol{\varepsilon}^0 \quad \text{for } \boldsymbol{L}_0 = \boldsymbol{L}_2 \tag{7.4.17}$$

where $\boldsymbol{\Phi}_r = -\left[\boldsymbol{S}_r + (\boldsymbol{L}_r - \boldsymbol{L}_0)^{-1}\boldsymbol{L}_0\right]^{-1}$. The strain concentration factor can be reduced to the form

$$\boldsymbol{T}^{(r)} = [\boldsymbol{I} + \boldsymbol{P}\,(\boldsymbol{L}_r - \boldsymbol{L})]^{-1} \quad \text{for } \boldsymbol{L}_0 = \boldsymbol{L}_2 = \boldsymbol{L},\ \ \Delta\boldsymbol{S} = \boldsymbol{0} \tag{7.4.18}$$

where $\boldsymbol{P} = \boldsymbol{S}\boldsymbol{L}^{-1}$. The same result is provided by the self-consistent method in (7.1.1).

Although the $\Delta\boldsymbol{S} = \boldsymbol{0}$ also holds for the double inhomogeneity used in the derivation of the generalized self-consistent method of Sect. 6.5, the present model predicts only the self-consistent result. This is a reminder of the approximation induced by application of the uniform equivalent eigenstrains (7.4.6) in the double inclusion, which do not reproduce the nonuniform local fields, derived for spherical and cylindrical double inhomogeneities by Christensen and Lo (1979). Moreover, since neither the tractions nor the displacements create homogeneous boundary conditions on $\partial\Omega_2$, the Hill lemma (3.8.19) does not apply, and the energy of the double inclusion cannot be exactly evaluated using the phase field averages, to confirm (7.4.14).

Alternate forms of the double inhomogeneity model, suggested by Hu and Weng (2000), are based on selections of comparison medium stiffness as $\boldsymbol{L}_0 \neq \boldsymbol{L}_2^{(r)}$ and $\boldsymbol{L}_g = \boldsymbol{L}_1$, the stiffness of the actual matrix surrounding the inhomogeneities $\boldsymbol{L}_r$. To examine the symmetry condition $\boldsymbol{L}_0\boldsymbol{\Phi}_2 = \boldsymbol{\Phi}_2^{\mathrm{T}}\boldsymbol{L}_0$ in (7.4.14), we denote

$$\left.\begin{aligned} \boldsymbol{F}_1 = (\boldsymbol{L}_1 - \boldsymbol{L}_0)^{-1} = \boldsymbol{E}_1\boldsymbol{L}_0^{-1} = \boldsymbol{F}_1^{\mathrm{T}} \quad \boldsymbol{F}_r = (\boldsymbol{L}_r - \boldsymbol{L}_0)^{-1} = \boldsymbol{E}_r\boldsymbol{L}_0^{-1} = \boldsymbol{F}_r^{\mathrm{T}} \\ \boldsymbol{S}_i = \boldsymbol{P}_i\boldsymbol{L}_0 \quad \text{for } i = r, 1, 2 \end{aligned}\right\} \tag{7.4.19}$$

Then, (7.4.7), (7.4.8) change to

$$\boldsymbol{L}_0\boldsymbol{\Phi}_g = -\left[\Delta\boldsymbol{P} + (\boldsymbol{P}_r + \boldsymbol{F}_r)\,(\boldsymbol{P}_r - \gamma\,\Delta\boldsymbol{P} + \boldsymbol{F}_r)^{-1}\,(\boldsymbol{P}_r - \gamma\,\Delta\boldsymbol{P} + \boldsymbol{F}_1)\right]^{-1} \tag{7.4.20}$$

$$\boldsymbol{L}_0\boldsymbol{\Phi}_r = -\left[(\boldsymbol{P}_r + \boldsymbol{F}_r) + \Delta\boldsymbol{P}(\boldsymbol{P}_r - \gamma\,\Delta\boldsymbol{P} + \boldsymbol{F}_1)^{-1}\,(\boldsymbol{P}_r - \gamma\,\Delta\boldsymbol{P} + \boldsymbol{F}_r)\right]^{-1} \tag{7.4.21}$$

where again $\gamma = f_r/(1-f_r)$, $f_r = \Omega_r/\Omega_0$. Both above terms need to be diagonally symmetric to assure that $\boldsymbol{L}_0\boldsymbol{\Phi}_2 = \boldsymbol{\Phi}_2^{\mathrm{T}}\boldsymbol{L}_0$ in (7.4.14), where

$$\boldsymbol{\Phi}_2 = f_r\,\boldsymbol{\Phi}_r + (1 - f_r)\,\boldsymbol{\Phi}_g \tag{7.4.13}$$

One configuration (*CA*) of this model stipulates that the ellipsoids Ω_r and Ω_2 are similar and have identical Eshelby tensors.

$$\left.\begin{aligned} &CA \equiv (\Delta \boldsymbol{P} = \boldsymbol{0}) \Rightarrow \boldsymbol{P}_2 = \boldsymbol{P}_r, \qquad \boldsymbol{L}_0\boldsymbol{\Phi}_g = -[\boldsymbol{P}_2 + (\boldsymbol{L}_1 - \boldsymbol{L}_0)]^{-1}, \\ &\boldsymbol{L}_0\boldsymbol{\Phi}_r = -[\boldsymbol{P}_2 + (\boldsymbol{L}_r - \boldsymbol{L}_0)]^{-1} \end{aligned}\right\} \tag{7.4.22}$$

Average strains in Ω_r, Ω_g and Ω_2 follow from (7.4.11), (7.4.12), (7.4.13). According to (7.4.14), effective stiffness of the double inhomogeneity is

$$\left.\begin{aligned} \left(\boldsymbol{L}_2^{(r)}\right)^{CA} &= \boldsymbol{L}_0 + \left(\left[f_r\left[\boldsymbol{P}_2 + (\boldsymbol{L}_r - \boldsymbol{L}_0)^{-1}\right]^{-1} - (1 - f_r)\right.\right. \\ &\left.\left. \times \left[\boldsymbol{P}_2 + (\boldsymbol{L}_1 - \boldsymbol{L}_0)^{-1}\right]^{-1}\right]^{-1} - \boldsymbol{P}_2\right)^{-1} = \left(\left(\boldsymbol{L}_2^{(r)}\right)^{CA}\right)^{\mathrm{T}} \end{aligned}\right\} \tag{7.4.23}$$

Configuration *CA* represents a double inhomogeneity consisting of a core $\boldsymbol{L}_r$ surrounded by a layer of matrix $\boldsymbol{L}_1$, such that both the core and outer ellipsoidal surfaces have the same aspect ratio and alignment. The comparison medium can have a different stiffness $\boldsymbol{L}_0$, selected in agreement with (6.2.16) or (6.2.24). Each inhomogeneity may have a certain stiffness $\boldsymbol{L}_r$ and volume fraction f_r, both different inside each double inhomogeneity, yielding different stiffnesses $(\boldsymbol{L}_2^{(r)})^{CA}$. However, the shape and alignment of all Ω_2 outer envelopes is the same, hence overall stiffness of the aggregate can be derived from a standard AFA procedure. If one identifies the comparison medium with the matrix $\boldsymbol{L}_0{=}\boldsymbol{L}_1$, then $\boldsymbol{L}_0\boldsymbol{\Phi}_g \to \boldsymbol{0}$ and

$$\left(\boldsymbol{L}_2^{(r)}\right)^{CA} = \boldsymbol{L}_{1'} + f_r\left[(\boldsymbol{L}_r - \boldsymbol{L}_1)^{-1} + (1 - f_r)\,\boldsymbol{P}_r\right]^{-1} \tag{7.4.24}$$

which for $f_r \to c_r = (1 - c_1)$ is the Mori-Tanaka estimate (7.2.5) of the stiffness of a two-phase composite reinforced by aligned inhomogeneities of single stiffness $\boldsymbol{L}_r$, and of the same shape Ω_r. Therefore, if the overall stiffness is selected as $\boldsymbol{L} = (\boldsymbol{L}_2^{(r)})^{CA}$, then the double inclusion model provides the Mori-Tanaka estimate of $\boldsymbol{L}$. This implies that an entire representative volume would be filled with double inhomogeneities of the same ellipsoidal shape and different size, arranged in the spirit of the CSA model, Fig. 7.6. Of course, the double inhomogeneities may be assigned only certain volume fractions $c_2^{(r)} < 1$ in the surrounding comparison medium or matrix $\boldsymbol{L}_0 = \boldsymbol{L}_1$. Since the shape of Ω_2 is specified by $\boldsymbol{P}_2 = \boldsymbol{P}_r$, the restrictions noted in Sect. 7.2.4 still apply in multi-phase systems. Aggregates reinforced by randomly orientated inhomogeneities can again be analyzed using orientation averaging in Sect. 2.2.10.

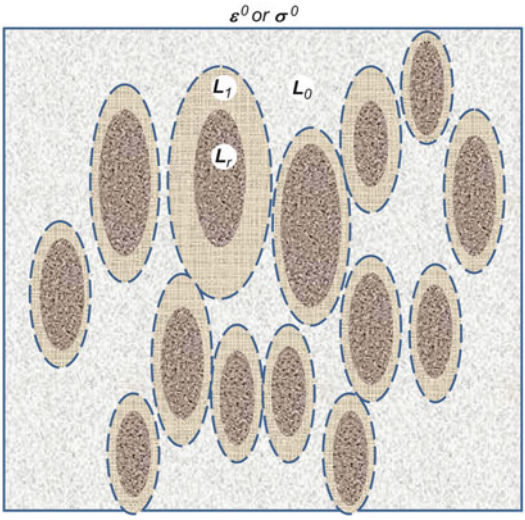

Fig. 7.6 The *CA* configuration of the double inhomogeneity model

7.4.4 *Multiphase Composites with Different Constituent Shapes and Alignments*

Another form of the double inhomogeneity model, that extends the capability of standard AFA models, is offered by the configuration *CB,* also suggested Hu and Weng (2000)

$$\left.\begin{aligned} &CB \equiv \left(\Delta \boldsymbol{P} \neq \boldsymbol{0},\ \boldsymbol{L}_0 = \boldsymbol{L}_g = \boldsymbol{L}_1\right) \Rightarrow \boldsymbol{L}_0\boldsymbol{\Phi}_g \to \boldsymbol{0}, \\ &\boldsymbol{L}_0\boldsymbol{\Phi}_r = -[\boldsymbol{P}_r + (\boldsymbol{L}_r - \boldsymbol{L}_0)]^{-1} \end{aligned}\right\} \tag{7.4.25}$$

Each inhomogeneity $\boldsymbol{L}_r$ is now embedded in a common matrix $\boldsymbol{L}_1$, and it may have its own shape and alignment described by a different $\boldsymbol{P}_r$. Since these three tensors follow from the known properties of a given matrix and reinforcements, one only needs to select a single $\boldsymbol{P}_2$ for all enclosures Ω_2, which have the same shape and alignment. This provides relief from making a 'suitable' choices of $\boldsymbol{L}_0$ and $\boldsymbol{L}_g$, required by the general double inhomogeneity model in Sect. 7.4.1. However, all $\boldsymbol{P}$ and $\boldsymbol{L}$ tensors that apply to inhomogeneities of different alignment need to be transformed into a single coordinate system that is used in the representative volume.

From (7.4.13) and (7.4.21)

$$\boldsymbol{L}_0\boldsymbol{\Phi}_2 = c_r\, \boldsymbol{L}_0\boldsymbol{\Phi}_r = -c_r\Big[\boldsymbol{P}_r + (\boldsymbol{L}_r - \boldsymbol{L}_1)^{-1}\Big]^{-1} = -c_r\,(\boldsymbol{L}_r - \boldsymbol{L}_1)\,\boldsymbol{T}_r \tag{7.4.26}$$

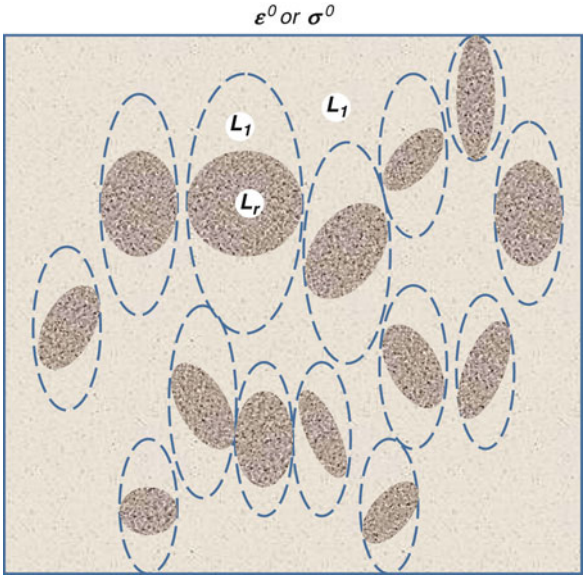

Fig. 7.7 The *CB* configuration of the double inhomogeneity model

where $c_r = (1 - c_1)$ is the actual volume fraction of inhomogeneities $\boldsymbol{L}_r$ in the matrix material $\boldsymbol{L}_1$. Here, the partial strain concentration factor $\boldsymbol{T}_r = [\boldsymbol{I} + \boldsymbol{P}_r\,(\boldsymbol{L}_r - \boldsymbol{L}_1)]^{-1}$ is that of a single-material inhomogeneity $\boldsymbol{L}_r$ in the matrix material $\boldsymbol{L}_1$, derived in (4.2.14). Average strains in Ω_r and Ω_2 follow from (7.4.2). The average strain in the double inhomogeneity is

$$\bar{\boldsymbol{\varepsilon}}_2^{(r)} = \left(\boldsymbol{I} - \boldsymbol{P}_2\Big[\boldsymbol{P}_r + (\boldsymbol{L}_r - \boldsymbol{L}_1)^{-1}\Big]^{-1}\right)\boldsymbol{\varepsilon}^0 = \boldsymbol{T}_2^{(r)}\boldsymbol{\varepsilon}^0 \tag{7.4.27}$$

Equation (7.4.14) yields the stiffness of the double inhomogeneity $\Omega_2^{(r)}$

$$\left.\begin{aligned}\left(\boldsymbol{L}_2^{(r)}\right)^{CB} &= \boldsymbol{L}_1 + f_r\Big[(\boldsymbol{L}_r - \mathbf{L}_1)^{-1} + \boldsymbol{P}_r - f_r\boldsymbol{P}_2\Big]^{-1}\\ &= \boldsymbol{L}_1 + f_r\Big[\boldsymbol{I} - f_r\,(\boldsymbol{L}_r - \boldsymbol{L}_1)\,\boldsymbol{T}_r\boldsymbol{P}_2\Big]^{-1}(\boldsymbol{L}_r - \boldsymbol{L}_1)\,\boldsymbol{T}_r\end{aligned}\right\} \tag{7.4.28}$$

where $f_r = \Omega_r/\Omega_2^{(r)}$. Also, $(\boldsymbol{L}_2^{(r)})^{CB} = \left((\boldsymbol{L}_2^{(r)})^{CB}\right)^{\mathrm{T}}$ for any $\boldsymbol{P}_r$ and $\boldsymbol{P}_2$ that define shapes of the ellipsoids Ω_r and Ω_2.

If all inhomogeneities Ω_r have the same shape and alignment, then all $(\boldsymbol{L}_2^{(r)})^{CB}$ are identical, and the overall stiffness of the composite aggregate can be selected as $\boldsymbol{L} = (\boldsymbol{L}_2^{(r)})^{CB}$, possibly with $f_r \to c_r = (1 - c_1)$. However, many distinct $(\boldsymbol{L}_2^{(r)})^{CB}$ may be admitted in modeling of matrix-based composites with misaligned

reinforcements, as long as the shape and alignment of all enclosures $\Omega_2^{(r)}$ are described by a single matrix $\boldsymbol{P}_2$. Short or long fibers combined with particles in a common matrix are among the systems that can be modeled in this manner. Overall stiffness or compliance can then be evaluated using an AFA procedure, based on (6.3.3), (6.3.4) and (6.3.5).

For a random distribution of orientations of inhomogeneities $\boldsymbol{L}_r$, the overall stiffness $\boldsymbol{L}$ of the composite aggregate is obtained in (7.4.29), as an orientation average of the terms associated with the inhomogeneities $r = 2, 3, \ldots n$, indicated by the $\{\}$ brackets; Sect. 2.2.10. The shape tensor $\boldsymbol{P}_2$ and matrix stiffness $\boldsymbol{L}_1$ remain unchanged.

$$\boldsymbol{L} = \left\{(\boldsymbol{L}_2^{(r)})^{CB}\right\} = \boldsymbol{L}_1 + (1-c_1)[\boldsymbol{I} - (1-c_1)\{(\boldsymbol{L}_r - \boldsymbol{L}_1)\boldsymbol{T}_r\}\boldsymbol{P}_2]^{-1}\{(\boldsymbol{L}_r - \boldsymbol{L}_1)\boldsymbol{T}_r\} \tag{7.4.29}$$

This stiffness formula was first found by a different procedure, as an estimate of Hashin-Shtrikman type, by Ponte Castaneda and Willis (1995), with variants valid for selected two-phase microstructures.

7.4.5 *Composites Containing Distributed Voids or Cracks*

When some or all reinforcements undergo complete decohesion from the matrix, they are replaced by cavities Ω_c that have the original inhomogeneity shape defined by $\boldsymbol{P}_r \equiv \boldsymbol{P}_c$, while $\boldsymbol{L}_r = \boldsymbol{L}_c \to 0$. In some cases the overall applied strain or stress may be associated with preferential decohesion of certain orientations and volume fractions of the originally bonded reinforcements. Then, the composite system can be modeled as a mixture of double inhomogeneities with solid and vacuous cores, each with prescribed orientation and volume fraction, possibly embedded in a common matrix.

In a completely debonded or porous aggregate, the matrix $\boldsymbol{L}_1$ is the comparison medium $\boldsymbol{L}_0^{(+)} = \boldsymbol{L}_1$, and $\boldsymbol{L}_r \to 0$, which leads to the following substitutions

$$\left.\begin{array}{l}\left[\boldsymbol{P}_r + (\boldsymbol{L}_r - \boldsymbol{L}_1)^{-1}\right] \to \boldsymbol{P}_r - \boldsymbol{M}_1 \quad \boldsymbol{T}_r \to (\boldsymbol{I} - \boldsymbol{P}_r\boldsymbol{L}_1)^{-1} \\ (\boldsymbol{L}_r - \boldsymbol{L}_1)\,\boldsymbol{T}_r \to (\boldsymbol{P}_r - \boldsymbol{M}_1)^{-1}\end{array}\right\} \tag{7.4.30}$$

Two geometries of porous media are of particular interest. When all cavities or cracks have the same shape and alignment, with $\boldsymbol{P}_r \equiv \boldsymbol{P}_2$, and the entire representative volume is filled with the double inhomogeneities, overall stiffness is predicted by the double inhomogeneity model *CA* in (7.4.24), with $f_c = \Omega_c/\Omega_2 \to c_c = (1-c_1)$. That provides an upper Hashin-Shtrikman bound on overall stiffness, identical with that in (6.3.21)

$$\boldsymbol{L}^{(+)} = \boldsymbol{L}_1 + (1-c_1)\,(c_1\boldsymbol{P} - \boldsymbol{M}_1)^{-1} \tag{7.4.31}$$

The *CB* variant yields stiffness of the double inhomogeneity with a vacuous core as

$$\boldsymbol{L}^{(+)} = \left(\boldsymbol{L}_2^{(c)}\right)^{CB} = \boldsymbol{L}_1 + (1-c_1)\left[\boldsymbol{P}_c - (1-c_1)\boldsymbol{P}_2 - \boldsymbol{M}_1\right]^{-1} \tag{7.4.32}$$

This represents another bound on the overall stiffness of a porous medium with different cavity shapes and orientations described by $\boldsymbol{P}_c$, and spatial distribution described by $\boldsymbol{P}_2$. For example, the geometry of Fig. 7.7 can be used, with some or all inhomogeneities replaced by cavities.

For randomly distributed cavities or cracks, orientation averaging in (7.4.29) provides the upper bound on overall stiffness

$$\boldsymbol{L}^{(+)} = \boldsymbol{L}_1 + (1-c_1)\left[\boldsymbol{I} - (1-c_1)\left\{(\boldsymbol{P}_c - \boldsymbol{M}_1)^{-1}\right\}\boldsymbol{P}_2\right]^{-1}\left\{(\boldsymbol{P}_c - \boldsymbol{M}_1)^{-1}\right\} \tag{7.4.33}$$

For both cavities and cracks, the $\boldsymbol{P}_c$ tensors are described in Sect. 4.6, together with the $\boldsymbol{P}_2$ tensors for spheres and with references to related publications. Since the $\boldsymbol{P} = \left(\boldsymbol{L}^* + \boldsymbol{L}_0\right)^{-1}$ tensors are positive definite, a comparison of (7.4.31) with (7.4.32) and (7.4.33) indicates that the latter upper bounds are tighter than the former, which agrees with the Mori-Tanaka estimate by Benveniste (1987a).

Simple forms of the bounds (7.4.33) for cracked solids have been derived by Ponte Castaneda and Willis (1995). A medium with a spherical distribution of randomly oriented cracks generates an isotropic solid with overall bulk and shear moduli K, G. Matrix moduli are $3K_1 = 2G_1(1+\nu_1)/(1-2\nu_1)$, and the volume fraction of the enclosures Ω_2 in a representative volume Ω_0 is denoted by $c_2 = \Omega_2/\Omega_0 \leq 1$. The upper bound on the two overall moduli is

$$\left.\begin{aligned} \frac{K^{(+)}}{K_1} &= 1 - \frac{12c_2(1-\nu_1^2)}{9\pi(1-2\nu_1) + 4c_2(1+\nu_1)^2} \\ \frac{G^{(+)}}{G_1} &= 1 - \frac{120c_2(1-\nu_1)(5-\nu_1)}{225\pi(2-\nu_1) + 16c_2(4-5\nu_1)(5-\nu_1)} \end{aligned}\right\} \tag{7.4.34}$$

Distributions of aligned circular cracks on planes perpendicular to the x_1-axis, in an isotropic matrix with moduli $E^{(1)} = 2(1+\nu^{(1)})G^{(1)}$, create a transversely isotropic material, where the cracks change only the longitudinal Young's and shear moduli E_{11} and $p = G_{12} = G_{13}$. The remaining three moduli $E_{22} = E_{33}$, $G_{23} = G_{32}$, $\nu_{23} = \nu_{32}$ are not changed by introduction of cracks aligned on parallel x_2x_3- planes. For a spherical distribution

$$\left.\begin{aligned} \frac{E_{11}^{(+)}}{E_{11}^{(1)}} &= 1 - \frac{60c_2(1-\nu_1^2)}{15\pi + 4c_2(7-15\nu_1^2)} \\ \frac{p^{(+)}}{p^{(1)}} &= 1 - \frac{60c_2(1-\nu_1)}{15\pi(2-\nu_1) + 8c_2(4-5\nu_1)} \end{aligned}\right\} \tag{7.4.35}$$

where elastic moduli of the isotropic matrix are $E_{11}^{(1)} = 2p^{(1)}(1 - \nu_1)$. Results for a flat distribution of cracks, where $\boldsymbol{P}_2$ is that for flat disks aligned with the cracks, can be found in Willis (1980).

7.4.6 Predictive Reliability of Micromechanical Methods

As one would expect in linear elasticity, methods described in Chap. 6, and especially the rigorous evaluations in Sects. 6.4 and 6.5, should deliver reliable magnitudes of overall properties. The approximate methods in Chap. 7 are useful in certain applications, as shown in Sect. 7.5. Among those, the Mori-Tanaka estimate appears to be most reliable when it coincides with the H-S lower bound. The self-consistent method requires care when there is large contrast between phase properties. The double inclusion model exhibits greater flexibility of property choices, and the *CB* form in Sect. 7.4.4, while allowing for different phase properties, shapes and alignments, also enjoys theoretical support as a H-S type estimate.

Of course, experimental verification of the different predictions is the ultimate test of their utility. That can be expected only when the following two conditions are satisfied:

(i) There is a nearly perfect bond everywhere between matrix and reinforcement or polycrystal grains, and the representative sample is free of voids or cracks that may degrade overall stiffness.
(ii) Elastic moduli measured on a large volume specimen of the matrix material actually prevail *in situ,* where matrix interlayers between fibers may be just few microns thick, and may locally disappear when interrupted by fiber contact, as in the "string of pearls" formations often observed on micrographs.

The first condition (*i*) should be satisfied in well-made materials, but it is useful to recall from Sect. 3.2.3 and (3.2.12) that the interface area is rather large in materials reinforced by small diameter fibers of particles. For example, $\boldsymbol{s}(\boldsymbol{\nu}_f) = c_f \times 0.4\,\mathrm{m}^2/1\,\mathrm{cm}^3$ in commonly used fiber composites reinforced by 10 μ diameter fibers. At the usual $c_f \doteq 0.6$ there is about $0.24\ \mathrm{m}^2/1\ \mathrm{cm}^3$ of interface area, which may accommodate localized interface debonds, impurities and other possible interruptions of perfect bond. The effect may not be significant under sustained loads, but it may be magnified under cyclic loading.

The second condition (*ii*) should again be satisfied in a large volume of well-made composite material, with a high volume fraction $c_m = 1 - c_f$ of matrix. However, the matrix polymer chains may often align around and along the fiber interface, yielding somewhat different matrix moduli *in situ*. Interface reactions producing a thin but distinct coating-like layer of a different material may also be observed, both in polymer and metal matrix systems. This may have an effect on actual overall properties, which can be accounted for by measuring effective moduli of the matrix in a material with well established fiber moduli.

Therefore, it is not unusual to find that measured moduli of composite specimens or plies are somewhat different from the predicted values, or that they may change from one batch of material to another. Measured strength magnitudes, both in tension and compression, provided by different sources, are often much larger than those found in the elastic moduli. Recourse to experimentally determined magnitudes for plies, laminate and particulate mixtures, such as can be found tabulated in Herakovich (1998) or Daniel and Ishai (2006) may provide useful guidance. However, designed properties of each material or part should be verified in each application.

In analyzing an available experimental result, on a material having a certain range of volume fractions, one may predict overall moduli as function of average volume fraction fluctuation by referring to Walpole's equations (6.3.25), (6.3.26) and (6.3.27). Those permit computation of the moduli of the underlying comparison medium from known overall and given phase properties. The expectation is that the same comparison medium properties prevail at all volume fractions in the selected range.

7.5 Applications of SCM and M-T to Functionally Graded Materials

Functionally graded materials (FGM) are particulate composites, with spatially variable phase volume fractions that gradually change in at least one material direction. In a typical single gradient two-phase system, $r = \alpha, \beta$, particles of phase β are added in a selected direction and in increasing concentrations to a continuous matrix of phase α, until the material is divided by a percolation threshold or by a transition zone. Beyond that zone, the matrix is a continuous phase β that contains dispersed α–phase particles in diminishing numbers. Such materials may remain dimensionally stable under the influence of stress or thermal gradients, for example in thermal barrier coatings. They may also facilitate joining of metal/ceramic interfaces.

Early developments in modeling of functionally graded materials relied on the elementary 'rule of mixtures' approximation, for example, by Fukui et al. (1994), Markworth and Saunders (1995), and in stress intensity factor evaluations in graded materials by Lee and Erdogan (1994, 1995). Giannakopoulos et al. (1995) and Finot and Suresh (1996) used this approach in elastic-plastic systems. Hirano et al. (1990) introduced a fuzzy-set estimate based on the Mori-Tanaka method, with an assumed transition function to account for the effect of changing volume fractions. The method was also used in modeling of thermoelastic behavior of FGM microstructures (Tanaka et al. 1993a, b). Reviews with additional references were written by Markworth et al. (1995) and Williamson et al. (1993).

A detailed description of the actual geometry of graded microstructures is usually not available, except perhaps for information on direction and magnitude of volume fraction distribution and approximate shape of the dispersed phase or phases.

Therefore, evaluation of overall response and local stresses and strains in graded materials must rely on idealized models. Those may be based on finite element analysis of selected discrete microstructures, or on estimates of locally homogenized properties of such microstructures obtained by the self-consistent or Mori-Tanaka schemes.

The major difference between application of these schemes to statistically homogeneous or graded materials is in selection of a representative volume, which has been identified in Sect. 3.3 as sufficiently large to have the properties of any larger volume. As suggested by Drugan and Willis (1996) and corroborated by numerical simulations by Gusev (1997), the diameter of the RVE should be equal to at least twice as large as that of spherical grains reinforcing isotropic matrix-based mixtures. Such representative volumes are not easily identified in systems with variable phase volume fractions, which may also be subjected to loading by nonuniform overall fields. However, application of AFA type methods appears to be justified by the slow density changes, and by the relatively small ratios of field gradients to field averages found in most graded systems. This is confirmed by the good agreement between results obtained using the two material models described below.

The present exposition is based on the work of Reiter et al. (1997) and Reiter and Dvorak (1998), designed to determine if the available analytical models can be applied with reasonable degree of confidence to prediction of homogenized properties of graded microstructures subjected to mechanical and thermal loads. To this end, selected two-phase microstructures with single composition gradients were modeled both by distributions of discrete phase subvolumes, and by a sequence of parallel homogenized layers with effective properties estimated by either the self-consistent or Mori-Tanaka methods. Overall response and phase field averages predicted by these discrete and layered models were compared under both mechanical loading, thermal changes and steady-state heat conduction. To make good agreement more difficult to achieve, a C/SiC composite system with large differences in phase properties and steep composition gradients was used in the comparisons.

7.5.1 Discrete and Layered Models of Graded Microstructures

Both the discrete and layered graded material models used in the comparative studies are based on planar arrays of hexagonal inhomogeneities in continuous matrices, which are more easily implemented in a discrete model.

Figure 7.8 shows the double array used in generating both graded material models. It is created by two overlapping honeycomb arrays, which have been separated in the x_2–direction by one half width of one hexagonal cell. A series of computer generated random distributions of the hexagons in the double array indicates percolation thresholds at $0.6 \leq c_r \leq 0.73$, much higher than the 0.5

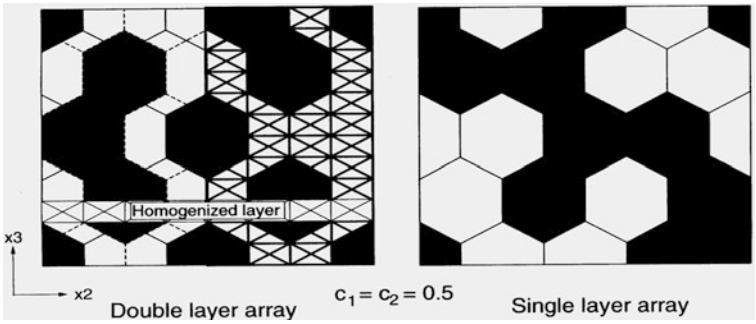

Fig. 7.8 Double and single honeycomb arrays. The double array is subdivided by 24 triangular elements per hexagonal cell, or by parallel layers that have effective properties estimated by the M-T or SCM procedures

threshold for the random distribution of uncorrelated hexagons in the adjacent single honeycomb array.

The composition gradients observed in actual microstructures are usually much smaller, equivalent to about 0.005–0.0025/row.

The double array is subdivided into thin material layers parallel to the x_2–axis. The thickness of three such layers is equal to that of one row of the hexagons. Phase volume fractions $c_r(x_3)$ indicate the number of phase parts in each layer. The finite element Model 3 further subdivides each layer into 320 triangular elements. Convergence with respect to coarseness of the mesh was established by comparisons of overall stiffness and field averages with those found using more refined meshes.

The layered model consists of 150 thin material layers, with effective layer properties evaluated by one of the averaging methods. The fine subdivision of the mesh and the small thickness of the homogenized layers relative to particle size cause oscillations in layer volume fractions and in estimated effective properties; these were reduced by superimposing a three-layer moving average on the computed results.

Figure 7.9 provides examples of three discrete microstructures, designated as Model 1_2 with a distinct percolation threshold, Model 2 with a wide skeletal transition zone, and Model 3 which has both a wide transition region and a threshold. Each micro-structure has 50 rows of hexagonal cells, with 40 cells per row. Five rows at both ends are filled with either homogeneous carbon or silicon carbide, then one hexagonal cell of the other phase is added in each next row, hence each new cell was added to a sufficiently large volume of constant composition. The resulting gradient is uniform, equal to 0.025/row, and of the same magnitude in all three models shown.

The graded microstructures were realized by the C/SiC system (Sasaki and Hirai 1991). Both phases were regarded as isotropic with the thermo-mechanical properties in Table 7.1, where E, ν are elastic moduli, α is the linear coefficient of thermal expansion and κ denotes heat conductivity. Several combinations of the SCM and M-T schemes were employed in finding effective property estimates of

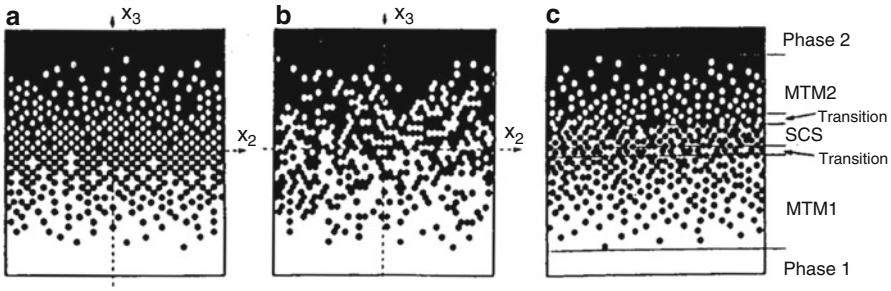

Fig. 7.9 Models of graded materials with the same linear composition gradient in the x_3−direction. (**a**) Model 1-2. (**b**) One of computer-generated random micro-structures of Model 2. (**c**) Microstructure used in the finite element analysis as Model 3 and as a layered model COMB3.1

Table 7.1 Phase properties of the carbon/silicon carbide system

	E (GPa)	ν	α (10^{-4}/°C)	κ (Wm^{-1}/°C)
C ($r=1$)	28	0.3	9.3	9.5
SiC ($r=2$)	320	0.3	4.2	135

individual layers in the layered models. At both matrix-rich regions at the upper and lower ends on the graded microstructures in Fig. 7.9, the Mori-Tanaka method was used in two versions, once with the matrix properties equal to those of phase 1, and once with those of phase 2; these estimates are labeled as MTM1 and MTM2 in the figures below. SCS denotes homogenization by the self-consistent method, which yields gradual property changes with the SiC volume fraction c_2.

Models COMB3.1 and COMB3.2 employed different transition functions between the three methods, to describe effective property changes with changing c_2; these can be found in Reiter and Dvorak (1998). The COMB3.1 model corresponds to the domain subdivision indicated in the right image of Fig. 7.9, where the self-consistent estimate is employed in the in the layers that have skeletal microstructures lacking a distinct matrix. Model COMB3.2 is suitable for materials with a narrow transition zone and distinct percolation threshold.

Figure 7.10 shows predictions by these models of the transverse Young's modulus E_{33} as a function of c_2, which is the volume fraction of SiC. Similar predictions for the coefficient of thermal expansion α_{eff} are shown in Figs. 7.11. In all three figures, the transitions are centered at $c_2 = 0.5$ and $c_2 = 0.65$ for model COMB3.1, and at $c_2 = 0.66$ for COMB3.2. Width of the transitions is equal to 0.05 on the c_2 scale. The modulus $E_{33} = E_{22}$ described in (2.3.5) was estimated using the Hill's moduli from Sect. 7.1.3 for the self-consistent method, and from Sect. 7.2.2 for the Mori-Tanaka method. The CTE is the transverse component of the eigenstrain in (3.6.18), where either the SCM or M-T estimates of the overall moduli are used to find $\boldsymbol{M}$. The phase eigenstrains are found as $\boldsymbol{\mu}_r = \boldsymbol{m}_r \Delta\theta$, where for the isotropic case, $\boldsymbol{m}_r = [\alpha_r,\ \alpha_r,\ \alpha_r,\ 0,\ 0,\ 0]^{\mathrm{T}}$, and α_r is the linear coefficient of thermal expansion of phase r. Heat conduction in the transverse direction of a

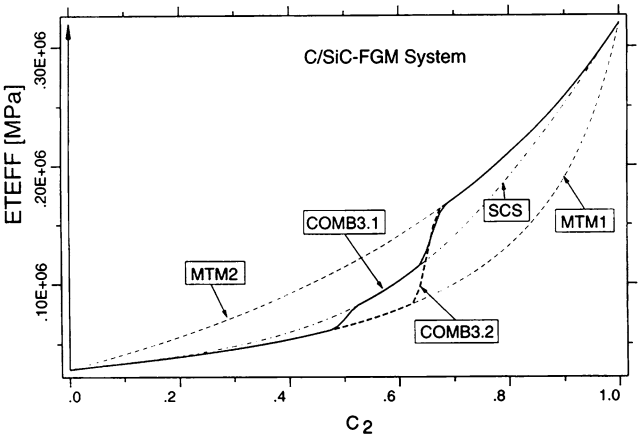

Fig. 7.10 Estimates of the overall transverse Young's modulus $E_{22} = E_{33}$ as functions of the SiC volume fraction c_2

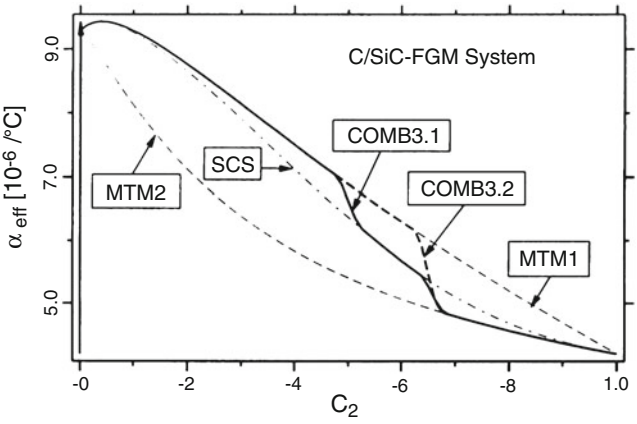

Fig. 7.11 Estimates of the overall coefficient of thermal expansion as functions of the SiC volume fraction c_2

fiber composite is governed by the same equations as the longitudinal shearing deformation. This axial shearing-transverse conduction analogy (Hashin 1968, 1972) allows writing down an expression for κ_T by exchanging κ_r for $p_r (r = 1,\ 2)$ in the self-consistent form of p in (7.1.8), and in the Mori-Tanaka form (7.2.13), where $(r = m,\ f)$. Results for particulate composites were derived by Hatta and Taya (1986), and for coated orthotropic fibers by Benveniste et al. (1990, 1991a). Models with homogenized layers were also analyzed by Ozisik (1968). Figure 7.12 illustrates the types of boundary conditions applied to both discrete and layered

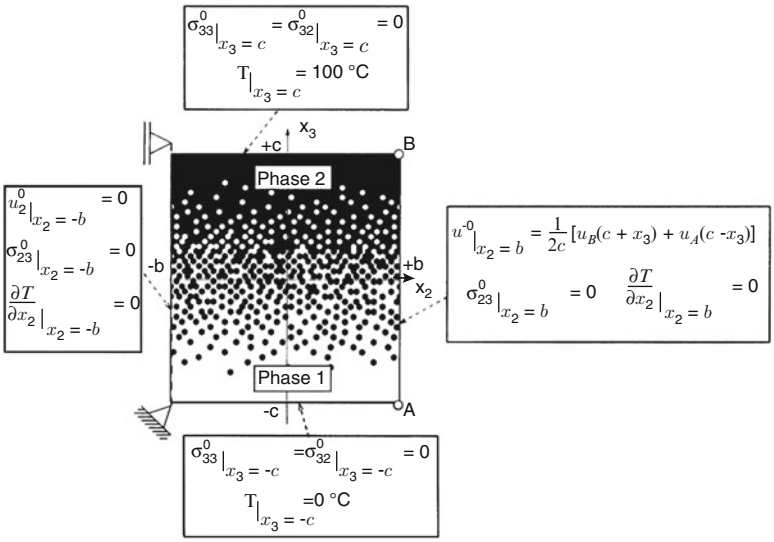

Fig. 7.12 Boundary conditions applied to the graded material subjected to a temperature gradient. Similar boundary conditions, with T = 100°C, were applied to impose the uniform change in temperature

models to simulate heat conduction in the x_3–direction, or a constant temperature change. The solution domain was bounded in the thickness direction by two parallel planes that allowed a uniform normal strain in the thickness direction; resultants of the external forces and moments on the bounding planes were equal to zero. In the finite element Model 3, the thermal and mechanical fields were obtained from a two-dimensional solution, using ABAQUS generalized plane strain elements.

7.5.2 *Selected Comparisons of Discrete and Homogenized Models*

Graded materials are often used in thermal barrier coatings that are subjected to both uniform changes in temperature and to thermal gradients. Of interest in such applications are temperature distributions in individual layers, as well as the overall and phase field averages of strain and stress fields, which may be useful in estimates of dimensional changes and life expectancy. Here we compare predictions obtained under the said conditions between the discrete finite element model Model 3 shown in Fig. 7.9c, and the layered model COMB3.1, which has layer overall properties of the kind shown in Figs. 7.10 and 7.11. It turns out that properties of layers with a distinct matrix phase are closely approximated by one of the two Mori-Tanaka estimates. The skeletal zone separating the distinct matrix layers is well represented

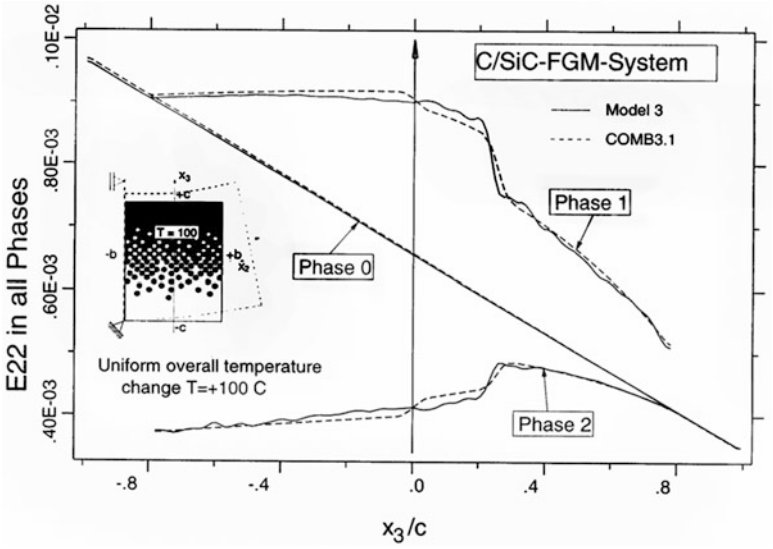

Fig. 7.13 Comparisons of average transverse strains $\varepsilon_{22}(x_3)$ caused by a uniform change in temperature. Phase 0 denotes the effective medium, Phase 1 is carbon, and Phase 2 is silicone carbide

by the self-consistent estimate and by the transition functions. Narrower transition zones in model COMB3.2 are indicated for systems with sharper boundaries, shown for example in Fig. 7.9a. Figure 7.13, shows close agreement between all phase strain averages computed with the discrete finite element Model 3 and the homogenized layer model COMB3.1.

Next, the graded layer was subjected to a thermal gradient. Assuming that the thermal and mechanical responses are not coupled, the steady state temperature distribution caused by the prescribed heat flow is evaluated first, and then applied together with the mechanical constraints to the solution domain. Figure 7.14 compares predictions of temperature distribution through the thickness of the graded layer under an applied temperature gradient. In this case, a close agreement is found between the finite element Model 3 and COMB3.1, while other layered models show small deviations.

Figure 7.15 shows the overall and phase transverse strain $\varepsilon_{22}(x_3)$ averages predicted by the two models. Notice that the overall transverse strain is near zero through the thickness of the layer, a desirable if fortuitous outcome, albeit under a small temperature difference. Steeper thermal gradients would generate overall transverse deformation. Finally, Fig. 7.16 shows the overall and phase transverse stress $\sigma_{22}(x_3)$ averages caused by the thermal gradient. Changes in material properties through the thickness cause very dissimilar trends in phase averages of transverse strain and stress, not observed in statistically homogeneous system.

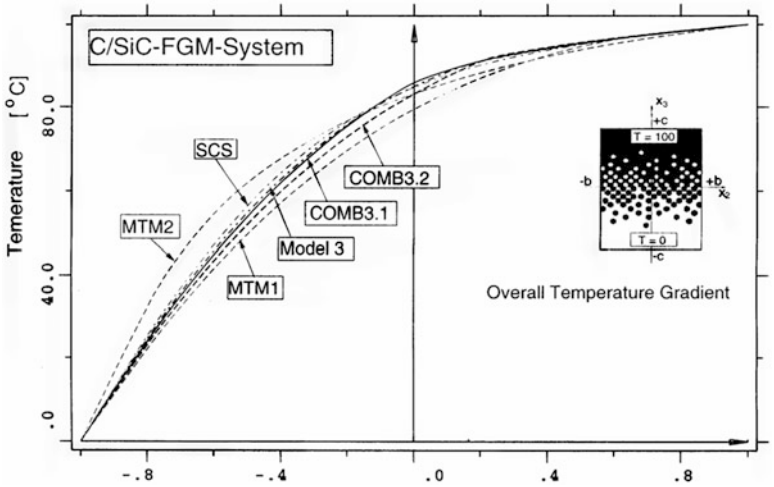

Fig. 7.14 Temperature distributions in the graded layer subjected to different surface temperatures, evaluated using discrete and homogenized layer models

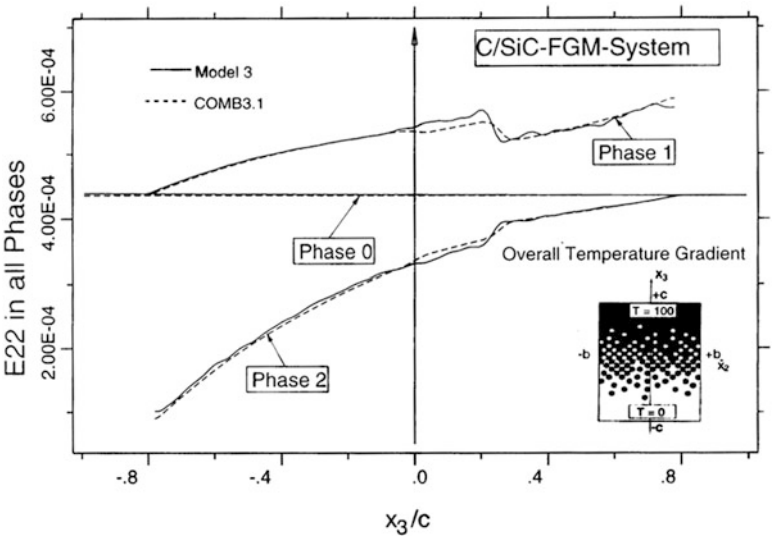

Fig. 7.15 Comparisons of average transverse strains $\varepsilon_{22}(x_3)$ caused by a temperature gradient of 100°C. Phase 0 denotes the effective medium, Phase 1 is carbon, and Phase 2 is silicone carbide

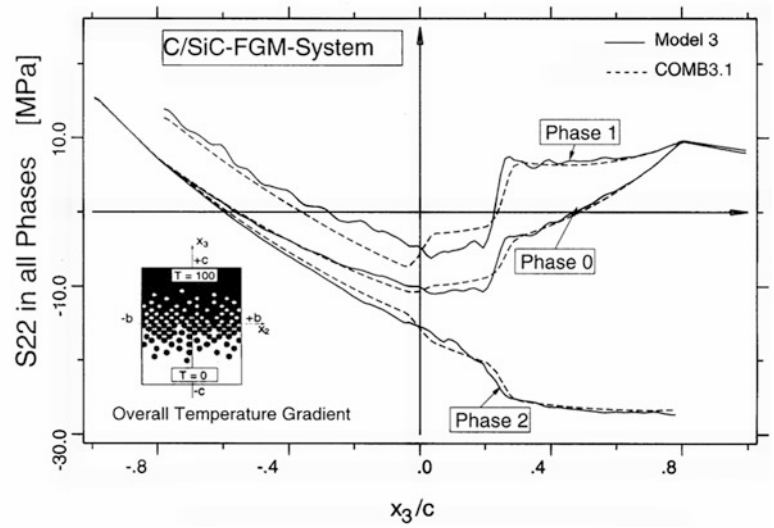

Fig. 7.16 Comparisons of average transverse stresses $\sigma_{22}(x_3)$ caused by a temperature gradient of 100°C. Phase 0 denotes the effective medium, Phase 1 is carbon, and Phase 2 is silicone carbide

These comparisons indicate the complex nature of strain and stress distributions in individual phases of the functionally graded materials. In single-gradient systems considered herein, the combined self-consistent and Mori-Tanaka estimates applied to layered models of the graded materials, provide fairly accurate predictions of both overall and phase strain and stress averages in systems subjected to mechanical and/or thermal changes and gradients.

Chapter 8
Transformation Fields

Together with the stresses caused by mechanical loads, composite materials must withstand stresses caused by distribution of transformation strains or eigenstrains in individual phases or subvolumes of each phase. As pointed out in Sect. 3.6.1, the former term applies here to all physically based deformations not caused by mechanical loads, including actual phase transformations. Frequent sources of transformation strains are changes in temperature and/or moisture content, piezoelectric and magneto-electro-elastic and pyroelectric effects (Benveniste 1992, 1993; Benveniste and Milton 2003), as well as diffusive and displacive transformations involved in kinetics of structural change in crystals and polycrystals (Ashby and Jones 1986), or martensitic phase transformations in steels, and shape memory alloys (Entchev and Lagudas 2002; Levitas and Javanbakh 2011). Inelastic deformations associated with plasticity, viscoelasticity and viscoplasticity will join this list in Chap. 12, but those will be analyzed in an entirely different setting.

As discussed in Sect. 3.6.1, regardless of their physical origin, all eigenstrains are regarded as deformations that would remain at a material point after instantaneous elastic unloading of that point to zero stress. Physically motivated eigenstrains are independent of current mechanical load. Equivalent eigenstrains may depend on both mechanical loads and physically based eigenstrains, and they vanish together with their sources. Although the said transformation strains are also present in polycrystalline metals and ceramics or polymers, their effect in composites and laminates is greatly magnified by the often high contrast between elastic moduli, coefficients of thermal expansion, and other physical properties of the constituents. Internal stresses caused by the eigenstrain fields can reach magnitudes that may compromise load bearing capacity or integrity of a composite material or structure. Therefore, they should be followed during fabrication, processing and service, and accounted for in structural analysis and design.

Results presented in Sect. 8.1 are mostly based on the method of uniform fields in two-phase heterogeneous media by Dvorak (1983, 1986), as summarized, rendered in contemporary notation and expanded by Benveniste and Dvorak (1989).

G.J. Dvorak, *Micromechanics of Composite Materials*, Solid Mechanics and Its Applications 186, DOI 10.1007/978-94-007-4101-0_8,

More general, adjustable uniform fields in elastic fiber reinforced system are described in Sect. 8.1.5. He (1999) extended the uniform field concept to nonlinear elastic fibrous composites. As the term suggests, uniform fields are independent of the geometry and material distribution in the microstructure, and therefore exact in that sense. Of course, the results they provide are in compliance with earlier work by Eshelby (1957), Levin (1967) and other writers named below.

Many transformation strains are caused by different but coupled field phenomena that are driven by independent sources at different rates. In multiphase composites and polycrytals, each transformation is assumed to be piecewise uniform and located in a particular volume fraction of the active phase. A local eigenstrain present in one phase or element of the representative volume may transmit a different amount of strain and stress to each other phase or element. Evaluation of the total local field average is based here on transformation influence functions or concentration factors, that monitor interaction between each pair of dissimilar eigenstrains in identical or different phase volume fractions. Section 8.2 shows their new derivation, for multiphase systems modeled by an average field approximation method.

Section 8.3 presents analysis of multiphase systems subjected to a uniform change in temperature. Section 8.4 summarizes different aspects of the overall and local elastic and transformation fields by inclusion-based averaging methods. It also mentions specific applications of the transformation field results to piezoelectric, magnetoelectric and other coupled field phenomena in composite media. Finally, certain other approaches to composites modeling will be noted.

The transformation influence function formalism will reappear in Chap. 12, on inelastic composite materials with elastic-plastic, viscoelastic or thermo-viscoplastic matrices, typical of metal matrix and certain polymer matrix composites. However, at each point in the matrix phase of such materials, the inelastic eigenstrains may reach dissimilar magnitudes which change during each step of an applied loading path. Therefore, the said formalism will be implemented using a finite element method, with the transformation influence functions derived for each pair of elements.

8.1 Uniform Change of Temperature in Two-Phase Composites and Polycrystals

Early efforts to estimate overall thermal expansion coefficients of composite materials, often with emphasis on two-phase systems, were reported by Schapery (1968), Rosen and Hashin (1970), Laws (1973, 1974). Later work includes contributions by Craft and Christensen (1981), Mikata and Taya (1986) and Takao and Taya (1985). Much of this early work used Eshelby's (1957) equivalent inclusion method and original Mori and Tanaka (1973) formalism. A general discussion and solutions of many thermoelastic problems can be found in several classic monographs, such as Boley and Wiener (1960) and Sneddon (1974).

Table 8.1 Thermal strain vectors of anisotropic solids

Isotropic or cubic	$\boldsymbol{m} = \{\alpha, \alpha, \alpha, 0, 0, 0\}^{\mathrm{T}}$
Transversely isotropic, trigonal, tetragonal	$\boldsymbol{m}=\{\alpha_A, \alpha_T, \alpha_T, 0, 0, 0\}^{\mathrm{T}}$
Orthogonal	$\boldsymbol{m}=\{\alpha_1, \alpha_2, \alpha_3, 0, 0, 0\}^{\mathrm{T}}$
Monoclinic ($x_3 = 0$)	$\boldsymbol{m}=\{\alpha_1, \alpha_2, \alpha_3, 0, 0, \alpha_6\}^{\mathrm{T}}$
Triclinic	$\boldsymbol{m}=\{\alpha_1, \alpha_2, \alpha_3, \alpha_4, \alpha_5, \alpha_6\}^{\mathrm{T}}$

8.1.1 Thermal Strain Vectors of Anisotropic Solids

Constitutive relations of isotropic solids, subjected to both a uniform deformation ε_{ij} and a uniform change in temperature $\Delta\theta = \theta - \theta_0$ from a reference temperature θ_0, can be written for any phase r in the form

$$\sigma_{ij}^r = \left(K_r - \frac{2}{3}G_r\right)\delta_{ij}\varepsilon_{mm}^r + 2G_r\varepsilon_{ij}^r - 3\alpha_r K_r \delta_{ij}\Delta\theta \tag{8.1.1}$$

where K_r, G_r are the phase bulk and shear moduli, and α_r is the linear coefficient of thermal expansion.

For all material symmetries, the corresponding relations follow from (3.6.1) and (3.6.15), with the phase and overall thermal strain vectors denoted by the symbol $\boldsymbol{m}_r$ and $\boldsymbol{m}$. Local and overall thermal eigenstrains are $\boldsymbol{\mu}_r = \boldsymbol{m}_r\Delta\theta$ and $\boldsymbol{\mu} = \boldsymbol{m}\Delta\theta$. Thermal eigenstresses are $\boldsymbol{\lambda}_r = \boldsymbol{l}_r\Delta\theta$ and $\boldsymbol{\lambda} = \boldsymbol{l}\Delta\theta$. Response of constituent phases is then described by

$$\left.\begin{aligned} \boldsymbol{\sigma}_r(\boldsymbol{x}) = \boldsymbol{L}_r\boldsymbol{\varepsilon}_r(\boldsymbol{x}) + \boldsymbol{l}_r\Delta\theta \quad \boldsymbol{\varepsilon}_r(\boldsymbol{x}) = \boldsymbol{M}_r\boldsymbol{\sigma}_r(\boldsymbol{x}) + \boldsymbol{m}_r\Delta\theta \\ \boldsymbol{l}_r = -\boldsymbol{L}_r\boldsymbol{m}_r \quad \boldsymbol{m}_r = -\boldsymbol{M}_r\boldsymbol{l}_r \end{aligned}\right\} \tag{8.1.2}$$

and of the composite as

$$\left.\begin{aligned} \boldsymbol{\sigma} = \boldsymbol{L}\boldsymbol{\varepsilon} + \boldsymbol{l}\Delta\theta \quad \boldsymbol{\varepsilon} = \boldsymbol{M}\boldsymbol{\sigma} + \boldsymbol{m}\Delta\theta \\ \boldsymbol{l} = -\boldsymbol{L}\boldsymbol{m} \quad \boldsymbol{m} = -\boldsymbol{M}\boldsymbol{l} \end{aligned}\right\} \tag{8.1.3}$$

These relations hold in temperature intervals which do not cause changes in the elastic moduli or coefficients of thermal expansion of the phases. Composites with temperature-dependent material properties can be treated as indicated in Sect. 8.3.2.

Coefficients of the thermal strain vectors are equal to the linear coefficients of thermal expansion of a phase or composite, and they have the dimension 1/°C. Their number and position depend on material symmetry, as explained in detail by Nye (1957, 1985, §5), and summarized in Table 8.1. The α_A, α_T denote longitudinal and transverse expansion coefficients of transversely isotropic, trigonal and tetragonal solids with $x_A \equiv x_1$ axis of rotational symmetry, such as aligned fiber composites.

In the monoclinic system, $\alpha_6 = \alpha_{12}$ describes thermal shear deformation in the $x_3 = 0$, or x_1x_2-plane of symmetry. Of course, this would be replaced by $\alpha_4 = \alpha_{23}$ for symmetry plane selected as $x_1 = 0$. The shear coefficients in the monoclinic and triclinic systems must comply with the contracted tensorial or engineering matrix notations currently used for mechanical strains, stiffness and compliance.

Notice that the thermal strain vectors of the first six symmetries in Table 8.1, excluding the monoclinic and triclinic, have only up to three nonzero coefficients of thermal expansion in the directions of normals to the planes of the particular material symmetry, and zero shear components. All of them also have only zero-valued coefficients in the second and third partitions of their stiffness and compliance matrices, which prevent coupling between normal and shear stress and strain components. These properties are exploited in evaluation of overall expansion coefficients of polycrystals and fiber composites.

8.1.2 Composites of Two Isotropic Phases

A representative volume V contains a two-phase composite $r = \alpha,\ \beta$, that has an arbitrary phase geometry. Both phases are isotropic and their spatial distribution in V guarantees statistical homogeneity of the aggregate. However, overall material symmetry can be represented by any of the eight symmetries described in Chap. 2. Our goal is to find the overall deformation of a representative volume V, caused by a uniform change in temperature $\Delta\theta$. Only reversible elastic deformation is allowed, possibly superimposed with a previously induced residual field. While the results follow as a special case from the general expressions (3.6.18) or (3.6.19), they can be found in a simpler, more transparent form as follows.

With reference to (3.6.9) and (8.1.1), let us create in the aggregate an auxiliary uniform isotropic stress $\hat{\sigma} = \hat{\sigma}_{kk}/3$ and a uniform isotropic strain $\hat{\varepsilon} = \hat{\varepsilon}_{kk}/3$

$$\hat{\varepsilon} = \hat{\sigma}/(3K_\alpha) + \alpha_\alpha \Delta\theta = \hat{\sigma}/(3K_\beta) + \alpha_\beta \Delta\theta \tag{8.1.4}$$

where α_r and K_r denote the linear coefficients of thermal expansion and bulk moduli of the phases. This yields the auxiliary overall isotropic stress and strain

$$\hat{\sigma} = \frac{3K_\alpha K_\beta}{K_\alpha - K_\beta}(\alpha_\alpha - \alpha_\beta)\Delta\theta \quad \hat{\varepsilon} = \frac{K_\alpha\alpha_\alpha - K_\beta\alpha_\beta}{K_\alpha - K_\beta}\Delta\theta \tag{8.1.5}$$

In matrix form, $\hat{\boldsymbol{\sigma}} = [\hat{\sigma},\ \hat{\sigma},\ \hat{\sigma},\ 0,\ 0,\ 0]^{\mathrm{T}}$ and $\hat{\boldsymbol{\varepsilon}} = [\hat{\varepsilon},\ \hat{\varepsilon},\ \hat{\varepsilon},\ 0,\ 0,\ 0]^{\mathrm{T}}$. Unloading from $\hat{\sigma}$ by application of a uniform overall stress $-\hat{\sigma}\,\delta_{ij}$ renders the aggregate free of surface tractions, leaving the overall strain caused by $\Delta\theta$. The remaining thermal strain is written in subscript and matrix forms as

$$m_{ij}\Delta\theta = \hat{\varepsilon}\delta_{ij} - M_{ijkl}\hat{\sigma}\delta_{kl} \quad \boldsymbol{m}\Delta\theta = \hat{\boldsymbol{\varepsilon}} - \boldsymbol{M}\hat{\boldsymbol{\sigma}} \tag{8.1.6}$$

where m_{ij} is the overall thermal strain tensor, M_{ijkl} is the overall compliance tensor. The thermal strain vector $\boldsymbol{m}$ and compliance $\boldsymbol{M}$ are (6×1) and (6×6) matrices, respectively, with nonzero coefficients determined by the overall material symmetry.

In addition to the overall coefficient of thermal expansion, it is often useful to determine the *averages of phase stresses* caused by a uniform change in temperature, and compare those with relevant strength magnitudes. The results are provided by the unloading steps

$$\boldsymbol{\sigma}_r = (\boldsymbol{I} - \boldsymbol{B}_r)\hat{\boldsymbol{\sigma}} \quad \boldsymbol{\varepsilon}_r = (\boldsymbol{I} - \boldsymbol{A}_r)\hat{\boldsymbol{\varepsilon}} \tag{8.1.7}$$

where $\boldsymbol{A}_r, \boldsymbol{B}_r$ are the mechanical concentration factors, which can be determined, for example, by one of the methods described in Chap. 7. For the self-consistent estimate, these factors appear in (7.1.1), and for the Mori-Tanaka method in (7.2.2), (7.2.7), or in (7.2.4), (7.2.9) for two-phase systems.

When the two-phase aggregate of two isotropic phases is also isotropic on the macroscale, the linear coefficient of thermal expansion is found by writing (8.1.4) or (8.1.6) as

$$\left.\begin{aligned} \alpha\Delta\theta &= \hat{\varepsilon} - \hat{\sigma}/(3K) = \hat{\sigma}[1/(3K_\alpha) - 1/(3K)] + \alpha_\alpha\Delta\theta \\ &= \hat{\sigma}[1/(3K_\beta) - 1/(3K)] + \alpha_\beta\Delta\theta \end{aligned}\right\} \tag{8.1.8}$$

where K is the overall bulk modulus, estimated in Sect. 6.4.3, as a function of the volume fractions $c_\alpha + c_\beta = 1$ of the phases. After unloading by $-\hat{\sigma}$ (Cribb 1968)

$$\alpha = \frac{1}{K(K_\alpha - K_\beta)}[K_\alpha(K - K_\beta)\alpha_\alpha - K_\beta(K - K_\alpha)\alpha_\beta] \tag{8.1.9}$$

This simplified form of (8.1.6) provides a connection between the overall expansion coefficient and the estimated or measured bulk modulus K of a representative volume of two-phase isotropic composites with isotropic phases of any microgeometry. An equivalent result that depends explicitly on phase volume fractions and on K follows from the Levin formula (Rosen and Hashin 1970)

$$\alpha = c_\alpha\alpha_\alpha + c_\beta\alpha_\beta + \frac{(\alpha_\alpha - \alpha_\beta)}{(1/K_\alpha - 1/K_\beta)}\left[\frac{1}{K} - \frac{c_\alpha}{K_\alpha} - \frac{c_\beta}{K_\beta}\right] \tag{8.1.10}$$

For $\alpha_\alpha = \alpha_\beta$, both forms yield $\alpha = \alpha_\alpha = \alpha_\beta$, indicating that application of a uniform thermal eigenstrain in the entire volume yields a uniform overall eigenstrain $\alpha\Delta\theta$.

Since α is a monotonic function of K, the upper [lower] bound on K provides a lower [upper] bound on α. In particular, using the bounds (6.3.22) for an arbitrary,

statistically homogeneous microstructure with well-ordered moduli, Levin (1967) and Rosen and Hashin (1970) show that the expansion coefficients are bracketed by

$$\frac{G_\beta}{3K_\alpha K_\beta + 4G_\beta \bar{K}} \geq \frac{\alpha - \bar{\alpha}}{4c_\alpha c_\beta (K_\alpha - K_\beta)(\alpha_\alpha - \alpha_\beta)} \geq \frac{G_\alpha}{3K_\alpha K_\beta + 4G_\alpha \bar{K}} \tag{8.1.11}$$

where $\bar{\alpha} = c_\alpha \alpha_\alpha + c_\beta \alpha_\beta$, $\bar{K} = c_\alpha K_\alpha + c_\beta K_\beta$, and $G_\alpha \leq G_\beta$.

8.1.3 Polycrystals

Connections between overall thermal expansion coefficients and overall elastic moduli can also be established for certain *multiphase aggregates*, such as polycrystals consisting of differently orientated grains of the same anisotropic material. As in Dvorak (1983), the procedure is again based on a uniform strain field, generated in the entire volume of the polycrystal by simultaneous application of an isotropic auxiliary stress $-\hat{p}$ and change in temperature $\Delta\theta$, both uniform, such that each constituent crystal grain undergoes pure dilatation of the same magnitude. This response is found in either trigonal, tetragonal, transversely isotropic or cubic crystals which exhibit axisymmetric deformation under the said loads. Auxiliary strain in each crystal grain can be made isotropic by adjusting the $\hat{p}/\Delta\theta$ ratio.

As indicated in Tables 2.2 and 2.3, the three material symmetries have similarly designated coefficients in the first (3×3) partition of their respective stiffness matrices. The same is true for stiffness coefficients of the cubic crystal, which are also connected by (2.2.18). All four compliance matrices have the same structure as the stiffness matrices, with M_{ij} coefficients replacing L_{ij}. Thermal strain vectors in Table 8.1 are also similar in that they do not include shear terms.

Suppose that each constituent single crystal is separated from the aggregate, and then subjected to a uniform auxiliary pressure $\hat{\sigma}_{kk}/3 = -\hat{p}$ and to a uniform temperature change $\Delta\theta$. As in the case of transverse isotropy in (2.3.8), both loads cause longitudinal and transverse strains $\varepsilon_A = \varepsilon_{11}$, $\varepsilon_T = (\varepsilon_{22} + \varepsilon_{33})/2$ in the principal material coordinates $x_1 \equiv x_A \perp x_T$ of each crystal. The auxiliary strain magnitudes are

$$\left.\begin{aligned} &\hat{\varepsilon}_A = -\eta_1 \hat{p} + \alpha_A \Delta\theta \quad \hat{\varepsilon}_T = -\eta_2 \hat{p} + \alpha_T \Delta\theta \\ &\eta_1 = M_{11} + M_{12} + M_{13} \quad \eta_2 = M_{21} + M_{22} + M_{23} \end{aligned}\right\} \tag{8.1.12}$$

where M_{ij} are coefficients of the compliance matrix of each crystal. For example, if each crystal exhibits hexagonal, or transversely isotropic material symmetry, the M_{ij} are taken from (2.3.2) to yield $(\eta_1 - \eta_2) = [(1 - \nu_{12})/E_{11} - (1 - \nu_{32})/E_{22}]$.

Isotropic dilatation of each grain is required, and it can be achieved by the auxiliary pressure

$$\hat{\varepsilon}_A = \hat{\varepsilon}_T \;\Rightarrow -(\eta_1 - \eta_2)\hat{p} = -(\alpha_A - \alpha_T)\Delta\theta \;\Rightarrow\; \hat{p}/\Delta\theta = \frac{\alpha_A - \alpha_T}{\eta_1 - \eta_2} \tag{8.1.13}$$

Substitution of this value of $\hat{p}$ in (8.1.12) yields local auxiliary strain in each grain as

$$\hat{\varepsilon}_A = \hat{\varepsilon}_T = \frac{\eta_1\alpha_T - \eta_2\alpha_A}{\eta_1 - \eta_2}\Delta\theta \tag{8.1.14}$$

Since all crystals undergo identical isotropic deformation while loaded by the above ratio of isotropic pressure $-\hat{p}$ and uniform thermal change $\Delta\theta$, the polycrystal can be reassembled as long as $-\hat{p}$ is applied at its outer boundary, and the entire aggregate is subjected to $\Delta\theta$. The overall auxiliary strain field then is $\hat{\bar{\varepsilon}} = \hat{\varepsilon}_A = \hat{\varepsilon}_T$.

The overall compliance $\boldsymbol{M} = \boldsymbol{L}^{-1}$ of the polycrystal is assumed to be known. No restrictions need to be placed on the overall material symmetry of the polycrystal, even though the symmetry of individual grains is higher or equal to trigonal. The overall thermal strain vector $\boldsymbol{m}$ has the nonzero coefficients shown in Table 8.1 for the overall material symmetry of the polycrystal.

Overall deformation of the polycrystal that is caused by the uniform thermal change is obtained by subtracting from the auxiliary strain field $\hat{\bar{\varepsilon}}$ the overall strain caused by the pressure $-\hat{p}$

$$\boldsymbol{\varepsilon} = \hat{\bar{\varepsilon}}\boldsymbol{\delta} + \hat{p}\boldsymbol{M}\boldsymbol{\delta} = \boldsymbol{m}\Delta\theta \tag{8.1.15}$$

where $\boldsymbol{\delta} = \{1, 1, 1, 0, 0, 0\}^{\mathrm{T}}$. This yields the overall strain vector

$$\boldsymbol{m} = \frac{\eta_1\alpha_T - \eta_2\alpha_A}{\eta_1 - \eta_2}\boldsymbol{\delta} + \frac{\alpha_A - \alpha_T}{\eta_1 - \eta_2}\boldsymbol{M}\boldsymbol{\delta} \tag{8.1.16}$$

This connection was obtained by Schulgasser (1987), as a generalization of an earlier result by Hashin (1984), valid for macroscopically isotropic polycrystals; see also Milton (2002). In an isotropic polycrystal, the overall expansion coefficient α and bulk modulus K are related by

$$\alpha = \frac{\alpha_A - \alpha_T}{(\eta_1 - \eta_2)K} + \frac{\eta_1\alpha_T - \eta_2\alpha_A}{\eta_1 - \eta_2} \tag{8.1.17}$$

Of course, $\hat{p} = 0$ for $\alpha_A = \alpha_T = \alpha$.

Benveniste (1996) applied the method of uniform fields to show that the Hashin and Schulgasser results apply also to polycrystals with imperfect interfaces that permit grain boundary sliding, providing that the sliding is reflected in the known overall compliance. He also shows that if the constituent crystals are cubic, then the polycrystal with grain boundary sliding has the same thermal expansion as the cubic single crystal.

Notice that the last two relations hold for any shape and orientation of the constituent grains, as long as they all have the same thermoelastic moduli. Applications of (8.1.16) can be found, for example, in rolled steel or aluminum plates, which have somewhat different elastic moduli in the rolling, transverse and thickness directions,

indicating orthotropic overall symmetry of a polycrystal consisting of cubic crystals. Notice that accuracy of $\boldsymbol{m}$ and $\bar{\alpha}$ can be degraded when $\eta_1 - \eta_2$ is very small.

8.1.4 Aligned Fiber Composites

In a transversely isotropic aligned fiber composite consisting of *two isotropic phases,* thermal change causes only longitudinal and transverse deformation, both uniform on the macroscale. The coefficients $\alpha_A,\ \alpha_T$ of the overall thermal strain vector can be found by utilizing the auxiliary uniform stress and strain fields in systems with isotropic phases, described by (8.1.4) and by

$$\hat{\sigma} = \frac{3K_\alpha K_\beta}{K_\alpha - K_\beta}(\alpha_\alpha - \alpha_\beta)\Delta\theta \quad \hat{\varepsilon} = \frac{K_\alpha\alpha_\alpha - K_\beta\alpha_\beta}{K_\alpha - K_\beta}\Delta\theta \qquad [8.1.5]$$

The elastic unloading to zero overall tractions, $\boldsymbol{m}\Delta\theta = \hat{\boldsymbol{\varepsilon}} - \boldsymbol{M}\hat{\boldsymbol{\sigma}}$, suggested by (8.1.6), is now based on the reduced (2×2) overall compliance matrix for axisymmetric deformation of a transversely isotropic solid that appears in $(2.3.8)_6$

$$\begin{bmatrix} \alpha_A \\ 2\alpha_T \end{bmatrix} = \begin{bmatrix} \hat{\varepsilon}_A/\Delta\theta \\ 2\hat{\varepsilon}_T/\Delta\theta \end{bmatrix} - \frac{1}{(kn - l^2)}\begin{bmatrix} k & -l \\ -l & n \end{bmatrix}\begin{bmatrix} \hat{\sigma}_A/\Delta\theta \\ \hat{\sigma}_T/\Delta\theta \end{bmatrix} \qquad (8.1.18)$$

where $\hat{\varepsilon}_A = \hat{\varepsilon}_{11},\quad \hat{\varepsilon}_T = (\hat{\varepsilon}_{22} + \hat{\varepsilon}_{33}),\quad \hat{\sigma}_A = \hat{\sigma}_{11},\quad \hat{\sigma}_T = (\hat{\sigma}_{22} + \hat{\sigma}_{33})/2$, and $k,\ n,\ l$ are the overall Hill's moduli of the transversely isotropic fibrous aggregate in (2.3.3), associated with axisymmetric deformation. For the fiber composite, k is bracketed by (6.4.1); when the matrix is the α–phase, and $m_\alpha < m_\beta$, one selects the lower bound. The moduli $n,\ l$ follow from the universal connections (3.9.4). The overall expansion coefficients of a fibrous composite of two isotropic phases are

$$\alpha_A = \hat{\varepsilon}/\Delta\theta - \frac{k - l}{kn - l^2}\hat{\sigma}/\Delta\theta \quad \alpha_T = \hat{\varepsilon}/\Delta\theta - \frac{n - l}{2(kn - l^2)}\hat{\sigma}/\Delta\theta \qquad (8.1.19)$$

where the $\hat{\sigma}$ and $\hat{\varepsilon}$ are given by (8.1.5).

Rosen and Hashin (1970) derived a more compact form using the Levin formula

$$\left.\begin{aligned} \alpha_A &= c_\alpha\alpha_\alpha + c_\beta\alpha_\beta + \frac{(\alpha_\alpha - \alpha_\beta)}{(1/K_\alpha - 1/K_\beta)}\left[\frac{3(k - l)}{k\,n - l^2} - \frac{c_\alpha}{K_\alpha} - \frac{c_\beta}{K_\beta}\right] \\ \alpha_T &= c_\alpha\alpha_\alpha + c_\beta\alpha_\beta + \frac{(\alpha_\alpha - \alpha_\beta)}{(1/K_\alpha - 1/K_\beta)}\left[\frac{3(n - l)}{2(k\,n - l^2)} - \frac{c_\alpha}{K_\alpha} - \frac{c_\beta}{K_\beta}\right] \end{aligned}\right\} \qquad (8.1.20)$$

They also pointed out that the universal connections (3.9.4) between phase and overall Hill's moduli can be used to show that the $\alpha_A,\ \alpha_T$ are monotonic functions of one of the moduli. Therefore, bounds on the moduli may be substituted into (8.1.20) in order to obtain bounds on the expansion coefficients.

Thermal expansion of aligned fiber composites of *two transversely isotropic phases*, $r = \alpha, \beta$, is also limited to uniform axisymmetric deformation in the longitudinal and transverse directions. Linear thermal expansion coefficients α_A, α_T of the overall thermal strain vector can be found by constructing an auxiliary stress field that is uniform in the entire aggregate. Equation (8.1.4) is now replaced by an expanded form of (8.1.18), describing a superposition of applied auxiliary tractions causing overall stresses $\hat{\sigma}_A$, $\hat{\sigma}_T$ with distinct thermal phase eigenstrains $\alpha_A^r \Delta\theta$, $\alpha_T^r \Delta\theta$ in the two phases. The auxiliary uniform strain field is

$$\left.\begin{aligned}\begin{bmatrix}\hat{\varepsilon}_A\\ 2\hat{\varepsilon}_T\end{bmatrix} &= \frac{1}{(k_\alpha n_\alpha - l_\alpha^2)}\begin{bmatrix}k_\alpha & -l_\alpha\\ -l_\alpha & n_\alpha\end{bmatrix}\begin{bmatrix}\hat{\sigma}_A\\ \hat{\sigma}_T\end{bmatrix} + \begin{bmatrix}\alpha_A^\alpha \Delta\theta\\ 2\alpha_T^\alpha \Delta\theta\end{bmatrix}\\ &= \frac{1}{(k_\beta n_\beta - l_\beta^2)}\begin{bmatrix}k_\beta & -l_\beta\\ -l_\beta & n_\beta\end{bmatrix}\begin{bmatrix}\hat{\sigma}_A\\ \hat{\sigma}_T\end{bmatrix} + \begin{bmatrix}\alpha_A^\beta \Delta\theta\\ 2\alpha_T^\beta \Delta\theta\end{bmatrix}\end{aligned}\right\} \tag{8.1.21}$$

Similar form can be written if one or both phases have trigonal or tetragonal material symmetry. Their stiffness matrices will be different, but the thermal strain vectors are similar. The auxiliary overall stress field components are found by solving $(8.1.21)_2$, as

$$\left.\begin{aligned}\hat{\sigma}_A &= -\frac{\eta(\alpha_A^\alpha - \alpha_A^\beta) + 2\lambda(\alpha_T^\alpha - \alpha_T^\beta)]}{\kappa\eta - \lambda^2}\Delta\theta\\ \hat{\sigma}_T &= -\frac{\lambda(\alpha_A^\alpha - \alpha_A^\beta) + 2\kappa(\alpha_T^\alpha - \alpha_T^\beta)}{\kappa\eta - \lambda^2}\Delta\theta\end{aligned}\right\} \tag{8.1.22}$$

where

$$\left.\begin{aligned}&\kappa = 1/E_{11}^\alpha - 1/E_{11}^\beta \quad \lambda = l_\alpha/(E_{11}^\alpha k_\alpha) - l_\beta/(E_{11}^\beta k_\beta)\\ &\eta = n_\alpha/(E_{11}^\alpha k_\alpha) - n_\beta/(E_{11}^\beta k_\beta)\end{aligned}\right\} \tag{8.1.23}$$

and $E_{11}^r = n_r - l_r^2/k_r$, according to (2.3.5). Notice that $\hat{\sigma}_A \neq 0$, $\hat{\sigma}_T \neq 0$ while $\alpha_A^\alpha \neq \alpha_A^\beta$, $\alpha_T^\alpha \neq \alpha_T^\beta$. When the CTEs are equal, the entire volume undergoes uniform thermal deformation at zero auxiliary tractions.

Unloading to zero overall tractions from the uniform fields (8.1.21), similar to that in (8.1.18), provides the two linear coefficients of thermal expansion

$$\left.\begin{aligned}\begin{bmatrix}\alpha_A\\ 2\alpha_T\end{bmatrix} &= \frac{1}{(k_r n_r - l_r^2)}\begin{bmatrix}k_r & -l_r\\ -l_r & n_r\end{bmatrix}\begin{bmatrix}\hat{\sigma}_A/\Delta\theta\\ \hat{\sigma}_T/\Delta\theta\end{bmatrix}\\ &+ \begin{bmatrix}\alpha_A^r \Delta\theta\\ 2\alpha_T^r \Delta\theta\end{bmatrix} - \frac{1}{(kn - l^2)}\begin{bmatrix}k & -l\\ -l & n\end{bmatrix}\begin{bmatrix}\hat{\sigma}_A/\Delta\theta\\ \hat{\sigma}_T/\Delta\theta\end{bmatrix}\end{aligned}\right\} \tag{8.1.24}$$

where $r = \alpha$ or $r = \beta$. In contrast to (8.1.20), the expansion coefficients in (8.1.19) and (8.1.24) depend on phase volume fractions only through the overall

moduli. Both are independent of the geometry of phase crossections, or on their distribution in the transverse plane. However, the latter may be needed in estimating the magnitudes of overall moduli $E_{11},\ k,\ l$ and n, when not available from direct measurement.

Averages of the strain and stress fields caused in the two phases by the thermal eigenstrains, in superposition with a uniform overall strain or stress, depend on the mechanical concentration factors $\boldsymbol{A}_r, \boldsymbol{B}_r$, and on the transformation concentration factors $\boldsymbol{D}_{rs}, \boldsymbol{F}_{rs}$, derived for two-phase systems in Sect. 3.6. In particular,

$$\boldsymbol{\varepsilon}_r = \boldsymbol{A}_r \boldsymbol{\varepsilon}^0 + \sum_{s=\alpha}^{s=\beta} \boldsymbol{D}_{rs} \boldsymbol{\mu}_s \quad \boldsymbol{\sigma}_r = \boldsymbol{B}_r \boldsymbol{\sigma}^0 + \sum_{s=\alpha}^{s=\beta} \boldsymbol{F}_{rs} \boldsymbol{\lambda}_s \tag{3.6.5}$$

$$\left.\begin{aligned} \boldsymbol{D}_{r\alpha}(\boldsymbol{x}) &= (\boldsymbol{I} - \boldsymbol{A}_r(\boldsymbol{x}))(\boldsymbol{L}_\alpha - \boldsymbol{L}_\beta)^{-1} \boldsymbol{L}_\alpha \\ \boldsymbol{D}_{r\beta}(\boldsymbol{x}) &= -(\boldsymbol{I} - \boldsymbol{A}_r(\boldsymbol{x}))(\boldsymbol{L}_\alpha - \boldsymbol{L}_\beta)^{-1} \boldsymbol{L}_\beta \end{aligned}\right\} \tag{3.6.8}$$

$$\left.\begin{aligned} \boldsymbol{F}_{r\alpha}(\boldsymbol{x}) &= (\boldsymbol{I} - \boldsymbol{B}_r(\boldsymbol{x}))(\boldsymbol{M}_\alpha - \boldsymbol{M}_\beta)^{-1} \boldsymbol{M}_\alpha \\ \boldsymbol{F}_{r\beta}(\boldsymbol{x}) &= -(\boldsymbol{I} - \boldsymbol{B}_r(\boldsymbol{x}))(\boldsymbol{M}_\alpha - \boldsymbol{M}_\beta)^{-1} \boldsymbol{M}_\beta \end{aligned}\right\} \tag{3.6.11}$$

The $\boldsymbol{A}_r, \boldsymbol{B}_r$ can be determined by one of the methods described in Chap. 7. For the self-consistent estimate, they are derived in (7.1.1), and for the Mori-Tanaka method in (7.2.2), (7.2.7), or in (7.2.4), (7.2.9) for two-phase systems. They also follow from (6.1.3) to (6.1.4).

8.1.5 Adjustable Uniform Fields in Fiber Composites

Next, recall from Sect. 3.9.2 that *a more general uniform field in aligned fiber composites* can be generated by allowing for different longitudinal normal stresses $\hat{\sigma}_{11}^{\alpha} \neq \hat{\sigma}_{11}^{\beta} \neq \hat{\sigma}_A$ in the two phases. This field provides useful connections between the auxiliary overall and phase stresses that are not revealed by (8.1.18) or (8.1.21).

The composite material consists of two distinct phases $r = \alpha,\ \beta$, that are perfectly bonded along interfaces aligned with the $x_1 -$ axis of the overall coordinates. Each phase may be at most transversely isotropic, with $x_1 -$ axis of rotational symmetry. Arbitrary geometry of the phases can be admitted in the transverse plane. Representative volume requirements outlined in Sect. 3.3 are assumed to be satisfied, implying monoclinic or higher effective material symmetry on the macroscale.

Initially free of both mechanical and residual stresses, the composite material is transformed by certain uniform phase eigenstrains $\boldsymbol{\mu}_\alpha \neq \boldsymbol{\mu}_\beta$, regarded in general as 12 independent loading parameters; $\boldsymbol{\mu}_r = [\mu_1^r,\ \mu_2^r,\ \mu_3^r,\ 2\mu_4^r,\ 2\mu_5^r,\ 2\mu_6^r]^{\mathrm{T}}, r =$

$\alpha,\ \beta$, written in the engineering matrix notation (1.1.11). For example, a uniform thermal change $\Delta\theta$ applied to a transversely isotropic phase generates there only three nonzero eigenstrains $\mu_1^r = \alpha_A \Delta\theta,\ \mu_2^r = \mu_3^r = \alpha_T \Delta\theta,\ \ \mu_4^r = \mu_5^r = \mu_6^r = 0$, see Table 8.1.

As in Sect. 3.9.2, an axisymmetric pair of auxiliary uniform surface tractions, denoted by $\hat{\sigma}_A$ and $\hat{\sigma}_T$, is applied such that the total strain field, generated by the eigenstrains and tractions, becomes uniform in the entire volume V. At all interior points, the total phase strain fields then satisfy

$$\hat{\boldsymbol{\varepsilon}}_\alpha(\boldsymbol{x}) = \hat{\boldsymbol{\varepsilon}}_\beta(\boldsymbol{x}) = \hat{\bar{\boldsymbol{\varepsilon}}} \tag{8.1.25}$$

where $\hat{\bar{\boldsymbol{\varepsilon}}}$ is an as yet unknown auxiliary overall strain. Since all interfaces are aligned with the x_1-axis, traction continuity can be satisfied by piecewise uniform auxiliary phase stress fields

$$\left.\begin{aligned} &\hat{\sigma}_1^\alpha \neq \hat{\sigma}_1^\beta \qquad \hat{\sigma}_1 = c_\alpha \hat{\sigma}_1^\alpha + c_\beta \hat{\sigma}_1^\beta \\ &\hat{\sigma}_j = \hat{\sigma}_j^\alpha = \hat{\sigma}_j^\beta \ \text{ for } \ j = 2,\ 3,\ ..6 \end{aligned}\right\} \tag{8.1.26}$$

Constitutive relations of the two phases are again written as $\hat{\boldsymbol{\varepsilon}}_r = \boldsymbol{M}_r \hat{\boldsymbol{\sigma}}_r + \boldsymbol{\mu}_r$. Together with the requirement $\hat{\boldsymbol{\varepsilon}}_\alpha - \hat{\boldsymbol{\varepsilon}}_\beta = \boldsymbol{0}$, they provide the expanded form of (3.9.7)

$$M_{i1}^\alpha \hat{\sigma}_1^\alpha - M_{i1}^\beta \hat{\sigma}_1^\beta + \sum_{j=2}^{6} (M_{ij}^\alpha - M_{ij}^\beta)\hat{\sigma}_j + \mu_i^\alpha - \mu_i^\beta = 0 \tag{8.1.27}$$

where $i = 1, 2, \ldots 6$. Solution of the six equations for the seven unknown phase stresses depends on one free parameter, which can be adjusted as needed for different applications.

The overall auxiliary stress $\hat{\boldsymbol{\sigma}}^0$ that generates the uniform strain field (8.1.25) in the transformed aggregate is again uniform, and specified by (3.9.8)

$$\left.\begin{aligned} &\hat{\boldsymbol{\sigma}}^0 = [\hat{\sigma}_A, \hat{\sigma}_T, \hat{\sigma}_T, 0, 0, 0]^{\mathrm{T}} \\ &\hat{\sigma}_A = \hat{\sigma}_1 = c_\alpha \hat{\sigma}_1^\alpha + c_\beta \hat{\sigma}_1^\beta \quad \hat{\sigma}_T = \frac{1}{2}(\hat{\sigma}_2 + \hat{\sigma}_3) \end{aligned}\right\} \tag{8.1.28}$$

With $\hat{\sigma}_T$ selected as the free parameter, the solution of (8.1.27) is (Dvorak 1990)

$$\hat{\sigma}_1^\alpha = q\{(l_\alpha \Delta l - n_\alpha \Delta k)\hat{\sigma}_T + k_\alpha E_{11}^\alpha [l_\beta \Delta\mu_1^r + k_\beta(\Delta\mu_2^r + \Delta\mu_3^r)]\} \tag{8.1.29}$$

$$\hat{\sigma}_1^\beta = q\{(l_\beta \Delta l - n_\beta \Delta k)\hat{\sigma}_T + k_\beta E_{11}^\beta [l_\alpha \Delta\mu_1^r + k_\alpha(\Delta\mu_2^r + \Delta\mu_3^r)]\} \tag{8.1.30}$$

$$\hat{\sigma}^r_{2,3} = \hat{\sigma}_T \mp m^*(\Delta\mu^r_2 - \Delta\mu^r_3) \tag{8.1.31}$$

$$\hat{\sigma}_4 = -m^*\Delta\mu^r_4 \quad \hat{\sigma}_5 = -p^*\Delta\mu^r_5 \quad \hat{\sigma}_6 = -p^*\Delta\mu^r_6 \tag{8.1.32}$$

where

$$\left.\begin{aligned} &m^* = -m_\alpha m_\beta/(m_\alpha - m_\beta) \quad p^* = -p_\alpha p_\beta/(p_\alpha - p_\beta) \\ &q^{-1} = (l_\alpha k_\beta - k_\alpha l_\beta) = 2k_\alpha k_\beta(\nu^\alpha_L - \nu^\beta_L) \neq 0 \\ &m_\alpha \neq m_\beta, p_\alpha \neq p_\beta \end{aligned}\right\} \tag{8.1.33}$$

Also, $\Delta\eta = \eta_\alpha - \eta_\beta$ for any quantity η_r, and $\Delta\mu^r_i = \mu^\alpha_i - \mu^\beta_i$. The $\nu^r_L = \nu^r_{12}$ are phase longitudinal Poisson's ratios. A different solution, for $(\nu^\alpha_L - \nu^\beta_L) = 0$, can be found in *op. cit*. For isotropic phases, Hill's moduli appearing in the above stress components are replaced by bulk and shear moduli K and G and by Poisson's ratio ν, according to

$$\left.\begin{aligned} &k + m = n = \frac{2G(1-\nu)}{1-2\nu} \quad k - m = l = \frac{2G\nu}{1-2\nu} \quad m = p = G \\ &k = K + G/3 \quad l = K - 2G/3 \quad n = K + 4G/3 \end{aligned}\right\} \tag{2.3.6}$$

It can be verified that the $\hat{\sigma}_A, \hat{\sigma}_T$ in (8.1.22) follow from (8.1.29) and (8.1.30) as a special case, by letting $\hat{\sigma}^\alpha_1 = \hat{\sigma}^\beta_1 = \hat{\sigma}_A, \hat{\sigma}^r_2 = \hat{\sigma}^r_3 = \hat{\sigma}_T$.

For any choice of the parameter $\hat{\sigma}_T$, the uniform strain field $\hat{\hat{\boldsymbol{\varepsilon}}}$ that is caused in the entire volume by the overall stress $\hat{\boldsymbol{\sigma}}^0 = [\hat{\sigma}_A,\ \hat{\sigma}_T,\ \hat{\sigma}_T,\ 0,\ 0,\ 0]^{\mathrm{T}}$ and by the phase eigenstrains $\boldsymbol{\mu}_r$, can be evaluated by changing (8.1.18) to

$$\begin{bmatrix} \hat{\varepsilon}_1 \\ \hat{\varepsilon}_2 + \hat{\varepsilon}_3 \end{bmatrix} = \frac{1}{(k_r n_r - l_r^2)} \begin{bmatrix} k_r & -l_r \\ -l_r & n_r \end{bmatrix} \begin{bmatrix} \hat{\sigma}_A \\ \hat{\sigma}_T \end{bmatrix} + \begin{bmatrix} \mu^r_1 \\ \mu^r_2 + \mu^r_3 \end{bmatrix} \tag{8.1.34}$$

where $r = \alpha,\ \beta$. This result also applies to aligned fibrous systems that may not comply with representative volume requirements.

Overall eigenstrain $\bar{\boldsymbol{\mu}}$ or overall residual strain is found by unloading to zero overall stress from the auxiliary overall strain state; $\bar{\boldsymbol{\mu}} = \hat{\hat{\boldsymbol{\varepsilon}}} - \boldsymbol{M}\hat{\boldsymbol{\sigma}}^0$. For composites exhibiting overall transverse isotropy, components of the overall eigenstrain follow from (8.1.34) as

$$\begin{bmatrix} \bar{\mu}_1 \\ \bar{\mu}_2 + \bar{\mu}_3 \end{bmatrix} = \begin{bmatrix} \hat{\varepsilon}_1 \\ \hat{\varepsilon}_2 + \hat{\varepsilon}_3 \end{bmatrix} - \frac{1}{(kn - l^2)} \begin{bmatrix} k & -l \\ -l & n \end{bmatrix} \begin{bmatrix} \hat{\sigma}_A \\ \hat{\sigma}_T \end{bmatrix} \tag{8.1.35}$$

where k, l, n are the overall moduli. When the phase eigenstrains are the thermal strains $\mu^r_1 = \alpha_A\Delta\theta,\ \mu^r_2 = \mu^r_3 = \alpha_T\Delta\theta$, the said unloading leaves the strain

$\bar{\boldsymbol{\mu}} = \boldsymbol{m}\Delta\theta$, where $\boldsymbol{m}$ is the overall thermal strain vector. The same result can be found using the Levin formula (3.8.16), providing that at least one of the mechanical concentration factors $\boldsymbol{B}_r$ is known. Since both auxiliary strain and stress fields depend on phase moduli, eigenstrains and volume fractions, the last equation can be expanded into universal connections between phase and overall moduli and eigenstrains, or coefficients of thermal expansion, analogous to those in Sect. 3.9.

Residual phase strain and stress averages caused by application of the phase eigenstrains are obtained in the unloading step, as

$$\boldsymbol{\varepsilon}_r = \hat{\bar{\boldsymbol{\varepsilon}}} - \boldsymbol{A}_r \boldsymbol{M} \hat{\boldsymbol{\sigma}}^0 = \boldsymbol{M}_r \boldsymbol{\sigma}_r + \boldsymbol{\mu}_r \quad \boldsymbol{\sigma}_r = \hat{\boldsymbol{\sigma}}_r - \boldsymbol{B}_r \hat{\boldsymbol{\sigma}}^0 = \boldsymbol{L}_r(\boldsymbol{\varepsilon}_r - \boldsymbol{\mu}_r) \quad (8.1.36)$$

Notice that the above residual phase stresses do not follow by simply letting $\hat{\sigma}_T \to 0$ in (8.1.29–8.1.30), because that still leaves $\hat{\sigma}_A \neq 0$.

The parameter $\hat{\sigma}_T$ can be selected to generate a certain auxiliary stress state in the matrix, while the composite is also subjected to prescribed phase eigenstrains. In particular, the longitudinal and transverse stress components can be related by

$$\hat{\sigma}_1^\alpha = \rho\hat{\sigma}_2^\alpha = \rho\hat{\sigma}_3^\alpha = \rho\hat{\sigma}_\mathrm{T} \quad (8.1.37)$$

The transverse overall stress that supports this stress ratio follows from (8.1.29) and (8.1.31) as

$$\hat{\sigma}_T = qk_\alpha E_{11}^\alpha [l_\beta \Delta\mu_1^r + k_\beta(\Delta\mu_2^r + \Delta\mu_3^r)][\rho - q(l_\alpha \Delta l - n_\alpha \Delta k)]^{-1} \quad (8.1.38)$$

The corresponding longitudinal traction is $\hat{\sigma}_A = \hat{\sigma}_1 = c_\alpha \hat{\sigma}_1^\alpha + c_\beta \hat{\sigma}_1^\beta$ with the normal stresses $\hat{\sigma}_1^r$ evaluated in (8.1.29–8.1.30) for this particular value of $\hat{\sigma}_T$.

For $\rho = 1$, the stress field in the $\alpha -$ phase is isotropic, although that or both phases may be transversely isotropic. However, if the $\alpha -$ phase is an isotropic matrix, and the local eigenstrains $\mu_1^\alpha = \mu_2^\alpha = \mu_3^\alpha$, then it undergoes an isotropic deformation $\hat{\boldsymbol{\varepsilon}}_\alpha$. Since the total auxiliary strain field $\hat{\bar{\boldsymbol{\varepsilon}}}$ is uniform in the entire aggregate, both phase strains and the overall strain $\hat{\bar{\boldsymbol{\varepsilon}}} = \hat{\boldsymbol{\varepsilon}}_\alpha$ are also isotropic. Of course, the stress field in an anisotropic fiber or $\beta -$ phase need not be isotropic. This particular solution is used in Chap. 11, in analysis of thermal hardening in composites with elastic-plastic matrices.

8.1.6 *Coated Fiber Composites*

Elastic moduli, thermal expansion coefficients and local thermomechanical fields in matrix-based composites reinforced by coated, cylindrically orthotropic fibers were derived by Dvorak and Chen (1989), who has used the method of uniform fields in the three-phase systems. Benveniste et al. (1989, 1991a) and Chen et al. (1990) have derived complete local thermomechanical fields, overall moduli and thermal

expansion coefficients of coated fiber composites, for both transversely isotropic fibers and coatings, and for cylindrically orthotropic fibers of Sect. 2.4. Hatta and Taya (1986), Mikata and Taya (1986) and many other writers derived related results.

Here we focus on determination of coefficients of thermal expansion of aligned, coated fiber composites, which are transversely isotropic on the macroscale. Their overall response to a uniform change in temperature is isotropic in the transverse plane and uniform in the longitudinal fiber direction. Their thermal expansion coefficients can be estimated by introducing replacement fibers, which have the effective axisymmetric elastic moduli and thermal expansion coefficients of the coated fibers.

The replacement fiber is a cylindrical composite element, with circular fiber phase (denoted by $r = f$) of radius γ_f, surrounded by a coating layer ($r = g$) of uniform thickness γ_g. Both phases are transversely isotropic, with $x_1 = x_A$ as the axis of rotational symmetry. Fiber and coating volume fractions are $\phi_f = [\gamma_f/(\gamma_f + \gamma_g)]^2$ and $\phi_g = 1 - \phi_f$. The effective elastic moduli of the replacement fiber then follow form

$$\left.\begin{aligned} k_R &= \frac{\phi_f k_f (k_g + m_g) + \phi_g k_g (k_f + m_g)}{\phi_f (k_g + m_g) + \phi_g (k_f + m_g)} \\ l_R &= \frac{\phi_f l_f (k_g + m_g) + \phi_g l_g (k_f + m_g)}{\phi_f (k_g + m_g) + \phi_g (k_f + m_g)} \\ n_R - \phi_f n_f - \phi_g n_g &= -\frac{\phi_f \phi_g (l_f - l_g)^2}{(\phi_f k_g + \phi_g k_f + m_g)} \end{aligned}\right\} \tag{8.1.39}$$

Derived by Hill (1964b), these moduli coincide with those of the composite cylinder assemblage (Hashin and Rosen 1964).

Notice that the effective axisymmetric moduli k_1 and l_1 of the possibly multilayer core are known from the previous homogenization step, and that all moduli of the coating layer are among the given values. Therefore, (8.1.39) can be extended to incorporate additional layers, and thus generate axisymmetric elastic moduli for replacement fibers containing several layers of different coatings, or with functionally graded coatings. Recursive formulae for such problems were written by Hervé and Zaoui (1995). Once all coating layers have been accounted for, the final replacement fibers are embedded in the actual matrix phase. Careful evaluation is needed of the volume fractions of the successive replacement fibers and coating layers, and of the final replacement fiber in the actual matrix.

Thermal expansion coefficients of a composite cylinder element coincide with those derived for two-phase fibrous solids; in (8.1.18–8.1.24) for transversely isotropic phases, and in (8.1.10) for isotropic phases. Therefore, the linear thermal expansion coefficients of the replacement fiber can be written by changing in the said equations the subscripts $\alpha \to f$, $\beta \to g$. For example, if both fiber and coating are isotropic, then according to (8.1.20), the expansion coefficients of the

replacement fiber are

$$\left.\begin{aligned}\alpha_R^A &= \phi_f\alpha_f + \phi_g\alpha_g + \frac{(\alpha_f-\alpha_g)}{(1/K_f-1/K_g)}\left[\frac{3(k_R-l_R)}{k_Rn_R-l_R^2}-\frac{\phi_f}{K_f}-\frac{\phi_g}{K_g}\right]\\ \alpha_R^T &= \phi_f\alpha_f + \phi_g\alpha_g + \frac{(\alpha_f-\alpha_g)}{(1/K_f-1/K_g)}\left[\frac{3(n_R-l_R)}{2(k_Rn_R-l_R^2)}-\frac{\phi_f}{K_f}-\frac{\phi_g}{K_g}\right]\end{aligned}\right\} \tag{8.1.40}$$

However, if the fibers and/or coatings are transversely isotropic, then the replacement coefficient of thermal expansion α_R^A and α_R^T need to be found using (8.1.22–8.1.24), again with the replacement moduli (8.1.39).

In addition to facilitating bonding between fiber and matrix, certain fiber coatings can also be employed to improve thermal expansion compatibility between fiber and matrix, to reduce interfacial thermal stresses. Those depend on both transverse thermal expansion of the matrix, and on the lateral strain induced in the matrix by the longitudinal constraint applied to the matrix by the fibers. Both effects may cooperate in creating either tensile or compressive stresses normal to the interface, and they can be examined using (8.3.7) below. A coating with a large expansion coefficient a_g^T would seem suitable, to elevate the transverse a_f^T of a less expansive fiber, toward and beyond that of the matrix. However, to stay bonded both to the fiber and matrix, it has to exhibit radial compression in the temperature interval of interest. In any event, it is evident from (8.1.40) that for a given fiber, the α_R^A and α_R^T may reach certain selected values only by adjustment of the volume fractions $\phi_g = 1-\phi_f$, and of the elastic moduli and CTEs of the coating. Therefore, few if any chemically admissible coatings may be found for significant thermal compatibility improvement in a given fiber/matrix system.

Strain and stress field averages caused by thermal changes and mechanical loads in the coating layers and in the fiber also depend on the geometry of the microstructure. They can be evaluated using the transformation and mechanical concentration factors, as described above, at the end of Sect. 8.1.4, or in what follows.

8.2 Transformation Influence Functions and Concentration Factors

8.2.1 Local and Overall Residual Fields

The representative volume of an elastic heterogeneous material considered consists of perfectly bonded ellipsoidal inhomogeneities in subvolumes V_r, each of which contains a single constituent phase, and is transformed by a possibly different

eigenstrain $\boldsymbol{\mu}_r$, uniform in V_r. The subscript $r = 1, 2, \ldots n$ also designates a particular subvolume V_r, as well as the stiffness $\boldsymbol{L}_r$ of the phase residing in V_r. Subject to the restrictions on shape and alignment in Sects. 7.1.2 and 7.2.4, each constituent phase $\boldsymbol{L}_r$ may be found in several inhomogeneities that are transformed by different eigenstrains. The material in each transformed inhomogeneity conforms to the elastic constitutive relations discussed in Sect. 3.6

$$\boldsymbol{\sigma}_r(\boldsymbol{x}) = \boldsymbol{L}_r[\boldsymbol{\varepsilon}_r(\boldsymbol{x}) - \boldsymbol{\mu}_r] \quad \boldsymbol{\varepsilon}_r(\boldsymbol{x}) = \boldsymbol{M}_r\boldsymbol{\sigma}_r(\boldsymbol{x}) + \boldsymbol{\mu}_r \tag{8.2.1}$$

The representative volume of the heterogeneous material is assumed to comply with the requirements outlined in Sect. 3.3, which specify that it contains all constituent phases and deforms in a macroscopically uniform manner when loaded either by a uniform overall stress $\boldsymbol{\sigma}^0$, or the piecewise uniform distribution of the eigenstrains $\boldsymbol{\mu}_r \in V_r$. Also, when uniformly deformed by an overall strain $\boldsymbol{\varepsilon}^0$, and/or by the transformations $\boldsymbol{\mu}_r \in V_r$, the representative volume responds by a macroscopically uniform overall stress. The uniform overall strain and stress are then found by superimposing the effect of applied overall fields with that caused by the local transformations, using (3.5.7) and the Levin formula (3.8.11)

$$\bar{\boldsymbol{\varepsilon}} = \boldsymbol{M}(\boldsymbol{\sigma}^0 - \bar{\boldsymbol{\lambda}}) = \boldsymbol{M}\boldsymbol{\sigma}^0 + \bar{\boldsymbol{\mu}} = \sum_{r=1}^{n} c_r \left[\boldsymbol{M}_r\boldsymbol{B}_r\boldsymbol{\sigma}^0 + \boldsymbol{B}_r^{\mathrm{T}}\boldsymbol{\mu}_r\right] \tag{8.2.2}$$

and

$$\bar{\boldsymbol{\sigma}} = \boldsymbol{L}(\boldsymbol{\varepsilon}^0 - \bar{\boldsymbol{\mu}}) = \boldsymbol{L}\boldsymbol{\varepsilon}^0 + \bar{\boldsymbol{\lambda}} = \sum_{r=1}^{n} c_r \left[\boldsymbol{L}_r\boldsymbol{A}_r\boldsymbol{\varepsilon}^0 + \boldsymbol{A}_r^{\mathrm{T}}\boldsymbol{\lambda}_r\right] \tag{8.2.3}$$

Here, $\bar{\boldsymbol{\mu}} = -\boldsymbol{M}\bar{\boldsymbol{\lambda}}$ is the overall eigenstrain caused by the distribution of $\boldsymbol{\mu}_r$, and $\bar{\boldsymbol{\lambda}}$ is the overall eigenstress $\bar{\boldsymbol{\lambda}} = -\boldsymbol{L}\bar{\boldsymbol{\mu}}$. The $\boldsymbol{L}\boldsymbol{M} = \boldsymbol{I}$ denote overall elastic stiffness and compliance, and $\boldsymbol{A}_r, \boldsymbol{B}_r$ are the mechanical strain and stress concentration factors derived by one of the AFA methods described in Sects. 7.1 and 7.2, or computed at integration points in a unit cell. For brevity and dimensional consistency, the loads applied in (8.2.2) or (8.2.3) will be referred to as load sets $\{\boldsymbol{\sigma}^0,\ \boldsymbol{\lambda}_r\}$ and $\{\boldsymbol{\varepsilon}^0,\ \boldsymbol{\mu}_r\}$, respectively.

To assess the effect of the above loads on the interior fields in the representative volume, we recall from (4.5.21) that the strain $\boldsymbol{\varepsilon}(\boldsymbol{x})$ caused in a homogeneous solid with stiffness $\boldsymbol{L}_0$ by an eigenstrain $\boldsymbol{\mu}(\boldsymbol{x}') = -\boldsymbol{M}_0\boldsymbol{\lambda}(\boldsymbol{x}')$ applied in a subvolume V_s is given by

$$\boldsymbol{\varepsilon}(\boldsymbol{x}) = \int_{V_s} \boldsymbol{\Gamma}(\boldsymbol{x} - \boldsymbol{x}')\boldsymbol{L}_0\boldsymbol{\mu}(\boldsymbol{x}')\mathrm{d}\boldsymbol{x}' \tag{8.2.4}$$

where

$$\Gamma_{mnij}(\boldsymbol{x}-\boldsymbol{x}') = -\frac{1}{2}[G_{mi,nj}(\boldsymbol{x}-\boldsymbol{x}') + G_{ni,mj}(\boldsymbol{x}-\boldsymbol{x}')] \qquad [4.5.22]$$

and $G_{ij}(\boldsymbol{x}-\boldsymbol{x}')$ is the Green's function in the medium $\boldsymbol{L}_0$. For example, in an isotropic solid, $G_{ij}(\boldsymbol{x}-\boldsymbol{x}')$ is given by (4.5.12).

This result can be extended to evaluation of $\boldsymbol{\varepsilon}(\boldsymbol{x})$ in a heterogeneous medium loaded by a superposition of an overall strain and local eigenstrains. As shown in Sect. 6.2.1, a local stress field $\boldsymbol{\sigma}(\boldsymbol{x}) = \boldsymbol{L}_r\boldsymbol{\varepsilon}(\boldsymbol{x})$ caused in a heterogeneous solid by an overall strain $\boldsymbol{\varepsilon}^0$ can be reproduced in an identical volume of a homogeneous comparison medium $\boldsymbol{L}_0$ by subjecting it to the same overall strain and to an eigenstress field $\boldsymbol{\lambda}(\boldsymbol{x}) = (\boldsymbol{L}_r - \boldsymbol{L}_0)\boldsymbol{\varepsilon}(\boldsymbol{x})$. In superposition with the field caused by the eigenstrain in (8.2.4), the strain field in a large volume V of the heterogeneous solid becomes

$$\boldsymbol{\varepsilon}(\boldsymbol{x}) = \boldsymbol{\varepsilon}^0 - \int_V \boldsymbol{\Gamma}(\boldsymbol{x}-\boldsymbol{x}')[(\boldsymbol{L}(\boldsymbol{x}') - \boldsymbol{L}_0)\boldsymbol{\varepsilon}(\boldsymbol{x}') - \boldsymbol{L}(\boldsymbol{x}')\boldsymbol{\mu}(\boldsymbol{x}')]\mathrm{d}\boldsymbol{x}' \qquad (8.2.5)$$

for $\boldsymbol{x}, \boldsymbol{x}' \in V$. Similar forms were used by Levin (1967), Willis (1978, 1981) and Walker et al. (1990). In actual solutions, the $\boldsymbol{\varepsilon}(\boldsymbol{x})$ and $\boldsymbol{\mu}(\boldsymbol{x})$ are approximated by volume averages over subvolumes V_r and V_s, respectively. Then, (8.2.5) is replaced by a system of n linear algebraic equations for the average local strains. As shown in Sect. 4.5, in the absence of mechanical loading, for $\boldsymbol{\varepsilon}^0 = \boldsymbol{0}$, the solution of (8.2.5) provides the Eshelby tensor $\boldsymbol{S} = \boldsymbol{P}\boldsymbol{L}_0$ that appears together with phase stiffness tensors in expression defining concentration factor tensors.

For the piecewise uniform distributions of the eigenstrains in subvolumes V_r and V_s of the representative volume V, the mechanical and residual strain and stress fields in V_r are sought in the form anticipated by (3.6.5)

$$\boldsymbol{\varepsilon}_r(\boldsymbol{x}) = \boldsymbol{A}_r(\boldsymbol{x})\boldsymbol{\varepsilon}^0 + \sum_{s=1}^{n} \boldsymbol{D}_{rs}(\boldsymbol{x})\boldsymbol{\mu}_s \quad \boldsymbol{\sigma}_r(\boldsymbol{x}) = \boldsymbol{L}_r[\boldsymbol{\varepsilon}_r(\boldsymbol{x}) - \boldsymbol{\mu}_r] \qquad (8.2.6)$$

$$\boldsymbol{\sigma}_r(\boldsymbol{x}) = \boldsymbol{B}_r(\boldsymbol{x})\boldsymbol{\sigma}^0 + \sum_{s=1}^{n} \boldsymbol{F}_{rs}(\boldsymbol{x})\boldsymbol{\lambda}_s \quad \boldsymbol{\varepsilon}_r(\boldsymbol{x}) = \boldsymbol{M}_r[\boldsymbol{\sigma}_r(\boldsymbol{x}) - \boldsymbol{\lambda}_r] \qquad (8.2.7)$$

where the transformation stress and strain influence functions $\boldsymbol{D}_{rs}(\boldsymbol{x})$ and $\boldsymbol{F}_{rs}(\boldsymbol{x})$ are (6×6) matrices representing fourth-rank tensors with dimensionless coefficients. They provide the contribution to the residual stress or strain averages in each subvolume r, caused by a uniform eigenstrain $\boldsymbol{\mu}_s$ or eigenstress $\boldsymbol{\lambda}_s$ applied in any subvolume s, including $s = r$, while the representative volume is under zero overall strain $\boldsymbol{\varepsilon}^0 = \boldsymbol{0}$ or stress $\boldsymbol{\sigma}^0 = \boldsymbol{0}$. Both sets include the self-induced terms $\boldsymbol{D}_{rr}(\boldsymbol{x})$ and $\boldsymbol{F}_{rr}(\boldsymbol{x})$ (no summation on r). The $\boldsymbol{D}_{rs}(\boldsymbol{x})$ matrices must comply with the contracted tensorial or engineering matrix notations adopted for the strain and eigenstrain vectors.

To connect (8.2.6) to the integral equation (8.2.5), the overall strain is set at $\boldsymbol{\varepsilon}^0 = \mathbf{0}$, and the strains caused by any eigenstrain field $\boldsymbol{\mu}(\boldsymbol{x})$ in a representative volume of a heterogeneous medium are described by the convolution

$$\boldsymbol{\varepsilon}(\boldsymbol{x}) = \boldsymbol{D}(\boldsymbol{x}, \boldsymbol{x}') * \boldsymbol{\mu}(\boldsymbol{x}') \tag{8.2.8}$$

Then, according to (8.2.5)

$$\boldsymbol{D}(\boldsymbol{x}, \boldsymbol{x}') * \boldsymbol{\mu}(\boldsymbol{x}') = -\int_V \boldsymbol{\Gamma}(\boldsymbol{x} - \boldsymbol{x}')[(\boldsymbol{L}(\boldsymbol{x}') - \boldsymbol{L}_0)\boldsymbol{D}(\boldsymbol{x}', \boldsymbol{x}') - \boldsymbol{L}(\boldsymbol{x}')]\boldsymbol{\mu}(\boldsymbol{x}')\mathrm{d}\boldsymbol{x}' \tag{8.2.9}$$

It is useful to keep in mind that the total local strain or stress fields in V_r, represented by (8.2.6) and (8.2.7), are superpositions of the mechanical load contributions $\boldsymbol{A}_r(\boldsymbol{x})\boldsymbol{\varepsilon}^0$ or $\boldsymbol{B}_r(\boldsymbol{x})\boldsymbol{\sigma}^0$, with the three components of residual fields which remain after mechanical unloading to $\boldsymbol{\varepsilon}^0 = \mathbf{0}$ or $\boldsymbol{\sigma}^0 = \mathbf{0}$. The latter consist of the contributions by $\boldsymbol{\mu}_s$ or $\boldsymbol{\lambda}_s$ transmitted from V_s, the self-induced contribution to local residual fields by $\boldsymbol{\mu}_r$ or $\boldsymbol{\lambda}_r$ applied in V_r, and the applied transformation strain $\boldsymbol{\mu}_r$ or eigenstress $\boldsymbol{\lambda}_r$.

In two-phase materials, the transformation influence functions $\boldsymbol{D}_{rs}(\boldsymbol{x})$ and $\boldsymbol{F}_{rs}(\boldsymbol{x})$ are related to their mechanical counterparts $\boldsymbol{A}_r(\boldsymbol{x})$, $\boldsymbol{B}_r(\boldsymbol{x})$ by the exact connections (3.6.8) and (3.6.11). For a dilute concentration of inhomogeneities, the results appear in Sect. 4.4. In unit cell models analyzed by the finite element method, the representative volume is subdivided into many subvolumes V_r, and the influence functions in (8.2.6) or (8.2.7) are replaced by transformation concentration factor tensors $\boldsymbol{D}_{rs}$ or $\boldsymbol{F}_{rs}$, that are averages of the respective functions taken over each subvolume V_r. Their evaluation in the context of finite element analysis is described in Chap. 12.

In materials reinforced by ellipsoidal inhomogeneities the $\boldsymbol{D}_{rs}$ and $\boldsymbol{F}_{rs}$ are connected to the known mechanical concentration factors by closed form expressions, which are derived next.

8.2.2 *Overall Strain $\boldsymbol{\varepsilon}^0$ and Phase Eigenstrains $\boldsymbol{\mu}_r$ Are Prescribed*

Strain averages caused in individual phase subvolumes V_r of a representative volume of a multiphase aggregate by an overall uniform strain $\boldsymbol{\varepsilon}^0$ and by piecewise uniform phase eigenstrains $\boldsymbol{\mu}_s$ in subvolumes V_s follow from (8.2.6) as

$$\boldsymbol{\varepsilon}_r = \boldsymbol{A}_r\boldsymbol{\varepsilon}^0 + \sum_{s=1}^{n} \boldsymbol{D}_{rs}\boldsymbol{\mu}_s = \boldsymbol{A}_r\boldsymbol{\varepsilon}^0 - \sum_{s=1}^{n} \boldsymbol{D}_{rs}\boldsymbol{M}_s\boldsymbol{\lambda}_s \quad \boldsymbol{\sigma}_r = \boldsymbol{L}_r(\boldsymbol{\varepsilon}_r - \boldsymbol{\mu}_r) \tag{8.2.10}$$

In two-phase composites, the transformation strain concentration factors $\boldsymbol{D}_{rs}$ were derived in (3.6.11), in terms of the mechanical concentration factors $\boldsymbol{A}_r$ and phase stiffnesses $\boldsymbol{L}_r$. That result holds for any phase geometry and distribution. In multiphase aggregates, $\boldsymbol{D}_{rs}$ are found next, again in terms of $\boldsymbol{A}_r$ and $\boldsymbol{L}_r$, providing that the inhomogeneities $r = 2, 3, \ldots n$, are modeled by ellipsoids. Each transformed ellipsoidal subvolume $V_r \equiv \Omega_r$ is first embedded at dilute concentration in a large volume Ω_0 of a certain homogeneous comparison medium $\boldsymbol{L}_0$, which is subjected to an as yet unknown uniform overall strain $\boldsymbol{\varepsilon}^0_\Omega$, applied by linearly varying displacements on the surface $\partial\Omega_0$. A prescribed eigenstrain $\boldsymbol{\mu}_r$ is applied in the subvolume Ω_r. Moreover, a certain uniform eigenstrain $\boldsymbol{\mu}_0$ of unknown magnitude is introduced in Ω_0, to represent the collective contribution of all phase eigenstrains $\boldsymbol{\mu}_s$ to the average transformation strain in the comparison medium $\boldsymbol{L}_0$. According to (4.3.2), the strain and stress caused by the load set $\{\boldsymbol{\varepsilon}^0_\Omega, \boldsymbol{\mu}_r, \boldsymbol{\mu}_0\}$ in a solitary ellipsoidal inhomogeneity Ω_r embedded in the comparison medium, are uniform and given by (4.3.2) and (4.3.7)

$$\left.\begin{aligned} &\boldsymbol{\varepsilon}_r = \boldsymbol{T}_r\boldsymbol{\varepsilon}^0_\Omega + \boldsymbol{R}_{rr}\boldsymbol{\mu}_r + \boldsymbol{R}_{r0}\boldsymbol{\mu}_0 \quad \boldsymbol{\sigma}_r = \boldsymbol{L}_r(\boldsymbol{\varepsilon}_r - \boldsymbol{\mu}_r) \\ &\boldsymbol{R}_{rr} = (\boldsymbol{I} - \boldsymbol{T}_r)(\boldsymbol{L}_r - \boldsymbol{L}_0)^{-1}\boldsymbol{L}_r = \boldsymbol{T}_r\boldsymbol{P}\boldsymbol{L}_r \\ &\boldsymbol{R}_{r0} = -(\boldsymbol{I} - \boldsymbol{T}_r)(\boldsymbol{L}_r - \boldsymbol{L}_0)^{-1}\boldsymbol{L}_0 = -\boldsymbol{T}_r\boldsymbol{P}\boldsymbol{L}_\mathbf{0} \end{aligned}\right\} \tag{8.2.11}$$

and $\boldsymbol{T}_r = [\boldsymbol{I} + \boldsymbol{P}(\boldsymbol{L}_r - \boldsymbol{L}_0)]^{-1}$ is the partial strain concentration factor (4.2.13) of a solitary inhomogeneity $\boldsymbol{L}_r$, surrounded by a large volume of $\boldsymbol{L}_0$. Components of the $\boldsymbol{P}$ tensors for different ellipsoidal shapes are given in Sect. 4.6.

Since both the comparison medium and the actual aggregate have to satisfy the same displacement boundary conditions, which now render $\boldsymbol{\varepsilon}^0 = \mathbf{0}$ on ∂V, we require that $\boldsymbol{\varepsilon}^0_\Omega + \boldsymbol{\mu}_0 = \mathbf{0}$ on $\partial\Omega_0$. The unknown eigenstrain $\boldsymbol{\mu}_0$ is thereby eliminated and the strain average is found to be

$$\boldsymbol{\varepsilon}_r = (\boldsymbol{T}_r - \boldsymbol{R}_{r0})\boldsymbol{\varepsilon}^0_\Omega + \boldsymbol{R}_{rr}\boldsymbol{\mu}_r \tag{8.2.12}$$

Using

$$\boldsymbol{\varepsilon}^0 = \sum_{s=1}^{n} c_s\boldsymbol{\varepsilon}_s = \sum_{s=1}^{n} c_s[(\boldsymbol{T}_s - \boldsymbol{R}_{s0})\boldsymbol{\varepsilon}^0_\Omega + \boldsymbol{R}_{ss}\boldsymbol{\mu}_s] = \mathbf{0} \tag{8.2.13}$$

and the $\boldsymbol{R}_{s0} = -\boldsymbol{T}_s\boldsymbol{P}\boldsymbol{L}_\mathbf{0} = -\boldsymbol{T}_s\boldsymbol{S}$ in (4.3.7), we evaluate the overall strain in the comparison medium

$$\boldsymbol{\varepsilon}^0_\Omega = -\left[\sum_{s=1}^{n} c_s\boldsymbol{T}_s(\boldsymbol{I} + \boldsymbol{S})\right]^{-1}\left[\sum_{s=1}^{n} c_s\boldsymbol{R}_{ss}\boldsymbol{\mu}_s\right] \tag{8.2.14}$$

The $\boldsymbol{S} = \boldsymbol{PL_0}$ matrix represents the Eshelby tensor of a transformed homogeneous inclusion Ω_r in $\boldsymbol{L}_0$. Substituting this result into (8.2.13) and comparing it with (8.2.6) at $\boldsymbol{\varepsilon}^0 = \boldsymbol{0}$, we arrive at

$$\boldsymbol{\varepsilon}_r = -\boldsymbol{T}_r \left[\sum_{s=1}^{n} c_s \boldsymbol{T}_s \right]^{-1} \left[\sum_{s=1}^{n} c_s \boldsymbol{R}_{ss} \boldsymbol{\mu}_s \right] + \boldsymbol{R}_{rr} \boldsymbol{\mu}_r = \sum_{s=1}^{n} \boldsymbol{D}_{rs} \boldsymbol{\mu}_s \tag{8.2.15}$$

Replacement of the leading product by $\boldsymbol{A}_r$ according to $(6.1.2)_1$, and reordering of the sums to separate the self-induced contributions, shows that

$$-\boldsymbol{A}_r \left[\sum_{s \neq r}^{n} c_s \boldsymbol{R}_{ss} \boldsymbol{\mu}_s \right] + (\boldsymbol{I} - c_r \boldsymbol{A}_r) \boldsymbol{R}_{rr} \boldsymbol{\mu}_r = \sum_{s \neq r}^{n} \boldsymbol{D}_{rs} \boldsymbol{\mu}_s + \boldsymbol{D}_{rr} \boldsymbol{\mu}_r \tag{8.2.16}$$

Since $\boldsymbol{\mu}_r$, $\boldsymbol{\mu}_s$ are independent variables, comparison of corresponding terms provides

$$\boldsymbol{D}_{rs} = (\delta_{rs} \boldsymbol{I} - c_s \boldsymbol{A}_r) \boldsymbol{R}_{ss} \tag{8.2.17}$$

where δ_{rs} is the Kronecker symbol, but the summation rule does not apply. The last term $\boldsymbol{R}_{ss} = \boldsymbol{T}_s \boldsymbol{PL}_s$ is now converted using $\boldsymbol{P} = (\boldsymbol{L}^* + \boldsymbol{L}_0)^{-1}$ in (4.2.9), and (4.2.14)

$$\boldsymbol{T}_s = (\boldsymbol{L}^* + \boldsymbol{L}_s)^{-1} (\boldsymbol{L}^* + \boldsymbol{L}_0) \quad \boldsymbol{A}_r = (\boldsymbol{L}^* + \boldsymbol{L}_r)^{-1} (\boldsymbol{L}^* + \boldsymbol{L}) \tag{8.2.18}$$

The eigenstrain concentration factors can then be expressed as

$$\left.\begin{aligned} \boldsymbol{D}_{rs} &= [\delta_{rs} \boldsymbol{I} - c_s (\boldsymbol{L}^* + \boldsymbol{L}_r)^{-1} (\boldsymbol{L}^* + \boldsymbol{L})] (\boldsymbol{L}^* + \boldsymbol{L}_s)^{-1} \boldsymbol{L}_s \\ \boldsymbol{D}_{rs} &= (\boldsymbol{I} - \boldsymbol{A}_r) (\boldsymbol{L}_r - \boldsymbol{L})^{-1} (\delta_{rs} \boldsymbol{I} - c_s \boldsymbol{A}_s^{\mathrm{T}}) \boldsymbol{L}_s \end{aligned}\right\} \tag{8.2.19}$$

This yields the (6×6) $\boldsymbol{D}_{rs}$ matrices in terms of the mechanical concentration factors $\boldsymbol{A}_r, \boldsymbol{A}_s$, stiffnesses $\boldsymbol{L}_r$, $\boldsymbol{L}_s$ of each pair of interacting phase subvolumes V_r and V_s, of the volume fraction c_s of the remote phase, and of the overall stiffness $\boldsymbol{L} = \Sigma c_r \boldsymbol{L}_r \boldsymbol{A}_r$ of the composite aggregate. Implicitly included are the coefficients of the $\boldsymbol{L}_0$ of an admissible comparison medium, which appear in $\boldsymbol{P} = (\boldsymbol{L}^* + \boldsymbol{L}_0)^{-1}$ and $\boldsymbol{S} = \boldsymbol{PL}_0$. After substitution into $(8.2.6)_1$, the $\boldsymbol{D}_{rs}$ tensors provide the magnitudes of strain averages caused in the subvolumes V_r, V_s by uniform eigenstrains $\boldsymbol{\mu}_r$, $\boldsymbol{\mu}_s$, under $\boldsymbol{\varepsilon}^0 = \boldsymbol{0}$.

For systems with low contrast between the phase elastic moduli, when $\boldsymbol{L}_r \to \boldsymbol{L}_0$, there is $\boldsymbol{T}_r \to \boldsymbol{I}$, and from (4.3.7), $\boldsymbol{R}_{rr} \doteq \boldsymbol{R}_{r0} \to \boldsymbol{S}$. Equation (8.2.17) is then reduced to $\boldsymbol{D}_{rs} = (\delta_{rs} - c_s) \boldsymbol{S}$.

In applications to two-phase ($r = \alpha, \beta$) statistically homogeneous systems of any micro-geometry, the above connections are replaced by (3.6.8), expanded here to

$$\left.\begin{aligned} \boldsymbol{D}_{\alpha\alpha}(\boldsymbol{x}) &= [\boldsymbol{I} - \boldsymbol{A}_\alpha(\boldsymbol{x})](\boldsymbol{L}_\alpha - \boldsymbol{L}_\beta)^{-1}\boldsymbol{L}_\alpha = -[\boldsymbol{I} - \boldsymbol{A}_\alpha(\boldsymbol{x})]\boldsymbol{M}_\beta(\boldsymbol{M}_\alpha - \boldsymbol{M}_\beta)^{-1} \\ \boldsymbol{D}_{\alpha\beta}(\boldsymbol{x}) &= -[\boldsymbol{I} - \boldsymbol{A}_\alpha(\boldsymbol{x})](\boldsymbol{L}_\alpha - \boldsymbol{L}_\beta)^{-1}\boldsymbol{L}_\beta = [\boldsymbol{I} - \boldsymbol{A}_\alpha(\boldsymbol{x})]\boldsymbol{M}_\alpha(\boldsymbol{M}_\alpha - \boldsymbol{M}_\beta)^{-1} \end{aligned}\right\} \tag{8.2.20}$$

Note the implied identity $(\boldsymbol{L}_\alpha - \boldsymbol{L}_\beta)^{-1}\boldsymbol{L}_\alpha = -\boldsymbol{M}_\beta(\boldsymbol{M}_\alpha - \boldsymbol{M}_\beta)^{-1}$ which holds in two-phase systems. The relations (8.2.20) become useful when the $\boldsymbol{A}_r(\boldsymbol{x})$ are known. It can be verified that for a single uniform eigenstrain $\boldsymbol{\mu}_r$ applied in an ellipsoidal subvolume V_r within a large volume V of a homogeneous medium, where $\boldsymbol{L}_\alpha \to \boldsymbol{L}_\beta$, the self-induced term $\boldsymbol{D}_{rr} \to \boldsymbol{S}$, the Eshelby tensor. In that case, the boundary condition $\boldsymbol{\varepsilon}^0 = \boldsymbol{0}$ is immaterial, since $V_r \ll V$ and $\bar{\boldsymbol{\sigma}} = \boldsymbol{0}$.

Evaluation of $\boldsymbol{D}_{r\alpha}$ and $\boldsymbol{D}_{r\beta}$ can be simplified when the phase volume fractions $c_\alpha + c_\beta = 1$, and the overall stiffness $\boldsymbol{L}$ are known. Then, the mechanical concentration factors $\boldsymbol{A}_r$, $\boldsymbol{B}_r$ of any two-phase aggregate can be derived from (3.5.13), in terms of local and overall stiffnesses and compliances, and phase volume fractions, as

$$c_\alpha \boldsymbol{A}_\alpha = (\boldsymbol{L}_\alpha - \boldsymbol{L}_\beta)^{-1}(\boldsymbol{L} - \boldsymbol{L}_\beta) \quad c_\beta \boldsymbol{A}_\beta = -(\boldsymbol{L}_\alpha - \boldsymbol{L}_\beta)^{-1}(\boldsymbol{L} - \boldsymbol{L}_\alpha) \tag{8.2.21}$$

For two-phase systems with low contrast, where $\boldsymbol{L}_\alpha \to \boldsymbol{L}_\beta \doteq \boldsymbol{L}$, application of uniform eigenstrains creates phase strain averages $\boldsymbol{\varepsilon}_\alpha = c_\beta \boldsymbol{S}(\boldsymbol{\mu}_\alpha - \boldsymbol{\mu}_\beta)$, $\boldsymbol{\varepsilon}_\beta = c_\alpha \boldsymbol{S}(\boldsymbol{\mu}_\alpha - \boldsymbol{\mu}_\beta)$ under $\boldsymbol{\varepsilon}^0 = \boldsymbol{0}$. The Eshelby matrix $\boldsymbol{S}$ is evaluated in either one of the two phases.

8.2.3 *Overall Stress $\boldsymbol{\sigma}^0$ and Phase Eigenstresses $\boldsymbol{\lambda}_r$ Are Applied*

Next, consider a representative volume of a heterogeneous aggregate with interacting subvolumes $r, s = 1, 2, \ldots n$, loaded by a uniform overall stress $\boldsymbol{\sigma}^0$ and by a piecewise uniform distribution of eigenstresses $\boldsymbol{\lambda}_s$ in subvolumes V_s or by the load set $\{\boldsymbol{\sigma}^0, \boldsymbol{\lambda}_s\}$. The subvolume stress averages caused by this load set are sought in the form (8.2.7) written as

$$\boldsymbol{\sigma}_r = \boldsymbol{B}_r\boldsymbol{\sigma}^0 + \sum_{s=1}^{n} \boldsymbol{F}_{rs}\boldsymbol{\lambda}_s = \boldsymbol{B}_r\boldsymbol{\sigma}^0 - \sum_{s=1}^{n} \boldsymbol{F}_{rs}\boldsymbol{L}_s\boldsymbol{\mu}_s \quad \boldsymbol{\varepsilon}_r = \boldsymbol{M}_r\boldsymbol{\sigma}_r + \boldsymbol{\mu}_r \tag{8.2.22}$$

where $\boldsymbol{B}_r$ are the mechanical stress concentration factor matrices and $\boldsymbol{F}_{rs}$ are eigenstress concentration factor matrices. Each $\boldsymbol{F}_{rs}$ matrix provides the contribution to stress average in subvolume V_r by a uniform eigenstress $\boldsymbol{\lambda}_s$ applied in subvolume V_s, while the representative volume is under zero overall stress $\boldsymbol{\sigma}^0 = \boldsymbol{0}$. The $\boldsymbol{F}_{rs}$ set includes the self-induced term $\boldsymbol{F}_{ss}$ (no summation on s).

Following a procedure analogous to that leading to the $\boldsymbol{D}_{rs}$, one can find that

$$\boldsymbol{F}_{rs} = [\delta_{rs}\boldsymbol{I} - c_r(\boldsymbol{M}^* + \boldsymbol{M}_r)^{-1}(\boldsymbol{M}^* + \boldsymbol{M})](\boldsymbol{M}^* + \boldsymbol{M}_s)^{-1}\boldsymbol{M}_s \tag{8.2.23}$$

and

$$\boldsymbol{F}_{rs} = (\boldsymbol{I} - \boldsymbol{B}_r)(\boldsymbol{M}_r - \boldsymbol{M})^{-1}(\delta_{rs}\boldsymbol{I} - c_s\boldsymbol{B}_s{}^{\mathrm{T}})\boldsymbol{M}_s \tag{8.2.24}$$

where $\boldsymbol{M} = \boldsymbol{L}^{-1}$ denote overall compliance and stiffness, and $\boldsymbol{M}^*$ is defined in (4.2.10). This gives the $\boldsymbol{F}_{rs}$ matrices in terms of the subvolume concentration factors, and phase and comparison medium stiffness matrices. Note that both $\boldsymbol{B}_r$ and $\boldsymbol{F}_{rs}$ are derived using a single comparison medium $\boldsymbol{L}_0$ that complies with the H-S bounds (6.2.16), and that the $\boldsymbol{B}_r, \boldsymbol{B}_s$ are related to $\boldsymbol{M}$ by (3.5.8).

Those results also apply to *two-phase systems* of any geometry in the representative volume, which were derived by the uniform fields method in Sect. 3

$$\left.\begin{aligned}\boldsymbol{F}_{r\alpha}(\boldsymbol{x}) &= (\boldsymbol{I} - \boldsymbol{B}_r(\boldsymbol{x}))(\boldsymbol{M}_\alpha - \boldsymbol{M}_\beta)^{-1}\boldsymbol{M}_\alpha \\ \boldsymbol{F}_{r\beta}(\boldsymbol{x}) &= -(\boldsymbol{I} - \boldsymbol{B}_r(\boldsymbol{x}))(\boldsymbol{M}_\alpha - \boldsymbol{M}_\beta)^{-1}\boldsymbol{M}_\beta\end{aligned}\right\} \qquad [3.6.11]$$

Again, if the phase volume fractions and overall compliance are known, then (3.5.12) provides $c_\alpha\boldsymbol{B}_\alpha = (\boldsymbol{M}_\alpha - \boldsymbol{M}_\beta)^{-1}(\boldsymbol{M} - \boldsymbol{M}_\beta)$, $c_\beta\boldsymbol{B}_\beta = -(\boldsymbol{M}_\alpha - \boldsymbol{M}_\beta)^{-1}$ $(\boldsymbol{M} - \boldsymbol{M}_\alpha)$, and the $\boldsymbol{F}_{rs}$ can be found without knowing the shape and alignment of the two phases.

A connection between $\boldsymbol{D}_{rs}$ and $\boldsymbol{F}_{rs}$ can be developed by applying to the total volume V a uniform overall stress $\boldsymbol{\sigma}^0$, and subvolume eigenstresses $\boldsymbol{\lambda}_r$ in $V_r \in V$. Local stresses in V_r are connected to $\boldsymbol{\varepsilon}_r$ and $\boldsymbol{\lambda}_r$ by (3.6.1), where the $\boldsymbol{\varepsilon}_r$ is now expressed by (8.2.6) while the overall strain $\bar{\boldsymbol{\varepsilon}} = \boldsymbol{M}\boldsymbol{\sigma}^0$. Together with the above equations, that yields

$$\boldsymbol{\sigma}_r = \boldsymbol{L}_r\boldsymbol{\varepsilon}_r + \boldsymbol{\lambda}_r = \boldsymbol{L}_r\boldsymbol{A}_r\boldsymbol{M}\boldsymbol{\sigma}^0 - \boldsymbol{L}_r\sum_{s=1}^{n}[(c_s\boldsymbol{A}_r\boldsymbol{B}_s^{\mathrm{T}} + \boldsymbol{D}_{rs})\boldsymbol{M}_s\boldsymbol{\lambda}_s] + \boldsymbol{\lambda}_r \tag{8.2.25}$$

for $r, s = 1, 2, \ldots n$. Recall from (3.5.11) that $\boldsymbol{L}_r\boldsymbol{A}_r\boldsymbol{M} = \boldsymbol{B}_r$, and rewrite the sum (8.2.7) in two parts, for $s \neq r$ and for $s = r$. Compare that with (8.2.25) to find that

$$\boldsymbol{F}_{rs} = \boldsymbol{L}_r[\delta_{rs}\boldsymbol{I} - c_s\boldsymbol{A}_r\boldsymbol{B}_s^{\mathrm{T}} - \boldsymbol{D}_{rs}]\boldsymbol{M}_s \tag{8.2.26}$$

We note in passing that the $\boldsymbol{D}_{rs}$ and $\boldsymbol{F}_{rs}$ in (8.2.19) and (8.2.24) are those first found by Dvorak and Benveniste (1992), in the context of the self-consistent and Mori-Tanaka methods. The present derivation is more compact and it admits any comparison medium $\boldsymbol{L}_0$ that complies with (6.2.16).

8.2.4 Properties of the Transformation Influence Functions

We first recall the expressions for local fields caused in a multi-phase heterogeneous aggregate of any microstructural geometry by application of the load sets $\{\boldsymbol{\varepsilon}^0,\ \boldsymbol{\mu}_s\}$ or $\{\boldsymbol{\sigma}^0,\ \boldsymbol{\lambda}_s\}$, where both $\boldsymbol{\mu}_s$ and $\boldsymbol{\lambda}_s$ are piecewise uniform in subvolumes V_s

$$\boldsymbol{\varepsilon}_r(\boldsymbol{x}) = \boldsymbol{A}_r(\boldsymbol{x})\boldsymbol{\varepsilon}^0 + \sum_{s=1}^{n} \boldsymbol{D}_{rs}(\boldsymbol{x})\boldsymbol{\mu}_s \quad \boldsymbol{\sigma}_r(\boldsymbol{x}) = \boldsymbol{L}_r[\boldsymbol{\varepsilon}_r(\boldsymbol{x}) - \boldsymbol{\mu}_r] \qquad [8.2.6]$$

$$\boldsymbol{\sigma}_r(\boldsymbol{x}) = \boldsymbol{B}_r(\boldsymbol{x})\boldsymbol{\sigma}^0 + \sum_{s=1}^{n} \boldsymbol{F}_{rs}(\boldsymbol{x})\boldsymbol{\lambda}_s \quad \boldsymbol{\varepsilon}_r(\boldsymbol{x}) = \boldsymbol{M}_r[\boldsymbol{\sigma}_r(\boldsymbol{x}) - \boldsymbol{\lambda}_r] \qquad [8.2.7]$$

and

$$\sum_{r=1}^{n} c_r \boldsymbol{\varepsilon}_r = \bar{\boldsymbol{\varepsilon}} \quad \sum_{r=1}^{n} c_r \boldsymbol{\sigma}_r = \bar{\boldsymbol{\sigma}} \qquad [3.5.5]$$

with $\Sigma_{r=1}^{n} c_r \boldsymbol{A}_r = \boldsymbol{I}$ and $\Sigma_{r=1}^{n} c_r \boldsymbol{B}_r = \boldsymbol{I}$. The strain and stress averages must be equal to the prescribed magnitudes, $\bar{\boldsymbol{\varepsilon}} = \boldsymbol{\varepsilon}^0$ and $\bar{\boldsymbol{\sigma}} = \boldsymbol{\sigma}^0$, while each $\boldsymbol{\mu}_s$ or $\boldsymbol{\lambda}_s$ can be prescribed independently of other transformations. Therefore, the transformation concentration factors in (8.2.6–8.2.7) must satisfy

$$\sum_{r=1}^{n} c_r \boldsymbol{D}_{rs} = \boldsymbol{0} \quad \sum_{r=1}^{n} c_r \boldsymbol{F}_{rs} = \boldsymbol{0} \qquad (8.2.27)$$

It can also be verified that

$$\int_V \boldsymbol{D}_{rs}(\boldsymbol{x})\mathrm{d}V = \boldsymbol{0} \quad \int_V \boldsymbol{F}_{rs}(\boldsymbol{x})\mathrm{d}V = \boldsymbol{0} \qquad (8.2.28)$$

Next, let a uniform eigenstrain $\boldsymbol{\mu}_q$ be prescribed in a single subvolume V_q, while the entire volume V of a multiphase aggregate is loaded by a uniform overall stress $\boldsymbol{\sigma}^0$. A piecewise uniform eigenstrain field $\boldsymbol{\mu}_r$ is applied in all $V_r \neq V_q$ to create an auxiliary uniform strain $\hat{\boldsymbol{\varepsilon}}$ and stress $\hat{\boldsymbol{\sigma}} = \boldsymbol{\sigma}^0$ everywhere in V. This is accomplished by letting

$$\hat{\boldsymbol{\varepsilon}} = \boldsymbol{M}_q\boldsymbol{\sigma}^0 + \boldsymbol{\mu}_q = \boldsymbol{M}_r\boldsymbol{\sigma}^0 + \boldsymbol{\mu}_r \Rightarrow \boldsymbol{\mu}_r = \boldsymbol{\mu}_q - (\boldsymbol{M}_r - \boldsymbol{M}_q)\boldsymbol{\sigma}^0 \qquad (8.2.29)$$

According to (8.2.6), the strain distribution $\boldsymbol{\varepsilon}_s(\boldsymbol{x})$ generated in a subvolume V_s by application of overall $\hat{\boldsymbol{\varepsilon}}$ and by $\boldsymbol{\mu}_r$ in V_r is

$$\boldsymbol{\varepsilon}_s(\boldsymbol{x}) = \boldsymbol{A}_s(\boldsymbol{x})\hat{\boldsymbol{\varepsilon}} + \sum_{r=1}^{n} \boldsymbol{D}_{sr}(\boldsymbol{x})\boldsymbol{\mu}_r \qquad (8.2.30)$$

where the sum is taken over all currently transformed subvolumes V_r. The $\hat{\boldsymbol{\varepsilon}}$ and $\boldsymbol{\mu}_r$ from (8.2.29) are now modified by letting $\boldsymbol{\mu}_q = \mathbf{0}$, and substituted in (8.2.30) to yield the uniform strain field $\boldsymbol{\varepsilon}(\boldsymbol{x}) = \hat{\boldsymbol{\varepsilon}}$ in V. The implication is that

$$\sum_{r=1}^{n} \boldsymbol{D}_{sr}(\boldsymbol{x})[\boldsymbol{M}_r - \boldsymbol{M}_q] = -[\boldsymbol{I} - \boldsymbol{A}_s(\boldsymbol{x})]\boldsymbol{M}_q \tag{8.2.31}$$

Since this must hold for any selected $\boldsymbol{M}_r$ and $\boldsymbol{M}_q$, it follows that

$$\sum_{r=1}^{n} \boldsymbol{D}_{sr}(\boldsymbol{x})\boldsymbol{M}_r = \mathbf{0} \quad \sum_{r=1}^{n} \boldsymbol{D}_{sr}(\boldsymbol{x}) = \boldsymbol{I} - \boldsymbol{A}_s(\boldsymbol{x}) \tag{8.2.32}$$

A similar derivation yields

$$\sum_{r=1}^{n} \boldsymbol{F}_{sr}(\boldsymbol{x})\boldsymbol{L}_r = \mathbf{0} \quad \sum_{r=1}^{n} \boldsymbol{F}_{sr}(\boldsymbol{x}) = \boldsymbol{I} - \boldsymbol{B}_s(\boldsymbol{x}) \tag{8.2.33}$$

Finally, let the overall strain applied to V be $\boldsymbol{\varepsilon}^0 = \mathbf{0}$, while a uniform eigenstress $\boldsymbol{\lambda}_r$ is induced in a single subvolume V_r. Separately, a uniform eigenstress $\boldsymbol{\lambda}'_s$ is applied in a single subvolume V_s under $\boldsymbol{\varepsilon}^0 = \mathbf{0}$. The strain caused by $\boldsymbol{\lambda}_r = -\boldsymbol{L}_r\boldsymbol{\mu}_r$ in any subvolume V_s, and the strain caused by $\boldsymbol{\lambda}'_s = -\boldsymbol{L}_s\boldsymbol{\mu}_s$ in any subvolume V_r, follow from (8.2.6) as

$$\boldsymbol{\varepsilon}_s(\boldsymbol{x}) = -\boldsymbol{D}_{sr}(\boldsymbol{x})\boldsymbol{M}_r\boldsymbol{\lambda}_r \quad \boldsymbol{\varepsilon}'_r(\boldsymbol{x}) = -\boldsymbol{D}_{rs}(\boldsymbol{x})\boldsymbol{M}_s\boldsymbol{\lambda}'_s \tag{8.2.34}$$

The reciprocal theorem in Sect. 3.7.3, and substitution of the last terms on both sides of (3.7.23) for the work of the primed on unprimed field, and vice versa, yields scalar products

$$\frac{1}{V}\int_{V_S} \boldsymbol{\lambda}'_s \bullet \boldsymbol{D}_{sr}(\boldsymbol{x})\boldsymbol{M}_r\boldsymbol{\lambda}_r \mathrm{d}V = \frac{1}{V}\int_{V_r} \boldsymbol{\lambda}_r \bullet \boldsymbol{D}_{rs}(\boldsymbol{x})\boldsymbol{M}_s\boldsymbol{\lambda}'_s \mathrm{d}V \tag{8.2.35}$$

Integration over V_s and V_r reflects the fact that $\boldsymbol{\lambda}'_s$ and $\boldsymbol{\lambda}_r$ are defined only in those respective volumes. Each side of the above equation is a scalar, equal to its transpose, and the $\boldsymbol{\lambda}_r$ and $\boldsymbol{\lambda}'_s$ are independent. Therefore,

$$c_r\boldsymbol{M}_s\boldsymbol{D}_{rs}^{\mathrm{T}} = c_s\boldsymbol{D}_{sr}\boldsymbol{M}_r \quad c_r\boldsymbol{D}_{rs}\boldsymbol{M}_s = c_s\boldsymbol{M}_r\boldsymbol{D}_{sr}^{\mathrm{T}} \tag{8.2.36}$$

A similar procedure involving application of uniform eigenstrains $\boldsymbol{\mu}_r \in V_r$ or $\boldsymbol{\mu}'_s \in V_s$ under $\boldsymbol{\sigma}^0 = \mathbf{0}$ provides the connections

$$c_r\boldsymbol{L}_s\boldsymbol{F}_{rs}^{\mathrm{T}} = c_s\boldsymbol{F}_{sr}\boldsymbol{L}_r \quad c_r\boldsymbol{F}_{rs}\boldsymbol{L}_s = c_s\boldsymbol{L}_r\boldsymbol{F}_{sr}^{\mathrm{T}} \tag{8.2.37}$$

For the self-induced transformation concentration factors, the above relations become

$$\boldsymbol{M}_s \boldsymbol{D}_{ss}^{\mathrm{T}} = \boldsymbol{D}_{ss} \boldsymbol{M}_s \quad \boldsymbol{L}_s \boldsymbol{F}_{ss}^{\mathrm{T}} = \boldsymbol{F}_{ss} \boldsymbol{L}_s \tag{8.2.38}$$

Notice that no summation is implied by the repeated subscripts.

Of course, the four connections derived in (8.2.27), (8.2.32–8.2.33) and (8.2.36–8.2.37) are not all independent. Rewrite $(8.2.36)_2$ as $c_r \boldsymbol{D}_{rs} = c_s \boldsymbol{M}_r \boldsymbol{D}_{sr}^{\mathrm{T}} \boldsymbol{L}_s$ and evaluate

$$\sum_{r=1}^{n} c_r \boldsymbol{D}_{rs} = c_s \left[\sum_{r=1}^{n} \boldsymbol{M}_r \boldsymbol{D}_{sr}^{\mathrm{T}} \right] \boldsymbol{L}_s = \boldsymbol{0} \tag{8.2.39}$$

where the term in square brackets is a transpose of $(8.2.32)_1$ and equal to zero. Therefore, (8.2.27) follows from $(8.2.32)_1$ and $(8.2.36)_2$.

Regardless of the method used in their derivation, the transformation influence functions and the concentration factors $\boldsymbol{D}_{rs}, \boldsymbol{F}_{rs}$ in a multi-phase heterogeneous medium have the following properties

$$\sum_{s=1}^{n} \boldsymbol{D}_{rs}(\boldsymbol{x}) = \boldsymbol{I} - \boldsymbol{A}_r(\boldsymbol{x}) \quad \sum_{s=1}^{n} \boldsymbol{F}_{rs}(\boldsymbol{x}) = \boldsymbol{I} - \boldsymbol{B}_r(\boldsymbol{x}) \tag{8.2.40}$$

$$\sum_{s=1}^{n} \boldsymbol{D}_{rs}(\boldsymbol{x}) \boldsymbol{M}_s = \boldsymbol{0} \quad \sum_{s=1}^{n} \boldsymbol{F}_{rs}(\boldsymbol{x}) \boldsymbol{L}_s = \boldsymbol{0} \tag{8.2.41}$$

$$\sum_{r=1}^{n} c_r \boldsymbol{D}_{rs} = \boldsymbol{0} \quad \sum_{r=1}^{n} c_r \boldsymbol{F}_{rs} = \boldsymbol{0} \tag{8.2.42}$$

$$c_r \boldsymbol{D}_{rs} \boldsymbol{M}_s = c_s \boldsymbol{M}_r \boldsymbol{D}_{sr}^{\mathrm{T}} \quad c_r \boldsymbol{F}_{rs} \boldsymbol{L}_s = c_s \boldsymbol{L}_r \boldsymbol{F}_{sr}^{\mathrm{T}} \tag{8.2.43}$$

Equations (8.2.40) and (8.2.42) represent $(2 \times n)$ independent relations that connect the $(n \times n)$ influence functions. Therefore, the transformation influence functions can be exactly related to their mechanical counterparts only in two-phase media, as shown in (3.6.8) and (3.6.11), or (8.2.20). In multi-phase system consisting of ellipsoidal inhomogeneities of the same shape and alignment, the transformation and mechanical concentration factors are connected by (8.2.19) and (8.2.23–8.2.24).

In systems consisting of three subvolumes, such as two-phase or three-phase composites loaded by three different eigenstrains, the mechanical and transformation influence functions can be connected by six relations

$$\boldsymbol{D}_{jk}(\boldsymbol{x})(\boldsymbol{M}_k - \boldsymbol{M}_l) = \boldsymbol{D}_{jj}(\boldsymbol{x})(\boldsymbol{M}_l - \boldsymbol{M}_j) - [\boldsymbol{I} - \boldsymbol{A}_j(\boldsymbol{x})]\boldsymbol{M}_l \tag{8.2.44}$$

For example,

$$\boldsymbol{D}_{12}(\boldsymbol{x})(\boldsymbol{M}_2 - \boldsymbol{M}_3) = \boldsymbol{D}_{11}(\boldsymbol{x})(\boldsymbol{M}_3 - \boldsymbol{M}_1) - [\boldsymbol{I} - \boldsymbol{A}_1(\boldsymbol{x})]\boldsymbol{M}_3 \tag{8.2.45}$$

where $j \neq k \neq l;\ j, k, l = 1, 2, 3$, and the summation rule does not apply. Notice that in a homogeneous medium, where $\boldsymbol{A}_r(\boldsymbol{x}) = \boldsymbol{I}$, this equation is reduced to an identity, and (8.2.40) yields $\sum_{s=1}^{n} \boldsymbol{D}_{rs}(\boldsymbol{x}) = \boldsymbol{0}$, $\sum_{s=1}^{n} \boldsymbol{F}_{rs}(\boldsymbol{x}) = \boldsymbol{0}$.

Finally, (8.2.40) and (3.5.8) provide an expression for the overall stiffness in terms of $\boldsymbol{D}_{rs}$

$$\boldsymbol{L} = \sum_{r=1}^{n} c_r \boldsymbol{L}_r \boldsymbol{A}_r = \sum_{r=1}^{n} \left[c_r \boldsymbol{L}_r \left(\boldsymbol{I} - \sum_{s=1}^{n} \boldsymbol{D}_{rs} \right) \right] \tag{8.2.46}$$

8.3 Uniform Change in Temperature in Multiphase Systems

8.3.1 Overall and Local Field Averages

Recall that the local and overall constitutive relations for multiphase systems are

$$\left.\begin{aligned} \boldsymbol{\sigma}_r(\boldsymbol{x}) = \boldsymbol{L}_r \boldsymbol{\varepsilon}_r(\boldsymbol{x}) + \boldsymbol{l}_r \Delta\theta \quad & \boldsymbol{\varepsilon}_r(\boldsymbol{x}) = \boldsymbol{M}_r \boldsymbol{\sigma}_r(\boldsymbol{x}) + \boldsymbol{m}_r \Delta\theta \\ \boldsymbol{l}_r = -\boldsymbol{L}_r \boldsymbol{m}_r \quad & \boldsymbol{m}_r = -\boldsymbol{M}_r \boldsymbol{l}_r \end{aligned}\right\} \tag{8.1.2}$$

and

$$\left.\begin{aligned} \boldsymbol{\sigma} = \boldsymbol{L}\boldsymbol{\varepsilon}^0 + \boldsymbol{l}\Delta\theta \quad & \boldsymbol{\varepsilon} = \boldsymbol{M}\boldsymbol{\sigma}^0 + \boldsymbol{m}\Delta\theta \\ \boldsymbol{l} = -\boldsymbol{L}\boldsymbol{m} \quad & \boldsymbol{m} = -\boldsymbol{M}\boldsymbol{l} \end{aligned}\right\} \tag{8.1.3}$$

The phase and overall thermal strain vectors are denoted by the symbol $\boldsymbol{m}_r$ and $\boldsymbol{m}$, and the thermal stress vectors by $\boldsymbol{l}_r = -\boldsymbol{L}_r \boldsymbol{m}_r$. Thermal eigenstrains that would be equal to total strains in a traction-free volume of a phase $r = 1, 2, \ldots n$ subjected to a uniform change of temperature $\Delta\theta$ are $\boldsymbol{\mu}_r = \boldsymbol{m}_r \Delta\theta, \bar{\boldsymbol{\mu}} = \boldsymbol{m}\Delta\theta$. Thermal eigenstress vectors are $\boldsymbol{\lambda}_r = \boldsymbol{l}_r \Delta\theta, \bar{\boldsymbol{\lambda}} = \boldsymbol{l}\Delta\theta$. Both $\boldsymbol{L}$, $\boldsymbol{M}$ and $\boldsymbol{l}$, $\boldsymbol{m}$ must satisfy admissibility conditions noted in Sect. 6.1, and summarized in Sect. 8.4.

Thermal strain vectors for the eight material symmetries appear in Table 8.1, in terms of linear coefficients of thermal expansion. Depending on the specific symmetry, these apply both to the phases and to homogenized aggregates. For given values of elastic moduli and thermal expansion coefficients of the phases, the following results provide the overall expansion coefficients that appear in thermal vectors $\boldsymbol{m}$ and $\boldsymbol{l}$, as well as estimates of the phase field averages, both in terms of the mechanical concentration factor tensors and overall stiffness or compliance.

The overall thermal vectors are represented by (6×1) matrices and they follow from the Levin formula (3.8.11) as

$$\boldsymbol{m} = \sum_{r=1}^{n} c_r \boldsymbol{B}_r^{\mathrm{T}} \boldsymbol{m}_r \quad \boldsymbol{l} = \sum_{r=1}^{n} c_r \boldsymbol{A}_r^{\mathrm{T}} \boldsymbol{l}_r \tag{8.3.1}$$

Coefficients of the $\boldsymbol{m}$ vector are linear coefficients of thermal expansion of the composite aggregate. The vector $\boldsymbol{l} = -\boldsymbol{L}\boldsymbol{m}$ collects the overall thermal stress components caused by thermal change in an aggregate that is prevented from deforming. As its relation to $\boldsymbol{m}$ suggests, it is the stress required to suppress the overall thermal deformation of an aggregate volume. Only in a homogeneous medium that undergoes a distribution of thermal deformations $\boldsymbol{m}\Delta\theta$ is the overall strain equal to the volume average of the local strains, because $\boldsymbol{A}_r = \boldsymbol{I}, \boldsymbol{B}_r = \boldsymbol{I}, \boldsymbol{m}_\mathbf{r} = \boldsymbol{m}, \boldsymbol{l}_r = \boldsymbol{l}$.

Local fields are conveniently described by introducing thermal strain and stress concentration factors, represented here by (6×1) column vectors, that determine the respective thermal contributions. For the load set $\{\boldsymbol{\varepsilon}^0,\ \Delta\theta\}$, the local field averages in each subvolume V_r are

$$\boldsymbol{\varepsilon}_r = \boldsymbol{A}_r\boldsymbol{\varepsilon}^{\mathbf{0}} + \boldsymbol{a}_r\Delta\theta \quad \boldsymbol{\sigma}_r = \boldsymbol{L}_r\left(\boldsymbol{\varepsilon}_r - \boldsymbol{m}_r\Delta\theta\right) \tag{8.3.2}$$

The $\boldsymbol{a}_r\Delta\theta$ is the local thermal strain average caused in subvolume r by a uniform temperature change $\Delta\theta$, applied while the aggregate is prevented from deforming, at $\boldsymbol{\varepsilon}^0 = \mathbf{0}$. For the load set $\{\boldsymbol{\sigma}^0,\ \Delta\theta\}$

$$\boldsymbol{\sigma}_r = \boldsymbol{B}_r\boldsymbol{\sigma}^0 + \boldsymbol{b}_r\Delta\theta \quad \boldsymbol{\varepsilon}_r = \boldsymbol{M}_r\boldsymbol{\sigma}_r + \boldsymbol{m}_r\Delta\theta \tag{8.3.3}$$

The $\boldsymbol{b}_r\Delta\theta$ is the local thermal stress average caused by $\Delta\theta$ in subvolume r, while the aggregate is free of external tractions, at $\boldsymbol{\sigma}^0 = \mathbf{0}$. Since $\sum_{r=1}^{n} c_r\boldsymbol{A}_r = \boldsymbol{I}, \sum_{r=1}^{n} c_r\boldsymbol{B}_r = \boldsymbol{I}$, the $\boldsymbol{a}_r,\ \boldsymbol{b}_r$ must satisfy

$$\sum\nolimits_{r=1}^{n} c_r\boldsymbol{a}_r = \mathbf{0} \quad \sum\nolimits_{r=1}^{n} c_r\boldsymbol{b}_r = \mathbf{0} \tag{8.3.4}$$

Notice that the dimension of the coefficients of both $\boldsymbol{a}_r$, $\boldsymbol{m}_r$ and $\boldsymbol{m}$ are $1/^0$C and those of $\boldsymbol{b}_r$, $\boldsymbol{l}_r$ and $\boldsymbol{l}$ are MPa/^{0}C. Of course, the coefficients of $\boldsymbol{A}_r$ and $\boldsymbol{B}_r$ are dimensionless. However, the coefficients in the last three rows of the $\boldsymbol{a}_r$ vectors must comply with the contracted tensorial or engineering matrix notations currently used for the strain vectors. Introduced by Laws (1973) for the self-consistent method, the present forms also apply to the Mori-Tanaka estimates and to those that follow from (6.3.5) and (6.3.6).

Additional connections relating $\boldsymbol{a}_r$ and $\boldsymbol{b}_r$ can be derived by letting $\boldsymbol{\varepsilon}^0 = \boldsymbol{m}\Delta\theta$, which implies that $\bar{\boldsymbol{\sigma}} = \mathbf{0}$. Then, $(8.3.2)_1$ and $(8.3.3)_2$ yield

$$\boldsymbol{a}_r - \boldsymbol{m}_r = \boldsymbol{M}_r\boldsymbol{b}_r - \boldsymbol{A}_r\boldsymbol{m} \quad \boldsymbol{b}_r - \boldsymbol{l}_r = \boldsymbol{L}_r\boldsymbol{a}_r - \boldsymbol{B}_r\boldsymbol{l} \tag{8.3.5}$$

Agreement between (8.3.3) and (8.2.6), (8.2.7) requires the thermal concentration factors to satisfy

$$\boldsymbol{a}_r = \sum_{s=1}^{n} \boldsymbol{D}_{rs}\boldsymbol{m}_s \quad \boldsymbol{b}_r = \sum_{s=1}^{n} \boldsymbol{F}_{rs}\boldsymbol{l}_s \tag{8.3.6}$$

where

$$\boldsymbol{D}_{rs} = (\boldsymbol{I} - \boldsymbol{A}_r)(\boldsymbol{L}_r - \boldsymbol{L})^{-1}(\delta_{rs}\boldsymbol{I} - c_s\boldsymbol{A}_s^{\mathrm{T}})\boldsymbol{L}_s \qquad [8.2.19]$$

and

$$\boldsymbol{F}_{rs} = (\boldsymbol{I} - \boldsymbol{B}_r)(\boldsymbol{M}_r - \boldsymbol{M})^{-1}(\delta_{rs}\boldsymbol{I} - c_s\boldsymbol{B}_s{}^{\mathrm{T}})\boldsymbol{M}_s \qquad [8.2.24]$$

As expected, equations (8.3.6) imply that the total thermal strain $\boldsymbol{\varepsilon}_r(\theta) = \boldsymbol{a}_r\Delta\theta$ or stress $\boldsymbol{\sigma}_r(\theta) = \boldsymbol{b}_r\Delta\theta$ are equal to the sum of all contributions transmitted from inhomogeneities $V_s \neq V_r$, including the self-induced parts in $V_s \equiv V_r$. Therefore, the $\boldsymbol{a}_r$ and $\boldsymbol{b}_r$ apply only to averages caused in the r-phase by all eigenstrains present in the system, imparted by the overall thermal and elastic moduli and mechanical concentration factors. In contrast, the transformation influence functions monitor interactions between each pair of individual phase subvolumes and their resident eigenstrains. They also enable replacement of the thermal eigenstrains by any uniform eigenstrain, using $\boldsymbol{\mu}_r = \boldsymbol{m}_r\Delta\theta, \boldsymbol{\lambda}_r = \boldsymbol{l}_r\Delta\theta$. After substitution in (8.3.6), and with regard to (8.1.3) and (8.3.1)

$$\left.\begin{aligned} \boldsymbol{a}_r &= (\boldsymbol{I} - \boldsymbol{A}_r)(\boldsymbol{L}_r - \boldsymbol{L})^{-1}(\boldsymbol{l}_r - \boldsymbol{l}) \\ \boldsymbol{b}_r &= (\boldsymbol{I} - \boldsymbol{B}_r)(\boldsymbol{M}_r - \boldsymbol{M})^{-1}(\boldsymbol{m}_r - \boldsymbol{m}) \end{aligned}\right\} \tag{8.3.7}$$

As long as the thermal concentration factors are related to the transformation influence functions of Sect. 8.2 by (8.3.6), they are valid for any inclusion based AFA method, where $\boldsymbol{A}_r$ and $\boldsymbol{L}$ or $\boldsymbol{B}_r$ and $\boldsymbol{M}$ satisfy the admissibility conditions already noted for the self-consistent and Mori-Tanaka methods in Chap. 7, and summarized in Sect. 8.4.

Although the overall thermal vectors can be found from (8.3.1) without prior knowledge of the thermal concentration factors, it is possible to derive separate connections that replace the $\boldsymbol{A}_r$ or $\boldsymbol{B}_r$ with $\boldsymbol{a}_r$ or $\boldsymbol{b}_r$. Using the overall constitutive relations (8.1.3) for the load set $\{\boldsymbol{\varepsilon}^0,\ \Delta\theta\}$ which is $\boldsymbol{\sigma} = \boldsymbol{L}\boldsymbol{\varepsilon}^0 + \boldsymbol{l}\Delta\theta$, and (8.3.3), we write

$$\left.\begin{aligned} -\boldsymbol{l}\Delta\theta = \boldsymbol{L}\boldsymbol{\varepsilon}^0 - \boldsymbol{\sigma} &= \boldsymbol{L}\boldsymbol{\varepsilon}^0 - \sum_{r=1}^{n} c_r\boldsymbol{\sigma}_r = \boldsymbol{L}\boldsymbol{\varepsilon}^0 - \sum_{r=1}^{n} c_r(\boldsymbol{L}_r\boldsymbol{\varepsilon}_r + \boldsymbol{l}_r\Delta\theta) \\ &= \boldsymbol{L}\boldsymbol{\varepsilon}^0 - \sum_{r=1}^{n} c_r\boldsymbol{L}_r(\boldsymbol{A}_r\boldsymbol{\varepsilon}^0 + \boldsymbol{a}_r\Delta\theta) - \sum_{r=1}^{n} c_r\boldsymbol{l}_r\Delta\theta \end{aligned}\right\} \tag{8.3.8}$$

A similar sequence can be developed for $\boldsymbol{m}$, and with (3.5.8), it yields

$$\left.\begin{aligned} \boldsymbol{l} &= \sum_{r=1}^{n} c_r(\boldsymbol{L}_r\boldsymbol{a}_r + \boldsymbol{l}_r) \quad \boldsymbol{L} = \sum_{r=1}^{n} c_r\boldsymbol{L}_r\boldsymbol{A}_r \\ \boldsymbol{m} &= \sum_{r=1}^{n} c_r(\boldsymbol{M}_r\boldsymbol{b}_r + \boldsymbol{m}_r) \quad \boldsymbol{M} = \sum_{r=1}^{n} c_r\boldsymbol{M}_r\boldsymbol{B}_r \end{aligned}\right\} \tag{8.3.9}$$

These connections confirm that both the local and overall thermal fields can be derived using either estimates of the overall elastic stiffness/compliance or of the mechanical concentration factors. They can also serve to verify accuracy of numerical evaluations of the thermal concentration factors and overall thermal vectors.

In two-phase systems $r = \alpha,\ \beta$, $c_\alpha + c_\beta = 1$, the overall thermal vectors (8.3.9) can be cast as (Benveniste et al. 1991a, b)

$$\left.\begin{aligned} \boldsymbol{l} &= \boldsymbol{l}_\alpha + \sum_{r=2}^{n} c_r\left[(\boldsymbol{l}_r - \boldsymbol{l}_\alpha) + (\boldsymbol{L}_r - \boldsymbol{L}_\alpha)\boldsymbol{a}_r\right] \\ \boldsymbol{m} &= \boldsymbol{m}_\alpha + \sum_{r=2}^{n} c_r\left[(\boldsymbol{m}_r - \boldsymbol{m}_\alpha) + (\boldsymbol{M}_r - \boldsymbol{M}_\alpha)\boldsymbol{b}_r\right] \end{aligned}\right\} \tag{8.3.10}$$

However, the overall thermal strain and stress vectors also follow by substituting thermal eigenstrains into the uniform field results (3.6.16), (3.6.17), (3.6.18), (3.6.19), or into the Levin formula (3.8.11) with the $\boldsymbol{A}_r, \boldsymbol{B}_r$ from (3.5.13) (Benveniste and Dvorak 1990). The results are

$$\left.\begin{aligned} \boldsymbol{m} &= (\boldsymbol{M} - \boldsymbol{M}_\beta)(\boldsymbol{M}_\alpha - \boldsymbol{M}_\beta)^{-1}\boldsymbol{m}_\alpha - (\boldsymbol{M} - \boldsymbol{M}_\alpha)(\boldsymbol{M}_\alpha - \boldsymbol{M}_\beta)^{-1}\boldsymbol{m}_\beta \\ \boldsymbol{m} &= c_\alpha\boldsymbol{m}_\alpha + c_\beta\boldsymbol{m}_\beta + (\boldsymbol{M} - c_\alpha\boldsymbol{M}_\alpha - c_\beta\boldsymbol{M}_\beta)(\boldsymbol{M}_\alpha - \boldsymbol{M}_\beta)^{-1}(\boldsymbol{m}_\alpha - \boldsymbol{m}_\beta) \end{aligned}\right\} \tag{8.3.11}$$

and

$$\left.\begin{aligned} \boldsymbol{l} &= (\boldsymbol{L} - \boldsymbol{L}_\beta)(\boldsymbol{L}_\alpha - \boldsymbol{L}_\beta)^{-1}\boldsymbol{l}_\alpha - (\boldsymbol{L} - \boldsymbol{L}_\alpha)(\boldsymbol{L}_\alpha - \boldsymbol{L}_\beta)^{-1}\boldsymbol{l}_\beta \\ \boldsymbol{l} &= c_\alpha\boldsymbol{l}_\alpha + c_\beta\boldsymbol{l}_\beta + (\boldsymbol{L} - c_\alpha\boldsymbol{L}_\alpha - c_\beta\boldsymbol{L}_\beta)(\boldsymbol{L}_\alpha - \boldsymbol{L}_\beta)^{-1}(\boldsymbol{l}_\alpha - \boldsymbol{l}_\beta) \end{aligned}\right\} \tag{8.3.12}$$

The latter equation was also derived by Laws (1973).

For the degenerate case in which $(\boldsymbol{M}_\alpha - \boldsymbol{M}_\beta)^{-1}$ or $(\boldsymbol{L}_\alpha - \boldsymbol{L}_\beta)^{-1}$ become singular, equations $(8.3.11\text{–}8.3.12)_1$ were examined in *op. cit*, for isotropic and transversely isotropic constituents. For isotropic phases, their results indicate that even though $(\boldsymbol{M}_\alpha - \boldsymbol{M}_\beta)^{-1}$ is singular when the shear moduli $G_\alpha = G_\beta$, the decompositions are well defined, but they fail if $K_\alpha = K_\beta$.

For fiber composites with two transversely isotropic phases, their results show that the uniform field results hold as long as the Hill's moduli of the phases satisfy $(k_\alpha - k_\beta)(n_\alpha - n_\beta) - (l_\alpha - l_\beta)^2 \neq 0$. Only in an elastically homogeneous medium loaded by a distribution of thermal strains, the $\boldsymbol{B}_r = \boldsymbol{I}$ and the overall thermal strain can be found as a simple weighed average $\boldsymbol{m} = \Sigma c_r \boldsymbol{m}_r$.

8.3.2 Temperature Dependent Phase Properties

Both elastic moduli and coefficients of thermal expansion of many materials depend on temperature. Often observed are gradual reductions in Young's moduli and small elevations of Poisson's ratios with increasing temperature, as well as increases in coefficients of thermal expansion. Actual magnitudes can be found in several on-line databases, such as *www.polymersdatabase.com*, and *www.jahm.com*. Interpretation of published data should exclude any time-dependent and other inelastic deformations that may have affected property measurements at higher temperatures, especially in polymers. Applications of temperature-dependent thermoelastic moduli are found in analysis of consolidation by hot isostatic pressing and heat treatment of metal matrix composites (Bahei-El-Din and Dvorak 1997).

As long as a given phase material responds by elastic deformation during loading and unloading in the temperature interval $\theta - \theta_0$ considered, changes in its moduli are reflected by simple monotonic functions $L^r_{\alpha\beta}(\theta)$, which may be different for each coefficient of $\boldsymbol{L}_r(\theta)$. Therefore, the several concentration factors that depend only on the moduli are also functions of current temperature. However, the thermally-induced deformation is accumulated incrementally in the said interval, and it is evaluated along the applied temperature path.

Phase constitutive relations (8.1.3) are modified to account for the deformation accumulated during a change $\theta - \theta_0$ from an initial to current temperature

$$\left.\begin{aligned} \boldsymbol{\varepsilon}_r(\theta) &= \boldsymbol{M}(\theta)\boldsymbol{\sigma}_r(\theta) + \int_{\theta_0}^{\theta} \boldsymbol{m}_r(\theta)\mathrm{d}\theta \\ \mathrm{d}\boldsymbol{\varepsilon}_r(\theta) &= \frac{\partial \boldsymbol{M}_r(\theta)}{\partial\theta}\mathrm{d}\boldsymbol{\sigma}_r(\theta) + \left[\boldsymbol{M}_r(\theta)\frac{\partial \boldsymbol{\sigma}_r(\theta)}{\partial\theta} + \boldsymbol{m}_r(\theta)\right]\mathrm{d}\theta \end{aligned}\right\} \tag{8.3.13}$$

and

$$\left.\begin{aligned} \boldsymbol{\sigma}_r(\theta) &= \boldsymbol{L}_r(\theta)\left[\boldsymbol{\varepsilon}_r(\theta) - \int_{\theta_0}^{\theta} \boldsymbol{m}_r(\theta)\mathrm{d}\theta\right] \\ \mathrm{d}\boldsymbol{\sigma}_r(\theta) &= \frac{\partial \boldsymbol{L}_r(\theta)}{\partial\theta}\left[\boldsymbol{\varepsilon}_r(\theta)\mathrm{d}\theta - \int_{\theta_0}^{\theta} \boldsymbol{m}_r(\theta)\mathrm{d}\theta\right] + \boldsymbol{L}_r(\theta)\left[\frac{\partial \boldsymbol{\varepsilon}_r(\theta)}{\partial\theta} - \boldsymbol{m}_r(\theta)\right]\mathrm{d}\theta \end{aligned}\right\} \tag{8.3.14}$$

Local strain averages and their increments at current temperature θ are

$$\left.\begin{aligned}\boldsymbol{\varepsilon}_r(\theta) &= \boldsymbol{A}_r(\theta)\boldsymbol{\varepsilon}^0(\theta) + \sum_{s=1}^{n}\left[\boldsymbol{D}_{rs}(\theta)\int_{\theta_0}^{\theta}\boldsymbol{m}_s(\theta)\mathrm{d}\theta\right]\\ \mathrm{d}\boldsymbol{\varepsilon}_r(\theta) &= \left[\dot{\boldsymbol{A}}_r(\theta)\boldsymbol{\varepsilon}^0(\theta)+\boldsymbol{A}_r(\theta)\dot{\boldsymbol{\varepsilon}}^0(\theta)\right]\mathrm{d}\theta+\sum_{s=1}^{n}\left[\dot{\boldsymbol{D}}_{rs}(\theta)\int_{\theta_0}^{\theta}\boldsymbol{m}_s(\theta)\mathrm{d}\theta+\boldsymbol{D}_{rs}\boldsymbol{m}_s(\theta)\mathrm{d}\theta\right]\end{aligned}\right\} \tag{8.3.15}$$

Notice that the $\boldsymbol{D}_{rs}(\theta)$ transmit the contribution of the accumulated thermal strain in subvolume V_s to the total strain in V_r, as a function of the current elastic moduli, hence it is not included in the integrals.

Overall stiffness then undergoes the rate of change

$$\left.\begin{aligned}\boldsymbol{L}(\theta) &= \sum_{r=1}^{n} c_r\boldsymbol{L}_r(\theta)\boldsymbol{A}_r(\theta)\\ \dot{\boldsymbol{L}} &= \sum_{r=1}^{n} c_r\left[\dot{\boldsymbol{L}}_r(\theta)\boldsymbol{A}_r(\theta)+\boldsymbol{L}_r(\theta)\dot{\boldsymbol{A}}_r(\theta)\right]\end{aligned}\right\} \tag{8.3.16}$$

Analogous derivatives can be found for the other concentration factors and stiffness estimates in Chap. 7. The Hashin-Shtrikman and other bounds on overall moduli and coefficients of thermal expansion are subject to similar temperature-induced changes.

The rate of change of phase stiffness coefficients with temperature, $\partial\boldsymbol{L}_r/\partial\theta = \dot{\boldsymbol{L}}_r(\theta)$, is reflected in both mechanical and transformation concentration factors, which depend on the elastic moduli. For a matrix $\boldsymbol{L}$ that has an inverse $\boldsymbol{L}^{-1}$, there is

$$\boldsymbol{L}\boldsymbol{L}^{-1} = \boldsymbol{I} \Rightarrow \dot{\boldsymbol{L}}\boldsymbol{L}^{-1} + \boldsymbol{L}\dot{\boldsymbol{L}}^{-1} = \boldsymbol{0} \Rightarrow \dot{\boldsymbol{L}}^{-1} = -\boldsymbol{L}^{-1}\dot{\boldsymbol{L}}\boldsymbol{L}^{-1} \tag{8.3.17}$$

The partial strain concentration factor $\boldsymbol{T}_r$ in (4.2.13) and its rate of change $\dot{\boldsymbol{T}}_r = \partial\boldsymbol{T}_r/\partial\theta$ are

$$\left.\begin{aligned}\boldsymbol{T}_r &= [\boldsymbol{I} + \boldsymbol{P}(\boldsymbol{L}_r - \boldsymbol{L}_0)]^{-1}\\ \dot{\boldsymbol{T}}_r &= -[\boldsymbol{I} + \boldsymbol{P}(\boldsymbol{L}_r - \boldsymbol{L}_0)]^{-1}[\dot{\boldsymbol{P}}(\boldsymbol{L}_r - \boldsymbol{L}_0) + \boldsymbol{P}(\dot{\boldsymbol{L}}_r - \dot{\boldsymbol{L}}_0)][\boldsymbol{I} + \boldsymbol{P}(\boldsymbol{L}_r - \boldsymbol{L}_0)]^{-1}\end{aligned}\right\} \tag{8.3.18}$$

where the coefficients of $\partial\boldsymbol{P}/\partial\theta = \dot{\boldsymbol{P}}$ can be obtained as derivatives of the $P_{\alpha\beta}$, shown for different ellipsoidal shapes in Sect. 4.6 (Suvorov and Dvorak 2002).

Similar derivatives can be found of the concentration factors utilized in the self-consistent and Mori-Tanaka estimates. In particular, from (7.2.1) for SCM:

$$\left.\begin{aligned} \boldsymbol{A}_r &= [\boldsymbol{I} + \boldsymbol{P}(\boldsymbol{L}_r - \boldsymbol{L}_0)]^{-1} \\ \dot{\boldsymbol{A}}_r &= -[\boldsymbol{I} + \boldsymbol{P}(\boldsymbol{L}_r - \boldsymbol{L}_0)]^{-1}[\dot{\boldsymbol{P}}(\boldsymbol{L}_r - \boldsymbol{L}_0) + \boldsymbol{P}(\dot{\boldsymbol{L}}_r - \dot{\boldsymbol{L}}_0)][\boldsymbol{I} + \boldsymbol{P}(\boldsymbol{L}_r - \boldsymbol{L}_0)]^{-1} \end{aligned}\right\} \tag{8.3.19}$$

and from (7.3.2) for M-T:

$$\left.\begin{aligned} \boldsymbol{A}_r &= \boldsymbol{T}_r \left[\sum_{s=1}^{N} c_s \boldsymbol{T}_s\right]^{-1} \\ \dot{\boldsymbol{A}}_r &= \dot{\boldsymbol{T}}_r \left[\sum_{s=1}^{N} c_s \boldsymbol{T}_s\right]^{-1} - \boldsymbol{T}_r \left[\sum_{s=1}^{N} c_s \boldsymbol{T}_s\right]^{-1} \left[\sum_{s=1}^{N} c_s \dot{\boldsymbol{T}}_s\right] \left[\sum_{s=1}^{N} c_s \boldsymbol{T}_s\right]^{-1} \end{aligned}\right\} \tag{8.3.20}$$

where the $\boldsymbol{T}_r$ is evaluated using (4.2.14) with $\boldsymbol{L}_0 = \boldsymbol{L}_1$, the matrix stiffness.

Derivatives of the transformation strain concentration factors (8.2.14), that apply to both methods are

$$\left.\begin{aligned} \boldsymbol{D}_{rs} &= (\boldsymbol{I} - \boldsymbol{A}_r)(\boldsymbol{L}_r - \boldsymbol{L})^{-1}(\delta_{rs}\boldsymbol{I} - c_s \boldsymbol{A}_s^{\mathrm{T}})\boldsymbol{L}_s \\ \dot{\boldsymbol{D}}_{rs} &= [-\dot{\boldsymbol{A}}_r(\boldsymbol{L}_r - \boldsymbol{L})^{-1} - (\boldsymbol{I} - \boldsymbol{A}_r)(\boldsymbol{L}_r - \boldsymbol{L})^{-1}(\dot{\boldsymbol{L}}_r - \dot{\boldsymbol{L}})(\boldsymbol{L}_r - \boldsymbol{L})^{-1}] \\ &\quad \times (\delta_{rs}\boldsymbol{I} - c_s \boldsymbol{A}_s^{\mathrm{T}})\boldsymbol{L}_s + (\boldsymbol{I} - \boldsymbol{A}_r)(\boldsymbol{L}_r - \boldsymbol{L})^{-1}[-c_s \dot{\boldsymbol{A}}_s^{\mathrm{T}} \boldsymbol{L}_s + (\delta_{rs}\boldsymbol{I} - c_s \boldsymbol{A}_s^{\mathrm{T}})\dot{\boldsymbol{L}}_s] \end{aligned}\right\} \tag{8.3.21}$$

Numerical evaluation of strain fields caused in composites with temperature dependent moduli and expansion coefficients by a thermal change $\theta - \theta_0$, and by a temperature-dependent overall strain $\boldsymbol{\varepsilon}^0(\theta)$ can be executed by integration of the increments in (8.3.20–21). Subdivision of the $\theta - \theta_0$ interval into parts where the elastic moduli and loading rates are approximately constant should reduce the effort.

8.4 Capabilities of Bounds and Estimates of Overall and Local Fields

This is a brief summary of certain aspects of the methods discussed in Chaps. 6, 7 and 8. The AFA or average field approximations for aggregates containing ellipsoidal inhomogeneities have the broadest range of applications. Overall stiffness estimates follow from

$$\left.\begin{aligned} \boldsymbol{L} &= \sum_{r=1}^{n} c_r \boldsymbol{L}_r \boldsymbol{A}_r = \sum_{r=1}^{n} c_r \boldsymbol{L}_r [\boldsymbol{I} + \boldsymbol{P}(\boldsymbol{L}_r - \boldsymbol{L}_0)]^{-1} \left[\sum_{s=1}^{n} c_s [\boldsymbol{I} + \boldsymbol{P}(\boldsymbol{L}_s - \boldsymbol{L}_0)]^{-1} \right]^{-1} \\ &= \sum_{r=1}^{n} c_r (\boldsymbol{L}^* + \boldsymbol{L}_r) \boldsymbol{A}_r - \boldsymbol{L}^* = \left[\sum_{r=1}^{n} c_r (\boldsymbol{L}^* + \boldsymbol{L}_r)^{-1} \right]^{-1} - \boldsymbol{L}^* = \boldsymbol{L}^{\mathrm{T}} \end{aligned} \right\} \tag{6.3.5}$$

$$\left.\begin{aligned} \boldsymbol{M} &= \sum_{r=1}^{n} c_r \boldsymbol{M}_r \boldsymbol{B}_r = \sum_{r=1}^{n} c_r \boldsymbol{M}_r [\boldsymbol{I} + \boldsymbol{Q}(\boldsymbol{M}_r - \boldsymbol{M}_0)]^{-1} \left[\sum_{s=1}^{n} c_s [\boldsymbol{I} + \boldsymbol{Q}(\boldsymbol{M}_s - \boldsymbol{M}_0)]^{-1} \right]^{-1} \\ &= \sum_{r=1}^{n} c_r (\boldsymbol{M}^* + \boldsymbol{M}_r) \boldsymbol{B}_r - \boldsymbol{M}^* = \left[\sum_{r=1}^{n} c_r (\boldsymbol{M}^* + \boldsymbol{M}_r)^{-1} \right]^{-1} - \boldsymbol{M}^* = \boldsymbol{M}^{\mathrm{T}} \end{aligned} \right\} \tag{6.3.6}$$

These expressions can be applied to either matrix-based or polycrystalline systems consisting of many different phases which may have different elastic moduli $\boldsymbol{L}_r$ and volume fractions $0 < c_r < 1$. However, proof of consistency $\boldsymbol{LM} = \boldsymbol{I}$ and diagonal symmetry in Sect. 6.3 requires all inhomogeneities $\boldsymbol{L}_r$, $\boldsymbol{M}_r$, $r = 1, 2, 3, \ldots n$ to have the same shape and alignment described by a single $\boldsymbol{P}$ matrix. Different $\boldsymbol{P}$ matrices can be selected in a dilutely reinforced system, where $c_r \ll 1$, as shown in (4.4.6) and (4.4.12). In matrix ($r = 1$) based systems, the single $\boldsymbol{P}$ is demanded only in $r = 2, 3, \ldots n$, according to (6.1.7).

At least three overall property estimates can be found from the above equations by selecting different stiffness $\boldsymbol{L}_0$ of the comparison medium. The first one is a pair of Hashin-Shtrikman upper and lower bounds, described in Sect. 6.2, where the choice of $\boldsymbol{L}_0$ or $\boldsymbol{M}_0$ is prescribed by (6.2.16) or (6.2.24). Bracketed by the H-S bounds are the self-consistent and Mori-Tanaka property estimates, which are obtained from (6.1.5) and (6.1.6) by letting $\boldsymbol{L}_0 = \boldsymbol{L}$ and $\boldsymbol{L}_0 = \boldsymbol{L}_1$, respectively; Sects. 7.1 and 7.2.

One exception to the same shape and alignment rule has been established in Sect. 7.2.4 for matrix-based two-phase systems, by rewriting the Mori-Tanaka overall stiffness expression in (7.2.26)

$$\boldsymbol{L} = \boldsymbol{L}_2 - c_1 \left[\sum_{s=1}^{n} c_s \left\{ (\boldsymbol{L}_2 - \boldsymbol{L}_1)^{-1} - [(\boldsymbol{L}_2 - \boldsymbol{L}_1) + (\boldsymbol{P}_s)^{-1}]^{-1} \right\} \right]^{-1} \tag{8.4.1}$$

The $\boldsymbol{P}_s = (\boldsymbol{L}_s^* + \boldsymbol{L}_1)^{-1} = \boldsymbol{P}_s^{\mathrm{T}}$ are different forms of $\boldsymbol{P}$ described in Sect. 4.6, for second-phase inhomogeneities $s = 2, 3, \ldots n$. A numerical evaluation of the self-consistent estimate of a certain three-phase matrix-based system in Sect. 7.1.4 also provided a diagonally symmetric stiffness matrix, but the result may not hold for other systems.

In well-ordered two-phase systems, where the difference $(\boldsymbol{L}_2 - \boldsymbol{L}_1)$ is either positive or negative semi-definite, the Mori-Tanaka estimate of overall stiffness coincides with the H-S upper or lower bound, which can be established with reference to (6.2.16) or (6.2.24). Therefore, (7.2.26) also provides the upper and lower H-S bound in the well-ordered systems. However, no definite conclusion can be reached about systems which are not well-ordered. Each such case requires a separate examination.

Another exception to the same shape and alignment rule is offered by the differential scheme in Sect. 7.3. As in the case of dilute approximation, diagonal symmetry of the overall stiffness is guaranteed for any combination of shapes and phase properties. Overall stiffness predicted by the differential scheme depends on the selected mixing sequence, which may impair its reliability.

Finally, the double inclusion and double inhomogeneity models of Sect. 7.4 enable estimates of overall stiffness and local field averages in system of many phases, shapes and alignment. This capability is offered by the *CB* configuration of the model, described in Fig. 7.7 and in Sect. 7.4.4. Although this approach has not been explored in the literature to the extent enjoyed by other methods, it may provide reliable results. For example, a stiffness estimate of the Hashin-Shtrikman type for randomly distributed reinforcement orientations is given by equation (7.4.29).

The limitations on shape and alignment of the reinforcements. as well as the diagonal symmetry of the AFA estimates and bounds are also required in extensions of the methods to problems involving application of eigenstrains in the phases. Overall response of a representative volume in Sect. 3.3, subjected to both mechanical and transformation loads follows from the Levin formula (3.8.12), written as

$$\bar{\boldsymbol{\varepsilon}} = \boldsymbol{M}(\boldsymbol{\sigma}^0 - \bar{\boldsymbol{\lambda}}) = \boldsymbol{M}\boldsymbol{\sigma}^0 + \bar{\boldsymbol{\mu}} = \sum_{r=1}^{n} c_r \left[\boldsymbol{M}_r \boldsymbol{B}_r \boldsymbol{\sigma}^0 + \boldsymbol{B}_r^{\mathrm{T}} \boldsymbol{\mu}_r\right] \qquad [8.2.2]$$

and

$$\bar{\boldsymbol{\sigma}} = \boldsymbol{L}(\boldsymbol{\varepsilon}^0 - \bar{\boldsymbol{\mu}}) = \boldsymbol{L}\boldsymbol{\varepsilon}^0 + \bar{\boldsymbol{\lambda}} = \sum_{r=1}^{n} c_r \left[\boldsymbol{L}_r \boldsymbol{A}_r \boldsymbol{\varepsilon}^0 + \boldsymbol{A}_r^{\mathrm{T}} \boldsymbol{\lambda}_r\right] \qquad [8.2.3]$$

These relations hold for any estimate of overall response, and can be readily converted to thermal response, by letting $\bar{\boldsymbol{\mu}} = \boldsymbol{m}\Delta\theta = -\boldsymbol{M}\bar{\boldsymbol{\lambda}}\Delta\theta$ and $\boldsymbol{\mu}_r = \boldsymbol{m}_r\Delta\theta = -\boldsymbol{M}_r\boldsymbol{\lambda}_r\Delta\theta$.

The same results should be reached when the overall strain or stress are derived by the particular averaging or other procedure employed in the stiffness or compliance estimate. In the AFA methods, the result follows from (8.3.9)

$$\boldsymbol{m} = \sum_{r=1}^{n} c_r(\boldsymbol{M}_r \boldsymbol{b}_r + \boldsymbol{m}_r) \quad \boldsymbol{l} = \sum_{r=1}^{n} c_r(\boldsymbol{L}_r \boldsymbol{a}_r + \boldsymbol{l}_r) \qquad (8.4.2)$$

For example, the thermo-elastic version of the Mori-Tanaka method regards each inhomogeneity as embedded in a large volume of the matrix $\boldsymbol{L}_1$ that is subjected to remotely applied uniform matrix strain $\boldsymbol{\varepsilon}_1$, as indicated by (7.2.1), and to a uniform temperature change $\Delta\theta$. The strain average in an inhomogeneity V_r is

$$\boldsymbol{\varepsilon}_r = \boldsymbol{T}_r\boldsymbol{\varepsilon}_1 + \boldsymbol{t}_r\Delta\theta \quad \boldsymbol{T}_r = [\boldsymbol{I} + \boldsymbol{P}(\boldsymbol{L}_r - \boldsymbol{L}_1)]^{-1} \tag{8.4.3}$$

The thermal strain concentration factor $\boldsymbol{t}_r$ can be derived as the sum of the self-induced strain caused by a uniform eigenstrain $\boldsymbol{\mu}_r = \boldsymbol{m}_r\Delta\theta = -\boldsymbol{M}_r\boldsymbol{l}_r\Delta\theta = -\boldsymbol{M}_r\boldsymbol{\lambda}_r$, and the strain caused by a similar eigenstrain or eigenstress, applied in the surrounding matrix. The inhomogeneity $\boldsymbol{L}_r$ in V_r is now embedded in a large volume of the matrix $\boldsymbol{L}_1$, hence we appeal to (4.3.2) and (4.3.7) to find

$$\boldsymbol{\varepsilon}_r(\theta) = \boldsymbol{R}_{rr}\boldsymbol{\mu}_r + \boldsymbol{R}_{r1}\boldsymbol{\mu}_1 = \boldsymbol{T}_r\boldsymbol{P}(\boldsymbol{L}_r\boldsymbol{\mu}_r - \boldsymbol{L}_1\boldsymbol{\mu}_1) \tag{8.4.4}$$

or

$$\boldsymbol{t}_r = -\boldsymbol{T}_r\boldsymbol{P}(\boldsymbol{l}_r - \boldsymbol{l}_1) \tag{8.4.5}$$

with $\boldsymbol{T}_1 = \boldsymbol{I}, \boldsymbol{t}_1 = \boldsymbol{0}$. Using $\Sigma c_r\boldsymbol{\varepsilon}_r = \boldsymbol{\varepsilon}^0$ and (8.3.2), we also find

$$\boldsymbol{a}_r = -\boldsymbol{T}_r\left[\sum_{s=1}^{n} c_s\boldsymbol{T}_s\right]^{-1}\left[\sum_{s=2}^{n} c_s\boldsymbol{t}_s\right] + \boldsymbol{t}_r \tag{8.4.6}$$

and

$$\boldsymbol{\varepsilon}_1 = \left[\sum_{s=1}^{n} c_s\boldsymbol{T}_s\right]^{-1}\left[\boldsymbol{\varepsilon}^0 - \Delta\theta\sum_{s=2}^{n} c_s\boldsymbol{t}_s\right] \tag{8.4.7}$$

Substitution of $\boldsymbol{a}_r$ from (8.4.6) into (8.4.2)^2 yields after some algebra

$$\boldsymbol{l} = \boldsymbol{L}\left[-\sum_{s=1}^{n} c_s\boldsymbol{t}_s\right] + \sum_{s=1}^{n} c_s(\boldsymbol{L}_s\boldsymbol{t}_s + \boldsymbol{l}_s) \tag{8.4.8}$$

On the other hand, the Levin-type form (8.2.2) is found in terms of the partial strain concentration factors in the matrix, as

$$\boldsymbol{l} = \left[\sum_{s=1}^{n} c_s\boldsymbol{T}_s^{\mathrm{T}}\right]^{-1}\left[\sum_{s=1}^{n} c_s\boldsymbol{T}_s^{\mathrm{T}}\boldsymbol{l}_s\right] \tag{8.4.9}$$

Derivation by Benveniste and Dvorak (1992a, b) shows that the two overall thermal stress vectors are equivalent as long as the all inhomogeneities are of the same shape and alignment, and the overall properties follow from those derived in Sect. 7.2.1. The same conclusion is reached with the self-consistent method.

For the Mori-Tanaka method applied to two-phase systems reinforced with inhomogeneities of different shape, one can write (8.4.5) as

$$\boldsymbol{t}_r = -\boldsymbol{T}_r \boldsymbol{P}_s(\boldsymbol{l}_r - \boldsymbol{l}_1) = -\boldsymbol{P}_1^s(\boldsymbol{l}_r - \boldsymbol{l}_1) \tag{8.4.10}$$

where $\boldsymbol{P}_s = (\boldsymbol{L}_s^* + \boldsymbol{L}_1)^{-1} = \boldsymbol{P}_s^{\mathrm{T}}$ and $\boldsymbol{P}_1^s = [(\boldsymbol{L}_2 - \boldsymbol{L}_1) + (\boldsymbol{P}_s)^{-1}]^{-1}$. The overall thermal stress vector is obtained then as

$$\boldsymbol{l} = \boldsymbol{l}_2 - c_1 \left[\sum_{s=1}^{n} c_s [(\boldsymbol{L}_2 - \boldsymbol{L}_1)^{-1} - \boldsymbol{P}_1^s] \right]^{-1} (\boldsymbol{L}_2 - \boldsymbol{L}_1)^{-1} (\boldsymbol{l}_2 - \boldsymbol{l}_1) \tag{8.4.11}$$

and can be shown to be equivalent to that from (8.4.9).

These observations suggest that correct overall transformations can be obtained from mechanical stiffness or compliance, local thermal stress vectors and mechanical concentration factors, as long as the latter satisfy their particular diagonal symmetry, consistency and shape and alignment requirements.

The composite assemblage or CCA/CSA bounds in Sect. 6.4 and the generalized self-consistent method or GSCM in Sect 6.5 provide the most reliable bounds and estimates of overall properties, albeit only for two-phase systems reinforced by spherical particles or aligned circular fibers. Their extension to evaluation of estimates of local field averages has not been a part of the original derivations. However, those can be obtained in terms of overall and phase moduli and volume fractions from (3.5.13). Section 8.1.4 shows that evaluation of coefficients of thermal expansion and averages of local fields caused by uniform changes in temperature can be accomplished by substitution of overall and phase moduli and volume fractions into established expressions. Similar procedure leads to phase field averages caused by uniform transformations of one or both phases.

8.5 Related Research Activities

This book covers only selected parts of micromechanics of heterogeneous media that have been investigated since the 1960s. Other areas which deserve attention include the methods developed in the Russian literature, first exposed by Kunin (1982, 1983) and in a major recent monograph by Buryachenko (2007). Also the homogenization method for systematic design of composite materials that exhibit certain optimal combinations of physical properties and material distribution in space, based on topology optimization (Bendsoe and Kikuchi 1988, Sigmund and Torquato 1999, Bendsoe and Sigmund 2004). This method can be used to

design material combinations and geometries that provide extreme values of overall thermal expansion, or thermal and electrical conductivity, or optimized piezoelectric microstructures.

Piezoelectric composites represent an important group of engineering materials, used in ultrasonic transducers, medical imaging and many other applications. Of interest are two-phase fiber systems with either arbitrary or aligned cylindrical fibers arranged at random or in close packed hexagonal or rectangular arrays. Such systems may have a large number of elastic, dielectric, piezoelectric, piezomagnetic and pyroelectric constants. By applying the method of uniform fields and related techniques, Benveniste and Dvorak (1992) have connected certain sets of the constants by microstructure-independent exact relations for the effective properties and point-wise fields. As in the elastic case of Sect. 3.9, such relations lead to a substantial reduction of independent overall properties of the fibrous piezoelectric systems. This was followed by a wider examination of micromechanics of piezoelectric composites. Computation of effective properties and local fields with transformation influence functions, and formulation of consistency conditions required from different micromechanical models were established by Benveniste (1993a, b, c). The magneto-electric effect in fibrous composites with piezoelectric and piezomagnetic phases, studied by Benveniste (1995) is drawing increasing attention due to the recent activity in magnetoelectric composites (Feibig 2005).

Chapter 9
Interfaces and Interphases

Several types of bonds may exist at the juncture between adjacent phases in contact. On the microscale of many composite materials, most desired is a perfect bond along a sharp spatial boundary S of vanishing thickness. It guarantees that both traction and displacement vectors remain continuous on S. Contact between phase surfaces may also involve presence of one or more interphases, thin bonded layers of additional homogeneous phases introduced, for example, as coatings on particles or fibers, or as products of an interfacial chemical reaction. During composites manufacture and/or loading, an interface is expected to transmit certain tractions between adjacent constituents. When the resolved tensile and/or shear stress reaches a high magnitude, the interface may become imperfect by allowing partial or complete decohesion, a displacement jump, possibly accompanied by a distribution of 'adhesive' tractions. In an opposite situation, a high compressive stress may cause radial cracking in one of the phases in contact, or in the surrounding matrix. While magnitudes of interface tractions determine material propensity to distributed damage, the work required by either decohesion or radial cracking must be provided by release of potential energy, which is proportional to phase volume; Chap. 5. Therefore, small inhomogeneities are less likely sources of damage than large ones.

At a high resolution, an interface is viewed as a multilayer of interacting atoms or polymer chains that form a complex bond between the adjacent materials. This area of current research is of interest in nanocomposites, which have a high specific surface area, often represented by interfacial zones that occupy a relatively large volume fraction, and may exercise significant influence on overall response; c.f. Sect. 3.2.3.

Here we first describe analysis of perfectly bonded planar and curved interfaces between two anisotropic elastic solids. That is followed by an example of separation models of imperfect interfaces. Their contribution to overall deformation or stress relaxation of particulate or fibrous composites is evaluated using damage-equivalent eigenstrains, similar to that in Sect. 4.3.4. A brief description of interphases and their models at the microscale and nanoscale completes the chapter.

G.J. Dvorak, *Micromechanics of Composite Materials*, Solid Mechanics and Its Applications 186, DOI 10.1007/978-94-007-4101-0_9,

9.1 Perfectly Bonded Interfaces

Analysis of coherent interfaces was developed primarily by Hill (1972, 1983) and Laws (1975, 1977). Their results show that a complete strain and stress field at surface points of, say, exterior or α–side of a perfectly bonded, planar or curved interface can be found in terms of known elastic stiffness $\boldsymbol{L}_\alpha$, and of the stress and strain components at the interior or β–side that remain continuous across the interface. As discussed in Chap. 4, the latter are uniform and easily evaluated in ellipsoidal inhomogeneities, which facilitates implementation of the results; Sects. 9.1.3, and 9.1.4.

9.1.1 Decomposition of Stress and Strain Tensors Relative to a Plane

Consider two adjacent elastic phases in contact along a perfectly bonded interface, where both tractions and displacements are continuous. Let ΔS be a planar interface segment separating the two bonded solids, referred to here as the α–phase and the β–phase. Local Cartesian coordinates ξ_i, $i=1, 2, 3$, are introduced such that $\xi_3 \perp \Delta S$, and ξ_1, ξ_2 are suitably selected in the ΔS plane.

Both strain, stress and any other second rank tensor τ_{jk} can be decomposed into interior and exterior parts with respect to the $\xi_1\xi_2-$ plane, as $\tau_{jk} = (\tau_{jk})_i + (\tau_{jk})_e$, where

$$(\tau_{jk})_i = \begin{bmatrix} \tau_{11} & \tau_{12} & 0 \\ \tau_{21} & \tau_{22} & 0 \\ 0 & 0 & 0 \end{bmatrix} \quad (\tau_{jk})_e = \begin{bmatrix} 0 & 0 & \tau_{13} \\ 0 & 0 & \tau_{23} \\ \tau_{31} & \tau_{32} & \tau_{33} \end{bmatrix} \tag{9.1.1}$$

and the scalar product $(\tau_{jk})_i \bullet (\tau_{jk})_e = 0$. The decomposition (9.1.1) is implemented by rearranging the coefficients of the stress and strain vectors as

$$\tilde{\boldsymbol{\tau}} = [\boldsymbol{\tau}_e, \boldsymbol{\tau}_i]^{\mathrm{T}} \quad \tilde{\tau}_j = [\tau_3, \tau_4, \tau_5, \tau_1, \tau_2, \tau_6]^{\mathrm{T}} \tag{9.1.2}$$

Contracted tensorial notation of Chap. 1, with the stress vector (1.1.9), is indicated by (9.1.2) and used in Sect. 9.1.

Continuity of displacements at the interface requires the in-plane strains, represented by the interior part of the strain tensor, to be equal on both sides of ΔS. The exterior strain component, normal to the interface, need not be continuous because by itself it causes no distortion of the interface. Continuity of tractions across the interface requires equality of the exterior part of the stress tensor. Therefore, strain and stress components in the α and β phases are related by

$$\left.\begin{aligned}\varepsilon_{jk}^{\alpha}&=\varepsilon_{jk}^{\beta}\\ \sigma_{jk}^{\alpha}&\neq\sigma_{jk}^{\beta}\end{aligned}\right\}\quad\text{for}\quad jk=11,12,22\qquad\left.\begin{aligned}\varepsilon_{jk}^{\alpha}&\neq\varepsilon_{jk}^{\beta}\\ \sigma_{jk}^{\alpha}&=\sigma_{jk}^{\beta}\end{aligned}\right\}\quad\text{for}\quad jk=31,32,33\tag{9.1.3}$$

In general, along an interface surface S joining two solids, the two parts of the strain and stress tensors, transformed to the ξ_j–coordinates are (Hill 1961)

$$(\varepsilon_{jk}^{\alpha}(\boldsymbol{\xi}))_i=(\varepsilon_{jk}^{\beta}(\boldsymbol{\xi}))_i\quad(\sigma_{jk}^{\alpha}(\boldsymbol{\xi}))_e=(\sigma_{jk}^{\beta}(\boldsymbol{\xi}))_e\quad\boldsymbol{\xi}\in S\tag{9.1.4}$$

These connections enable evaluation of the discontinuous parts of stress and strain at one side of the interface, from fields known at the other side. In particular, if the said fields are known inside or at the surface points $S(\xi)_\beta$ of an inhomogeneity $r=\beta$, then it is possible to determine all field values at matrix points $S(\xi)_\alpha$, located across the interface. The elastic constitutive relation of phase α, and connections (9.1.4) imply that

$$(\boldsymbol{\sigma}_i^{\alpha}+\boldsymbol{\sigma}_e^{\alpha})=\boldsymbol{L}_\alpha(\boldsymbol{\varepsilon}_i^{\alpha}+\boldsymbol{\varepsilon}_e^{\alpha})\Rightarrow(\boldsymbol{\sigma}_i^{\alpha}+\boldsymbol{\sigma}_e^{\beta})=\boldsymbol{L}_\alpha(\boldsymbol{\varepsilon}_i^{\beta}+\boldsymbol{\varepsilon}_e^{\alpha})\tag{9.1.5}$$

Solution is sought for the unknown $\boldsymbol{\sigma}_i^{\alpha}$ and $\boldsymbol{\varepsilon}_e^{\alpha}$, to complete the entire stress and strain state at points located along the α–side of the interface, in terms of the known exterior stress $\boldsymbol{\sigma}_e^{\beta}$ and interior strain $\boldsymbol{\varepsilon}_i^{\beta}$ components along the β–side of the interface, and of the α–phase stiffness $\boldsymbol{L}_\alpha$. Constitutive relations of the β–phase need not be specified, since the coefficients L_{ij}^{β} do not appear in (9.1.5) or (9.1.7).

For example, when the α–phase is *isotropic*,

$$\sigma_{jk}^{\alpha}=\lambda_\alpha\varepsilon_{ll}^{\alpha}\delta_{jk}+2\mu_\alpha\varepsilon_{jk}^{\alpha}\tag{9.1.6}$$

The λ_α, μ_α are Lamé constants, Sect. 2.2.8, and $\xi_3\perp\Delta S$. Then, components of $\boldsymbol{\sigma}_i^{\alpha}$ and $\boldsymbol{\varepsilon}_e^{\alpha}$ at points adjacent to ΔS can be found by solving (9.1.5) as (Hill 1972)

$$\left.\begin{aligned}\sigma_{11}^{\alpha}&=\frac{\lambda_\alpha}{\lambda_\alpha+2\mu_\alpha}\left\{\sigma_{33}^{\beta}+2\mu_\alpha\left(\varepsilon_{11}^{\beta}+\varepsilon_{22}^{\beta}\right)\right\}+2\mu_\alpha\varepsilon_{11}^{\beta}\\ \sigma_{22}^{\alpha}&=\frac{\lambda_\alpha}{\lambda_\alpha+2\mu_\alpha}\left\{\sigma_{33}^{\beta}+2\mu_\alpha\left(\varepsilon_{11}^{\beta}+\varepsilon_{22}^{\beta}\right)\right\}+2\mu_\alpha\varepsilon_{22}^{\beta}\\ \sigma_{12}^{\alpha}&=2\mu_\alpha\varepsilon_{12}^{\beta}\qquad2\mu_\alpha\varepsilon_{13}^{\alpha}=\sigma_{13}^{\beta}\qquad2\mu_\alpha\varepsilon_{23}^{\alpha}=\sigma_{23}^{\beta}\\ \varepsilon_{33}^{\alpha}&=\frac{1}{\lambda_\alpha+2\mu_\alpha}\left\{\sigma_{33}^{\beta}-\lambda_\alpha\left(\varepsilon_{11}^{\beta}+\varepsilon_{22}^{\beta}\right)\right\}\end{aligned}\right\}\tag{9.1.7}$$

When both phases are linearly elastic and isotropic, similar relations can be written for the β–phase components in terms of λ_β and μ_β.

Connections (9.1.7) apply to any interface between two isotropic solids, as long as all stress and strain components are defined in the local coordinates ξ_i, with ξ_3

normal to the interface. Since the β–phase components are typically evaluated in the overall x_j system, the connections are useful when the two systems are or are made coaxial. When this is not the case, the exterior and interior parts are derived in (9.1.52) and (9.1.53).

Next, when the α–phase is *anisotropic*, with known material symmetry in the $\boldsymbol{\xi}$-system, the constitutive relation of the α–phase is modified to reflect the continuity condition $(9.1.5)_2$ and the rearrangement of the coefficients in (9.1.2) indicated by the top tildes. The result is written as a partition of $\tilde{\boldsymbol{\sigma}}_\alpha = \boldsymbol{\Lambda}_\alpha \tilde{\boldsymbol{\varepsilon}}_\alpha$

$$\begin{bmatrix} \boldsymbol{\sigma}_e^\beta \\ \boldsymbol{\sigma}_i^\alpha \end{bmatrix} = \begin{bmatrix} \boldsymbol{\Lambda}_{ee}^\alpha & \boldsymbol{\Lambda}_{ei}^\alpha \\ \boldsymbol{\Lambda}_{ie}^\alpha & \boldsymbol{\Lambda}_{ii}^\alpha \end{bmatrix} \begin{bmatrix} \boldsymbol{\varepsilon}_e^\alpha \\ \boldsymbol{\varepsilon}_i^\beta \end{bmatrix} \tag{9.1.8}$$

where $\boldsymbol{\varepsilon}_i^\beta = \boldsymbol{\varepsilon}_i^\alpha$ and $\boldsymbol{\sigma}_e^\beta = \boldsymbol{\sigma}_e^\alpha$ are (3×1) vectors (9.1.3), and the $\boldsymbol{\Lambda}$ matrices are

$$\left.\begin{aligned} \boldsymbol{\Lambda}_{ii} &= \begin{bmatrix} L_{11} & L_{12} & L_{16} \\ L_{21} & L_{22} & L_{26} \\ L_{61} & L_{62} & L_{66} \end{bmatrix} \quad \boldsymbol{\Lambda}_{ie} = \begin{bmatrix} L_{13} & L_{14} & L_{15} \\ L_{23} & L_{24} & L_{25} \\ L_{63} & L_{64} & L_{65} \end{bmatrix} \\ \boldsymbol{\Lambda}_{ei} &= \begin{bmatrix} L_{31} & L_{32} & L_{36} \\ L_{41} & L_{42} & L_{46} \\ L_{51} & L_{52} & L_{56} \end{bmatrix} \quad \boldsymbol{\Lambda}_{ee} = \begin{bmatrix} L_{33} & L_{34} & L_{35} \\ L_{43} & L_{44} & L_{45} \\ L_{53} & L_{54} & L_{55} \end{bmatrix} \end{aligned}\right\} \tag{9.1.9}$$

Equation 9.1.8 is solved for the exterior strain and interior stress components on the $\alpha -$ side.

$$\left.\begin{aligned} \boldsymbol{\varepsilon}_e^\alpha &= \boldsymbol{\Lambda}_{ee}^{-1}\boldsymbol{\sigma}_e^\beta - \boldsymbol{\Lambda}_{ee}^{-1}\boldsymbol{\Lambda}_{ei}\boldsymbol{\varepsilon}_i^\beta \\ \boldsymbol{\sigma}_i^\alpha &= \boldsymbol{\Lambda}_{ie}\boldsymbol{\Lambda}_{ee}^{-1}\boldsymbol{\sigma}_e^\beta + (\boldsymbol{\Lambda}_{ii} - \boldsymbol{\Lambda}_{ie}\boldsymbol{\Lambda}_{ee}^{-1}\boldsymbol{\Lambda}_{ei})\boldsymbol{\varepsilon}_i^\beta \end{aligned}\right\} \tag{9.1.10}$$

Laws (1975) writes that using (6×1) stress and strain vectors

$$\tilde{\boldsymbol{\varepsilon}}_\alpha = \boldsymbol{C}\tilde{\boldsymbol{\varepsilon}}_\beta + \boldsymbol{D}\tilde{\boldsymbol{\sigma}}_\beta \quad \tilde{\boldsymbol{\sigma}}_\alpha = \boldsymbol{F}\tilde{\boldsymbol{\varepsilon}}_\beta + \boldsymbol{G}\tilde{\boldsymbol{\sigma}}_\beta \tag{9.1.11}$$

where the top tilde indicates rearrangement of the coefficients (9.1.2) and the (6×6) matrices are

$$\left.\begin{aligned} \boldsymbol{C} &= \begin{bmatrix} \mathbf{0} & -\boldsymbol{\Lambda}_{ee}^{-1}\boldsymbol{\Lambda}_{ei} \\ \mathbf{0} & \mathbf{I} \end{bmatrix}_\alpha \quad \boldsymbol{D} = \begin{bmatrix} \boldsymbol{\Lambda}_{ee}^{-1} & \mathbf{0} \\ \mathbf{0} & \mathbf{0} \end{bmatrix}_\alpha \\ \boldsymbol{F} &= \begin{bmatrix} \mathbf{0} & \mathbf{0} \\ \mathbf{0} & (\boldsymbol{\Lambda}_{ii} - \boldsymbol{\Lambda}_{ie}\boldsymbol{\Lambda}_{ee}^{-1}\boldsymbol{\Lambda}_{ei}) \end{bmatrix}_\alpha \quad \boldsymbol{G} = \begin{bmatrix} \mathbf{I} & \mathbf{0} \\ \boldsymbol{\Lambda}_{ie}\boldsymbol{\Lambda}_{ee}^{-1} & \mathbf{0} \end{bmatrix}_\alpha \end{aligned}\right\} \tag{9.1.12}$$

This result does not depend on $\boldsymbol{\varepsilon}_e^\beta$ and $\boldsymbol{\sigma}_i^\beta$ which nevertheless appear in $\tilde{\boldsymbol{\varepsilon}}_\beta$ and $\tilde{\boldsymbol{\sigma}}_\beta$.

By writing the constitutive law in the α–phase for the stress and strain vectors in the modified form (9.1.8), as $\tilde{\boldsymbol{\sigma}}_\alpha = \boldsymbol{\Lambda}_\alpha \tilde{\boldsymbol{\varepsilon}}_\alpha$, and by observing that it must hold even if the interface is located in a homogeneous solid, where $\tilde{\boldsymbol{\sigma}}_\alpha = \tilde{\boldsymbol{\sigma}}_\beta$, $\tilde{\boldsymbol{\varepsilon}}_\alpha = \tilde{\boldsymbol{\varepsilon}}_\beta$, one can verify that (9.1.3) imply the connections

$$\boldsymbol{F} = \boldsymbol{\Lambda}_a \boldsymbol{C} \quad \boldsymbol{G} = \boldsymbol{\Lambda}_a \boldsymbol{D} \quad \boldsymbol{C} + \boldsymbol{D}\boldsymbol{\Lambda}_a = \boldsymbol{\Lambda}_a \boldsymbol{D} + \boldsymbol{F}\boldsymbol{\Lambda}_a{}^{-1} = \boldsymbol{I} \tag{9.1.13}$$

and

$$\tilde{\boldsymbol{\varepsilon}}_\alpha - \tilde{\boldsymbol{\varepsilon}}_\beta = \boldsymbol{D}(\tilde{\boldsymbol{\sigma}}_\beta - \boldsymbol{\Lambda}_\alpha \tilde{\boldsymbol{\varepsilon}}_\beta) \quad \tilde{\boldsymbol{\sigma}}_\alpha - \tilde{\boldsymbol{\sigma}}_\beta = \boldsymbol{F}(\tilde{\boldsymbol{\varepsilon}}_\beta - \boldsymbol{\Lambda}_\alpha^{-1} \tilde{\boldsymbol{\sigma}}_\beta) \tag{9.1.14}$$

where $\boldsymbol{D} = \boldsymbol{D}^{\mathrm{T}}$, $\boldsymbol{F} = \boldsymbol{F}^{\mathrm{T}}$. Notice that $\boldsymbol{C}$, $\boldsymbol{F}$, $\boldsymbol{G}$ each depend only on $\boldsymbol{D}\boldsymbol{\Lambda}_\alpha = \boldsymbol{\Lambda}_\alpha \boldsymbol{D}$.

The above results hold at any point of a perfectly bonded planar interface whose normal is perpendicular to a $\xi_1\xi_2$–plane. As noted above, both the β–phase fields and the α–phase field and stiffness components have to be specified in the same coordinate system. Next, results analogous to (9.1.7) and (9.1.14) are derived for curved interfaces, with variable orientation of the interface normal.

9.1.2 *Decomposition of Stress and Strain Tensors Relative to a Surface*

We now consider an interface S that describes a smooth boundary between two distinct, perfectly bonded media. In certain overall Cartesian coordinates x_i ($i = 1$, 2, 3), the interface is no longer planar, but defined by some function $\Theta(\boldsymbol{x}) = 0$. At each point P of the interface, we again define local or intrinsic Cartesian coordinates ξ_k, such that ξ_3 points toward the α–phase, in the direction normal to the tangential $\xi_1\xi_2$–plane. A unit normal vector $\boldsymbol{n}$ to S has the components $n_j = \cos(\xi_3, x_j)$ in an overall x_j system. For example, $\boldsymbol{n} = [\cos\theta, \sin\theta, 0]^{\mathrm{T}}$ along an interface of a matrix with a circular cylindrical fiber, aligned with the x_3–axis, where θ is measured counterclockwise from $\theta = 0$ at $\xi_3 \equiv x_1$. The same normal defines points along the circumference of a sphere or spheroid centered at $x_j = 0$. The goal is to find a general form of (9.1.4) valid at an interface point with any normal $\boldsymbol{n}$. The original derivation by Laws (1975) is replaced here by a later one by Hill (1983).

Decomposition (9.1.1) of the stress or strain tensors into exterior and interior parts follows from a well known resolution of a surface traction vector $t_j = \sigma_{jk} n_k$, applied at P, into components normal and tangential to S

$$t_j = (n_k t_k) n_j + (\delta_{jk} - n_j n_k) t_k \tag{9.1.15}$$

For a symmetric tensor, this decomposition is (Hill 1972)

$$t_i n_j = \sigma_{ik} n_k n_j + \sigma_{jk} n_k n_i = t_j n_i \tag{9.1.16}$$

It can be easily verified that in the special case $n_k = [n_1,\ n_2,\ n_3]^{\mathrm{T}} = [0,\ 0,\ 1]^{\mathrm{T}}$, the intrinsic components of this tensor are $t_j n_3 = \sigma_{j3}$ for $j = 1,\ 2$, equal to the two exterior parts of $(\sigma_{ij})_e$ in (9.1.1). However, $t_{33} = 2(\sigma_{33})$, which rectified by subtracting $\sigma_{33} = n_k n_l \sigma_{kl}$ from (9.1.16). The invariant formula for the exterior part in (9.1.1) then is

$$\left.\begin{aligned}(\sigma_{ij})_e &= (n_k\sigma_{ik})n_j + (n_k\sigma_{jk})n_i - (n_k n_l \sigma_{kl})n_i n_j \\ &= (n_i\delta_{jk} + n_j\delta_{ik} - n_i n_j n_k)n_l\sigma_{kl}\end{aligned}\right\} \tag{9.1.17}$$

The interior part is the difference $\sigma_{ij} - (\sigma_{ij})_e$, which can be reduced to

$$(\sigma_{ij})_i = (\delta_{ik} - n_i n_k)(\delta_{jl} - n_j n_l)\sigma_{kl} \tag{9.1.18}$$

The same decomposition is applied to obtain the exterior and interior parts of the infinitesimal strain tensor.

A more general for of this decomposition was introduced by (Hill 1983) in the form

$$(\sigma_{ij})_e = E_{ijkl}\sigma_{kl} \quad (\sigma_{ij})_i = N_{ijkl}\sigma_{kl} \tag{9.1.19}$$

where

$$E_{ijkl}\sigma_{kl} = [n_i(\delta_{jk} - n_j n_k) + n_j(\delta_{ik} - n_i n_k) + n_i n_j n_k]n_l\sigma_{kl} \tag{9.1.20}$$

$$N_{ijkl}\sigma_{kl} = (\delta_{ik} - n_i n_k)\left(\delta_{jl} - n_j n_l\right)\sigma_{kl} \tag{9.1.21}$$

and

$$\left.\begin{aligned}&E_{ijkl} + N_{ijkl} = I_{ijkl} = \frac{1}{2}(\delta_{ik}\delta_{jl} + \delta_{jk}\delta_{il}) \\ &E_{ijkl} = E_{jikl} = E_{ijlk} = E_{klij} \quad N_{ijkl} = N_{jikl} = N_{ijlk} = N_{klij} \\ &E_{ijkl}N_{lkmn} = N_{ijkl}E_{lkmn} = \mathbf{0} \quad E_{ijkl}E_{lkmn} = E_{ijmn} \quad N_{ijkl}N_{lkmn} = N_{ijmn}\end{aligned}\right\} \tag{9.1.22}$$

The E_{ijkl} and N_{ijkl} have the same symmetries as stiffness and compliance tensors, and their products show that they are idempotent, similar but not identical to the projection tensors (1.1.16). In numerical work, they are represented by (6×6) matrices $\bar{\boldsymbol{E}}$ and $\bar{\boldsymbol{N}}$, derived as $\bar{\boldsymbol{N}}$ and $\bar{\boldsymbol{E}} = \boldsymbol{I} - \bar{\boldsymbol{N}}$. When the tensorial component notations (1.1.9) and (1.1.10) are used for both strain and stress, the $\bar{\boldsymbol{E}}$ or $\bar{\boldsymbol{N}}$ matrices can be employed in evaluation of exterior or interior components of both quantities.

By applying the contraction rules (1.1.8), the N_{ijkl} matrix can be reduced to a (6×6) matrix $\bar{N}_{RS} = \bar{N}_{SR}$, $R, S = 1, 2, \ldots 6$. In particular, (9.1.21) can be

written as $N_{ijkl}\sigma_{kl} = \mathrm{N}_{ik}\mathrm{N}_{jl}\sigma_{kl}$ when $k = l = 11, 22, 33$, and $N_{ijkl}\sigma_{kl} = (\mathrm{N}_{ik}\mathrm{N}_{jl} + \mathrm{N}_{il}\mathrm{N}_{jk})\sigma_{kl}$ when $k \neq l$. For example, $N_{1122} = \bar{N}_{12}$, $N_{2223} = 2\bar{N}_{24}$. The N_{ik}, N_{jl} are (9×1) arrays, evaluated as $\mathrm{N}_{ik} = (1 - n_i^2)$ for $i = k$, $\mathrm{N}_{jl} = (1 - n_j^2)$ for $j = l$, and $\mathrm{N}_{ik} = -n_i n_k = \mathrm{N}_{ki}$ for $i \neq k$, $\mathrm{N}_{jl} = -n_j n_l$ for $j \neq l$. Coefficients of the (6×6) matrix $\bar{\boldsymbol{N}}$ then follow from the above forms for N_{ik}, N_{jl}, with the first row and all diagonal terms shown here as examples.

$$\left.\begin{aligned}
&\bar{N}_{11} = \left(1 - n_1^2\right)^2 \quad \bar{N}_{12} = (n_1 n_2)^2 \quad \bar{N}_{13} = (n_1 n_3)^2 \\
&\bar{N}_{14} = 2n_1^2 n_2 n_3 \quad \bar{N}_{15} = -2\left(1 - n_1^2\right) n_1 n_3 \quad \bar{N}_{16} = -2\left(1 - n_1^2\right) n_1 n_2 \\
&\bar{N}_{22} = \left(1 - n_2^2\right)^2 \quad \bar{N}_{33} = \left(1 - n_3^2\right)^2 \quad \bar{N}_{44} = 2(n_2 n_3)^2 \\
&\bar{N}_{55} = 2(n_1 n_3)^2 \quad \bar{N}_{66} = 2\left(1 - n_1^2\right)\left(1 - n_2^2\right)
\end{aligned}\right\} \tag{9.1.23}$$

In the special case when $n_i = [0,\ 0,\ 1]^{\mathrm{T}}$, $\bar{\boldsymbol{E}}$ preserves the components of σ_{kl} having index $i = 3$, and $\bar{\boldsymbol{N}}$ preserves those of σ_{kl} lacking index $i = 3$, which yields the decomposition (9.1.1). Nonzero components then are $\bar{E}_{33} = \bar{E}_{44} = \bar{E}_{55} = 1$ and $\bar{N}_{11} = \bar{N}_{22} = \bar{N}_{66} = 1$.

In this manner, any second rank tensor $\sigma_{jk}(\boldsymbol{x})$ or $\varepsilon_{jk}(\boldsymbol{x})$ at an interface point S can be decomposed into exterior and interior parts, with respect to a plane. The normal ξ_3 points toward the $\alpha-$phase, in the direction normal to the tangential $\xi_1\xi_2-$ plane in the intrinsic Cartesian coordinates ξ_k at each interface point.

The continuity conditions (9.1.3) are now written for an interface S between two solids $r = \alpha,\ \beta$, defined by a certain function $\Theta(\boldsymbol{x}) = 0$. They apply to the exterior part of the stress tensor and to the interior part of the strain tensor

$$E_{ijkl}\sigma_{kl}^{\alpha}(\boldsymbol{x}) = E_{ijkl}\sigma_{kl}^{\beta}(\boldsymbol{x}) \quad N_{ijkl}\varepsilon_{kl}^{\alpha}(\boldsymbol{x}) = N_{ijkl}\varepsilon_{kl}^{\beta}(\boldsymbol{x}) \quad \boldsymbol{x} \in S \tag{9.1.24}$$

where $\boldsymbol{\sigma}_e^{\beta}$ and $\boldsymbol{\varepsilon}_i^{\beta}$ are known at the $\beta-$side of the interface. Together with the elastic stiffness $\boldsymbol{L}_{\alpha}$, these continuity conditions are sufficient for determination of all $\boldsymbol{\sigma}_{\alpha}$ and $\boldsymbol{\varepsilon}_{\alpha}$ components at the $\alpha-$side of the interface.

Evaluation of complete $\boldsymbol{\sigma}_{\alpha}$ and $\boldsymbol{\varepsilon}_{\alpha}$ fields proceeds as follows. Suppose that at a certain point P the interface is not stretched, so that the interior part of the strain vanishes, $\boldsymbol{N}\boldsymbol{\varepsilon}_{\alpha} = \boldsymbol{N}\boldsymbol{\varepsilon}_{\beta} = \boldsymbol{0}$, while the exterior part of the stress remains continuous, $\boldsymbol{E}\boldsymbol{\sigma}_{\alpha} = \boldsymbol{E}\boldsymbol{\sigma}_{\beta} \neq \boldsymbol{0}$. The top bars on $\bar{\boldsymbol{E}}$ and $\bar{\boldsymbol{N}}$ are no longer used. The complete strain tensor at the $\alpha-$side, written only in terms of the continuous stress components, as $\boldsymbol{\varepsilon}_{\alpha} = \boldsymbol{\mathcal{D}}\boldsymbol{\sigma}_{\beta}$. This expression must also hold in a homogeneous medium $\boldsymbol{L}_{\alpha}$ where $\boldsymbol{\varepsilon}_{\alpha} = \boldsymbol{\varepsilon}_{\beta}$ and $\boldsymbol{\sigma}_{\alpha} = \boldsymbol{\sigma}_{\beta}$, in the form $\boldsymbol{\varepsilon}_{\beta} = \boldsymbol{\mathcal{D}}\boldsymbol{L}_{\alpha}\boldsymbol{\varepsilon}_{\beta}$, and when $\boldsymbol{\varepsilon}_{\beta}$ is unrestricted. Subtracting these two solutions yields connections analogous to (9.1.14)

$$\boldsymbol{\varepsilon}_{\alpha} - \boldsymbol{\varepsilon}_{\beta} = \boldsymbol{\mathcal{D}}(\boldsymbol{\sigma}_{\beta} - \boldsymbol{L}_{\alpha}\boldsymbol{\varepsilon}_{\beta}) \tag{9.1.25}$$

A similar result for the difference $\boldsymbol{\sigma}_\alpha - \boldsymbol{\sigma}_\beta$ is obtained by letting $\boldsymbol{E}\boldsymbol{\sigma}_\alpha = \boldsymbol{E}\boldsymbol{\sigma}_\beta = \boldsymbol{0}$ and $\boldsymbol{N}\boldsymbol{\varepsilon}_\alpha = \boldsymbol{N}\boldsymbol{\varepsilon}_\beta \neq \boldsymbol{0}$, and by constructing the solution in the form $\boldsymbol{\sigma}_\alpha = \boldsymbol{\mathcal{F}}\boldsymbol{\varepsilon}_\beta$. The general solution, where $\boldsymbol{\sigma}_\beta$ is unrestricted, can then be written in the form

$$\boldsymbol{\sigma}_\alpha - \boldsymbol{\sigma}_\beta = \boldsymbol{\mathcal{F}}(\boldsymbol{\varepsilon}_\beta - \boldsymbol{M}_\alpha \boldsymbol{\sigma}_\beta) \tag{9.1.26}$$

Both $\boldsymbol{\mathcal{D}}$ and $\boldsymbol{\mathcal{F}}$ are fourth rank tensors; $\boldsymbol{\mathcal{D}}$ is determined in (9.1.36) and (9.1.37) below. They provide an evaluation of the interface fields which is different from the decomposition in (9.1.8), (9.1.9), (9.1.10), (9.1.11), and (9.1.12), but which leads to similar results. Indeed, the last two equations can be rearranged into the form similar to (9.1.11), as

$$\boldsymbol{\varepsilon}_\alpha = \boldsymbol{\mathcal{C}}\boldsymbol{\varepsilon}_\beta + \boldsymbol{\mathcal{D}}\boldsymbol{\sigma}_\beta \quad \boldsymbol{\sigma}_\alpha = \boldsymbol{\mathcal{F}}\boldsymbol{\varepsilon}_\beta + \boldsymbol{\mathcal{G}}\boldsymbol{\sigma}_\beta \tag{9.1.27}$$

where

$$\left.\begin{aligned} &\boldsymbol{\mathcal{C}} = \boldsymbol{I} - \boldsymbol{\mathcal{D}}\boldsymbol{L}_\alpha \quad \boldsymbol{\mathcal{F}} = \boldsymbol{L}_\alpha(\boldsymbol{I} - \boldsymbol{\mathcal{D}}\boldsymbol{L}_\alpha) \quad \boldsymbol{\mathcal{G}} = \boldsymbol{L}_\alpha\boldsymbol{\mathcal{D}} \\ &\boldsymbol{L}_\alpha\boldsymbol{\mathcal{D}} + \boldsymbol{\mathcal{F}}\boldsymbol{M}_\alpha = \boldsymbol{I} = \boldsymbol{\mathcal{D}}\boldsymbol{L}_\alpha + \boldsymbol{M}_\alpha\boldsymbol{\mathcal{F}} \end{aligned}\right\} \tag{9.1.28}$$

Therefore

$$\left.\begin{aligned} \boldsymbol{\varepsilon}_\alpha &= \boldsymbol{\mathcal{D}}\boldsymbol{\sigma}_\beta + \boldsymbol{M}_\alpha\boldsymbol{\mathcal{F}}\boldsymbol{\varepsilon}_\beta = \boldsymbol{\mathcal{D}}(\boldsymbol{E}\boldsymbol{\sigma}_\beta) + \boldsymbol{M}_\alpha\boldsymbol{\mathcal{F}}(\boldsymbol{N}\boldsymbol{\varepsilon}_\beta) \\ \boldsymbol{\sigma}_\alpha &= \boldsymbol{L}_\alpha\boldsymbol{\mathcal{D}}\boldsymbol{\sigma}_\beta + \boldsymbol{\mathcal{F}}\boldsymbol{\varepsilon}_\beta = \boldsymbol{L}_\alpha\boldsymbol{\mathcal{D}}(\boldsymbol{E}\boldsymbol{\sigma}_\beta) + \boldsymbol{\mathcal{F}}(\boldsymbol{N}\boldsymbol{\varepsilon}_\beta) \end{aligned}\right\} \tag{9.1.29}$$

The last terms indicate that the $\boldsymbol{\varepsilon}_\alpha$, $\boldsymbol{\sigma}_\alpha$ are insensitive to the terms $\boldsymbol{N}\boldsymbol{\sigma}_\beta$, $\boldsymbol{E}\boldsymbol{\varepsilon}_\beta$ which are not bound by (9.1.25). Hill (1983) and Walpole's (1981) also derived algebraic properties of the above idempotent operators. In particular

$$\left.\begin{aligned} \boldsymbol{\mathcal{D}}\boldsymbol{N} = \boldsymbol{0} = \boldsymbol{N}\boldsymbol{\mathcal{D}} \quad \boldsymbol{\mathcal{F}}\boldsymbol{E} = \boldsymbol{0} = \boldsymbol{E}\boldsymbol{\mathcal{F}} \quad \boldsymbol{\mathcal{D}}\boldsymbol{\mathcal{F}} = \boldsymbol{0} = \boldsymbol{\mathcal{F}}\boldsymbol{\mathcal{D}} \\ \boldsymbol{\mathcal{D}}\boldsymbol{E} = \boldsymbol{\mathcal{D}} = \boldsymbol{E}\boldsymbol{\mathcal{D}} \quad \boldsymbol{\mathcal{F}}\boldsymbol{N} = \boldsymbol{\mathcal{F}} = \boldsymbol{N}\boldsymbol{\mathcal{F}} \end{aligned}\right\} \tag{9.1.30}$$

This indicates that $\boldsymbol{\mathcal{D}}$ [$\boldsymbol{\mathcal{F}}$] generates exterior [interior] tensors and annihilates interior [exterior] tensors. Therefore, $\boldsymbol{\mathcal{D}}\boldsymbol{\sigma}_\beta$ contributes the exterior part of $\boldsymbol{\varepsilon}_\alpha$, and $\boldsymbol{\mathcal{F}}\boldsymbol{\varepsilon}_\beta$ to the interior part of $\boldsymbol{\sigma}_\alpha$. The $\boldsymbol{\mathcal{D}}$ and $\boldsymbol{\mathcal{F}}$ are both orthogonal.

Derivation of the component form of $\boldsymbol{\mathcal{D}}$ was first outlined by Hill (1961), and later by Kunin and Sosnina (1973), Laws (1977) and Hill (1983). We follow here the two latter procedures. Continuity of the interior strain components in (9.1.3) can be written as $\boldsymbol{N}(\boldsymbol{\varepsilon}_\alpha - \boldsymbol{\varepsilon})_\beta = \boldsymbol{0}$, with $\boldsymbol{N}$ from (9.1.21). Then, the jump of the strain components at the interface is limited to the exterior part

$$\varepsilon_{ij}^\alpha - \varepsilon_{ij}^\beta = \frac{1}{2}\left(\zeta_i n_j + \zeta_j n_i\right) \tag{9.1.31}$$

This result also follows from Hadamard's (1903) lemma for discontinuities in derivatives of continuous functions, or displacements u_i, at an interface. The vector

ζ_j is determined by invoking continuity of tractions, $\sigma^{\alpha}_{ik} n_k = \sigma^{\beta}_{ik} n_k$, which restricts only the exterior stress components. Together with (9.1.31), it implies that

$$\left.\begin{aligned} L^{\alpha}_{ijkl}(\varepsilon^{\alpha}_{kl} - \varepsilon^{\beta}_{kl}) n_j &= (\sigma^{\beta}_{ij} - L^{\alpha}_{ijkl}\varepsilon^{\beta}_{kl}) n_j = L^{\alpha}_{ijkl}\zeta_k n_l n_j \\ L^{\alpha}_{ijkl} n_l n_j \zeta_k &= K_{ik}\zeta_k = (\sigma^{\beta}_{ij} - L^{\alpha}_{ijkl}\varepsilon^{\beta}_{kl}) n_j \\ \zeta_k &= K^{-1}_{ik}(\sigma^{\beta}_{ij} - L^{\alpha}_{ijmn}\varepsilon^{\beta}_{mn}) n_j \end{aligned}\right\} \tag{9.1.32}$$

where $K_{ik} = L^{\alpha}_{ijkl} n_j n_l = K_{ki}$ is the acoustic tensor. For real materials, L^{α}_{ijkl} is symmetric and positive definite, hence K_{ik} is invertible. From (9.1.25), (9.1.31)

$$\varepsilon^{\alpha}_{kl} - \varepsilon^{\beta}_{kl} = \zeta_k n_l = (K_{ik})^{-1}(\sigma^{\beta}_{ij} - L_{ijmn}\varepsilon^{\beta}_{nm})\, n_j n_l = D_{klij}\,(\sigma^{\beta}_{ij} - L_{ijmn}\varepsilon^{\beta}_{nm}) \tag{9.1.33}$$

The symmetric form of the $\mathcal{D}$ tensor is

$$\mathcal{D}_{ijkl} = \frac{1}{4}(n_j K^{-1}_{ik} n_l + n_j K^{-1}_{il} n_k + n_i K^{-1}_{jk} n_l + n_i K^{-1}_{jl} n_k) \tag{9.1.34}$$

Reduction to a (6×6) matrix $\mathcal{D}$ is left for an exercise.

These components posses the same symmetries as do $\boldsymbol{L}$, $\boldsymbol{E}$ and $\boldsymbol{N}$. Since all operators in (9.1.26) and (9.1.28) depend on $\mathcal{D}$ and $\boldsymbol{L} = \boldsymbol{L}_{\alpha}$, this completes the evaluation of the stresses and strains at the $\alpha-$side of a general interface $S \perp \boldsymbol{n}$. We recall that in the intrinsic or local coordinates ξ_i, the normal is aligned with ξ_3, while in the fixed x_i-system, $n_i = \cos(\xi_3,\ x_i)$.

For an arbitrarily anisotropic medium, the acoustic tensor is a complicated function of the unit normal of the interface and of the $\alpha-$phase elastic moduli, hence it is best evaluated numerically. However, simple evaluation of the complete fields (9.1.27) is possible at selected points where $n_i = [0,\ 0,\ 1]^{\mathrm{T}}$, and where interface traction maxima or minima are expected. Moreover, the explicit inverse of $\boldsymbol{K}$ can be derived for isotropic materials, together with the following forms of forms of $\mathcal{D}$ and $\mathcal{F}$ (Hill 1983)

$$K_{ik} = \mu\delta_{ik} + (\lambda + \mu) n_i n_k \qquad \mu K^{-1}_{ik} = \delta_{ik} - \frac{\lambda + \mu}{\lambda + 2\mu} n_i n_k \tag{9.1.35}$$

$$2\mu\mathcal{D}_{ijkl} = E_{ijkl} - \frac{\lambda}{\lambda + 2\mu} n_i n_j n_k n_l \tag{9.1.36}$$

$$\frac{1}{2\mu}\mathcal{F}_{ijkl} = N_{ijkl} + \frac{\lambda}{\lambda + 2\mu}\left(\delta_{ij} - n_i n_j\right)(\delta_{kl} - n_k n_l) \tag{9.1.37}$$

where λ, μ are Lame's constants, and $\boldsymbol{E}$, $\boldsymbol{N}$ are defined in (9.1.20) and (9.1.21). When assembled in (9×9) matrices, with rows designated by ij and columns by kl, all elements of $\mathcal{D}$ [$\mathcal{F}$], not involving [involving] index 3 are zero, while others depend on $\boldsymbol{K}^{-1}$.

9.1.3 Interface Fields at Anisotropic Ellipsoidal Inhomogeneities and Cavities

Application of the above results to a perfectly bonded interface between an ellipsoidal inhomogeneity and a large volume V of a matrix provides a useful illustration of their utility. The volume is loaded by surface displacements or tractions on ∂V which create an overall uniform strain $\boldsymbol{\varepsilon}^0$, or stress $\boldsymbol{\sigma}^0$. The inhomogeneity is the β–phase, with elastic stiffness $\boldsymbol{L}_\beta$ and compliance $\boldsymbol{M}_\beta$. The matrix is the α–phase, with properties $\boldsymbol{L}_\alpha$, $\boldsymbol{M}_\alpha$. Both phases can be anisotropic, each with a different material symmetry defined in the overall x_i system of coordinates. Recall that under the uniform overall loads, the local strain and stress fields in the inhomogeneity are both uniform, and given by (4.2.13), now written as

$$\boldsymbol{\varepsilon}_\beta = [\boldsymbol{I} + \boldsymbol{P}(\boldsymbol{L}_\beta - \boldsymbol{L}_\alpha)]^{-1}\boldsymbol{\varepsilon}^0 \quad \boldsymbol{\sigma}_\beta = [\boldsymbol{I} + \boldsymbol{Q}(\boldsymbol{M}_\beta - \boldsymbol{M}_\alpha)]^{-1}\boldsymbol{\sigma}^0 \tag{9.1.38}$$

The $\boldsymbol{P}$ and $\boldsymbol{Q}$ matrices are defined in (4.2.9), and their forms for selected ellipsoidal shapes are described in Sect. 4.6. Both $\boldsymbol{P}$ and $\boldsymbol{Q}$ are evaluated in the matrix, in the α–phase, and are connected by $\boldsymbol{P}\boldsymbol{L}_\alpha + \boldsymbol{M}_\alpha\boldsymbol{Q} = \boldsymbol{I}$. Inside the inhomogeneity, $\boldsymbol{\varepsilon}_\beta = \boldsymbol{M}_\beta\boldsymbol{\sigma}_\beta$ and $\boldsymbol{\sigma}_\beta = \boldsymbol{L}_\beta\boldsymbol{\varepsilon}_\beta$.

The $\beta-$phase fields (9.1.38) are now substituted into (9.1.25) and (9.1.26), to yield the $\alpha-$phase fields in terms of the overall loads (Laws 1975).

$$\boldsymbol{\varepsilon}_\alpha = [\boldsymbol{I} + \boldsymbol{\mathcal{D}}(\boldsymbol{L}_\beta - \boldsymbol{L}_\alpha)][\boldsymbol{I} + \boldsymbol{P}(\boldsymbol{L}_\beta - \boldsymbol{L}_\alpha)]^{-1}\boldsymbol{\varepsilon}^0 \tag{9.1.39}$$

and

$$\boldsymbol{\varepsilon}_\alpha = [\boldsymbol{I} + \boldsymbol{\mathcal{F}}(\boldsymbol{M}_\beta - \boldsymbol{M}_\alpha)][\boldsymbol{I} + \boldsymbol{Q}(\boldsymbol{M}_\beta - \boldsymbol{M}_\alpha)]^{-1}\boldsymbol{\sigma}^0 \tag{9.1.40}$$

The conjugate fields follow from $\boldsymbol{\sigma}_\alpha = \boldsymbol{L}_\alpha\boldsymbol{\varepsilon}_\alpha$ and $\boldsymbol{\varepsilon}_\alpha = \boldsymbol{M}_\alpha\boldsymbol{\sigma}_\alpha$, respectively. Notice that the strain and stress fields at points on the α–side of the interface depend on the orientation of the normal n_i at each point, which is reflected in the (6×6) matrices $\boldsymbol{\mathcal{D}}$ and $\boldsymbol{\mathcal{F}} = \boldsymbol{L}_\alpha(\boldsymbol{L} - \boldsymbol{\mathcal{D}}\boldsymbol{L}_\alpha)$ that now represent the tensors in (9.1.28) and (9.1.34). Analytical evaluation is possible for spherical and circular cylindrical shapes, but only a numerical evaluation appears feasible for other shapes.

Next, suppose that under overall strain $\boldsymbol{\varepsilon}^{\boldsymbol{0}} = \boldsymbol{0}$, the matrix $\boldsymbol{L}_\alpha$ is transformed by a uniform eigenstrain $\boldsymbol{\mu}_\alpha$, while the ellipsoidal inhomogeneity $\boldsymbol{L}_\beta$ undergoes a uniform trans-formation $\boldsymbol{\mu}_\beta$. Corresponding eigenstress vectors are $\boldsymbol{\lambda}_\alpha = -\boldsymbol{L}_\alpha\boldsymbol{\mu}_\alpha$ and $\boldsymbol{\lambda}_\beta = -\boldsymbol{L}_\beta\boldsymbol{\mu}_\beta$. The stress in the inhomogeneity is $\boldsymbol{\sigma}_\beta = \boldsymbol{L}_\beta(\boldsymbol{\varepsilon}_\beta - \boldsymbol{\mu}_\beta)$, hence (9.1.25), (9.1.39) change to

$$\boldsymbol{\varepsilon}_\alpha = [\boldsymbol{I} + \boldsymbol{\mathcal{D}}(\boldsymbol{L}_\beta - \boldsymbol{L}_\alpha)]\boldsymbol{\varepsilon}_\beta - \boldsymbol{\mathcal{D}}\boldsymbol{L}_\beta\boldsymbol{\mu}_\beta \tag{9.1.41}$$

Local fields in the inhomogeneity are derived from (4.3.2), in the form

$$\boldsymbol{\varepsilon}_\beta = \boldsymbol{R}_{\beta\beta}\boldsymbol{\mu}_\beta + \boldsymbol{R}_{\beta\alpha}\boldsymbol{\mu}_\alpha \quad \boldsymbol{\sigma}_\beta = \boldsymbol{L}_\beta(\boldsymbol{\varepsilon}_\beta - \boldsymbol{\mu}_\beta) \tag{9.1.42}$$

where

$$\boldsymbol{R}_{\beta\beta} = [\boldsymbol{I} + \boldsymbol{P}(\boldsymbol{L}_\beta - \boldsymbol{L}_\alpha)]^{-1}\boldsymbol{P}\boldsymbol{L}_\beta \quad \boldsymbol{R}_{\beta\alpha} = -[\boldsymbol{I} + \boldsymbol{P}(\boldsymbol{L}_\beta - \boldsymbol{L}_\alpha)]^{-1}\boldsymbol{P}\boldsymbol{L}_\alpha \tag{9.1.43}$$

according to (4.3.7), with $\boldsymbol{T}_r$ derived from (4.2.14). Therefore, the eigenstrains $\boldsymbol{\mu}_\alpha$, $\boldsymbol{\mu}_\beta$ at $\boldsymbol{\varepsilon}^0 = \boldsymbol{0}$ deform points along the matrix or $\alpha-$side of the interface by

$$\boldsymbol{\varepsilon}_\alpha = [\boldsymbol{I} + \mathcal{D}(\boldsymbol{L}_\beta - \boldsymbol{L}_\alpha)][\boldsymbol{I} + \boldsymbol{P}(\boldsymbol{L}_\beta - \boldsymbol{L}_\alpha)]^{-1}\boldsymbol{P}(\boldsymbol{L}_\beta\boldsymbol{\mu}_\beta - \boldsymbol{L}_\alpha\boldsymbol{\mu}_\alpha) - \mathcal{D}\boldsymbol{L}_\beta\boldsymbol{\mu}_\beta \tag{9.1.44}$$

The stress generated at the matrix points adjoining the interface is $\boldsymbol{\sigma}_\alpha = \boldsymbol{L}_\alpha(\boldsymbol{\varepsilon}_\alpha - \boldsymbol{\mu}_\alpha)$.

Application of $\boldsymbol{\mu}_\alpha$, $\boldsymbol{\mu}_\beta$ at $\boldsymbol{\sigma}^0 = \boldsymbol{0}$ yields $\boldsymbol{\varepsilon}_\beta = \boldsymbol{M}_\beta\boldsymbol{\sigma}_\beta + \boldsymbol{\mu}_\beta = \boldsymbol{M}_\beta(\boldsymbol{\sigma}_\beta - \boldsymbol{\lambda}_\beta)$, hence (9.1.26), (9.1.40) change to

$$\boldsymbol{\sigma}_\alpha = [\boldsymbol{I} + \mathcal{F}(\boldsymbol{M}_\alpha - \boldsymbol{M}_\beta)]\boldsymbol{\sigma}_\beta - \mathcal{F}\boldsymbol{M}_\beta\boldsymbol{\lambda}_\beta \tag{9.1.45}$$

Local stress caused in the inhomogeneity by $\boldsymbol{\lambda}_\alpha$, $\boldsymbol{\lambda}_\beta$ at $\boldsymbol{\sigma}^0 = \boldsymbol{0}$ follows from (4.3.3) and (4.3.8) as

$$\boldsymbol{\sigma}_\beta = [\boldsymbol{I} + \boldsymbol{Q}(\boldsymbol{M}_\beta - \boldsymbol{M}_\alpha)]^{-1}\boldsymbol{Q}(\boldsymbol{M}_\beta\boldsymbol{\lambda}_\beta - \boldsymbol{M}_\alpha\boldsymbol{\lambda}_\alpha) \tag{9.1.46}$$

After substitution into (9.1.45),

$$\boldsymbol{\sigma}_\alpha = [\boldsymbol{I} + \mathcal{F}(\boldsymbol{M}_\alpha - \boldsymbol{M}_\beta)][\boldsymbol{I} + \boldsymbol{Q}(\boldsymbol{M}_\beta - \boldsymbol{M}_\alpha)]^{-1}\boldsymbol{Q}(\boldsymbol{M}_\beta\boldsymbol{\lambda}_\beta - \boldsymbol{M}_\alpha\boldsymbol{\lambda}_\alpha) - \mathcal{F}\boldsymbol{M}_\beta\boldsymbol{\lambda}_\beta \tag{9.1.47}$$

Interface fields caused in the matrix by the complete loading set $\{\boldsymbol{\varepsilon}^0, \boldsymbol{\mu}_\alpha, \boldsymbol{\mu}_\beta\}$ are the superposition of (9.1.39) with (9.1.44). For the loading set $\{\boldsymbol{\sigma}^0, \boldsymbol{\lambda}_\alpha, \boldsymbol{\lambda}_\beta\}$ one has to superimpose (9.1.40) with (9.1.47).

Finally, we use the above results to derive strain and stress fields at the surface of a *loaded ellipsoidal cavity* in the matrix $\boldsymbol{L}_\alpha$. Applied loads include overall strain $\boldsymbol{\varepsilon}^0$ or stress $\boldsymbol{\sigma}^0$ at infinity, tractions at cavity surface that are in equilibrium with a uniform stress $\bar{\boldsymbol{\sigma}}_r^c = \boldsymbol{\sigma}_\beta$, and a uniform eigenstrain $\boldsymbol{\mu}_\alpha$ in the matrix. Under these loads, local strain $\bar{\boldsymbol{\varepsilon}}_r^c = \boldsymbol{\varepsilon}_\beta$ derived from displacements of the cavity wall is uniform, and it is connected to the overall fields by (9.1.39), (9.1.40), and (9.1.41), written now as

$$\boldsymbol{\varepsilon}^0 - \boldsymbol{\varepsilon}_\beta = \boldsymbol{P}[\boldsymbol{\sigma}_\beta - \boldsymbol{L}_\alpha(\boldsymbol{\varepsilon}_\beta - \boldsymbol{\mu}_\alpha)] \quad \boldsymbol{\sigma}^0 - \boldsymbol{\sigma}_\beta = \boldsymbol{Q}(\boldsymbol{\varepsilon}_\beta - \boldsymbol{\mu}_\alpha - \boldsymbol{M}_\alpha\boldsymbol{\sigma}_\beta) \tag{9.1.48}$$

or as

$$\boldsymbol{\varepsilon}_\beta = (\boldsymbol{I} - \boldsymbol{S})^{-1}[\boldsymbol{\varepsilon}^0 - \boldsymbol{P}(\boldsymbol{\sigma}_\beta + \boldsymbol{L}_\alpha\boldsymbol{\mu}_\alpha)] \quad \boldsymbol{\varepsilon}_\beta = \boldsymbol{M}_\alpha\boldsymbol{\sigma}_\beta + \boldsymbol{Q}^{-1}(\boldsymbol{\sigma}^0 - \boldsymbol{\sigma}_\beta) + \boldsymbol{\mu}_\alpha \tag{9.1.49}$$

The strain $\boldsymbol{\varepsilon}_\alpha$ and stress $\boldsymbol{\sigma}_\alpha$ at the surface of the cavity follow from (9.1.25) and (9.1.26) as

$$\boldsymbol{\varepsilon}_\alpha = \boldsymbol{\mathcal{D}}\boldsymbol{\sigma}_\beta + (\boldsymbol{I} - \boldsymbol{\mathcal{D}}\boldsymbol{L}_\alpha)\boldsymbol{\varepsilon}_\beta \quad \boldsymbol{\sigma}_\alpha = (\boldsymbol{I} - \boldsymbol{\mathcal{F}}\boldsymbol{M}_\alpha)\boldsymbol{\sigma}_\beta + \boldsymbol{\mathcal{F}}\boldsymbol{\varepsilon}_\beta \tag{9.1.50}$$

Substitution of each of the distinct forms of $\boldsymbol{\varepsilon}_\beta$ from (9.1.49) into both expressions then yields the fields caused along the cavity surface by the load sets $\{\boldsymbol{\varepsilon}^0,\ \boldsymbol{\sigma}_\beta,\ \boldsymbol{\mu}_\alpha\}$ or $\{\boldsymbol{\sigma}^0,\ \boldsymbol{\sigma}_\beta,\ \boldsymbol{\mu}_\alpha\}$, respectively.

9.1.4 *Interface Fields at Isotropic Inhomogeneities and Cavities*

Evaluation of complete distributions along an entire interface is seldom needed, since points of traction maxima or minima can be often identified for typical shapes of reinforcements and for simple applied stress or strain states and for uniform phase eigenstrains of interest. As mentioned above, simple evaluation of the fields in matrix points adjoining an ellipsoidal inhomogeneity is possible at selected points on the circumference of spheres, spheroids and cylinders with normals aligned with the direction of principal overall normal stress in the transverse plane.

In particular, the uniform interior strain fields in an isotropic spherical particle residing in an isotropic matrix have already been evaluated in (4.4.26) with the concentration factors from (4.4.23) and (4.4.27). In the dilute case, the overall strain $\boldsymbol{\varepsilon}^0$ can be applied such as to generate overall simple tension stress $\bar{\sigma}_{11}$ Corresponding components of the uniform stress and strain field in the particle are then substituted as the β–phase components into (9.1.7), to find the complete fields in the matrix at selected interface points. An illustrative example appears in Sect. 9.1.5.

General forms of the above results for any normal direction at interfaces between isotropic elastic constituents had been derived by Hill (1972), with α–phase moduli $\lambda_\alpha,\ \mu_\alpha$ in the constitutive relation (9.1.6). Continuity of interface tractions $t_i = \sigma_{ik}n_k$ and of the interior part of the strain are written in general or fixed x_i–system, $n_i = \cos(\xi_3,\ x_i)$, as

$$(\sigma^\alpha_{kl} - \sigma^\beta_{kl})n_l = 0 \quad (\delta_{ik} - n_i n_k)(\delta_{jl} - n_j n_l)(\varepsilon^\alpha_{kl} - \varepsilon^\beta_{kl}) = 0 \tag{9.1.51}$$

where the second relation follows from (9.1.18), and the continuous parts of $\boldsymbol{\sigma}_\beta,\ \boldsymbol{\varepsilon}_\beta$ are known. The interior part of the stress is found from (9.1.6) into (9.1.18). The total stress is written according to (9.1.27), as $\boldsymbol{\sigma}_\alpha = \boldsymbol{\mathcal{F}}\boldsymbol{\varepsilon}_\beta + \boldsymbol{\mathcal{G}}\boldsymbol{\sigma}_\beta$, where

$$\left.\begin{aligned} \mathcal{F}_{ijkl}\varepsilon^\beta_{kl} &= 2\mu_\alpha\left[(\delta_{ik} - n_i n_k)(\delta_{jl} - n_j n_l) + \frac{\lambda_\alpha}{\lambda_\alpha + 2\mu_\alpha}(\delta_{ij} - n_i n_j)(\delta_{kl} - n_k n_l)\right]\varepsilon^\beta_{kl} \\ \mathcal{G}_{ijkl}\sigma^\beta_{kl} &= \left[n_i\delta_{jk} + n_j\delta_{ik} - n_i n_j n_k + \frac{\lambda_\alpha}{\lambda_\alpha + 2\mu_\alpha}(\delta_{ij} - n_i n_j)n_k\right]n_l\sigma^\beta_{kl} \end{aligned}\right\} \tag{9.1.52}$$

The last term in $\mathcal{G}_{ijkl}$ belongs to the interior part of $\boldsymbol{\sigma}_\alpha$.

Total strain $\boldsymbol{\varepsilon}_\alpha = \boldsymbol{\mathcal{C}}\boldsymbol{\varepsilon}_\beta + \boldsymbol{\mathcal{D}}\boldsymbol{\sigma}_\beta$ is obtained from

$$\left.\begin{aligned} \mathcal{C}_{ijkl}\varepsilon^\beta_{kl} &= \left[(\delta_{ik}-n_in_k)(\delta_{jl}-n_jn_l) - \frac{\lambda_\alpha}{\lambda_\alpha+2\mu_\alpha}n_in_j(\delta_{kl}-n_kn_l)\right]\varepsilon^\beta_{kl} \\ \mathcal{D}_{ijkl}\sigma^\beta_{kl} &= \frac{1}{2\mu_\alpha}\left[n_i\delta_{jk}+n_j\delta_{ik}-\frac{2(\lambda_\alpha+\mu_\alpha)}{\lambda_\alpha+2\mu_\alpha}n_in_jn_k\right]n_l\sigma^\beta_{kl} \end{aligned}\right\} \tag{9.1.53}$$

These results hold at any smooth part of a perfectly bonded interface between two arbitrarily shaped isotropic solids.

The above operators $\mathcal{D}_{ijkl}$ and $\mathcal{F}_{ijkl}$ can also be used in (9.1.40) and (9.1.44) to find the fields caused by uniform phase eigenstrains and overall mechanical loads. They are equally useful in evaluation of fields (9.1.50) at the surface of a *loaded cavity*, where $\boldsymbol{\varepsilon}_\beta$ are given by (9.1.49) and $\boldsymbol{\sigma}_\beta$ is a prescribed cavity stress. Hill (1972) derived the complete stress state at the surface of both loaded and traction free cavities. For a traction-free spherical cavity in an isotropic matrix, with Poisson's ratio ν_α, loaded by a uniform stress $\boldsymbol{\sigma}^0$ applied at infinity, his result is

$$\begin{aligned} \sigma^\alpha_{ij} = \frac{15}{7-5\nu_\alpha}\Bigg[&(1-\nu_\alpha)(\delta_{ik}-n_in_k)(\delta_{jl}-n_jn_l) \\ &-\left(\frac{1-5\nu_\alpha}{10}\delta_{kl}+\nu_\alpha n_kn_l\right)(\delta_{ij}-n_in_j)\Bigg]\sigma^0_{kl} \end{aligned} \tag{9.1.54}$$

This agrees with an earlier but different form found by Eshelby (1957).

For a traction-free circular cylindrical cavity, the surface stresses were found in terms of overall uniform fields by Laws (1975). In $(r,\ \varphi,\ z)$ coordinates, where z is aligned with the cylinder axis, his results are

$$\left.\begin{aligned} &\sigma^\alpha_{rr}=\sigma^\alpha_{r\varphi}=\sigma^\alpha_{rz}=0 \quad \sigma^\alpha_{\varphi\varphi}=-\sigma^0_{rr}+3\sigma^0_{\varphi\varphi} \\ &\sigma^\alpha_{zz}=2\nu_\alpha(\sigma^0_{\varphi\varphi}-\sigma^0_{rr})+\sigma^0_{zz} \quad \sigma^\alpha_{\varphi z}=2\,\sigma^0_{\varphi z} \end{aligned}\right\} \tag{9.1.55}$$

The σ^0_{ij} are components of the overall uniform stress applied at infinity.

In the context of steady state conduction, results parallel to the formulation of elasticity were obtained by Chen (1993a). Also, combining elasticity with conduction by constructing appropriate augmented matrices, Chen (1993b) established systematically interface conditions for coupled electro-elastic piezoelectric solids.

9.1.5 *Evaluation of Interface Stresses in a S-Glass/Epoxy Composite*

Significance of the mechanical and thermal contributions to the interface stresses can be illustrated by evaluating their magnitudes in an S-glass/epoxy fiber composite with isotropic phases. Phase moduli are (Herakovich 1998)

$$\left.\begin{aligned} E_f &= 87.0 \text{ GPa}, K_f = 51.8 \text{ GPa}, \ \alpha_f = 1.6 \times 10^{-6}/^{\circ}\text{C} \\ E_m &= 4.1 \text{ GPa}, \ K_m = 4.6 \text{ GPa}, \ \alpha_m = 63 \times 10^{-6}/^{\circ}\text{C} \end{aligned}\right\} \tag{9.1.56}$$

Their contrast appears high, but it is quite moderate when the present $E_f = 87.0$ GPa is compared to the longitudinal Young's moduli $E_L^f = 124$ GPa of Kevlar 49, or to $E_L^f = 235$ GPa of the AS4 fiber. However, the latter fibers are anisotropic, with low transverse moduli of 15 and 7 GPa and longitudinal CTEs of -2.0 and $-0.5 \times 10^{-6}/^{\circ}$C, but with higher transverse CTEs of 60 and $15 \times 10^{-6}/^{\circ}$C, respectively.

The Mori-Tanaka method of Sect. 7.2 will be used in evaluation of the phase and overall field averages. According to (7.2.9) and (7.2.10), the fiber and matrix stress concentration factors $\boldsymbol{B}_r$, $r = f, \ m$, and the overall compliance $\boldsymbol{M}$ follow from

$$\boldsymbol{B}_f = [\boldsymbol{I} + c_m \boldsymbol{Q}(\boldsymbol{M}_f - \boldsymbol{M}_m)]^{-1} \quad \boldsymbol{B}_m = \Big[c_m \boldsymbol{I} + c_f [\boldsymbol{I} + \boldsymbol{Q}(\boldsymbol{M}_f - \boldsymbol{M}_m)]^{-1}\Big]^{-1} \tag{9.1.57}$$

$$\boldsymbol{M} = \boldsymbol{M}_m + c_f (\boldsymbol{M}_f - \boldsymbol{M}_m)[\boldsymbol{I} + c_m \boldsymbol{Q}(\boldsymbol{M}_f - \boldsymbol{M}_m)]^{-1} \tag{9.1.58}$$

where $\boldsymbol{M}_f$, $\boldsymbol{M}_m$ are phase compliance matrices, and $c_f + c_m = 1$ are phase volume fractions. The $\boldsymbol{Q} = \boldsymbol{L}_m(\boldsymbol{I} - \boldsymbol{P}\boldsymbol{L}_m)$ matrix in (4.2.9) is found with reference to (4.6.6), which provides coefficients of the $\boldsymbol{P}$ matrix in terms of the stiffness coefficients L_{ij}^m, and the aspect ratio of fiber crossection, selected here as $\rho = 1$ for a circular fiber. Overall stiffness can be found using (7.2.5), or the expressions (7.2.11, 7.2.12, 7.2.13, 7.2.14) for the overall Hill's moduli, which can be substituted into (2.3.3). However, since (4.6.6) specifies the $x_A^f \equiv x_3$ as the fiber direction in the overall coordinate system, the stiffness matrix (2.3.3), written for $x_A^f \equiv x_1$, needs to be modified by exchange of the $1 \leftrightarrow 3$ rows and columns. The consistency condition $\boldsymbol{M}\boldsymbol{L} = \boldsymbol{I}$ should always be verified.

The stress and strain components in the fiber are nearly uniform at low and moderate fiber densities, and approximated as such at higher densities. They follow from (7.2.7) as $\boldsymbol{\sigma}_f = \boldsymbol{B}_f \boldsymbol{\sigma}^0$ and $\boldsymbol{\varepsilon}_f = \boldsymbol{M}_f \boldsymbol{\sigma}_f$, where $\boldsymbol{\sigma}^0$ is the overall applied stress. In the present illustrative example, we select the overall stress as simple tension, applied to the composite aggregate in the x_1-direction, perpendicular to the fiber axis $x_A^f \equiv x_3$. The overall stress vector is $\boldsymbol{\sigma}^0 = [1, \ 0, \ 0, \ 0, \ 0, \ 0]^{\mathrm{T}}$, hence all resulting fiber and matrix stress components indicate stress concentrations under the single overall unit stress.

Substitution of the fiber fields for the $\beta-$phase components in equations (9.1.7), relabeled using the $3 \leftrightarrow 1$ exchange, provide the three stresses in the matrix phase, at the interface with the fiber. The contact point has the normal $\boldsymbol{n} = [1, 0, 0]^{\mathrm{T}}$ aligned with the overall loading direction, instead of the original interface normal $\xi_3 \perp \Delta S$, or $\boldsymbol{n} = [0, \ 0, \ 1]^{\mathrm{T}}$ in (9.1.7).

Table 9.1 Matrix interface and fiber stresses caused by transverse overall stress $\sigma^0_{11} = 1$ in a S-glass/epoxy composite

c_f	$\sigma^{mi}_{11} = \sigma^{f}_{11}$	σ^{mi}_{22}	$\sigma^{mi}_{kk}/3$	σ^{f}_{22}	σ^{f}_{33}
0.01	2.052	0.9482	1.271	−1.640	−6.078
0.1	1.732	0.8276	1.140	−1.234	−2.303
0.3	1.324	0.6489	0.8918	−0.7405	−0.8545
0.5	1.125	0.5622	0.7643	−0.4576	−0.4387
0.7	1.028	0.5228	0.7017	−0.2557	−0.2219
0.9	0.9952	0.5153	0.6823	−0.08426	−0.06863

Table 9.1 shows numerical values of the normal and tangential matrix interface (mi) and fiber stress components caused at the contact point by the applied unit mechanical load. The volume fractions include the very low $c_f = 0.01$, relevant in measurement of interface strength in pull-out and fragmentation tests on single fiber specimens

The continuous normal stress $\sigma^{mi}_{11} = \sigma^{f}_{11}$, which promotes interface decohesion, is elevated at low fiber volume fractions, but close to the applied overall stress $\sigma^0_{11} = 1$ at typical $c_f = 0.5 - 0.7$ concentrations found in fibrous plies.

The hoop stress σ^{mi}_{22}, which may support radial cracks, is also low. As expected under overall transverse tension, the fiber supports high axial compression stress, which is further elevated in systems reinforced with high modulus fibers. Actual stress magnitudes applied in service are limited by the transverse strength $\sigma^0_{ult} \doteq 50$ MPa of typical S-glass/epoxy plies. At that point, localized interface separation may lead to ply failure.

Thermal stresses and deformations caused by cooling from matrix curing temperatures and by exposure in service can evaluated using (8.3.7) and (8.3.10) or (8.3.11). To that end, the matrix and fiber thermal strain vectors $\boldsymbol{m}_r$ are assembled, using the CTEs from (9.1.56) in the isotropic form of the vectors in Table 8.1. The mechanical stress concentration factors and phase and overall stiffness needed in (8.3.7) are already available from the earlier calculations. Of course, under a uniform change of temperature, the fiber stress and strain are both uniform and complying with the constitutive relation (8.1.1). Therefore, thermally induced radial, hoop and axial stresses in the matrix layer next to the fiber interface are also uniform along a circular fiber circumference.

Table 9.2 shows the fiber stress and strain components caused at the above contact point by $\Delta\theta = +1°\text{C}$, together with the linear overall coefficients of thermal expansion. Overall transverse isotropy of the composite promotes rapid reduction of the longitudinal or axial coefficient α_A with increasing fiber volume fraction. Similar, but much weaker effect is recorded by the values of the transverse overall coefficient α_T, which is actually higher than that of the matrix ($\alpha_m = 63 \times 10^{-6}/°\text{C}$) even at $c_f = 0.3$, due to the constraint imposed by the fiber on longitudinal expansion.

Table 9.2 Fiber thermal stress (kPa/°C) and strain (10^{-6}/°C) and overall CTEs in a S-glass/epoxy composite; $\Delta\theta = +1°\text{C}$ $\boldsymbol{n} = [1, 0, 0]^{\text{T}}$

c_f	$\sigma_{11}^f = \sigma_{11}^{mi}$	σ_{33}^f	$\varepsilon_{11}^f = \varepsilon_{22}^f$	α_A	α_T
0.01	−410.8	4199	−12.70	51.94	66.47
0.1	−412.8	1333	−5.473	19.02	74.08
0.3	−365.2	283.0	−2.389	6.700	68.00
0.5	−296.4	36.42	−1.149	3.517	55.97
0.7	−204.9	−36.63	−0.144	2.215	39.35
0.9	−80.42	−28.16	0.951	1.681	16.45

Table 9.3 Matrix thermal stress (kPa/°C) and strain (10^{-6}/°C) at fiber interface in S-glass/epoxy composite; $\Delta\theta = +1°\text{C}$ $\boldsymbol{n} = [1, 0, 0]^{\text{T}}$

c_f	σ_{22}^{mi}	σ_{33}^{mi}	$\sigma_{kk}^{mi}/3$	ε_{11}^{mi}
0.01	−195.6	−45.1	−201.9	−83.56
0.1	−216.7	−142.3	−257.3	−70.02
0.3	−196.9	−169.2	−243.8	−57.82
0.5	−159.2	−145.0	−200.2	−46.31
0.7	−107.4	−100.2	−137.5	−32.25
0.9	−36.11	−33.89	−50.14	−13.64

Of course, magnitudes of overall CTEs depend on those of the constituents. The $\alpha_f = 1.6 \times 10^{-6}/°\text{C}$ for S-glass in (9.1.56) is on the low side of reported values, which are as high as $\alpha_f = 5.6 \times 10^{-6}/°\text{C}$ (Daniel and Ishai 2006). However, in systems reinforced by high-modulus fibers, such as Kevlar 49 and AS4, which also have small negative longitudinal expansion coefficients, the effect of axial compression on transverse expansion will dominate overall response, while the mismatch in lateral expansion will be reduced.

Thermal stresses in the fiber and at the matrix interface are listed in the first column of Table 9.2, where $\sigma_{11}^f = \sigma_{11}^{mi}$, and in Table 9.3, which includes the remaining matrix interface stresses at the contact point and the discontinuous strain component ε_{11}^{mi}. The computed values indicate that temperature changes may generate significant stress magnitudes. In particular, cooling from typical curing temperatures of 120–175°C to room temperature of 20°C causes interface tension stress $\sigma_{11}^f = \sigma_{11}^{mi} = 29.64 - 37.05$ MPa at $c_f = 0.5$. The matrix hoop stress at the interface is 15.9–19.8 MPa, and the isotropic tension stress there is 20–25 MPa. Those values are well below the nominal epoxy matrix strength of 70–90 MPa, but they may substantially reduce the strength reserve available to support mechanical loads. The above temperature intervals are magnified in aerospace structural composites exposed to low temperatures.

In service, the thermal tension stress may be superimposed with local interface tension caused by overall transverse mechanical stress. Under $\sigma_{ult}^0 \doteq 50$ MPa, the interface stress at $c_f = 0.5$ is $\sigma_{11}^f = \sigma_{11}^{mi} = 1.125 \times 50 = 56.25$ MPa, Table 9.1.

After superposition with the above interfacial thermal stresses of 29.64–37.05 MPa, the combined mechanical and thermal stresses may exceed strength of the interface.

At allowed mechanical load levels, well below σ^0_{ult}, the thermal contribution may dominate interface stress magnitudes. Part of the thermal stress may be relieved by viscous deformation under slow cooling rate from curing temperature. In any case, interface and phase stresses may be very different but still of concern in other composite systems, hence their magnitudes should be examined in each application.

The fiber volume fraction may fluctuate in actual composite systems, where fiber and matrix rich regions often coexist in individual plies. However, the overall stiffness, compliance and the thermal strain and stress vectors depend on the average volume fractions, not on their local fluctuations. Since each fiber is embedded in a certain sense in an effective medium that has the said overall properties, changes of the interface stresses with local density changes should be rather subdued, limited to nearest neighbor interactions.

9.2 Imperfectly Bonded Inhomogeneities and Cavities

Under increasing overall loads and/or phase eigenstrains, an inhomogeneity may experience gradual or complete separation from its neighbors or from the surrounding matrix. This may involve extension of a sharp crack, or a gradual decohesion of bonds between the two surfaces, still connected by certain ligaments that transmit tractions dependent on the magnitude and direction of displacement differences or jumps between pairs of originally bonded points on the two sides of the interface. The latter contribute to overall deformation of a progressively damaged aggregate. Interface tractions remain continuous, but they undergo changes that are reflected in the overall stress supported by the aggregate at a given overall strain; Sect. 9.2.2.

Several imperfect interface models have been proposed to relate local tractions to the displacement jumps along the interface or a thin interphase layer. The simple spring-layer model postulates that interface tractions increase in proportion to the magnitude of the displacement jumps (Hashin 1990, 1991), and an improved version allows for direct contact under compression and prevents interpenetration (Achenbach and Zhu 1989). Modeling of imperfect interfaces by thin elastic interphases was described by Hashin (2002). Several other interface conditions were proposed and analyzed in the technical literature, for example, by Jasiuk et al. (1993), Jasiuk and Kouider (1993) and Qu (1993). More advanced models of the interfacial traction-displacement relations have been inspired by interatomic potentials; they allow for an initial increase of the interfacial tractions up to a certain maximum, followed by gradual softening until complete separation. Two such models appear in Sect. 9.2.2. Overall response of an aggregate damaged by interfacial decohesion is described in Sect. 9.2.3.

9.2.1 Interface Tractions and Displacements

Suppose that a prescribed program of both mechanical loads and phase transformations is applied to the total volume V of a heterogeneous aggregate, such that an inhomogeneity r of stiffness $\boldsymbol{L}_r$ undergoes gradual decohesion from the surrounding 'matrix' $\boldsymbol{L}_1$. Small displacements are assumed, hence the volumes of the inhomogeneity and the surrounding cavity are approximately equal, $V_r \doteq V_{rc}$, but each may accommodate a different average strain. The surface of the inhomogeneity and its area are denoted by ∂V_r and those of the cavity wall by ∂V_{rc}. Relative stretching is neglected, hence the surface areas $\partial V_r \doteq \partial V_{rc}$.

Interface displacement jumps are differences in displacements of each pair of points that were originally in contact.

$$[u_i] = u_i^{rc} - u_i^{rd} \tag{9.2.1}$$

where u_i^{rc}, u_i^{rd} are displacements of the cavity wall and of the debonded inhomogeneity surface, respectively, constrained such that interpenetration is prohibited. Average strain increment (3.4.5) caused by the displacement jumps (9.2.1) inside the cavity volume V_{rc} is equal to the difference between the total strain averages in the cavity and partially debonded inhomogeneity.

$$\Delta\bar{\varepsilon}_{ij}^{rd} = (\bar{\varepsilon}_{ij}^{rc} - \bar{\varepsilon}_{ij}^{rd}) = \frac{1}{2V}\int\limits_{\partial V_{rc}} \left\{[u_i]n_j + [u_j]n_i\right\} \mathrm{d}S \tag{9.2.2}$$

Where n_j denotes a unit normal to the cavity wall, pointing into the matrix $\boldsymbol{L}_1$.

Traction continuity across $\partial V_r \doteq \partial V_{rc}$ is preserved, hence average stresses in both inhomogeneity and cavity are equal and follow from (3.4.2), applied to interface tractions $t_i^d(\boldsymbol{\xi})$, $\boldsymbol{\xi} \in \partial V_{rc}$, taken as forces per unit reference area. They are also connected to the cavity average elastic strain $(\bar{\varepsilon}_{kl}^{rd} - \mu_{kl}^r)$ in the inhomogeneity, where μ_{ij}^r is a uniform, physically motivated local eigenstrain that is a part of the applied loads.

$$\bar{\sigma}_{ij}^{rd} = \bar{\sigma}_{ij}^{rc} = \frac{1}{2V}\int\limits_{\partial V_{rc}} (t_i^d \xi_j + t_j^d \xi_i)\mathrm{d}S = L_{ijkl}^r(\bar{\varepsilon}_{kl}^{rd} - \mu_{kl}^r) \tag{9.2.3}$$

Total strain average in the partially debonded inhomogeneity is $\bar{\varepsilon}_{ij}^{rd} = M_{ijkl}^r \bar{\sigma}_{kl}^{rd} + \mu_{ij}^r$.

Evaluation of the average strain $\bar{\varepsilon}_{ij}^{rc}$ of the loaded cavity generally follows from (9.2.2) applied to the displacements of the cavity wall. The contribution of the displacement jumps to the average strain in the cavity volume can then be found in terms of surface integrals of both tractions and displacements on the cavity wall.

$$\Delta\bar{\varepsilon}_{ij}^{rd} = (\bar{\varepsilon}_{ij}^{rc} - \bar{\varepsilon}_{ij}^{rd}) = \frac{1}{2V}\int\limits_{\partial V_{rc}} \Big[(u_i^{rc} n_j + u_j^{rc} n_i) - M_{ijkl}^{r}(t_k^d \xi_l + t_l^d \xi_k)\Big] \mathrm{d}S - \mu_{ij}^{r} \tag{9.2.4}$$

However, for cavities of ellipsoidal shape, one can appeal to

$$\left.\begin{aligned} \bar{\boldsymbol{\varepsilon}}_r^c &= (\boldsymbol{I} - \boldsymbol{S})^{-1}\left(\boldsymbol{\varepsilon}_\Omega^0 - \boldsymbol{S}\boldsymbol{\mu}_0\right) - \boldsymbol{M}^* \bar{\boldsymbol{\sigma}}_r^c \\ &= (\boldsymbol{I} - \boldsymbol{S})^{-1}\left[\boldsymbol{\varepsilon}_\Omega^0 - \boldsymbol{S}\left(\boldsymbol{\mu}_0 + \boldsymbol{M}_0 \bar{\boldsymbol{\sigma}}_r^c\right)\right] \end{aligned}\right\} \qquad [4.3.27]$$

where $S = \boldsymbol{P}\boldsymbol{L}_0$ is the Eshelby tensor determined by cavity shape, with $\boldsymbol{P}$ taken from Sect. 4.6, and $\boldsymbol{L}_0$ selected as an effective stiffness of the medium surrounding the cavity. For example, when the aggregate is modeled by the Mori-Tanaka method of Sect. 7.2, one selects $\boldsymbol{L}_0 = \boldsymbol{L}_1, \boldsymbol{M}_0 = \boldsymbol{M}_1$, the stiffness and compliance of the matrix. Also, $(\boldsymbol{\varepsilon}_\Omega^0 - \boldsymbol{S}\boldsymbol{\mu}_0) = (\boldsymbol{\varepsilon}_1 - \boldsymbol{S}\boldsymbol{\mu}_1)$. Similar selections can be made in the context of the self-consistent and other methods. The modified form of (4.3.27) connects $\bar{\boldsymbol{\sigma}}_r^c$ or $\bar{\sigma}_{ij}^{rd} = \bar{\sigma}_{ij}^{rc}$ to $\bar{\boldsymbol{\varepsilon}}_r^c$ or $\bar{\varepsilon}_{ij}^{rc}$, which yields $\bar{\varepsilon}_{ij}^{rd} = M_{ijkl}^{r}\bar{\sigma}_{kl}^{rd} + \mu_{ij}^{r}$. Then, evaluation of either displacements or tractions on each cavity wall provides the magnitude of the average displacement jump at $V_r \doteq V_{rc}$.

9.2.2 *Needleman's Imperfect Interface Models*

Specific descriptions of traction-displacement relations along an imperfect bi-material interface, e.g., between an inhomogeneity and surrounding matrix, can be derived from atomistic calculations (Rose et al. 1981; Ferrante et al. 1982), reconstructed at the continuum scale by one of two cohesive zone models by Needleman (1987, 1990), as described next.

By being independent of the constitutive relations of the originally bonded materials, such relations introduce additional material parameters. To reduce their number, the cohesive zone models assume that the tractions may not exceed a certain maximum $\sigma_{\max}$ in normal separation at any point along the interface, and that the total work of separation $\mathcal{W}_{\max}^s$ per unit interface area is path and model independent. This admits existence of a potential, chosen either as a power-law or exponential function of normal and shear displacement differences between each pair of points in contact prior to separation. Dimensional considerations imply existence of a characteristic length $\delta \approx \mathcal{W}_{\max}^s/\sigma_{\max}$, which is related to maximum displacement jump $[u]_{\max}$ at separation. Actual values of δ are provided below.

For brevity, the components of the displacement difference in (9.2.1) are described by dimensionless variables $\upsilon_i = [u_i]/\delta,\ i = n,\ t,\ b$, in local coordinates $\xi_i = (\xi_n,\ \xi_t,\ \xi_b)$ at any point of the interface. The ξ_n points from the inhomogeneity as normal to the interface, and $\xi_t,\ \xi_b$ are in the tangential plane. A proportionality

factor α, the ratio of shear to normal stiffness of the interface is also introduced. The *power-law potential* is selected as

$$\left.\begin{aligned}\mathcal{W}([u_i]) &= -\int_0^{[u]*} t_i \,\mathrm{d}u_i = -\int_{\tau_0}^{\tau*} t_i^d\,[u_i]\,\mathrm{d}\tau \\ &= \frac{27}{8}\sigma_{\max}\delta\left[\upsilon_n^2\left(1-\frac{4}{3}\upsilon_n+\frac{1}{2}\upsilon_n^2\right)+\alpha\left(\upsilon_t^2+\upsilon_b^2\right)(1-\upsilon_n)^2\right]\end{aligned}\right\} \tag{9.2.5}$$

Interface tractions are obtained as $t_i = -\partial\mathcal{W}/\partial[u_i]$, for $[u_n] \le [u_n^*] \equiv \delta$, where $[u_n^*]$ is the maximum displacement difference in normal separation.

$$\left.\begin{aligned} t_n &= -\frac{27}{4}\sigma_{\max}\left[\upsilon_n(1-\upsilon_n)^2-\alpha\left(\upsilon_t^2+\upsilon_b^2\right)(1-\upsilon_n)\right] \\ t_t &= -\frac{27}{4}\sigma_{\max}\left[\alpha\upsilon_t\,(1-\upsilon_n)\right] \quad t_b = -\frac{27}{4}\sigma_{\max}\left[\alpha\upsilon_b\,(1-\upsilon_n)\right]\end{aligned}\right\} \tag{9.2.6}$$

Tractions $t_i \equiv 0$ for $[u_n] > \delta$. Work of separation is evaluated as $\mathcal{W}_{\max}^s = (9/16)\sigma_{\max}\delta$, and by assumption, it is independent if the separation path.

The *exponential potential* is selected in the form

$$\mathcal{W}([u_n],[u_t],[u_b]) = \frac{9}{16}\sigma_{\max}\delta\left[1-\left(1+z\upsilon_n-\frac{1}{2}\alpha z^2\upsilon_t^2\right)\exp\left(-z\upsilon_n\right)\right] \tag{9.2.7}$$

where $z = 16e/9$, $e = \exp(1)$, and $\mathcal{W}(0,0,0) = 0$, $\mathcal{W} \to \mathcal{W}_{\max}^s$ as $[u_n] \to \infty$. This form yields the same total work of separation $\mathcal{W}_{\max}^s$ as the power-law potential, but it does not predict a finite displacement at complete separation. Interface tractions are again found as derivatives $t_i = -\partial\mathcal{W}/\partial[u_i]$

$$\left.\begin{aligned} t_n &= -\sigma_{\max}e\left(z\upsilon_n-\frac{1}{2}\alpha z^2\upsilon_t^2\right)\exp\left(-z\upsilon_n\right) \\ t_t &= -\sigma_{\max}e\left(\alpha z\upsilon_t\right)\exp\left(-z\upsilon_n\right) \qquad t_b = -\sigma_{\max}e\left(\alpha z\upsilon_b\right)\exp\left(-z\upsilon_n\right)\end{aligned}\right\} \tag{9.2.8}$$

Figure 9.1 shows interface tractions as functions of normalized displacement difference. Following the onset of separation, interface tractions increase with the displacement up to a certain maximum and then decrease to zero value at complete separation. Normal traction maximum $t_n = \sigma_{\max}$ is reached at $u_n = \delta/3$ for the power law form, and at $u_n = 9\delta/(16e) \approx 0.207\delta$ for the exponential form. A finite separation distance, at $[u_n]/\delta = 1$, is predicted by the power law, but both forms predict the work of separation per unit area as $\mathcal{W}_{\max}^s = (9/16)\sigma_{\max}\delta$. In the exponential potential, about 0.95 $\mathcal{W}_{\max}^s$ is reached at $[u_n]/\delta = 1$.

This and similar imperfect interface models are useful in finite element analysis of elastic or inelastic heterogeneous media, both at small and finite strains. They

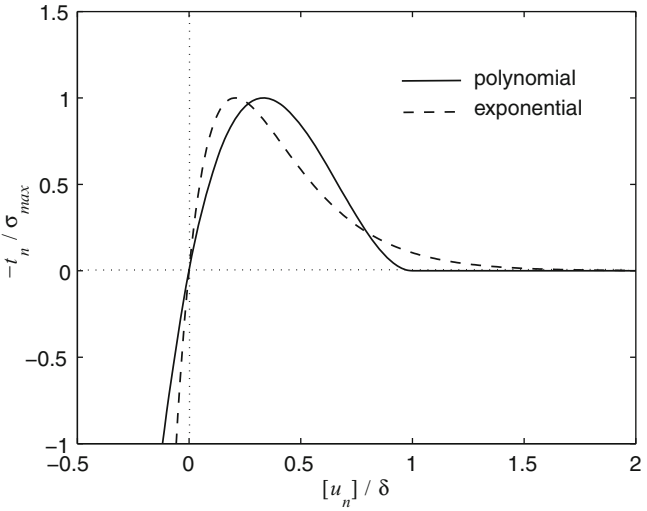

Fig. 9.1 Needleman's (1990) traction-displacement models of interface separation (Reproduced with permission)

are usually implemented in a unit cell model, which may imply synchronized decohesion of groups or of all inhomogeneities in a representative volume. That may not occur in real materials, where interface properties fluctuate both along and among different interfaces

However, the two constitutive relations for an imperfect interface provide a useful tool for studies of void nucleation from precipitates, inclusions and other inhomogeneities in metallic or polymeric matrices characterized by either elastic or inelastic constitutive relations at both small and finite strains. Tvergaard (1991, 2003) used this approach in finite element studies of decohesion of stiff particles from an elastic-plastic metal matrix. They can also be used in simulations of deformation and failure adhesive bonds and interlayers. Information about actual values of the parameters $\sigma_{\max}$ and $\mathcal{W}^s_{\max}$, required in an implementation of the models in specific material systems, are not generally available, and are often introduced as educated estimates. Levy (2001, 2003) had found that the models may predict unstable decohesion of an inhomogeneity, related to different bifurcation mechanisms. That implies the possibility of spontaneous and essentially complete separation of inhomogeneities from the now cavity-filled matrix.

Another class of imperfect interfaces is found in granular materials bonded at certain contact points under overall pressure. Those are also of interest in powder metallurgy where growth of the contact points under elevated temperature and pressure leads to formation of perfectly bonded interfaces between polycrystal grains. Elastic modeling of such cohesive aggregates was described, for example, by Jefferson et al. (2002).

9.2.3 Overall Response

Evaluation of the influence of the local displacement jumps and local stress changes on overall response is difficult because the magnitude and direction of the jump vectors may change under continued loading, and both are hidden from direct observation. As long as the evolution of local displacements and tractions on all cavity walls can be predicted by selected models, an incremental analysis can be formulated to compute current overall strain or stress, along a loading path prescribed by tractions or displacements on the surface of the aggregate. Solutions of this problem have been examined in numerous investigations. Among the first influential papers on the subject are those by Horii and Nemat-Nasser (1983) and Benveniste (1985). The approach followed by these and many other authors attempts to find an instantaneous effective overall stiffness $\boldsymbol{L}_d$ of the damaged aggregate, which exhibits load or damage induced anisotropy. That is well illustrated by the energy approach to evaluation of overall stiffness in *op. cit.*, where the total strain energy of an aggregate volume V, subjected to a prescribed overall strain $\boldsymbol{\varepsilon}^0$ follows from the results of Sect. 5.1.1, as

$$\mathcal{W} = \frac{1}{2}\left(\boldsymbol{\varepsilon}^0\right)^{\mathrm{T}} \boldsymbol{L}_d \boldsymbol{\varepsilon}^0 V = \frac{1}{2}\left(\boldsymbol{\varepsilon}^0\right)^{\mathrm{T}} \boldsymbol{L}\boldsymbol{\varepsilon}^0 (V - V_C) + \frac{1}{2}\int_{S_C} \left(t_i u_i^0 - t_i^0 u_i\right) \mathrm{d}S \qquad (9.2.9)$$

The total aggregate volume V is divided into the volume V_C of all cavities filled by the partially or fully debonded inhomogeneities, and the part $V - V_C$ of the homogenized, undamaged aggregate, which retains its original stiffness $\boldsymbol{L}$. The last integral is the Eshelby formula (5.1.8) for interaction energy between the homogenized aggregate and the filled cavities. The t_i and u_i are the actual tractions and displacements at individual points of total surface S_C which includes all surfaces of cavities that contain the imperfectly bonded inhomogeneities, while the t_i^0, u_i^0 are evaluated along the same surface S_C, drawn in a homogeneous medium $\boldsymbol{L}$. All terms in the surface integral depend upon and change along the applied loading path. An equation similar to (9.2.9) can be written for the total potential energy and overall compliance $\boldsymbol{M}_d$ of the damaged aggregate, following the derivations in Sect. 5.1.2. In any case, evaluation of the overall instantaneous stiffness along the loading path requires possibly laborious monitoring of the evolution of tractions and displacements t_i and u_i on cavity walls S_C, and of their counterparts on S_C drawn in a homogeneous medium $\boldsymbol{L}$, subjected to the current magnitude of overall strain.

In both the direct and energy approaches to evaluation of overall stiffness, the opening, closing and sliding of the imperfect interfaces under variable overall loads may imperil the physically expected consistency $\boldsymbol{M}_d = \boldsymbol{L}_d^{-1}$ of the overall properties. Therefore, it is often preferable to estimate overall response of damaged aggregates by simulating the effect of displacement jumps by application of *damage-equivalent eigenstrains* $\boldsymbol{\mu}_r^{dq}$ to the fully bonded aggregate, as outlined for dilute approximation of overall properties in Sect. 4.3.4, and for other heterogeneous aggregates by Dvorak and Zhang (2001).

In this approach, a uniform eigenstrain $\boldsymbol{\mu}_r^{dq} = \Delta\bar{\varepsilon}_{ij}^{rd}$ (9.2.2), (9.2.4) is applied to those inhomogeneities in a perfectly bonded aggregate which undergo partial or complete decohesion in the damaged aggregate. The $\boldsymbol{\mu}_r^{dq}$ is equal to the average strain generated by the displacement jump along each partially debonded interface, and $\boldsymbol{\mu}_r$ is a physically induced eigenstrain in the inhomogeneity. Addition of this eigenstrain to the load-induced strain in a bonded inhomogeneity generates there the strain average $\bar{\boldsymbol{\varepsilon}}_r^c$ of the surrounding cavity.

$$\bar{\boldsymbol{\varepsilon}}_r = \bar{\boldsymbol{\varepsilon}}_r^c = \boldsymbol{M}_r\bar{\boldsymbol{\sigma}}_r^c + \boldsymbol{\mu}_r + \boldsymbol{\mu}_r^{dq} \tag{9.2.10}$$

Evaluation of the damage-equivalent eigenstrain requires computation of the $\bar{\boldsymbol{\varepsilon}}_r^c$ and $\bar{\boldsymbol{\sigma}}_r^c$ or of $\boldsymbol{\varepsilon}_r^d = \boldsymbol{M}_r\boldsymbol{\sigma}_r^c$ during evolution of the damage. That should be simpler than finding the interaction energy integral in (9.2.9). Moreover, analysis of ellipsoidal inhomogeneities can take advantage of (4.3.27), which connects the stress and stain averages.

Introduction of the damage-equivalent eigenstrains does not change the original overall material symmetry or stiffness of the fully bonded aggregate. Instead, overall response is evaluated using the expressions (8.2.2) or (8.2.3). Under applied overall stress $\boldsymbol{\sigma}^0$ and uniform phase eigenstrains $\boldsymbol{\mu}_r + \boldsymbol{\mu}_r^{dq}$, the overall strain follows as

$$\bar{\boldsymbol{\varepsilon}} = \boldsymbol{M}\left(\boldsymbol{\sigma}^0 - \bar{\boldsymbol{\lambda}}\right) = \boldsymbol{M}\boldsymbol{\sigma}^0 + \bar{\boldsymbol{\mu}} = \sum_{r=1}^{n} c_r\left[\boldsymbol{M}_r\boldsymbol{B}_r\boldsymbol{\sigma}^0 + \boldsymbol{B}_r^{\mathrm{T}}\left(\boldsymbol{\mu}_r^{dq} + \boldsymbol{\mu}_r\right)\right] \tag{9.2.11}$$

Under uniform overall strain $\boldsymbol{\varepsilon}^0$ and $\boldsymbol{\lambda}_r + \boldsymbol{\lambda}_r^{dq} = -\boldsymbol{L}_r(\boldsymbol{\mu}_r + \boldsymbol{\mu}_r^{dq})$, the overall stress is

$$\bar{\boldsymbol{\sigma}} = \boldsymbol{L}\left(\boldsymbol{\varepsilon}^0 - \bar{\boldsymbol{\mu}}\right) = \boldsymbol{L}\boldsymbol{\varepsilon}^0 + \bar{\boldsymbol{\lambda}} = \sum_{r=1}^{n} c_r\left[\boldsymbol{L}_r\boldsymbol{A}_r\boldsymbol{\varepsilon}^0 + \boldsymbol{A}_r^{\mathrm{T}}\left(\boldsymbol{\lambda}_r + \boldsymbol{\lambda}_r^{dq}\right)\right] \tag{9.2.12}$$

The concentration factors $\boldsymbol{A}_r$, $\boldsymbol{B}_r$ are evaluated in the undamaged aggregate. The overall eigenstrain $\bar{\boldsymbol{\mu}}$ can be decomposed into the physically motivated contribution due to $\boldsymbol{\mu}_r$ and the damage-induced addition to the overall strain.

The effect of damage on stress and strain averages caused in the phase r by damage and physically motivated eigenstrains in inhomogeneities of phase s, is then found from (8.2.6) and (8.2.7)

$$\boldsymbol{\varepsilon}_r = \boldsymbol{A}_r\boldsymbol{\varepsilon}^0 + \sum_{s=1}^{n}\boldsymbol{D}_{rs}\left(\boldsymbol{\mu}_s + \boldsymbol{\mu}_s^{dq}\right) \quad \boldsymbol{\sigma}_r = \boldsymbol{L}_r\left(\boldsymbol{\varepsilon}_r - \boldsymbol{\mu}_r - \boldsymbol{\mu}_r^{dq}\right) \tag{9.2.13}$$

or

$$\boldsymbol{\sigma}_r = \boldsymbol{B}_r\boldsymbol{\sigma}^0 + \sum_{s=1}^{n}\boldsymbol{F}_{rs}\left(\boldsymbol{\lambda}_s + \boldsymbol{\lambda}_s^{dq}\right) \quad \boldsymbol{\varepsilon}_r = \boldsymbol{M}_r\left(\boldsymbol{\sigma}_r - \boldsymbol{\lambda}_r - \boldsymbol{\lambda}_r^{dq}\right) \tag{9.2.14}$$

Complete interface separation is represented by the value of $\boldsymbol{\mu}_r^{dq}$ which makes $\boldsymbol{\sigma}_r \to 0$.

The damage-equivalent eigenstrain approach to modeling of overall response of composites undergoing interface decohesion relies on standard results derived for phase transformation problems in Chap. 8. The $\boldsymbol{\mu}_r^{dq} = \Delta\bar{\varepsilon}_{ij}^{rd}$ in (9.2.4) depends only on surface integrals of tractions and displacements on the cavity wall, which follow from selected decohesion rules implemented in unit cell models subjected to a prescribed overall loading path.

Another approach to modeling of damage by a distribution of eigenstrains was described by Hatami-Marbini and Picu (2009), for a random location of defects in a regular fiber network.

9.3 Interphases

This designation refers to a wide range of contact configurations between two solids, which are not perfect bonds or well-defined imperfect bonds. In general, interphases are either inserted as coatings or interlayers of one or more distinct phases, or generated by physical and/or chemical interactions between the two surfaces in contact. In both cases, material composition and properties are affected within some distance from the ideal interface. As long as this distance is small relative to the size or diameter of a typical phase or constituent, it is often possible to reproduce the interface properties by prescribing certain jump conditions at a thin interface. On the other hand, when the affected distance is comparable in size to that of the constituents, typically encountered at the nanoscale, it is necessary to consider in detail the mutual interactions and their effect on overall properties of the mixture. Here we describe some typical models of interphases at both ratios of their thickness to particle or fiber size.

9.3.1 Thin Interphases with Assigned Properties

Analysis of a contact configuration between two surfaces, joined by an interlayer which is of very thin relative to the size of the joined parts, is often simplified by expressing its effect on the adjoining constituents by appropriate interface conditions. That enables solutions for strain, stress, temperature and other fields inside the joined phases, without the need to solve inside the interlayer. A comprehensive study of such conditions for elastic contact in two and three dimensions was conducted by Benvensite and Miloh (2001) and Benveniste and Berdichevsky (2010).

In two dimensions, a thin curved isotropic layer of constant radial thickness is placed between two elastic solids under plane strain conditions. Properties of this layer are allowed to change in the tangential direction, and are classified as soft or

stiff, depending on the magnitude of Lamé surface moduli (λ_s, μ_s). For example, when in-plane orthogonal coordinates in a surface are denoted by α, β the stress and strain tensor components in a thin interphase are connected by Hooke's law

$$\left.\begin{aligned}\sigma_{\alpha\alpha} &= (\lambda_s + 2\mu_s)\varepsilon_{\alpha\alpha} + \lambda_s\varepsilon_{\beta\beta} \\ \sigma_{\beta\beta} &= (\lambda_s + 2\mu_s)\varepsilon_{\beta\beta} + \lambda_s\varepsilon_{\alpha\alpha} \\ \sigma_{\alpha\beta} &= 2\mu_s\varepsilon_{\alpha\beta}\end{aligned}\right\} \tag{9.3.1}$$

The surface moduli λ_s, μ_s have the dimensions of N/m, different from the standard Lame constants (N/m^2). Their magnitudes can be used to classify several distinct interfaces at the microscale. For example, Benveniste and Miloh (2001) identified seven types of interfaces, two of the 'soft' type which preserve only traction continuity, and 'stiffer' interfaces which allow traction discontinuity when represented by an extensible or inextensible membrane, inextensible shell, or rigid contact. The latter are useful in certain elasticity and conductivity problems. A perfectly bonded interface of Sect. 9.1 separates the two types.

The membrane-type interface with assigned surface moduli has found applications in continuum modeling of nanocomposites, where it supports a surface stress caused by interaction of the joined surfaces. The concept of surface stress dates back to two centuries ago, when it was introduced by the Young-Laplace equation in fluids (Young 1805; Laplace 1806). This equation states that the hydrostatic pressure across a spherical surface is proportional to the surface tension and the mean curvature. Surface tension in fluids is defined as a force per unit length along the perimeter of the interface. The concept of surface stress in solids, first introduced by Gibbs (1928), is defined through the change in excess free energy of deformation of the interface at constant referential area. It is associated with the differences in configuration of atoms at the surface and in the bulk. In contrast to fluids, surface stress in solids is generally non-hydrostatic and may depend on the crystallographic directions of the solids joined at the interface.

The surface stress in mechanics correlates with the electron distribution in quantum mechanics. Electrons redistribute on surfaces, leading to bond saturation and thereby elastic stiffening Zhou and Huang (2004). For some solids particularly covalent solids, surface reconstruction takes places, accompanying the electron redistribution Shim et al. (2005). The surface stress or electron redistribution on surfaces also trigger non-linear elastic deformation under the surface Liang et al. (2005). In ceramic or metal systems with large specific surface at the nanometer scale, the interphases at grain boundaries are usually amorphous, containing uncoordinated atoms. Their thickness is equal to two or three lattice sizes from both faces, or approximately 1.5–2 nm, and it may increase with temperature. Material symmetry and other properties of both free surfaces and interphases have been estimated by several atomistic and continuum simulations (Wolf 1991; Shenoy and Freund 2002; Freund and Suresh 2003; Sun and Zhang 2003; Diao et al. 2004; Park et al. 2006). It remains an area of active research, outside the present scope.

Theoretical framework for analysis of interface stresses between two different solids was established by Gurtin and Murdoch (1975) within the classical theory of membranes (see also Gurtin et al. 1998; Povstenko 1993; Landau and Lifshitz 1987; Benveniste 2006). More recently, the subject has attracted attention of an interdisciplinary community of materials, physical chemistry, and continuum mechanics researchers (Nix and Gao 1998; Cammarata et al. 2000a; Miller and Shenoy 2000; Spaepen 2000; Duan et al. 2005a).

Applications have been identified in following of stress evolution during thin film deposition (Freund and Suresh 2003), and also in modeling of overall behavior of nanocomposites. For example, Sharma et al. (2003) derived solutions for the elastic state of transformed spherical inhomogeneities with surface effects using a variational approach. Yang (2004) found effective bulk and shear moduli of composites containing spherical nanosized cavities at dilute concentrations, in which the surface behavior is modeled by a constant residual tension. Sharma and Ganti (2004) constructed closed-form expressions for the Eshelby's tensor for spherical and cylindrical inclusions. Duan et al. (2005a, b) derived the interior and exterior field solutions for a spherical inhomogeneity with an interface stress and eigenstress effect, subjected to a uniform eigenstrain in the inclusion and/or to a remote uniform stress. All such studies indicate that the strain energy of a heterogeneous nano-structure can be dramatically influenced by surface effects, which alter both its local response and macroscopic properties.

Chen et al. (2006, 2007a) derived a generalized Young-Laplace equation for solids, for an in-plane interface stress acting in the tangent plane of a curved surface, and for traction vectors on the top and bottom of this surface that are in equilibrium with stresses in the three-dimensional bulk neighborhood. This equation was applied to analysis of overall elastic behavior of solids containing spherical inclusions with interface stress effects, and also to composites with aligned cylindrical inclusions (Chen et al. 2007b). In both applications, effective elastic moduli were derived in closed form, and the transverse shear moduli by the generalized self-consistent method of Sect. 6.5.

In a fiber system with surface effects, the results satisfy universal connections between the overall and local axisymmetric moduli and phase volume fractions of unidirectional two-phase composites, similar to those in Sect. 3.9. One can also find a uniform strain field created by application of a certain combination of external isotropic strain and uniform change in temperature, or by piecewise uniform eigenstrains in the phases. Mechanical unloading to zero overall strain then reveals the existence of exact size-dependent connections that provide the effective thermal expansion coefficient as a function of the phase and overall moduli, in agreement with a modified Levin's formula.

Modeling of an interphase by a thin interface with surface effects allows closed form solutions of surface interactions in particle and fiber nanocomposites. However, evaluation of the surface moduli and of their connection to actual interphase properties is often uncertain. Applications are usually limited to the effect of surface stress in small cavities, where surface effects become significant when

cavity diameter is 5–10 nm. In contrast, as shown below, observed thickness of actual interphases often approaches or exceed this size especially in polymer matrix systems.

9.3.2 Interphase Regimes in Polymer Nanocomposites

In such systems, matrix polymer chains are preferentially aligned in parallel with the surface of a stiff filler, such that they surround each inclusion with a graded and possibly anisotropic interfacial layer (Ozmusul and Picu 2002). Overall elastic moduli of the composite can be derived with regard to the geometry and linearly varying properties of the layer, elastic moduli and volume fraction of the filler, and strength of the filler/matrix bond. Finite element evaluations of effective layer and filler properties can be used to determine a larger equivalent diameter of the filler, to enable application of standard homogenization methods to the converted geometry of the two-phase system having original or bulk phase moduli.

A subsequent study by Picu and Ozmusul (2003) examined in more detail by lattice Monte Carlo simulations the bond–scale and chain-scale structure of linear polymers in the interfacial layer between impenetrable, closely spaced spherical walls. For evaluation of overall elastic moduli, the effective size of the equivalent filler was determined for various types of interactions (entropic, cohesive in the bulk polymer, attraction to filler surface) and chain length, density and wall curvature. Viscoelasticity of such systems was investigated by Sarvestani and Picu (2005), who considered the effect of dynamic mobility of polymer melts and concentrated solutions in nanocomposites with low filler volume fraction. In their model, the strain rate sensitivity was associated with the thermal motion of chains, with entanglement constraints, and with polymer/filler attachment or detachment process. Picu et al. (2004) modeled the effect of confinement by fillers on chain conformations along interfaces by an atomistic model of the polymer material. An extensive overview of these and related results by Dionne et al. (2005, 2006), Ozmusul et al. (2005) and others was presented by Picu (2009).

Another method to quantify the mechanical properties of the polymer interphase layer near surfaces was proposed by Watcharotone et al. (2011). Using a model system to represent the interaction between embedded nanoparticle surfaces and polymer, ultra-thin polymer films supported on substrates were probed by nanoindentation. A coupled finite element analysis removed the effect of the substrate on the force-displacement data to reveal the elastic property changes of the polymer in the 100 nm regime near an attractive interface. Results demonstrated modulus increases by a factor of two due to the combined effect of geometric confinement and chemical interaction.

Different interphase regimes exist in polymer nanocomposites reinforced by carbon nanotubes or graphitic nanofiller, which allow interpenetration of polymer chains. As shown by L. C. Brinson and her co-workers, both elastic moduli and

the glass transition temperature of polymer nanocomposites can change much more than the theoretical prediction of potential property changes due to inclusion of small reinforcement loadings; <1 wt% or less (Ramanathan et al. 2005, 2008). The hypothesis is that there is an extensive regime of altered polymer, the interphase, in the vicinity of the nanoparticles which arises due to a combination of geometric and chemical interactions between the molecular network and the nanoparticle surfaces. For smaller polymer-particle interactions, the interphase can be discrete, leading to a broadening of the relaxation spectra of the material and modest property improvements. However, for appropriately tuned polymer-particle interactions, the interphase can extend for 100's of nanometers from the nanoparticles to form, even at very low loadings of particles, a percolated interphase zone. The ability to tune the surface chemistry and morphology to adjust the interphase extent is supported by studies on ultrathin polymer films on interphase/altered polymer formation, and it may offer significant property improvements for focused applications.

The subject is of course much broader than can be described here. The references cited offer an insight into some current developments in this active research area.

Chapter 10
Symmetric Laminates

Laminated plates and shells are made by laying up and co-curing unidirectionally reinforced fibrous composite plies or laminae, which have different in-plane orientation and are ordered in a certain stacking sequence. Ply thicknesses are material system specific and their final magnitudes may depend on the fabrication procedure. Most polymer matrix composites are made using pre-impregnated or prepreg tapes or sheets, reinforced by tows consisting of many small diameter (<20 μm) fibers, which typically form $\sim$0.127 mm (0.005 in.) thick plies. Metal matrix laminates are often reinforced by monolayers of large diameter (150 μm) filaments, which yield ply thicknesses of $\sim$0.200 mm (0.008 in.). Therefore, many plies are required to build up section thicknesses required in larger structures.

In most applications, all layers are made of the same material and in the same thickness. However, hybrid laminates that contain two or more different material systems, perhaps one with high stiffness and another possessing high elongation and strength are also used. So are laminates reinforced by fabrics of various weaves.

Applied loads may include membrane forces, bending and twisting moments, and through-the-thickness shear forces, as well as thermal and other eigenstrains in individual plies. In analysis of the overall response and interior fields in laminated structures, each ply is regarded as a homogenized anisotropic layer. Both traction and displacement continuity are enforced at all ply interfaces. However, this only assures continuity of the exterior stress and the interior strain components in adjacent anisotropic layers of different orientations, while the remaining stress and strain components may assume different magnitudes. Therefore, complex interior stress and deformation states may exist in multilayer laminates.

Different laminated plate and shell theories have been proposed to predict overall deflections, buckling loads and frequencies. Accuracy of predicted stress and strain distributions in individual plies is often reduced by simplifying assumptions about overall or local deformation. For example, often promoted and used, is the 'classical' laminated plate theory, based on the Kirchhoff hypothesis for homogeneous plates, which stipulates that transverse normals remain straight, inextensible, and perpendicular to the midsurface during deformation that is limited

G.J. Dvorak, *Micromechanics of Composite Materials*, Solid Mechanics and Its Applications 186, DOI 10.1007/978-94-007-4101-0_10,

to small strains. However, as shown early on by Pagano (1969) the classical theory provides erroneous predictions of interior fields even in a simple three-layer cross-ply plate under cylindrical bending. More reliable higher-order theories that rely on fewer restrictions are described, for example, by Lekhnitskii (1968), Ambartsumyan (1970), Librescu (1975), Panc (1975), Whitney (1987), Noor and Burton (1989), Kovarik (1989), Ochoa and Reddy (1992), Reddy (1997), and in numerous technical papers. Vel and Batra (1999, 2000a, 2001a) derived an analytical solution in the form of infinite series for cylindrical bending of elastic laminated plates subjected to different (clamped, simply supported or traction free) boundary conditions at individual edges of each ply. The approach has been extended to hybrid laminates with one or more plies made of a piezoelectric material, and to thermo-mechanical deformation (Vel and Batra 2000b, 2001b, Vel et al. 2004). They reduced the three-dimensional problem to plane strain, and obtained its solution by Eshelby et al. (1953) and Stroh (1958) formalism described, for example, by Ting (1996), Chap. 5.

Here we focus on an important class of laminates that have a plane of symmetry and are loaded by uniformly distributed in-plane forces and by thermal and other eigenstrains that cause only uniform, in-plane overall strains. Symmetric laminates are widely used in composite structures, to support membrane forces in plates or shells. They are also preferred in experimental characterization of laminate moduli, ductility, endurance and strength. Their analysis is not encumbered by the assumptions and restrictions employed by different laminated plate theories, and is closely related to micromechanics. It is both simple and accurate, yielding interior and overall fields in closed form. In the present context, symmetric laminates will be used to illustrate interactions between constituent, ply and laminate response under different loading conditions, and in the presence of thermal and other physically based eigenstrains in the fiber and matrix phases. That enables applications of such laminates in creating dimensionally stable plates and auxetic materials, and in reducing free edge stresses. Moreover, laminates with optimized fiber prestress and laminates damaged by transverse cracking will be described in Sects. 9.9 and 10.10.

10.1 Constitutive Relations of Fibrous Plies

The laminates considered here have a midplane, or plane of symmetry, such that each layer on one side of this plane is paired with an identical layer on the other side. Both layers have the same orientation, elastic moduli, thickness and distance from the midplane, and each is regarded as a homogenized transversely isotropic layer of constant thickness. The derivations that follow apply to a representative element of a laminated plate removed from free edges and supports, where both the plate and each individual ply experience the state of plane stress, generated by uniform overall normal and shear in-plane tractions. Uniform stress or strain normal to the outer plane surfaces can be also applied, together with distributions of uniform thermal strains and other eigenstrains in each symmetric pair of plies. The results can be extended to representative elements of shells with low thickness/radius ratios.

10.1.1 Plane Stress Stiffness and Compliance

Stiffness and compliance matrices of individual ply pairs are derived in a form corresponding to the state of plane stress, where $\sigma_{33} = \sigma_{31} = \sigma_{32} = 0$, and $\varepsilon_{33} = \text{const.}$, $\varepsilon_{31} = \varepsilon_{32} = 0$. *Engineering strains* (1.1.11) *are used in this chapter*. They are denoted here by boldface Roman letters. In particular, in each ply of pair (i), the (6×6) stiffness matrix $\boldsymbol{L}_i$ of the fibrous composite material of the ply is reduced to the (3×3) matrix $\mathbf{L}_i$, and the compliance $\boldsymbol{M}_i$ to $\mathbf{M}_i = \mathbf{L}_i^{-1}$. That is consistent with our adopted notation, but it differs from that accepted in much of the literature on laminates, where $\mathbf{L}_i = \mathbf{Q}_i$ and $\mathbf{M}_i = \mathbf{S}_i$. The indexes (i) and (j) are reserved for ply identification.

The (3×1) plane stress and strain vectors are denoted by $\boldsymbol{\sigma}_i$ and $\boldsymbol{\varepsilon}_i$, and elastic constitutive relations of each ply (i) are written in analogy to (3.4.9) as

$$\boldsymbol{\sigma}_i = \mathbf{L}_i \boldsymbol{\varepsilon}_i \quad \boldsymbol{\varepsilon}_i = \mathbf{M}_i \boldsymbol{\sigma}_i \tag{10.1.1}$$

In component form, similar to (2.3.2)–(2.3.3), this reads as

$$\begin{bmatrix} \sigma_1^{(i)} \\ \sigma_2^{(i)} \\ \sigma_6^{(i)} \end{bmatrix} = \begin{bmatrix} \mathrm{L}_{11}^{(i)} & \mathrm{L}_{12}^{(i)} & 0 \\ \mathrm{L}_{12}^{(i)} & \mathrm{L}_{22}^{(i)} & 0 \\ 0 & 0 & \mathrm{L}_{66}^{(i)} \end{bmatrix} \begin{bmatrix} \varepsilon_1^{(i)} \\ \varepsilon_2^{(i)} \\ \varepsilon_6^{(i)} \end{bmatrix} \quad \begin{bmatrix} \varepsilon_1^{(i)} \\ \varepsilon_2^{(i)} \\ \varepsilon_6^{(i)} \end{bmatrix} = \begin{bmatrix} M_{11}^{(i)} & M_{12}^{(i)} & 0 \\ M_{12}^{(i)} & M_{22}^{(i)} & 0 \\ 0 & 0 & M_{66}^{(i)} \end{bmatrix} \begin{bmatrix} \sigma_1^{(i)} \\ \sigma_2^{(i)} \\ \sigma_6^{(i)} \end{bmatrix} \tag{10.1.2}$$

where $\varepsilon_6^{(i)} = 2\varepsilon_{12}^{(i)}$, and the stiffness coefficients are expressed as functions of overall moduli of the ply material

$$\left.\begin{aligned} \mathrm{L}_{11}^{(i)} &= (E_{11}^{(i)} k^{(i)} + m^{(i)} n^{(i)})/(k^{(i)} + m^{(i)}) = E_{11}^{(i)}/(1 - \nu_{12}^{(i)} \nu_{21}^{(i)}) \\ \mathrm{L}_{12}^{(i)} &= 2l^{(i)} m^{(i)}/(k^{(i)} + m^{(i)}) = \nu_{12}^{(i)} E_{22}^{(i)}/(1 - \nu_{12}^{(i)} \nu_{21}^{(i)}) \\ \mathrm{L}_{22}^{(i)} &= 4k^{(i)} m^{(i)}/(k^{(i)} + m^{(i)}) = E_{22}^{(i)}/(1 - \nu_{12}^{(i)} \nu_{21}^{(i)}) \\ \mathrm{L}_{66}^{(i)} &= p^{(i)} = G_{12}^{(i)} = 1/M_{66}^{(i)} \end{aligned}\right\} \tag{10.1.3}$$

The compliance matrix $\mathbf{M}_i$ is obtained by deleting third to fifth rows and columns from (2.3.2), while the remaining coefficients are preserved.

$$\left.\begin{aligned} M_{11}^{(i)} &= 1/E_{11}^{(i)} = \mathrm{L}_{22}^{(i)}/\Lambda \quad M_{12}^{(i)} = -\nu_{21}^{(i)}/E_{22}^{(i)} = -\nu_{12}^{(i)}/E_{11}^{(i)} = -\mathrm{L}_{12}^{(i)}/\Lambda \\ M_{22}^{(i)} &= 1/E_{22}^{(i)} = \mathrm{L}_{11}^{(i)}/\Lambda \quad M_{66}^{(i)} = 1/G_{12}^{(i)} \quad \Lambda = \mathrm{L}_{11}^{(i)} \mathrm{L}_{22}^{(i)} - (\mathrm{L}_{12}^{(i)})^2 \end{aligned}\right\} \tag{10.1.4}$$

The first three terms in the above stiffness matrix $\mathbf{L}_i$ were derived from (2.3.3) by writing the stress components as

$$\left.\begin{array}{ll} \sigma_1 = n\varepsilon_1 + l(\varepsilon_2 + \varepsilon_3) & \sigma_2 = l\varepsilon_1 + (k+m)\varepsilon_2 + (k-m)\varepsilon_3 \\ \sigma_3 = l\varepsilon_1 + (k-m)\varepsilon_2 + (k+m)\varepsilon_3 = 0 & \sigma_6 = p\varepsilon_6 \end{array}\right\} \tag{10.1.5}$$

then solving for ε_3, and noting that $n = E_{11} + l^2/k$. The remaining terms follow from (2.3.4) and (2.3.5).

Specific magnitudes of the ply moduli can be estimated by one of the methods described in Chaps. 6 and 7, in terms of fiber and matrix moduli and their volume fractions, or obtained from experimental measurements in Table 2.4. Typical values for widely used material systems can be found in several references, such as Daniel and Ishaii (2006) and Herakovich (1998). Actual ply moduli magnitudes depend on those of both phases and their interfaces, and on fabrication and processing conditions. Different magnitudes can be found even in testing of specimens cut from a single large sheet of ply material.

10.1.2 Thermal and Eigenstrain Ply Vectors

Together with mechanical loading, each ply pair may be transformed by a different, physically based eigenstrain. One source is a change in temperature $\Delta\theta = \theta - \theta_0$, from a reference to the current value θ, applied over a certain time period, until it becomes uniform in the entire representative element of the laminate. In-plane response of each ply is described by a thermal strain vector $\mathbf{m}_i$ or a stress vector $\mathbf{l}_i$, which are reduced forms of $\boldsymbol{m}$ and $\boldsymbol{l}$ in (8.3.1). Linear coefficients of thermal expansion of a unidirectional fiber composite have the transversely isotropic form in Table 8.1. The thermal vectors now are

$$\mathbf{m}_i = \{\alpha_A^{(i)}, \alpha_T^{(i)}, 0\}^{\mathrm{T}} = -\mathbf{M}_i\mathbf{l}_i \quad \mathbf{l}_i = \{l_1^{(i)}, l_2^{(i)}, l_6^{(i)}\}^{\mathrm{T}} = -\mathbf{L}_i\mathbf{m}_i \tag{10.1.6}$$

Another source are piecewise uniform eigenstrains in individual ply pairs, applied symmetrically with respect to the midplane. They may represent moisture or temperature gradients that are symmetric about the midplane, or inelastic deformation of certain ply pairs. In each case, they are derived in terms of the local eigenstrains in the fiber and matrix, using the Levin formula (3.8.11), and reduced to the form $\{\mu_{11}^{(i)},\ \mu_{22}^{(i)},\ 2\mu_{12}^{(i)}\}^{\mathrm{T}}$. A $\mu_{33}^{(i)}$ component may also be admitted, as indicated in (10.1.10) below.

A transverse normal compressive stress $-\sigma_{33}$, which is often encountered in clamped joints, is not a part of the stress state applied in (10.1.2). Of course, continuity of normal stress components at the planar interfaces guarantees that each

ply supports the same magnitude of $-\sigma_{33} = -\sigma_{33}^{(i)}$. If free from in-plane constraints and tractions, the stress σ_{33} would deform each ply according to (2.3.2)

$$\varepsilon_{11}^{(i)} = -(\nu_{21}^{(i)}/E_{22}^{(i)})\sigma_{33} \quad \varepsilon_{33}^{(i)} = -(\nu_{32}^{(i)}/E_{22}^{(i)})\sigma_{33} \quad \varepsilon_{33}^{(i)} = (1/E_{22}^{(i)})\sigma_{33} \tag{10.1.7}$$

Since they are not caused by one of the stresses in (10.1.2), these components can be regarded in the present context as stress-free strains, or ply eigenstrain components that simulate in each ply the effect of uniform transverse normal stress applied to the laminate.

Superposition of the last two sources provides the total eigenstrain in symmetric ply pairs

$$\boldsymbol{\mu}_i = \left\{ [\mu_{11}^{(i)} - (\nu_{21}^{(i)}/E_{22}^{(i)})\sigma_{33}],\ [\mu_{22}^{(i)} - (\nu_{32}^{(i)}/E_{22}^{(i)})\sigma_{33}],\ 2\mu_{12}^{(i)} \right\}^{\mathrm{T}} = -\mathbf{M}_i \boldsymbol{\lambda}_i \tag{10.1.8}$$

where the thermal parts of the eigenstrains are $\mu_{11}^{(i)} = \alpha_A^{(i)}\Delta\theta$, $\mu_{22}^{(i)} = \mu_{33}^{(i)} = \alpha_T^{(i)}\Delta\theta$, and $\mu_6 = 2\mu_{12}$ can be added as a part of a physically motivated eigenstrain.

10.1.3 Ply Load Sets

Constitutive relations for in-plane deformation of each ply pair include both mechanical loads, uniform thermal change and distinct eigenstrains in individual ply pairs. These can be arranged in dimensionally consistent load sets $\{\boldsymbol{\sigma}_i,\ \mathbf{l}_i\Delta\theta,\ \boldsymbol{\lambda}_i\}$ or $\{\boldsymbol{\varepsilon}_i,\ \mathbf{m}_i\Delta\theta,\ \boldsymbol{\mu}_i\}$, corresponding to either traction or displacement boundary conditions applied to the plies and laminate. Of course, the thermal and eigenstrain terms are independent of mechanical loads, and are interrelated by (10.1.6) and (10.1.8).

The two load sets are related by

$$\boldsymbol{\varepsilon}_i = \mathbf{M}_i(\boldsymbol{\sigma}_i - \mathbf{l}_i\Delta\theta - \boldsymbol{\lambda}_i) \quad \boldsymbol{\sigma}_i = \mathbf{L}_i(\boldsymbol{\varepsilon}_i - \mathbf{m}_i\Delta\theta - \boldsymbol{\mu}_i) \tag{10.1.9}$$

Each ply also undergoes a through-the-thickness normal strain, caused by the above loads. With reference to (2.3.2), the total out-of-plane normal strain is

$$\varepsilon_{33}^{(i)} = -(\nu_{12}^{(i)}/E_{11}^{(i)})\sigma_{11}^{(i)} - (\nu_{23}^{(i)}/E_{22}^{(i)})\sigma_{22}^{(i)} + (1/E_{22}^{(i)})\sigma_{33} + \alpha_T^{(i)}\Delta\theta + \mu_{33}^{(i)} \tag{10.1.10}$$

Notice that for $E_{11}^{(i)} \gg E_{22}^{(i)}$ and $\nu_{23}^{(i)} > \nu_{12}^{(i)}$, the transverse stress $\sigma_{22}^{(i)}$ has a major influence on the magnitude of $\varepsilon_{33}^{(i)}$. Laminates that exhibit large contrast in ply moduli and may have auxetic properties are described in Sect. 10.7.

10.2 Coordinate Systems and Transformations

Two systems of coordinates are required in laminate analysis. *A local or material system* $(x_1^{(i)},\ x_2^{(i)},\ x_3^{(i)})$ in each lamina or ply (i), utilized in Sect. 10.1, where $x_1^{(i)}$ coincides with the fiber direction and $x_3 \equiv x_3^{(i)}$ with the normal to the plane of a flat lamina, or to a tangential plane. A *global or laminate coordinate system* $(\bar{x}_1,\ \bar{x}_2,\ \bar{x}_3)$, where the $\bar{x}_1\,\bar{x}_2 -$ plane is parallel to but not necessarily aligned with the $x_1^{(i)}x_2^{(i)} -$ plane, and $\bar{x}_3 \parallel x_3$; Fig. 10.1.

The angle θ_i, measured counter-clockwise from the global $\bar{x}_1 -$ direction to the local $x_1^{(i)}-$direction, defines orientation of each ply pair. A shorthand notation is used to describe the *stacking sequence*. Starting typically from the top or outer surface of the plate or shell, each ply (i) is designated, in turn, by its θ_i angle relative to the global $\bar{x}_1 -$ axis. Numerical subscripts at the angle value indicate the number of adjacent plies of a given orientation and the $(.)_S$ subscript indicates presence of a plane of symmetry.

For example, the sequence $(0_2/+45/-45/90)_S$ or $(0_2/\pm 45/90)_S$ describes a symmetric laminate that has $\mathrm{n} = 2$ or two 0−degree plies with $x \equiv x_1^{(i)}$ at each surface, followed toward the interior by one pair of $+45^{\mathrm{o}}$ and one pair of -45^{o} plies, and by a symmetry plane or midplane between a pair 90^{o} plies.

A number of different laminate configurations, both symmetric and asymmetric can be described in this manner. They include cross-ply $(0_{\mathrm{n}}/90_{\mathrm{n}})_S$ or $(+45_{\mathrm{n}}/-45_{\mathrm{n}})_S$, angle-ply $(+\theta_{\mathrm{n}}/-\theta_{\mathrm{n}})_S$, and balanced laminates with equal numbers (n) of $+\theta$ and $-\theta$ plies. Quasi-isotropic laminates have at least three $N = 3$ planes of reflection symmetry separated by equal angles π/N, $N \geq 3$, which guarantee that the overall laminate moduli do not depend on in-plane orientation, c. f., Sect. 2.2.6. For example, a $(0/\pm 60)_S$ with $N = 3$, is quasi-isotropic, and so is a $(0/\pm 45/90)_S$ laminate, $N = 4$.

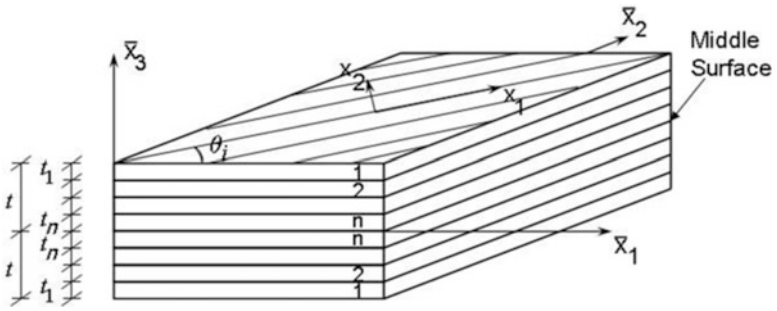

Fig. 10.1 Geometry of a symmetric laminated plate

Counterclockwise rotations by θ_i about the $x_3 \equiv \bar{x}_3$−axis, from the global $(\bar{x}_1,\ \bar{x}_2,\ \bar{x}_3)$ to the local $(x_1^{(i)},\ x_2^{(i)},\ x_3^{(i)})$ coordinates, will be described by two matrices, with coefficients that depend on $m = \cos\theta_i,\ n = \sin\theta_i$.

$$\mathbf{X}_i = \begin{bmatrix} m^2 & n^2 & 2mn \\ n^2 & m^2 & -2mn \\ -mn & mn & (m^2 - n^2) \end{bmatrix} \quad \mathbf{Y}_i = \begin{bmatrix} m^2 & n^2 & -2mn \\ n^2 & m^2 & 2mn \\ mn & -mn & (m^2 - n^2) \end{bmatrix} \tag{10.2.1}$$

Notice that $\mathbf{X}_i = \mathbf{Y}_i^{-1}$ is a reduced form of the (6×6) $\boldsymbol{X}$ matrix in (1.1.32), and that it conforms with the transformation (1.1.33), which applies to both stress and strain tensor coefficients. Recall from Chap. 1 that the transformations can be written as $\sigma'_{ij} = a_{ik}a_{jl}\sigma_{kl}$ or as $\boldsymbol{\sigma'} = \mathbf{a}\,\boldsymbol{\sigma}\,\mathbf{a}^{\mathrm{T}}$, and in the same form for the strain tensor. However, while the contracted stress vector follows from $\boldsymbol{\sigma'} = \mathbf{X}\,\boldsymbol{\sigma}$ as in (1.1.27), the contracted engineering strain vector transforms as $\boldsymbol{\varepsilon}'_{EG} = (\mathbf{X}^{-1})^{\mathrm{T}}\boldsymbol{\varepsilon}_{EG}$, according to (1.1.29).

Strain and stress vectors as well as stiffness and compliance matrices, defined in the global or laminate coordinate system $(\bar{x}_1,\ \bar{x}_2,\ \bar{x}_3)$, are denoted by *top bars, which no longer indicate volume averages*. Ply strains and stresses caused by in-plane mechanical loads applied to the laminate are first evaluated in the global coordinates, where we denote them by $\bar{\boldsymbol{\varepsilon}}_i = \{\bar{\varepsilon}_{11}^{(i)},\ \bar{\varepsilon}_{22}^{(i)},\ \bar{\varepsilon}_{12}^{(i)}\}^{\mathrm{T}}$ and $\bar{\boldsymbol{\sigma}}_i = \{\bar{\sigma}_{11}^{(i)},\ \bar{\sigma}_{22}^{(i)},\ \bar{\sigma}_{12}^{(i)}\}^{\mathrm{T}}$, and then they are transformed to $\boldsymbol{\varepsilon}_i,\ \boldsymbol{\sigma}_i$ in the local system. In contrast, the thermal strain or stress vectors $\mathbf{m}_i = -\mathbf{M}_i\,\mathbf{l}_i$ and the eigenstrains $\boldsymbol{\mu}_i = -\mathbf{M}_i\,\boldsymbol{\lambda}_i$ originate in the local or material system and are then transformed into $\bar{\mathbf{m}}_i = -\bar{\mathbf{M}}_i\bar{\mathbf{l}}_i$ and $\bar{\boldsymbol{\mu}}_i = -\bar{\mathbf{M}}_i\,\bar{\boldsymbol{\lambda}}_i$ in the global system. Rules for stress and engineering strain transformations between the ply and overall coordinate systems are

$$\left.\begin{aligned} &\boldsymbol{\varepsilon}_i = \mathbf{Y}_i^{\mathrm{T}}\bar{\boldsymbol{\varepsilon}}_i \quad \boldsymbol{\sigma}_i = \mathbf{X}_i\bar{\boldsymbol{\sigma}}_i \quad \bar{\mathbf{m}}_i\,\Delta\theta + \bar{\boldsymbol{\mu}}_i = \mathbf{X}_i^{\mathrm{T}}(\mathbf{m}_i\,\Delta\theta + \boldsymbol{\mu}_i) \\ &\bar{\mathbf{l}}_i\,\Delta\theta + \bar{\boldsymbol{\lambda}}_i = \mathbf{Y}_i(\mathbf{l}_i\,\Delta\theta + \boldsymbol{\lambda}_i) \end{aligned}\right\} \tag{10.2.2}$$

Response of a ply to each of the dimensionally consistent applied load sets $\{\bar{\boldsymbol{\sigma}}_i,\ \bar{\mathbf{l}}_i\,\Delta\theta,\ \bar{\boldsymbol{\lambda}}_i\}$ or $\{\bar{\boldsymbol{\varepsilon}}_i,\ \bar{\mathbf{m}}_i\,\Delta\theta,\ \bar{\boldsymbol{\mu}}_i\}$ is now written as in (10.1.9)

$$\bar{\boldsymbol{\varepsilon}}_i = \bar{\mathbf{M}}_i(\bar{\boldsymbol{\sigma}}_i - \bar{\mathbf{l}}_i\,\Delta\theta - \bar{\boldsymbol{\lambda}}_i) \quad \bar{\boldsymbol{\sigma}}_i = \bar{\mathbf{L}}_i(\bar{\boldsymbol{\varepsilon}}_i - \bar{\mathbf{m}}_i\,\Delta\theta - \bar{\boldsymbol{\mu}}_i) \tag{10.2.3}$$

where the stiffness and compliance matrices in the global coordinates follow from (10.2.2) as

$$\bar{\mathbf{L}}_i = \mathbf{Y}_i\mathbf{L}_i\mathbf{Y}_i^{\mathrm{T}} \quad \bar{\mathbf{M}}_i = \mathbf{X}_i^{\mathrm{T}}\mathbf{M}_i\mathbf{X}_i \tag{10.2.4}$$

It is often convenient to have expressions for the coefficients of the ply stiffness and compliance matrices in the global coordinates, written in terms of the local stiffness and compliance coefficients, with $m = \cos\theta_i,\ n = \sin\theta_i$.

$$\left.\begin{aligned}
\bar{\mathrm{L}}_{11} &= \mathrm{L}_{11}m^4 + 2(\mathrm{L}_{12} + 2\mathrm{L}_{66})m^2n^2 + \mathrm{L}_{22}n^4 \\
\bar{\mathrm{L}}_{12} &= (\mathrm{L}_{11} + \mathrm{L}_{22} - 4\mathrm{L}_{66})m^2n^2 + \mathrm{L}_{12}(m^4 + n^4) \\
\bar{\mathrm{L}}_{22} &= \mathrm{L}_{11}n^4 + 2(\mathrm{L}_{12} + 2\mathrm{L}_{66})m^2n^2 + \mathrm{L}_{22}m^4 \\
\bar{\mathrm{L}}_{16} &= (\mathrm{L}_{11} - \mathrm{L}_{12} - 2\mathrm{L}_{66})m^3n + (\mathrm{L}_{12} - \mathrm{L}_{22} + 2\mathrm{L}_{66})mn^3 \\
\bar{\mathrm{L}}_{26} &= (\mathrm{L}_{11} - \mathrm{L}_{12} - 2\mathrm{L}_{66})mn^3 + (\mathrm{L}_{12} - \mathrm{L}_{22} + 2\mathrm{L}_{66})m^3n \\
\bar{\mathrm{L}}_{66} &= (\mathrm{L}_{11} + \mathrm{L}_{22} - 2\mathrm{L}_{12} - 2\mathrm{L}_{66})m^2n^2 + \mathrm{L}_{66}(m^4 + n^4)
\end{aligned}\right\} \tag{10.2.5}$$

and

$$\left.\begin{aligned}
\bar{\mathrm{M}}_{11} &= M_{11}m^4 + (2M_{12} + M_{66})m^2n^2 + M_{22}n^4 \\
\bar{\mathrm{M}}_{12} &= (M_{11} + M_{22} - M_{66})m^2n^2 + M_{12}(m^4 + n^4) \\
\bar{\mathrm{M}}_{22} &= M_{11}n^4 + (2M_{12} + M_{66})m^2n^2 + M_{22}m^4 \\
\bar{\mathrm{M}}_{16} &= (2M_{11} - 2M_{12} - M_{66})m^3n + (2M_{12} - 2M_{22} + M_{66})mn^3 \\
\bar{\mathrm{M}}_{26} &= (2M_{11} - 2M_{12} - M_{66})mn^3 + (2M_{12} - 2M_{22} + M_{66})m^3n \\
\bar{\mathrm{M}}_{66} &= 4(M_{11} - 2M_{12} + M_{22})m^2n^2 + M_{66}(m^2 - n^2)^2
\end{aligned}\right\} \tag{10.2.6}$$

Notice that the same numerical subscripts indicate distinct directions when attached to either global or local stiffness or compliance coefficients. The local coefficients L_{kl} and M_{kl}, in terms of the $(i)-$ply moduli, are given by (10.1.3) and (10.1.4), respectively.

Following the rotation (10.2.4), a ply that is transversely isotropic in the material system may be left with only one plane of symmetry, parallel to the $\bar{x}_1\bar{x}_2-$midplane in the global system. Therefore, it exhibits monoclinic symmetry in the global $(\bar{x}_1,\ \bar{x}_2,\ \bar{x}_3)$ coordinates, which is reflected in the form of $\bar{\mathbf{L}}_i$ and $\bar{\mathbf{M}}_i$ matrices. In contrast to (10.1.2), both matrices now have nonzero coupling terms at $kl = 16,\ 26$. For example, $\bar{\mathrm{L}}_{16}^{(i)}$ and $\bar{\mathrm{L}}_{26}^{(i)}$ generate contributions to in-plane normal stresses $\bar{\sigma}_{11}^{(i)},\ \bar{\sigma}_{22}^{(i)}$ by a shear strain $\bar{\varepsilon}_6^{(i)} = 2\bar{\varepsilon}_{12}^{(i)}$.

10.3 Overall Response and Ply Stresses in Symmetric Laminates

Expressions for the overall properties of laminated plates need to be derived in terms of their counterparts in each ply. Force equilibrium is satisfied if all in-plane forces $\bar{\mathbf{N}}_i$, supported by each symmetric ply pair, have the same resultant $\bar{\mathbf{N}} = \{\bar{N}_1,\ \bar{N}_2,\ \bar{N}_6\}^{\mathrm{T}}$ as in-plane tractions applied to the laminate. Continuity of displacements across the ply interfaces applies to the interior components of the

strain tensor, hence all plies must undergo the same in-plane deformation. Both conditions are satisfied by

$$\bar{\boldsymbol{\varepsilon}} = \bar{\boldsymbol{\varepsilon}}_i \quad \bar{\boldsymbol{\sigma}} = \sum_{i=1}^{n} c_i \bar{\boldsymbol{\sigma}}_i = \sum_{i=1}^{n} c_i \bar{\mathbf{N}}_i / t_i \quad c_i = t_i / t \tag{10.3.1}$$

where $\bar{\boldsymbol{\varepsilon}}$ and $\bar{\boldsymbol{\sigma}}$ denote the overall deformation and stress of the laminate in global coordinates $(\bar{x}_1,\ \bar{x}_2,\ \bar{x}_3)$. Their components are

$$\bar{\boldsymbol{\varepsilon}} = \{\bar{\varepsilon}_1, \bar{\varepsilon}_2, \bar{\varepsilon}_6\}^T \quad \bar{\boldsymbol{\sigma}} = \{\bar{\sigma}_1, \bar{\sigma}_2, \bar{\sigma}_6\}^T = \bar{\mathbf{N}}/(2t) \tag{10.3.2}$$

The $i = 1,\ 2,\ \ldots\ n$ denote the number of symmetric pairs of plies. Each ply in a given pair has a thickness t_i /2, hence the pair volume fraction c_i has the value indicated, and $\Sigma_{i=1}^{n} c_i = 1$; $2t$ is the total thickness of the plate.

The macroscopic or overall constitutive relations of a symmetric laminate have the same form as the ply relations (10.2.3). For the overall load sets $\{\bar{\boldsymbol{\sigma}},\ \bar{\mathbf{l}}\,\Delta\theta,\ \bar{\boldsymbol{\lambda}}\}$ or $\{\bar{\boldsymbol{\varepsilon}},\ \bar{\mathbf{m}}\Delta\theta,\ \bar{\boldsymbol{\mu}}\}$, those are

$$\bar{\boldsymbol{\varepsilon}} = \bar{\mathbf{M}}\,(\bar{\boldsymbol{\sigma}} - \bar{\mathbf{l}}\,\Delta\theta - \bar{\boldsymbol{\lambda}}) \qquad \bar{\boldsymbol{\sigma}} = \bar{\mathbf{L}}(\bar{\boldsymbol{\varepsilon}} - \bar{\mathbf{m}}\Delta\theta - \bar{\boldsymbol{\mu}}) \tag{10.3.3}$$

where $\bar{\mathbf{L}}$ and $\bar{\mathbf{M}} = \bar{\mathbf{L}}^{-1}$ denote the (3×3) laminate plane stress stiffness and compliance matrices, and $\bar{\mathbf{m}} = -\bar{\mathbf{L}}^{-1}\bar{\mathbf{l}} = \{\bar{\alpha}_1,\ \bar{\alpha}_2,\ \bar{\alpha}_6\}^{\mathrm{T}}$ is the laminate thermal strain vector. The $\bar{\alpha}_k$ are in-plane linear coefficients of thermal expansion of a laminate; of course, $\bar{\alpha}_6 = 2\bar{\alpha}_{12} = 0$ in orthotropic or quasi-isotropic laminates. The overall eigenstress $\bar{\boldsymbol{\lambda}} = (\bar{\lambda}_1,\ \bar{\lambda}_2,\ \bar{\lambda}_6)^{\mathrm{T}}$ is related to the overall eigenstrain $\bar{\boldsymbol{\mu}}$ by $\bar{\boldsymbol{\lambda}} = -\bar{\mathbf{L}}\,\bar{\boldsymbol{\mu}}$; it is equal to the overall in-plane stress caused by $\bar{\boldsymbol{\mu}}$ at $\bar{\boldsymbol{\varepsilon}} = 0$.

In-plane stiffness, compliance, and the thermal strain and stress vectors of the laminate are found by reducing $(10.2.3)_2$ to $\bar{\boldsymbol{\sigma}}_i = \bar{\mathbf{L}}_i\bar{\boldsymbol{\varepsilon}} + \bar{\mathbf{l}}_i\,\Delta\theta$, and by substituting for $\bar{\boldsymbol{\sigma}}_i$ into $(10.3.1)_2$. Since $\bar{\boldsymbol{\sigma}}$ and $\Delta\theta$ are independent, the results are

$$\bar{\mathbf{L}} = \sum_{i=1}^{n} c_i \bar{\mathbf{L}}_i \quad \bar{\mathbf{M}} = \bar{\mathbf{L}}^{-1} \quad \bar{\mathbf{l}} = \sum_{i=1}^{n} c_i \bar{\mathbf{l}}_i = -\sum_{i=1}^{n} c_i \bar{\mathbf{L}}_i \bar{\mathbf{m}}_i \quad \bar{\mathbf{m}} = -\bar{\mathbf{L}}^{-1}\bar{\mathbf{l}} \tag{10.3.4}$$

Of course, the first equation is analogous to $(3.5.7)_1$, while the third equation agrees with the Levin formula (3.8.11–3.8.12), with $\boldsymbol{A}_r = \boldsymbol{I}$, implied by the constraint $\bar{\boldsymbol{\varepsilon}} = \bar{\boldsymbol{\varepsilon}}_i$. Relations between the overall and ply eigenstrains follow from a modified version of the Levin formula, which requires information about stress distribution among ply pairs.

Stress distribution factors $\bar{\mathbf{H}}_i$ and $\bar{\mathbf{h}}_i$ are (3×3) and (3×1) matrices which evaluate in-plane ply stresses $\bar{\boldsymbol{\sigma}}_i$ caused by application of mechanical loads (10.3.1) and a uniform thermal change $\Delta\theta$.

$$\bar{\boldsymbol{\sigma}}_i = \bar{\mathbf{H}}_i\bar{\boldsymbol{\sigma}} + \bar{\mathbf{h}}_i\,\Delta\theta \tag{10.3.5}$$

Referring to (10.3.3)$_2$ and letting $\bar{\boldsymbol{\mu}} = \mathbf{0}$, we find at $\bar{\boldsymbol{\sigma}} \neq \mathbf{0}$, $\Delta\theta = 0$:

$$\bar{\boldsymbol{\varepsilon}} = \bar{\boldsymbol{\varepsilon}}_i \;\Rightarrow\; \bar{\mathbf{M}}\,\bar{\boldsymbol{\sigma}} = \bar{\mathbf{M}}_i\,\bar{\boldsymbol{\sigma}}_i \;\Rightarrow\; \bar{\boldsymbol{\sigma}}_i = \bar{\mathbf{M}}_i^{-1}\,\bar{\mathbf{M}}\,\bar{\boldsymbol{\sigma}} = \bar{\mathbf{L}}_i\,\bar{\mathbf{M}}\bar{\boldsymbol{\sigma}} \tag{10.3.6}$$

And at $\bar{\boldsymbol{\sigma}} = \mathbf{0}$, $\Delta\theta \neq 0$:

$$\bar{\boldsymbol{\varepsilon}} = \bar{\boldsymbol{\varepsilon}}_i \;\Rightarrow\; \bar{\mathbf{m}}\Delta\theta = \bar{\mathbf{M}}_i\,\bar{\boldsymbol{\sigma}}_i + \bar{\mathbf{m}}_i\Delta\theta \;\Rightarrow\; \bar{\boldsymbol{\sigma}}_i = \bar{\mathbf{M}}_i^{-1}(\bar{\mathbf{m}} - \bar{\mathbf{m}}_i)\Delta\theta \tag{10.3.7}$$

Therefore

$$\left.\begin{aligned} &\bar{\mathbf{H}}_i = \bar{\mathbf{L}}_i\,\bar{\mathbf{L}}^{-1} \quad \bar{\mathbf{h}}_i = \bar{\mathbf{L}}_i(\bar{\mathbf{m}} - \bar{\mathbf{m}}_i) = \bar{\mathbf{L}}_i\,\bar{\mathbf{L}}^{-1}\,\bar{\mathbf{L}}\bar{\mathbf{m}} + \bar{\mathbf{l}}_i = -\bar{\mathbf{H}}_i\bar{\mathbf{l}} + \bar{\mathbf{l}}_i \\ &\sum_{i=1}^{n} c_i\,\bar{\mathbf{H}}_i = \mathbf{I} \quad \sum_{i=1}^{n} c_i\,\bar{\mathbf{h}}_i = \mathbf{0} \end{aligned}\right\} \tag{10.3.8}$$

All are expressed as functions of the quantities given in (10.3.4). According to (10.3.1)$_1$, the strain distribution factor is a unit matrix.

Eigenstress distribution factors determine ply stresses caused in laminates by eigenstrains $\boldsymbol{\mu}_i = -\mathbf{M}_i\boldsymbol{\lambda}_i$ in (10.1.8), applied in symmetric pairs of plies. They may represent inelastic, moisture-induced, and other ply eigenstrains that do not depend on a single parameter, such as $\Delta\theta$. According to (10.2.2), they transform into global coordinates as

$$\bar{\boldsymbol{\mu}}_i = \mathbf{X}_i^{\mathrm{T}}\boldsymbol{\mu}_i = -\bar{\mathbf{M}}_i\,\bar{\boldsymbol{\lambda}}_i \quad \bar{\boldsymbol{\lambda}}_i = \mathbf{Y}_i\,\boldsymbol{\lambda}_i = -\bar{\mathbf{L}}_i\,\bar{\boldsymbol{\mu}}_i \tag{10.3.9}$$

The contribution made by each eigenstrain to residual stresses in all plies of a laminate free of in-plane tractions is sought in the form

$$\bar{\boldsymbol{\sigma}}_i = \sum_{j=1}^{n} \bar{\mathbf{F}}_{ij}\,\bar{\boldsymbol{\lambda}}_j \tag{10.3.10}$$

where $\bar{\mathbf{F}}_{ij}$ is the eigenstress distribution factor that provides the stress $\bar{\boldsymbol{\sigma}}_i$ in ply (i) caused by an eigenstress $\bar{\boldsymbol{\lambda}}_j$ in ply (j) while the overall stress $\bar{\boldsymbol{\sigma}} = \mathbf{0}$. Self-induced contributions are included through $\bar{\mathbf{F}}_{ii}$.

To find $\bar{\mathbf{F}}_{ij}$, let us apply an eigenstrain $\bar{\boldsymbol{\mu}}_j$ in ply pair (j), while keeping the laminate at $\bar{\boldsymbol{\varepsilon}} = \bar{\boldsymbol{\varepsilon}}_i = \mathbf{0}$ by an external constraint. In plies $i = j$, this eigenstrain generates ply stresses $\bar{\boldsymbol{\sigma}}'_j = \bar{\boldsymbol{\lambda}}_j = -\bar{\mathbf{L}}_j\,\bar{\boldsymbol{\mu}}_j$, and zero stresses $\bar{\boldsymbol{\sigma}}'_i = \mathbf{0}$ in plies $i \neq j$. Total stress supported by the external constraint is $\bar{\boldsymbol{\sigma}}' = c_j\,\bar{\boldsymbol{\lambda}}_j$. Upon removal of the constraint, the laminate must return to traction-free state, which requires application of an auxiliary overall stress $\bar{\boldsymbol{\sigma}}'' = -c_j\,\bar{\boldsymbol{\lambda}}_j$. In superposition with the ply stresses present under constraint, the ply stresses caused by application of $\bar{\boldsymbol{\mu}}_j$ are

$$\bar{\boldsymbol{\sigma}}_i = -c_j\,\bar{\mathbf{H}}_i\,\bar{\boldsymbol{\lambda}}_j \quad \text{for } i \neq j \qquad \bar{\boldsymbol{\sigma}}_j = (\mathbf{I} - c_j\,\bar{\mathbf{H}}_j)\bar{\boldsymbol{\lambda}}_j \quad \text{for } i = j \tag{10.3.11}$$

Comparing that with (10.3.10), we find the eigenstress distribution factor

$$\bar{\mathbf{F}}_{ij} = \delta_{ij}\,\mathbf{I} - c_j\,\bar{\mathbf{H}}_i \tag{10.3.12}$$

where δ_{ij} is the Kronecker symbol, but the summation rule does not apply. Using (10.3.10), (10.3.11) and (10.3.5), one can confirm the derivation of the vector $\bar{\mathbf{h}}_i$ in (10.3.8) from the above expression for $\bar{\mathbf{F}}_{ij}$.

Ply stresses generated by the load set $\{\bar{\boldsymbol{\sigma}},\ \bar{\mathbf{l}}_i\Delta\theta,\ \bar{\boldsymbol{\lambda}}_i\}$ are obtained from the above as

$$\bar{\boldsymbol{\sigma}}_i = \bar{\mathbf{H}}_i\,\bar{\boldsymbol{\sigma}} + \bar{\mathbf{h}}_i\Delta\theta - \sum_{j=1}^{n}(\delta_{ij}\,\mathbf{I} - c_j\,\bar{\mathbf{H}}_i)\,\bar{\boldsymbol{\lambda}}_j \tag{10.3.13}$$

Finally, the overall in-plane strain, caused by an eigenstrain $\bar{\boldsymbol{\mu}}_i$ applied in ply pairs (i), is made equal to the deformation that the laminate undergoes during relaxation of the initial in-plane constraint, while the overall stress is reduced from the eigenstress $\bar{\boldsymbol{\lambda}}$ to $\bar{\boldsymbol{\sigma}} = \mathbf{0}$. The resulting forms of the in-plane eigenstress and eigenstrain introduced by the above load set are

$$\bar{\boldsymbol{\mu}} = -\bar{\mathbf{L}}^{-1}\bar{\boldsymbol{\lambda}} = -\bar{\mathbf{L}}^{-1}\sum_{i=1}^{n} c_i\bar{\boldsymbol{\lambda}}_i = \sum_{i=1}^{n} c_i\bar{\mathbf{L}}^{-1}\bar{\mathbf{L}}_i\,\bar{\boldsymbol{\mu}}_i = \sum_{i=1}^{n} c_i\bar{\mathbf{H}}_i^{\mathrm{T}}\,\bar{\boldsymbol{\mu}}_i \tag{10.3.14}$$

This is another form of the Levin formula (3.8.11), where the stress distribution factor $\bar{\mathbf{H}}_j$ has been substituted for the stress concentration factor $\boldsymbol{B}_r$. Of course, the strain concentration factor would be replaced here by a unit tensor, as required by $(10.3.1)_1$.

Together with (10.3.4), eqns. (10.3.14) enable writing (10.3.3) in terms of the i−th ply pair contributions described in Sect. 10.2.

$$\bar{\boldsymbol{\varepsilon}} = \bar{\mathbf{M}}\,(\bar{\boldsymbol{\sigma}} - \bar{\mathbf{l}}\,\Delta\theta - \bar{\boldsymbol{\lambda}}) \quad \bar{\boldsymbol{\sigma}} = \bar{\mathbf{L}}(\bar{\boldsymbol{\varepsilon}} - \bar{\mathbf{m}}\Delta\theta - \bar{\boldsymbol{\mu}}) \tag{10.3.3}$$

$$\bar{\boldsymbol{\varepsilon}} = \left[\sum_{i=1}^{n} c_i\bar{\mathbf{L}}_i\right]^{-1}\left[\bar{\boldsymbol{\sigma}} - \sum_{j=1}^{n} c_j\,(\bar{\mathbf{l}}_j\Delta\theta + \bar{\boldsymbol{\lambda}}_j)\right] \quad \bar{\boldsymbol{\sigma}} = \sum_{i=1}^{n} c_i\bar{\mathbf{L}}_i\,(\bar{\boldsymbol{\varepsilon}} - \bar{\mathbf{m}}_i\Delta\theta - \bar{\boldsymbol{\mu}}_i) \tag{10.3.15}$$

The latter are the laminate constitutive relations for the load sets $\{\bar{\boldsymbol{\sigma}},\ \bar{\mathbf{l}}_i\Delta\theta,\ \bar{\boldsymbol{\lambda}}_i\}$ or $\{\bar{\boldsymbol{\varepsilon}},\ \bar{\mathbf{m}}_i\Delta\theta,\ \bar{\boldsymbol{\mu}}_i\}$, where $c_i = t_i/t$ is the ply pair volume fraction, $\bar{\mathbf{L}}_i$ is the stiffness matrix and $\bar{\mathbf{m}}_i = -\bar{\mathbf{L}}_i^{-1}\bar{\mathbf{l}}_i$ is the thermal strain vector of the plies in ply pair (i); $\bar{\boldsymbol{\mu}}_i = -\bar{\mathbf{L}}_i^{-1}\,\bar{\boldsymbol{\lambda}}_i$ is the uniform eigenstrain vector applied in this ply pair. Connections of the load set components to ply properties and eigenstrains in the local material system are shown in (10.2.2).

10.4 Ply and Constituent Stress and Strain Averages

10.4.1 Load Set $\{\bar{\boldsymbol{\sigma}}, \bar{\mathbf{l}}_i \Delta\theta, \bar{\boldsymbol{\lambda}}_i\}$ Is Applied

In-plane ply stresses caused in the laminate by the load set that represents independent loads $\bar{\boldsymbol{\sigma}} = \bar{\mathbf{N}}/2t$ in (10.3.1), $\Delta\theta$, and $\boldsymbol{\mu}_i$ in (10.1.8) are obtained by transforming (10.3.13) from the global to local coordinates. The in-plane ply stresses in the material system of each ply pair are

$$\boldsymbol{\sigma}_i = \mathbf{X}_i \bar{\boldsymbol{\sigma}}_i = \mathbf{X}_i \left[\bar{\mathbf{H}}_i \, \bar{\boldsymbol{\sigma}} + \bar{\mathbf{h}}_i \Delta\theta - \sum_{j=1}^{n} (\delta_{ij} \mathbf{I} - c_j \bar{\mathbf{H}}_i) \, \bar{\boldsymbol{\lambda}}_j \right] \tag{10.4.1}$$

Useful connections derived in $(10.2.4)_1$, (10.3.4) and (10.3.8) are

$$\left.\begin{gathered} \bar{\mathbf{H}}_i = \bar{\mathbf{L}}_i \bar{\mathbf{L}}^{-1} \quad \bar{\mathbf{h}}_i = \bar{\mathbf{L}}_i (\bar{\mathbf{m}} - \bar{\mathbf{m}}_i) = -\bar{\mathbf{H}}_i \bar{\mathbf{l}} + \bar{\mathbf{l}}_i \\ \bar{\mathbf{L}} = \sum_{i=1}^{n} c_i \bar{\mathbf{L}}_i \quad \bar{\mathbf{L}}_i = \mathbf{Y}_i \mathbf{L}_i \mathbf{Y}_i^{\mathrm{T}} \quad \bar{\mathbf{l}} = \sum_{i=1}^{n} c_i \bar{\mathbf{l}}_i \quad \bar{\mathbf{l}}_i = \mathbf{Y}_i \mathbf{l}_i = -\mathbf{Y}_i \mathbf{L}_i \mathbf{m}_i \end{gathered}\right\} \tag{10.4.2}$$

Material property information, the stiffness $\mathbf{L}_i$ and the ply thermal strain vector $\mathbf{m}_i = \{\alpha_A^{(i)}, \alpha_T^{(i)}, 0\}^{\mathrm{T}}$, are specified in (10.1.2), (10.1.3) and (10.1.6). Other physically induced eigenstrains appear in (10.1.8). If preferred, the thermal strains can be included in $\boldsymbol{\mu}_j$.

The in-plane laminate strain $\bar{\boldsymbol{\varepsilon}} = \bar{\boldsymbol{\varepsilon}}_i$ caused by $\{\bar{\boldsymbol{\sigma}}, \bar{\mathbf{l}}_i \Delta\theta, \bar{\boldsymbol{\lambda}}_i\}$ is given by (10.3.15). After transformation into local coordinates, the ply strains are

$$\boldsymbol{\varepsilon}_i = \mathbf{Y}_i^{\mathrm{T}} \bar{\boldsymbol{\varepsilon}} = \mathbf{Y}_i^{\mathrm{T}} \bar{\mathbf{L}}^{-1} \left[\bar{\boldsymbol{\sigma}} - \sum_{j=1}^{n} c_j \, (\bar{\mathbf{l}}_j \Delta\theta + \bar{\boldsymbol{\lambda}}_j) \right] \tag{10.4.3}$$

The through-the-thickness strain $\bar{\varepsilon}_{33}$ is the sum of the transverse ply strains generated by the in-plane stresses, and of any applied eigenstrain components, as shown in (10.1.10). The overall average is found as

$$\left.\begin{aligned} \bar{\varepsilon}_{33} = \sum_{i=1}^{n} c_i \varepsilon_{33}^{(i)} = \sum_{i=1}^{n} c_i \Big[& -(\nu_{12}^{(i)}/E_{11}^{(i)}) \sigma_{11}^{(i)} - (\nu_{23}^{(i)}/E_{22}^{(i)}) \sigma_{22}^{(i)} \\ & + \sigma_{33}/E_{22}^{(i)} + \alpha_T^{(i)} \Delta\theta + \mu_{33}^{(i)} \Big] \end{aligned}\right\} \tag{10.4.4}$$

Ply stresses $\sigma_{11}^{(j)}$, $\sigma_{22}^{(j)}$ in local material coordinates are derived from the $\boldsymbol{\sigma}_i$ in (10.4.1), where they depend on both overall stress and in-plane ply eigenstrains. The remaining contributions to (10.4.4) are independent of $\boldsymbol{\sigma}_i$.

Strain and stress averages in the fiber and matrix phases of individual plies are found by regarding the in-plane stresses $\boldsymbol{\sigma}_i$ in (10.4.1), and the uniform transverse normal stress $\sigma_{33}^{(i)} = \sigma_{33}$, as macroscopic or overall stress components applied to each ply pair. Since the $\boldsymbol{\sigma}_i$ are (3×1) vectors, they need to be augmented, together with $\sigma_{33}^{(i)}$, to (6×1) vectors, that in the previous Chapters were denoted by $\boldsymbol{\sigma}^0$. With $r, s = f, m$ denoting the two phases, we write the phase stress and strain field averages in individual plies (i)

$$\boldsymbol{\sigma}_r^{(i)} = \boldsymbol{B}_r^{(i)} \ (U\boldsymbol{\sigma}_i + \boldsymbol{\sigma}_3) + \boldsymbol{b}_r^{(i)} \Delta\theta + \sum_{s=f}^{s=m} \boldsymbol{F}_{rs}^{(i)} \boldsymbol{\lambda}_s^{(i)} \tag{10.4.5}$$

where

$$\boldsymbol{U}^{\mathrm{T}} = \begin{bmatrix} 1 & 0 & 0 & 0 & 0 & 0 \\ 0 & 1 & 0 & 0 & 0 & 0 \\ 0 & 0 & 0 & 0 & 0 & 1 \end{bmatrix} \quad \boldsymbol{\sigma}_3 = \{0,\ 0,\ \sigma_{33},\ 0,\ 0,\ 0\}^{\mathrm{T}} \tag{10.4.6}$$

and $\boldsymbol{\sigma}_i$ is given by (10.4.1). The $\boldsymbol{B}_r^{(i)}$, $\boldsymbol{F}_{rs}^{(i)}$ and $\boldsymbol{b}_r^{(i)}$ are the mechanical, thermal and transformation stress concentration factors for the fiber composite material of the ply. In the two-phase fiber-matrix system of a ply, they appear in (3.5.4), (3.6.5) and (8.3.3), and are adjusted here to

$$\left.\begin{aligned} &c_m \boldsymbol{B}_m = (\boldsymbol{M}_m - \boldsymbol{M}_f)^{-1}(\boldsymbol{M} - \boldsymbol{M}_f) && c_f \boldsymbol{B}_f = -(\boldsymbol{M}_m - \boldsymbol{M}_f)^{-1}(\boldsymbol{M} - \boldsymbol{M}_m) \\ &\boldsymbol{b}_m = \boldsymbol{F}_{mf}\boldsymbol{l}_f + \boldsymbol{F}_{mm}\boldsymbol{l}_m && \boldsymbol{b}_f = \boldsymbol{F}_{fm}\boldsymbol{l}_m + \boldsymbol{F}_{ff}\boldsymbol{l}_f \\ &\boldsymbol{F}_{mf} = -(\boldsymbol{I} - \boldsymbol{B}_m)(\boldsymbol{M}_m - \boldsymbol{M}_f)^{-1}\boldsymbol{M}_f && \boldsymbol{F}_{mm} = (\boldsymbol{I} - \boldsymbol{B}_m)(\boldsymbol{M}_m - \boldsymbol{M}_f)^{-1}\boldsymbol{M}_m \end{aligned}\right\} \tag{10.4.7}$$

where the volume fractions $c_f + c_m = 1$. $\boldsymbol{M}$ and $\boldsymbol{M}_r$ are (6×6) overall compliances of the ply and phase materials, respectively. The overall compliance $\boldsymbol{M}$ can be bounded or estimated by one of the methods in Chaps. 6 or 7. The (6×1) phase thermal stress vector is $\boldsymbol{l}_r = -\boldsymbol{L}_r \boldsymbol{m}_r$, and $\boldsymbol{m}_r$ is the thermal strain vector of linear coefficients of thermal expansion of the fiber and matrix phases, Table 8.1. $\boldsymbol{L}_r$ denotes stiffness matrix of each phase.

Final form of the phase stress and strain averages caused in each ply by the load set $\{\bar{\boldsymbol{\sigma}},\ \bar{\mathbf{I}}_i \Delta\theta,\ \bar{\boldsymbol{\lambda}}_i\}$ is

$$\boldsymbol{\sigma}_r^{(i)} = \boldsymbol{B}_r^{(i)} U \mathbf{X}_i \left[\bar{\mathbf{H}}_i\, \bar{\boldsymbol{\sigma}} + \bar{\mathbf{h}}_i \Delta\theta - \sum_{j=1}^{n} (\delta_{ij}\, \mathbf{I} - c_j\, \bar{\mathbf{H}}_i)\, \bar{\boldsymbol{\lambda}}_j \right]$$
$$+ \boldsymbol{B}_r^{(i)} \boldsymbol{\sigma}_3 + \boldsymbol{b}_r^{(i)} \Delta\theta + \sum_{s=f}^{s=m} \boldsymbol{F}_{rs}^{(i)} \boldsymbol{\lambda}_s^{(i)} \tag{10.4.8}$$

and

$$\boldsymbol{\varepsilon}_r^{(i)} = \boldsymbol{M}_r^{(i)}\boldsymbol{\sigma}_r^{(i)} + \boldsymbol{m}_r^{(i)}\Delta\theta + \boldsymbol{\mu}_r^{(i)} \tag{10.4.9}$$

This shows the distinct contributions of the mechanical loads, thermal changes and other phase and ply eigenstrains to the fiber and matrix field averages in each ply.

As expected, the overall stress $\bar{\boldsymbol{\sigma}}$ is first allocated to individual plies by the ply stress distribution factors $\bar{\mathbf{H}}_i$ in (10.3.5) and (10.4.2). Then, both $\bar{\boldsymbol{\sigma}}_i$ and $\boldsymbol{\sigma}_3$, contribute to each of the two phase stress averages through the local concentration factors $\boldsymbol{B}_r^{(i)}$; $r = f,\ m$. The deformation and stress fields generated by a uniform change in temperature $\Delta\theta$ and by phase eigenstrains $\boldsymbol{\mu}_s^{(i)}$ in the fiber and matrix, contribute both to the local phase stresses $\boldsymbol{\sigma}_r^{(i)}$ through ply stresses $\boldsymbol{\sigma}_i$, in the form of and ply thermal terms $\bar{\mathbf{h}}_i\,\Delta\theta$, and to ply eigenstrains $\boldsymbol{\mu}_j$. The latter follow from the Levin formula, applied to phase eigenstrains in each ply pair (i). They also make a direct or self-induced contribution to the phase field averages in each transformed ply by the last two terms in (10.4.8). Ply strains (10.4.3) are derived from the stress and eigenstrain fields, and so are the phase strains in (10.4.9).

10.4.2 Load Set $\{\bar{\boldsymbol{\varepsilon}},\ \bar{\mathbf{m}}_i\,\Delta\theta,\ \bar{\boldsymbol{\mu}}_i\}$ Is Applied

According to $(10.3.1)_1$, all plies experience the same in-plane deformation $\bar{\boldsymbol{\varepsilon}}_i = \bar{\boldsymbol{\varepsilon}}$. In the local material coordinates of each ply, the in-plane strain and stress then follow from (10.1.9) and (10.2.2) as

$$\boldsymbol{\varepsilon}_i = \mathbf{Y}_i^{\mathrm{T}}\bar{\boldsymbol{\varepsilon}} \quad \boldsymbol{\sigma}_i = \mathbf{L}_i(\boldsymbol{\varepsilon}_i - \mathbf{m}_i\Delta\theta - \boldsymbol{\mu}_i) \tag{10.4.10}$$

where $\mathbf{m}_i\Delta\theta + \boldsymbol{\mu}_i = \mathbf{Y}_i^{\mathrm{T}}(\bar{\mathbf{m}}_i\Delta\theta + \bar{\boldsymbol{\mu}}_i)$. Moreover, each ply deforms by the uniform amount $\varepsilon_{33}^{(i)}$ in (10.1.10). In evaluation of strain averages in the fiber and matrix constituents, $\varepsilon_{33}^{(i)}$ can be regarded as an overall strain component applied to each ply (i). Total overall strain vector $\boldsymbol{\varepsilon}_i$ applied to the ply consists of the in-plane contribution augmented by the matrix $\boldsymbol{U}$ in (10.4.6), and a new vector $\boldsymbol{\varepsilon}_3^{(i)}$

$$\boldsymbol{\varepsilon}_i = \boldsymbol{U}\varepsilon_i + \boldsymbol{\varepsilon}_3^{(i)} \qquad \boldsymbol{\varepsilon}_3^{(i)} = \{0,\ 0,\ \boldsymbol{\varepsilon}_{33}^{(i)},\ 0,\ 0,\ 0\}^{\mathrm{T}} \tag{10.4.11}$$

where the $\boldsymbol{\varepsilon}_{33}^{(i)}$, given by (10.1.10), now depends on the in-plane strains

$$\varepsilon_{33}^{(i)} = -\nu_{13}^{(i)}\varepsilon_{11} - \nu_{23}^{(i)}\varepsilon_{22} + \sigma_{33}/E_{22}^{(i)} + \alpha_T^{(i)}\Delta\theta + \mu_{33}^{(i)} \tag{10.4.12}$$

The strain and stress averages in the fiber and matrix of each ply (i) are written with additional terms caused by a change in temperature $\Delta\theta$ and phase eigenstrains $\boldsymbol{\mu}_s^{(i)}$

$$\left.\begin{aligned}\boldsymbol{\varepsilon}_r^{(i)} &= \boldsymbol{A}_r^{(i)}(\boldsymbol{U}\varepsilon_i + \boldsymbol{\varepsilon}_3^{(i)}) + \boldsymbol{a}_r^{(i)}\Delta\theta + \sum_{s=f}^{s=m} \boldsymbol{D}_{rs}^{(i)}\boldsymbol{\mu}_s^{(i)} \\ \boldsymbol{\sigma}_r^{(i)} &= \boldsymbol{L}_i(\boldsymbol{\varepsilon}_r^{(i)} - \boldsymbol{m}_r^{(i)}\Delta\theta - \boldsymbol{\mu}_r^{(i)})\end{aligned}\right\} \tag{10.4.13}$$

where $r,\ s = f,\ m$; $\boldsymbol{a}_r^{(i)}$ and $\boldsymbol{D}_{rs}^{(i)}$ are the thermal strain and eigenstrain concentration factors that evaluate the fiber and matrix strains under $\boldsymbol{\varepsilon}_i$, defined in Sect. 3.6.2.

Of course, for a given set of loads, (10.4.8), (10.4.9) or (10.4.12) yield the same phase field averages. However, evaluation relying on the latter appears to be simpler, because in contrast to the different in-plane ply stresses, the in-plane ply strains are all equal to overall laminate strains in the global coordinate system.

10.5 Design of Laminates for Cylindrical Pressure Vessels

Symmetric laminates can be designed to respond to proportional in-plane loads by a selected deformation path. For example, a thin-walled cylindrical pressure vessel can be made to undergo isotropic in-plane deformation in its wall when loaded by normal stresses prescribed in a certain ratio q, such that

$$q\bar{\sigma}_{11} = \bar{\sigma}_{22} \quad q \geq 1 \quad \bar{\varepsilon}_{11} = \bar{\varepsilon}_{22} \quad \bar{\varepsilon}_{12} = 0 \tag{10.5.1}$$

where the $\bar{x}_1-$axis is aligned with the cylinder axis of symmetry, and the $\bar{x}_2-$axis is tangential to the hoop direction. Application of either internal or external hydrostatic pressure makes the ratio of the hoop to longitudinal normal stress $q = 2$. A different q value can be caused by additional axisymmetric mechanical loads. In any case, as long as the laminate responds by isotropic in-plane deformation (10.5.1), then regardless of the particular layup, each ply is subjected to the same deformation and stress states in its material system, and all fibers support the same stress. An optimal design criterion may incorporate this property.

Candidate laminate layups should be orthotropic, with constitutive relation for in-plane response having the same form as that for a single ply in (10.1.2)

$$\begin{bmatrix}\bar{\sigma}_1 \\ \bar{\sigma}_2 \\ \bar{\sigma}_6\end{bmatrix} = \begin{bmatrix}\bar{\mathrm{L}}_{11} & \bar{\mathrm{L}}_{12} & 0 \\ \bar{\mathrm{L}}_{12} & \bar{\mathrm{L}}_{22} & 0 \\ 0 & 0 & \bar{\mathrm{L}}_{66}\end{bmatrix}\begin{bmatrix}\bar{\varepsilon}_1 \\ \bar{\varepsilon}_2 \\ \bar{\varepsilon}_6\end{bmatrix} \tag{10.5.2}$$

where the top bars denote laminate stiffness, stress and strain coefficients in the global coordinate system. It can be shown that the conditions (10.5.1) are satisfied when

$$q\,\bar{\mathrm{L}}_{11} - (1-q)\,\bar{\mathrm{L}}_{12} - \bar{\mathrm{L}}_{22} = 0 \tag{10.5.3}$$

This condition can be satisfied by several laminate layups, with appropriate orientation and volume fractions of the ply pairs. The latter are denoted by c_θ, where θ is the angle between ply fiber direction and the 0° or $\bar{x}_1-$axis in the global coordinate system.

First, let us consider a crossply $(0_{C0}/90_{C90})_s$ laminate, made using the same fibrous composite material in all plies. The stiffness matrix of the laminate is obtained from (10.1.2) as

$$\begin{bmatrix} \bar{\mathrm{L}}_{11} & \bar{\mathrm{L}}_{12} & 0 \\ \bar{\mathrm{L}}_{12} & \bar{\mathrm{L}}_{22} & 0 \\ 0 & 0 & \bar{\mathrm{L}}_{66} \end{bmatrix} = c_0 \begin{bmatrix} \mathrm{L}_{11}^{(0)} & \mathrm{L}_{12}^{(0)} & 0 \\ \mathrm{L}_{12}^{(0)} & \mathrm{L}_{22}^{(0)} & 0 \\ 0 & 0 & \mathrm{L}_{66}^{(0)} \end{bmatrix} + c_{90} \begin{bmatrix} \mathrm{L}_{22}^{(0)} & \mathrm{L}_{12}^{(0)} & 0 \\ \mathrm{L}_{12}^{(0)} & \mathrm{L}_{11}^{(0)} & 0 \\ 0 & 0 & \mathrm{L}_{66}^{(0)} \end{bmatrix} \tag{10.5.4}$$

where $c_0 + c_{90} = 1$ and $\mathrm{L}_{ij}^{(0)}$ are stiffness coefficients of each composite ply in the local system. Notice the $\mathrm{L}_{11}^{(0)} \leftrightarrow \mathrm{L}_{22}^{(0)}$ exchange in the 90° stiffness matrix. Substitution into (10.6.3) provides ply volume fractions

$$c_0 = (1 - c_{90}) = \left[\mathrm{L}_{11}^{(0)} - q\mathrm{L}_{22}^{(0)} + (1-q)\mathrm{L}_{12}^{(0)}\right]\left[(1+q)(\mathrm{L}_{11}^{(0)} - \mathrm{L}_{22}^{(0)})\right]^{-1} \tag{10.5.5}$$

In terms of ply moduli in (10.1.3)

$$c_0 = \left[E_{11}^{(0)} - E_{22}^{(0)}[q(1+\nu_{12}) - \nu_{12}]\right]\left[(1+q)(E_{11}^{(0)} - E_{22}^{(0)})\right]^{-1} \tag{10.5.6}$$

subject to $0 < c_0 < 1$. This condition limits the stress ratio q that can admitted for each specific choice of the ply composite material. Useful values of q are provided by fiber-dominated composite plies where $E_{11}^{(0)}/E_{22}^{(0)} \gg 1$.

As an example, we select a carbon/epoxy (AS4/3501-6) material with elastic moduli

$$E_{11}^{(0)} = 142.0 \text{ GPa},\ E_{22}^{(0)} = 10.3 \text{ GPa},\ E_{12}^{(0)} = 7.2 \text{ GPa},\ \nu_{12}^{(0)} = 0.28,\ \nu_{21}^{(0)} = 0.02 \tag{10.5.7}$$

For the stress ratio $q = 2$, (10.5.6) yields volume fractions $c_0 \doteq 0.3, c_{90} \doteq 0.7$. Therefore, if this material were selected for building a thin-walled pressure vessel, one would use 70 plies in the 90° hoop direction and 30 plies in the longitudinal direction in each 100 plies of wall thickness. This ratio is too biased and would result in thicker 90° plies, susceptible to transverse cracking.

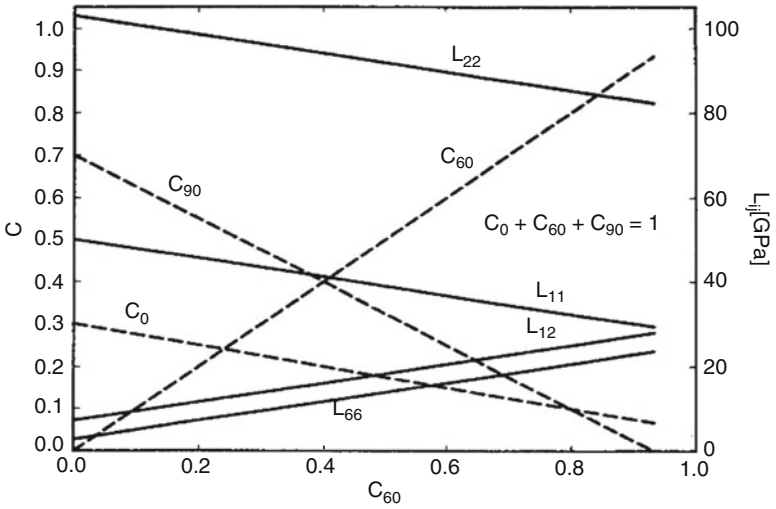

Fig. 10.2 Stiffness coefficients $\bar{L}_{ij}$ of $(0_{C0}/\pm 60_{C60}/90_{C90})_s$ laminates as functions of ply volume fraction of the ±60−degree plies. All such laminates respond by an isotropic in-plane deformation $\bar{\varepsilon}_{11} = \bar{\varepsilon}_{22}$ to biaxial in-plane normal stress $2\bar{\sigma}_{11} = \bar{\sigma}_{22}$ (Dvorak et al. 1999)

A better distribution of ply orientations is obtained by adding ±45° or ±60° to the 0° and 90° plies (Dvorak et al. 1999). This requires expansion of (10.5.3) in agreement with $(10.3.4)_1$ to

$$\bar{\mathbf{L}} = c_0\bar{\mathbf{L}}^{(0)} + (c_{60}/2)[\bar{\mathbf{L}}^{(+60)} + \bar{\mathbf{L}}^{(-60)}] + c_{90}\bar{\mathbf{L}}^{(90)} \tag{10.5.8}$$

where c_{60} is the volume fraction of the ±60° ply pairs. A similar expression can be written for ±45° plies. After substitution of the coefficients of $\bar{\mathbf{L}}$ required in (10.5.3), at $q = 2$, the ply pair volume fractions are connected by

$$277.95\, c_0 - 19.95 c_{60} - 119.25\, c_{90} = 0 \quad c_0 + c_{60} + c_{90} = 1 \tag{10.5.9}$$

Specific volume fractions and laminate stiffness coefficients can be selected as functions of a parameter, such as c_{60}.

Figure 10.2 shows the changes in ply volume fractions on the left vertical axis, and coefficients of the laminate stiffness on the right vertical axis. For each value of c_{60}, the diagram indicates the volume fractions c_0 and c_{90} and the laminate longitudinal $\bar{L}_{11}$, hoop $\bar{L}_{22}$ and shear stiffness coefficients that appear in the expanded form of $\bar{\mathbf{L}}$ on the left hand side of equation (10.5.4). A suitable selection for most applications appears to be $c_{60} = c_{90} = 0.4$, $c_0 = 0.2$, arranged, for example, in multiple layers of $(0/90/+60/90/-60)_s$ layups. Of course, this applies only to the prismatic, cylindrical part of the vessel. End caps can be made using the continuing 0 and ±60−degree plies, which can form an isotropic laminate. However, a separate analysis is needed to determine if the applied pressure and selected cap shape may require additional reinforcement.

10.6 Dimensionally Stable Laminates

Symmetric laminates can be designed to undergo small or zero in-plane deformations when subjected to a uniform change in temperature. At first glance, this appears to be enabled by the axial thermal contraction of certain carbon and aramid fibers. However, it turns out that other factors, such as longitudinal ply stiffness and reduced thermal expansion in ply transverse direction also play a significant role.

Consider a single fibrous ply (i), with known linear longitudinal and transverse coefficients of thermal expansion arranged as in (10.1.6), in the vector $\mathbf{m}_i = \{\alpha_A^{(i)},\ \alpha_T^{(i)},\ 0\}^{\mathrm{T}}$. Transformation from local to global coordinates of the ply thermal vector is shown in (10.2.2). A substitution for the coordinate transformation matrix $\mathbf{X}_i$ in (10.2.1), yields this vector in the form

$$\bar{\mathbf{m}}_i = \mathbf{X}_i^{\mathrm{T}}\mathbf{m}_i = \begin{bmatrix} m^2\alpha_A^{(i)} + n^2\alpha_T^{(i)} \\ n^2\alpha_A^{(i)} + m^2\alpha_T^{(i)} \\ 2mn(\alpha_A^{(i)} - \alpha_T^{(i)}) \end{bmatrix} \tag{10.6.1}$$

where $m = \cos\theta_i$, $n = \sin\theta_i$, and the angle θ_i indicates orientation of ply pair (i), Fig. 10.1.

Overall thermal strain vector of a symmetric laminate follows from (10.3.4) as

$$\bar{\mathbf{m}} = \bar{\mathbf{L}}^{-1}\sum_{i=1}^{n} c_i\bar{\mathbf{L}}_i\bar{\mathbf{m}}_i = \{\bar{\alpha}_1,\ \bar{\alpha}_2,\ \bar{\alpha}_6\}^{\mathrm{T}} \tag{10.6.2}$$

where the $\bar{\alpha}$ denote linear coefficients of thermal expansion in the indicated directions of global coordinates.

Of interest in applications are balanced angle-ply laminates of the $(\pm\theta)_s$ layup, where ply volume fractions $c_{(+\theta)} = c_{(-\theta)} = 0.5$. Many interdispersed ply pairs should be used to minimize the small torsion moment caused by different pair separation distances. For laminates of this kind, nonzero coefficients of the overall stiffness $\bar{\mathbf{L}}$ in $(10.3.4)_1$ are equal to the $\bar{L}_{11}^{(i)}, \bar{L}_{12}^{(i)}, \bar{L}_{22}^{(i)}, \bar{L}_{56}^{(i)}$ coefficients of the constituent plies, because those do not change signs with θ in (10.2.5). The vector $\bar{\mathbf{m}}$ can then be written in a more transparent form, using (10.1.4), as

$$\bar{\mathbf{m}}(\pm\theta) = \begin{bmatrix} \bar{m}_1^{(i)} + (\bar{L}_{22}^{(i)}\bar{L}_{16}^{(i)} - \bar{L}_{12}^{(i)}\bar{L}_{26}^{(i)})\bar{m}_6^{(i)}/\bar{\Lambda} \\ \bar{m}_2^{(i)} + (\bar{L}_{11}^{(i)}\bar{L}_{26}^{(i)} - \bar{L}_{12}^{(i)}\bar{L}_{16}^{(i)})\bar{m}_6^{(i)}/\bar{\Lambda} \\ 0 \end{bmatrix} \tag{10.6.3}$$

where $\bar{\Lambda} = \bar{L}_{11}^{(i)}\bar{L}_{22}^{(i)} - (\bar{L}_{12}^{(i)})^2$, and $\bar{m}_6^{(i)} = 2mn(\alpha_A^{(i)} - \alpha_T^{(i)})$, from (10.6.1). The stiffness coefficients (10.1.3) of each ply transform to global coordinates according

to (10.2.5), where $\bar{L}_{16}^{(i)}$ and $\bar{L}_{26}^{(i)}$ change signs with the sign of θ_i and the same is true for $\bar{m}_6^{(i)}$. Therefore, the magnitude of $\bar{\mathbf{m}}$ depends only on the absolute value of the angle θ.

Local stresses caused in individual plies of the laminate by a uniform temperature change $\Delta\theta$, are from (10.4.1)

$$\boldsymbol{\sigma}_i = \mathbf{X}_i \bar{\boldsymbol{\sigma}}_i = \mathbf{X}_i \bar{\mathbf{h}}_i \Delta\theta = \mathbf{X}_i \bar{\mathbf{L}}_i (\bar{\mathbf{m}} - \bar{\mathbf{m}}_i)\Delta\theta \tag{10.6.4}$$

where $\bar{\mathbf{m}}_i = \mathbf{X}_i^{\mathrm{T}} \mathbf{m}_i$ is given by (10.6.1).

Two types of dimensionally stable laminates can be constructed. One type is the $(\pm\theta_n)_s$ layup that displays zero thermal expansion in one, say, longitudinal direction $\bar{x}_1$. The required angle θ is found by solving the equation

$$\bar{m}_1^{(i)} + \left(\bar{L}_{22}^{(i)}\bar{L}_{16}^{(i)} - \bar{L}_{12}^{(i)}\bar{L}_{26}^{(i)}\right)\bar{m}_6^{(i)}/\bar{\Lambda} = 0 \tag{10.6.5}$$

Solutions can be obtained in systems with stiff fibers that have low or negative CTE. For example, Bahei-El-Din et al. (1992) found that in the elastic deformation range, a $(\pm\theta)_s$ P100 graphite/aluminum laminate had zero thermal expansion in the $\bar{x}_1$-direction at $\theta = 12^o$ and $\theta = 38^o$. Herakovich (1998) reports this property for a $(\pm\theta = 42^o)_s$ T300/5208 carbon/epoxy laminate.

Another type of dimensionally stable laminates are $(\pm 45)_s$ or crossply layups that have zero or very low thermal expansion coefficients in both $\bar{x}_1$, $\bar{x}_2-$directions. As an example, consider a Kevlar/epoxy ($c_f = 0.55$), and a T300/5208 ($c_f = 0.62$) carbon epoxy, with material properties in Table 10.1 (Herakovich 1998).

The first two coefficients of the overall thermal strain vector $\bar{\mathbf{m}}(\pm 45)_S$ of the laminate in (10.6.3) are equal. The terms $\bar{m}_1^{(i)} = \bar{m}_2^{(i)}$ are the ply CTEs transformed into global coordinates. For $\theta = \pm 45$ there is $2\sin\theta\cos\theta = 1$, hence $\bar{m}_6^{(i)} = (\alpha_A - \alpha_T)$. The through-the-thickness coefficient of thermal expansion $\bar{\alpha}_{33}$ is found using (10.1.10), where the ply stresses in material coordinates are given by (10.6.4).

Figure 10.3 shows the longitudinal and transverse coefficients of thermal expansion of the Kevlar-epoxy laminate that has ply properties listed in Table 10.1. Response of the T300/5208 laminate is similar.

Table 10.2 presents the magnitudes of $\bar{m}_1^{(i)} = \bar{m}_2^{(i)}$ and of the overall in-plane coefficients of thermal expansion $\bar{\alpha}_{11} = \bar{\alpha}_{22}$ defined by (10.6.2), and the out-of-plane CTE $\bar{\alpha}_{33}$. Also shown are thermal stress magnitudes caused by $\Delta\theta = +1^o$C, in 10^{-6}GPa. The small positive magnitudes of $\bar{\alpha}_{11} = \bar{\alpha}_{22}$ shown in the table can be reduced further by making small adjustments in the tabulated properties. For example, increasing the longitudinal ply modulus of Kevlar/epoxy plies by 10%, to $1.1\,E_{11}$ yields $\bar{\alpha}_{11} = \bar{\alpha}_{22} = 0.8$. Reductions in both axial and transverse CTEs of the plies causes similar effects. Such property changes may be induced in a hybrid system with added stiffer and/or less expansive fibers or matrices. It should

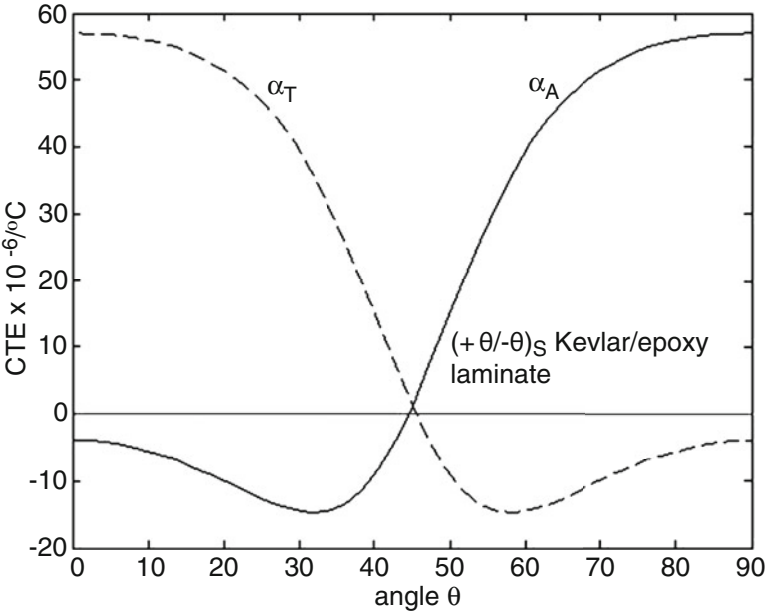

Fig. 10.3 Longitudinal and transverse linear coefficients of thermal expansion of the $(\pm\theta)_S$ Kevlar/epoxy laminate

Table 10.1 Thermoelastic moduli of fibrous plies

	E_{11}	E_{22}	G_{12}	G_{23}	ν_{12}	α_A	α_T
Kevlar/epoxy	76.8	5.5	2.07	1.4	0.34	−4	57
T300/5208	132	10.8	5.65	3.38	0.24	−0.77	25

$E_{11}, E_{22}, G_{12}, G_{23}$ are shown in GPa; $\alpha_{A,}$, α_T in $10^{-6}/°C$

Table 10.2 Thermoelastic response of $(\pm 45)_s$ laminates

	$\bar{m}_1^{(i)} = \bar{m}_2^{(i)}$	$\bar{\alpha}_{11} = \bar{\alpha}_{22}$	$\bar{\alpha}_{33}$	$\sigma_{11} = -\sigma_{22}$
Kevlar/epoxy	26.5	1.22	72.6	299.5
T300/5208	12.1	1.56	38.3	248.3

$\bar{m}_k$ and α_{kk} are shown in $10^{-6}/°C$ and σ_{kk} in Pa/°C

be noted that small variations in ply moduli and CTEs are frequently reported in commonly used composite material systems, hence each particular application requires a separate evaluation.

Under a thermal change $\Delta\theta > 0$, all plies of a $(\pm 45)_S$ laminate support the same in-plane stresses $\sigma_{11} = -\sigma_{22}$, tensile in the fiber direction and compressive in the transverse direction. However, the signs change when $\Delta\theta < 0$, potentially exposing the plies to transverse tension that may cause matrix cracks and related

changes in ply thermoelastic moduli. For the nominal transverse tensile strength of Kevlar/epoxy of 27.6 MPa, transverse cracks may appear at $\Delta\theta \leq -92^{o}$C from processing temperature. In the T300/5208 system, the transverse strength is equal to 43.4 MPa, allowing for $\Delta\theta \leq -175^{o}$C.

10.7 Auxetic Laminates

As discussed in Sect. 2.6, auxetic materials have at least one negative Poisson's ratio. This property is displayed by certain balanced angle-ply laminates, which undergo through-the-thickness expansion when loaded by a tensile in-plane normal stress. Moreover, at two magnitudes of the $\pm\theta$ angles, the laminates exhibit zero through-the-thickness deformation under uniaxial in-plane tension or compression.

Consider again a $(\pm\theta_n)_s$ laminate loaded by the uniform in-plane overall normal stresses $\bar{\sigma}_1$ and $\bar{\sigma}_2$ defined in (10.3.1). Since all symmetric ply pairs have the same volume fraction in the $+\theta$ and $-\theta$ orientations, one can select $n = 2$, $c_i = 0.5$. The normal strains in the directions of the global coordinate system follow from (10.3.3), (10.4.4), with $\bar{\mathbf{M}} = \bar{\mathbf{L}}^{-1}$ from (10.1.4).

$$\left.\begin{aligned} \bar{\varepsilon}_1 = (\bar{L}_{22}^{(i)}\bar{\sigma}_1 - \bar{L}_{12}^{(i)}\bar{\sigma}_2)/\bar{\Lambda} \quad \bar{\varepsilon}_2 = (-\bar{L}_{12}^{(i)}\bar{\sigma}_1 + \bar{L}_{11}^{(i)}\bar{\sigma}_2)/\bar{\Lambda} \\ \bar{\varepsilon}_{33} = -(\nu_{12}^{(i)}/E_{11}^{(i)})\sigma_{11}^{(i)} - (\nu_{23}^{(i)}/E_{22}^{(i)})\sigma_{22}^{(i)} \end{aligned}\right\} \tag{10.7.1}$$

where $\bar{\Lambda} = \bar{L}_{11}^{(i)}\bar{L}_{22}^{(i)} - (\bar{L}_{12}^{(i)})^2$.

We note for future reference that the ply stress vector in the global coordinates, derived from (10.3.5) to (10.3.8), is

$$\bar{\boldsymbol{\sigma}}_i = \{\bar{\sigma}_{11}^{(i)},\ \bar{\sigma}_{22}^{(i)},\ \bar{\sigma}_{12}^{(i)}\}^{\mathrm{T}} \quad \bar{\sigma}_{11}^{(i)} = \bar{\sigma}_1 \quad \bar{\sigma}_{22}^{(i)} = \bar{\sigma}_2 \quad \bar{\sigma}_{12}^{(i)} = (\bar{Q}_1^{(i)}\ \bar{\sigma}_{11}^{(i)} + \bar{Q}_2^{(i)}\ \bar{\sigma}_{22}^{(i)})/\bar{\Lambda} \tag{10.7.2}$$

where

$$\bar{Q}_1^{(i)} = (\bar{L}_{22}^{(i)}\bar{L}_{16}^{(i)} - \bar{L}_{12}^{(i)}\bar{L}_{26}^{(i)}),\ \ \bar{Q}_2^{(i)} = (\bar{L}_{11}^{(i)}\bar{L}_{26}^{(i)} - \bar{L}_{12}^{(i)}\bar{L}_{16}^{(i)}) \tag{10.7.3}$$

In the local or material coordinates, the stress $\boldsymbol{\sigma}_i = \{\sigma_{11}^{(i)},\ \sigma_{22}^{(i)},\ \sigma_{12}^{(i)}\}^{\mathrm{T}}$ in each ply pair (i) is expressed in (10.2.2) and (10.3.5), or (10.6.4). Its components are

$$\boldsymbol{\sigma}_i = \mathbf{X}_i\bar{\mathbf{L}}_i\bar{\mathbf{L}}^{-1}\bar{\boldsymbol{\sigma}} = \begin{bmatrix} m^2 + 2mn\,\bar{Q}_1/\bar{\Lambda} \\ n^2 - 2mn\,\bar{Q}_1/\bar{\Lambda} \\ -mn + (m^2 - n^2)\,\bar{Q}_1/\bar{\Lambda} \end{bmatrix}\bar{\sigma}_1 + \begin{bmatrix} n^2 + 2mn\,\bar{Q}_2/\bar{\Lambda} \\ m^2 - 2mn\,\bar{Q}_2/\bar{\Lambda} \\ mn + (m^2 - n^2)\,\bar{Q}_2/\bar{\Lambda} \end{bmatrix}\bar{\sigma}_2 \tag{10.7.4}$$

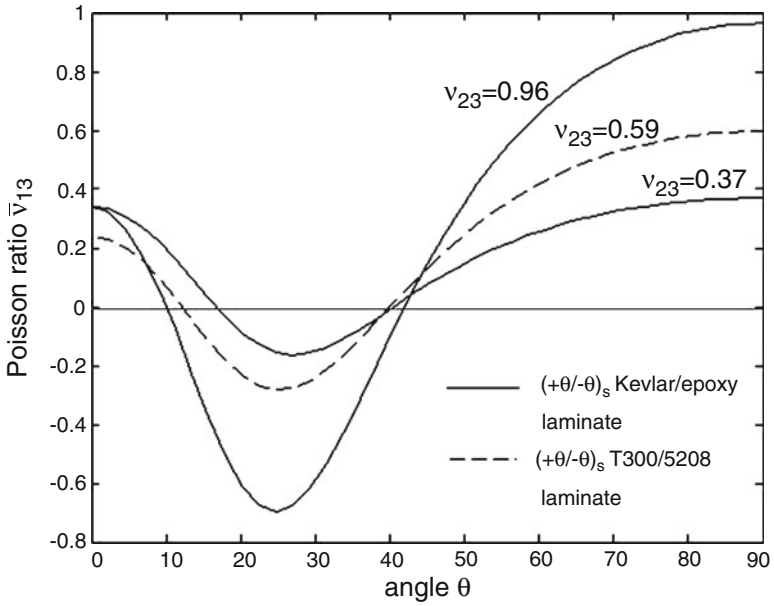

Fig. 10.4 Poisson's ratios $\bar{\nu}_{13}$ of Kevlar/epoxy and T300/5208 $(\pm\theta)_S$ laminates

Table 10.3 Poisson's ratios of auxetic $(\pm\theta)$ laminates

	θ $(\bar{\nu}_{13}=0)$		θ $(\bar{\nu}_{13}=\min.)$	θ $(\bar{\nu}_{12}=\max.)$	ν_{12}	ν_{21}	ν_{23}
Kevlar/epoxy	16.715°	40.541°	27.016° (−0.164)	26.017° (+1.545)	0.34	0.0244	0.37
T300/5208	12.278°	39.970°	25.180° (−0.279)	26.995° (+1.265)	0.24	0.0196	0.59

where $m=\cos\theta$, $n=\sin\theta$. Together with (10.6.4), this provides component form of thermomechanical ply stresses in $(\pm\theta_n)_s$ laminates. Poisson's ratios of interest are $\bar{\nu}_{13}=-\bar{\varepsilon}_3/\bar{\varepsilon}_1$ and $\bar{\nu}_{12}=-\bar{\varepsilon}_2/\bar{\varepsilon}_1$, where the strains are caused by $\bar{\sigma}_1>0$ at $\bar{\sigma}_2=0$. Figures 10.4 and 10.5 show the results for the two laminates introduced in Table 10.1. In Fig. 10.4, the $\nu_{23}=0.96$ was derived from E_{22} and G_{23} in Table 10.1 and (2.3.5), while $\nu_{23}=0.37$ was reported by Herakovich (1998) (Fig. 10.5). See also Table 2.4.

Table 10.3 shows the θ−angles where $\bar{\nu}_{13}=0$ and where it reaches a minimum, and where $\bar{\nu}_{12}$ reaches a maximum. The negative $\bar{\nu}_{13}$ have small absolute values, but the maxima of $\bar{\nu}_{12}>1$, as anticipated in Sect. 2.5. Magnitudes of reported ply Poisson's ratios are listed in the last three columns.

The $\bar{\nu}_{13}=$ min. coincides with a minimum value of $\sigma_{22}^{(i)}\approx -0.1\,\bar{\sigma}_1$, while $\sigma_{11}^{(i)}\approx 1.05\,\bar{\sigma}_1$. However, since the coefficients $(\nu_{12}^{(i)}/E_{11}^{(i)})\ll(\nu_{23}^{(i)}/E_{22}^{(i)})$ in $(10.7.1)_2$, both laminates exhibit auxetic response. Such response may not be obtained in laminates with lower contrast in ply moduli.

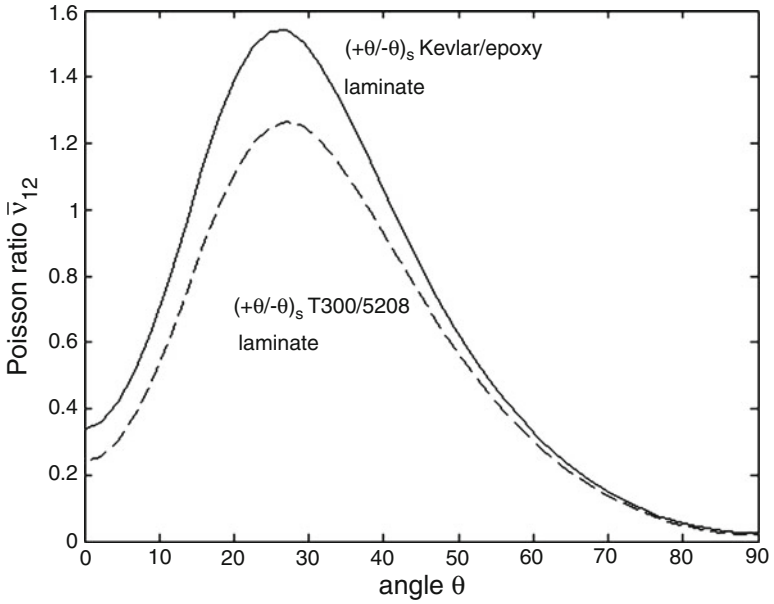

Fig. 10.5 Poisson's ratios $\bar{\nu}_{12}$ of Kevlar/epoxy and T300/5208 $(\pm\theta)_S$ laminates

The $\bar{\nu}_{12} = \max.$ is associated with a sharp rise in $\bar{\varepsilon}_2$ and delayed rise in $\bar{\varepsilon}_1$. Although both $\bar{\nu}_{12} = \max.$ and $\bar{\nu}_{13} = \min.$ are observed at similar values of θ, they may not be attributed to the same source.

10.8 Laminates with Reduced Free Edge Stresses

It is well known that under applied loads, laminated plates and shells can experience high, concentrated interlaminar stresses at and a small distance from free edges. The source of these stresses are image tractions $t_k = -\bar{\sigma}_{kl} n_l$ at a free edge with unit normal n_l, that remove those that would be generated in the absence of the free edge, inside the plate, by the in-plane ply stresses $\bar{\sigma}_{kl}$. Of course, the latter do not cause iterlaminar stresses. For example, let the laminate shown in Fig. 10.1 represent a part of a prismatic specimen of width $-d \leq \bar{x}_2 \leq +d$, which is loaded by an overall stress $\bar{\sigma}_1$, and by a uniform change in temperature $\Delta\theta$. Ply stresses created by these loads in the interior of the laminate are limited to the in-plane intralaminar components derived in (10.3.5)–(10.3.8), as

$$\bar{\boldsymbol{\sigma}}_i = \bar{\mathbf{H}}_i \bar{\boldsymbol{\sigma}} + \bar{\mathbf{h}}_i \Delta\theta = \{\bar{\sigma}_{11}^{(i)},\ \bar{\sigma}_{22}^{(i)},\ \bar{\sigma}_{12}^{(i)}\}^{\mathrm{T}} \quad \bar{\boldsymbol{\sigma}} = \{\bar{\sigma}_{11}, 0,\ 0\}^{\mathrm{T}} \tag{10.8.1}$$

The lateral surfaces are made traction free by superposition of $\bar{\boldsymbol{\sigma}}_i$ with image tractions $\bar{\mathbf{t}}_i = \{0, -\bar{\sigma}_{22}^{(i)}, -\bar{\sigma}_{12}^{(i)}\}^{\mathrm{T}}$ applied to each ply at $\bar{x}_2 = \pm d$. Displacement continuity at ply interfaces under loading by $\bar{\mathbf{t}}_i$ is enforced by shear and normal stresses $\bar{\sigma}_{13}$, $\bar{\sigma}_{23}$ and $\bar{\sigma}_{33}$ that need to be continuous across each interface and ply thickness, but may be variable through the thickness. Since each ply is regarded as an anisotropic layer with different orientation of principal planes in the global coordinate system, the interlaminar stress components near ply interfaces may reach very high magnitudes at $\bar{x}_2 = \pm d$.

Analysis of free edge stresses had been developed by several researchers since the 1960s, starting with Hayashi (1967), Pagano and Pipes (1970), Pagano (1978a, b), Wang and Choi (1982), Yen (1990). The variational approach developed by Pagano was based on Reissner's (1950) principle. It satisfies traction and displacement continuity conditions at interfaces between adjacent layers, and stress equilibrium in the sense of vanishing resultant forces and moments in each layer of the laminate. More recent work has employed the minimum complementary energy principle by using admissible fields that satisfy equilibrium and traction continuity pointwise, but not displacement continuity at ply interfaces. They were developed for uniaxial tension and cylindrical bending by Kassapoglou and Lagace (1986), Rose and Herakovich (1993), Yin (1994a, b), Flanagan (1994), Kim and Atluri (1995a, b) and Wang and Choi (1982). An extensive list of references on the subject can be found, for example, in Herakovich (1998) and in Suvorov and Dvorak (2001).

Reductions of free edge stresses in laminates can be achieved by selecting certain ply stacking sequences or layups (Herakovich 1998; Christensen and DeTeresa 1992). Kim and Atluri (1995b) found that interlaminar stresses caused by uniaxial tension can be minimized by applying a through-the-thickness thermal gradient. Use of optimized fiber prestress for reduction of free edge stresses caused by mechanical and thermal loads was examined by Suvorov and Dvorak (2001), with Yin's (1994a, b) analysis. The objective function was selected to minimize the differences between ply surface tractions caused by fiber prestress, and by the thermomechanical loads. Results had shown that free edge stresses caused by selected tensile and thermal loads can be nearly eliminated by application of optimized fiber prestress to suitably chosen ply stacking sequences.

Here we make contact with the work of Christensen and DeTeresa (1992), which is related to the discussion of auxetic laminates in Sect. 10.7. Their results have shown that very low interlaminar stresses exist at the $\bar{x}_2 = \pm d$ free edges in $(0_n/\pm\theta_m)_S$ laminates that are made of identical plies and are loaded by simple tension or compression $\bar{\sigma}_1$ in the 0−degree direction, providing that

$$\theta = \tan^{-1}\left(\nu_{12}^{(-1/2)}\right) \tag{10.8.2}$$

where ν_{12} is the longitudinal Poisson's ratio of a lamina.

Two distinct conditions need to be satisfied for this result to hold. One assures that both 0−degree and the $(\pm\theta)_S$ laminates, when not in contact, undergo the same lateral deformation under $\bar{\varepsilon}_1$ applied to the entire $(0_n/\pm\theta_m)_S$ laminate. The

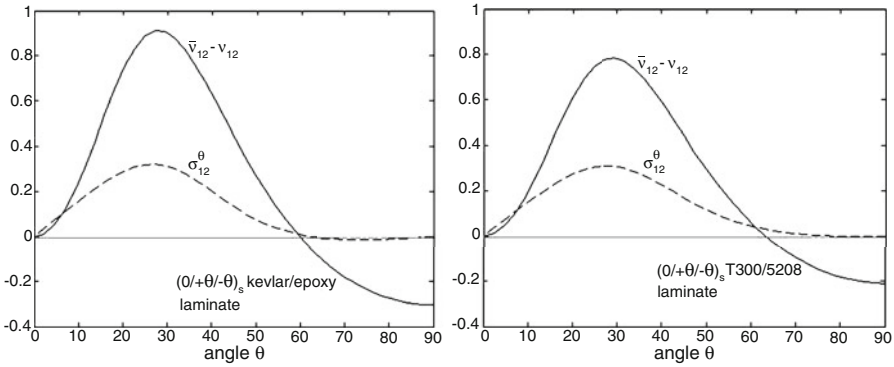

Fig. 10.6 Difference $(\bar{\nu}_{12} - \nu_{12})$ in the laminate and ply Poisson's ratios, and the shear stress $\bar{\sigma}_{12}$ (GPa) in the $\pm 60^{\circ}$ plies of $(0/\pm\theta)_S$ laminates loaded by simple tension in the $0^{\circ}-$direction

longitudinal and transverse strains of both laminates are identical when they have the same longitudinal Poisson's ratios. This condition can be written as

$$\nu_{12} = -\varepsilon_{22}/\varepsilon_{11} = -\bar{\varepsilon}_2/\bar{\varepsilon}_1 = \bar{\nu}_{12} \tag{10.8.3}$$

where $-\varepsilon_{22}/\varepsilon_{11}$ is the strain ratio in the 0° ply. An examination of Fig. 10.6, which has similar appearance for other laminates, indicates that $\bar{\nu}_{12} = \nu_{12}$ when $\theta \simeq 60^{\circ}$.

The second condition applies to the shear stress $\bar{\sigma}_{12}$ in each of the $+\theta$ and $-\theta$ plies, where absence of unloading shear tractions at the free lateral surfaces requires the ply shear stresses in (10.7.2) to comply with

$$\bar{\sigma}_{12}^{(+\theta)} = \bar{\sigma}_{12}^{(-\theta)} = (\bar{Q}_1^{(i)}\ \bar{\sigma}_{11}^{(i)} + \bar{Q}_2^{(i)}\ \bar{\sigma}_{22}^{(i)})/\bar{\Lambda} = 0 \tag{10.8.4}$$

Both conditions can be satisfied by appealing to simplified constitutive relations of fibrous plies, based on distinct contributions of fiber dominated ($E_{11} = E_A,\ \nu_{12} = \nu_A$) and matrix dominated ($E_{22} = E_T,\ G_{12},\ G_{23}$) elastic moduli to ply response (Christensen 1998; Christensen and Zywicz 1990). All comply with the connections between the engineering and Hill's moduli derived in Sect. 2.3.

This theory makes no attempt to relate ply to phase properties and volume fractions. Instead, it treats the ply as an isotropic solid, with generalized moduli, that deforms in parallel with an elastic spring aligned in the $x_A = x_1-$direction of the fiber. Such ply response appears to prevail in certain quasi-isotropic laminates made of identical plies, and loaded by overall normal in-plane tractions.

When all n ply pairs (i) have the same moduli and thickness, the response of the laminate to uniform in-plane deformation is assumed to be

$$\bar{\sigma}_{jk} = \widehat{\lambda}\bar{\varepsilon}_{qq}\delta_{jk} + 2\widehat{\mu}\bar{\varepsilon}_{jk} + \frac{1}{n}(E_{11} - \widehat{E})\sum_{i=1}^{n} q_j^{(i)} q_k^{(i)} q_l^{(i)} q_m^{(i)} \bar{\varepsilon}_{lm} \tag{10.8.5}$$

where $\widehat{\lambda}$ and $\widehat{\mu}$ are the generalized moduli

$$[q_p^{(i)}] = [\cos\,\theta_i, \sin\theta_i, 0] \tag{10.8.6}$$

and the range of free subscripts is 1, 2, ... 6.

The generalized elastic ply moduli, denoted by $(\widehat{\cdot})$, are defined in terms of the actual ply moduli as

$$\widehat{\mu} = \frac{1}{6}\left[\frac{3(1-\nu_{12})E_{22}}{2(1-\nu_{12}^2 E_{22}/E_{11})} + 2G_{12} + G_{23}\right] \tag{10.8.7}$$

and

$$\widehat{\lambda} = \frac{2\nu_{12}}{1-2\nu_{12}}\widehat{\mu} \quad \widehat{E} = 2(1+\nu_{12})\widehat{\mu} \tag{10.8.8}$$

The form of $\widehat{\mu}$ is suggested by the relative contributions of matrix-dominated moduli to the strain energy of an idealized transversely isotropic ply that has $\nu_{12} = \nu_{23} = 0$. The moduli ratio is $(E_{22}/2) : 2G_{12} : G_{23} \propto 3{:}2{:}1$, which is reflected inside the bracket in (10.8.7). Apart from the coefficient L_{11}, the ply stiffness matrix is similar to that for an isotropic solid in (2.2.21). Indeed, if one selects

$$G_{12} = G_{23} = \frac{(1-\nu_{12})E_{22}}{2(1-\nu_{12}^2 E_{22}/E_{11})} \tag{10.8.9}$$

the generalized stiffness coefficients $\widehat{\mathrm{L}}_{jk} \neq \widehat{\mathrm{L}}_{11}$ regain their 'exact' connections between isotropic elastic moduli.

The constitutive relation (10.8.5) can be used either in its original 3D form, or reduced to plane stress form. In the latter case, the plane stress stiffness coefficients for each ply (i) in $(10.1.2)_1$ are

$$\left.\begin{aligned} &\widehat{\mathrm{L}}_{11}^{(i)} = \widehat{\mathrm{L}}_{22}^{(i)} - E_{11}^{(i)} - \widehat{E}^{(i)} \qquad \widehat{\mathrm{L}}_{12}^{(i)} = \widehat{\mathrm{L}}_{21}^{(i)} = \widehat{\lambda}^{(i)}[1 - \widehat{\lambda}^{(i)}/(\widehat{\lambda}^{(i)} + 2\widehat{\mu}^{(i)})] \\ &\widehat{\mathrm{L}}_{22}^{(i)} = 2\widehat{\mu}^{(i)} + \widehat{\lambda}^{(i)}[1 - \widehat{\lambda}^{(i)}/(\widehat{\lambda}^{(i)} + 2\widehat{\mu}^{(i)})] \qquad \widehat{\mathrm{L}}_{66}^{(i)} = \widehat{\mu}^{(i)} \end{aligned}\right\} \tag{10.8.10}$$

Agreement well within the experimental error range of ply properties was reported by Christensen and Zywicz (1990), in comparisons of laminate moduli predicted by the approximate form (10.8.5) and by standard lamination theory, both applied to quasi-isotropic $(0/\pm 60)_s$ glass/epoxy and carbon/epoxy laminates. As expected, the largest discrepancies (6 − 16%) between the laminate moduli predictions were found in E_{33}, ν_{12} and $\nu_{13} = \nu_{23}$.

Applications of (10.8.5) should be limited to quasi-isotropic laminates. To derive ply stresses in the $+\theta$ or $-\theta$ plies of the $(0_n/\pm\theta_m)_S$ laminate, each ply is considered separated from the laminate and subjected to strains

$$\bar{\varepsilon}_{11}^{(\pm\theta)} = 1 \quad \bar{\varepsilon}_{22}^{(\pm\theta)} = \bar{\varepsilon}_{33}^{(\pm\theta)} = -\nu_{12} \quad \bar{\varepsilon}_{12}^{(\pm\theta)} = \bar{\varepsilon}_{23}^{(\pm\theta)} = \bar{\varepsilon}_{31}^{(\pm\theta)} = 0 \tag{10.8.11}$$

After substitution into (10.8.5), the ply stresses of interest are

$$\left.\begin{aligned} \bar{\sigma}_{22}^{(\pm\theta)} &= (E_{11} - \widehat{E})\sin^2\theta\,(\cos^2\theta - \nu_{12}\sin^2\theta) \\ \bar{\sigma}_{12}^{(\pm\theta)} &= (E_{11} - \widehat{E})\sin\theta\cos\theta\,(\cos^2\theta - \nu_{12}\sin^2\theta) \end{aligned}\right\} \tag{10.8.12}$$

It is seen that both $\bar{\sigma}_{22}^{(\pm\theta)} = \bar{\sigma}_{12}^{(\pm\theta)} = 0$ when $\theta = \tan^{-1}(\nu_{12})^{-1/2}$, as anticipated by (10.8.2). Since the strains applied in (10.8.11) are also consistent with those experienced by the $\theta = 0^o$ plies, the entire laminate should not exhibit any free edge stresses at $\bar{x}_2 = \pm d$.

Comparisons of the approximate theory with accurate evaluation (10.8.4) of the ply shear stress are shown in Fig. 10.6, which presents combined plots of actual $(\bar{\nu}_{12} - \nu_{12})$ and shear stress $\bar{\sigma}_{12}^{(\pm\theta)}$ (in units of GPa) in a perfectly bonded six-ply $(0/\pm\theta)_S$ Kevlar/epoxy and T300/5208 laminates described in Table 10.1. In both systems, $(\bar{\nu}_{12} - \nu_{12}) \to 0$ is found fairly close to θ-values predicted by (10.8.2). Those are $\theta = 59.75$ for $\nu_{12} = 0.34$, and $\theta = 63.90$ for $\nu_{12} = 0.24$, where the shear stresses $\bar{\sigma}_{12}^{(\pm\theta)}$ have very low values.

In conclusion, (10.8.2) offers simple and fairly accurate predictions of the $\theta-$ angle for $(0/\pm\theta)_S$ laminates which exhibit vanishing free edge stresses at $\bar{x}_2 = \pm d$, while loaded by simple tension or compression in the $0-$ degree direction. As long as this favorable layup is obtained at $\theta \simeq 60^o$, low interlaminar stresses can also be expected to exist at free edges aligned with $+60^o$ or -60^o loading directions (Alberski 2000).

10.9 Laminates with Fiber Prestress

Prestressing of structural components for improvement of internal stress distributions and overall deflections is widely used in concrete structures, and to a lesser degree in steel structures. Typically, high-strength steel cables are inserted during construction and then anchored in the finished structure while subjected to tension forces which generate desirable residual stresses in those parts of the structure which may have a relatively low strength reserve under applied service loads. In concrete structures, the residual field, in superposition with stresses from service loads, is designed to distribute the total field between the concrete 'matrix' and steel reinforcement according to their respective strength.

Fiber prestress in composite plies and laminates offers similar advantages when it is designed for reaching a particular goal, such as protecting the matrix from

Table 10.4 Forces that generate 1,000 MPa tension stress in a fiber tow

Fiber	Diam., μm	Filaments/tow	Force, N (lbs)	Fiber strength, MPa
S-2 glass	14	2,000	308 (69)	4,600
Kevlar 49	12	1,000	113 (25)	3,600
Carbon AS4	8	12,000	603 (135)	3,600
Graphite P100S	10	2,000	157 (35)	2,200

damage, or reducing fiber waviness to enhance compressive strength, or equalizing total fiber stress in cylindrical pressure vessels. Such applications will be briefly described.

In fabrication of prestressed composite parts, certain tensile stress is applied to pre-impregnated fiber tows and released after matrix consolidation. That can be accomplished, for example, by widely used fiber placement operations with in-situ matrix cure, adjusted for application of variable force magnitudes. Forces corresponding to 1,000 MPa prestress in commonly used fiber tows are shown in Table 10.4.

10.9.1 Prestressed Laminated Plates

First, we evaluate the effect of fiber prestress on ply and phase stress distributions, and on position of damage envelopes in symmetric laminated plates. Uniform in-plane tractions and temperature changes are applied to each or all ply pairs, such that the laminate undergoes only in-plane and through-the-thickness deformation. As long as the already deposited plies remain elastic during prestress removal and cooling from the matrix curing temperature, application and removal of prestress, and matrix cure and cooling, can be assumed to take place simultaneously in all plies.

At the beginning of the process, prior to matrix consolidation, a certain tensile prestress $\left(\sigma_{11}^{f}\right)_{p}^{(i)}$ is applied to the fiber tows which will reinforce plies (i). The fibers are assumed to be at most transversely isotropic, as in Sect. 8.1.4. A thermal strain $\mathbf{m}_f \Delta\theta$, caused by heating the fibers to matrix curing temperature, is superimposed with the mechanical strain caused by the prestress.

Total ply stress and fiber strain fields in each ply (i) before consolidation are

$$\left.\begin{aligned}
\boldsymbol{\sigma}_i^{\,p} &= \left\{ c_f^{(i)} \left(\sigma_{11}^{f}\right)_{p}^{(i)}, 0, 0 \right\}^{\mathrm{T}} \qquad \bar{\boldsymbol{\sigma}}_i^{\,p} = \mathbf{Y}_i \left\{ c_f^{(i)} \left(\sigma_{11}^{f}\right)_{p}^{(i)}, 0, 0 \right\}^{\mathrm{T}} \qquad \bar{\boldsymbol{\sigma}}^{\,p} = \sum_{i=1}^{n} c_i \bar{\boldsymbol{\sigma}}_i^{\,p} \\
\left(\boldsymbol{\varepsilon}_i^{f}\right)^{p} &= \left\{ \left[\mathrm{M}_{11}^{(f)} \left(\sigma_{11}^{f}\right)_{p}^{(i)} + \alpha_A^f \Delta\theta \right], \left[\mathrm{M}_{12}^{(f)} \left(\sigma_{11}^{f}\right)_{p}^{(i)} + \alpha_T^f \Delta\theta \right], \right. \\
&\qquad \left. \left[\mathrm{M}_{12}^{(f)} \left(\sigma_{11}^{f}\right)_{p}^{(i)} + \alpha_T^f \Delta\theta \right], 0, 0, 0 \right\}^{T}
\end{aligned}\right\} \tag{10.9.1}$$

where the rotation matrix $\mathbf{Y}_i$ of the ply is given by (10.2.1), and $\bar{\boldsymbol{\sigma}}^p$ is the resultant of all in-plane ply prestresses, to be removed after matrix consolidation.

Next, the matrix is cured at a certain temperature, while the ply fibers support the prestress $(\sigma_{11}^f)_p^{(i)}$. The matrix is assumed to be free of stress after cure, while the fibers are deformed by $(\boldsymbol{\varepsilon}_i^f)^p$. Overall strain of the laminate is set to zero. The temperature of the new laminate is then reduced by $-\Delta\theta$ to ambient or to another desired magnitude, where the fiber prestress is removed. The uniform thermal change $-\Delta\theta$ and unloading by the in-plane overall stress $-\bar{\boldsymbol{\sigma}}^p$ in (10.9.1) cause laminate and ply strains and stresses in global and ply coordinates

$$\left.\begin{aligned} \bar{\boldsymbol{\varepsilon}} = \bar{\boldsymbol{\varepsilon}}_i &= -\left(\bar{\mathbf{L}}^{-1}\bar{\boldsymbol{\sigma}}^p + \bar{\mathbf{m}}\Delta\theta\right) \qquad \boldsymbol{\varepsilon}_i = \mathbf{Y}^{\mathrm{T}}\bar{\boldsymbol{\varepsilon}}_i \\ \bar{\boldsymbol{\sigma}}_i &= -\left(\bar{\mathbf{H}}_i\bar{\boldsymbol{\sigma}}^p + \bar{\mathbf{h}}_i\Delta\theta\right) \qquad \boldsymbol{\sigma}_i = \mathbf{X}\bar{\boldsymbol{\sigma}}_i \end{aligned}\right\} \tag{10.9.2}$$

Those are evaluated according to (10.3.3–5). The $\bar{\mathbf{L}}$ and $\bar{\mathbf{m}}$ matrices denote respectively the overall in-plane stiffness matrix and thermal strain vector of the elastic laminate, and $\bar{\mathbf{H}}_i$, $\bar{\mathbf{h}}_i$ are the mechanical and thermal ply stress distribution factors in (10.3.8).

The laminate is free of mechanical tractions after prestress release. However, the latter applies normal and shear tractions $-\bar{\boldsymbol{\sigma}}_i^p$ in (10.9.1) to the free edges of each homogenized ply in the global or laminate coordinate system. The residual stress averages that are left in the plies and phases follow from (10.4.1) and (10.4.8), for loading of the laminate by the overall stress in (10.9.2). Fiber strain is equal to the difference between $\left(\boldsymbol{\varepsilon}_i^f\right)^p$ from the original prestress at $+\Delta\theta$, and the unloading strain due to $-\bar{\boldsymbol{\sigma}}^p$ and $-\Delta\theta$, while the fibers reside in the already consolidated plies. This difference is expected to be very small relative to fiber strength. However, release of fiber prestress generates a possibly significant compressive stress state in the matrix, due to the overall unloading by $\bar{\boldsymbol{\sigma}}_i$ in (10.9.2). Evaluation of all field averages in both constituents and plies follows the procedure described in Sect. 10.4.2.

10.9.2 Damage Envelopes of Prestressed Laminated Plates

A generic damage envelope of a laminate is determined by the strength magnitudes of each ply in longitudinal and transverse tension or compression ($\sigma_{11}^{i(T)}$, $\sigma_{22}^{i(T)}$, $\sigma_{11}^{i(C)}$, $\sigma_{22}^{i(C)}$), and in longitudinal shear (σ_{12}^i). When plotted in a selected global stress plane of the laminate, each strength value traces a straight line Dvorak and Sejnoha (1995, 1996). The example shown in Fig. 10.7 shows these lines for a nine ply $\left[(0/90)_2/\bar{0}\right]_{\mathrm{S}}$ S-glass/epoxy laminate, in the plane of biaxial normal overall in-plane tractions S_{11}, S_{22}. The respective ply strength values were selected as 1,280 MPa and 690 MPa in longitudinal tension and compression, 49 MPa and 158 MPa in transverse tension and compression of a single ply, and

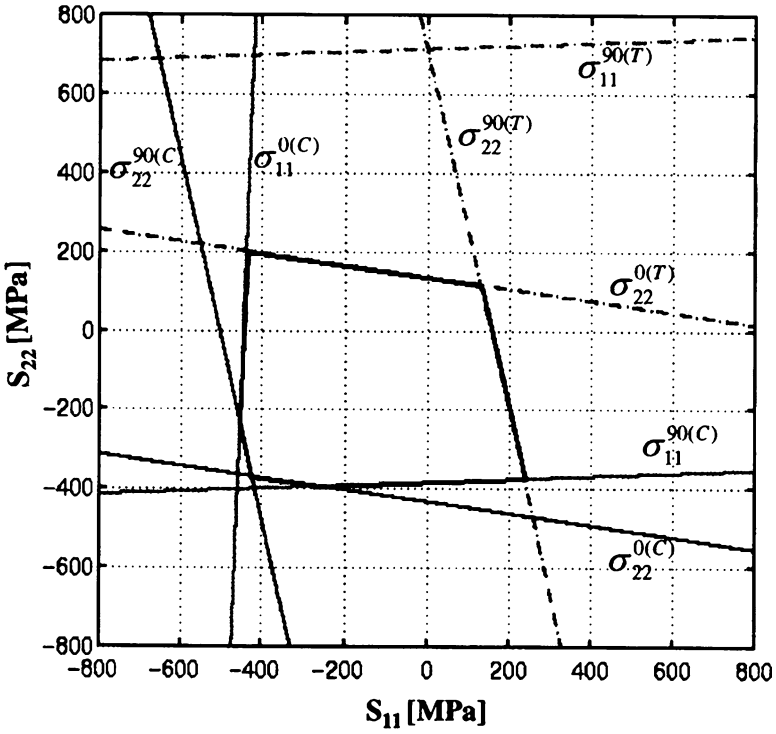

Fig. 10.7 Initial damage envelope of a S-glass/epoxy $\left[(0/90)_s/\bar{0}\right]_s$ laminate. The effect of cooling from curing temperature is neglected (Dvorak and Suvorov 2000)

69 MPa in longitudinal shear. It should be noted that the transverse compression strength of plies embedded in a laminated plate may be higher than that measured on an unconstrained ply. Ply and phase properties, details of the analysis and damage envelopes for other laminate layups can be found in Dvorak and Suvorov (2000).

The damage envelope in Fig. 10.7 surrounds the damage-free interior part of the S_{11}, S_{22} laminate stress plane, which contains the origin, where the laminate is traction-free. The effect of cooling from curing temperature is neglected in this figure. Most of the envelope's lower and left edges correspond to the longitudinal compression branches of the 0-degree and 90-degree plies, designated by $\left(\sigma_{11}^{0(C)}, \sigma_{11}^{90(C)}\right)$, with a minor contribution by the transverse compression branches $\left(\sigma_{22}^{0(C)}, \sigma_{22}^{90(C)}\right)$ of the two plies. As expected, the upper and right edges are traces of the transverse tensile strengths $\left(\sigma_{22}^{0(T)}, \sigma_{22}^{90(T)}\right)$ of the two plies. The envelope contains the laminate stress origin $S_{11} = S_{22} = 0$, but the tension range is small.

More elaborate envelopes with similar features may be constructed by utilizing the same strength magnitudes in different theoretical strength criteria. Examples of the latter can be found on R.M. Christensen's website www.FailureCriteria.com.

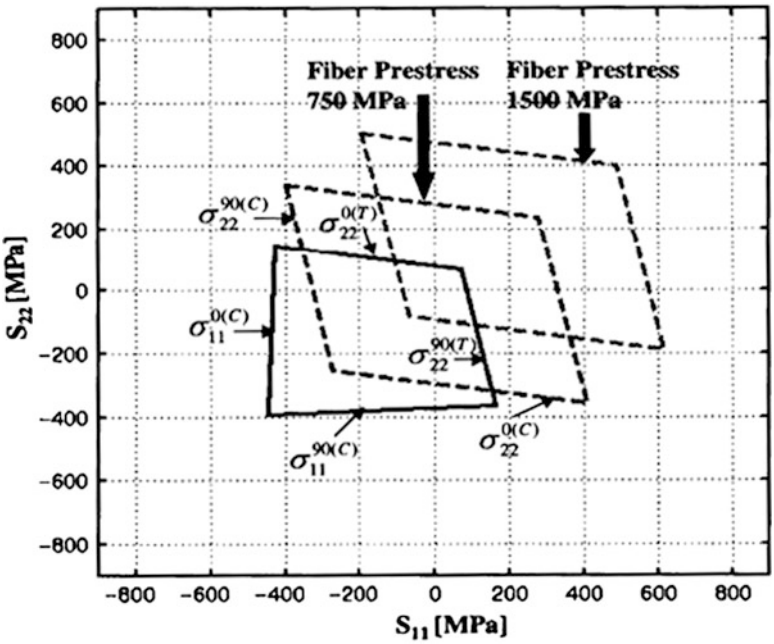

Fig. 10.8 Damage envelopes of a prestressed S-glass/epoxy $\left[(0/90)_s/\bar{0}\right]_s$ laminate. The effect of cooling from curing temperature is included (Dvorak and Suvorov 2000)

The effect of fiber prestress and cooling by $\Delta\theta = -150^{o}$C from matrix curing temperature on the position of the damage envelopes is illustrated in Fig. 10.8. The initial damage envelope has shifted somewhat due to the thermal change, and is now formed only by the four dominant branches shown in Fig. 10.7. Then, prestress is applied to both 0 and 90-degree plies, at 750 MPa or at 1,500 MPa. Damage envelopes of the prestressed laminate consist only of the transverse tension and compression branches of the plies.

As expected, application of the biaxial prestress translates the damage envelope in the $S_{11} = S_{22}$ in-plane laminate stress direction, away from the origin, and thus provides a larger tensile stress range where the laminate should remain free of damage. However, the envelopes do not expand as a result of prestress, hence the range allowed for transverse compression is smaller.

Figure 10.9 illustrates the effect of prestress on fiber failure envelopes, constructed from ply strength values in longitudinal tension and compression. Solid lines denote the envelope before application of prestress, the left and bottom branches indicate possible failure in compression, as they did in Fig. 10.8. The two tension branches at the top and at right suggest onset of tensile failure of the respective plies. Prestress translates the fiber damage envelopes in the direction opposite to that of the matrix damage envelopes, but at a much lower rate. For the

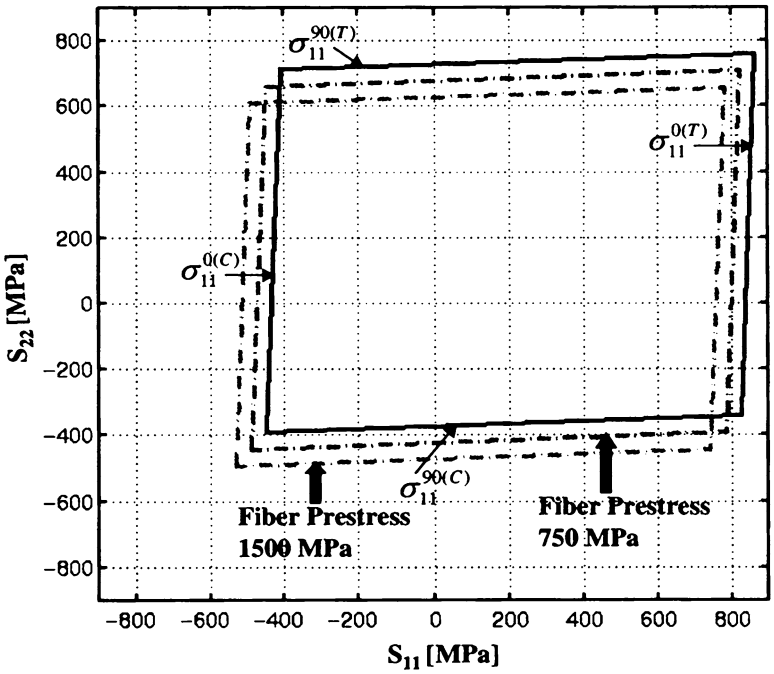

Fig. 10.9 Fiber failure envelopes of a prestressed S-glass/epoxy $\left[(0/90)_s/\bar{0}\right]_s$ laminate (Dvorak and Suvorov 2000)

selected prestress magnitudes, the matrix damage envelopes are contained within their fiber failure counterparts.

Ply strengths $\sigma_{11}^{0(C)}, \sigma_{11}^{90(C)}$ in longitudinal compression and the resulting positions of the compression branches of the envelopes depend on fiber alignment in the ply. Even seemingly minor fiber misalignment of few degrees from the longitudinal axis facilitates fiber microbuckling, kinking and related failure mechanisms, which significantly reduce compressive strength (Budiansky and Fleck 1993, 1994; Kyriakides et al. 1995; Fleck 1997). For example, Christensen and DeTeresa (1997) suggest that the ratio of longitudinal compressive strength to the longitudinal shear modulus p in a carbon/epoxy composite may decrease from $\sigma_{11}^C/p = 0.45$ at 1 degree misalignment to $\sigma_{11}^C/p = 0.15$ at 4 degrees; still a respectable magnitude. Since fiber prestress improves fiber alignment, it should also elevate ply compressive strength and thus lead to expansion of the compression branches of the damage and fiber failure envelopes in Fig. 10.9. However, this effect will not be reflected in the damage envelopes of the pretressed plies in Fig. 10.8, which are surrounded by transverse strength branches.

The above examples demonstrate the effect of simple biaxial fiber prestress on the position and translation of the damage and fiber failure envelopes of

elastic laminated plates. Some composite matrices may become viscoelastic and undergo time-dependent deformation that relaxes a part of the prestress-induced matrix stress; such situations were analyzed by Suvorov and Dvorak (2002). Other applications of prestressing of elastic laminates can be directed to reduction of free-edge stresses in laminates, as discussed next.

10.9.3 Fiber Prestress for Suppression of Free Edge Stress Concentrations

External loads and temperature changes in fabrication and service may cause stress concentrations between adjacent homogenized plies at free edges of laminated plates. In Sect. 10.8, we had shown that certain ply layups reduce those concentrations, at least under uniaxial loading of the laminate. Here we describe how similar reductions can be produced under more general loading conditions by applying fiber prestress.

Consider a laminated plate of any layup that has been subjected to fiber prestress in certain plies before matrix consolidation, then cured and brought by $-\Delta\theta$ to a lower service temperature. Each ply is regarded as homogenized thin plate, not necessarily bonded to the other plies, with effective thermoelastic moduli of the aligned fiber composite. The latter are assumed to be identical in all plies. Thermal expansion of the isotropic matrix is assumed to exceed that of the fibers, hence cooling of a free ply causes larger contraction in the direction transverse to the fibers. Then, in superposition with the thermal change, prestress release can create an isotropic in-plane strain state of the same magnitude in all plies of the finished laminate. In the absence of differential deformation, the homogenized plies do not experience interfacial stress concentrations at free ends. However, localized stresses due to prestress release are left at the fiber-matrix interfaces, within a small distance of about two fiber diameters from their ends.

Let us now determine fiber prestress $\left(\sigma_{11}^{f}\right)_{p}^{(j)}$ that creates an isotropic in-plane strain after application of $-\Delta\theta$ to a traction-free laminate (Dvorak 2001, Suvorov and Dvorak 2001a). During and immediately after matrix cure, each ply is subjected to longitudinal stress $c_f\left(\sigma_{11}^{f}\right)_{p}^{(i)}$ by the fiber prestress, as in (10.9.1). The fibers are deformed by $\left(\boldsymbol{\varepsilon}_i^{f}\right)^{p}$, but the newly formed plies are regarded as free of strain. An isotropic strain state in each consolidated ply will be created by the prestress magnitude that satisfies

$$\left.\begin{aligned}
&\varepsilon_{11}^{(i)}=\varepsilon_{22}^{(i)}=-\mathrm{M}_{11}^{(i)}c_f\left(\sigma_{11}^{f}\right)_{p}^{(i)}-\alpha_A^{(i)}\Delta\theta=-\mathrm{M}_{21}^{(i)}c_f\left(\sigma_{11}^{f}\right)_{p}^{(i)}-\alpha_T^{(i)}\Delta\theta\\
&\left(\sigma_{11}^{f}\right)_{p}^{(i)}=\frac{1}{c_f\left(\mathrm{M}_{21}^{(i)}-\mathrm{M}_{11}^{(i)}\right)}\left(\alpha_A^{(i)}-\alpha_T^{(i)}\right)\Delta\theta\geq 0
\end{aligned}\right\}\tag{10.9.3}$$

The $M_{11}^{(i)}$ and $M_{21}^{(i)} = M_{12}^{(i)}$ are the local in-plane compliances of ply (i) from (10.1.2), and $\alpha_A^{(i)}$, $\alpha_T^{(i)}$ are the linear thermal expansion coefficients in (10.1.6). In a typical ply, there is $\left(M_{21}^{(i)} - M_{11}^{(i)}\right) = -\left(1 + \nu_{12}^{(i)}\right)/E_{11}^{(i)}$ from (10.1.4), and $\alpha_A^{(i)} < \alpha_T^{(i)}$, hence the inequality should be satisfied.

After prestress release and cooling by $-\Delta\theta$, each ply exhibits the following uniform isotropic in-plane deformation $\varepsilon_{11}^{(i)} = \varepsilon_{22}^{(i)}$, relative to the strain-free state at matrix curing temperature $+\Delta\theta$ and prestress $c_f \left(\sigma_{11}^f\right)_p^{(i)}$.

$$\left.\begin{aligned} \varepsilon_{11}^{(i)} &= \left\{ M_{11}^{(i)} \left[\left(M_{11}^{(i)} - M_{21}^{(i)} \right)^{-1} \left(\alpha_T^{(i)} - \alpha_A^{(i)} \right) \right] + \alpha_A^{(i)} \right\} \Delta\theta \\ \varepsilon_{22}^{(i)} &= \left\{ M_{21}^{(i)} \left[\left(M_{11}^{(i)} - M_{21}^{(i)} \right)^{-1} \left(\alpha_T^{(i)} - \alpha_A^{(i)} \right) \right] + \alpha_T^{(i)} \right\} \Delta\theta \end{aligned}\right\} \tag{10.9.4}$$

The laminate is now traction-free, and all plies exhibit the same isotropic in-plane strain relative to the strain-free state at matrix consolidation. That precludes development of stress concentrations between the homogenized plies at laminate free edges.

In simple $(0/90)_S$ or crossply laminates, the prestress may be adjusted to generate an isotropic in-plane strain when the finished laminate is loaded by uniform mechanical tractions that cause constant biaxial in-plane normal strains. Of course, that is possible only if, after incorporating those strains in (10.9.3), the prestress magnitude that yields the same isotropic deformation in all plies is positive, similar to that in (10.9.4). Free edge stress concentrations between homogenized adjacent plies could thus be eliminated while the laminate is subjected to selected service loads.

More elaborate applications of fiber prestress for reduction of free edge stresses in symmetric laminated plates were described by Suvorov and Dvorak (2001a). Using polynomial approximations stress functions by Yin (1994a, b), they had developed an optimization procedure for evaluation of fiber prestress in individual plies which keep the stresses in both laminate interior and at free edges within allowable limits, while the applied mechanical load may change within a certain interval or inside a damage envelope. Mechanical loading by both in-plane tractions and bending or twisting moments was considered, together with thermal and general ply eigenstrains.

The prestress magnitudes released at a free edge were required to minimize the objective function

$$I = \sum_{i=1}^{n} \left[\left(\sum_{q=p,m,\theta} \left(\sigma_{yy}^{si,q} - \sigma_{yy}^{\ell i,q} \right) \right)^2 + \left(\sum_{q=p,m,\theta} \left(\sigma_{xy}^{si,q} - \sigma_{xy}^{\ell i,q} \right) \right)^2 \right] \to \min. \tag{10.9.5}$$

where i is the ply number, the $\sigma_{yy}^{si,q}$ and $\sigma_{xy}^{si,q}$ are the normal and shear tractions caused at the lateral surface or the free edge of each homogenized ply (i) by either prestress ($q = p$), or by mechanical loads ($q = m$), or by ply thermal eigenstrains ($q = \theta$). The components $\sigma_{yy}^{\ell i,q}$ and $\sigma_{xy}^{\ell i,q}$ are computed using the laminated plate theory of Sect. 10.3, on interior planes removed from but parallel to the free edge. The prestress release is thus designed to minimize the difference between applied surface and resulting interior tractions, both resolved on parallel surfaces. Objective functions designed to directly minimize the interfacial stress concentrations at free edges were found to be less useful. Interlaminate stress limits were included in the constraints, to assure that prescribed strength criteria were not violated anywhere in the laminate. Since ply stresses undergo large changes within a certain small distance from the free edge, the computed distributions need to be sampled within that distance, to capture the interfacial stress maxima. Examples were presented for crossply and $(0/+45/-45/90/0)_S$ S-glass epoxy laminates, to show that interlaminar stresses caused at free edges by thermal or mechanical loads can be reduced to near zero by release of optimized fiber prestress.

10.9.4 Prestressed Laminates for Cylindrical Pressure Vessels

Multilayered laminates are often used in construction of cylindrical pressure vessels or submersibles, loaded by internal or external pressure. They are manufactured by winding layers $j = 2, 3, \ldots N$ of a prepreg fiber tape on a fixed elastic mandrel $j = 1$, such that the tape is cured at contact with already consolidated layers, Fig. 10.10. In this process, the fibers are subjected to a certain tensile force P_j, to reduce fiber waviness. Moreover, the force can be designed for optimized fiber prestress, that eliminates or improves fabrication related residual stresses in the cylinder wall. That is of particular value in submerged structures under external pressure, which rely on high compressive strength of the laminate. In such applications, preference should be given to symmetric laminates described in Sect. 10.5, which respond by uniform isotropic in-plane deformation to loading by a uniform biaxial overall in-plane stress $2\bar{\sigma}_{zz} = \bar{\sigma}_{\phi\phi}$, for example, the $(0_{C0}/\pm 60_{C60}/90_{C90})_s$ layup of Fig. 10.2.

The laminated cylinder exhibits overall cylindrical orthotropy described in Sect. 2.4. Ply elastic constants can be derived by identifying the cylinder wall with a laminated plate of the same layup. Overall moduli are evaluated using the classical laminated plate theory of Sect. 10.3, and then transformed into cylindrical coordinates, as suggested by Sun and Li (1988) and Luo and Sun (1991). Applications to submersibles exposed to both external and axial pressure need to consider exposure to buckling, described for example by Kardomateas and Philobox (1995).

Analysis of prestressed cylinders, developed by Dvorak and Prochazka (1996), Dvorak et al. (1999) and by Srinivas et al. (1999), is now briefly reviewed. The

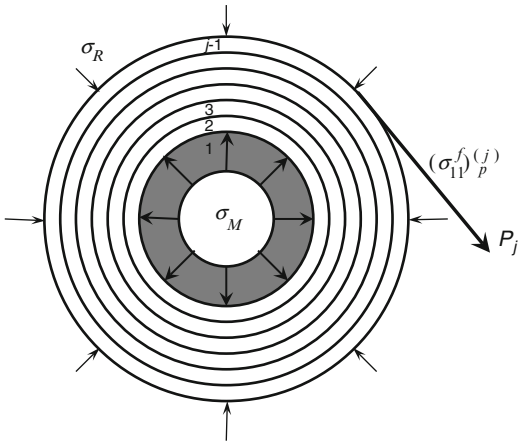

Fig. 10.10 Winding of a laminated cylinder on a fixed elastic mandrel

$(r,\ \phi,\ z)$ overall coordinate system is attached to the cylinder, to denote radial, hoop and longitudinal components. Fiber prestress is induced by forces P_j, applied to the fibers of each layer j before matrix cure, c.f., (10.9.1). The forces may change from layer to layer, in both prescribed magnitude and direction on the tangential plane to the cylinder wall. Together with ply orientation, each P_j contains an angle ψ_j with the longitudinal z-axis of the cylinder. Ply magnitudes P_j are collected in a $((N-1)\times 1)$ vector $\boldsymbol{P}$. Notice that the $\boldsymbol{P}$, $\boldsymbol{S}$ and $\boldsymbol{T}$ symbols used in this section are not related to similar symbols used earlier for the Eshelby and Hill tensors.

Figure 10.10 shows the loads that generate the following three types $\kappa = \alpha,\ \beta,\ \delta$ of stress vectors $\boldsymbol{\sigma}^{\kappa}$ in each ply during buildup of the cylinder. They are resolved into hoop and longitudinal components $\boldsymbol{\sigma}^{\kappa}_{\phi\phi},\ \boldsymbol{\sigma}^{\kappa}_{zz}$, all represented by $((N-1)\times 1)$ vectors. Their coefficients ultimately depend on the longitudinal and hoop components of $\boldsymbol{P}$. An in-plane self-stress $\boldsymbol{\sigma}^{\alpha}$ is caused, in part, by the prestress and by thermal stresses, both left in the ply after the $\pm\,\Delta\theta$ heating and cooling cycle to cure the matrix. Winding of a prestressed ply on the layers of the partially completed cylinder causes an exterior pressure σ_R, which induces an in-plane relaxation stresses $\boldsymbol{\sigma}^{\beta}$ in each of the already placed ply. An interior pressure σ_M is supported by the mandrel and eventually removed, leaving an in-plane stress $\boldsymbol{\sigma}^{\delta}$ in each ply.

The three stress types can be written as

$$\left.\begin{aligned} \boldsymbol{\sigma}^{\kappa}_{\phi\phi} &= \boldsymbol{S}^{\kappa}_{\phi\phi}\boldsymbol{P}^{\phi} + \boldsymbol{S}^{\kappa}_{\phi z}\boldsymbol{P}^{z} \quad \boldsymbol{\sigma}^{\kappa}_{zz} = \boldsymbol{S}^{\kappa}_{z\phi}\boldsymbol{P}^{\phi} + \boldsymbol{S}^{\kappa}_{zz}\boldsymbol{P}^{z} \\ P^{\phi}_{j} &= P_j \sin\psi_j \quad P^{z}_{j} = P_j \cos\psi_j \quad \kappa = \alpha,\beta,\delta \end{aligned}\right\} \tag{10.9.6}$$

where the $\boldsymbol{S}$ matrices are $((N-1)\times(N-1))$ influence functions that evaluate the corresponding stresses caused in each ply by the P^{ϕ}_{j} and P^{z}_{j} components of the applied force P_j of unit magnitude. Evaluation of the influence functions and their

constraints was described in detail by Srinivas et al. (1999). The force components are related to the vector $\boldsymbol{P}$ of ply prestress forces P_j by diagonal matrices

$$\left.\begin{aligned} \boldsymbol{P}^{\phi} &= \boldsymbol{T}_{\phi}\boldsymbol{P} \qquad \boldsymbol{P}^{z} = \boldsymbol{T}_{z}\boldsymbol{P} \\ \boldsymbol{T}_{\phi} &= \mathrm{diag}(\sin\psi_2, \sin\psi_3, \ldots \sin\psi_N) \\ \boldsymbol{T}_{z} &= \mathrm{diag}(\cos\psi_2, \cos\psi_3, \ldots \cos\psi_N) \end{aligned}\right\} \tag{10.9.7}$$

Total residual stresses in the plies then are

$$\left.\begin{aligned} \boldsymbol{\sigma}_{\phi\phi} &= \boldsymbol{S}_{\phi\phi}\boldsymbol{P}^{\phi} + \boldsymbol{S}_{\phi z}\boldsymbol{P}^{z} = \left(\boldsymbol{S}_{\phi\phi}\boldsymbol{T}_{\phi} + \boldsymbol{S}_{\phi z}\boldsymbol{T}_{z}\right)\boldsymbol{P} = \boldsymbol{S}_{\phi}\boldsymbol{P} \\ \boldsymbol{\sigma}_{zz} &= \boldsymbol{S}_{z\phi}\boldsymbol{P}^{\phi} + \boldsymbol{S}_{zz}\boldsymbol{P}^{z} = \left(\boldsymbol{S}_{z\phi}\boldsymbol{T}_{\phi} + \boldsymbol{S}_{zz}\boldsymbol{T}_{z}\right)\boldsymbol{P} = \boldsymbol{S}_{z}\boldsymbol{P} \\ \boldsymbol{S}_{\phi\phi} &= \boldsymbol{S}^{\alpha}_{\phi\phi} + \boldsymbol{S}^{\beta}_{\phi\phi} + \boldsymbol{S}^{\delta}_{\phi\phi} \quad \boldsymbol{S}_{\phi z} = \boldsymbol{S}^{\alpha}_{\phi z} + \boldsymbol{S}^{\beta}_{\phi z} + \boldsymbol{S}^{\delta}_{\phi z} \\ \boldsymbol{S}_{z\phi} &= \boldsymbol{S}^{\alpha}_{z\phi} + \boldsymbol{S}^{\beta}_{z\phi} + \boldsymbol{S}^{\delta}_{z\phi} \quad \boldsymbol{S}_{zz} = \boldsymbol{S}^{\alpha}_{zz} + \boldsymbol{S}^{\beta}_{zz} + \boldsymbol{S}^{\delta}_{zz} \end{aligned}\right\} \tag{10.9.8}$$

When they are resolved on a radial plane, their resultants must vanish.

Final magnitudes of residual ply stresses $\boldsymbol{\sigma}_{\phi\phi}$ and $\boldsymbol{\sigma}_{zz}$ in the completed cylindrical laminate can be found either directly, for a prescribed distribution of prestress magnitudes in individual plies, or by optimization. For example, application of a constant prestress force often generates compressive residual stresses in the interior plies and tensile stresses at the exterior plies. A more favorable, optimized distribution of the P_j magnitudes requires that ply stresses satisfy a certain objective function I and related constraints. The goal can be to minimize only the residual stresses due to fabrication, by demanding that

$$I = \sum_{j=2}^{N}\left[\left(\sigma^{j}_{\phi\phi}\right)^2 + \left(\sigma^{j}_{zz}\right)^2\right] \rightarrow \min. \tag{10.9.9}$$

Constraints imposed on the solution admit only tensile forces $P_j > 0$, and they may include limits imposed on the final residual stresses by a selected ply strength criterion.

In certain cases, the analysis leading to (10.9.9) can be augmented by superposition of the fabrication and load-induced stresses. Prestress force distribution may then be found that minimizes total stresses generated in the cylinder wall by both sources.

It should be noted that effective mandrel stiffness has a significant influence on the final state of residual stress, caused either by constant or optimized prestress forces. Under constant prestress, very stiff mandrels reduce residual stress gradients across wall thickness, while under optimized prestress they reduce analogous prestress force gradients. Relatively compliant mandrels, which may be more common in fabrication of large structures, produce opposite effects. After constant prestress, they leave residual stress gradients, which may reduce or eliminate the

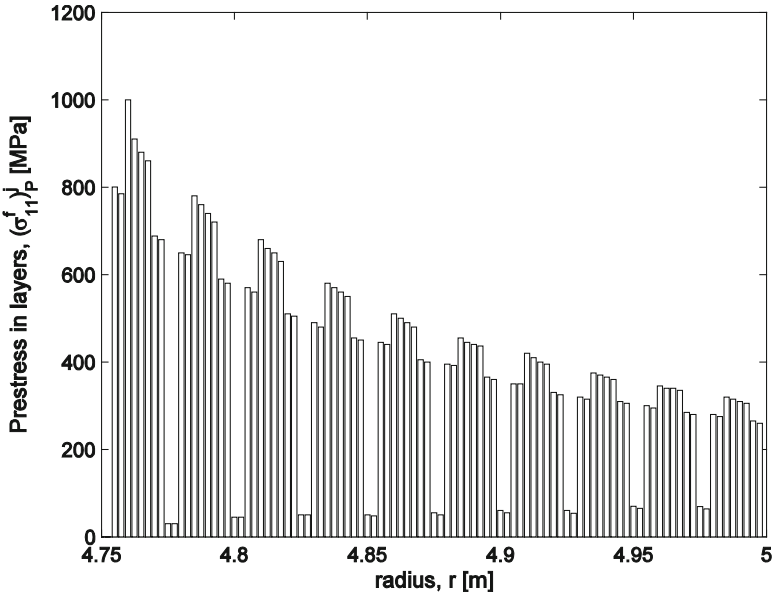

Fig. 10.11 Optimal prestress distribution in a 100 ply wall of a cylindrical pressure vessel (Srinivas et al. 1999)

compressive strength advantage gained by improved fiber alignment. That is not of concern when residual stress magnitudes are controlled by optimized prestress which accounts for mandrel stiffness.

A numerical solution to the optimization problem, based on the active set method of quadratic programming, described by Gill et al. (1981, 1984), was outlined and implemented by Srinivas et al. (1999). The $(0/90/+60/90/-60)_S$ ply layup was designed according to (10.5.8–9) for a carbon/epoxy (AS4/3501-6) material with elastic moduli listed in (10.5.7).

Figure 10.11 shows magnitudes of optimized prestress that were found in the 0.25 m thick wall of a cylindrical pressure vessel with external diameter of 10.0 m, built on rather compliant 0.05 m thick steel mandrel. They drop from the inner to outer plies, in the range 1000 MPa $> \left(\sigma^f_{11}\right)^{(j)}_p >$ 300 MPa, however, when mandrel thickness changed to 1.0 m, the drop range was only 1000 MPa $> \left(\sigma^f_{11}\right)^{(j)}_p >$ 730 MPa. Remarkably, the optimized solution provides a sequence of fiber prestress in the differently oriented plies, which renders the completed cylinder essentially free of residual stresses.

Vanishing prestress magnitudes are present in the zero-degree or longitudinal plies. However, their coupling with the dominant 60° and 90° or hoop plies is weak, hence prestress elevation in longitudinal plies does not have an appreciable effect on stresses in the adjacent plies. The difference of prestress between the 60° and 90° plies is small, and when neglected, the prestress distribution may follow a nearly parabolic curve through wall thickness. The implication is that

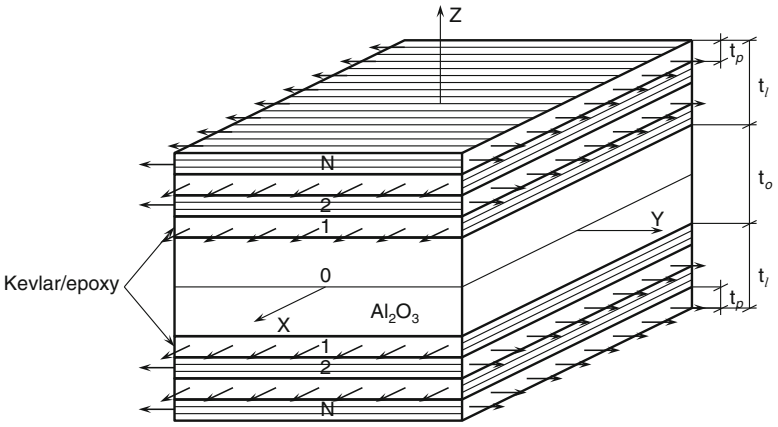

Fig. 10.12 Element of a ceramic plate encapsulated by prestressed Kevlar/epoxy laminate

several direct evaluations of residual stresses caused by slowly or rapidly decreasing parabolic prestress distributions may uncover a satisfactory distribution of final residual stresses, without the need to find an optimized distribution.

10.9.5 Prestress of Ceramic Armor Plates

Fiber prestress may also be used to induce a significant magnitude of biaxial in-plane compression and confinement to armor grade ceramic tiles and plates. In this application, the fiber tows or tapes are wound over opposite edges of a rectangular plate in a 0/90 layup, such that the laminate layers eventually encapsulate the plate. An element of such plate appears on Fig. 10.12. The residual stress in already deposited layers is reduced somewhat by prestress of subsequent layers, and also by matrix creep, hence the prestress forces should be optimized, as described by Suvorov and Dvorak (2001b).

Force equilibrium in the two in-plane directions provides a simple connection between fiber and plate stresses, and of total fiber area required to support a certain biaxial compressive stress in the plate.

The ratio of the plate compression to average tension in each fiber direction of the 0/90 laminate is $\sigma_{11}^{o(C)} / \sigma_{11}^{\ell(T)} = t_\ell / t_o$, the ratio of each laminate face thickness to total thickness of the plate. In the example shown for Kevlar/epoxy laminate in Fig. 10.12, the fiber volume fraction is $c_f = 0.6$, the average stress in each ply direction is $\sigma_{11}^{\ell(T)} \doteq -1.2\,\sigma_{11}^{o(C)}$, hence $t_o/2 \doteq 1.2 t_\ell/2$ and $2t_\ell \doteq 1.7 t_o$. Total thickness of the assembly is $t_o + 2t_\ell = 2.7 t_o$. Area density is found to rise by about 60% above that of the alumina plate. Such increases in bulk and weight could be accommodated in vehicle and equipment armor design.

The ceramic/laminate assembly combines several elements of armor design described, for example, in recent reviews by Gooch (2010) and Chen et al. (2007). It provides for highly pressurized confinement of the ceramic and strong laminate backing, analogous to, among others, the heat-shrunk metal/ceramic tiles assembly described by Hauver et al. (2005) and Malaise et al. (2000) for defeating a long rod penetrator. Moreover, the front plate keeps cracked and shattered parts inside, to suppress crack growth and reduce ejection of pulverized debris which accelerate erosion of projectiles during penetration. That was documented for membrane confinement by Sarva et al. (2007). Finally, the in-plane pressure should provide a significant improvement of dynamic compression and shear strengths of the ceramic. For example, an increase of the former from about 0.4 GPa at no lateral confinement to 1.4 GPa at 230 MPa confinement pressure was observed on Macor by in Hopkinson bar experiments. Similar results were obtained on aluminum nitride, where the maximum shear strength increases linearly until reaches about 3.3 GPa at ∼3.0 GPa of pressure. (Chen and Ravichandran 1996, 1997, 2000). However, viscoelastic prestress release may render the Kevlar/epoxy laminate confinement less effective then that provided by the heat shrunk metal/ceramic constraint.

10.10 Laminates with Transverse Cracks

10.10.1 Cracks in Polymer and Metal Matrix Plies

Slit or tunneling cracks frequently extend on planes aligned with the longitudinal fiber directions and perpendicular to the interfaces of unidirectional composite plies embedded in laminates, as well as in surface plies. Figure 10.13 shows micrograph of a crossection of such cracks in a crossply glass-epoxy composite; it also reveals several dark dry spots between imperfectly bonded fibers in the longitudinal plies, which may serve as initial flaws. Crack extension into adjacent plies is prevented or hindered by the differently oriented fiber walls, resulting in systems of parallel cracks, commonly called transverse cracks, although they extend primarily in the longitudinal fiber direction.

Transverse cracking in polymer matrix plies can be attributed to the generally lower magnitude of the ultimate transverse tensile strain in comparison with the ultimate longitudinal tensile strain, and to the equality of in-plane strains in (10.3.1). Also, to the availability of a free crack path through the matrix, and to the mechanical extension that compensates for the relatively larger transverse thermal contraction of each ply during cooling of the laminate from matrix cure.

In laminates with ductile metal matrices, transverse cracking can be induced by low cycle fatigue of the matrix, and it may be prevented or arrested in certain systems by shakedown to elastic state (Dvorak and Johnson 1980; Dvorak et al.

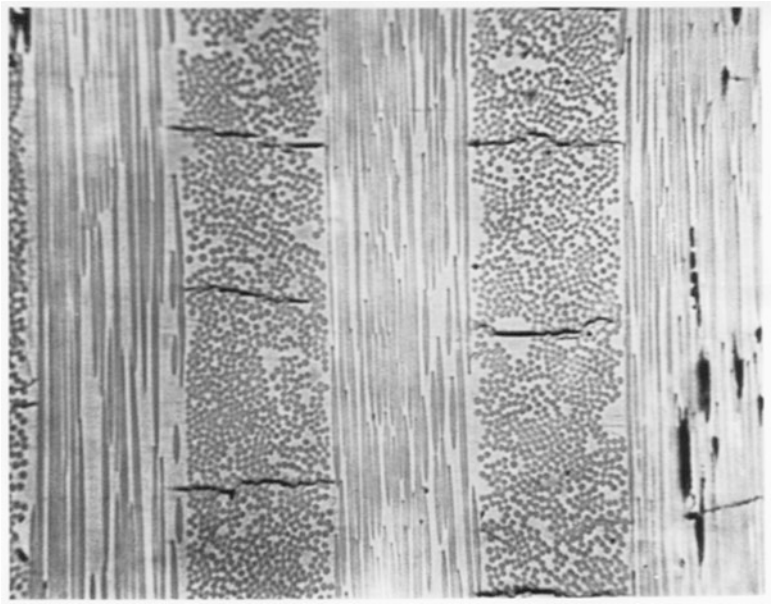

Fig. 10.13 Transverse cracks in plies of a glass/epoxy laminate

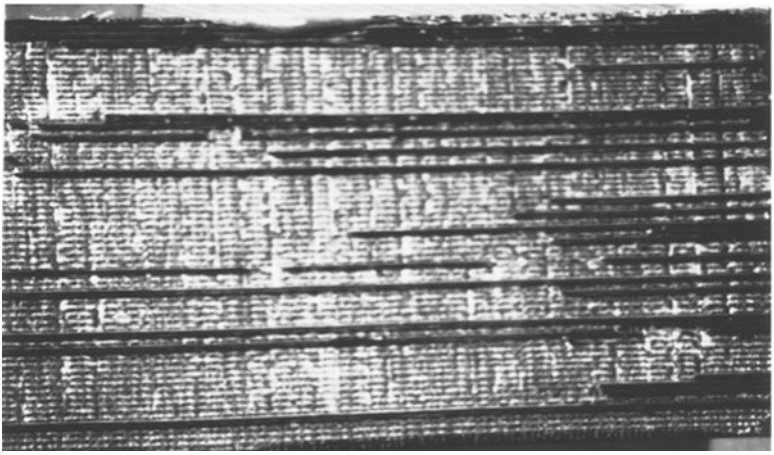

Fig. 10.14 Transverse fatigue cracks in the 90-degree ply of a B/Al laminate (Dvorak and Johnson 1980)

1994). Figure 10.14 presents a system of such low cycle fatigue cracks in a 90-degree ply of a boron/aluminum laminate, revealed by etching away most of the 0-degree fibers of the surface ply.

Transverse cracks usually grow and multiply in suitably orientated plies, under increasing overall strain applied to the laminate, and/or its duration. A schematic

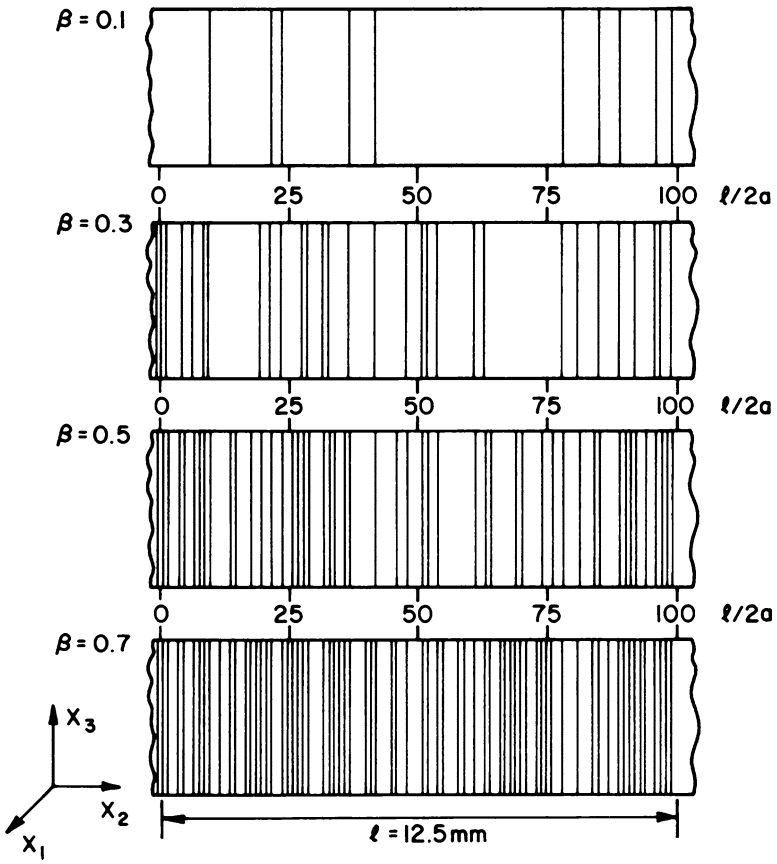

Fig. 10.15 Simulated evolution of transverse crack density in a composite ply

illustration of a damaged ply appears in Fig. 10.15, where the crack lines have been randomly generated at different average crack densities $\beta = 2a/d$, the ratio of ply thickness $2a$ to average distance d between cracks. As long as the individual cracks do not interact at low and medium average densities, $\beta < 0.5$, new cracks may appear when the overall laminate strain, resolved on transverse plane of each ply, becomes sufficiently large to activate additional pre-existing flaws. Availability of such flaws may become exhausted at higher densities, where the strain energy available to drive new cracks through the remaining ligaments is also reduced, by the increasing proximity of existing cracks. That is evident in the figure at $\beta = 0.5$. A certain saturation density is then reached, where no new cracks may appear, and the ply carries near vanishing magnitudes of normal and shear stresses on the transverse plane.

Experimental observation and modeling of cracked plies has attracted interest of many investigators. Bailey et al. (1979), Crossman and Wang (1982), and

Wang (1984), visualized transverse cracks in both glass/epoxy and carbon or graphite/epoxy systems, and were thus able to determine transverse crack densities as functions of applied load.

Modeling of local fields and stiffness changes caused by different crack densities were often focused on $(0/90)_S$ crossply laminates (Garrett and Bailey 1977; Highsmith and Reifsnider 1982; Hashin 1985; Praveen and Reddy 1998; McCartney and Schoeppner 2002; Nairn 2006). Cracks in arbitrary laminate layups have been modeled by Laws et al. (1983), Dvorak et al. (1985) and Dvorak and Laws (1987), who had identified thermoelastic properties of cracked plies with those estimated by the self-consistent method for an infinite transversely isotropic fibrous medium. Gudmundson and Zhang (1993), utilized existing analytical solutions for a row of cracks in an infinite homogeneous isotropic medium. Many numerical studies of transverse cracking have been completed in recent years, as discussed for example by Zhang et al. (2007).

Although theoretical predictions of crack densities as functions of applied strain involve a rich selection of interesting problems, their utility in applications is limited by their dependence on several uncertain parameters. Transverse cracks typically initiate at preexisting flaws, which may have a different distribution of strength magnitudes in each material system. In the absence of direct observation, the strength distribution needs to be assumed, which makes the prediction unreliable. Also required is the distribution of longitudinal ply toughness, which can be measured only once on a single ply. However, actual crack opening displacements, and strain energy released inside a laminate are not generally known. While stiff fiber walls may reduce the crack opening displacement and released energy, they may under different circumstances deflect the crack edge along ply interfaces, form an H crack, and elevate energy release (Cook and Erdogan 1972; Delale and Erdogan 1979; Lu and Erdogan 1983; Gupta et al. 1992; Dvorak and Suvorov 2006).

Moreover, as long as the fibers are not damaged, longitudinal strength and stiffness of a ply are not substantially reduced by transverse cracking, especially in polymer matrix laminates, where matrix contribution to ply and overall properties is relatively small. Therefore, in a conservative approach, the effect of unknown parameters can be circumvented by assuming that each cracked ply may reach a maximum or saturation crack density, and estimate the crack-induced stiffness changes accordingly. Finally, it is well known that transverse cracking can be entirely suppressed by reducing ply thickness such that the tunneling crack cannot release enough strain energy to overcome ply toughness (Dvorak et al. 1985; Dvorak and Laws 1987; Ho and Suo 1993).

Next, we discuss a simple approach to determination of asymptotic limits on ply stiffness when the crack density $\beta \to \infty$, and separately, the effect of ply thickness on the said release of strain energy.

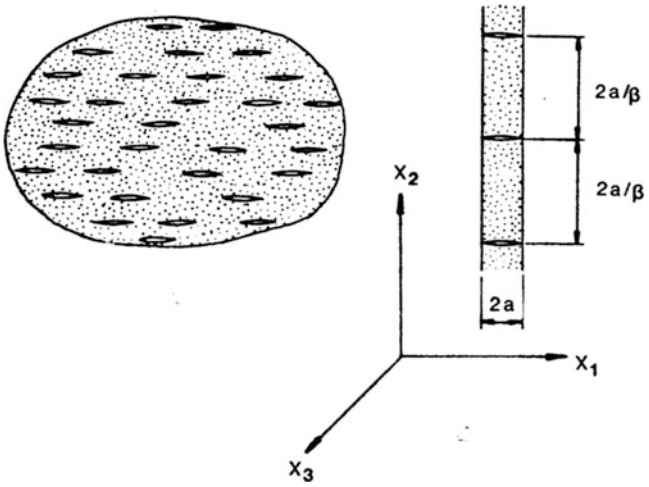

Fig. 10.16 An infinite medium and a fiber ply with aligned slit cracks (Dvorak et al. 1985)

10.10.2 Ply Stiffness at Large Crack Density

An approximate model of a cracked ply was developed by Laws et al. (1983), based on identification of the ply elastic properties with those of an infinite orthotropic medium that contains a certain density of aligned slit cracks of constant width, Fig. 10.16. The latter were estimated by the self-consistent method.

In particular, the self-consistent estimate of overall stiffness and compliance of a two-phase medium of a certain volume V, consisting of a distribution of aligned slit cracks of identical size in a transversely isotropic fibrous matrix $\boldsymbol{L}_0$ was derived by Laws et al. (1983), using the potential and interaction energies of a single crack in an orthotropic medium.

$$\mathcal{V}_0 = -\frac{1}{2}\left(\boldsymbol{\sigma}^0\right)^{\mathrm{T}} \boldsymbol{M}_0 \boldsymbol{\sigma}^0 V \qquad \mathcal{V}_I = -\frac{1}{2}\pi a^2 \eta \left(\boldsymbol{\sigma}^0\right)^{\mathrm{T}} \boldsymbol{\Lambda} \boldsymbol{\sigma}^0 V \qquad [5.4.8]$$

For the medium containing a certain crack density β, the total potential energy is

$$-\frac{1}{2}\left(\boldsymbol{\sigma}^0\right)^{\mathrm{T}} \boldsymbol{M}(\beta) \boldsymbol{\sigma}^0 V = -\frac{1}{2}\left(\boldsymbol{\sigma}^0\right)^{\mathrm{T}} \boldsymbol{M}_0 \boldsymbol{\sigma}^0 V - \frac{1}{2}\pi a^2 \eta \left(\boldsymbol{\sigma}^0\right)^{\mathrm{T}} \boldsymbol{\Lambda}(\beta) \boldsymbol{\sigma}^0 V \qquad (10.10.1)$$

Overall compliance $\boldsymbol{M}$ is then inverted using the identities $\boldsymbol{M}\boldsymbol{L} = \boldsymbol{M}_0 \boldsymbol{L}_0 = \boldsymbol{I}$, to yield the overall stiffness

$$\boldsymbol{M} = \boldsymbol{M}_0 + \bar{\beta}\boldsymbol{\Lambda} \qquad \boldsymbol{L} = \boldsymbol{L}_0 - \bar{\beta}\boldsymbol{L}_0 \boldsymbol{\Lambda} \boldsymbol{L} \qquad (10.10.2)$$

As in (5.4.2), $\bar{\beta} = \pi\beta/4$, and the crack density $\beta = 4\eta a^2 = 2a/d$, the ratio of ply thickness $2a$ to average distance $d = 2a/\beta$ between cracks.

Nonzero coefficients of $\boldsymbol{\Lambda}$ are

$$\left.\begin{aligned} \Lambda_{22} &= \frac{L_{11}\left(\alpha_1^{1/2} + \alpha_2^{1/2}\right)}{L_{11}L_{22} - L_{12}^2} \qquad \Lambda_{44} = \frac{1}{(L_{44}L_{55})^{1/2}} \\ \Lambda_{66} &= \frac{(L_{11}L_{22})^{1/2}\left(\alpha_1^{1/2} + \alpha_2^{1/2}\right)}{L_{11}L_{22} - L_{12}^2} \end{aligned}\right\} \qquad [5.4.6]$$

where $\alpha_1,\ \alpha_2$ are roots of

$$L_{11}L_{66}\alpha^2 - \left(L_{11}L_{22} - L_{12}^2 - 2L_{12}L_{66}\right)\alpha + L_{22}L_{66} = 0 \qquad [4.6.8]$$

These results imply that the overall material symmetry of the cracked medium is that of an orthotropic solid with nine stiffness and compliance coefficients, Table 2.1. In particular, the compliance $\boldsymbol{M}$ in (10.10.1) is changed by the crack density only in M_{22}, M_{44} and M_{66}, in three of the nine components, while the six other compliance coefficients retain their original or undamaged magnitudes M_{ij}^0 of the fibrous matrix. The nonzero coefficients of $\boldsymbol{\Lambda}$ are recast in terms of the compliances M_{ij}^0, and the three variable coefficients of $\boldsymbol{M}$ are found as

$$\left.\begin{aligned} M_{22} &= M_{22}^0 + \bar{\beta}\left[M_{22}M_{33}^0 - \left(M_{23}^0\right)^2\right]\left(\alpha_1^{1/2} + \alpha_2^{1/2}\right)/M_{33}^0 \\ M_{44} &= M_{44}^0 + \bar{\beta}\left(M_{44}M_{55}^0\right)^{1/2} \\ M_{66} &= M_{66}^0 + \bar{\beta}\left[M_{22}M_{33}^0 - \left(M_{23}^0\right)^2\right]^{1/2}\left[M_{11}^0M_{33}^0 - \left(M_{13}^0\right)^2\right]^{1/2}\left(\alpha_1^{1/2} + \alpha_2^{1/2}\right)/M_{33}^0 \end{aligned}\right\} \qquad (10.10.3)$$

Notice that the nonzero coefficient of $\boldsymbol{\Lambda}$ now appear as second terms, in agreement with $\boldsymbol{M}$ in (10.10.2, 10.10.3). An analytical form of M_{44} can be found, and a numerical solution of M_{22} and M_{26} was described together with the thermal and mechanical field averages by Dvorak et al. (1985).

The $\boldsymbol{M}^*$ now denotes the overall compliance of the cracked medium at large values of crack density. It is evaluated from the self-consistent solution for $\beta \to \infty$, which yields

$$M_{22}^*,\ M_{44}^*,\ M_{66}^* \to \infty \qquad (10.10.4)$$

The corresponding overall stiffness is a singular matrix, found at the same limit of β.

$$\left.\begin{aligned} L_{11}^{*} &= M_{33}^{0}/\gamma = L_{11}^{0} - \left(L_{12}^{0}\right)^{2}/L_{22}^{0} \quad L_{12}^{*} = L_{22}^{*} = L_{23}^{*} = 0 \\ L_{13}^{*} &= -M_{13}^{0}/\gamma = L_{13}^{0} - L_{12}^{0}L_{23}^{0}/L_{22}^{0} \quad L_{44}^{*} = L_{66}^{*} = 0 \\ L_{33}^{*} &= M_{11}^{0}/\gamma = L_{33}^{0} - \left(L_{23}^{0}\right)^{2}/L_{22}^{0} \quad L_{55}^{*} = L_{55}^{0} \\ \gamma &= M_{11}^{0}M_{33}^{0} - \left(M_{13}^{0}\right)^{2} \end{aligned}\right\} \tag{10.10.5}$$

These relations provide fairly accurate estimates of ply stiffnesses L_{ij}; $i, j = 1, 2, 3$, at medium and higher crack concentrations.

Local strain field averages in the cracked ply can be divided between those contributed by the cracks and by the fibrous matrix, with the latter possibly containing a thermal strain component. Since the stress field is continuous, the matrix average is equal to the overall average. The self-consistent prediction of the crack accommodation strain is found from the instantaneous compliance $\boldsymbol{M}$ in (10.10.2) under overall applied stress and from $(10.3.3)_2$ where $\mathbf{L}$ is replaced by $\boldsymbol{L}$

$$\bar{\boldsymbol{\varepsilon}}_c = \bar{\beta}\boldsymbol{\Lambda}\boldsymbol{L}(\bar{\boldsymbol{\varepsilon}} - \boldsymbol{m}\Delta\theta) \tag{10.10.6}$$

where $\bar{\boldsymbol{\varepsilon}}$ is the overall strain average and $\boldsymbol{m}$ is the overall thermal vector of the fibrous 'matrix', which is not changed by presence of empty or closed cracks. However, the thermal stress vector $\boldsymbol{l} = -\boldsymbol{L}\boldsymbol{m}$ depends on the variable stiffness of the cracked medium.

In applications of the above results to the ply constitutive relations in (10.1.2–4), it is necessary to change the coordinate system with $x_3 = x_A$ shown in Fig. 10.16 to that used in Sect. 10.1, which identifies the fiber axis with $x_1 = x_A$. The x_2-axis is not affected. The said change is accomplished by taking the above stiffness coefficient L_{33}^{*} to stand for $\left(L_{11}^{*}\right)^{(i)}$ in (10.1.2). Also, $L_{22}^{*} = L_{23}^{*} = 0$ for $\left(L_{22}^{*}\right)^{(i)}$, $\left(L_{12}^{*}\right)^{(i)}$, and L_{44}^{*} for $\left(L_{66}^{*}\right)^{(i)}$. Coefficients L_{13}^{*} and L_{55}^{*} are not included in the plane stress constitutive relation of a ply. In the relations for the global coordinate system, those changes carry over to (10.2.5). Similar changes need to be implemented in the crack accommodation strain (10.10.6).

10.10.3 Effect of Ply Thickness on Energy Release by Transverse Cracks

Evolution of an initial flaw into a crack, which then extends by tunneling along the fiber direction through a ply, is shown schematically in Fig. 10.17. Transverse cracking is the result of accumulation of many stage (3) tunneling cracks in a ply. Of course, those cracks can propagate only if they release enough strain energy to overcome the longitudinal fracture toughness of the ply. Therefore, the energy released per unit length of crack extension depends on ply thickness $2a$, and on stiffnesses of the adjacent plies which may either reduce or enlarge the crack

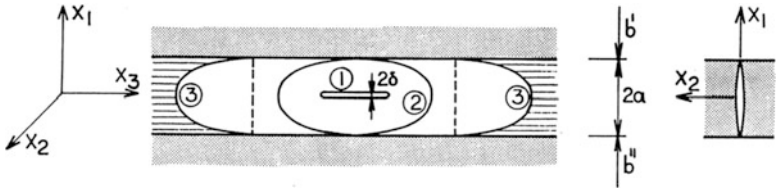

Fig. 10.17 Evolution of an initial flaw (1) into ply crack (2) and tunneling crack (3). (Dvorak and Laws 1987)

opening displacement. Evaluation of the released energy has been the subject of numerous model simulation in the references cited above, which most often favored crossply laminates.

Simplified procedures neglect the effect of adjacent plies, which may be reduced by crack deflection along ply interfaces. In particular, in the model of Fig. 10.16, the focus is on a certain volume fraction of aligned slit cracks in the fibrous matrix. Under overall applied stress $\boldsymbol{\sigma}^0$, the potential energy per unit thickness $|x_3| = 1$ of the cracked medium was found in Sect. 5.4 as $\mathcal{V} = \mathcal{V}_0 + \mathcal{V}_I$

$$\mathcal{V}_0 = -\frac{1}{2}(\boldsymbol{\sigma}^0)^{\mathrm{T}}\boldsymbol{M}_1\boldsymbol{\sigma}^0 V \qquad \mathcal{V}_I = -\frac{1}{2}\pi a^2\eta(\boldsymbol{\sigma}^0)^{\mathrm{T}}\boldsymbol{\Lambda}\boldsymbol{\sigma}^0 V \qquad [5.4.8]$$

and after substitution for Λ_{ij} from (5.4.6), and with $\eta = \beta/4a^2 = \bar{\beta}/(\pi a^2)$, the interaction energy released by tunneling crack of unit length $|x_3| = 1$ is expressed in terms of the ply stress averages $\sigma_2 = \sigma_{22}, \sigma_4 = \sigma_{32}, \sigma_6 = \sigma_{21}$ as

$$\mathcal{V}_I = \frac{1}{2}\bar{\beta}\left[\Lambda_{22}\left(\sigma^0_{22}\right)^2 + \Lambda_{44}\left(\sigma^0_{32}\right)^2 + \Lambda_{66}\left(\sigma^0_{12}\right)^2\right] V \qquad [5.4.9]$$

The interaction energy depends on the second powers of applied ply stress components that activate the three crack opening modes, and on $\bar{\beta} = \pi a^2\eta$, where η is the average number of cracks of length $2a$ in a square of side $2a$. However, actual crack nucleation, multiplication or extension of existing cracks may be observed only in Mode I, and usually not in the other two modes due to surface roughness.

Similar results were found by Ho and Suo (1993) who had also considered periodic and kinked, tunnels and thermal cracking in laminates with isotropic glass or ceramic plies.

Experimental confirmation of the effect of ply thickness on onset of transverse cracking, or first ply failure, was provided by several early experiments by Bailey et al. (1979), Crossman and Wang (1982) and Wang (1984). The results are displayed in Fig. 10.18, where the experimental points at low ply thicknesses were approximated by continuous curves corresponding to constant toughness or energy release values $G_{ic} = \mathcal{V}_I$. The dashed lines approximate the experimental points at high thickness values, and are apparently equal to the transverse strength of single

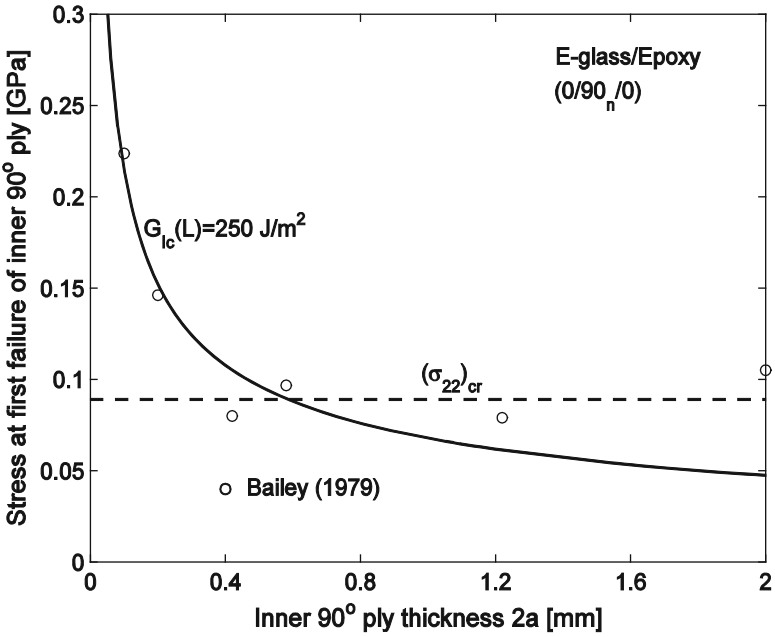

Fig. 10.18 Stress at first ply failure as a function of ply thickness in an E-glass/epoxy crossply laminate (Dvorak and Laws 1987)

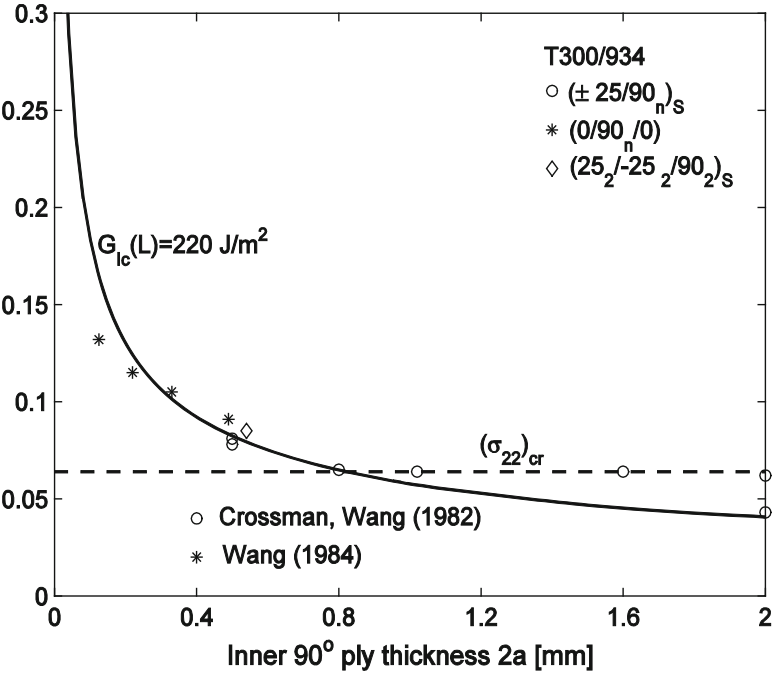

Fig. 10.19 Stress at first ply failure as a function of ply thickness in a carbon/epoxy crossply laminate (Dvorak and Laws 1987)

plies. Intersection of the solid and dashed lines separates thin and thick plies. In the two systems shown, very thin 0.1–0.2 mm thick plies are resistant to transverse cracking. Actual ply thickness that offers similar resistance in a particular composite systems should be confirmed by experiments (Fig. 10.19).

Our unpublished tension and torsion experiments were obtained on glass-epoxy laminated tubes with $(0_2/90/0_2)$, $q = 1.0,\ 2.0,\ 4.0$ layups, all 4.0 in. in diameter. Transverse cracks appeared prior to fiber failure in tension only in tubes containing two and four inner plies, where they reduced only the $E_{22}^{(i)}$ and $L_{22}^{(i)}$ modulus and stiffness. The longitudinal and transverse shear moduli were not affected, since the crack surfaces meandered among the intact fibers, which resisted the crack opening displacement of the two faces in both longitudinal and transverse modes. For the same reason, torsion loads did not produce or extend existing transverse cracks at zero tension, but they eventually caused extensive interface delamination. However, no cracks were observed in tubes containing only single 90-degree plies, at $q = 1.0$. Those had experienced only fiber failure in the 0-degree plies, without any transverse cracks or visible ply delamination.

Chapter 11
Elastic – Plastic Solids

This chapter provides a short introduction to constitutive relations for materials that exhibit incremental elastic-plastic deformation in response to an applied loading path which extends beyond their initial yield surface. In a certain sense, it is analogous to Chap. 2 on Anisotropic Elastic Solids, with which it shares the results pertaining to isotropic elasticity. Moreover, the instantaneous tangential stiffness or compliance matrices may have as many as 21 nonzero coefficients, as in triclinic elastic materials. In preparation for Chap. 12, attention is focused on those parts of incremental plasticity theory that are useful in modeling of metal matrix composites.

All derivations are executed in tensorial component notation. Final results are converted into matrix notation suitable for numerical evaluations. More complete expositions of the subject appear in one of many books on phenomenological theories of plasticity, for example, in Hill (1950), who also describes early development of the field, or in Drucker (1967) and Lubliner (1990). A comprehensive treatment of modern plasticity appears in the monograph by Jirasek and Bazant (2002). Research efforts that connect overall response to microstructural deformation mechanisms are described by Dawson (2000), Hutchinson (2000) and McDowell (2000), and in many later publications.

11.1 Yield and Loading Surfaces, Normality and Convexity

A material point or a certain volume of a homogeneous, isotropic elastic material is initially free of stress and any strain. When subjected to a uniform stress σ_{ij}, this material may exhibit elastic and plastic deformation that both evolve along a prescribed loading path. The elastic part of the deformation is always governed by the constitutive relations described in Sect. 2.2.8 and its magnitude is proportional to σ_{ij}. Plastic deformation is described by entirely different rules, that can be divided

G.J. Dvorak, *Micromechanics of Composite Materials*, Solid Mechanics and Its Applications 186, DOI 10.1007/978-94-007-4101-0_11,

into three groups. (a) Initial yield and subsequent loading surfaces that surround the part of the applied stress space where the material deforms only elastically. (b) Convexity and normality conditions that indicate the shape of the loading surface and the direction of the plastic strain increment vector, caused by application of a stress increment directed toward the exterior of the current loading surface. (c) Hardening and flow rules that govern evolution of size, shape and position of the loading surfaces, and of plastic strain increment magnitudes during active plastic loading. Supported by the early experiments by Bridgman (1952) and by many later results, the theories discussed below neglect the contribution, if any, of the isotropic plastic strain component, $\varepsilon^p_{kk} = 0$, hence $\varepsilon^p_{ij} = e^p_{ij}$, the plastic strain deviator. However, elastic dilatation continues as part of the elastic deformation that accompanies plastic flow, and during unloading into the interior of the current yield surface from the most recent loading point.

In contrast to elastic behavior, which is well defined by constant moduli, plastic deformation is described by phenomenological theories which may include assumed or hidden variables, and utilize material parameters whose values depend on the applied loading path. Material characterization is limited to experiments in uniaxial or biaxial tension and/or compression, which may be augmented by torsion of pressurized thin-walled tubes. In most applications the actual loading path is more complex than that used in the characterization, hence agreement between theoretical predictions and observed behavior is often far from perfect.

11.1.1 Mises Yield and Loading Surfaces

Plastic deformation is caused by a state of stress that reaches an *initial yield surface* or a subsequent *loading surface* in the six-dimensional stress space σ_{ij}, or in the deviatoric stress space $s_{ij} = \sigma_{ij} - (1/3)\sigma_{kk}\delta_{ij}$. In particular, the Mises loading surface frequently adopted for metals is

$$f(s_{ij}, a_{ij},\ Y(\varepsilon^p_{eq}, \theta)) = \frac{1}{2}(s_{ij} - a_{ij})(s_{ij} - a_{ij}) - \frac{1}{3}Y^2(\varepsilon^p_{eq}, \theta) \leq 0 \qquad (11.1.1)$$

where the first term is the second invariant $\tilde{J}_2 = \tilde{s}_{ij}\tilde{s}_{ij}/2$ of the deviatoric stress tensor $\tilde{s}_{ij} = (s_{ij} - a_{ij})$, the s_{ij} is the current loading point, a_{ij} describes the position of the current center of the surface, and $Y(\varepsilon^p_{eq},\ \theta)/\sqrt{3} = \tau_0(\varepsilon^p_{eq},\ \theta)$ are the current yield stresses in simple tension, and shear. Both a_{ij} and Y or τ_0 have certain initial magnitudes at the onset of first plastic deformation. Those usually change during plastic flow, according to different hardening rules.

Among the several definitions of the yield stress in frequent use, we adopt the stress magnitude which causes first deviation from linearly elastic response, determined by back extrapolation to zero plastic strain, Fig. 12.7. The material may have been exposed to previous periods of plastic straining, possibly followed

by elastic unloading. The yield stress may depend on temperature θ, and on the invariant of accumulated equivalent plastic strain ε^p_{eq}, defined in (11.1.3). In addition to those appearing in (11.1.1), the loading surface may also depend on certain internal variables, which represent various processes that may be observed on the microscale, but are beyond the scope of direct measurement or modeling on the macroscale.

Convenient forms of J_2 and its derivatives are

$$\left.\begin{aligned} J_2 &= \frac{1}{2}s_{ij}s_{ij}=\frac{1}{2}(s_{11}^2+s_{22}^2+s_{33}^2+2s_{23}^2+2s_{31}^2+2s_{12}^2)\\ J_2 &= \frac{1}{6}[(\sigma_{11}-\sigma_{22})^2+(\sigma_{22}-\sigma_{33})^2+(\sigma_{33}-\sigma_{11})^2]+\sigma_{23}^2+\sigma_{31}^2+\sigma_{12}^2\\ \frac{\partial J_2}{\partial \sigma_{ij}} &= \frac{\partial J_2}{\partial s_{ij}} = [s_{11},\ s_{22},\ s_{33},\ 2s_{23},\ 2s_{31},\ 2s_{12}]^{\mathrm{T}}\\ \mathrm{d}J_2 &= \frac{\partial J_2}{\partial s_{ij}}\mathrm{d}s_{ij} = s_{ij}\mathrm{d}s_{ij} \end{aligned}\right\} \tag{11.1.2}$$

Similar expressions describing yield and loading surfaces can be written in principal stress components, which are normal stresses on principal planes of σ_{ij}, where shear stresses vanish. Under isotropic stress, $\sigma_{ij}=\sigma_{11}=\sigma_{22}=\sigma_{33}$, $J_2=0$, hence the Mises yield criterion does not depend on the isotropic part of the stress tensor. This feature offers a simple image of the Mises surface, as a circular cylinder of radius $\rho_0=(\sqrt{2/3})\,Y$, with the hydrostatic axis in the principal stress space. In simple tension σ_{11}, $J_2=\sigma_{11}^2/3$, and $\mathrm{d}J_2=(2/3)\sigma_{11}\mathrm{d}\sigma_{11}=(2J_2/\sigma_{11})\mathrm{d}\sigma_{11}$.

The Mises yield criterion is often interpreted in terms of a critical magnitude of the octahedral shear stress $\tau^2_{\mathrm{oct}}=2J_2/3$, resolved on planes which form a regular octahedron in the 3D principal stress space, with normals $\mathbf{n}=(3)^{-1}(\pm\mathbf{e}_1,\ \pm\mathbf{e}_2,\ \pm\mathbf{e}_3)$. While the τ_{oct} remains constant at all points of the yield or loading surface, the principal stress directions and the said normals change from point to point along the surface contour. Therefore, if τ_{oct} activates a certain slip system related to the current alignment of the principal stress axes, then each point on the yield surface should be associated with a different slip system. This association may prove useful in selecting a suitable hardening rule. A less insightful or scalar interpretation of the Mises yield condition is based on a critical magnitude of the distortional part of the strain energy (2.1.5), which is equal to $\mathcal{W}_D=s_{ij}e_{ij}/2=s_{ij}s_{ij}/(4G)=J_2/(2G)$.

As long as the time rate of plastic deformation is sufficiently slow, with typical dwell periods of few minutes, material response appears not to depend on the loading rate. Under such circumstances assumed here, time derivatives of stress and strain indicated by top dots $(\dot{\cdot})$, can be used to denote their increments along a loading path.

The *equivalent or effective plastic strain* ε^p_{eq} in (11.1.1) is an integral of invariant plastic strain increments $\dot{\varepsilon}^p_{ij}=\dot{e}^p_{ij}$, accumulated during the total 'time' $0\le\tau\le T$

of possibly intermittent plastic deformation that starts at a certain reference state. The *equivalent stress* σ_{eq} is defined by the applied stress deviator components s_{ij}

$$\varepsilon^p_{eq} = \int_0^T \dot{\varepsilon}^p_{eq} \mathrm{d}\tau = \int_0^T \left(\frac{2}{3} \dot{\varepsilon}^p_{ij} \dot{\varepsilon}^p_{ij} \right)^{1/2} \mathrm{d}\tau \quad \sigma_{eq} = \left(\frac{3}{2} s_{ij} s_{ij} \right)^{1/2} \tag{11.1.3}$$

Under both uniaxial and multiaxial stress states, these two evolving invariants trace an *equivalent stress/plastic strain curve* for a given material subjected to a prescribed loading path. The numerical factors are selected such that in simple tension, $\varepsilon^p_{eq} = \varepsilon^p_{11}$ and $\sigma_{eq} = \sigma_{11}$, indicating logarithmic strain and true stress, which approximately coincide with engineering strain components (1.1.11) at the small deformations assumed herein.

Any incremental change in plastic strain yields a positive increment $\dot{\varepsilon}^p_{eq} > 0$, regardless of the actual strain sign, hence ε^p_{eq} is a measure of a *cumulative* plastic strain. The σ_{eq} is also positive under similar circumstances. However, the loading path in stress space may include unloading excursions into the interior of the current loading surface, followed by loading periods, as in cyclic loading. The equivalent stress is equal to the current yield stress at temperature θ only during each plastic loading period, $\sigma_{eq} = Y(\varepsilon^p_{eq}, \theta)$. Therefore, the equivalent stress/plastic strain curve is effectively generated under ε^p_{eq} strain control. When thermal changes are applied as secondary loads, the equivalent stress/plastic strain relation becomes a function of the current temperature θ, measured from a certain reference value θ_0.

The time derivative of the equivalent stress/plastic strain curve defines the *plastic tangent modulus*

$$H(\varepsilon^p_{eq}, \theta) = [\dot{\sigma}_{eq} - (\partial Y / \partial \theta) \dot{\theta}] / \dot{\varepsilon}^p_{eq} \tag{11.1.4}$$

which provides the slope of a tangent to this curve at the current $\sigma_{eq} = Y(\varepsilon^p_{eq}, \theta)$. In the above formula, the yield stress is assumed to decrease, $\partial Y / \partial \theta < 0$ with $\dot{\theta} > 0$, causing a contraction of the yield surface and amplification of the effective stress increment. Notice that $H(\varepsilon^p_{eq}, \theta)$ is distinct from the *plastic secant modulus* $H_S = \sigma_{eq} / \varepsilon^p_{eq}$ that connects the total equivalent quantities in certain plasticity theories, but is not used in the incremental theory described here.

Apart from the elastic moduli, the $Y(\varepsilon^p_{eq}, \theta)$ and $H(\varepsilon^p_{eq}, \theta)$ are among very few measurable parameters that represent material response under inelastic deformation. In most applications, $H(\varepsilon^p_{eq}, \theta)$ is derived from a tension or compression test, where $\sigma_{eq} = \sigma_{11}$ and $\varepsilon^p_{eq} = \varepsilon^p_{11}$, or it is assumed to follow a certain form, e.g., a power-law. Whenever possible the plastic tangent modulus should be evaluated with regard to the expected loading regime. Among the several different theories that have been proposed to adaptively estimate $H(\varepsilon^p_{eq}, \theta)$ under combined multiaxial loading, a suitable choice is offered by the Dafalias and Popov (1976) two-surface model, described briefly in Sect. (11.2.4) below.

The sign of plastic tangent modulus is often used to classify three different types of inelastic material response. $H = 0$ describes perfectly plastic or non-hardening materials. Linear work hardening is implied by a constant $H > 0$, and the more common nonlinear work hardening by $H = H(\varepsilon^p_{eq},\theta) > 0$. Strain softening, often caused by local cavitation or other distributed damage in the material, is indicated by $H = H(\varepsilon^p_{eq},\theta) < 0$. Other symbols, such as $E^p_{\tan}$ or h have also been used to denote H in technical papers on plasticity.

11.1.2 Normality and Convexity of the Loading Surface

Application of stress increments $\dot{\sigma}_{ij}$ or $\dot{s}_{ij}$ along a loading path directed to the exterior of the initial or current yield surface is possible in materials where the current yield stress is elevated during plastic deformation. The initial yield surface evolves into a *loading surface* which may change shape and/or position, such that it always contains the current loading point. Loading points located outside the current loading surface can not be reached in time-independent plasticity, but they are admitted in viscoplasticity theories for time-dependent inelastic deformations, applied to metals at elevated temperatures. Such theories have been described, for example, by Chaboche (1989), Freed et al. (1991), Freed and Walker (1993), Lemaitre and Chaboche (1990) and Krempl (2000).

Finding the loading point on a current loading surface is assured by satisfying the *consistency condition* where

$$\left.\begin{aligned} \dot{f} &= \frac{\partial f}{\partial \tilde{s}_{ij}}\dot{\tilde{s}}_{ij} - \frac{\partial f}{\partial Y}\dot{Y} = \tilde{s}_{ij}\dot{\tilde{s}}_{ij} - \frac{2}{3}Y\dot{Y} \le 0 \\ \tilde{s}_{ij} &= s_{ij} - a_{ij} \qquad \dot{Y} = \left[\frac{\partial Y}{\partial \varepsilon^p_{eq}}\dot{\varepsilon}^p_{eq} + \frac{\partial Y}{\partial \theta}\dot{\theta}\right] \end{aligned}\right\} \tag{11.1.5}$$

Since $Y = \sigma_{eq}$ during plastic loading, the expression for $\dot{Y}$ above and in (11.1.4) suggest that $\partial Y/\partial \varepsilon^p_{eq} = H(\varepsilon^p_{eq},\ \theta)$.

Material responses described above by the plastic tangent modulus H are reflected in the following criteria defining *plastic loading, neutral loading and unloading* with respect to the current loading surface.

$$\begin{aligned} &\dot{\varepsilon}^p_{ij} \neq 0 \quad \text{if and only if } f = 0, \quad \dot{f} > 0 \\ &\dot{\varepsilon}^p_{ij} = 0 \quad \text{if } f \le 0 \text{ and } \dot{f} < 0, \quad \text{or if } f = 0 \text{ and } \quad \dot{f} = 0 \end{aligned} \tag{11.1.6}$$

These criteria are sometimes interpreted as the Kuhn and Tucker (1951) conditions associated with the solution of a convex linear programming problem.

Notice that unloading and reloading to the current loading surface, at $f \le 0$ and $\dot{f} < 0$, elicits only an elastic response. The same is formally true during neutral loading, when $f = 0$ and $\dot{f} = 0$, and the loading vector coincides with

a tangent to the loading surface. However, experiments often show that under such circumstances, the loading surface tends to translate away from a neutral loading point, to reposition the loading vector to a nearby regular loading point.

As long as the total strain is of infinitesimal magnitude, it can be additively decomposed into elastic and inelastic or plastic parts. The total strain is then evaluated as the integral of the increments $\dot{\boldsymbol{\varepsilon}} = \dot{\boldsymbol{\varepsilon}}^e + \dot{\boldsymbol{\varepsilon}}^\theta + \dot{\boldsymbol{\varepsilon}}^p$ taken along a thermo-mechanical loading path, as shown in (11.1.11) below. The elastic and thermal strain increments $\dot{\boldsymbol{\varepsilon}}^e = \boldsymbol{L}\dot{\boldsymbol{\sigma}}, \dot{\boldsymbol{\varepsilon}}^\theta = \boldsymbol{m}\dot{\theta}$ are derived using the stiffness and thermal strain vector or expansion coefficient of an *isotropic* material in Table 8.1. Coefficients of the plastic strain increment vector $\dot{\boldsymbol{\varepsilon}}^p$ follow from one of the flow rules described below. They are constrained by the plastic incompressibility assumption $\dot{\varepsilon}^p_{kk} = 0$, hence they contribute only to the deviatoric components the total strain increment.

The *direction* of the plastic strain increment during loading follows from the *Drucker postulate* (1950, 1951). Consider an elastic loading/unloading cycle applied to a material point, or a small volume of material, by a certain device that creates there a uniform state of stress $\boldsymbol{\sigma}^*$. This stress is inside the current loading surface so that $f \leq 0$. Additional stress $(\boldsymbol{\sigma} - \boldsymbol{\sigma}^*)$ is applied by the device inside the elastic domain, until $\boldsymbol{\sigma}$ reaches a point on the current loading surface, $f = 0$, while other variables in (11.1.1) are held constant. Next, an 'external agency', not connected to the loading device, is called upon to apply and then remove a small stress increment $\pm\Delta\boldsymbol{\sigma}$ directed to the exterior of the current loading surface, such that $f = 0$, $\dot{f} > 0$. This generates both an elastic strain increment, which disappears upon removal of the stress increment, $\Delta\boldsymbol{\varepsilon}^e = +\Delta\boldsymbol{\varepsilon}^e - \Delta\boldsymbol{\varepsilon}^e = 0$, and a plastic strain increment $\Delta\boldsymbol{\varepsilon}^p$, that remains as a total strain increment, $\Delta\boldsymbol{\varepsilon} = \Delta\boldsymbol{\varepsilon}^p$. The elastic part of the loading cycle is completed when the loading device returns the stress state back to $\boldsymbol{\sigma}^*$, not necessarily along the same path.

The *Drucker postulate* requires the total work performed by the loading device and by the 'external agency' along the closed path $0 \leq \tau \leq T$ to be positive

$$\mathcal{W} = \mathcal{W}^e + \mathcal{W}^p = \int_0^T [\sigma_{ij}(\tau) - \sigma^*_{ij} + \Delta\sigma_{ij}][\varepsilon_{ij}(\tau) + \Delta\varepsilon_{ij}]\mathrm{d}\tau \geqslant 0 \tag{11.1.7}$$

where the equality holds only when $\dot{\varepsilon}^p_{ij} = 0$. Since $\sigma_{ij}(0) = \sigma_{ij}(T)$ and $\varepsilon^e_{ij}(0) = \varepsilon^e_{ij}(T)$

$$\left.\begin{aligned} \mathcal{W}^e &= \int_0^T [\sigma_{ij}(\tau) - \sigma^*_{ij} + \Delta\sigma_{ij}][\varepsilon^e_{ij}(\tau) + \Delta\varepsilon^e_{ij}]\mathrm{d}\tau = 0 \\ \mathcal{W} = \mathcal{W}^p &\doteq \int_0^T [\sigma_{ij}(\tau) - \sigma^*_{ij}]\Delta\varepsilon^p_{ij}\mathrm{d}\tau \geqslant 0 \end{aligned}\right\} \tag{11.1.8}$$

where $\Delta\sigma_{ij} \ll (\sigma_{ij} - \sigma^*_{ij})$ is neglected. For $\Delta\boldsymbol{\sigma} \to \dot{\boldsymbol{\sigma}}$, $\Delta\boldsymbol{\varepsilon}^p \to \dot{\boldsymbol{\varepsilon}}^p$, the above equations provide the following work inequalities

$$\dot{\sigma}_{ij}(\dot{\varepsilon}^e_{ij} + \dot{\varepsilon}^p_{ij}) > 0 \quad \sigma_{ij}\dot{\varepsilon}^p_{ij} \geqslant 0 \quad (\sigma_{ij} - \sigma^*_{ij})\dot{\varepsilon}^p_{ij} \geqslant 0 \tag{11.1.9}$$

Materials that satisfy (11.1.9) are *stable in Drucker's sense*.

The last inequality also follows from the *maximum dissipation postulate*, first proposed by von Mises (1928), which plays an important role in plasticity theory. In particular, when regarded as a scalar product $(\boldsymbol{\sigma} - \boldsymbol{\sigma}^*) \bullet \dot{\boldsymbol{\varepsilon}}^p \geqslant 0$ of the stress vector inside the yield surface and the plastic strain increment, the inequality suggests that the *yield surface must be convex*, and that the direction of the *plastic strain increment coincides with a normal to the yield surface*. This property is typical of an associative flow rule, or associative plasticity, exhibited by most but not all materials or plasticity theories. It applies only at a material point or in a uniformly deformed homogeneous material volume.

Definition of the direction of the plastic strain increment vector $\dot{\boldsymbol{\varepsilon}}^p$ implies a superposition of a six-dimensional engineering strain space on the coaxial deviatoric stress space. It states that the unit normal n_{ij} to the yield surface in the stress space coincides with the direction of the $\dot{\boldsymbol{\varepsilon}}^p$. In the tensorial component notation, the direction of n_{ij} is interpreted as the derivative $\partial J_2/\partial\sigma_{ij} = \partial J_2/\partial s_{ij} = s_{ij}$ of J_2 with respect to the nine-dimensional vector with components s_{ij}. After scaling to unity

$$n_{ij} = \frac{\partial J_2/\partial s_{ij}}{\sqrt{s_{ij}s_{ij}}} = \frac{s_{ij}}{\sqrt{2J_2}} \qquad n_{ij}n_{ij} = 1 \tag{11.1.10}$$

The normality and convexity conditions are also satisfied at singular loading points or corners of the loading surface, created by several intersecting branches that represent uniformly deforming subvolumes. At such points, the plastic strain increment vector is the resultant of the several subvolume contributions, and it is confined inside a cone of normals to the intersecting branches (Hill 1967). For example, as will be shown in Chap. 12, such branches appear in the overall stress space of composite materials with elastic-plastic matrices, as projections of many local yield surfaces at different points of a subdivided nonuniform deformation field.

Constitutive relations for elastic-plastic deformation described by the Mises or J_2 theory, also called the Prandtl-Reuss equations, are usually written as

$$\left.\begin{aligned} \dot{\varepsilon}_{ij} &= \dot{\varepsilon}^e_{ij} + \dot{\varepsilon}^\theta_{ij} + \dot{\varepsilon}^p_{ij} = M_{ijkl}\dot{\sigma}_{kl} + m_{ij}\dot{\theta} + \dot{\lambda}\, s_{ij} \\ \dot{\sigma}_{ij} &= L_{ijkl}(\dot{\varepsilon}_{kl} - \dot{\varepsilon}^\theta_{kl} - \dot{\varepsilon}^p_{kl}) = L_{ijkl}(\dot{\varepsilon}_{kl} - m_{kl}\dot{\theta} - \dot{\lambda}\, s_{kl}) \end{aligned}\right\} \tag{11.1.11}$$

where L_{ijkl} and M_{ijkl} are elastic stiffness and compliance tensors, which satisfy $L_{ijkl}M_{klmn} = I_{ijmn}$, and m_{ij} is the thermal strain tensor, all for an isotropic solid. The normality condition is satisfied by the coaxiality of n_{ij} and $s_{ij} = (2J_2)^{-1/2}n_{ij}$. The scalar multiplier $\dot{\lambda}$ is proportional to the magnitude of $|\,\dot{\varepsilon}^p_{ij}\,|$, and $\dot{\theta}$ is a temperature increment. Specific forms of $\dot{\varepsilon}^p_{ij} = \dot{\lambda}s_{ij}$ related to different hardening rules are described next.

11.2 Hardening and Flow Rules

During plastic loading $(11.1.6)_1$, the consistency condition (11.1.5) is satisfied by changes in the shape and/or position of the loading surface according to certain isotropic and/or kinematic hardening rules. Any current loading point $\sigma_{ij} + \dot{\sigma}_{ij}$ or $s_{ij} + \dot{s}_{ij}$ on the prescribed loading path must lie on the loading surface, and unloading from the last loading point takes place along a path that lies entirely within the current loading surface, where material response is determined by the original elastic moduli. Reloading to the last or to any other point on the current loading surface also causes only elastic strains. A loading path that extends beyond the current loading surface must be accompanied by expansion and/or translation of the surface such that it contains the loading point. This accommodation process is directed by several hardening rules, with associated definitions of the magnitudes and directions of the plastic strain increments at each loading point of a prescribed stress path.

11.2.1 Isotropic Hardening and Flow Rules

Isotropic hardening implies expansion of the initial yield surface, in which its original shape is retained but the yield stress is allowed to increase as a certain function of accumulated equivalent plastic strain ε^p_{eq}, or of the total work dissipated by plastic deformation. Both criteria yield similar predictions of material response. The center of the loading surface does not translate, hence $a_{ij} = 0$ and the loading surface can only expand, according to (11.1.1)

$$f(s_{ij}, Y(\varepsilon^p_{eq}, \theta)) = \frac{1}{2} s_{ij} s_{ij} - \frac{1}{3} Y^2(\varepsilon^p_{eq}, \theta) \leq 0 \tag{11.2.1}$$

The plastic strain increment $\dot{\varepsilon}^p_{ij} = \dot{\lambda} s_{ij}$ in (11.1.11) is derived as a vector normal to this yield surface, such that its invariant $\dot{\varepsilon}^p_{eq}$, defined in (11.1.3) satisfies (11.1.4), while $\sigma_{eq} = Y(\varepsilon^p_{eq}, \theta)$. The current value of the plastic tangent modulus $H(\varepsilon^p_{eq}, \theta)$ determines the rate of change of the yield stress, or of the expansion of the yield surface, at the current loading point.

The scalar multiplier $\dot{\lambda}$ can be evaluated by several procedures. A very simple one employs definitions of $\dot{\varepsilon}^p_{eq}$ and σ_{eq} in (11.1.3), written as

$$\dot{\varepsilon}^p_{eq} = \left(\frac{2}{3} \dot{\varepsilon}_{ij} \dot{\varepsilon}_{ij} \right)^{1/2} = \dot{\lambda} \left(\frac{2}{3} s_{ij} s_{ij} \right)^{1/2} = \frac{2}{3} \dot{\lambda} \sigma_{eq} \tag{11.2.2}$$

According to (11.1.4), $H(\varepsilon^p_{eq}, \theta) \dot{\varepsilon}^p_{eq} = \dot{\sigma}_{eq} - (\partial Y / \partial \theta) \dot{\theta}$, hence

$$\dot{\lambda} = \frac{3}{2 H(\varepsilon^p_{eq}, \theta) \sigma_{eq}} \left[\dot{\sigma}_{eq} - \frac{\partial Y}{\partial \theta} \dot{\theta} \right] \tag{11.2.3}$$

Moreover, whether found under simple or combined, monotonic or cyclic loading, the tangent plastic modulus $H(\varepsilon^p_{eq}, \theta)$ also describes material response under simple tension, where

$$\left.\begin{aligned} &\sigma_{11} \neq 0 \Rightarrow s_{11} = 2\sigma_{11}/3, \quad s_{22} = s_{33} = -\sigma_{11}/3 \quad J_2 = \sigma_{11}^2/3 \\ &\sigma_{11} = \sigma_{eq} \quad \dot{\varepsilon}^p_{11} = \dot{\varepsilon}^p_{eq} \quad \dot{\sigma}_{11} = H(\varepsilon^p_{eq},\theta)\dot{\varepsilon}^p_{11} + (\partial Y/\partial\theta)\dot{\theta} \end{aligned}\right\} \tag{11.2.4}$$

Then

$$\left.\begin{aligned} \dot{\varepsilon}^p_{11} = \dot{\lambda} s_{11} = \frac{2}{3}\dot{\lambda}\sigma_{11} = \frac{1}{H(\varepsilon^p_{eq},\theta)}\left[\dot{\sigma}_{11} - \frac{\partial Y}{\partial\theta}\dot{\theta}\right] \\ \Rightarrow \dot{\lambda} = \frac{3}{2H(\varepsilon^p_{eq},\theta)\sigma_{eq}}\left[\dot{\sigma}_{eq} - \frac{\partial Y}{\partial\theta}\dot{\theta}\right] \end{aligned}\right\} \tag{11.2.5}$$

This derivation of $\dot{\lambda}$ for isotropic hardening can be extended to any loading path, with the same result written in terms of the equivalent variables. Of course, different $H(\varepsilon^p_{eq}, \theta)$ values may be encountered during loading along dissimilar loading paths applied to a given elastic-plastic material.

Frequently used but more laborious way to find $\dot{\lambda}$ relies on the consistency equation for the isotropic hardening yield function (11.1.12), which follows from (11.1.5) with $a_{ij} = 0$, $s_{ij} = \tilde{s}_{ij}$.

$$\dot{f} = \frac{\partial f}{\partial s_{ij}}\dot{s}_{ij} - \frac{\partial f}{\partial Y}\dot{Y} = s_{ij}\dot{s}_{ij} - \frac{2}{3}Y\left[\frac{\partial Y}{\partial\varepsilon^p_{eq}}\dot{\varepsilon}^p_{eq} + \frac{\partial Y}{\partial\theta}\dot{\theta}\right] \leq 0 \tag{11.2.6}$$

Here we only need to show that the $\dot{\lambda}$ derived above satisfies this equation. Using again $\dot{\varepsilon}^p_{eq} = (2/3)\dot{\lambda}\sigma_{eq}$, and $H(\varepsilon^p_{eq},\theta) = [\dot{\sigma}_{eq} - (\partial Y/\partial\theta)\dot{\theta}]/\dot{\varepsilon}^p_{eq} = (\partial Y/\partial\varepsilon^p_{eq})$ from (11.1.4), we find after some algebra that for $\dot{f} \to 0^+$

$$\dot{\lambda} = \frac{9(s_{ij}\dot{s}_{ij})/(2\sigma_{eq}) - 3(\partial Y/\partial\theta)\dot{\theta}}{2H(\varepsilon^p_{eq},\theta)\sigma_{eq}} = \frac{3}{2H(\varepsilon^p_{eq},\theta)\sigma_{eq}}\left[\dot{\sigma}_{eq} - \frac{\partial Y}{\partial\theta}\dot{\theta}\right] \tag{11.2.7}$$

where according to (11.1.12), $\sigma_{eq} = Y = \sqrt{3J_2}$, and $\dot{\sigma}_{eq} = \sqrt{3/(4J_2)}\; s_{ij}\dot{s}_{ij}$ during plastic loading. This provides another form of the consistency equation

$$\dot{f} = s_{ij}\dot{s}_{ij} - \frac{2}{3}\sigma_{eq}\dot{\sigma}_{eq} \leq 0 \tag{11.2.8}$$

A substitution for $s_{ij}\dot{s}_{ij}$ into (11.2.7) then confirms the last equality there, which reproduces (11.2.3) and (11.2.5).

A convenient form of the plastic strain increment can be found using the above expressions for $\dot{\lambda}$, σ_{eq} and $\dot{\sigma}_{eq}$, and the unit normal to the yield surface. As shown

in (11.1.10), the unit normal is written in the tensorial component notation as $n_{ij} = s_{ij}/\sqrt{2J_2}$. The plastic strain increment is

$$\dot{\varepsilon}^p_{ij} = \dot{\lambda} s_{ij} = \frac{3}{4H(\varepsilon^p_{eq},\theta)J_2}\left[s_{kl}\dot{s}_{kl} - \sqrt{\frac{2}{3}}\frac{\partial Y}{\partial \theta}\dot{\theta}\right]s_{ij} = \frac{3}{2H(\varepsilon^p_{eq},\theta)}\left[n_{kl}\dot{s}_{kl} - \sqrt{\frac{2}{3}}\frac{\partial Y}{\partial \theta}\dot{\theta}\right]n_{ij} \tag{11.2.9}$$

where $\dot{s}_{kl}$ is the applied deviatoric stress increment and $\dot{\theta}$ is the rate of temperature change.

An inverse relation that evaluates the plastic part of an applied total strain increment $\dot{\varepsilon}_{ij}$ is obtained using $\dot{s}_{ij} = 2G(\dot{e}_{ij} - \dot{e}^\theta_{ij} - \dot{\varepsilon}^p_{ij})$, where $\dot{e}_{ij} = \dot{\varepsilon}_{ij} - (\dot{\varepsilon}_{kk}/3)\delta_{ij}$.

$$\left.\begin{aligned}\dot{\varepsilon}^p_{ij} &= \frac{3}{2H(\varepsilon^p_{eq},\theta)}\left[n_{kl}\dot{s}_{kl} - \sqrt{\frac{2}{3}}\frac{\partial Y}{\partial \theta}\dot{\theta}\right]n_{ij} \\ &= \frac{3G}{H(\varepsilon^p_{eq},\theta)}n_{kl}(\dot{e}_{kl} - \dot{e}^\theta_{kl} - \dot{\varepsilon}^p_{kl})n_{ij} - \sqrt{\frac{3}{2}}\frac{1}{H(\varepsilon^p_{eq},\theta)}\frac{\partial Y}{\partial \theta}\dot{\theta}n_{ij}\end{aligned}\right\} \tag{11.2.10}$$

It can be shown from the definition of n_{ij} that $n_{ij}\delta_{ij} = 0$, hence $n_{ij}e_{kl}n_{kl} = n_{ij}\varepsilon_{kl}n_{kl}$ and $n_{kl}\dot{s}_{kl}n_{ij} = n_{kl}\dot{\sigma}_{kl}n_{ij}$. Also, $n_{kl}\dot{\varepsilon}^p_{kl}n_{ij} = \dot{\varepsilon}^p_{ij}$, since n_{ij} and $\dot{\varepsilon}^p_{kl}$ are coaxial. That finally yields

$$\left.\begin{aligned}\dot{\varepsilon}^p_{ij} &= \frac{3}{2H(\varepsilon^p_{eq},\theta)}\left[n_{kl}\dot{\sigma}_{kl} - \sqrt{\frac{2}{3}}\frac{\partial Y}{\partial \theta}\dot{\theta}\right]n_{ij} \\ \dot{\varepsilon}^p_{ij} &= \frac{1}{[1 + H(\varepsilon^p_{eq},\theta)/(3G)]}\left[n_{kl}(\dot{\varepsilon}_{kl} - \dot{\varepsilon}^\theta_{kl}) - \frac{1}{\sqrt{6}G}\frac{\partial Y}{\partial \theta}\dot{\theta}\right]n_{ij}\end{aligned}\right\} \tag{11.2.11}$$

where $\dot{\sigma}_{kl}$ and $\dot{\varepsilon}_{kl}$ are the applied stress and total strain increments, and $\dot{\varepsilon}^\theta_{kl} = m_{kl}\dot{\theta}$, $m_{kl} = \alpha\delta_{kl}$ for an isotropic material, Table 8.1.

Different, often more elaborate but equivalent forms of $\dot{\varepsilon}^p_{ij}$ can be found in books and papers on plasticity. The results presented here, in terms of the normals to the current yield surface, are convenient in numerical work, as shown in Sect. 11.3.

11.2.2 Kinematic Hardening and Flow Rules

Kinematic hardening retains the shape and size of the initial yield surface (11.1.1), but it allows its translation in the six-dimensional stress or deviatoric stress spaces. The loading surface is described by

$$f((s_{ij} - a_{ij}),\ Y(\theta)) = \frac{1}{2}(s_{ij} - a_{ij})(s_{ij} - a_{ij}) - \frac{1}{3}Y^2(\theta) \le 0 \tag{11.2.12}$$

where a_{ij} indicates position of the current center of the loading surface in the deviatoric stress space; it is often regarded as a back stress, which is examined in Sect. 12.1.4. The actual yield stress is again derived from an equivalent stress/temperature/plastic strain relation, hence it increases with accumulated ε_{eq}^{p} and it changes with $\dot{\theta}$. In kinematic hardening, this increase is accommodated by the translation vector a_{ij}, while $Y(\theta)$ determines the constant size or 'diameter' of the yield surface. The translation vector a_{ij} is derived from one of the following hardening rules.

The Prager-Ziegler hardening rule (Ziegler 1959) postulates that application of a deviatoric stress increment $\dot{s}_{ij}$ at a current loading point s_{ij} causes translation of the loading surface in the direction of the current stress vector $(s_{ij} - a_{ij})$

$$\dot{a}_{ij} = \dot{\eta}(s_{ij} - a_{ij}) \tag{11.2.13}$$

where the scalar multiplier

$$\dot{\eta} = \frac{(s_{pq} - a_{pq})}{(s_{rs} - a_{rs})(s_{rs} - a_{rs})}[\dot{s}_{pq} - (\partial Y/\partial\theta)\dot{\theta}] \tag{11.2.14}$$

is found at the current stress s_{ij} such that the translated yield surface meets the stress increment at the new loading point $s_{ij} + \dot{s}_{ij}$. This is guaranteed by projecting the stress increment onto the translation vector via the scalar product appearing in the numerator. In the original version of this rule, proposed by Prager (1956), the direction of both the translation $\dot{a}_{ij}$ and the plastic strain increment $\dot{\varepsilon}_{ij}$ were assumed to coincide with that of the normal n_{ij}. That led to certain inconsistencies that were discovered and resolved by Shield and Ziegler (1958).

The *Phillips hardening rule* (Phillips et al. 1972, 1974; Phillips 1986) specifies that the translation is equal to the stress increment itself

$$\dot{a}_{ij} = \rho\dot{s}_{ij} \tag{11.2.15}$$

where ρ shows the effect of a temperature change. From the consistency condition (11.1.5), ρ is found as

$$(s_{ij} - a_{ij})(\dot{s}_{ij} - \rho\dot{s}_{ij}) - \frac{2}{3}Y\frac{\partial Y}{\partial\theta}\dot{\theta} \le 0 \Rightarrow \rho = 1 - \frac{2Y}{3(s_{ij} - a_{ij})\dot{s}_{ij}}\frac{\partial Y}{\partial\theta}\dot{\theta} \tag{11.2.16}$$

Extensive experimental investigations on aluminum by Phillips and coworkers, as well as by Dvorak et al. (1988) and Nigam et al. (1994) on metal matrix composites, and by Ellyin (1989) on titanium, show that this rule provides a good qualitative prediction of observed locations of yield and loading surfaces, which are often entirely different from those predicted by the Prager-Ziegler rule. The said experiments detected the yield surfaces at very small deviations from elastic strains, at several points of a combined normal and shear stress loading/unloading

path that generated plastic strains of moderate magnitude. However, actual shapes and sizes of so detected loading surfaces undergo changes during continuing plastic deformation, that are at best only approximated by the Phillips kinematic hardening rule.

Notice that during application of any stress increment, the Phillips rule retains the original position of the loading point on the translated loading surface, together with the magnitude and principal directions of the stress $(s_{ij} - a_{ij})$. Preservation of the principal stress directions by this hardening rule suggests that the current slip system may continue to operate during active plastic loading. This appears to be physically more appealing, at least at very small plastic strains, than the sudden changes in loading point position, principal stress directions and possible slip system orientations, implied by the isotropic and Prager-Ziegler hardening rules under non-proportional loading.

In materials undergoing kinematic hardening, the current yield stress $Y(\theta)$ no longer appears as a function of the plastic strain rate $\dot{\varepsilon}^p_{eq}$. To reintroduce this rate into the yield function and in the consistency equation, Ziegler (1959) proposed to make its magnitude proportional to a_{ij}

$$\dot{a}_{ij}\frac{\partial f}{\partial s_{ij}} = c\dot{\varepsilon}^p_{ij}\frac{\partial f}{\partial s_{ij}} = c\dot{\lambda}\frac{\partial f}{\partial s_{ij}}\frac{\partial f}{\partial s_{ij}} \tag{11.2.17}$$

That modifies the consistency equation (11.1.5) and it yields the $\dot{\lambda}$ multiplier

$$\left.\begin{aligned}(s_{ij} - a_{ij})[\dot{s}_{ij} - c\,\dot{\lambda}(s_{ij} - a_{ij})] - \frac{2}{3}Y\frac{\partial Y}{\partial\theta}\dot{\theta} \le 0\\ \dot{\lambda} = \frac{(s_{ij} - a_{ij})\dot{s}_{ij} - \frac{2}{3}Y\frac{\partial Y}{\partial\theta}\dot{\theta}}{c\,(s_{kl} - a_{kl})(s_{kl} - a_{kl})}\end{aligned}\right\} \tag{11.2.18}$$

together with

$$\dot{\varepsilon}^p_{ij} = \dot{\lambda}(s_{ij} - a_{ij}) = \frac{1}{c}\left[n_{kl}\dot{s}_{kl} - \sqrt{\frac{2}{3}}\frac{\partial Y}{\partial\theta}\dot{\theta}\right]n_{ij} \tag{11.2.19}$$

according to the connections $n_{ij} = (s_{ij} - a_{ij})/\sqrt{2J_2}$ from (11.1.10), and $Y = \sqrt{3J_2}$ from (11.1.1).

The proportionality constant c is derived again with reference to deformation under simple tension. With $\sigma_{11} \neq 0 \;\Rightarrow\; s_{11} = 2\sigma_{11}/3$, $s_{22} = s_{33} = -\sigma_{11}/3$, $J_2 = \sigma^2_{11}/3$, equations (11.2.19) and (11.1.4) provide

$$\dot{\varepsilon}^p_{11} = \frac{2}{3c}\left[\dot{\sigma}_{11} - \frac{\partial Y}{\partial\theta}\dot{\theta}\right] \Rightarrow c = \frac{2}{3\dot{\varepsilon}^p_{11}}\left[\dot{\sigma}_{11} - \frac{\partial Y}{\partial\theta}\dot{\theta}\right] = \frac{2}{3}H(\varepsilon^p_{eq}, \theta) \tag{11.2.20}$$

The plastic strain increment (11.2.19) has the final form

$$\dot{\varepsilon}_{ij}^{p} = \frac{3}{2H(\varepsilon_{eq}^{p},\ \theta)}\left[n_{kl}\dot{s}_{kl} - \sqrt{\frac{2}{3}}\frac{\partial Y}{\partial\theta}\dot{\theta}\right]n_{ij} \tag{11.2.21}$$

which is the same result as that obtained with isotropic hardening. Therefore, application of a stress increment $\dot{\sigma}_{kl}$, or a total strain increment $\dot{\varepsilon}_{kl}$, generate the plastic strain rates

$$\left.\begin{aligned}\dot{\varepsilon}_{ij}^{p} &= \frac{3}{2H(\varepsilon_{eq}^{p},\theta)}\left[n_{kl}\dot{\sigma}_{kl} - \sqrt{\frac{2}{3}}\frac{\partial Y}{\partial\theta}\dot{\theta}\right]n_{ij}\\ \dot{\varepsilon}_{ij}^{p} &= \frac{1}{[1+H(\varepsilon_{eq}^{p},\theta)/(3G)]}\left[n_{kl}(\dot{\varepsilon}_{kl}-\dot{\varepsilon}_{kl}^{\theta}) - \frac{1}{\sqrt{6}G}\frac{\partial Y}{\partial\theta}\dot{\theta}\right]n_{ij}\end{aligned}\right\} \quad [11.2.11]$$

where $\dot{\varepsilon}_{kl}^{\theta} = m_{kl}\dot{\theta}$, $m_{kl} = \alpha\delta_{kl}$ in an isotropic material, Table 8.1.

11.2.3 Mixed Isotropic and Kinematic Hardening Rules

This type of hardening is often observed under cyclic loading, where the yield surface may expand with the number of cycles, while exhibiting translations within each cycle. Models of mixed hardening modify the kinematic hardening rules by either retarding the translation a_{ij} of the yield surface center, or by expanding the surface, both as functions of the accumulated equivalent plastic strain ε_{eq}^{p}. The first choice is illustrated by the Armstrong and Frederick (1966) rule, which specifies evolution of the back stress by the differential equation

$$\dot{a}_{ij} = \frac{2}{3}H(\varepsilon_{eq}^{p},\ \theta)\dot{\varepsilon}_{ij}^{p} + g\dot{\varepsilon}_{eq}^{p}a_{ij} \tag{11.2.22}$$

where g is a material parameter. The first term evolves a_{ij} as implied by (11.2.17) and the second part is the retardation term.

The second choice, examined below, involves enhancement of the yield stress in the kinematic hardening rule (11.2.12), by adding an isotropic internal stress $Q\left(\theta, \varepsilon_{eq}^{p}\right)$, with the loading surface assuming the form

$$f(s_{ij},a_{ij},Y(\varepsilon_{eq}^{p},\theta)) = \frac{1}{2}(s_{ij}-a_{ij})(s_{ij}-a_{ij}) - \frac{1}{3}[Y_m(\theta,\ \varepsilon_{eq}^{p})]^2 \le 0 \tag{11.2.23}$$

where the modified yield stress is $Y_m(\theta,\ \varepsilon_{eq}^{p}) = [Y(\theta) + Q(\theta,\ \varepsilon_{eq}^{p})]$. Evolution of $Q\left(\theta, \varepsilon_{eq}^{p}\right)$ was studied by Chan et al. (1988), Lindholm et al. (1984). Chaboche (1989) and Zaverl and Lee (1978), who suggested the differential form

$$\dot{Q}(\theta,\ \varepsilon_{eq}^{p}) = q(\theta)[Q_a(\theta) - Q]\,\dot{\varepsilon}_{eq}^{p} \tag{11.2.24}$$

with initial conditions $Q = 0$ at $\varepsilon^p_{eq} = 0$. That can be integrated to yield

$$Q(\theta,\ \varepsilon^p_{eq}) = Q_a(\theta)[1 - \exp(-q(\theta)\,\varepsilon^p_{eq})] \tag{11.2.25}$$

The Q rises with plastic strain until it reaches an asymptotic value $Q_a(\theta)$, at a rate indicated by $q(\theta)$. Both $Q_a(\theta)$ and $q(\theta)$ can be evaluated by monitoring yield stress changes in cyclic tests at different constant temperatures θ.

The consistency condition (11.1.5) and (11.2.2), together with (11.2.24), now yield

$$\left.\begin{aligned} \dot f &= \tilde s_{ij}\dot{\tilde s}_{ij} - \frac{2}{3}Y_m\left[\frac{\partial Y_m}{\partial \varepsilon^p_{eq}}\dot\varepsilon^p_{eq} + \frac{\partial Y_m}{\partial\theta}\dot\theta\right] \\ &= \tilde s_{ij}\dot{\tilde s}_{ij} - \frac{2}{3}Y_m\left[\frac{2}{3}q(\theta)(Q_a - Q)\dot\lambda\sigma_{eq} + \frac{\partial Y_m}{\partial\theta}\dot\theta\right] \le 0 \end{aligned}\right\} \tag{11.2.26}$$

Recall that $\tilde s_{ij} = (s_{ij} - a_{ij})$, $3\tilde s_{ij}\dot{\tilde s}_{ij}/2 = \dot{\tilde\sigma}_{eq}\sqrt{3\tilde J_2}$ and $Y = \sqrt{3\tilde J_2}$, and write the final form of $\dot\lambda$ as

$$\dot\lambda = \frac{3}{2}\frac{\left[\frac{3}{2}\tilde s_{ij}\dot{\tilde s}_{ij} - Y_m\frac{\partial Y_m}{\partial\theta}\dot\theta\right]}{Y_m q(\theta)(Q_a - Q)\tilde\sigma_{eq}} = \frac{3}{2q(\theta)(Q_a - Q)\tilde\sigma_{eq}}\left[\tilde\sigma_{eq} - \frac{\partial Y_m}{\partial\theta}\dot\theta\right] \tag{11.2.27}$$

Proceeding as in (11.2.10) and (11.2.11), we find the plastic strain increments caused by applied deviatoric stress or by total strain increment

$$\left.\begin{aligned} \dot\varepsilon^p_{ij} &= \frac{3}{2q(\theta)(Q_a - Q)}\left[n_{kl}\dot{\tilde s}_{kl} - \sqrt{\frac{2}{3}}\frac{\partial Y_m}{\partial\theta}\dot\theta\right]n_{ij} \\ \dot\varepsilon^p_{ij} &= \frac{1}{\{1 + [q(\theta)(Q_a - Q)]/(3G)\}}\left[n_{kl}(\dot\varepsilon_{kl} - \dot\varepsilon^\theta_{kl}) - \frac{1}{\sqrt{6}G}\frac{\partial Y_m}{\partial\theta}\dot\theta\right]n_{ij} \end{aligned}\right\} \tag{11.2.28}$$

where as in (11.2.11), $n_{kl}\dot s_{kl}n_{ij} = n_{kl}\dot\sigma_{kl}n_{ij}$. Notice that these results are similar to those in (11.2.11), where the $H(\varepsilon^p_{eq},\theta)$ tangent modulus (11.1.4) has now been replaced by $\dot Q(\theta,\ \varepsilon^p_{eq})/\dot\varepsilon^p_{eq} = q(\theta)[Q_a(\theta) - Q]$ from (11.2.24).

To incorporate the Armstrong-Frederick back stress retardation term in this result, one can rewrite (11.2.22) as

$$\dot a_{ij} = \frac{2}{3}\dot\lambda[H(\varepsilon^p_{eq},\ \theta)s_{ij} + g\sigma_{eq}a_{ij}] \tag{11.2.29}$$

and substitute that into $\dot{\tilde s}_{ij} = (\dot s_{ij} - \dot a_{ij})$. The expression in square brackets will then appear in the denominators of (11.2.28).

11.2.4 The Dafalias-Popov Model for Adaptive Estimate of the Tangent Modulus

Originally invented for applications to cyclic loading (Dafalias and Popov 1976), this model was found to be useful in interpretation of combined loading experiments on fibrous metal matrix composites. Several other models of this kind prefer to employ additional loading surfaces and hidden variables, which may be open to subjective interpretation.

Under simple tension cycles, applied stress σ and plastic strain ε^p are connected as indicated in Fig. 11.1. The yield stress increases from an initial value at a very small plastic strain, to a bounding value indicated by a linear or nonlinear function of larger plastic strain. The difference $\delta(\varepsilon^p)$, between the current and bounding values of the applied stress at points $\boldsymbol{s}$ and $\bar{\boldsymbol{s}}$, changes from an initial maximum δ_{in} at the onset of yielding to $\delta(\varepsilon^p) \to 0$ when a bound is reached. In particular, $H(\varepsilon^p) \to \infty$ at $\delta(\varepsilon^p) \to \delta_{\text{in}}$, and $H(\varepsilon^p) \to H_0$ at $\delta(\varepsilon^p) \to 0$.

The uniaxial model describes the plastic tangent modulus $H(\varepsilon^p)$ by a function of $\delta(\varepsilon^p)$

$$H(\varepsilon^p,\ \theta) = H_0(\theta) + h(\theta)\,\delta(\varepsilon^p)/[\delta_{\text{in}} - \delta(\varepsilon^p)] \tag{11.2.30}$$

where h is added as a material parameter to those designated by δ_{in} and H_0. The initial stress distance δ_{in} may have a different value in the loading and unloading branches of the stress-plastic strain curve, and also in subsequent load cycles. Of course, after $\delta \to 0$, the $H(\varepsilon^p)$ can be described by another function of plastic strain that admits nonlinear hardening at larger strains.

In the six-dimensional stress space, the diagram in Fig. 11.1 is represented by a pair of loading surfaces shown in Fig. 11.2, which may again be described by functions of deviatoric stress, with two constant yield stresses in simple tension.

$$\left.\begin{aligned} f((s_{ij} - a_{ij}),\ Y(\theta)) &= \frac{1}{2}(s_{ij} - a_{ij})(s_{ij} - a_{ij}) - \frac{1}{3}Y^2(\theta) \le 0 \\ F((\bar{s}_{ij} - b_{ij}),\ \bar{Y}(\theta)) &= \frac{1}{2}(\bar{s}_{ij} - b_{ij})(\bar{s}_{ij} - b_{ij}) - \frac{1}{3}\bar{Y}^2(\theta) \le 0 \end{aligned}\right\} \tag{11.2.31}$$

The top bar now denotes quantities associated with the bounding surface F. The interior yield surface f always surrounds the present elastic deformation region in stress space. As long as the current loading point, denoted by s at σ_{ij}, resides on the yield surface f, plastic strain is determined by the flow rule associated with f. The exterior bounding surface F indicates onset of larger plastic strains, along the bound lines in the uniaxial diagram. Once the loading point s approaches and merges with $\bar{s}$ at $\bar{\sigma}_{ij}$ on the bounding surface, the plastic strain increment is derived from the flow rule associated with F. The bounding surface retains this role while the two surfaces are in contact. Experimental evidence of the bounding surface can be found in Phillips and Lee (1979).

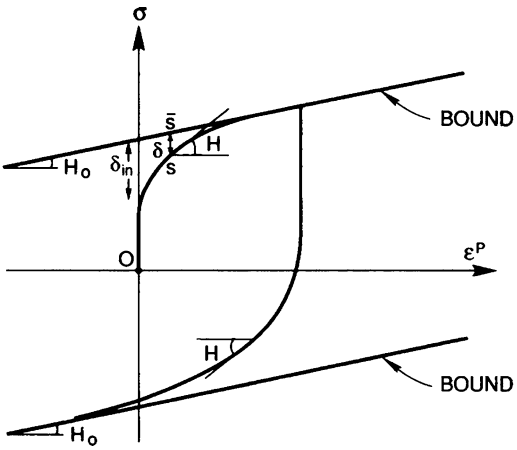

Fig. 11.1 Schematic representation of the quantities δ, δ_{in}, H, H_0 in a uniaxial test

Before inelastic deformation, the bounding surface F is usually defined as an isotropic expansion of the yield surface

$$(\bar{s}_{ij} - b_{ij}) = \xi(s_{ij} - a_{ij}) \tag{11.2.32}$$

where $\xi > 1$ is a similarity ratio. While the centers of the two surfaces coincide, this expansion carries the point at $\boldsymbol{s}$ on the yield surface to its position $\bar{\boldsymbol{s}}$ on the bounding surface, hence the normals to the two surfaces at points $\boldsymbol{s}$ and $\bar{\boldsymbol{s}}$ have the same direction. The distance δ between points $\boldsymbol{s}$ and $\bar{\boldsymbol{s}}$ corresponds to that from δ_{in} in the uniaxial test in Fig. 11.1.

During plastic loading, both surfaces undergo coupled simultaneous translations in stress space, and possible shape or size changes if mixed hardening is considered. They approach each other along a vector η_{ij} directed from $\boldsymbol{s}$ toward $\bar{\boldsymbol{s}}$. The yield surface translates by $\dot{a}_{ij}$ derived from a selected kinematic or mixed hardening rule, while the center of the bounding surface translates according to

$$\dot{b}_{ij} = \dot{a}_{ij} - \dot{C}\,\eta_{ij} \quad \eta_{ij}\eta_{ij} = 1 \tag{11.2.33}$$

The scalar factor $\dot{C}$ follows from the hardening and flow rules that apply to the two surfaces in stress space, and from possible shape or size changes in mixed hardening. As long as the loading point $s \neq \bar{s}$, the translating bounding surface serves only as a carrier of the point $\bar{\boldsymbol{s}}$. Current distance δ between the two points is

$$\delta = [(\bar{s}_{ij}^{\bar{s}} - s_{ij}^{s})(\bar{s}_{ij}^{\bar{s}} - s_{ij}^{s})]^{1/2} \tag{11.2.34}$$

This distance, together with H_0 and δ_{in} found prior to any plastic deformation as $\delta = \delta_{\text{in}}$, yields the instantaneous value of the plastic tangent modulus

$$H(\varepsilon^p, \theta) = H_0(\theta) + h\,\delta(\varepsilon^p)/[\delta_{\text{in}} - \delta(\varepsilon^p)] \tag{11.2.30}$$

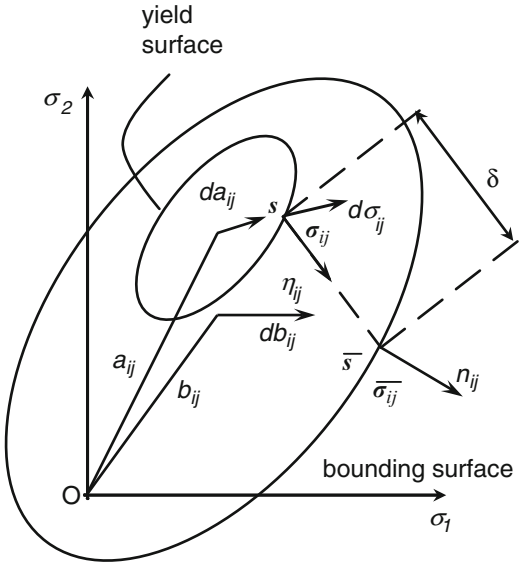

Fig. 11.2 Yield and bounding surfaces during plastic flow

which is then used to relate current $\dot{\sigma}_{eq}$, $\dot{\varepsilon}^p_{eq}$ and $\dot{\theta}$ by

$$H(\varepsilon^p_{eq},\theta) = [\dot{\sigma}_{eq} - (\partial Y/\partial\theta)\dot{\theta}]/\dot{\varepsilon}^p_{eq} \qquad [11.1.4]$$

Once the two surfaces come into contact at points $\boldsymbol{s} \to \bar{\boldsymbol{s}}$ with the same normal, they translate together as long as plastic loading continues, while the flow rule associated with the bounding surface determines the plastic strain increment. Upon unloading, followed by reverse loading at another point on the yield surface, the two surfaces may separate and translate again toward possible contact at another pair of points with aligned normals.

In particular, when the Phillips kinematic hardening rule (11.2.10) is adopted for both surfaces, and the translation rates are described by the first term in (11.2.22), the Dafalias and Popov model stipulates that

$$\left.\begin{aligned}
&\dot{a}_{ij}n_{ij} = \frac{2}{3}H(\varepsilon^p_{eq},\theta)(\dot{\varepsilon}^p_{ij}\dot{\varepsilon}^p_{ij})^{1/2} = \sqrt{\frac{2}{3}}\,H(\varepsilon^p_{eq},\theta)\dot{\varepsilon}^p_{eq} \qquad \dot{b}_{ij}n_{ij} = \sqrt{\frac{2}{3}}\,H_0(\theta)\dot{\varepsilon}^p_{eq} \\
&\dot{b}_{ij}n_{ij} = \dot{a}_{ij}n_{ij} - \dot{C}\,\eta_{ij}n_{ij} \Rightarrow \dot{C}\,\eta_{ij}n_{ij} = \sqrt{\frac{2}{3}}\left(1 - \frac{H_0(\theta)}{H(\varepsilon^p_{eq},\theta)}\right)(\dot{\sigma}_{eq} - (\partial Y/\partial\theta)\dot{\theta}) \\
&\dot{C} = \sqrt{\frac{2}{3}}\left(1 - \frac{H_0(\theta)}{H(\varepsilon^p_{eq},\theta)}\right)\frac{[\dot{\sigma}_{eq} - (\partial Y/\partial\theta)\dot{\theta}]}{\eta_{kl}n_{kl}}
\end{aligned}\right\} \qquad (11.2.35)$$

The hardening rule for the bounding surface finally is

$$\dot{b}_{ij} = \dot{a}_{ij} - \dot{C}\,\eta_{ij} = \dot{s}_{ij} - \sqrt{\frac{2}{3}}\left(1 - \frac{H_0(\theta)}{H(\varepsilon^p_{eq},\,\theta)}\right)\frac{[\dot{\sigma}_{eq} - (\partial Y/\partial\theta)\dot{\theta}]}{\eta_{kl}n_{kl}}\eta_{ij} \qquad (11.2.36)$$

where $\dot{s}_{ij}$ is the applied deviatoric stress increment that also evaluates $\dot{\sigma}_{eq}$.

The distance between any two loading points can also be written as $\delta\eta_{ij} = \bar{\sigma}_{ij} - \sigma_{ij}$. The derivation utilizes $\eta_{ij}\eta_{ij} = 1$, $\dot{\eta}_{ij}\eta_{ij} = 0$ and equations that follow (11.2.32), and it yields

$$\left.\begin{aligned}\dot{\delta}\eta_{ij} &= (\dot{\bar{\sigma}}_{ij} - \dot{\sigma}_{ij})\eta_{ij} = \xi(\dot{\sigma}_{ij} - \dot{\alpha}_{ij})\eta_{ij} + (\dot{\beta}_{ij} - \dot{\sigma}_{ij})\eta_{ij}\\ &= (\xi - 1)(\dot{\sigma}_{ij} - \dot{\alpha}_{ij})\eta_{ij} - \dot{C}\,\eta_{ij}\end{aligned}\right\} \qquad (11.2.37)$$

Since $\xi > 1$, the first term can change signs according to the direction of $\dot{\sigma}_{ij}$. However, $\dot{C} > 0$ in the second term, making this term with the minus sign always negative. This result indicates the rate of approach or separation of the surfaces during loading and unloading, and the corresponding rate of change of the $H(\varepsilon^p_{eq},\,\theta)$ according to (11.2.30).

The two surface model can be easily modified for applications to systems where the bounding surface F undergoes mixed or purely isotropic hardening during those loading periods when the two surfaces are in contact. In the latter case, $b_{ij} = 0$ in $(11.2.35)_2$, which is replaced by the isotropic form (11.1.12) with the associated flow rule. The yield surface f may translate in purely kinematic mode inside the bounding surface, which remains stationary during separation and approach periods but may expand when it acquires the loading point. Such behavior was implied by experiments on aluminum in plane stress, conducted by Phillips and co-workers. However, experimental support for this or other models describing the evolution of $H(\varepsilon^p_{eq},\,\theta)$ under general loading conditions does not appear to be available.

11.3 Matrix Form and Consistency of the Instantaneous Tangent Stiffness

The results found in the preceding sections show that expressions evaluating the plastic strain rate $\dot{\varepsilon}^p_{ij}$ associated with the Mises yield and loading surfaces are not dependent on the distinctions between isotropic, kinematic or mixed hardening, except for the separate plastic tangent modulus specified in (11.2.24). However, the different hardening rules determine changes in size or position that the surfaces experience in response to loading. This implies changes in the direction of the current normal n_{ij}, which is coaxial with the plastic strain rate in superimposed engineering strain coordinates, and is a function of the current value of the applied deviatoric stress during plastic loading. The magnitude of $\dot{\varepsilon}^p_{ij}$ depends on the current values of the stress increment $\dot{s}_{ij}$, and on the plastic tangent modulus $H(\varepsilon^p_{eq},\,\theta)$ or $q(\theta)[Q_a(\theta) - Q]$. When caused by an applied strain increment $\dot{e}_{ij}$, it also depends on the elastic shear modulus G.

Numerical evaluations of the elastic and plastic strain increments generated in each loading step are facilitated by using a matrix form of the constitutive relations derived for different hardening rules in (11.2.10–11.2.11), (11.2.19) and (11.2.28). *The tensorial component notation and its contracted form of Sect. 2.1 are used, instead of the engineering matrix notation.*

First, recall from (11.1.10) that $n_{ij} = s_{ij}/\sqrt{s_{ij}s_{ij}} = s_{ij}/\sqrt{2J_2}$. The $n_{ij}n_{kl}$ which appears in the said constitutive relations, represents a fourth-order projector tensor, denoted here by $\boldsymbol{E}$, with the following properties that assure consistency of the relations

$$E_{ijkl} = n_{ij}n_{kl} = n_{kl}n_{ij} = \frac{\tilde{s}_{kl}\tilde{s}_{ij}}{\tilde{s}_{pq}\tilde{s}_{pq}} = E_{klij} \tag{11.3.1}$$

$$\boldsymbol{E} : \boldsymbol{E} = (n_{ij}n_{kl})\,(n_{kl}n_{pq}) = \frac{\tilde{s}_{ij}\tilde{s}_{kl}}{\tilde{s}_{rs}\tilde{s}_{rs}}\,\frac{\tilde{s}_{kl}\tilde{s}_{pq}}{\tilde{s}_{rs}\tilde{s}_{rs}} = \frac{(\tilde{s}_{kl}\tilde{s}_{kl})\tilde{s}_{ij}\tilde{s}_{pq}}{(\tilde{s}_{rs}\tilde{s}_{rs})^2} = \frac{\tilde{s}_{ij}\tilde{s}_{pq}}{\tilde{s}_{rs}\tilde{s}_{rs}} = \boldsymbol{E} \tag{11.3.2}$$

where $\tilde{s}_{ij} = s_{ij} - a_{ij}$ can is used when needed in a particular hardening rule. The idempotent matrix that satisfies these requirements and reproduces the tensorial component result in contracted tensorial notation is

$$\boldsymbol{E} = \frac{\tilde{\boldsymbol{s}}\tilde{\boldsymbol{s}}^{\mathrm{T}}}{\tilde{\boldsymbol{s}}^{\mathrm{T}}\tilde{\boldsymbol{s}}} = \left(\sum_{\alpha=1}^{6}\tilde{s}_\alpha^2\right)^{-1}\begin{bmatrix} \tilde{s}_1^2 & \tilde{s}_1\tilde{s}_2 & \tilde{s}_1\tilde{s}_3 & \tilde{s}_1\tilde{s}_4 & \tilde{s}_1\tilde{s}_5 & \tilde{s}_1\tilde{s}_6 \\ & \tilde{s}_2^2 & \tilde{s}_2\tilde{s}_3 & \tilde{s}_2\tilde{s}_4 & \tilde{s}_2\tilde{s}_5 & \tilde{s}_2\tilde{s}_6 \\ & & \tilde{s}_3^2 & \tilde{s}_3\tilde{s}_4 & \tilde{s}_3\tilde{s}_5 & \tilde{s}_3\tilde{s}_6 \\ & & & \tilde{s}_4^2 & \tilde{s}_4\tilde{s}_5 & \tilde{s}_4\tilde{s}_6 \\ & & & & \tilde{s}_5^2 & \tilde{s}_5\tilde{s}_6 \\ & \text{sym.} & & & & \tilde{s}_6^2 \end{bmatrix} \tag{11.3.3}$$

The leading denominator $1/(\tilde{s}_\alpha\tilde{s}_\alpha)$ assures compliance with $\boldsymbol{EE} = \boldsymbol{E}$, which parallels (11.3.2). In some technical papers on plasticity, this denominator is replaced by $1/(2\tilde{J}_2)$ or by a yield stress equivalent of $1/(2\tilde{J}_2)$, with $\tilde{J}_2$ from (11.1.2). Since $\tilde{\boldsymbol{s}} = 2G\boldsymbol{e}$, the above matrix can also be evaluated as originally suggested by Ponte Castaneda (1996); $\boldsymbol{E} = (\boldsymbol{e}\boldsymbol{e}^{\mathrm{T}})/(\boldsymbol{e}^{\mathrm{T}}\boldsymbol{e})$. The n_{ij} in (11.1.10) is transcribed as $\tilde{\boldsymbol{s}}/\sqrt{\tilde{\boldsymbol{s}}^{\mathrm{T}}\tilde{\boldsymbol{s}}}$, hence carrying this result into (11.3.1) should yield the correct form of $\boldsymbol{E}$.

The plastic strain increments associated with Mises or J_2 yield surfaces that undergo either isotropic or kinematic hardening were derived under applied overall rates of stress or strain and temperature change as

$$\left.\begin{aligned} \dot{\varepsilon}_{ij}^p &= \frac{3}{2H(\varepsilon_{eq}^p,\ \theta)}\left[n_{kl}\dot{\sigma}_{kl} - \sqrt{\frac{2}{3}}\frac{\partial Y}{\partial\theta}\dot{\theta}\right]n_{ij} \\ \dot{\varepsilon}_{ij}^p &= \frac{1}{[1 + H(\varepsilon_{eq}^p, \theta)/(3G)]}\left[n_{kl}(\dot{\varepsilon}_{kl} - \dot{\varepsilon}_{kl}^\theta) - \frac{1}{\sqrt{6}G}\frac{\partial Y}{\partial\theta}\dot{\theta}\right]n_{ij} \end{aligned}\right\} \quad [11.1.22]$$

Under traction boundary conditions, the total strain increment $\dot{\boldsymbol{\varepsilon}} = \dot{\boldsymbol{\varepsilon}}^e + \dot{\boldsymbol{\varepsilon}}^\theta + \dot{\boldsymbol{\varepsilon}}^p$, caused by application of a stress increment $\dot{\boldsymbol{\sigma}}$ and thermal change $\dot{\theta}$, follows from

the standard thermoelastic relations (11.1.11). Both elastic and plastic strains are generated by the independent loads $\dot{\boldsymbol{\sigma}}$ and $\dot{\theta}$. The thermomechanical elastic-plastic constitutive relations are written in the tensorial component and contracted tensorial notations.

$$\left.\begin{aligned} &\dot{\varepsilon}_{ij} = \mathcal{M}_{ijkl}\dot{\sigma}_{kl} + m_{ij}\dot{\theta} \quad \mathcal{M}_{ijkl} = M^e_{ijkl} + \frac{3}{2H(\varepsilon^p_{eq},\,\theta)} n_{ij}n_{kl} = \mathcal{M}_{klij} \\ &m_{ij} = m^e_{ij} - \sqrt{\frac{3}{2}}\frac{(\partial Y/\partial\theta)}{H(\varepsilon^p_{eq},\,\theta)} n_{ij} \end{aligned}\right\} \tag{11.3.4}$$

$$\dot{\boldsymbol{\varepsilon}} = \boldsymbol{\mathcal{M}}\dot{\boldsymbol{\sigma}} + \boldsymbol{m}\dot{\theta} \quad \boldsymbol{\mathcal{M}} = \boldsymbol{M}^e + \frac{3}{2H(\varepsilon^p_{eq},\,\theta)}\boldsymbol{E} \quad \boldsymbol{m} = \boldsymbol{m}^e - \sqrt{\frac{3}{2}}\frac{(\partial Y/\partial\theta)}{H(\varepsilon^p_{eq},\,\theta)}\left(\frac{\tilde{\boldsymbol{s}}}{\sqrt{\tilde{\boldsymbol{s}}^{\mathrm{T}}\tilde{\boldsymbol{s}}}}\right) \tag{11.3.5}$$

where $\boldsymbol{\mathcal{M}} = \boldsymbol{M}^e + \boldsymbol{\mathcal{M}}^p$ and $\boldsymbol{m} = \boldsymbol{m}^e + \boldsymbol{m}^p$ are the (6×6) instantaneous elastic-plastic compliance matrix and the (6×1) thermal strain vector. $\boldsymbol{M}^e$ is the elastic compliance matrix and $\dot{\varepsilon}^\theta_{kl} = m_{kl}\dot{\theta}$, $m^e_{kl} = \alpha\delta_{kl}$, is the thermal strain vector for isotropic materials, $\boldsymbol{m}^e = [\alpha,\ \alpha,\ \alpha,\ 0,\ 0,\ 0]^{\mathrm{T}}$, Table 8.1.

Under displacement boundary conditions, the stress increment caused by an applied total strain increment, which includes thermal and plastic parts, is

$$\dot{\sigma}_{ij} = L^e_{ijkl}(\dot{\varepsilon}_{kl} - \dot{\varepsilon}^\theta_{kl} - \dot{\varepsilon}^p_{kl}) \tag{11.3.6}$$

where L^e_{ijkl} is the elastic stiffness of an isotropic material, and $\dot{\varepsilon}_{kl}$ is the total applied strain. The plastic strain increment caused by an applied total strain increment is given by $(11.2.11)_2$. Since the tensor $\dot{\varepsilon}^p_{kl}$ has zero isotropic part, $\dot{\varepsilon}^p_{kk} = 0$, its contribution to the isotropic stress is $\dot{\sigma}_{kk} = 3K\dot{\varepsilon}^p_{kk} = 0$, and the product $L^e_{ijkl}\dot{\varepsilon}^p_{kl} = 2G\dot{\varepsilon}^p_{ij}$. Therefore, the stress rate can be expressed as

$$\left.\begin{aligned} \dot{\sigma}_{ij} =& \mathcal{L}_{ijkl}\dot{\varepsilon}_{kl} + \ell_{ij}\dot{\theta} = \left[L^e_{ijkl} - \frac{2G\, n_{kl}n_{ij}}{[1 + H(\varepsilon^p_{eq},\theta)/(3G)]}\right]\dot{\varepsilon}_{kl} \\ &+ \left[-L^e_{ijkl}m^e_{kl} + \frac{2G}{[1 + H(\varepsilon^p_{eq},\theta)/(3G)]}\left(n_{kl}m^e_{kl} + \frac{1}{\sqrt{6}G}\frac{\partial Y}{\partial\theta}\right)n_{ij}\right]\dot{\theta} \end{aligned}\right\} \tag{11.3.7}$$

In matrix form, with $\boldsymbol{\mathcal{L}} = \boldsymbol{L}^e + \boldsymbol{\mathcal{L}}^p$, $\boldsymbol{\ell} = \boldsymbol{l}^e + \boldsymbol{\ell}^p$

$$\left.\begin{aligned} &\dot{\boldsymbol{\sigma}} = \boldsymbol{\mathcal{L}}\,\dot{\boldsymbol{\varepsilon}} + \boldsymbol{\ell}\,\dot{\theta} \quad \boldsymbol{\mathcal{L}} = \boldsymbol{L}^e - \frac{2G}{[1 + H(\varepsilon^p_{eq},\theta)/(3G)]}\boldsymbol{E} \\ &\boldsymbol{\ell} = -\boldsymbol{L}^e\boldsymbol{m}^e + \frac{2G}{[1 + H(\varepsilon^p_{eq},\theta)/(3G)]}\left[\boldsymbol{E}\,\boldsymbol{m}^e + \frac{1}{\sqrt{6}G}\frac{\partial Y}{\partial\theta}\left(\frac{\tilde{\boldsymbol{s}}}{\sqrt{\tilde{\boldsymbol{s}}^{\mathrm{T}}\tilde{\boldsymbol{s}}}}\right)\right] \end{aligned}\right\} \tag{11.3.8}$$

where $\boldsymbol{\mathcal{L}} = \boldsymbol{L}^e + \boldsymbol{\mathcal{L}}^p = \boldsymbol{\mathcal{L}}^{\mathrm{T}}$ denotes the (6×6) instantaneous elastic-plastic tangent stiffness, and $\boldsymbol{\ell} = \boldsymbol{l}^e + \boldsymbol{\ell}^p$ the related (6×1) thermal stress vector.

Coefficients of the $\boldsymbol{E}$ matrix depend on the current deviatoric stresses at the loading point, with many or all of the six coefficients $\tilde{s}_\alpha$ possibly assuming values different from zero. Therefore, during plastic loading, the instantaneous tangent stiffness and compliance matrices may have few if any zero valued coefficients among the 21, as in triclinic materials. However, isotropic material symmetry prevails in definition of the elastic stiffness matrix during loading, and upon elastic unloading. As long as the position of the loading point and thus the direction of the normal to the loading surface remain fixed during continuing loading, the coefficients of both the instantaneous tangential stiffness $\boldsymbol{\mathcal{L}}$ and thermal stress vector $\boldsymbol{\ell}$ retain their magnitudes. Therefore, such loading can be regarded as proportional loading. That type of loading is implied by Phillips-type kinematic hardening.

Consistency of the elastic-plastic constitutive relations requires the instantaneous tangential stiffness and compliance tensors and thermal vectors to comply with

$$\mathcal{L}_{ijkl}\mathcal{M}_{klmn} = I_{ijmn} \quad m_{ij} = -\mathcal{M}_{ijkl}\ell_{kl} \quad \ell_{ij} = -\mathcal{L}_{ijkl}m_{kl} \tag{11.3.9}$$

Proving these relations is facilitated by the projector tensors described in (1.1.16), and by the projector tensor $\boldsymbol{E}$.

$$J_{ijkl} = \frac{1}{3}\delta_{ij}\delta_{kl} \quad K_{ijkl} = \frac{1}{2}(\delta_{ik}\delta_{jl} + \delta_{il}\delta_{jk}) - J_{ijkl} = I_{ijkl} - J_{ijkl} \quad E_{ijkl} = n_{ij}n_{kl} \tag{11.3.10}$$

The elastic plastic constitutive relations (11.3.5) and (11.3.8) can be written as

$$\boldsymbol{\mathcal{L}} = 3K\boldsymbol{J} + 2G\boldsymbol{K} - \frac{2G}{1 + (H/3G)}\boldsymbol{E} \quad \boldsymbol{\mathcal{M}} = \frac{1}{3K}\boldsymbol{J} + \frac{1}{2G}\boldsymbol{K} + \frac{3}{2H}\boldsymbol{E} \tag{11.3.11}$$

where the $\boldsymbol{J}$ and $\boldsymbol{K}$ matrices are evaluated in (1.1.19). The two leading terms on the right hand sides represent the isotropic elastic stiffness $\boldsymbol{L}^e$ and compliance $\boldsymbol{M}^e$ of the elastic-plastic material. The projector tensors and matrices have the properties shown in (2.2.28) augmented here to include those of the $\boldsymbol{E}$ tensor (Ponte Castaneda 1996).

$$\left.\begin{array}{l} \boldsymbol{JJ} = \boldsymbol{J} \quad \boldsymbol{KK} = \boldsymbol{K} \quad \boldsymbol{KJ} = \boldsymbol{0} \quad \boldsymbol{J} + \boldsymbol{K} = \boldsymbol{I} \quad \boldsymbol{K} - \boldsymbol{E} = \boldsymbol{F} \\ \boldsymbol{FF} = \boldsymbol{F} \quad \boldsymbol{EF} = \boldsymbol{0} \quad \boldsymbol{EJ} = \boldsymbol{0} \quad \boldsymbol{FJ} = \boldsymbol{0} \\ \boldsymbol{KE} = \boldsymbol{EK} = \boldsymbol{EE} = \boldsymbol{E} \end{array}\right\} \tag{11.3.12}$$

Proof of consistency follows from

$$\left.\begin{aligned}\boldsymbol{\mathcal{L}}\boldsymbol{\mathcal{M}} &= \boldsymbol{JJ} + \boldsymbol{KK} + [6G/(2H)]\boldsymbol{KE} - [1 + H/(3G)]^{-1}\boldsymbol{EK} \\ &\quad - [3G/H][1 + H/(3G)]^{-1}\boldsymbol{EE} \\ &= \boldsymbol{J} + \boldsymbol{K} = \boldsymbol{I}\end{aligned}\right\} \tag{11.3.13}$$

In the contracted tensorial notation of Sect. 2.1, the Kronecker symbol is $\boldsymbol{\delta} = [1,\ 1,\ 1,\ 0,\ 0,\ 0]^{\mathrm{T}}$, the projection matrices $\boldsymbol{J} = \boldsymbol{\delta}\boldsymbol{\delta}^{\mathrm{T}}/3$ and $\boldsymbol{K} = \boldsymbol{I} - \boldsymbol{J}$ are both diagonally symmetric and idempotent, and together with $\boldsymbol{E}$ in (11.3.3), they satisfy the connections implied by (11.3.12). Therefore, the above proof applies in both tensorial component and in contracted tensorial notation. Since the $\boldsymbol{E}$ matrix typically has nonzero off-diagonal coefficients, connections between the contracted tensorial matrices $\boldsymbol{\mathcal{L}}^p$ and their engineering forms no longer follow from (1.1.22). However, similar connections can be established by modification of the stiffness matrix.

Separation of the elastic and plastic parts of the instantaneous tangential stiffness and compliance tensors, $\boldsymbol{\mathcal{L}} = \boldsymbol{L}^e + \boldsymbol{\mathcal{L}}^p$, $\boldsymbol{\mathcal{M}} = \boldsymbol{M}^e + \boldsymbol{\mathcal{M}}^p$, shows that

$$\boldsymbol{\mathcal{L}}^p = -\frac{2G}{1 + (H/3G)}\boldsymbol{E} \quad \boldsymbol{\mathcal{M}}^p = \frac{3}{2H}\boldsymbol{E} \quad \boldsymbol{\mathcal{L}}^p\boldsymbol{\mathcal{M}}^p = -\frac{3G/H}{[1 + (H/3G)]}\boldsymbol{E} \tag{11.3.14}$$

That confirms that only the elastic and total instantaneous stiffness and compliance are consistent, while the plastic parts by themselves are not. The last two connections between the thermal vectors in (11.3.9) are verified by multiplying the respective tensors, while using the relation $L^e_{ijkl}n_{kl} = 2Gn_{ij}$.

Equations (11.3.11) provide the instantaneous elastic-plastic tangent stiffness and compliance derived by differentiation of the constitutive relation. Evaluation of plastic strain increments in each next loading step requires application of a selected stress and temperature increments, of the yield condition, hardening rule and loading/unloading criteria, followed by construction of the current $\boldsymbol{E}$ projection matrix. Different incremental iterative solution procedures can be used in finding a numerical solution. To preserve the quadratic rate of convergence of the Newton-Raphson equilibrium iteration, it is preferable to replace the tangent stiffness by an algorithmic stiffness obtained by differentiation of the numerical algorithm used in stress evaluation. This consistent linearization technique was developed by Hughes and Pister (1978), Hughes and Taylor (1978) and Simo and Hughes (1998). A flowchart for equilibrium solution using the secant Newton method with algorithmic moduli can be found in Box 6.6, Sect. 6.4.7 in Belytschko et al. (2000).

Chapter 12
Inelastic Composite Materials

Initial applications of elastic–plastic and other inelastic constitutive relations in predicting overall response of heterogeneous materials had focused on polycrystalline metals, modeled as a multiphase system of randomly orientated single crystal grains which were assigned certain yield conditions and slip mechanisms. Early work includes the slip theory of Batdorf and Budiansky (1949), the rigid-plastic single crystal system of Bishop and Hill (1951), the elastic–plastic K.B.W. model of Kröner (1961) and the self-consistent approximation by Hershey (1954) and by Budiansky and Wu (1962). Further developed by Hill (1965c, 1967) and implemented by Hutchinson (1970), the SCM approximation extended the elasticity form of the method to polycrystals and two-phase composites. That and numerous other extensions of elastic micromechanical methods to inelastic systems provide an interface with the latter. However, they often assume uniform elastic and inelastic deformation in each grain, or in the entire matrix of a particulate or fibrous composite, according to a specified constitutive relation. Since local deformation is not uniform, the overall response predicted by such theories is not supported by experiments, as shown in Sect. 12.2.2. Nonuniform local deformation was examined on composite cylinders under axisymmetric and thermal loads, and in shakedown state, by Dvorak and Rao (1976a, b), Tarn, et al. (1975). General loading effects were investigated with models which constrained only longitudinal deformation by elastic fibers (Dvorak and Bahei-El-Din 1979, 1980, 1982). More recent work, supported by numerical methods, has focused on realistic aspects of deformation mechanisms of polycrystals and composites, as reviewed by Dawson, Hutchinson, Torquato and others in a report on research trends in solid mechanics (Dvorak 1999).

An alternative early approach by Mulhern et al. (1967, 1969) and Spencer (1972, 1987) focused on macroscopic behavior of unidirectional ‘ideal fiber reinforced materials’ at finite inelastic strain. In that regime, the material was subjected to kinematic constraints of fiber inextensibility and overall incompressibility, inspired by modeling of large deformations of elastic materials such as rubber reinforced by inextensible cords, which was proposed in the 1950s by Adkins and Rivlin and summarized by Green and Adkins (1960). Yield conditions and associated flow

G.J. Dvorak, *Micromechanics of Composite Materials*, Solid Mechanics and Its Applications 186, DOI 10.1007/978-94-007-4101-0_12,

rules were written as functions overall invariants of transverse isotropy (2.2.15), analogous to those in Hill's (1948) anisotropic plasticity theory. The methodology was extended to laminates by Smith and Spencer (1970) and by other investigators. The implied independence of overall shear deformation on the longitudinal normal stress component was later confirmed, but only at small strains, by experimental results of Dvorak et al. (1988), shown later in Figs. 12.9 and 12.10, and examined by Spencer (1992).

Plastic deformations of fiber composite structures are typically restricted in the longitudinal direction by the elastic fibers, with maximum strain of 1–2%. Large strains can be present in unidirectional materials, on planes aligned with the fibers, especially at notch or crack tips. Those instances were analyzed and confirmed by experiments on unidirectional laminates by Dvorak et al. (1988), Bahei-El-Din et al. (1989), and Farez and Dvorak (1989, 1993). Large plastic deformations are also found in polycrystals and other situations, as reviewed by Nemat-Nasser (1992, 2004). Damage and plasticity of fibrous composites was studied by Kattan and Voyijadis (1993), Fish et al. (1999) among many others. More recent application of numerical methods, especially those based the fast Fourier transform by Moulinec and Suquet (1994) identified localized slip bands on planes aligned with stiff fibers in metal matrices with low hardening, at small overall strain.

A different research direction has been pursued on nonlinear composite materials, where the inelastic matrix phase is assumed to follow a power law with a single material parameter, such as the instantaneous shear modulus in deformation theory of plasticity. This class of materials was investigated by Talbot and Willis (1985, 1992, 1997), Willis (1991), Ponte-Castaneda (1991, 1996), Ponte-Castaneda and Willis (1995), deBotton and Ponte-Castaneda (1993). Review of this work, which attracted large attention in numerous papers, can be found in Ponte-Castaneda and Suquet (1998).

This chapter focuses on modeling of fibrous metal matrix composites at small elastic–plastic strains. The actual materials have an aluminum matrix and they are reinforced by relatively large, $\sim$150 μm diameter fibers, or particles of similar size. Matrix local deformation is not assumed to be uniform, since the actual local fields depend on the deformation history of each material point, as described in Chap. 11. Elastic–plastic deformation is treated by numerical methods based on unit cell models discretized by finite elements. In particular, local and overall inelastic deformation is analyzed here by the transformation field analysis method in Sect. 12.1. In Sect. 12.2 we review the bimodal plasticity theory and experimental evidence that illustrates the capability of different modeling techniques to predict at least certain parts of actual response. Section 12.3 examines translations of yield and loading surface clusters due to thermal hardening, caused by temperature induced changes in local stress states. Utility and limitations of different modeling techniques are summarized in a closing section.

12.1 Transformation Field Analysis (TFA) of Inelastic Deformation

This method is based on a particular interpretation of the well-known elastic–plastic response of a material point or small volume V_η, to a loading step applied by a uniform stress increment $\dot{\boldsymbol{\sigma}}_\eta^k$ from a current stress state $\boldsymbol{\sigma}_\eta^k$ to a new state $\boldsymbol{\sigma}_\eta^{k+1} = \boldsymbol{\sigma}_\eta^k + \dot{\boldsymbol{\sigma}}_\eta^k$. According to (11.3.5), the total strain caused in V_η by the loading step is

$$\left.\begin{aligned} &\boldsymbol{\varepsilon}_\eta^{k+1} = \boldsymbol{\varepsilon}_\eta^k + \boldsymbol{\mathcal{M}}_\eta^k \dot{\boldsymbol{\sigma}}_\eta^k = \boldsymbol{\varepsilon}_\eta^k + \dot{\boldsymbol{\varepsilon}}_\eta^{ke} + \dot{\boldsymbol{\varepsilon}}_\eta^{kp} \\ &\dot{\boldsymbol{\varepsilon}}_\eta^{ke} = \left[\frac{1}{3K_\eta}\boldsymbol{J} + \frac{1}{2G_\eta}\boldsymbol{K}\right]\dot{\boldsymbol{\sigma}}_\eta^k \quad \dot{\boldsymbol{\varepsilon}}_\eta^{kp} = \frac{3}{2H_\eta^k}\boldsymbol{E}_\eta^k \dot{\boldsymbol{\sigma}}_\eta^k \end{aligned}\right\} \tag{12.1.1}$$

The instantaneous compliance $\boldsymbol{\mathcal{M}}_\eta^k$ is derived from (11.3.11), where the deviatoric components of $\boldsymbol{\sigma}_\eta^k$ provide coefficients of the $\boldsymbol{E}_\eta^k$ matrix in (11.3.3). Application of a selected yield condition and hardening rule during the loading step assures that the $\boldsymbol{\sigma}_\eta^{k+1}$ is located on the new loading surface. Instantaneous elastic unloading of V_η to $\boldsymbol{\sigma}_\eta \to 0$ would reveal the total plastic strain $\boldsymbol{\varepsilon}_\eta^p$ which has accumulated in V_η along the loading path leading to the new stress state $\boldsymbol{\sigma}_\eta^{k+1}$.

From this perspective, an elastic–plastic solid in a volume V, consisting of many subvolumes V_η, responds to plastic loading by accommodating an interacting distribution of variable plastic strains or eigenstrains $\boldsymbol{\varepsilon}_\eta^p$, in the original elastic material. The accommodation is facilitated by elastic transformation influence functions, evaluated in preprocessing as (6×6) matrices for each pair of Gauss points or uniform strain elements subdividing the solution domain. These functions provide the strain or stress caused in each element by application of a unit eigenstrain or eigenstress in the other element of the pair. They depend only on elastic moduli, geometry, and refinement of the subdivision of both elastic and inelastic phases. Their derivation appears in Sect. 12.1.3.

For two-phase and multiphase systems such functions were derived in Sects. 3.6.2 and 8.2, where they only monitor interactions between individual phases, or their volume fractions. Here they are replaced by a different set of influence functions, for evaluation of the effect of *nonuniform eigenstrain distributions in the phases.*

Total strain fields caused in V at any point of the loading path are derived by superimposing the current eigenstrain $\boldsymbol{\varepsilon}_\eta^p$ and elastic strain fields. The latter include those generated by mechanical loads, and the residual fields that enforce compatibility of total strain fields in the presence of usually incompatible eigenstrains. Although certain eigenstrains may result from processes that depend on past or current inelastic deformation and on time, at the end of each loading step their interactions and local and overall effects are determined by the elastic response of the host material or structure to both applied and eigenstrain loads, c. f. Sect. 3.6.1.

The transformation field analysis is implemented in a finite element program, as described by Dvorak (1993), Dvorak et al. (1994) and Dvorak and Bahei-El-Din (2000). The overall and local eigenstrains are found by an iterative computation which assures compliance with local constitutive relations, equilibrium and compatibility, at each Gauss point and in each step of the loading path. Response to applied loads is then determined using a selected homogenization approach, outlined here for the instantaneous overall tangent stiffness and for the underlying local fields. A specific strategy for equilibrium solution using the secant Newton method with algorithmic moduli, presented at the end of Chap. 11, can be adopted for computation of the overall algorithmic stiffness and local fields. The TFA method provides the same simulation of inelastic behavior of a unit cell as does a standard finite element program for elastic–plastic or other inelastic materials, usually at much less expense.

Oskay and Fish (2007) and other authors emphasize the large savings in computational cost in comparison with standard finite element programs for inelastic analysis. As an illustration, they consider a square composite panel with a centered elastic fiber and a blunt notch at the panel edge. Four reduced order models with different numbers of interface and phase partitions were compared with the direct homogenization. The computational cost of one of the four models that showed 85% accuracy in crack growth rates was found to be roughly 3,000 times lower than that of direct homogenization. The saving is realized by retaining the mechanical and transformation concentration factor magnitudes in each step, and without regard to the number of times that the inelastic unit cell problem has to be solved.

Numerous applications and modifications of the method have appeared since its 1992–1994 debut, available on Google search for "transformation field analysis." Papers that illustrate applications of the method are, among others, by Prochazka (1997) on slope optimization, by Baweja et al. (1998) for creep of concrete, by Benveniste (1987a, b) and Dvorak and Benveniste (1997) on piezoelectric composites, by Dvorak (2001) on damage modeling, by Franciosi and Berberinni (2007) on polycrystal plasticity, by Sacco (2009) on periodic masonry, and by Bahei-El-Din (2009) and Bahei-El-Din et al. (2010) on electromechanical coupling in woven composites exhibiting damage, and on multiscale damage mechanics.

12.1.1 Periodic Unit Cell Models

Materials with random distributions of aligned fibers in the transverse plane had been modeled by unit cells containing several dozen fibers, for example, by Brockenbrough et al. (1991) and by others. Overall response, as illustrated by computed stress–strain diagrams, depends primarily on the fiber volume fractions when a unit cell is loaded by normal stress in the longitudinal direction. However, when the fiber volume fraction grows beyond $c_f > 0.20$, and a given unit cell is loaded by transverse tension or shear, inelastic response depends on both fiber distribution in the transverse plane and on fiber shape, and also on the direction of applied stress. In particular, rotation of a given cell by a different angle around

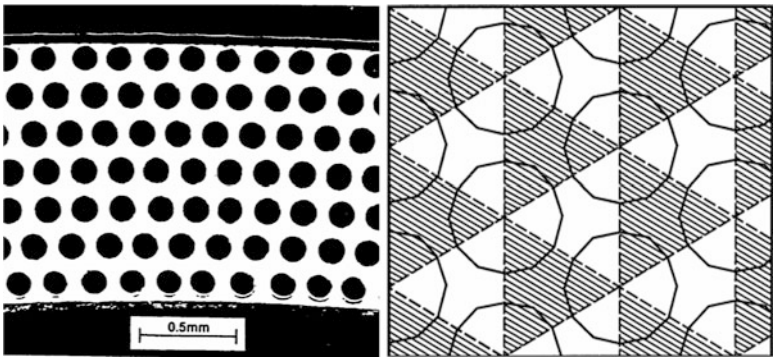

Fig. 12.1 High contrast micrograph of a transverse crosssection B/Al composite, $c_f = 0.45$, and its representation by the periodic hexagonal array model

the longitudinal axis, with respect to a fixed transverse stress state, generates very distinct stress–strain diagrams in the inelastic range. Such behavior can be attributed to the particular local slip mechanisms created in the apparently random microstructures by the different loading directions. It implies that even large unit cells containing many fibers may not be regarded as representative volumes.

This deficiency is often remedied by modeling of inelastic heterogeneous materials as microstructures with a periodic distribution of particulate or fiber reinforcements. Actual fiber distributions of this kind are found in metal matrix composites fabricated using directed fiber layup on a matrix foil, followed by consolidation under transverse pressure at elevated temperature. Examples of periodic models for fiber composites can be found in Accorsi and Nemat-Nasser (1986), Suquet (1987, 1997), Wu et al. (1989) Teply and Reddy (1990), Aboudi (1991), Teply et al. (1992), Walker (1993), Nemat-Nasser and Hori (1999), Fish et al. (1997). They offer a good approximation of the microgeometry of fibrous materials with periodic, transversely isotropic distributions of aligned fibers in the transverse plane.

A micrograph of such composite and of its representation by the periodic hexagonal array (PHA) model are shown in Fig. 12.1 (Dvorak and Teply 1985, Teply and Dvorak 1987, 1988). The material volume is subdivided into similar unit cells, each containing only one or fractions of a single fiber. Inelastic response depends again on the fiber shape and on the loading direction, but not on the spatial distribution of the fibers, only on their volume fraction. Since all unit cells undergo the same deformation under given load, each cell can be regarded as a representative volume. The transverse plane of the model is divided into shaded and clear triangular cells, with vertices in the fiber centers. Figure 12.2 shows such cell with supports and loads.

The dimensions imply that the size of each triangle area is equal to unity, and c_f denotes the fiber volume fraction. Model geometry can be adjusted to represent periodic distributions of aligned ribbons of polygonal crossections, or composites reinforced by aligned short fibers or particles.

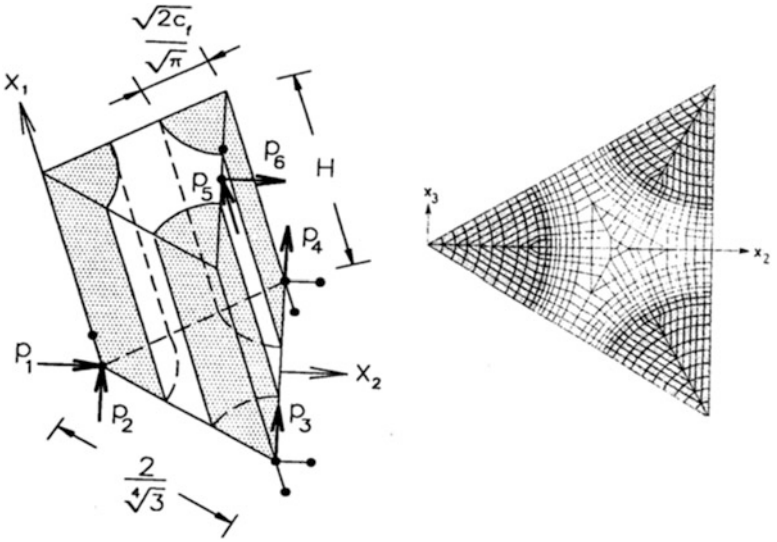

Fig. 12.2 Geometry, constraints and loading, and an example of subdivision of the unit cell of the periodic hexagonal array model

Displacement boundary conditions applied to the unit cell include six constraints to eliminate rigid body motion, multipoint constraints at the triangular boundary derived from the assumed periodic geometry of the microstructure, and generalized plane strain boundary conditions. Vertices and midpoints of the sides of the top and bottom triangles of the prismatic cell undergo relative displacements that would generate the same uniform strain field $\boldsymbol{\varepsilon}^0$ in a homogeneous solid. This guarantees that the deformation fields in the clear triangles are the same as those in the shaded triangles, rotated by $-\pi$. Analysis of a single triangular prismatic unit cell then provides the periodic fields in the entire volume. Derivation of the periodic displacement boundary conditions is described in detail by Teply and Dvorak (1988).

The unit cell of volume V is divided into subvolumes represented by finite elements, V_η, η, $\rho = 1, 2, \ldots, M$, interconnected at nodes i, $j = 1, 2, \ldots, R$, such that each subvolume belongs either to the matrix or to the fiber. Assuming a linear displacement field in an equivalent macroscopically homogeneous volume, the method of virtual work can be used to compute the nodal forces, P_k, $k = 1, 2, \ldots, 6$, applied as shown in Fig. 12.2, from the overall stresses (Bahei-El-Din and Dvorak 2000). The mesh refinement shown provides a detailed description of the local fields, but close estimate of overall response can be obtained from unit cells with lower mesh density.

12.1.2 Mechanical and Transformation Influence Functions

Local strain or stress fields generated by application of uniform overall strain $\boldsymbol{\varepsilon}^0 = \bar{\boldsymbol{\varepsilon}}$ or overall uniform stress $\boldsymbol{\sigma}^0 = \bar{\boldsymbol{\sigma}}$, and a by distribution of inelastic strains in the subelements of a unit cell, are described by equations similar to those used in (3.6.5) and in analysis of thermal fields. In the present application, they are written for the two distinct boundary conditions as

$$\left.\begin{aligned} \boldsymbol{\varepsilon}_\eta &= \boldsymbol{A}_\eta \bar{\boldsymbol{\varepsilon}} + \sum_{\rho=1}^{M} \boldsymbol{D}_{\eta\rho} \left(\boldsymbol{\varepsilon}_\rho^{in} + \boldsymbol{\varepsilon}_\rho^{\theta} \right) \\ \boldsymbol{\sigma}_\eta &= \boldsymbol{B}_\eta \bar{\boldsymbol{\sigma}} + \sum_{\rho=1}^{M} \boldsymbol{F}_{\eta\rho} \left(\boldsymbol{\sigma}_\rho^{re} + \boldsymbol{\sigma}_\rho^{\theta} \right) \end{aligned}\right\} \tag{12.1.2}$$

Prior to proceeding with solution of the above equations, we outline evaluation of the two pairs of mechanical and transformation influence functions $\boldsymbol{A}_\eta$, $\boldsymbol{D}_{\eta\rho}$ and $\boldsymbol{B}_\eta$, $\boldsymbol{F}_{\eta\rho}$. These influence functions and their connections with the Green's function were described in Sect. 8.2.1. In the present context, they are derived for use in a unit cell, subdivided by three-dimensional constant strain elements V_η, $\eta, \rho = 1, 2, \ldots, M$, interconnected at nodes $i, j = 1, 2, \ldots, R$.

Coefficients of the (6×6) *mechanical stress and strain concentration factor* matrices $\boldsymbol{A}_\eta$ and $\boldsymbol{B}_\eta$ are computed by solving in turn six elastic problems. Solutions are sought in a unit cell that is free of any initial stresses or eigenstrains. Load applied in each solution of the six problems is limited to one (6×1) overall uniform strain or stress vector $\bar{\boldsymbol{\varepsilon}}_k = \bar{\boldsymbol{i}}_k$, or $\bar{\boldsymbol{\sigma}}_k = \bar{\boldsymbol{i}}_k$, $1 \le k \le 6$, where $\bar{\boldsymbol{i}}_k$ is the k-th column of the identity matrix $\boldsymbol{I}$. The six local strain $\boldsymbol{\varepsilon}_\eta^k = \boldsymbol{A}_\eta \bar{\boldsymbol{i}}_k$ or stress $\boldsymbol{\sigma}_\eta^k = \boldsymbol{B}_\eta \bar{\boldsymbol{i}}_k$ components found in each of the M elements V_ρ, in response to application of $\bar{\boldsymbol{i}}_k$, comprise the k-th column of the $\boldsymbol{A}_\eta$ or $\boldsymbol{B}_\eta$ matrix. For example, application of the load vector $\bar{\boldsymbol{\varepsilon}}_4 = [0,\ 0,\ 0,\ 1,\ 0,\ 0]^{\mathrm{T}}$ to the unit cell generates (6×1) strain vectors in each element V_η, which are equal to the fourth columns of $\boldsymbol{A}_\eta$ or $\boldsymbol{B}_\eta$. The elastic mechanical concentration factors remain in effect during any loading program that may involve inelastic deformation, but preserves the magnitude of the original elastic moduli.

Coefficient of *the transformation concentration factors* are generated in a similar manner. The eigenstrain concentration factor is a (6×6) matrix $\boldsymbol{D}_{\eta\rho}$, which evaluates the contribution to the strain in all elements V_η by a uniform eigenstrain applied in element V_ρ at $\bar{\boldsymbol{\varepsilon}} = \boldsymbol{0}$. During evaluation of the eigenstrain influence functions, the unit cell undergoes only elastic deformation, under displacement boundary conditions that guarantee zero overall strain. The goal is to construct individual columns $\boldsymbol{d}_{\eta\rho}^k$ of (6×6) matrices $\boldsymbol{D}_{\eta\rho}$, which are local strains $\boldsymbol{\varepsilon}_\eta = \boldsymbol{D}_{\eta\rho}\boldsymbol{\mu}_\rho$ in all elements V_η caused by one of six unit-valued eigenstrain vectors $\boldsymbol{\mu}_\rho = \boldsymbol{i}_\rho^{\,k}$, applied in turn in each single V_ρ, while all other elements are free of any

transformations. Columns of the self-induced $\boldsymbol{D}_{\eta\eta}$ matrices are obtained in response to $\boldsymbol{\mu}_\eta = \boldsymbol{i}_\eta^k$. Again, the transformation concentration factors remain constant as long as the original elastic moduli of each element are preserved. Construction of $\boldsymbol{D}_{\rho\eta}$ for all M elements requires solving $6M$ elasticity problems, which may become time-consuming in large or densely subdivided unit cells. This effort can be reduced in cells with one or more planes of symmetry.

In the following derivation of the columns $\boldsymbol{d}_{\eta\rho}^k$, top tildes ($\sim$) are used to distinguish FEM terms from similarly denoted micromechanics terms. The strain vector in each element is related to the vector nodal displacements $\tilde{\boldsymbol{\alpha}}_\eta = [\alpha_i^\eta,\ \alpha_j^\eta, \ldots]^{\mathrm{T}}$ by

$$\boldsymbol{\varepsilon}_\eta = \tilde{\boldsymbol{S}}\boldsymbol{u}_\eta = \tilde{\boldsymbol{S}}\tilde{\boldsymbol{N}}_\eta\tilde{\boldsymbol{\alpha}}_\eta = \tilde{\boldsymbol{B}}_\eta\tilde{\boldsymbol{\alpha}}_\eta \tag{12.1.3}$$

where $\tilde{\boldsymbol{S}}$ is the kinematic linear differential operator, $\boldsymbol{u}_\eta$ is the displacement field, $\tilde{\boldsymbol{N}}_\eta = [\boldsymbol{N}_i^\eta,\ \boldsymbol{N}_j^\eta, \ldots]^{\mathrm{T}}$ are prescribed shape functions, linear in the Cartesian coordinates for a uniform strain field in each element, and $\tilde{\boldsymbol{B}}_\eta$ is a matrix with constant coefficients.

Local stress $\boldsymbol{\sigma}_\eta$ in each element that has been transformed by an eigenstrain $\boldsymbol{\mu}_\eta$ and the tractions on the element surface are reproduced by subjecting the element to the nodal force $\tilde{\boldsymbol{q}}_\eta = [\tilde{\boldsymbol{q}}_{\mathbf{i}}^\eta,\ \tilde{\boldsymbol{q}}_j^\eta, \ldots]^{\mathrm{T}}$, statically equivalent to the boundary tractions causing element stress, and derived from virtual work.

$$\boldsymbol{\sigma}_\eta = \tilde{\boldsymbol{L}}_\eta\left(\boldsymbol{\varepsilon}_\eta - \boldsymbol{\mu}_\eta\right) \quad \boldsymbol{q}_\eta = \int_{\Omega_\eta} \tilde{\boldsymbol{B}}_\eta^{\mathrm{T}}\boldsymbol{\sigma}_\eta \mathrm{d}\Omega_\eta \tag{12.1.4}$$

where $\tilde{\boldsymbol{L}}_\eta$ is the element stiffness matrix. Nodal forces $\tilde{\boldsymbol{q}}_\eta$ at each node i of element V_η are a sum of stresses contributed by the total strain and eigenstrain vectors.

$$\tilde{\boldsymbol{q}}_{\mathbf{i}}^\eta = \sum_{j=1}^{P} \tilde{\boldsymbol{K}}_{ij}^\eta\tilde{\boldsymbol{\alpha}}_j^\eta + \tilde{\boldsymbol{f}}_i^\eta \quad \tilde{\boldsymbol{K}}_{ij}^\eta = \int_{\Omega_\eta} \left(\tilde{\boldsymbol{B}}_i^\eta\right)^{\mathrm{T}}\boldsymbol{L}_\eta\tilde{\boldsymbol{B}}_j^\eta \,\mathrm{d}\Omega_\eta \quad \tilde{\boldsymbol{f}}_i^\eta = -\int_{\Omega_\eta} \left(\tilde{\boldsymbol{B}}_i^\eta\right)^{\mathrm{T}}\boldsymbol{L}_\eta\boldsymbol{\mu}_\eta \,\mathrm{d}\Omega_\eta \tag{12.1.5}$$

where P is the total number of element nodes, $\tilde{\boldsymbol{K}}_{ij}^\eta$ is the ij-partition of the element stiffness matrix, and $\tilde{\boldsymbol{f}}_i^\eta$ are nodal forces caused at node i by the uniform eigenstrains $\boldsymbol{\mu}_\eta$. Since the unit eigenstrains $\boldsymbol{\mu}_\rho$ are columns $\boldsymbol{i}_k$, $k = 1, 2, \ldots, 6$ of the identity matrix $\boldsymbol{I}$, such that, for example, $\mathbf{i}_4 = [0,\ 0,\ 0,\ 1,\ 0,\ 0]^{\mathrm{T}}$, the load vector in (12.1.5) generated by each such eigenstrain component is $\tilde{\boldsymbol{f}}_i^\eta = -\left(\tilde{\boldsymbol{B}}_i^\eta\right)^{\mathrm{T}}\tilde{\boldsymbol{l}}_k^\eta\,\Omega_\eta$, where $\tilde{\boldsymbol{l}}_k^\eta$ is the k-th column of $\boldsymbol{L}_\eta$.

In the absence of external loads, the sum of forces contributed by all M elements to an interconnecting node must vanish.

$$\sum_{\eta=1}^{M} \tilde{\boldsymbol{q}}_{\mathbf{i}}^{\eta} = \sum_{\eta=1}^{M} \left[\sum_{j=1}^{P} \tilde{\boldsymbol{K}}_{ij}^{\eta} \tilde{\boldsymbol{\alpha}}_{j}^{\eta} + \tilde{\boldsymbol{f}}_{i}^{\eta} \right] = 0 \tag{12.1.6}$$

These matrix equations, for all nodes R of the M elements, can be augmented and written as

$$\tilde{\boldsymbol{K}}\tilde{\boldsymbol{\alpha}} = \tilde{\boldsymbol{f}} \quad \tilde{K}_{ij} = \sum_{\eta=1}^{M} \tilde{K}_{ij}^{\eta} \quad \tilde{\boldsymbol{f}}_{i} = -\sum_{\eta=1}^{M} \tilde{\boldsymbol{f}}_{i}^{\eta} \tag{12.1.7}$$

where $\tilde{\boldsymbol{K}} = \tilde{\boldsymbol{K}}^{\mathrm{T}}$ is the overall stiffness matrix of the domain, which is symmetric and can be decomposed into upper and lower triangular factors $\boldsymbol{K}_U = \boldsymbol{K}_L^{\mathrm{T}}$, using Cholesky's method. The overall load vector is denoted by $\tilde{\boldsymbol{f}}$, and $\tilde{\boldsymbol{\alpha}} = [\tilde{\boldsymbol{\alpha}}_1, \tilde{\boldsymbol{\alpha}}_2, \ldots, \tilde{\boldsymbol{\alpha}}_R]^{\mathrm{T}}$ is the vector of as yet unknown nodal displacements. Those follow from forward and backward solutions of the equations

$$\left.\begin{aligned} \tilde{\boldsymbol{K}}_L \left[\boldsymbol{y}^{(1)}, \boldsymbol{y}^{(2)}, \ldots, \boldsymbol{y}^{(6M)}\right]^{\mathrm{T}} &= \left[\tilde{\boldsymbol{f}}^{(1)}, \tilde{\boldsymbol{f}}^{(2)}, \ldots, \tilde{\boldsymbol{f}}^{(6M)}\right]^{\mathrm{T}} \\ \tilde{\boldsymbol{K}}_U \left[\tilde{\boldsymbol{\alpha}}^{(1)}, \tilde{\boldsymbol{\alpha}}^{(2)}, \ldots, \tilde{\boldsymbol{\alpha}}^{(6M)}\right]^{\mathrm{T}} &= \left[\boldsymbol{y}^{(1)}, \boldsymbol{y}^{(2)}, \ldots, \boldsymbol{y}^{(6M)}\right]^{\mathrm{T}} \end{aligned}\right\} \tag{12.1.8}$$

Finally, the element nodal displacements $\tilde{\boldsymbol{\alpha}}_\eta$ are extracted from the solutions for $\tilde{\boldsymbol{\alpha}}^{(i)}$ and substituted in (12.1.3), yielding the components $\boldsymbol{\varepsilon}_\eta$ of the strain caused in the element Ω_η by a unit component $\boldsymbol{i}_k^{\rho}$ of the eigenstrain $\boldsymbol{\mu}_\rho$. This strain is the k-th column $\boldsymbol{d}_{\eta\rho}^{k}$ of the eigenstrain concentration factor matrix $\boldsymbol{D}_{\eta\rho}$. It can be written symbolically as

$$\boldsymbol{d}_{\eta\rho}^{k} = \tilde{\boldsymbol{B}}_\eta \tilde{\boldsymbol{P}}_\eta \tilde{\boldsymbol{\alpha}}^{(i)} = \tilde{\boldsymbol{B}}_\eta \tilde{\boldsymbol{P}}_\eta \tilde{\boldsymbol{K}}^{-1} \tilde{\boldsymbol{f}} \tag{12.1.9}$$

where $\tilde{\boldsymbol{B}}_\eta$ is the matrix in (12.1.3) and $\tilde{\boldsymbol{\alpha}}_\eta = \tilde{\boldsymbol{P}}_\eta \tilde{\boldsymbol{\alpha}}^{(i)}$ are the nodal displacements of element η caused by the overall displacements. The overall load vector $\tilde{\boldsymbol{f}}$ in (12.1.5) is a function of the unit-valued eigenstrain components applied in turn in each element of the unit cell. Therefore, the $\boldsymbol{D}_{\eta\rho}$ matrix has constant coefficients that depend only on the geometry and subdivision of the unit cell, and on stiffness coefficients of the phases.

Derivation of the stress transformation factor matrices $\boldsymbol{F}_{\eta\rho}$ follows a similar procedure, but under load vectors derived from $6M$ unit eigenstress vectors $\boldsymbol{\lambda}_\eta = -\boldsymbol{L}_\eta \boldsymbol{\mu}_\eta = \boldsymbol{i}_k, k = 1, 2, \ldots, 6$.

As already mentioned, evaluation of the concentration factor matrices can be simplified in unit cell that have one or more planes of symmetry. For example, the cell shown in Fig. 12.2 can be divided into six identical triangles. Therefore, the $\boldsymbol{A}_\eta$ and $\boldsymbol{D}_{\eta\rho}$ or $\boldsymbol{B}_\eta$ and $\boldsymbol{F}_{\eta\rho}$ found in the entire domain during application of the unit eigenstrains $\boldsymbol{i}_k$ in one of the six triangles can serve in determination of the complete set of concentration factors for all M elements. The required transformations of the single triangle results are described in detail by Dvorak et al. (1994).

As expected, the strength of interaction decreases when element V_η is far removed from element V_ρ where the eigenstrain $\boldsymbol{\mu}_\rho$ is applied. That does not indicate that computation of the $\boldsymbol{D}_{\eta\rho}$ or $\boldsymbol{F}_{\eta\rho}$ should be reduced to certain areas, because even weak interaction may transmit a significant contribution to $\boldsymbol{\varepsilon}_\eta$ by a large eigenstrain $\boldsymbol{\mu}_\rho$. However, those products $\boldsymbol{D}_{\eta\rho}\boldsymbol{\mu}_\rho$ or $\boldsymbol{F}_{\eta\rho}\boldsymbol{\lambda}_\rho$ which make only negligible contributions to the total local strain or stress in (11.3.1) may be discarded. In elements V_η, where no eigenstrains $\boldsymbol{\mu}_\eta$ are to be generated, such as those in an elastic fiber held at constant temperature, it is only necessary to find the $\boldsymbol{D}_{\eta\rho}\boldsymbol{\mu}_\rho$ or $\boldsymbol{F}_{\eta\rho}\boldsymbol{\lambda}_\rho$ transmitted by any $\boldsymbol{\mu}_\rho$ from elements V_ρ .

Influence functions similar to those above are also used in the boundary element method, to develop a fundamental solution which describes the effect of a concentrated force applied at an interior point, on displacements at boundary points. In contrast, the present 'fundamental solution' applies to eigenstrain interactions in each pair of elements of a discretized domain, including those on the boundary.

12.1.3 Local and Overall Yield Surfaces

During elastic deformation or after complete unloading of a unit cell, any local uniform stress vector $(\sigma_{ij}^\eta - \alpha_{ij}^\eta)$, contained within the local yield surface of each element V_η, is related to a uniform overall stress vector $(\bar{\sigma}_{kl} - \bar{\alpha}_{kl})$ by the stress concentration factor B_{ijkl}^η that depends on elastic moduli, geometry and volume fractions of the phases. By substituting the element stress into the yield condition (11.1.1), one can derive the yield surface of each element in both local and overall stress space. These relations are

$$\left.\begin{aligned} \left(\sigma_{ij}^\eta - \alpha_{ij}^\eta\right) &= B_{ijkl}^\eta \left(\bar{\sigma}_{kl} - \bar{\alpha}_{kl}^\eta\right) \\ g_\eta\left(\sigma_{ij}^\eta - \alpha_{ij}^\eta\right) &= \tilde{J}_2\left(s_{ij}^\eta\right) - Y_\eta^2\left(\varepsilon_{eq}^p, \theta\right) = 0 \\ G_\eta\left(\bar{\sigma}_{ij} - \bar{\alpha}_{ij}^\eta\right) &= g_\eta\left[B_{ijkl}^\eta \left(\bar{\sigma}_{kl} - \bar{\alpha}_{kl}^\eta\right)\right] = 0 \end{aligned}\right\} \tag{12.1.10}$$

The σ_{ij}^η is current stress in V_η, and α_{ij}^η is the position of the center of the yield surface in the local σ_{ij}^η −space. The second equation applies when the local stress satisfies the element yield condition $g_\eta = 0$, where $\tilde{J}_2$ is the second invariant of the deviatoric stress, written as a function of s_{ij}^η, according to (11.1.1), and Y_η is the current yield stress of the material element in the matrix phase. The third equation evaluates the yield surface G_η of element V_η, centered at $\bar{\alpha}_{ij}^\eta$ in the overall stress space. Since the concentration factor B_{ijkl}^η is different in each element, overall yield surfaces G_η are branches of a cluster of element yield surfaces in the overall stress space. An example of such clusters of element yield surfaces in the overall stress space is shown later in Fig. 12.15. In a unit cell that is in unloaded state, or has not yet experienced inelastic deformation, the interior envelope of the

cluster represents a current loading or yield surface, of the aggregate. As long as the overall stress path is contained within this interior envelope, the cluster of the unit cell remains in elastic state and the G_η yield surfaces remains fixed in the $\bar{\sigma}_{ij}$ −space.

If a unit cell is free of thermal or other residual stresses, then both translation vectors α_{ij}^{η} and $\bar{\alpha}_{ij}^{\eta}$ are equal to zero. Next, suppose that a uniform overall stress increment $\Delta\bar{\sigma}_{ij} = \Delta\bar{\sigma}_{ij}^{0}$ has been applied to cause inelastic deformation in some or all elements of the aggregate. As indicated in Sect. 11.2, the elements that yield under $\Delta\bar{\sigma}_{ij}^{0}$ follow their own hardening and flow rules. Guided by experimental results described in Sect. 12.2.2, we follow here the Phillips rule that requires local yield surface center translation (11.2.15). According to $(12.1.10)_1$ both local and overall element loading surfaces translate by

$$\left(\Delta\alpha_{ij}^{\rho}\right)^{(h)} = \Delta\sigma_{ij}^{\rho} \Rightarrow \left(\Delta\bar{\alpha}_{ij}^{\rho}\right)^{(h)} = \Delta\bar{\sigma}_{ij}^{0} \tag{12.1.11}$$

for any stress increment $\Delta\bar{\sigma}_{ij}^{0}$ that causes plastic loading in elements $V_\rho = V_\rho^p$. The superscript (h) indicates that this translation is required by the adopted hardening rule. Kinematic hardening of the local element yield surfaces implies that both the local surfaces and the corresponding branches of the overall surface in (12.1.10) do not change shape or size during plastic loading. Evaluation of the $\Delta\sigma_{ij}^{\rho}$ is deferred to Sect. 12.1.4.

At the end of the loading step $\Delta\bar{\sigma}_{ij} = \Delta\bar{\sigma}_{ij}^{0}$, all elements $V_\rho = V_\rho^p$ which had experienced inelastic straining contain new plastic increments $(\Delta\varepsilon_{ij}^{\rho})^p$. Those are considered as element eigenstrains $\left(\Delta\varepsilon_{ij}^{\rho}\right)^p = \Delta\mu_{ij}^{\rho}$. According to (3.6.1), they are related to element eigenstresses by $\Delta\lambda_{ij}^{\rho} = -L_{ijkl}^{\rho}\Delta\mu_{ij}^{\rho}$. This distribution of residual eigenstresses is a load separate from but superimposed with stresses caused by the applied $\Delta\bar{\sigma}_{ij}^{0}$ in elements $V_\rho = V_\rho^p$.

As in (12.1.2), the superposition takes place in an elastic unit cell, where the effect of element eigenstrains on total local field is described by the eigenstress influence function $F_{ijkl}^{\eta\rho}$, which transmit eigenstress contributions from elements V_ρ^p to all V_η, $\eta = 1,\ 2, \ldots,\ M$. The resulting local stress increment is

$$\Delta\sigma_{ij}^{\eta} = B_{ijkl}^{\eta}\Delta\bar{\sigma}_{kl}^{0} + \sum_{\rho=1}^{M} F_{ijkl}^{\eta\rho}\Delta\lambda_{kl}^{\rho} \tag{12.1.12}$$

The $F_{ijkl}^{\eta\rho}$ include the self-induced $F_{ijkl}^{\eta\eta}$ which is activated when the element V_η also yields, and $\left(\Delta\varepsilon_{ij}^{\eta}\right)^p = \Delta\mu_{ij}^{\eta}$.

The overall stress increment can now be reversed by applying an overall unloading step $\Delta\bar{\sigma}_{ij}^{u} = -\Delta\bar{\sigma}_{ij}^{0}$ directed inside the current cluster of overall yield surfaces, such that the unit cell undergoes only elastic deformation. That eliminates the overall stress contribution to the local stress and it leaves a permanent or back

stress change in all elements. The latter is reflected by translations of current centers of element yield surfaces, from their original positions α_{ij}^{ρ} preceding application of $\pm\Delta\bar{\sigma}_{ij}^{0}$, to $\alpha_{ij}^{\eta} + \left(\Delta\alpha_{ij}^{\eta}\right)^{(\lambda)}$, where

$$\left(\Delta\alpha_{ij}^{\eta}\right)^{(\lambda)} = \left(\Delta\sigma_{ij}^{\eta}\right) - \left(\Delta\sigma_{ij}^{\eta}\right)^{u} = \sum_{\rho=1}^{M} F_{ijkl}^{\eta\rho}\Delta\lambda_{kl}^{\rho} \tag{12.1.13}$$

The $\left(\Delta\alpha_{ij}^{\eta}\right)^{(\lambda)}$ is the *residual or back stress contribution* to the total translation of all element yield surfaces caused by the eigenstress field $\Delta\lambda_{kl}^{\rho}$ distributed in $V_{\rho} = V_{\rho}^{p}$.

Since $(12.1.10)_1$ connects any pair of local and overall stress vectors in an elastic unit cell, local changes in element yield surface centers can be projected into the overall stress space. All braches of the overall yield surface cluster $G_{\eta}\left(\bar{\sigma}_{ij} - \bar{\alpha}_{ij}^{\eta}\right)$, including those which remain elastic under $\Delta\bar{\sigma}_{ij}^{0}$, are translated due to the back stress changes (12.1.13), by the increments

$$\Delta\bar{\alpha}_{ij}^{\eta} = \left(\Delta\bar{\alpha}_{ij}^{\eta}\right)^{(\lambda)} = \left(B_{ijpq}^{\eta}\right)^{-1} \sum_{\rho=1}^{M} F_{pqkl}^{\eta\rho}\Delta\lambda_{kl}^{\rho} \tag{12.1.14}$$

Moreover, those branches of the overall surface that correspond to the plastically deforming elements V_{ρ}^{p} are all translated by $\left(\Delta\bar{\alpha}_{ij}^{\rho}\right)^{(h)} = \Delta\bar{\sigma}_{ij}^{0}$ in compliance with the hardening rule (12.1.11). Their local and overall stress vectors reside on their respective loading surfaces, hence they are connected by $\left(\Delta\sigma_{ij}^{\rho} - \Delta\alpha_{ij}^{\rho}\right) = B_{ijpq}^{\rho}\left(\Delta\bar{\sigma}_{ij}^{0} - \Delta\bar{\alpha}_{ij}^{\rho}\right)$. Total translation vectors in the overall stress space then are

$$\Delta\bar{\alpha}_{ij}^{\rho} = \left(\Delta\bar{\alpha}_{ij}^{\rho}\right)^{(h)} + \left(\Delta\bar{\alpha}_{ij}^{\rho}\right)^{(\lambda)} = \Delta\bar{\sigma}_{ij}^{0} + \left(B_{ijpq}^{\eta}\right)^{-1} \sum_{\rho=1}^{M} F_{pqkl}^{\eta\rho}\Delta\lambda_{kl}^{\rho} \tag{12.1.15}$$

The respective increments serve to update positions of stress points and yield surface centers in the yield conditions (12.1.10) during plastic loading. In applications, which are illustrated in Sect. 12.2, the $\left(\Delta\bar{\alpha}_{ij}^{\rho}\right)^{(h)} = \Delta\bar{\sigma}_{ij}^{0}$ provide the major contribution to translations of the affected overall branches. The back stress contributes to cluster rearrangement during plastic loading, which is more evident among the overall surfaces belonging to the plastically deforming elements and to their possibly elastic neighbors. Those far removed should experience only minor loading surface translations due to the weaker eigenstress interactions. That is seen in the numerical simulation of yield surface clusters in Fig. 12.15. Additional results of that simulation appear in Dvorak et al. (1991) and Shah (1991).

12.1.4 Thermoplastic Deformation of Unit Cell Models

The transformation field analysis method is illustrated in the context of elastic–plastic and thermal deformation in the subelements of a unit cell. Two distinct load rate sets are applied, denoted by $\{\dot{\boldsymbol{\varepsilon}}^0, \dot{\theta}\}$ or $\{\dot{\boldsymbol{\sigma}}^0, \dot{\theta}\}$. Total local strain or stress field increments generated by such applications are described by equations similar to those used in analysis of thermal fields. However, in the present application, the eigenstrains include both inelastic and total thermal strains, $\boldsymbol{\mu} \rightarrow \dot{\boldsymbol{\varepsilon}}^{in} + \dot{\boldsymbol{\varepsilon}}^{\theta}$. The eigenstresses consist of relaxation and thermal stresses $\boldsymbol{\lambda} \rightarrow \boldsymbol{\sigma}^{re} + \boldsymbol{\sigma}^{\theta}$. In each subvolume where the eigenstrains are locally uniform, total increments are

$$\left.\begin{aligned} \dot{\boldsymbol{\varepsilon}}_\eta &= \boldsymbol{A}_\eta \dot{\boldsymbol{\varepsilon}}^0 + \sum_{\rho=1}^{M} \boldsymbol{D}_{\eta\rho} \left(\dot{\boldsymbol{\varepsilon}}_\rho^{in} + \dot{\boldsymbol{\varepsilon}}_\rho^{\theta} \right) \\ \dot{\boldsymbol{\sigma}}_\eta &= \boldsymbol{B}_\eta \dot{\boldsymbol{\sigma}}^0 + \sum_{\rho=1}^{M} \boldsymbol{F}_{\eta\rho} \left(\dot{\boldsymbol{\sigma}}_\rho^{re} + \dot{\boldsymbol{\sigma}}_\rho^{\theta} \right) \end{aligned}\right\} \qquad [12.1.2]$$

According to Sect. 12.1.1, the $\boldsymbol{A}_\eta$ and $\boldsymbol{B}_\eta$ are the elastic strain and stress concentration factors of elements V_η, computed by applying, in turn, six unit values of the overall stain or stress vector to the unit cell. The $\boldsymbol{L}_\eta$ and $\boldsymbol{M}_\eta$ are elastic stiffness and compliance matrices of the phase material residing in V_η. The eigenstrain concentration factor matrices $\boldsymbol{D}_{\eta\rho}$ are assembled from the six columns $\boldsymbol{d}_{\eta\rho}^k$ derived in (12.1.9). A similar derivation provides the eigenstress concentration factors $\boldsymbol{F}_{\eta\rho}$. Both follow from a series of elastic solutions for unit applied eigenstrains or eigenstresses in elements V_ρ, and are evaluated only once, in the preprocessing stage.

Next, the eigenstrain and eigenstress contributions, caused at each material point by either one of the applied load sets, are expressed as functions of total strain and stress, respectively. Using the local instantaneous compliances and stiffnesses defined in (11.3.5) and (11.3.8), the total increments are decomposed into elastic, inelastic and thermal parts

$$\left.\begin{aligned} &\dot{\boldsymbol{\varepsilon}}_\rho = \boldsymbol{\mathcal{M}}_\rho \dot{\boldsymbol{\sigma}}_\rho + \boldsymbol{m}_\rho \dot{\theta} = \left(\boldsymbol{M}_\rho^e + \boldsymbol{\mathcal{M}}_\rho^p\right) \dot{\boldsymbol{\sigma}}_\rho + \boldsymbol{m}_\rho \dot{\theta} = \dot{\boldsymbol{\varepsilon}}_\rho^e + \dot{\boldsymbol{\varepsilon}}_\rho^{in} + \dot{\boldsymbol{\varepsilon}}_\rho^{\theta} \\ &\dot{\boldsymbol{\varepsilon}}_\rho^{in} + \dot{\boldsymbol{\varepsilon}}_\rho^{\theta} = \boldsymbol{\mathcal{M}}_\rho^p \dot{\boldsymbol{\sigma}}_\rho + \boldsymbol{m}_\rho \dot{\theta} \end{aligned}\right\} \qquad (12.1.16)$$

and

$$\left.\begin{aligned} &\dot{\boldsymbol{\sigma}}_\rho = \boldsymbol{\mathcal{L}}_\rho \dot{\boldsymbol{\varepsilon}}_\rho + \boldsymbol{\ell}_\rho \dot{\theta} = \left(\boldsymbol{L}_\rho^e + \boldsymbol{\mathcal{L}}_\rho^p\right) \dot{\boldsymbol{\varepsilon}}_\rho + \boldsymbol{\ell}_\rho \dot{\theta} = \dot{\boldsymbol{\sigma}}_\rho^e + \dot{\boldsymbol{\sigma}}_\rho^{re} + \dot{\boldsymbol{\sigma}}_\rho^{\theta} \\ &\dot{\boldsymbol{\sigma}}_\rho^{re} + \dot{\boldsymbol{\sigma}}_\rho^{\theta} = \boldsymbol{\mathcal{L}}_\rho^p \dot{\boldsymbol{\varepsilon}} + \boldsymbol{\ell}_\rho \dot{\theta} \end{aligned}\right\} \qquad (12.1.17)$$

The eigenstrains include inelastic and total thermal strains, and they are related to the relaxation and total thermal stress or eigenstress by the general connections (3.6.1).

$$\left.\begin{aligned}\dot{\boldsymbol{\sigma}}_\rho^{re}+\dot{\boldsymbol{\sigma}}_\rho^{\theta}&=-\boldsymbol{L}_\rho\left(\dot{\boldsymbol{\varepsilon}}_\rho^{in}+\dot{\boldsymbol{\varepsilon}}_\rho^{\theta}\right)=-\boldsymbol{L}_\rho\left(\boldsymbol{\mathcal{M}}_\rho^{p}\dot{\boldsymbol{\sigma}}_\rho+\boldsymbol{m}_\rho\dot{\theta}\right)\\ \dot{\boldsymbol{\varepsilon}}_\rho^{in}+\dot{\boldsymbol{\varepsilon}}_\rho^{\theta}&=-\boldsymbol{M}_\rho\left(\dot{\boldsymbol{\sigma}}_\rho^{re}+\dot{\boldsymbol{\sigma}}_\rho^{\theta}\right)=-\boldsymbol{M}_\rho\left(\boldsymbol{\mathcal{L}}_\rho^{p}\dot{\boldsymbol{\varepsilon}}+\boldsymbol{\ell}_\rho\dot{\theta}\right)\end{aligned}\right\}\tag{12.1.18}$$

Substitution into (12.1.2) provides one system of equations for each of the two loading sets $\left\{\dot{\boldsymbol{\varepsilon}}^0,\dot{\theta}\right\}$ or $\left\{\dot{\boldsymbol{\sigma}}^0,\ \dot{\theta}\right\}$ that can be solved for the respective rates of local strain $\dot{\boldsymbol{\varepsilon}}_\eta$ or local stress $\dot{\boldsymbol{\sigma}}_\eta$.

$$\dot{\boldsymbol{\varepsilon}}_\eta-\sum_{\rho=1}^{M}\boldsymbol{D}_{\eta\rho}\boldsymbol{M}_\rho\boldsymbol{\mathcal{L}}_\rho^{P}\dot{\boldsymbol{\varepsilon}}_\rho=\boldsymbol{A}_\eta\dot{\boldsymbol{\varepsilon}}^0+\sum_{\rho=1}^{M}\boldsymbol{D}_{\eta\rho}\boldsymbol{M}_\rho\boldsymbol{\ell}_\rho\dot{\theta}\tag{12.1.19}$$

$$\dot{\boldsymbol{\sigma}}_\eta-\sum_{\rho=1}^{M}\boldsymbol{F}_{\eta\rho}\boldsymbol{L}_\rho\boldsymbol{\mathcal{M}}_\rho^{p}\dot{\boldsymbol{\sigma}}_\rho=\boldsymbol{B}_\eta\dot{\boldsymbol{\sigma}}^0+\sum_{\rho=1}^{M}\boldsymbol{F}_{\eta\rho}\boldsymbol{L}_\rho\boldsymbol{m}_\rho\dot{\theta}\tag{12.1.20}$$

In numerical solutions, under uniform overall rate of applied strain and temperature, or the load set $\left\{\dot{\boldsymbol{\varepsilon}}^0,\dot{\theta}\right\}^k$, the array of strain increments in elements V_η is

$$\left\{\dot{\boldsymbol{\varepsilon}}_\eta\right\}=\left[\operatorname{diag}\left(\boldsymbol{I}\right)+\sum_{\rho=1}^{M}\boldsymbol{D}_{\eta\rho}\boldsymbol{M}_\rho\boldsymbol{\mathcal{L}}_\rho^{P}\right]^{-1}\left\{\boldsymbol{A}_\eta\dot{\boldsymbol{\varepsilon}}^0+\sum_{\rho=1}^{M}\boldsymbol{D}_{\eta\rho}\boldsymbol{M}_\rho\boldsymbol{\ell}_\rho^{k}\dot{\theta}\right\}\tag{12.1.21}$$

Accuracy of the solution depends on the size of applied overall increments, which needs to be adjusted to satisfy a selected tolerance criterion. A series of solutions for different overall increments is usually used to identify the acceptable load rate values. An iteration procedure that may be employed to find the local strain rates in agreement with instantaneous constitutive relations and yield conditions of the elements is described in Dvorak et al. (1994).

For element rate $\dot{\boldsymbol{\varepsilon}}_\eta$ extracted for each V_η, the corresponding stress and plastic strain rates are

$$\left.\begin{aligned}\dot{\boldsymbol{\sigma}}_\eta&=\boldsymbol{\mathcal{L}}_\eta\dot{\boldsymbol{\varepsilon}}_\eta+\boldsymbol{\ell}_\eta\dot{\theta}=\boldsymbol{L}_\eta\left[\dot{\boldsymbol{\varepsilon}}_\eta-\dot{\boldsymbol{\varepsilon}}_\eta^{in}-\dot{\boldsymbol{\varepsilon}}_\eta^{\theta}\right]\\ \dot{\boldsymbol{\varepsilon}}_\eta^{in}&=\boldsymbol{M}_\eta\left(\boldsymbol{L}_\eta-\boldsymbol{\mathcal{L}}_\eta\right)\dot{\boldsymbol{\varepsilon}}_\eta\\ \dot{\boldsymbol{\varepsilon}}_\eta^{\theta}&=-\boldsymbol{M}_\eta\boldsymbol{\ell}_\eta\dot{\theta}\end{aligned}\right\}\tag{12.1.22}$$

Local strain rate can be expressed by instantaneous mechanical and thermal concentration factors of elements V_η, (6×6) and (6×1) matrices

$$\dot{\boldsymbol{\varepsilon}}_\eta = \boldsymbol{\mathcal{A}}_\eta \dot{\boldsymbol{\varepsilon}}^0 + \boldsymbol{a}_\eta \dot{\theta} \quad \sum_{\eta=1}^{M} c_\eta \boldsymbol{\mathcal{A}}_\eta = \boldsymbol{I} \quad \sum_{\eta=1}^{M} c_\eta \boldsymbol{a}_\eta = \boldsymbol{0} \tag{12.1.23}$$

Overall instantaneous stress rate and tangent stiffness are then

$$\left.\begin{aligned} &\dot{\bar{\boldsymbol{\sigma}}} = \boldsymbol{\mathcal{L}} \dot{\boldsymbol{\varepsilon}}^0 + \boldsymbol{\ell} \dot{\theta} = \boldsymbol{L} \left(\dot{\boldsymbol{\varepsilon}}^0 - \dot{\bar{\boldsymbol{\mu}}} \right) \quad \dot{\bar{\boldsymbol{\mu}}} = \sum_{\eta=1}^{M} c_\eta \boldsymbol{B}_\eta^{\mathrm{T}} \left(\dot{\boldsymbol{\varepsilon}}_\eta^{in} + \dot{\boldsymbol{\varepsilon}}_\eta^{\theta} \right) \\ &\boldsymbol{\mathcal{L}} = \sum_{\eta=1}^{M} c_\eta \boldsymbol{\mathcal{L}}_\eta \boldsymbol{\mathcal{A}}_\eta \quad \boldsymbol{\ell} = \sum_{\eta=1}^{M} c_\eta \boldsymbol{\ell} c_\eta \end{aligned}\right\} \tag{12.1.24}$$

The overall eigenstrain rate $\dot{\bar{\boldsymbol{\mu}}}$ follows from the Levin formula. Integration of the respective rates along the loading path of overall strain and temperature change provides the current local and overall strain and stress.

For the load set $\left\{\dot{\boldsymbol{\sigma}}^0, \dot{\theta}\right\}$, similar sequence of equations yields

$$\left\{\dot{\boldsymbol{\sigma}}_\eta\right\} = \left[\operatorname{diag}(\boldsymbol{I}) + \sum_{\rho=1}^{M} \boldsymbol{F}_{\eta\rho} \boldsymbol{L}_\rho \boldsymbol{\mathcal{M}}_\rho^p \right]^{-1} \left\{ \boldsymbol{B}_\eta \dot{\boldsymbol{\sigma}}^0 + \sum_{\rho=1}^{M} \boldsymbol{F}_{\eta\rho} \boldsymbol{L}_\rho \boldsymbol{m}_\rho \dot{\theta} \right\} \tag{12.1.25}$$

In terms of instantaneous mechanical and thermal concentration factors of V_η

$$\left.\begin{aligned} &\dot{\boldsymbol{\sigma}}_\eta = \boldsymbol{\mathcal{B}}_\eta \dot{\boldsymbol{\sigma}}^0 + \boldsymbol{b}_\eta \dot{\theta} \quad \dot{\boldsymbol{\varepsilon}}_\eta = \boldsymbol{M}_\eta \left(\dot{\boldsymbol{\sigma}}_\eta - \dot{\boldsymbol{\sigma}}_\eta^{re} - \dot{\boldsymbol{\sigma}}_\eta^{\theta} \right) = \boldsymbol{M}_\eta \boldsymbol{B}_\eta \boldsymbol{\sigma}^0 \\ &\sum_{\eta=1}^{M} c_\eta \boldsymbol{\mathcal{B}}_\eta = \boldsymbol{I} \qquad \sum_{\eta=1}^{M} c_\eta \boldsymbol{b}_\eta = \boldsymbol{0} \end{aligned}\right\} \tag{12.1.26}$$

Overall instantaneous strain rate and tangent compliance for the load set $\left\{\dot{\boldsymbol{\sigma}}^0, \dot{\theta}\right\}$ are

$$\left.\begin{aligned} &\dot{\bar{\boldsymbol{\varepsilon}}} = \boldsymbol{\mathcal{M}} \dot{\boldsymbol{\sigma}}^0 + \boldsymbol{m}\, \dot{\theta} = \boldsymbol{M} \left(\dot{\boldsymbol{\sigma}}^0 - \dot{\bar{\boldsymbol{\lambda}}} \right) \quad \dot{\bar{\boldsymbol{\lambda}}} = \sum_{\eta=1}^{M} c_\eta \boldsymbol{A}_\eta^{\mathrm{T}} \left(\dot{\boldsymbol{\sigma}}_\eta^{re} + \dot{\boldsymbol{\sigma}}_\eta^{\theta} \right) \\ &\boldsymbol{\mathcal{M}} = \sum_{\eta=1}^{M} c_\eta \boldsymbol{\mathcal{M}}_\eta \boldsymbol{\mathcal{B}}_\eta \quad \boldsymbol{m} = \sum_{\eta=1}^{M} c_\eta \boldsymbol{\mathcal{B}}_\eta^{\mathrm{T}} \boldsymbol{m}_\eta \end{aligned}\right\} \tag{12.1.27}$$

For completeness, we repeat here expressions for the instantaneous overall stiffness, compliance and thermal vectors of individual elements V_ρ that are needed above.

$$\left.\begin{aligned}\dot{\boldsymbol{\sigma}}_\rho &= \boldsymbol{\mathcal{L}}_\rho \dot{\boldsymbol{\varepsilon}}_\rho + \boldsymbol{\ell}_\rho \dot{\theta} \qquad & \boldsymbol{\mathcal{L}}_\rho &= \boldsymbol{L}^e_\rho - \frac{2G_\rho}{\left[1 + H_\rho\left(\varepsilon^p_{eq}, \theta\right)/\left(3G_\rho\right)\right]}\boldsymbol{E}_\rho \\ \boldsymbol{\ell}_\rho &= -\boldsymbol{L}^e_\rho \boldsymbol{m}^e_\rho + \frac{2G_\rho}{\left[1 + H_\rho\left(\varepsilon^p_{eq}, \theta\right)/\left(3G_\rho\right)\right]}\left[\boldsymbol{E}_\rho \boldsymbol{m}^e_\rho + \frac{1}{\sqrt{6}G_\rho}\frac{\partial Y_\rho}{\partial \theta}\left(\frac{\tilde{\boldsymbol{s}}_\rho}{\sqrt{\tilde{\boldsymbol{s}}^{\mathrm{T}}_\rho \tilde{\boldsymbol{s}}_\rho}}\right)\right]\end{aligned}\right\} \qquad [11.3.8]$$

and

$$\left.\begin{aligned}\dot{\boldsymbol{\varepsilon}}_\rho &= \boldsymbol{\mathcal{M}}_\rho \dot{\boldsymbol{\sigma}}_\rho + \boldsymbol{m}_\rho \dot{\theta} \qquad & \boldsymbol{\mathcal{M}}_\rho &= \boldsymbol{M}^e_\rho + \frac{3}{2H_\rho\left(\varepsilon^p_{eq}, \theta\right)}\boldsymbol{E}_\rho \\ \boldsymbol{m}_\rho &= \boldsymbol{m}^e_\rho - \sqrt{\frac{3}{2}}\frac{\left(\partial Y_\rho/\partial\theta\right)}{H_\rho\left(\varepsilon^p_{eq}, \theta\right)}\left(\frac{\tilde{\boldsymbol{s}}_\rho}{\sqrt{\tilde{\boldsymbol{s}}^{\mathrm{T}}_\rho \tilde{\boldsymbol{s}}_\rho}}\right)\end{aligned}\right\} \qquad [11.3.5]$$

12.1.5 Viscoelastic Deformation of Unit Cell Models

Composite materials with viscoelastic, viscoplastic and other time and temperature dependent inelastic constituents can be analyzed in a similar manner. The concentration factors and influence functions are still derived from an elasticity solution, but the phase constitutive relations (11.3.5) and (11.3.8) are replaced by those describing the response under consideration.

First investigations of composites with linear viscoelastic matrices were carried out by Hashin (1970), Christensen (1969), Schapery (1974), and many other authors. Those relied primarily on AFA elasticity solutions described in Chaps. 6 and 7, their Laplace or Fourier transforms, and inversions. The transformation field analysis of such time-dependent problems is not limited to linear constitutive theories, which seldom capture all aspects of actual material behavior. In its finite element implementation, the method follows the different deformation histories of all matrix and reinforcement elements, which contribute to overall response but are not accessible to inclusion based averaging methods.

Material response to a stress-time path $\boldsymbol{\sigma}_\eta(\tau)$ applied in each element V_η, starting at $\boldsymbol{\sigma}_\eta(0) = 0$, can be described by the constitutive equation.

$$\boldsymbol{\varepsilon}_\eta(\tau) = \boldsymbol{M}_\eta \boldsymbol{\sigma}_\eta(\tau) + \int_0^t \boldsymbol{J}_\eta(t-\tau)\frac{\mathrm{d}\boldsymbol{\sigma}_\eta(\tau)}{\mathrm{d}\tau}\mathrm{d}\tau \qquad (12.1.28)$$

The creep compliance function J_{ijkl} is a fourth rank tensor, assumed to have the symmetries as the elastic compliance $\boldsymbol{M}_\eta$. Therefore, it can be represented by a diagonally symmetric (6×6) matrix $\boldsymbol{J}_\eta = \boldsymbol{J}_\eta{}^{\mathrm{T}}$, with at most 21 independent

coefficients. Instantaneous elastic response may also be present, with $\boldsymbol{J}_\eta(0) = \boldsymbol{M}_\eta$. Specific forms of creep compliance can be found, for example, in Findley et al. (1976), Knauss and Emri (1981), Schapery (1997), Christensen (1998, 2003) and Brinson and Brinson (2008). Experimental verification of the selected form within the time and stress range of interest may be required for reliable evaluation of overall response.

Application of a strain-time path $\boldsymbol{\varepsilon}_\eta(\tau)$ in each element V_η, starting at $\boldsymbol{\varepsilon}_\eta(0) = 0$, is described by

$$\boldsymbol{\sigma}_\eta(\tau) = \boldsymbol{L}_\eta \boldsymbol{\varepsilon}_\eta(\tau) + \int_0^t \boldsymbol{G}_\eta(t-\tau)\,\frac{\mathrm{d}\boldsymbol{\varepsilon}_\eta(\tau)}{\mathrm{d}\tau}\mathrm{d}\tau \tag{12.1.29}$$

where the local relaxation function $\boldsymbol{G}_\eta(t-\tau)$ has the same symmetries as does the above creep compliance, hence it can be represented by a (6×6) matrix $\boldsymbol{G}_\eta = \boldsymbol{G}_\eta{}^{\mathrm{T}}$. Instantaneous elastic response is governed by $\boldsymbol{G}_\eta(0) = \boldsymbol{L}_\eta$, the local elastic stiffness matrix.

The total local strain rate is obtained by taking the time derivative of (12.1.28)

$$\dot{\boldsymbol{\varepsilon}}_\eta(t) = \boldsymbol{M}_\eta \dot{\boldsymbol{\sigma}}_\eta(t) + \dot{\boldsymbol{J}}_\eta(0)\,\boldsymbol{\sigma}_\eta(t) + \int_{0^+}^t \ddot{\boldsymbol{J}}_\eta(t-\tau)\,\boldsymbol{\sigma}_\eta(\tau)\,\mathrm{d}\tau \tag{12.1.30}$$

Local stress rate follows from (12.1.29) as

$$\dot{\boldsymbol{\sigma}}_\eta(t) = \boldsymbol{L}_\eta \dot{\boldsymbol{\varepsilon}}_\eta(t) + \dot{\boldsymbol{G}}_\eta(0)\,\boldsymbol{\varepsilon}_\eta(t) + \int_{0^+}^t \ddot{\boldsymbol{G}}_\eta(t-\tau)\,\boldsymbol{\varepsilon}_\eta(\tau)\,\mathrm{d}\tau \tag{12.1.31}$$

Next, the elastic contribution is separated from the viscous part, which is now regarded as a local eigenstrain, applied in each element V_η of the subdivided representative volume. After addition of the thermal eigenstrains the total local strain and stress rates are found as

$$\dot{\boldsymbol{\varepsilon}}_\eta(t) = \boldsymbol{A}_\eta \dot{\boldsymbol{\varepsilon}}^0(t) - \sum_{\rho=1}^M \boldsymbol{D}_{\eta\rho}\boldsymbol{M}_\rho \left[\dot{\boldsymbol{G}}_\rho(0)\,\boldsymbol{\varepsilon}_\rho(t) + \int_{0^+}^t \ddot{\boldsymbol{G}}(t-\tau)\,\dot{\boldsymbol{\varepsilon}}_\rho(t)\mathrm{d}\tau + \boldsymbol{\ell}_\rho \dot{\theta}(t) \right] \tag{12.1.32}$$

$$\dot{\boldsymbol{\sigma}}_\eta(t) = \boldsymbol{B}_\eta \dot{\boldsymbol{\sigma}}^0(t) - \sum_{\rho=1}^M \boldsymbol{F}_{\eta\rho}\boldsymbol{L}_\rho \left[\dot{\boldsymbol{J}}_\rho(0)\,\boldsymbol{\sigma}_\rho(t) + \int_{0^+}^t \ddot{\boldsymbol{J}}(t-\tau)\,\dot{\boldsymbol{\sigma}}_\rho(t)\mathrm{d}\tau + \boldsymbol{m}_\rho \dot{\theta}(t) \right] \tag{12.1.33}$$

Solution of either equation involves updating of the $\boldsymbol{J}(t)$ or $\boldsymbol{G}(t)$ functions and their derivatives after each loading step, according to the constitutive relation of each element. The elastic terms, which include the mechanical and transformation influence functions and elastic moduli, remain constant. Again, a series of solutions for different time steps that determine the magnitude of load increments is used to satisfy a selected error criterion.

Composite materials with matrices or phases that exhibit viscoplastic response under elevated temperature can be analyzed in the same manner, after identification of the inelastic transformation components of the phase constitutive relations. Those can be found in the work of Krempl (1985, 2000), Chaboche (1989), Freed and Walker (1993) and many others. An example of the analysis can be found in Bahei-El-Din (1996).

12.1.6 Modified Transformation Field Analysis Methods

Here we briefly describe two improvements and extensions of the TFA, as proposed in an analytical procedure by Chaboche et al. (Chaboche et al. 1998, 2001, 2005), Kanoute et al. (2009) and in the numerical nonuniform transformation field analysis method, or NTFA, by Michel and Suquet (2003, 2004).

In the original two-phase form of TFA, the matrix plastic strain was assumed to be uniform, and the equivalent eigenstrain, introduced there to reduce average matrix stress, elevated the fiber and total stress, as shown in Sect. 4.3.3. That made overall response too stiff (Dvorak 1992). To rectify this, Chaboche adjusted the stress by embedding the fiber in a homogeneous inelastic matrix that has a varying instantaneous tangent stiffness $\boldsymbol{\mathcal{L}}_1$, as originally suggested by Hill (1965c).

A representative volume V of a two-phase composite is considered, consisting of a homogeneous matrix ($r=1$) that has the elastic stiffness $\boldsymbol{L}_1$, and a homogeneous, elastic reinforcement phase ($r=2$), with stiffness $\boldsymbol{L}_2$. The two phases are present in known volume fractions $c_r = V_r/V$, $\Sigma_r c_r = 1$; their compliance matrices are denoted by $\boldsymbol{M}_r = \boldsymbol{L}_r{}^{-1}$. Individual reinforcement fibers or particles are perfectly bonded to the matrix along their interfaces, and spatially distributed such as to assure statistical homogeneity of the aggregate. Application of surface displacements derived from a uniform overall strain rate $\dot{\boldsymbol{\varepsilon}}^0$ generates on the surface of the RVE certain surface tractions that are in equilibrium with a uniform overall stress rate $\dot{\bar{\boldsymbol{\sigma}}}$. Moreover, a distribution of piecewise uniform inelastic eigenstrain rates $\dot{\boldsymbol{\varepsilon}}_r^{in}$ in the phases of a traction-free representative volume is assumed to produce a uniform overall inelastic strain rate $\dot{\bar{\boldsymbol{\varepsilon}}}^{in}$. If the representative volume was prevented from deforming by a rigid constraint imposed on its boundary, the inelastic strain rates would generate an overall inelastic eigenstress $\dot{\bar{\boldsymbol{\sigma}}}^{in} = -\boldsymbol{L}\dot{\bar{\boldsymbol{\varepsilon}}}^{in}$.

Phase averages of total local strain rates in the phases are related to the applied total average strain rates in the phases by $\dot{\bar{\boldsymbol{\varepsilon}}}_r = \boldsymbol{\mathcal{A}}_r\,\dot{\boldsymbol{\varepsilon}}^0$, where the instantaneous strain concentration factors $\boldsymbol{\mathcal{A}}_r$, $\Sigma_r c_r \boldsymbol{\mathcal{A}}_r = \boldsymbol{I}$, are functions of the tangential moduli of

the inelastic matrix phase. Since accurate evaluation of the inelastic concentration factors is difficult under most circumstances, the improved version of TFA adopts the suggestion of Hill (1965c). Specifically, an approximate value of $\mathcal{A}_2$ is found in analogy with the elastic $\boldsymbol{A}_2$, by embedding an ellipsoidal inhomogeneity of $\boldsymbol{L}_2$ in a homogeneous but plastically anisotropic matrix that has an instantaneous tangent stiffness $\mathcal{L}_1$, derived from the averages of the matrix stress and strain rates.

The Mori-Tanaka method is preferred to Hill's choice of the self-consistent method. As in Sect. 7.2.1, the strain rate average in the elastic phase is determined by the instantaneous partial strain concentration factor $\mathcal{T}_2$, such that

$$\dot{\bar{\boldsymbol{\varepsilon}}}_2 = \mathcal{T}_2\,\dot{\bar{\boldsymbol{\varepsilon}}}_1 \qquad \mathcal{T}_2 = [\boldsymbol{I} + \mathcal{P}\,(\boldsymbol{L}_2 - \mathcal{L}_1)]^{-1} \tag{12.1.34}$$

where $\mathcal{P}$ is computed for the selected ellipsoidal shape in the instantaneous matrix stiffness $\mathcal{L}_1$, and $\mathcal{T}_1 = \boldsymbol{I}$. Instantaneous values of the total strain concentration factors and of the overall stiffness are

$$\left.\begin{aligned} \mathcal{A}_1 &= [c_1\boldsymbol{I} + c_2\mathcal{T}_2]^{-1} = \left\{c_1\boldsymbol{I} + c_2[\boldsymbol{I} + \mathcal{P}\,(\boldsymbol{L}_2 - \mathcal{L}_1)]^{-1}\right\}^{-1} \\ \mathcal{A}_2 &= [\boldsymbol{I} + c_1\mathcal{P}\,(\boldsymbol{L}_2 - \mathcal{L}_1)]^{-1} \\ \mathcal{L} &= \mathcal{L}_1 + c_2\,(\boldsymbol{L}_2 - \mathcal{L}_1)\,[\boldsymbol{I} + c_1\mathcal{P}\,(\boldsymbol{L}_2 - \mathcal{L}_1)]^{-1} \end{aligned}\right\} \tag{12.1.35}$$

Local and overall strain and stress rates are then approximated as

$$\left.\begin{aligned} \dot{\bar{\boldsymbol{\varepsilon}}}_1 &= \dot{\bar{\boldsymbol{\varepsilon}}}_1^{e} + \dot{\bar{\boldsymbol{\varepsilon}}}_1^{in} = \mathcal{A}_1\dot{\boldsymbol{\varepsilon}}^0 = (\mathcal{L}_1)^{-1}\dot{\bar{\boldsymbol{\sigma}}}_1 \qquad \dot{\bar{\boldsymbol{\sigma}}}_1 = \boldsymbol{L}_1\left(\dot{\bar{\boldsymbol{\varepsilon}}}_1 - \dot{\bar{\boldsymbol{\varepsilon}}}_1^{in}\right) \\ \dot{\bar{\boldsymbol{\varepsilon}}}_2 &= \mathcal{A}_2\dot{\boldsymbol{\varepsilon}}^0 = \frac{1}{c_2}\,(\boldsymbol{I} - c_1\mathcal{A}_1)\,\dot{\boldsymbol{\varepsilon}}^0 \qquad \dot{\bar{\boldsymbol{\sigma}}}_2 = \boldsymbol{L}_2\dot{\bar{\boldsymbol{\varepsilon}}}_2 \\ \dot{\bar{\boldsymbol{\sigma}}} &= \sum_{r=1}^{2} c_r\dot{\bar{\boldsymbol{\sigma}}}_r = [\mathcal{L}_1 + c_2\,(\boldsymbol{L}_2 - \mathcal{L}_1)\,\mathcal{A}_2]\,\dot{\boldsymbol{\varepsilon}}^0 = \mathcal{L}\dot{\boldsymbol{\varepsilon}}^0 \end{aligned}\right\} \tag{12.1.36}$$

Different auxiliary solutions have been proposed for evaluation of $\mathcal{A}_2$, both for the self-consistent estimate or the Mori-Tanaka method. As indicated in (11.3.3), $\mathcal{L}_1$ may have low material symmetry, not necessarily included in the analytical solutions listed in Sect. 4.6. Instead, the instantaneous Eshelby and/or $\mathcal{P}$ tensor would need to be computed after each loading step, using the procedures of Ghahremani (1977) or Gavazzi and Lagoudas (1990). That may require much effort, however, simplified evaluations of $\mathcal{P}$ can be found when $\mathcal{L}_1$ assumes a constant asymptotic magnitude. Chaboche, et al. (2001, 2005) suggested this approach for certain applications, such as monotonic transverse shear deformation of a unidirectional fibrous composite tube under internal pressure. They reduce the asymptotic stiffness to an isotropic form, similar to that adopted by deformation theory of plasticity. By adding $\alpha_s(\boldsymbol{K}$–$\boldsymbol{E})$ to $(11.3.11)_1$ and letting $\alpha_s = -2G_1\,/(1 + H\,/3G_1)$ to eliminate $\boldsymbol{E}$, one

recovers $(2.2.29)_1$ with a different shear modulus $2\gamma_s = 2G_1H/(3G_1+H)$. The instantaneous matrix tangent stiffness is then described by an isotropic medium with variable tangent modulus H

$$\boldsymbol{\mathcal{L}}_1 = 3K_1\boldsymbol{J} + \frac{2G_1H}{(3G_1+H)}\boldsymbol{K} \tag{12.1.37}$$

where the projection matrices $\boldsymbol{J}$ and $\boldsymbol{K}$ were evaluated in (1.1.19).

This approximations of the instantaneous matrix stiffness $\boldsymbol{\mathcal{L}}_1$ and of the instantaneous concentration factor $\boldsymbol{\mathcal{A}}_2$ is utilized to modify the original two-phase form of the transformation field analysis. Chaboche et al. (2001, 2005) proposed to write the local strain rate averages as

$$\left.\begin{aligned}
&\dot{\bar{\boldsymbol{\varepsilon}}}_1 = \boldsymbol{A}_1\dot{\boldsymbol{\varepsilon}}^0 + \boldsymbol{D}_{11}\boldsymbol{N}_1\dot{\bar{\boldsymbol{\varepsilon}}}_1^{\,in} = \boldsymbol{\mathcal{A}}_1\dot{\boldsymbol{\varepsilon}}^0 \qquad \dot{\bar{\boldsymbol{\varepsilon}}}_2 = \boldsymbol{A}_2\dot{\boldsymbol{\varepsilon}}^0 + \boldsymbol{D}_{21}\boldsymbol{N}_1\dot{\bar{\boldsymbol{\varepsilon}}}_1^{\,in} = \boldsymbol{\mathcal{A}}_2\dot{\boldsymbol{\varepsilon}}^0\\
&\boldsymbol{D}_{11}\boldsymbol{N}_1\dot{\bar{\boldsymbol{\varepsilon}}}_1^{\,in} = (\boldsymbol{A}_1-\boldsymbol{\mathcal{A}}_1)\,\dot{\boldsymbol{\varepsilon}}^0 = \boldsymbol{D}_{11}\boldsymbol{N}_1\left(\boldsymbol{\mathcal{L}}_1^{-1}-\boldsymbol{L}_1^{-1}\right)\boldsymbol{\mathcal{L}}_1\boldsymbol{\mathcal{A}}_1\dot{\boldsymbol{\varepsilon}}^0\\
&\dot{\bar{\boldsymbol{\varepsilon}}}_1^{\,in} = \left(\boldsymbol{\mathcal{L}}_1^{in}\right)^{-1}\dot{\bar{\boldsymbol{\sigma}}}_1 = \left(\boldsymbol{\mathcal{L}}_1^{-1}-\boldsymbol{L}_1^{-1}\right)\boldsymbol{\mathcal{L}}_1\boldsymbol{\mathcal{A}}_1\dot{\boldsymbol{\varepsilon}}^0
\end{aligned}\right\} \tag{12.1.38}$$

where $\boldsymbol{N}_1$ is a correction matrix that changes the average eigenstrain in the matrix phase to $\dot{\boldsymbol{\mu}}_1 = \boldsymbol{N}_1\dot{\bar{\boldsymbol{\varepsilon}}}_1^{in}$. The reinforcement phase is elastic, $\dot{\boldsymbol{\mu}}_2 = 0$. Since $\boldsymbol{D}_{11} = (\boldsymbol{I}-\boldsymbol{A}_1)(\boldsymbol{L}_1-\boldsymbol{L}_2)^{-1}\boldsymbol{L}_1$, the correction matrix

$$\boldsymbol{N}_1 = (\boldsymbol{I}-\boldsymbol{M}_1\boldsymbol{L}_2)\left(\boldsymbol{I}-\boldsymbol{A}_1^{-1}\right)^{-1}\left(\boldsymbol{\mathcal{A}}_1^{-1}-\boldsymbol{A}_1^{-1}\right)(\boldsymbol{I}-\boldsymbol{M}_1\boldsymbol{\mathcal{L}}_1)^{-1} \tag{12.1.39}$$

Overall and local stress rates are

$$\dot{\bar{\boldsymbol{\sigma}}} = \boldsymbol{L}\left(\dot{\boldsymbol{\varepsilon}}^0 - \dot{\bar{\boldsymbol{\varepsilon}}}^{in}\right) \qquad \dot{\bar{\boldsymbol{\sigma}}}_1 = \boldsymbol{L}_1\left(\dot{\bar{\boldsymbol{\varepsilon}}}_1 - \dot{\bar{\boldsymbol{\varepsilon}}}_1^{in}\right) \qquad \dot{\bar{\boldsymbol{\sigma}}}_2 = \boldsymbol{L}_2\dot{\bar{\boldsymbol{\varepsilon}}}_2 \tag{12.1.40}$$

Moreover

$$\left.\begin{aligned}
\boldsymbol{L}\dot{\bar{\boldsymbol{\varepsilon}}}^{in} &= \boldsymbol{L}\dot{\boldsymbol{\varepsilon}}^0 - \dot{\bar{\boldsymbol{\sigma}}} = (c_1\boldsymbol{L}_1\boldsymbol{A}_1 + c_2\boldsymbol{L}_2\boldsymbol{A}_2)\,\dot{\boldsymbol{\varepsilon}}^0 - c_1\dot{\bar{\boldsymbol{\sigma}}}_1 - c_2\dot{\bar{\boldsymbol{\sigma}}}_2\\
&= (c_1\boldsymbol{L}_1\boldsymbol{A}_1 + c_2\boldsymbol{L}_2\boldsymbol{A}_2)\,\dot{\boldsymbol{\varepsilon}}^0 - c_1\boldsymbol{L}_1\boldsymbol{A}_1\dot{\boldsymbol{\varepsilon}}^0 - c_1\boldsymbol{L}_1\boldsymbol{D}_{11}\boldsymbol{N}_1\dot{\bar{\boldsymbol{\varepsilon}}}_1^{\,in}\\
&\quad + c_1\boldsymbol{L}_1\dot{\bar{\boldsymbol{\varepsilon}}}_1^{in} - c_2\boldsymbol{L}_2\boldsymbol{A}_2\dot{\boldsymbol{\varepsilon}}^0 - c_2\boldsymbol{L}_2\boldsymbol{D}_{21}\boldsymbol{N}_1\dot{\bar{\boldsymbol{\varepsilon}}}_1^{\,in}\\
\boldsymbol{L}\dot{\bar{\boldsymbol{\varepsilon}}}^{in} &= c_1\boldsymbol{L}_1\dot{\bar{\boldsymbol{\varepsilon}}}_1^{in} - (c_1\boldsymbol{L}_1\boldsymbol{D}_{11} + c_2\boldsymbol{L}_2\boldsymbol{D}_{21})\,\boldsymbol{N}_1\dot{\bar{\boldsymbol{\varepsilon}}}_1^{\,in}
\end{aligned}\right\} \tag{12.1.41}$$

According to (3.5.11), (3.6.12) and (3.6.14) $\boldsymbol{L}_r\boldsymbol{A}_r = \boldsymbol{B}_r\boldsymbol{L}$ and $\sum_{r=1}^{2} c_r\boldsymbol{L}_r\boldsymbol{D}_{rs} = c_s\left(\boldsymbol{I}-\boldsymbol{A}_s^{\mathrm{T}}\right)\boldsymbol{L}_s$. The overall inelastic strain rate is then found as

$$\dot{\bar{\boldsymbol{\varepsilon}}}^{in} = c_1\boldsymbol{B}_1^{\mathrm{T}}\boldsymbol{N}_1\dot{\bar{\boldsymbol{\varepsilon}}}_1^{in} + c_1\boldsymbol{L}^{-1}\boldsymbol{L}_1(\boldsymbol{I}-\boldsymbol{N}_1)\,\dot{\bar{\boldsymbol{\varepsilon}}}_1^{in} \tag{12.1.42}$$

first term corresponds to Levin's prediction (3.8.16). The second term is caused by the assumptions in (12.1.36). Agreement with Levin's formula can be reached by accepting $\boldsymbol{N}_1\dot{\bar{\boldsymbol{\varepsilon}}}_1^{in}$ as the corrected matrix eigenstrain, and by disregarding the last term in (12.1.42). However, comparisons with finite element computations show good agreement with the improved TFA, at least under monotonic transverse stress.

The Nonlinear Transformation Field Analysis or NTFA, proposed by Michel and Suquet (2003, 2004), extends the finite element version of TFA to large structural problems. A more accurate description of the method may emphasize its macroscopic character, as in MTFA.

The original implementation of TFA in Sect. 12.1.1 yields a distribution of inelastic strains in the phases within a unit cell that serves as representative volume of a periodic composite material. Accurate evaluation of local fields requires a fine subdivision. Therefore, direct extension of the method to many unit cells that subdivide a larger composite structure would multiply the number of unknown inelastic strains and magnify computational cost. Approaches to extension of TFA to large solution domains subjected to nonuniform overall boundary conditions prefer to reduce the local subdivision to the matrix and fiber phases within each unit cell, and accept uniform plastic and total strains in each of the two phases. For example, Fish et al. (1997) developed a two-point homogenization scheme and Fish and Shek (1999) proposed decomposition of the plastic strain into several shape functions. Such approaches may not provide satisfactory response predictions in every application, hence there is a need for more accurate computational schemes that can be implemented at reasonable cost.

A promising strategy for solution of large scale heterogeneous material problems is offered by the NTFA. Two length scales are utilized, one within a unit cell and another on a structure, with coordinates $\boldsymbol{x}$ and $\boldsymbol{X}$. A standard elasticity solution of the finely subdivided cell is performed, yielding an overall stiffness $\boldsymbol{L}$ and strain plus eigenstrain influence functions $\boldsymbol{A}_\eta, \boldsymbol{D}_{\eta\rho}$, as described in Sect. 12.1.3. Next, elastic–plastic solutions of the unit cell are obtained under several $k = 1, 2, \ldots, K$ overall stress state components, each applied monotonically in a single direction up to a level where a well developed plastic strain field is found. Any suitable method that provides plastic strains at integration points of the selected subdivision can be used in this task. The fast Fourier transform (FFT) method of Moulinec and Suquet (1994) and Michel et al. (1999) was used in the original presentation, but the finite element or the TFA method with a single set of precomputed influence functions for all plastic modes could be used as well.

For example, in preparation for a structure scale generalized plane strain problem in the $\bar{x}_2\bar{x}_3$ −plane, one may find the plastic mode fields by applying, in turn, four overall normal components $\bar{\sigma}_{11}^0$, $\bar{\sigma}_{22}^0$, $\bar{\sigma}_{33}^0$, $\bar{\sigma}_{23}^0$. Each application generates a *plastic mode* $\boldsymbol{\mu}_r^{(k)}(\boldsymbol{x})$, a nonuniform strain field that becomes a part of the superposition

$$\boldsymbol{\varepsilon}_r^{in}(\boldsymbol{x},t) = \sum_{k=1}^{K} \boldsymbol{\varepsilon}_k^{in}(t)\boldsymbol{\mu}_r^{(k)}(\boldsymbol{x}) \tag{12.1.43}$$

where $\boldsymbol{\varepsilon}_r^{in}(\boldsymbol{x},\ t)$ is the inelastic strain at point $\boldsymbol{x}$ and time t in each inelastic phase r, typically the matrix. In reference to crystal plasticity, the $\boldsymbol{\mu}_r^{(k)}(\boldsymbol{x})$ would represent a specific slip system and $\boldsymbol{\varepsilon}_k^{in}$ the magnitude of slip on that system, the latter dependent on a certain scalar magnitude τ_k of a resolved shear stress. Each plastic mode is limited to the volume of the particular inelastic phase r, and it conforms to the constitutive relation of that phase. In particular, it must be purely deviatoric and incompressible, $tr\left(\boldsymbol{\mu}_r^{(k)}\right) = 0$. Any two modes $k = p, q$ present in each single phase r are orthogonal, $\left(\boldsymbol{\mu}_r^{(p)}\right)^{\mathrm{T}}\boldsymbol{\mu}_r^{(q)} = \mathbf{0}$ when $p \neq q$. Finally, the equivalent magnitude (11.1.3) of each plastic mode function is normalized over inelastic phase volume V_r.

$$\left\langle \mu_{eq}^{(k)} \right\rangle = \frac{1}{V_r}\int_{V_r} \mu_{eq}^{(k)}(\boldsymbol{x})\,\mathrm{d}V = 1 \tag{12.1.44}$$

Modified constitutive relations of each phase volume V_r are introduced for each mode, by the following scalar products of respective (6×6) stress, strain and mode eigenstrain vectors, averaged over V_r.

$$\tau_k = \left\langle \boldsymbol{\sigma}^{\mathrm{T}}\boldsymbol{\mu}^{(k)} \right\rangle \quad e_k = \left\langle \boldsymbol{\varepsilon}^{\mathrm{T}}\boldsymbol{\mu}^{(k)} \right\rangle \quad e_k^{in} = \left\langle \left(\boldsymbol{\varepsilon}^{in}\right)^{\mathrm{T}}\boldsymbol{\mu}^{(k)} \right\rangle \tag{12.1.45}$$

Local fields in each phase, originally computed as a nonuniform distribution, are now replaced by phase volume averages for each mode.

$$e_k = \boldsymbol{a}_k^{\mathrm{T}}\boldsymbol{\varepsilon}^0 + \sum_{l=1}^{K} D_{kl}^N \varepsilon_l^{in} \tag{12.1.46}$$

where

$$\boldsymbol{a}_k = \left\langle \boldsymbol{A}(\boldsymbol{x})\,\boldsymbol{\mu}^{(k)} \right\rangle \quad D_{k\ell}^N = \left\langle \left(\boldsymbol{\mu}^{(k)}\right)^{\mathrm{T}} \sum_{\rho=1}^{M} \boldsymbol{D}_{\eta\rho}\boldsymbol{\mu}_\rho^{(\ell)} \right\rangle \tag{12.1.47}$$

The $\boldsymbol{A}(\boldsymbol{x})$ is the elastic mechanical influence function, derived together with $\boldsymbol{D}_{\eta\rho}$ for finite elements in the phases, Sect. 12.1.2. The sum in the last term yields the contributions of eigenstrains $\boldsymbol{\mu}_\rho^{(\ell)}(\boldsymbol{x})$ generated in each single $\ell-$ mode in all elements V_ρ to the total strain in V_η After volume averaging (12.1.44) of the local scalar products, one obtains the $D_{k\ell}^N$, a scalar multiplier that brings in the respective contributions of all ε_l^{in} mode eigenstrains to the scaled total strain e_k in the inelastic phase.. The superscript N identifies $D_{k\ell}^N$ with NTFA. The $\boldsymbol{a}_k$ and $D_{k\ell}^N$ are new mechanical and transformation concentration factors of each phase.

The current value of the resolved shear stress $\tau_k^{(r)}$, that drives inelastic deformation in elastically isotropic phase r, is evaluated as $\tau_k^{(r)} = 2G_r(e_k^{(r)} - (e_k^{(r)})^{in})$ where G_r is shear elastic modulus. The inelastic strain in each element for each

mode evolves according to (12.1.47). A mode coupling assumption that affects all above variables can also be introduced.

On the structural level, local fields in each phase of the composite material are again uniform, represented by the quantities (12.1.46) for each mode. The standard two-phase TFA solution is enhanced by inclusion of $k = 1, 2, \ldots, K$ plastic modes, which the above reduction of variables (12.1.45) converts to K scalars in each phase. Details of the finite element implementation of the NTFA method can be found together with examples in Michel and Suquet (2003). They considered overall response of a square block of unidirectional fiber composite transversely compressed by attached, rigid dies, and found both NTFA and TFA two-point solutions. The former was more compliant, but comparisons based on other schemes may yield different results.

The method is an extension and enhancement of TFA. Response of a structure under non-proportional or cyclic loading may require participation of several sets of plastic mode functions, each for a different part of the applied loading path. Even under monotonic loading of a structure, computing of the plastic modes for NTFA may require substantial effort. An alternative approach may be developed, for example, by decomposing the structure into periodic hexagonal array or other unit cells, with minimal subdivision that allows enough degrees of freedom needed for inelastic deformation of each cell (Teply and Dvorak 1988). The subdivisions may be adjusted in locations where large deformation gradients are expected to develop in the structure.

12.2 Experimental Support of Theoretical Predictions

Published analytical or computational models of inelastic behavior of composite materials are seldom supported by experimental evidence. Attempts to verify model results are usually limited to tension tests of unidirectional or symmetric laminate specimens, which produce simple stress–strain curves that can be easily matched by several different predictions. More extensive comparisons of predictions with actual behavior of metal or other inelastic composites subjected to multiaxial loading are rare. To partially remedy this situation, we present here a part of experimental investigations undertaken by Dvorak et al. (1988) and Nigam et al. (1994). The observed behavior is interpreted both with analytical and unit cell models. The former is based on the bimodal plasticity theory for fiber composites by Dvorak and Bahei-El-Din (1987), which was inspired by the earlier experimental results. The unit cell model is the periodic hexagonal array or PHA model of Sect. 12.1.1. Both models provide good approximation of the shape and position of loading surfaces detected in experiments. Along the entire loading path, the observed plastic strain increment directions and magnitudes compare reasonably well with those computed using the PHA model. The bimodal theory predictions may agree only along several initial loading segments. Complete results of the comparative studies can be found in Dvorak (1990) and Shah (1991).

12.2.1 Bimodal Plasticity of Fiber Composites

As is well known, deformation of an unreinforced metal matrix layer may admit several slip systems of different orientation. In contrast, reinforcement by aligned fibers may limit the available slip systems in a ply to planes that are parallel to the direction of the fiber axis. Frequently used boron or silicon carbide fibers have high longitudinal and transverse stiffness that promotes their bending resistance. Under certain loads applied to the fibrous ply, they channel plastic slip into planes aligned with the fiber axis. That gives rise to the matrix-dominated or MDM deformation mode. However, both fibers and matrix participate in overall deformation under loads which cause high normal stress in the direction close to that of the fiber axis, and thus favor the fiber-dominated or FDM mode. In both modes, the composite is regarded as homogenized elastic continuum, with overall moduli and local stresses estimated by the self-consistent, Mori-Tanaka or other averaging method. Two yield conditions are prescribed to generate branches of the overall yield surface.

The FDM yield condition is derived from an estimate of average matrix stress and the Mises criterion (11.1.1). For convenience in subsequent applications, total stress is used in place of the deviatoric components. In the elastic deformation range, within the overall yield surface, the matrix stress vector is related to the overall vector by (12.1.10), written as

$$(\boldsymbol{\sigma}_m - \boldsymbol{\alpha}_m) = \boldsymbol{B}_m\,(\bar{\boldsymbol{\sigma}} - \bar{\boldsymbol{\alpha}}) \tag{12.2.1}$$

where $\boldsymbol{B}_m$ is a stress concentration factor of the matrix and the top bars denote current overall stress average. Positions of the centers of the matrix and overall loading surfaces are denoted by $\boldsymbol{\alpha}_m$ and $\bar{\boldsymbol{\alpha}}$. The overall branch of the FDM mode follows from the matrix yield condition (11.2.12), and is translated here by the Phillips rule as.

$$\begin{aligned} f &\equiv (\bar{\boldsymbol{\sigma}} - \bar{\boldsymbol{\alpha}})^{\mathrm{T}} \boldsymbol{B}_m^{\mathrm{T}} \boldsymbol{Q}\, \boldsymbol{B}_m\,(\bar{\boldsymbol{\sigma}} - \bar{\boldsymbol{\alpha}}) - Y_m^2\,(\theta) = 0 \\ \mathrm{d}\bar{\boldsymbol{\alpha}} &= \mathrm{d}\bar{\boldsymbol{\sigma}} \end{aligned} \tag{12.2.2}$$

Nonzero coefficients of the (6×6) symmetric matrix $\boldsymbol{Q}$ are: $Q_{11} = Q_{22} = Q_{33} = 1$, $Q_{12} = Q_{13} = Q_{23} = -1/2$, $Q_{44} = Q_{55} = Q_{66} = 3$; $Y_m\,(\theta)$ is the matrix yield stress, which may depend on temperature. The stress concentration factor $\boldsymbol{B}_m$ makes the size of the FDM branch dependent on the elastic moduli and volume fractions of the fiber and matrix constituents. It can be evaluated by an averaging method of Chap. 7, or derived from known overall and phase compliances and volume fractions, as shown in (3.5.13).

The FDM yield condition can be applied to any general deformation mode of the composite, as it has been in numerous plasticity studies based on extensions of standard averaging methods. However, it is restricted in certain systems by the MDM yield condition.

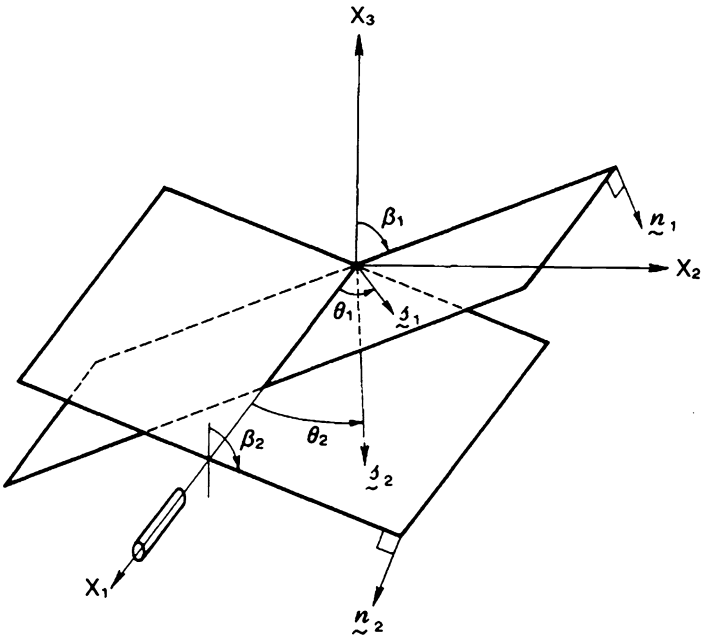

Fig. 12.3 Geometry of conjugate slip systems in the matrix-dominated deformation mode (Dvorak and Bahei-El-Din 1987)

The MDM branch reduces the elastic deformation region of the composite by allowing inelastic deformation on two conjugate slip systems $k = 1, 2$, aligned with the fiber direction, Fig. 12.3. The scalar magnitude of the resolved shear stress on the k system is derived from the Schmid law for crystalline slip

$$\tau_{ns}^{(k)} = n_i^{(k)} \bar{\sigma}_{ij} s_j^{(k)} \tag{12.2.3}$$

The $n_i^{(k)}$ is the normal to the slip plane, $s_j^{(k)}$ is the slip direction, and $\bar{\sigma}_{ij}$ is the same overall stress applied to the ply as that in (12.2.1). The initial yield condition on the k- plane compares the maximum resolved shear stress to matrix yield stress in simple shear, $\tau_m^2 = Y_m^2/3$.

$$f\left(\tau^{(k)}\right) \equiv \left(\max \tau_{ns}^{(k)}\right)^2 - \tau_m^2(\theta) = 0 \tag{12.2.4}$$

Overall plane stress deformation is assumed to occur in the $x_1 x_2$ −plane, where $\bar{\sigma}_{22}$, $\bar{\sigma}_{33}$ are the transverse normal stresses and $\bar{\sigma}_{21}$ is the longitudinal shear stress applied to the ply. Using the slip system angles in Fig. 12.3, one can find the shear stress resolved on the slip planes (1) and (2)

$$\tau_{ns}^{(1)} = \frac{1}{2}\sin 2\beta \sin\theta \left(\bar{\sigma}_{22} - \bar{\sigma}_{33}\right) + \cos\beta \cos\theta \, \bar{\sigma}_{21} = -\tau_{ns}^{(2)} \tag{12.2.5}$$

Derivatives $\partial\tau_{ns}^{(1)}/\partial\beta = 0$ and $\partial\tau_{ns}^{(1)}/\partial\theta = 0$ eventually yield (max $\tau_{ns}^{(k)}$) as

$$\left.\begin{array}{ll} \max\ \tau_{ns}^{(1)} = \dfrac{1}{2}\left(1-q^2\right)\left(\bar{\sigma}_{22}-\bar{\sigma}_{33}\right)+q\bar{\sigma}_{21} = -\max\ \tau_{ns}^{(2)} & \text{for } |q| \le 1 \\ \max\ \tau_{ns}^{(1)} = \bar{\sigma}_{21} = -\max\ \tau_{ns}^{(2)} & \text{for } |q| \ge 1 \\ q = \bar{\sigma}_{21}/(\bar{\sigma}_{22}-\bar{\sigma}_{33}) & \text{for } \bar{\sigma}_{22} \ne \bar{\sigma}_{33} \end{array}\right\} \tag{12.2.6}$$

Substitution into the yield condition (12.2.4) provides two parts of the MDM branch.

$$\left.\begin{array}{l} f_a\left(\bar{\boldsymbol{\sigma}}-\bar{\boldsymbol{\alpha}}\right) \equiv \dfrac{1}{4}\left[\left(\bar{\sigma}_{22}-\bar{\alpha}_{22}\right)-\left(\bar{\sigma}_{33}-\bar{\alpha}_{33}\right)\right]^2\left(1+q^2\right)^2-\tau_m^2 \\ = \left(\dfrac{\left[\left(\bar{\sigma}_{22}-\bar{\alpha}_{22}\right)-\left(\bar{\sigma}_{33}-\bar{\alpha}_{33}\right)\right]}{\tau_m} \mp 1\right)^2+\left(\dfrac{\bar{\sigma}_{21}-\bar{\alpha}_{21}}{\tau_m}\right)^2-1=0 \quad \text{for } |q| \le 1 \end{array}\right\} \tag{12.2.7}$$

and

$$f_b\left(\bar{\boldsymbol{\sigma}}-\bar{\boldsymbol{\alpha}}\right) \equiv \left(\bar{\sigma}_{21}-\bar{\alpha}_{21}\right)^2-\tau_m^2=0 \quad \text{for } |q| \ge 1 \tag{12.2.8}$$

Kinematic hardening causes translation of the loading surface branches, which follows the Phillips rule on the FDM branch, and on the semi-circular segments of the MDM branch. The flat segments of MDM branches, respond only to the component $\bar{\sigma}_{21}$ that is perpendicular to the segments. With reference to the two loading conditions, the hardening rules are

$$\begin{array}{lll} \mathrm{d}\bar{\alpha}_{21} = \mathrm{d}\bar{\sigma}_{21} & \mathrm{d}\bar{\alpha}_{22} = \mathrm{d}\bar{\sigma}_{22} & \text{for } f_a = 0, |q| \le 1 \\ \mathrm{d}\bar{\alpha}_{21} = \mathrm{d}\bar{\sigma}_{21} & \mathrm{d}\bar{\alpha}_{22} \to 0 & \text{for } f_b = 0, |q| \ge 1 \end{array} \tag{12.2.9}$$

Plastic strain increments can be easily formulated but not reliably predicted by the bimodal theory or by another averaging method. That is documented in the discussion of computed and experimentally observed increments that follows Figs. 12.15 and 12.16.

Figure 12.4 shows the semicircular and flat parts of the initial MDM yield surface. Each point on the surface corresponds to a particular orientation of the slip system normals and directions. Varying stress magnitudes in the plane of the ply could promote or suppress the matrix or fiber deformation mode in different parts of the ply. However, changes in fiber orientation within ply or other composite volume are not allowed, because they would lead to interactions between misaligned pairs of slip systems, which are not considered by the bimodal plasticity theory.

Size of both FDM and MDM branches depends on the magnitude of the matrix shear yield stress $\boldsymbol{\tau}_m$ in (12.2.7, 12.2.8), but size of the FDM branch also depends on the elastic moduli and volume fraction of the fiber and matrix, through the stress concentration factor $\boldsymbol{B}_m$ in (12.2.1, 12.2.2). Therefore, different composite

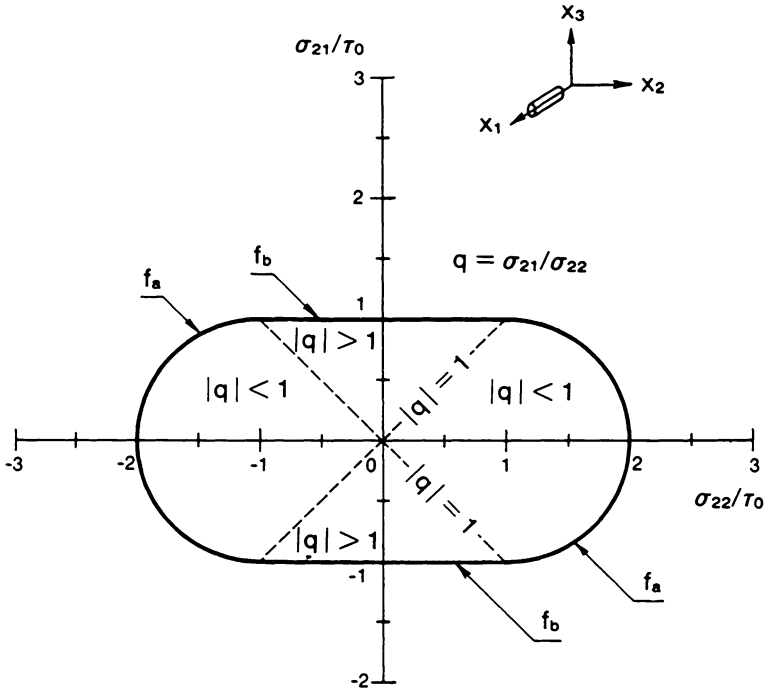

Fig. 12.4 Crossection of the MDM branch of the overall yield surface (Dvorak and Bahei-El-Din 1987)

material systems have FDM branches which may either cap the MDM cylinder, or be surrounded by it, Fig. 12.5. At a given τ_m, the deciding factor are the magnitudes of transverse and longitudinal shear moduli of the fiber. High moduli magnitudes are found in nearly isotropic boron and silicon carbide (SCS-2) fibers manufactured by chemical vapor deposition or CVD. In contrast, the anisotropic carbon and graphite fibers have high longitudinal Young's modulus, but low transverse moduli. Composites reinforced by such fibers have FDM plane stress yield surface represented by elongated spheroids contained inside the MDM cylinder.

Both branches of the overall surface are superimposed in Fig. 12.5. The left image is typical for metal composites reinforced by stiff, inflexible fibers. In that case, the FDM ellipsoid provides end caps on the MDM cylinder. The right image in Fig. 12.5 is typical for metal composites reinforced by flexible fibers, with a high Young's modulus. The circumferential diameter but not the longitudinal size of the FDM cylinder becomes smaller than the distance between the two MDM planes in Fig. 12.4. The interior elastic region of the composite is surrounded by those branches of the overall yield surface which are closest to the stress-free state at the origin. The FDM and MDM branches do not translate relative to each other or separate during plastic deformation, hence they do not represent independent material models of fibrous material deformation.

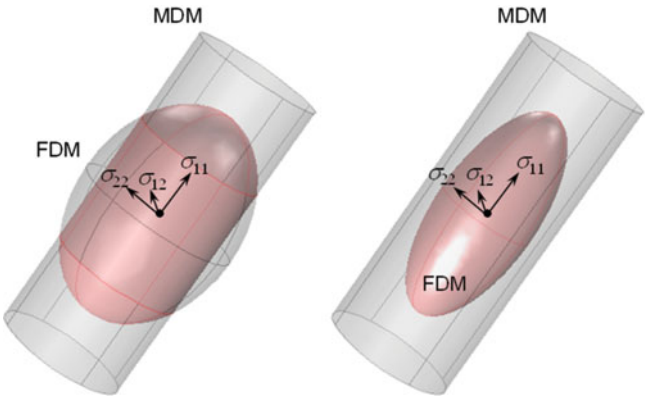

Fig. 12.5 Superimposed FDM and MDM branches of the bimodal yield surface. The MDM branch trims the FDM branch in the left image. In the right image, the FDM branch precludes the matrix mode of plastic deformation

Moulinec and Suquet (1994) performed a numerical analysis of plastic slip in a large samples of a unidirectional aluminum matrix composite reinforced by a moderate volume fraction of unidirectional fibers, randomly distributed in the transverse plane. The sample was loaded by transverse tension. In systems with a low yield stress and tangent modulus of the matrix, the load generated a dense distribution of discrete, narrow slip bands on planes aligned with the fibers axis, as anticipated in the MDM deformation mode. In a system with a higher tangent modulus, the bands were still visible but somewhat diffused.

12.2.2 Comparison of Experimental Results with Predictions

Figure 12.6 shows one of several thin-walled cylindrical specimens used in evaluation of actual elastic–plastic response of a metal matrix composite. A micrograph of the cylinder wall, made with unidirectional boron fiber in a 6061 aluminum matrix, appears in Fig. 12.1. Fiber diameter is 142 μm. Both constituents were isotropic, with thermoelastic moduli $E_f = 400$ GPa, $G_f = 167$ GPa, $\alpha_f = 4.7 \times 10^{-6}/°\text{C}$, $E_m = 72.5$ GPa, $G_m = 27.3$ GPa, $\alpha_m = 24 \times 10^{-6}/°\text{C}$. Initial yielding of the annealed matrix was detected at $Y_m = 36$ MPa. The instantaneous plastic tangent modulus $H(\varepsilon^p)$ was determined from experiments, shown for example in Fig. 12.8, and from the Dafalias-Popov model in Sect. 11.2.4.

Each specimen tube was manufactured by diffusion bonding of fiber monolayers, mechanically deposited on matrix foils, in process similar to that used for the tubular frame truss of space shuttle orbiter (Miller et al. 1973). The monolayer was wrapped several times on a cylindrical mandrel and then subjected to external pressure of 30 MPa at 500°C for 40 min. The same procedure was used in manufacture of aluminum material specimens, tested to yield matrix yield and loading surfaces

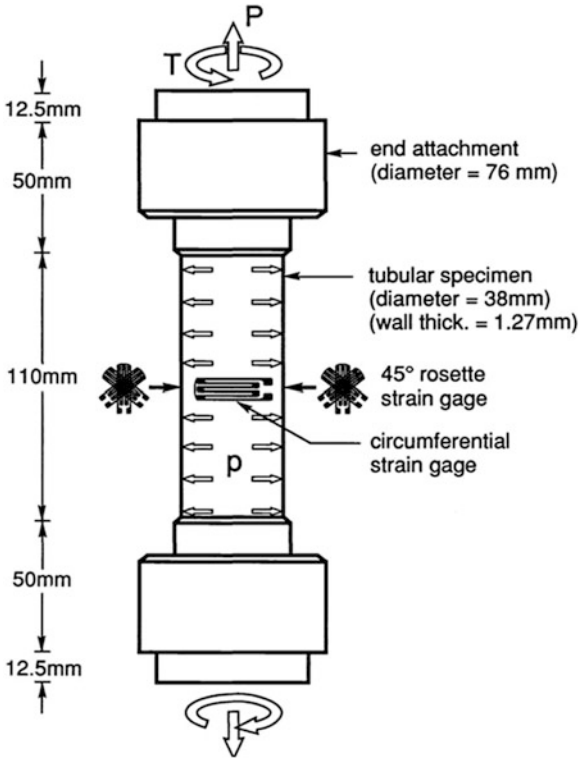

Fig. 12.6 Loads and dimensions of the composite and matrix test specimens (Bahei-El-Din and Dvorak 2000)

and plastic strains. For partial relief of residual stresses, both the composite and matrix specimens were annealed at 500°C for 2 h., then cooled at the rate of 10°C/h to 260°C and finally air cooled. A computer-controlled MTS multi-axial test system was used in the experiments under combined tension, torsion and internal pressure loads. Complete information about manufacture, specimen instrumentation and experimental techniques and results can be found in Dvorak et al. (1988), Liu (1988) and Nigam et al. (1994).

Individual yield points on the initial and subsequent loading surfaces were determined by incremental loading from certain starting points within the elastic region. A sample of actual recordings appears in Fig. 12.7. Small stress increments of 1–2 MPa were applied in sequence at the rate of 3–4 MPa/min. Strain magnitudes were recorded after a 30s. waiting period, and detected with the accuracy of approximately 2×10^{-6} Measured elastic strains were closely matched by self-consistent predictions. Onset of plastic deformation was determined by back-extrapolation of a linear interpolation of 3–4 plastic strain measurements.

Small excursion into the plastic region caused minor distortions of the current loading surface, which were minimized by selecting load directions symmetric to

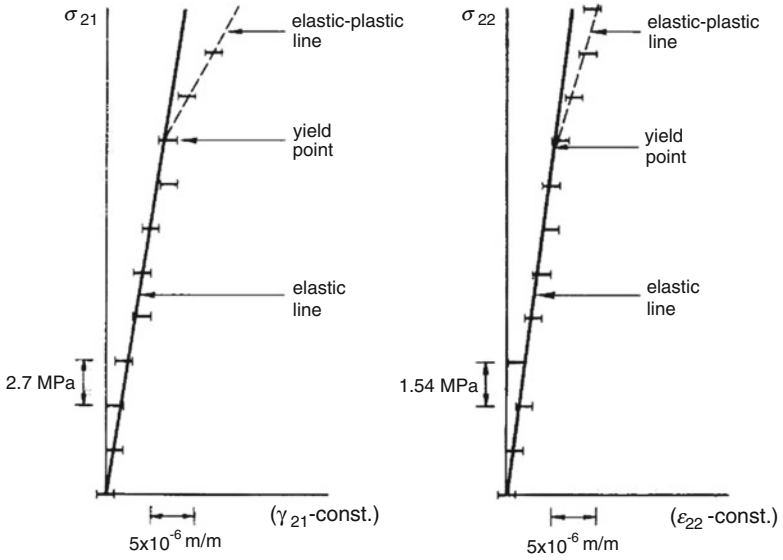

Fig. 12.7 Examples of actual stress–strain records used in detection of the yield points (Dvorak et al. 1988)

the anticipated position of the principal axes of the loading surface. In contrast, a more recent study by Lissenden (2010) shows that shape and size of loading surfaces may depend on the particular loading sequence when the yield points are defined by permanent strain magnitude of 20×10^{-6}.

Figure 12.8 shows the initial and subsequent loading surfaces of the matrix material. Pronounced kinematic hardening of the Phillips type in (11.2.15) is evident, together with some elongation of the initial circular shape drawn at the origin, also observed and analyzed by Phillips and Weng (1975). Although not in perfect agreement with standard plasticity theory predictions, these and similar experiments provide good confirmation of the hardening rule, as close as one may expect to find along a non-proportional loading path.

Figure 12.9 shows two sections of the first yield surface detected on the annealed composite specimen, under transverse tension σ_{22}/τ_0, combined either with longitudinal tension σ_{11}/τ_0, or with longitudinal shear σ_{21}/τ_0 and longitudinal compression that compensates for the internal pressure. Experimental yield points were found along the interior loading path indicated by their numerical sequence. Related theoretical predictions include the bimodal surface branches, and surfaces predicted by the unit cell PHA model of Sect. 12.1.1.

The (UB) and (LB) labels refer to uniform strain and uniform stress boundary conditions, originally applied in finding upper and lower bounds on the instantaneous stiffness (Teply and Dvorak 1988). Computed yield points were found at first deviation from linearity of stress–strain curves generated by the PHA model along the same loading directions, and joined by the respective surface contours.

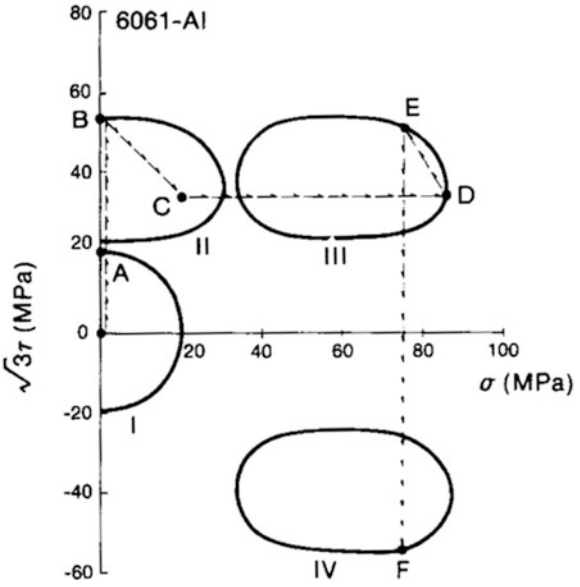

Fig. 12.8 Initial and subsequent loading surfaces of the annealed 6061 aluminum matrix (Dvorak et al. 1988)

As expected, the normalizing shear stress τ_0 was gradually elevated by the small plastic strains generated in the detection process. After adjustment, the experimental yield points are on or very close to the predicted surfaces. Both figures are dominated by the MDM branch; the FDM branch appears only as an end cap. Residual thermal stresses after annealing caused the center of the FDM branch to be located at $\sigma_{11}/\tau_0 = -0.53$, and the axis of the MDM cylinder at small value of σ_{22}/τ_0.

Hardening of the composite was examined for both MDM and FDM branches under many loading sequences, as described in the references by Dvorak et al. (1988, 1991), Shah (1991) and in Nigam et al. (1994). A sequence is presented in Fig. 12.10 and continued in Fig. 12.11. First loading surface was detected at the end of the loading path 1–4. No axial compression was applied to compensate for longitudinal normal stress $\sigma_{11} = \sigma_{22}/2$ caused in the specimen wall by internal pressure, hence the magnitude of the resulting normal stress in the wall is equal to $(\sqrt{5}/2)\sigma_{22}$, as indicated on the horizontal axis.

After application of the next cycle 4-C-D-E-A-B, the loading surface was found to nearly coincide with the first one. The experimentally detected yield points are denoted by empty or black circles. Loading surfaces and plastic strain increment directions detected by experiment appear at the end of the loading segments C-D and D-E-A, Fig. 12.11. Both PHA and MDM predictions of the loading surfaces are included, and help to complete the upper left surface which extends into $\sigma_{22}/\tau_0 < 0$ or external pressure range, not applied in this experiment.

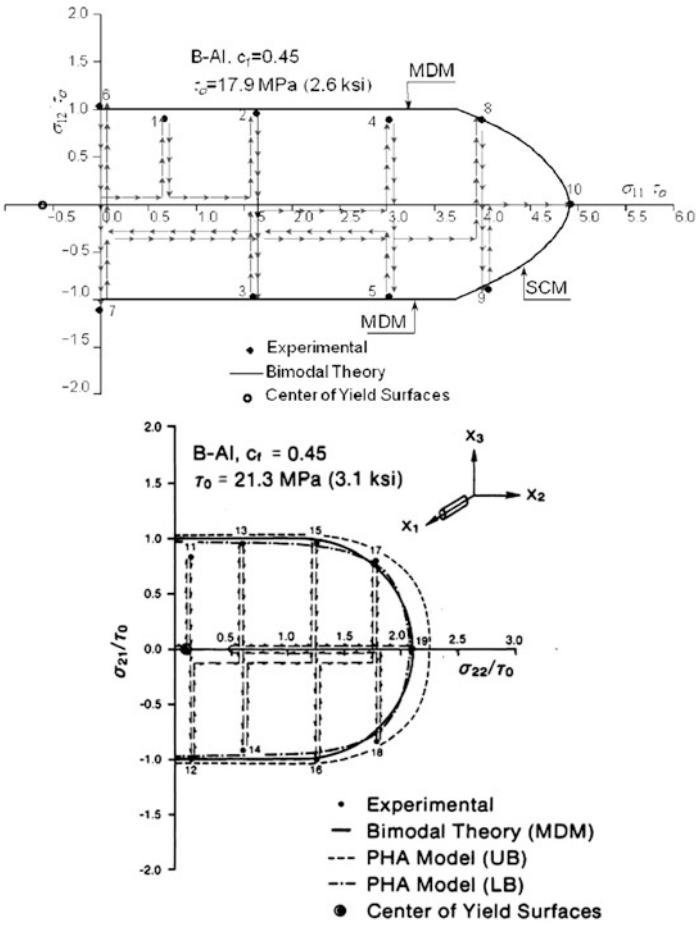

Fig. 12.9 First FDM and MDM yield surfaces of the composite under longitudinal $({}_{11}\sigma)$ or transverse $({}_{22}\sigma)$ tension and longitudinal shear $({}_{12}\sigma)$ loading

Response in the fiber-dominates mode is similar. Figure 12.12 shows four surfaces obtained along a loading path in the $\sigma_{11}\sigma_{21}-$plane. The first two surfaces are confirmed experimentally only for the FDM caps on the tension or right end. More reliable are surfaces III and IV, where both FDM caps were confirmed. The last surface IV has a cap supported by several yield points at longitudinal compression. Detection of the caps is often aided by combining normal and shear stresses, since the slope of the stress–strain record under purely longitudinal inelastic deformation is less distinct than those shown in Fig. 12.7.

Figures 12.9 to 12.12, show excellent agreement of the bimodal plasticity theory with experimentally detected shape and translation of both FDM and MDM branches of initial and subsequent loading surfaces. Kinematic hardening of the

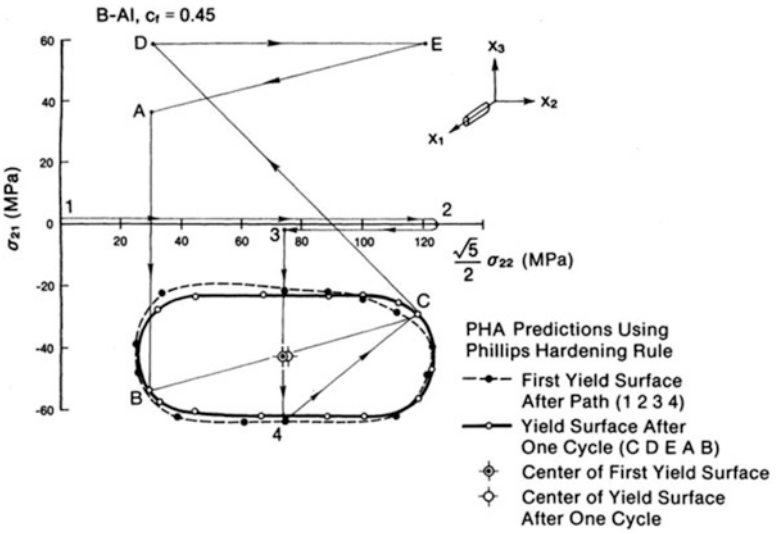

Fig. 12.10 Loading path and load cycle leading to a first and final yield surface (Shah 1991)

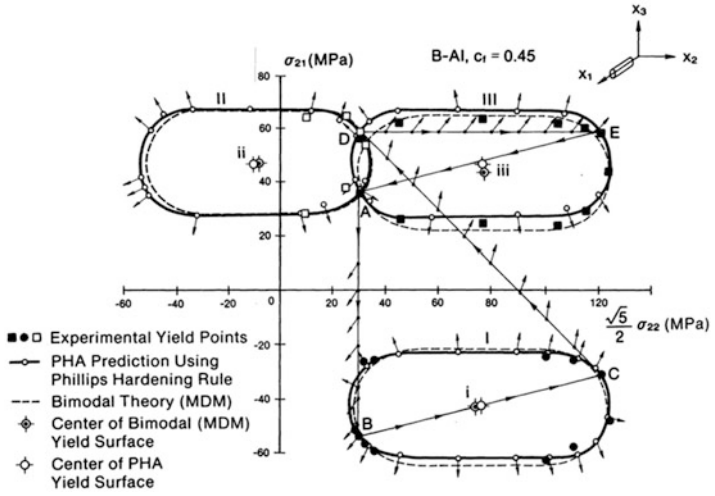

Fig. 12.11 Plastic strain increment directions and yield surfaces detected during a load cycle. Comparison with predicted MDM and PHA branches (Shah 1991)

Phillips type is evident in both modes, consistent with matrix hardening in Fig. 12.8. The Prager-Ziegler rule fails to predict the results. However, measured plastic strain increments often show significant deviation from normality to the MDM branches, and from bimodal theory predictions of their magnitudes. This is not unexpected in the results that follow.

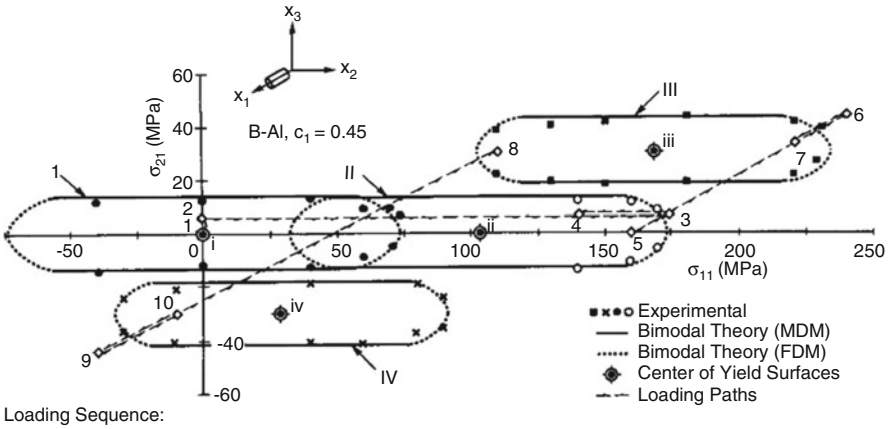

Fig. 12.12 FDM/MDM branches detected at several point of a loading path in the axial tension and shear plane (Nigam et al. 1994)

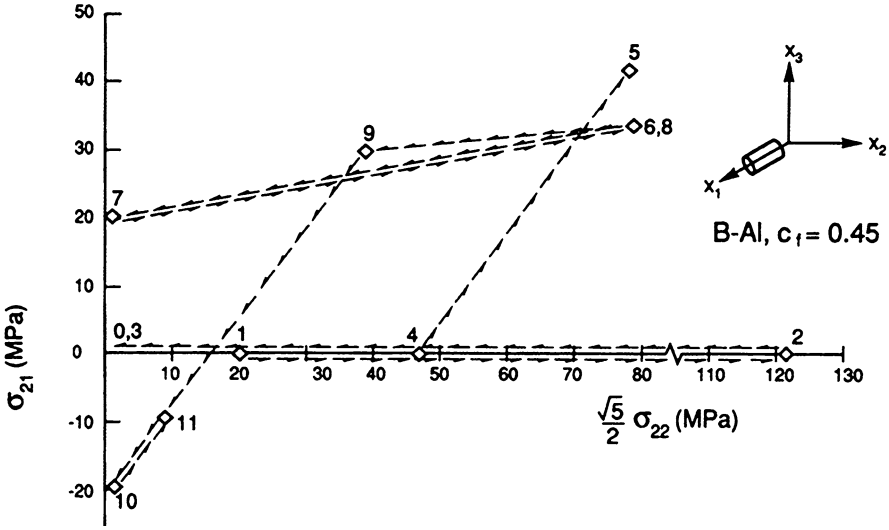

Fig. 12.13 A general loading path in the longitudinal shear and scaled transverse tension plane

Finally, we describe some of the comparisons of experimentally detected loading surfaces and plastic strains with their predictions, conducted along the loading paths shown in Fig. 12.13 (Dvorak et al. 1991). This study included both experiments and computational modeling of the clusters of loading surface branches of individual elements of the subdivided unit cell of the PHA model, Figure 12.14 shows the cluster in the elastic state, derived from (12.1.10). Each element branch indicates the

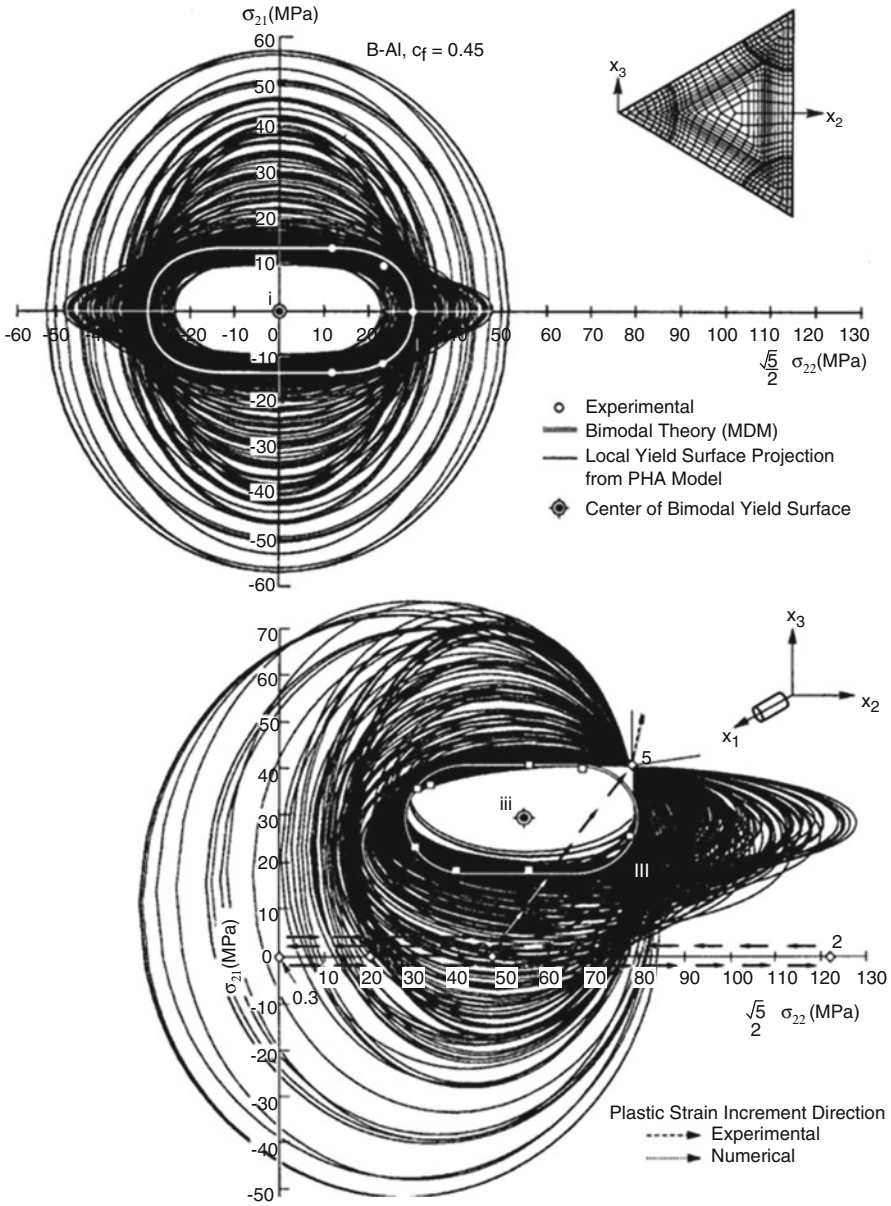

Fig. 12.14 Initial and subsequent clusters of element yield branches are compared with MDM surfaces and experimentally detected yield points. Computed and measured overall plastic strain increments coincide inside local yield cones (Dvorak et al. 1991)

overall stress magnitude that would cause onset of local plastic deformation. The initial MDM branch is shown together with several experimentally detected yield points in the top figure. Penetration of the cluster surfaces inside the MDM surface branch is not surprising; it indicates possible microscale yielding in the matrix which has not yet generated the overall $1 - 2 \times 10^{-6}$ magnitude of plastic strain available to detection.

In the bottom image, the cluster had been rearranged by local stress changes caused, in part, by plastic strains accumulated along the path 1–5. A yield point #5 is detected on loading from an elastic region. All branches of the cluster pass through the corner point in the overall stress plane, which indicates that plastic yielding is present in all elements of the unit cell. The bimodal surface fitted to other loading points is pierced by the loading path, which is not unusual. A cone of normals to the exterior branches of the cluster forms at the corner point. Local plastic strain increments at each point of the loading path were computed using Dafalias-Popov model of Sect. 11.2.4, and the experimental equivalent plastic strain and stress record of the matrix test specimen. Their resultant appears as one of the two arrows inside the cone. Fairly good agreement in both magnitude and direction of the computed and measured plastic strains was observed at all points of the path shown in Fig. 12.13. Elastic moduli of each specimen were repeatedly verified in small unloading steps for detection of their deterioration due to possible damage to the fiber/matrix interfaces generated during the loading program.

Observed deviation from normality to estimated overall loading surfaces is to be expected in plasticity of heterogeneous media, which only limits the overall increment vectors to cones of normals. Local normality remains valid for all branches corresponding to homogeneous material elements, and it is enforced in computations. Therefore, attempts to predict overall plastic strains by averaging, by normality to detected or modeled smooth yield surfaces, or by other methods that do not reproduce the distribution in direction and magnitude of local plastic strains in the matrix, are misguided.

That is illustrated in Fig.12.15, which collects several predictions and a measurement of overall plastic strains along the general path of Fig. 12.13. The Mori-Tanaka estimates shown in the figure are typical of those provided by other averaging approaches, and are very different from the magnitudes detected even in the early segments of the path. On the other hand, overall plastic strains ε^p_{22} computed with the PHA unit cell show good agreement with those measured in the transverse direction. Larger than predicted overall plastic strain ε^p_{21} was detected in the longitudinal shear direction. However, the agreement between the computed and measured loading surfaces and plastic strains is very good, considering the long and variable loading path and the phenomenological character of the plasticity theory used in modeling of matrix response. That may be attributed to the simplifying effect of stiff isotropic boron fibers on plastic deformation of the matrix, that is embodied in the bimodal theory.

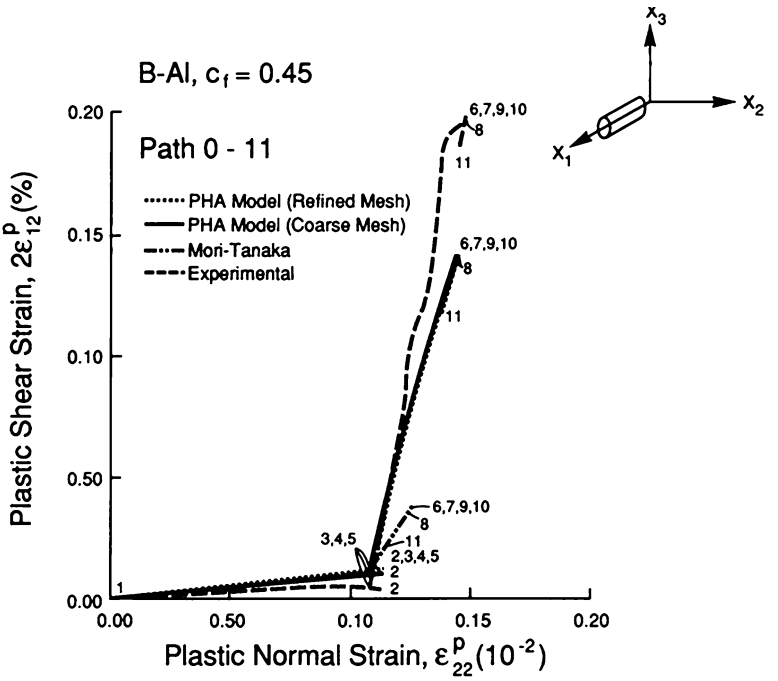

Fig. 12.15 Plastic strains along the general loading path, detected and predicted by different methods (Dvorak et al. 1991)

12.3 Thermal Hardening

Application of a uniform temperature change to a traction-free polycrystalline metallic material generates a macroscopically uniform thermal strain or eigenstrain, and it may also reduce or elevate the yield stress. A similar situation prevails in all perfectly bonded heterogeneous materials, but differential thermal expansion of the phases produces a distribution of piecewise uniform eigenstrains, and residual thermal stresses. The latter cause changes in shape and position of both phase and overall yield surface branches in their respective stress spaces. Not observed in nominally homogeneous materials, this type of hardening is called *thermal hardening, or elastic thermal hardening*. It is a form of constraint hardening caused by interactions of the phases, independent of phase hardening because it need not involve plastic deformation. In two-phase systems, thermal hardening of a unidirectional fiber composite was first identified by finite element modeling of overall yield surfaces at different temperatures (Dvorak et al. 1973, 1974). Analytical understanding follows from the uniform fields discussed in Chap. 3 (Dvorak 1997). Transformation fields described in Sect. 8.2 can be used for multiphase systems.

12.3.1 Thermal Hardening in Composites of Two Isotropic Phases

Thermoelastic constitutive relations of an isotropic phase are written as

$$\sigma_{ij}^r = \left(K_r - \frac{2}{3}G_r\right)\delta_{ij}\varepsilon_{mm}^r + 2G_r\varepsilon_{ij}^r - 3\alpha_r^\theta K_r\delta_{ij}\Delta\theta \qquad [8.1.1]$$

where K_r, G_r are the phase bulk and shear moduli, α_r^θ is the linear coefficient of thermal expansion, ε_{ij} is a uniform applied strain, and $\Delta\theta = \theta - \theta_0$ is a uniform change in temperature from a reference value θ_0. Phase property magnitudes of K_r, G_r and α_r^θ are assumed to be independent of $\Delta\theta$.

First, we consider a representative volume V of a two-phase composite that consists of two perfectly bonded isotropic phases of arbitrary geometry, distributed such that the aggregate is statistically homogeneous on the macroscale. The aggregate is traction free, but a uniform thermal change $\Delta\theta$ is applied in V, creating a nonuniform distribution of purely elastic strains in the phases. Details of this distribution may not be easily determined, since they depend on the specific geometry and thermoelastic moduli of the phases. However, the effect of $\Delta\theta$ on the position of the element branches of the overall yield surface can be found by elementary means. In particular, as shown in Sect. 8.1.2, a superposition of the interior stress field caused by the uniform thermal change $\Delta\theta$, with that generated by application of a certain overall isotropic auxiliary strain or stress to the aggregate, provides interior stress and strain fields that are uniform and isotropic in the entire representative volume. These uniform fields may coexist with an initial stress and strain state present in the aggregate.

In a composite of two isotropic phases with arbitrary geometry of the microstructure, the auxiliary uniform isotropic stress $\hat{\sigma} = \hat{\sigma}_{kk}/3$ and a uniform isotropic strain $\hat{\varepsilon} = \hat{\varepsilon}_{kk}/3$ were found from

$$\hat{\varepsilon} = \hat{\sigma}/(3K_\alpha) + \alpha_\alpha\Delta\theta = \hat{\sigma}/\left(3K_\beta\right) + \alpha_\beta\Delta\theta \qquad [8.1.4]$$

where α_r and K_r denote the linear coefficient of thermal expansion and bulk modulus of the phases. The auxiliary overall stress and strain are

$$\hat{\sigma} = \frac{3K_\alpha K_\beta}{K_\alpha - K_\beta}\left(\alpha_\alpha - \alpha_\beta\right)\Delta\theta \qquad \hat{\varepsilon} = \frac{K_\alpha\alpha_\alpha - K_\beta\alpha_\beta}{K_\alpha - K_\beta}\Delta\theta \qquad [8.1.5]$$

Unloading from $\hat{\sigma}$ by application of a uniform overall stress $-\hat{\sigma}\,\delta_{ij}$ renders the aggregate free of surface tractions, leaving the overall strain caused by $\Delta\theta$. The remaining thermal strain is written in subscript and matrix forms as

$$m_{ij}\Delta\theta = \hat{\varepsilon}\delta_{ij} - M_{ijkl}\hat{\sigma}\delta_{kl} \qquad \boldsymbol{m}\Delta\theta = \hat{\boldsymbol{\varepsilon}} - \boldsymbol{M}\hat{\boldsymbol{\sigma}} \qquad [8.1.6]$$

where m_{ij} is the overall thermal strain tensor. In matrix form, $\hat{\boldsymbol{\sigma}} = [\hat{\sigma},\ \hat{\sigma},\ \hat{\sigma},\ 0,\ 0,\ 0]^{\mathrm{T}}$, $\hat{\boldsymbol{\varepsilon}} = [\hat{\varepsilon},\ \hat{\varepsilon},\ \hat{\varepsilon},\ 0,\ 0,\ 0]^{\mathrm{T}}$, and the overall compliance $\boldsymbol{M}$ of the composite is a known (6×6) matrix evaluated as described in Chaps. 6 or 7.

Since the superimposed local fields due to $\hat{\sigma}$ and $\Delta\theta$ are uniform and isotropic, they have no effect on the position or size of the initial or current yield surfaces of the elements subdividing the inelastic phase in local stress space, or on the corresponding branches of the overall yield surface. Therefore, the yield surface cluster that was in existence before application of $\Delta\theta$ remains undisturbed while the aggregate is subjected to both $\Delta\theta$ and $\hat{\sigma}$.

The auxiliary stress $\hat{\sigma}$ is now removed by applying a uniform overall stress $\bar{\sigma}_{ij} = -\hat{\sigma}\,\delta_{ij}$ to the representative volume, while $\Delta\theta$ is preserved. In each subelement this unloading step causes the local stress change $\Delta\sigma_{ij}^{\eta} = -B_{ijkl}^{\eta}\hat{\sigma}\,\delta_{kl}$. As long as this unloading step does not cause any plastic deformation, its effect on the overall strain is described by (8.1.6). Before application of temperature change, and after elastic unloading the clusters of element yield surfaces are described by (12.1.10) and by

$$\left.\begin{aligned} G_{\eta}\left(\bar{\sigma}_{ij} - \bar{\alpha}_{ij}^{\eta}\right) &= g_{\eta}\left[B_{ijkl}^{\eta}\left(\bar{\sigma}_{kl} - \bar{\alpha}_{kl}^{\eta}\right)\right] = 0 \\ G_{\eta}\left(\bar{\sigma}_{ij} - \hat{\sigma}\,\delta_{ij} - \bar{\alpha}_{ij}^{\eta}\right) &= g_{\eta}\left[B_{ijkl}^{\eta}\left(\bar{\sigma}_{kl} - \hat{\sigma}\,\delta_{kl} - \bar{\alpha}_{kl}^{\eta}\right)\right] = 0 \end{aligned}\right\} \tag{12.3.1}$$

Each G_{η} function describes the η-branch of the cluster of element yield branches while the aggregate is subjected to $\Delta\theta$. The overall unloading step has the same effect on all branches of the cluster in the overall stress space. Therefore, application of $\Delta\theta$ causes a rigid body translation of the original cluster by $-\hat{\sigma}\,\delta_{ij}$, in the direction of the overall hydrostatic stress. Rigid body translation is also observed in all two-phase system where the uniform auxiliary stress field $\hat{\sigma}$ can be found such that its superposition with the thermal stresses generates an isotropic stress field in the matrix phase. Anisotropic fields can also be found; the uniform fields in (8.1.22) for aligned fiber composite of two transversely isotropic phases, and in (8.1.14) for polycrystals, are not necessarily isotropic.

As an illustration of thermal hardening, Fig. 12.16 shows a subdivided unit cell designed to model the response of an aluminum matrix composite reinforced by periodically distributed silicone carbide particles. This cell is similar to the PHA model in Fig. 12.1. Displacement boundary conditions allow uniform deformation of the cell under the applied uniform thermal change, with zero force resultants on each face. The left image in Fig. 12.17 shows a section of the cluster of element yield surfaces in the axisymmetric overall stress plane, in a stress-free state, with no external tractions or thermal changes applied. Scales on the coordinate axes are given by the stress invariants $I_1 = \sigma_{11},\ I_2 = (\sigma_{22} + \sigma_{33})/2$. The element branches of the overall yield surface cluster in the $I_1\,I_2$ −plane are found from (12.3.1). The interior envelope of the cluster is the initial yield surface of the composite. The right image shows the same cluster after application of a uniform thermal change $\Delta\theta = +24.95°\mathrm{C}$, which brings the interior envelope of the cluster into contact with the

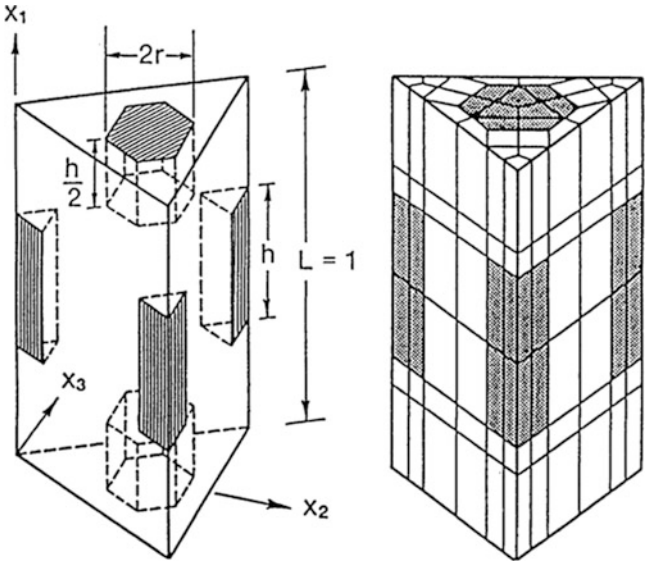

Fig. 12.16 Geometry and finite element subdivision of a unit cell in the PHA model of a particulate composite (Dvorak et al. 1991)

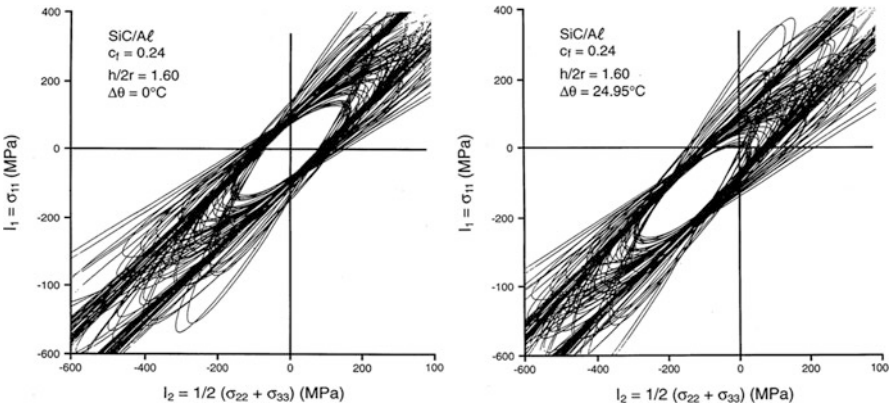

Fig. 12.17 Translation of yield surface clusters in the axisymmetric overall stress plane caused by thermal hardening of a particulate SiC/Al composite (Dvorak 1991)

origin, the current mechanical loading point at $I_1 = I_2 = 0$. A similar effect was first observed by Dvorak et al. (1974) and in current form by Dvorak et al. (1991), Dvorak (1992).

Further increase in temperature would cause local inelastic deformation in the elements whose yield surface branches come into contact with the origin. A distribution of inelastic strains in the affected elements would augment the local thermal eigenstrain field in each element. The cluster would become rearranged

by the changing total local stress field, as it proceeds to move toward the origin. When the temperature change causes yielding in all elements, the rearranged cluster forms a corner at the stationary origin, where all the translated and deformed loading surface branches come into contact or intersect.

A numerical simulation of yield surface clusters and plastic strains that develop during complex loading of a particle reinforced composite, modeled by the unit cell in Fig. 12.16, can be found in Dvorak et al. (1991).

12.3.2 Thermal Hardening in Two-Phase Aligned Fiber Composites

The systems considered here have an elastically isotropic matrix, which is reinforced by aligned, transversely isotropic fibers. Analysis of thermal hardening follows in the steps outlined in the preceding paragraph, but the isotropic uniform field in the aggregate is no longer given by (8.1.4). Instead, we refer to the more general, uniform fields in Sect. 8.1.5, which can be adjusted to create an isotropic uniform strain field in a fiber systems with transversely isotropic phases.

A uniform change in temperature $\Delta\theta$ is applied to the composite aggregate together with an overall auxiliary stress $\hat{\boldsymbol{\sigma}}^0$, which is axisymmetric with respect to the fiber direction $x_A \equiv x_1$, and has the longitudinal or axial and transverse components

$$\left.\begin{aligned} &\hat{\boldsymbol{\sigma}}^0 = [\hat{\sigma}_A,\ \hat{\sigma}_T,\ \hat{\sigma}_T,\ 0,\ 0,\ 0]^{\mathrm{T}} \\ &\hat{\sigma}_A = \hat{\sigma}_1 = c_\alpha \hat{\sigma}_1^\alpha + c_\beta \hat{\sigma}_1^\beta \qquad \hat{\sigma}_T = \frac{1}{2}(\hat{\sigma}_2 + \hat{\sigma}_3) \end{aligned}\right\} \qquad [8.1.28]$$

The temperature change generates thermal strains or eigenstrains $\boldsymbol{\mu}_r$, which are also axisymmetric, and are given by

$$\boldsymbol{\mu}_r = \boldsymbol{m}_r \Delta\theta \qquad \boldsymbol{m}_r = \left[\alpha_A^r,\ \alpha_T^r,\ \alpha_T^r,\ 0,\ 0,\ 0\right]^{\mathrm{T}} \qquad (12.3.2)$$

where $\boldsymbol{m}_r$ is the thermal strain vector of phases $r = \alpha, \beta$, c. f., Table 8.1.

Our objective is to find the components $\hat{\sigma}_A,\ \hat{\sigma}_T$ of the auxiliary overall stress $\hat{\boldsymbol{\sigma}}^0$ such that application of the load set $\{\hat{\boldsymbol{\sigma}}^0, \boldsymbol{m}\Delta\theta\}$ creates a uniform and isotropic stress field in the $r = \alpha$ phase, which is selected to represent the metal matrix. The interior strain field is also uniform in the entire volume, $\hat{\boldsymbol{\varepsilon}}_\alpha(\boldsymbol{x}) = \hat{\boldsymbol{\varepsilon}}_\beta(\boldsymbol{x}) = \hat{\bar{\boldsymbol{\varepsilon}}}$. Since the α-phase is isotropic, an isotropic stress state may exist there only if the uniform strain field is isotropic in the entire volume. The thermal strain $\boldsymbol{m}_\alpha \Delta\theta$ already satisfies this requirement in the isotropic α-phase.

A general solution of this problem was derived in Sect. 8.1.5. The transverse stress $\hat{\sigma}_T$ is uniform in the entire volume and it serves as a free parameter in the solution. The longitudinal normal stresses (8.1.29, 8.1.30) are written in the present application as

$$\hat{\sigma}_1^{\alpha} = q\left[\left(l_\alpha \Delta l - n_\alpha \Delta k\right)\hat{\sigma}_T + k_\alpha E_{11}^{\alpha}\left(l_\beta \Delta\alpha_A^r + 2k_\beta \Delta\alpha_T^r\right)\Delta\theta\right] \tag{12.3.3}$$

$$\hat{\sigma}_1^{\beta} = q\left[\left(l_\beta \Delta l - n_\beta \Delta k\right)\hat{\sigma}_T + k_\beta E_{11}^{\beta}\left(l_\alpha \Delta\alpha_A^r + 2k_\alpha \Delta\alpha_T^r\right)\Delta\theta\right] \tag{12.3.4}$$

where

$$q^{-1} = \left(l_\alpha k_\beta - k_\alpha l_\beta\right) = 2k_\alpha k_\beta\left(\nu_L^{\alpha} - \nu_L^{\beta}\right) \neq 0 \tag{12.3.5}$$

Also, $\Delta k = k_\alpha - k_\beta$, $\Delta l = l_\alpha - l_\beta$ and $\Delta\alpha_j^r = \alpha_j^{\alpha} - \alpha_j^{\beta}$, $j = A, T$. The k_r, l_r, n_r are Hill's elastic moduli of the phases defined in Sect. 2.3.1, and $\nu_L^r = \nu_{12}^r$ are phase longitudinal Poisson's ratios.

The auxiliary overall stress components $\hat{\sigma}_A$ and $\hat{\sigma}_T$ that create a selected axisymmetric stress state in phase α, are found from the following condition and then substituted into (12.3.4).

$$\hat{\sigma}_1^{\alpha} = \hat{\sigma}_2^{\alpha} = \hat{\sigma}_3^{\alpha} = \hat{\sigma}_T \tag{12.3.6}$$

That yields the transverse overall stress components that supports the isotropic stress field, in superposition with the thermal stresses due to $\Delta\theta$.

$$\hat{\sigma}_T = \left[1 - q\left(l_\alpha \Delta l - n_\alpha \Delta k\right)\right]^{-1}\left\{q k_\alpha E_{11}^{\alpha}\left[\left(l_\beta \Delta\alpha_A^r + 2k_\beta \Delta\alpha_T^r\right)\Delta\theta\right]\right\} \tag{12.3.7}$$

The corresponding longitudinal traction is $\hat{\sigma}_A = \hat{\sigma}_1 = c_\alpha \hat{\sigma}_1^{\alpha} + c_\beta \hat{\sigma}_1^{\beta}$, where the normal stress $\hat{\sigma}_1^{\beta}$ evaluated from (12.3.4) for this particular value of $\hat{\sigma}_T$. The stress field in an anisotropic fiber or β-phase need not be isotropic. The transverse and longitudinal normal stress components create the auxiliary overall stress $\hat{\boldsymbol{\sigma}}^{(\theta)} = [\hat{\sigma}_A,\ \hat{\sigma}_T,\ \hat{\sigma}_T,\ 0,\ 0,\ 0]^{\mathrm{T}}$, that in superposition with the thermal stresses creates and isotropic stress in the matrix $r = \alpha$.

Next, we retrace the steps leading to the rigid body translation of the cluster of initial yield surface branches of a fibrous ply, similar to that shown in Fig. 12.17 for a particulate composite made of isotropic phases. The total volume of the composite is represented by a single unit cell subjected to displacement boundary conditions that allow uniform deformation of the cell. The cell is subdivided into $\eta,\ \rho = 1, 2, \ldots, M$ finite elements, where the local stress vectors and yield conditions comply with

$$\left.\begin{aligned}\left(\sigma_{ij}^{\eta} - \alpha_{ij}^{\eta}\right) &= B_{ijkl}^{\eta}\left(\bar{\sigma}_{kl} - \bar{\alpha}_{kl}^{\eta}\right)\\ g_\eta\left(\sigma_{ij}^{\eta} - \alpha_{ij}^{\eta}\right) &= \tilde{J}_2\left(s_{ij}^{\eta}\right) - Y_\eta^2\left(\varepsilon_{eq}^{p}, \theta\right) = 0\\ G_\eta\left(\bar{\sigma}_{ij} - \bar{\alpha}_{ij}^{\eta}\right) &= g_\eta\left[B_{ijkl}^{\eta}\left(\bar{\sigma}_{kl} - \bar{\alpha}_{kl}^{\eta}\right)\right] = 0\end{aligned}\right\} \tag{12.1.10}$$

The σ_{ij}^{η} is current stress in V_η and α_{ij}^{η} is the position of the center of the yield surface in the local σ_{ij}^{η} −space, $\tilde{J}_2(s_{ij}^{\eta})$ is the second invariant of the deviatoric stress, and Y_η is the current yield stress of the matrix material in V_η.

In the overall $\bar{\sigma}_{ij}$ −space of the ply, the element yield surface branches form a cluster, similar to that in Fig. 12.14. This cluster remains undisturbed when the composite is subjected to the load set $\{\hat{\boldsymbol{\sigma}}^{(\theta)},\ \boldsymbol{m}\Delta\theta\}$, because $\hat{\boldsymbol{\sigma}}^{(\theta)}$ now adjusts the thermal stress to an isotropic stress state in the matrix phase $r = \alpha$. Unloading by application of an overall stress $-\hat{\boldsymbol{\sigma}}^{(\theta)} = -[\hat{\sigma}_A,\ \hat{\sigma}_T,\ \hat{\sigma}_T,\ 0,\ 0,\ 0]^{\mathrm{T}}$ leaves only the thermal stress distribution, and it translates the cluster in the overall stress space to

$$G_\eta\left(\bar{\sigma}_{ij} - \hat{\sigma}_{ij}^{(\theta)} - \bar{\alpha}_{ij}^{\eta}\right) = g_\eta\left[B_{ijkl}^{\eta}\left(\bar{\sigma}_{kl} - \hat{\sigma}_{ij}^{(\theta)} - \bar{\alpha}_{kl}^{\eta}\right)\right] = 0 \tag{12.3.8}$$

The $\hat{\sigma}_T$ comes from (12.3.7) and $\hat{\sigma}_A = \hat{\sigma}_1 = c_\alpha\hat{\sigma}_1^{\alpha} + c_\beta\hat{\sigma}_1^{\beta}$, with the two longitudinal normal stresses from (12.3.3, 12.3.4, 12.3.5) for the said $\hat{\sigma}_T$. Of course, when the fiber is also isotropic, phase elastic moduli change according to (2.3.6) and the translation vector coincides with $-\hat{\sigma}\delta_{ij}$.

12.3.3 Thermal Hardening in Laminated Plates

The auxiliary stress components (12.3.3, 12.3.4, 12.3.5, 12.3.6, 12.3.7) can be utilized in analysis of thermal hardening of laminated plates consisting of unidirectional fibrous plies made of the same two-phase composite material. Ply thickness and layup sequence can be selected at will, with or without a defined midplane. Initially separated from the plate, each planar ply is loaded by a uniform change in temperature $\Delta\theta$ and by the auxiliary stress $\hat{\boldsymbol{\sigma}} = [\hat{\sigma}_A,\ \hat{\sigma}_T,\ \hat{\sigma}_T]^{\mathrm{T}}$. In all plies, the $\hat{\sigma}_T$ is applied on all four ply surface planes aligned with the fiber direction, together with the corresponding stress $\hat{\sigma}_A$ applied on the two surfaces perpendicular to the fiber. Since all plies now undergo the same isotropic deformation, and the tractions on their lateral surfaces are known, the laminate can be reassembled, provided that $\hat{\sigma}_A$ and $\hat{\sigma}_T$ remain applied to the external edges of each ply, and that $\hat{\sigma}_T$ is also applied as normal stress σ_{33} to both exterior in-plane surfaces of the laminated plate. Recall from (10.1.8) that the latter part of $\hat{\sigma}_T$ can be represented by an in-plane eigenstrain and thus incorporated into the constitutive relation (10.1.9) of each ply.

After reassembly, the $\hat{\sigma}_A$ and $\hat{\sigma}_T$ are transformed by $(10.2.2)_2$ from the local coordinates $x_j^{(i)}$ of each ply, into ply tractions $\hat{\bar{\sigma}}_1$, $\hat{\bar{\sigma}}_2$ and a shear $\hat{\bar{\sigma}}_6$ in the global or laminate system of coordinates $\bar{x}_j$, $j = 1, 2, 3$. The transformed ply tractions are then substituted into (10.3.1, 10.3.2), to yield their global resultant $\hat{\bar{\boldsymbol{\sigma}}} = \sum c_i[\hat{\bar{\sigma}}_1^{(i)},\ \hat{\bar{\sigma}}_2^{(i)},\ \hat{\bar{\sigma}}_6^{(i)}]^{\mathrm{T}}$. The contribution of a thermal change $\Delta\theta$ to the stress state in each ply is now denoted by $\bar{\boldsymbol{\sigma}}_i^{(\theta)}$, which is the in-plane stress remaining in each ply (i) after unloading of the laminate by in-plane stress $-\hat{\bar{\boldsymbol{\sigma}}}$ and transverse stress $\bar{\sigma}_{33} = -\hat{\sigma}_T$. The unloading step follows from (10.1.10) and (10.3.13).

$$\left.\begin{aligned} \bar{\boldsymbol{\sigma}}_i^{(\theta)} &= \left(\mathbf{I} - \bar{\mathbf{H}}_i\right)\hat{\bar{\boldsymbol{\sigma}}} + \sum_{j=1}^{n}\left(\delta_{ij}\,\mathbf{I} - c_j\,\bar{\mathbf{H}}_i\right)\bar{\mathbf{L}}_j\,\bar{\boldsymbol{\mu}}_j \\ \bar{\boldsymbol{\mu}}_j &= -\hat{\sigma}_T\left\{-\left(\nu_{12}^{(i)}\Big/E_{11}^{(i)}\right), -\left(\nu_{23}^{(i)}\Big/E_{22}^{(i)}\right),\ 0\right\}^{\mathrm{T}} \end{aligned}\right\} \tag{12.3.11}$$

The transverse stress $\bar{\sigma}_{33}$ vanishes in the unloading step. Corresponding stress averages in the fiber and matrix phases $r = f, m$ are, from (10.4.5)

$$\boldsymbol{\sigma}_r^{(i)} = \boldsymbol{B}_r^{(i)}\boldsymbol{U}\,\bar{\boldsymbol{\sigma}}_i^{(\theta)} + \boldsymbol{b}_r\,\Delta\theta \tag{12.3.12}$$

Onset of global yielding in each ply can be determined by one or more yield surfaces that may be assigned to the ply. The bimodal surfaces described in Sect. 12.2.1 are a convenient choice. However, they now need to be derived directly from the matrix yield condition and from the matrix stress average (12.3.12). The latter causes their rigid body translation, because both contributions to $\boldsymbol{\sigma}_r^{(i)}$ depend on $\Delta\theta$. In the first term, $\Delta\theta$ is introduced through $\hat{\sigma}_T$. Translation of ply yield surfaces in the global coordinates is not necessarily limited to in-plane directions, because $\bar{\boldsymbol{\sigma}}_i^{(\theta)}$ also depends on the $\bar{\sigma}_{33} = -\hat{\sigma}_T$ applied to laminate surfaces. Initial and translated loading surfaces of each ply need to be converted from ply to global coordinate systems. Implementation and results of the outlined procedure, with yield surfaces of each ply represented by the bimodal plasticity theory of Sect. 12.2, were described by Bahei-El-Din (1992).

Here we show selected results of the said procedure, obtained for a $(0/\pm 45)_S$ laminated plate, made of a silicon carbide (SCS6) fiber, $c_f = 0.35$, in a titanium aluminate (Ti_3Al) matrix. Matrix yield stress increases linearly from 200 MPa at the fabrication temperature of 920 °C, where the laminate was assumed to be stress-free, to 624 MPa at room temperature. Branches of the bimodal yield surface were constructed in the global system for each ply of the laminate. The initial cluster of ply branches of the stress-free laminate at fabrication temperature is symmetric about the origin, which is the center of all branches. The top image in Fig. 12.18 shows a section of the cluster in the global coordinate plane $\bar{\sigma}_{11}\bar{\sigma}_{22}$.

Cooling of the laminate from the fabrication to room temperature has not caused plastic deformation, since the matrix yield stress had increased at a faster rate than the temperature-induced translations of the branches. The elastic thermal hardening of the laminate causes large size expansion and rearrangement of the branches. Bottom part of Fig. 12.18 shows the cluster at 21 °C, in the global stress coordinates $\bar{\sigma}_{11}\bar{\sigma}_{22}$. Since both the fiber and matrix constituents are isotropic, one part of the rigid body translation of the branches proceeds in the isotropic stress direction of each ply, as in Fig. 12.17. Another part is induced by ply stress changes caused by the global unloading (12.3.11). Both are projected into global stress space of the laminate and superimposed. The magnitude of translation due to thermal hardening in the global stress space is proportional to $\Delta\theta$. The direction is not in the ply stress plane.

Interior envelopes of the clusters surround the elastic deformation region of the plate. They are subdivided into FDM and MDM segments, and shown at the fabrication and room temperatures in Fig. 12.19. Similar initial and translated surfaces were found in the $\bar{\sigma}_{11}\bar{\sigma}_{21}$–plane. Both figures appear in the same stress scale, and the interior envelopes coincide on the $\bar{\sigma}_{11}$–axis. The initial surfaces are of the MDM mode, while FDM branches, projected from the local caps in certain plies, form sections the interior envelopes at room temperature.

These examples show the large effect that a change from processing to room temperature may have on the size and position of the branches of ply and overall loading surfaces. Activation of either fiber or matrix dominated mode on the interior surface also indicates where to expect either more compliant or stiffer response.

12.3.4 Thermal Hardening in Polycrystals and Multiphase Systems

Uniform strain and stress fields which were used to find simple thermal hardening rules in two-phase systems and multilayer laminates of identical two-phase fiber plies, are also available in polycrystals consisting of randomly orientated grains with identical elastic properties, described in Sect. 8.1.3. Each grain may have trigonal, tetragonal. hexagonal or cubic material symmetry. Mechanical stress averages σ_{ij}^{η}, caused in each grain $r = \eta$ by a uniform overall stress $\bar{\sigma}_{ij}$ can be determined as $\sigma_{ij}^{\eta} = B_{ijkl}^{\eta}\bar{\sigma}_{ij}$, where the local stress concentration factors B_{ijkl}^{η} can be determined, for example, by the self-consistent method using (7.1.1).

A uniform thermal change $\Delta\theta = \theta - \theta_0$ applied to a polycrystal will cause thermal stresses in individual grains. However, superposition of $\Delta\theta$ with an applied overall stress $\hat{\sigma}_{ij} = \hat{p}\delta_{ij}$ from (8.1.13), creates an auxiliary isotropic uniform overall strain $\hat{\varepsilon}_{kl}$ (8.1.14) in the entire aggregate. Local stress average in each η-grain is $\hat{\sigma}_{ij}^{\eta} = L_{ijkl}^{\eta}\left(\hat{\varepsilon}_{kl} - m_{kl}^{\eta}\Delta\theta\right)$, where L_{ijkl}^{η} is the local stiffness and m_{kl}^{η} the local thermal strain vector, found for each material symmetry of the grains from Table 8.1. Unloading by the overall stress $\bar{\sigma}_{ij} = -\hat{p}\delta_{ij}$ returns the polycrystal to traction-free state, and it changes the local stress to

$$\sigma_{ij}^{\eta} = \hat{\sigma}_{ij}^{\eta} - B_{ijkl}^{\eta}\hat{p}\delta_{kl} \tag{12.3.13}$$

Onset of plastic deformation in each grain should be defined by a certain yield function $g_{\eta}\left(\sigma_{ij}^{\eta} - \alpha_{ij}^{\eta}\right)$ of local invariants of σ_{ij}^{η}, consistent with the particular material symmetry of the grains. Branches of the yield surfaces of individual grains in the overall stress space $\bar{\sigma}_{kl}$ can be generated by describing each branch by

$$G_{\eta}\left(\bar{\sigma}_{ij} - \bar{\alpha}_{ij}^{\eta}\right) = g_{\eta}\left[\hat{\sigma}_{ij}^{\eta} - B_{ijkl}^{\eta}\left(\hat{p}\delta_{kl} - \bar{\alpha}_{kl}^{\eta}\right)\right] = 0 \tag{12.3.14}$$

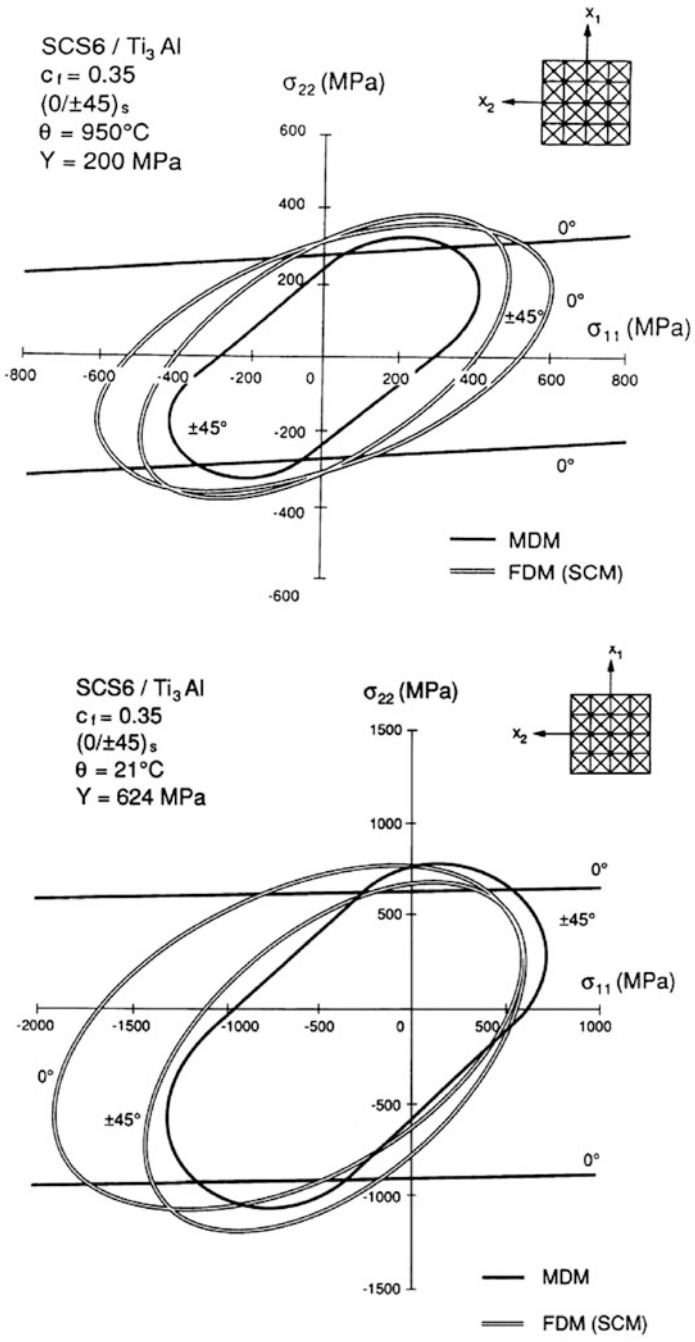

Fig. 12.18 Clusters of initial ply yield surfaces at fabrication temperature and of translated yield surfaces at room temperature of a SCS6/Ti_3Al composite. Reprinted with permission from Bahei-El-Din (1992)

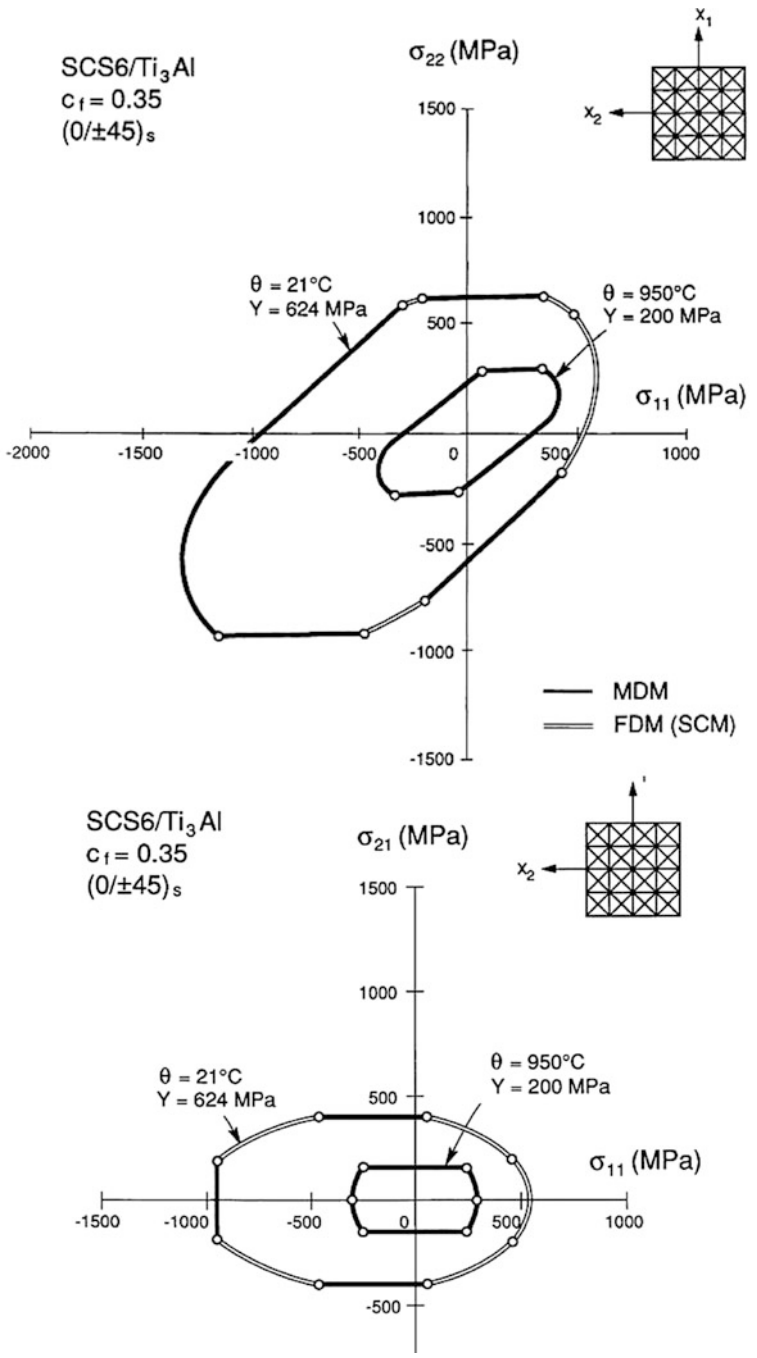

Fig. 12.19 Internal envelopes of ply surfaces of a SCS6/Ti_3Al composite at fabrication and room temperature in $\bar{\sigma}_{11}\bar{\sigma}_{22}$−plane and in $\bar{\sigma}_{11}\bar{\sigma}_{21}$−plane. Reprinted with permission from Bahei-El-Din (1992)

where $\hat{\sigma}_{ij}^{\eta} = L_{ijkl}^{\eta}\left(\hat{\varepsilon}_{kl} - m_{kl}^{\eta}\Delta\theta\right)$ and $\hat{p}$ brings in the effect of temperature change. The $\bar{\alpha}_{ij}^{\eta}$ denote again current positions of the centers of the individual branches, as indicated by the specific form of the local yield function.

Multi-phase aggregates do not lend themselves to evaluation of local thermal stress fields by a uniform field method. Instead, these fields need to be found using (8.2.22), as

$$\sigma_{ij}^{\eta} = B_{ijkl}^{\eta}\bar{\sigma}_{kl} + \sum_{\rho=1}^{n} F_{ijkl}^{\eta\rho} L_{klrs}^{\rho} m_{rs}^{\rho}\Delta\theta \tag{12.3.15}$$

or from (8.3.3)

$$\sigma_{ij}^{\eta} = B_{ijkl}^{\eta}\bar{\sigma}_{kl} + b_{ij}^{\eta}\Delta\theta \tag{12.3.16}$$

The $\lambda_{kl}^{\rho} = l_{kl}^{\rho}\Delta\theta = -L_{klrs}^{\rho} m_{rs}^{\rho}\Delta\theta$ is the thermal eigenstress in each grain $r = \rho$. As shown in (8.2.23, 8.2.24), the $F_{ijkl}^{\eta\rho}$ can be found in terms of the B_{ijkl}^{η} and B_{ijkl}^{ρ}, and compliances M_{ijkl}^{η}, M_{ijkl}^{ρ}, while b_{ij}^{η} is given in (8.3.7). The local stresses can be used to generate local yield surfaces in each elastic phase or subelement V_{η}. Projection of the local surfaces as branches of the overall yield surface follows again in the steps leading to (12.3.14).

12.4 Utility of Plasticity Theories of Composite Materials

Modeling of inelastic composite materials has attracted substantial attention over the last 40 years. Many early papers had extended elastic averaging approaches and standard plasticity theories to evaluation of yield functions and plastic strain directions and magnitudes of both fibrous and particle systems. More recent work shows that predictions indicated by averaging methods are not in agreement with experiments, numerical simulations, or with the bimodal theory. Therefore, such predictions can now be regarded as a self-contained body of work of limited significance in applications.

More recent finite element work has shown that even large domains, consisting of a matrix and many aligned fibers randomly distributed in the transverse plane, cannot be regarded as representative volumes. Their response to constant transverse uniform stress changes with rotation of the domain about the direction of the fibers. That limits numerical simulations to unit cells subjected to periodic boundary conditions. Since the metal matrix composites that have been used in actual aerospace structures exhibit nearly periodic distribution of boron or silicon carbide fibers, they can be represented by unit cell models designed as representative volumes, such as the PHA model in Sect. 12.1.1.

The results outlined in this chapter apparently represent the most complete set of comparisons between controlled multiaxial experiments and both analytical and numerical simulations. The bimodal plasticity and the Phillips hardening rule appear to yield reasonably accurate predictions of the shapes and positions of overall yield

and loading surfaces observed in experiments. The MDM yield condition suggests that the yield stress is independent of the slip system involved, which is confirmed by comparison with experiments in Fig. 12.9. However, the experimentally detected directions of the plastic strain increments shown in Fig. 12.11 are not quite perpendicular to the MDM branch segments. That is most pronounced along the D-E segment in the figure, but is also evident on other parts of the several MDM branches. We note that similar deviations from normality were found in detection of plastic strain increments of the polycrystal aluminum matrix along the path shown in Fig. 12.8, and also in the cited work by Phillips and associates.

Deviations from normality can be explained by inspecting the cluster of loading surfaces computed with the PHA model in Fig. 12.14. The MDM branch of the bimodal surface provides a good approximation to the observed yield points. However, each such point is a corner of the currently loaded branches of the cluster, and the plastic strain increment direction is only required to lie within the cone of normals at each such corner. However, the bimodal theory and Phillips rule alone can approximate the experimentally observed shapes and positions of both MDM and FDM yield and loading surfaces along a complex loading path. Such approximation cannot be expected from the averaging method, which would predict only the FDM branch of the bimodal surface.

The bimodal theory can be useful in predicting the stress range loads which may cause primarily elastic deformation of a composite structure, even under variable loads. Of course, elastic response is desirable in most applications, since frequent excursions into the plastic region cause low cycle fatigue (Dvorak and Johnson 1980). That response is assured when the material and structure shake down to an elastic state, possibly after some excursions into the plastic region (Maier 1969, 1973; Tarn et al. 1975). On the other hand, absence of shakedown allows repeated inelastic straining, which may lead to structural failure in relatively few cycles. The cyclic loading sequence leading to shakedown may also be accompanied by development of damage by transverse cracking, as indicated in Sect. 10.10. Such process has been modeled in several metal matrix laminates by Dvorak, Lagoudas and Huang (1994, 2000). Thermal hardening may play a significant role in shakedown processes at elevated temperatures. Shakedown as well as thermal hardening are precluded by constrains on elastic or total deformation, such as the fiber inextensibility and overall incompressibility assumed for the ‘ideal materials’ by Mulhern et al. (1967, 1969) and Spencer (1972, 1987).

In conclusion, reliable parts of the predictions include yield and loading surfaces evaluated with the bimodal theory and Phillips hardening rule. Also, inelastic strain magnitudes evaluated for a subdivided unit cell, by the transformation field analysis or by a finite element program. The flow rule for evaluation of plastic strain magnitude can be based on data obtained in combined loading experiments in Sect. 12.2.2, but not necessarily from standard uniaxial tests.

Far removed from reality is the assumption of normality of plastic strain increments to a model-predicted smooth loading surface, and the plastic strain magnitude evaluation on the basis of uniaxial tension experiments on bulk matrix material.

References

Aboudi, J. (1991). *Mechanics of composite materials – A unified micromechanical approach*. Amsterdam: Elsevier.

Accorsi, M. L., & Nemat-Nasser, S. (1986). Bounds on the overall elastic and instantaneous elastoplastic moduli of periodic composites. *Mechanics of Materials, 5*, 209–220.

Achenbach, J. D., & Zhu, H. (1989). Effect of interfacial zone on mechanical behavior and failure of fiber-reinforced composites. *Journal of the Mechanics and Physics of Solids, 37*, 381–393.

Ahmad, F. (2002). Invariants and structural invariants of the anisotropic elasticity tensor. *Quarterly Journal of Mechanics and Applied Mathematics, 55*, 597–606.

Alberski, T.C. (2000). The role of fiber prestress in improving damage resistance of composite laminates. Ph.D. Dissertation, Rensselaer Polytechnic Institute.

Almgren, R. F. (1985). An isotropic three-dimensional structure with Poisson's ratio $= -1$. *Journal of Elasticity, 15*, 427–430.

Ambartsumyan, S. A. (1970). *Theory of anisotropic plates. Strength, stability, vibration* (T. Cheron, Trans.). Stamford: Technomic Publishing.

Arfken, G. B., & Weber, H. J. (1995). *Mathematical methods for physicists*. San Diego: Academic.

Armstrong, P. J., & Frederick, C. O. (1966). *A mathematical representation of the multiaxial Bauschinger effect* (Report RD/B/N 731, C.E.G.B).

Asaro, R. J., & Barnett, D. M. (1975). The non-uniform transformation strain problem for an anisotropic ellipsoidal inclusion. *Journal of the Mechanics and Physics of Solids, 23*, 77–83.

Ashby, M. F., & Jones, D. R. H. (1986). *Engineering materials 2. An introduction to microstructures, processing and design*. Oxford: Pergamon Press.

Ashby, M. F., Evans, A., Fleck, N. A., Gibson, L. J., Hutchinson, J. W., & Wadley, H. N. G. (2000). *Metal foams. A design guide*. Boston: Butterworth Heinemann.

Babuska, I. (1975). Homogenization and application: Mathematical and computational problems. In B. Hubbard (Ed.), *Numerical solution of partial differential equations – III*. New York: Academic.

Backus, G. A. (1970). Geometrical picture of anisotropic elastic tensors. *Reviews of Geophysics and Spacephysics, 8*, 633–671.

Bacon, D. J., Barnett, D. M., & Scattergood, R. O. (1979). Anisotropic continuum theory of lattice defects. *Progress in Material Science, 23*, 51–262.

Baerheim, R. (1993). Harmonic decomposition of the anisotropic elasticity tensor. *Quarterly Journal of Mechanics and Applied Mathematics, 46*, 511–523.

Bahei-El-Din, Y. A. (1992). Uniform fields, yielding and thermal hardening in fibrous composite laminates. *International Journal of Plasticity, 8*, 867–892.

Bahei-El-Din, Y. A. (1996). Finite element analysis of viscoplastic composite materials and structures. *Mechanics of Composite Materials and Structures, 3*, 1–28.

G.J. Dvorak, *Micromechanics of Composite Materials*, Solid Mechanics and Its Applications 186, DOI 10.1007/978-94-007-4101-0,

Bahei-El-Din, Y. A. (2009). Modeling electromechanical coupling in woven composites exhibiting damage. *Journal of Aerospace Engineering, Proceedings of the Institution of Mechanical Engineering, 223*(Part G), 485–495.

Bahei-El-Din, Y. A., & Dvorak, G. J. (1997). Isothermal fatigue of sigma/timetal 21S laminates: II. Modeling and numerical analysis. *Mechanics of Composite Materials and Structures, 4*, 131–158.

Bahei-El-Din, Y. A., & Dvorak, G. J. (2000). Micromechanics of inelastic composite materials. In A. Kelly & C. Zweben (Eds.), *Comprehensive composite materials*. In T.-W. Chou (Eds.), *I: Fiber Reinforcements and General Theory of Composites*, Ch. 1.14. Amsterdam: Elsevier Science B. V., pp. 403–430.

Bahei-El-Din, Y. A., Dvorak, G. J., & Wu, J. F. (1989). Fracture of fibrous metal matrix composites – II. Modeling and numerical analysis. *Engineering Fracture Mechanics, 34*, 105–123.

Bahei-El-Din, Y. A., Dvorak, G. J., & Wu, J.-F. (1992). Dimensional stability of metal-matrix laminates. *Composites Science and Technology, 43*, 207–219.

Bahei-El-Din, Y. A., Ibrahim, I. A., & Botrous, A. G. (1998). Micromechanical analysis of inelastic laminates. In Y. A. Bahei-El-Din & G. J. Dvorak (Eds.), *IUTAM symposium on transformation problems in composite and active materials* (pp. 45–60). Dordrecht: Kluwer Academic.

Bahei-El-Din, Y. A., Khire, R., & Hajela, P. (2010). Multiscale transformation field analysis of progressive damage in fibrous laminates. *International Journal of Multiscale Computational Engineering, 8*, 69–80.

Bailey, J. E., Curtis, P. T., & Parvizi, A. (1979). On the transverse cracking and longitudinal splitting behaviour of glass and carbon fibre reinforced epoxy cross ply laminates and the effect of Poisson and thermally generated strain. *Proceedings of the Royal Society London*, *A366*, 599.

Barnett, D. M. (1972). The precise evaluation of derivatives of the anisotropic elastic Green's functions. *Physica Status Solidi, 49*, 741–748.

Batdorf, S. B., & Budiansky, B. (1949). *A matrhmatical theory of plasticity based on the concept of slip* (Techical Note 1871). Washington, DC: National Advisory Committee for Aeronautics.

Baughman, R. H., Shacklette, J. M., Zakhidov, A. A., & Stafstrom, S. (1998). Negative Poisson's ratio as a common feature of cubic materials. *Nature, 426*, 667.

Baweja, S., Dvorak, G. J., & Bazant, Z. P. (1998). Composite model for basic creep of concrete. *Journal of Engineering Mechanics, 124*, 959–965.

Behrens, E. (1971). Elastic constants of fiber-reinforced composites with transversely isotropic constituents. *ASME Journal of Applied Mechanics, 38*, 1062–1065.

Belytschko, T., Liu, W. K., & Moran, B. (2000). *Nonlinear finite elements for continua and structures*. Chichester: Wiley.

Bendsoe, M. P., & Kikuchi, N. (1988). Generating optimal topologies in optimal design using a homogenization method. *Computer Methods in Applied Mechanics and Engineering, 71*, 197–224.

Bendsoe, M. P., & Sigmund, O. (2004). *Topology Optimization: Theory, Methods and Applications.* Springer-Verlag, Berlin.

Bensoussan, A., Lions, J. L., & Papanicolaou, G. (1978). *Asymptotic analysis for periodic structures*. Amsterdam: Nort Holland.

Benveniste, Y. (1985). The effective mechanical behaviour of composite materials with imperfect contact between the constituents. *Mechanics of Materials, 4*, 197–208.

Benveniste, Y. (1987a). A new approach to the application of Mori-Tanaka theory in composite materials. *Mechanics of Materials, 6*, 147–157.

Benveniste, Y. (1987b). A differential effective medium theory with a composite sphere embedding. *ASME Journal of Applied Mechanics, 54*, 466–468.

Benveniste, Y. (1992). The determination of the elastic and electric fields in a piezoelectric inhomogeneity. *Journal of Applied Physics, 72*, 1086–1095.

Benveniste, Y. (1993). Exact results in the micromechanics of fibrous piezoelectric composites exhibiting pyroelectricity. *Proceedings of the Royal Society London, A441*, 1–22.

Benveniste, Y. (1993a). Universal relations in piezoelectric composites with eigenstress and polarization fields. I. Binary media: Local fields and effective behavior. *ASME Journal of Applied Mechanics*, *60*, 265–269.

Benveniste, Y. (1993b). Universal relations in piezoelectric composites with eigenstress and polarization fields. II. Multiphase media.: Effective behavior. *ASME Journal of Applied Mechanics, 60*, 270–275.

Benveniste, Y. (1993c). Exact results in the micromechanics of fibrous piezoelectric composites exhibiting pyroelectricity. *Proceedings of the Royal Society London, A 441*, 59–81.

Benveniste, Y. (1995). Magnetoelectric effect in fibrous composites with piezoelectric and piezomagnetic phases. *Physics Review B., 51*, 16424–16427

Benveniste, Y. (1996). Thermal expansion of polycrystalline aggregates consisting of elongated crystals and containing cylindrical pores or inclusions. *Journal of the Mechanics and Physics of Solids, 44*, 137–153.

Benveniste, Y. (2006). A general interface model for a three-dimensional curved thin anisotropic interphase between two anisotropic media. *Journal of the Mechanics and Physics of Solids*, *54*, 708–734.

Benveniste, Y. (2008). Revisiting the generalized self-consistent scheme in composites: Clarification of some aspects and a new formulation. *Journal of the Mechanics and Physics of Solids, 56*, 2984–3002.

Benveniste, Y., & Berdichevsky, O. (2010). On two models of arbitrarily curved three-dimensional thin interphases in elasticity. *International Journal of Solids and Structures, 47*, 1899–1915.

Benveniste, Y., & Dvorak, G. J. (1989). On a correspondence between mechanical and thermal effects in two-phase composites. In *Micromechanics and inhomogeneity* (The Toshio Mura 65th anniversary volume, pp. 65–81). New York: Springer.

Benveniste, Y., & Dvorak, G. J. (1992a). Uniform fields and universal relations in piezoelectric composites. *Journal of the Mechanics and Physics of Solids, 40*, 1295–1312.

Benveniste, Y., & Dvorak, G. J. (1992b). Some remarks on a class of uniform fields in fibrous composites. *Journal of Applied Mechanics, 59*, 1030–1032.

Benveniste, Y., & Miloh, T. (2001). Imperfect soft and stiff interfaces in two-dimensional elasticity. *Mechanics of Materials, 33*, 309–323.

Benveniste, Y., & Milton, G. W. (2003). New exact results for the effective electric, elastic, piezoelectric and other properties of composite ellipsoid assemblages. *Journal of the Mechanics and Physics of Solids, 51*, 1773–1813.

Benveniste, Y., Dvorak, G. J., & Chen, T. (1989). Stress fields in composites with coated inclusions. *Mechanics of Materials, 7*, 305–317.

Benveniste, Y., Chen, T., & Dvorak, G. J. (1990). The effective thermal conductivity of composites reinforced by coated cylindrically orthotropic fibers. *Journal of Applied Physics, 67*, 2878–2884.

Benveniste, Y., Dvorak, G. J., & Chen, T. (1991a). On the effective properties of composites with coated cylindrically orthotropic fibers. *Mechanics of Materials, 12*, 289–297.

Benveniste, Y., Dvorak, G. J., & Chen, T. (1991b). On diagonal and elastic symmetry of the approximate effective stiffness tensor of heterogeneous media. *Journal of the Mechanics and Physics of Solids, 39*, 927–946.

Beran, M. J. (1968). *Statistical continuum theories*. New York: Interscience Publishers.

Berryman, J. G. (1980). Long wavelength propagation in composite elastic media II, Ellipsoidal inclusions. *Journal of the Acoustical Society of America, 68*, 1820–1831.

Berryman, J. G. (1987). Relationship between specific surface area and spatial correlation functions for anisotropic porous media. *Journal of Mathematics and Physics, 28*, 244–245.

Betti, E. (1872). Teori della elasticita. *Il Nnuovo Cimento* (Series 2), pp. 7–10.

Biot, M. A. (1941). General theory of three-dimensional consolidation. *Journal of Applied Physics, 12*, 155–164.

Bishop, J. F. W., & Hill, R. (1951). A theory of the plastic distortion of a polycrystalline aggregate under combined stress. *Philosophical Magazine, 42*, 414–427.

Bo, Z., & Lagodas, D. C. (1999). Thermomechanical modeling of polycrystalline SMAs under cyclic loading, Part I: Theoretical derivations. *International Journal of Engineering Science, 37*, 1089–1140.

Boley, B. A., & Wiener, J. H. (1960). *Theory of thermal stresses*. New York: Wiley.

Boucher, S. (1974). On the effective moduli of isotropic two-phase elastic composites. *Journal of Composite Materials, 8*, 82–89.

Boulanger, P., & Hayes, M. (1998). Poisson's ratio for orthotropic materials. *Journal of Elasticity, 50*, 87–89.

Brdička, M. (1959). *Mechanika kontinua* (in Czech), ČSAV, Czechoslovak Academy of Sciences, Prague.

Bridgman, P. W. (1952). *Studies in large plastic flow and fracture*. New York: McGraw-Hill.

Brinson, H. F., & Brinson, L. C. (2008). *Polymer Engineering Science and Viscoelasticity: An Introduction.* Springer Science, New York.

Brockenbrough, J. R., Suresh, S., & Wienecke, H. A. (1991). Deformation of fiber-reinforced metal-matrix composites: Geometrical effects of fiber shape and distribution. *Acta Metallurgica et Materialia, 39*, 735–752.

Bruggeman, D. A. G. (1935). Berechnung verschiedener physikalisher Konstanten von heterogenen Substanzen I. *Annalen der Physik, 24*, 636–663.

Budiansky, B. (1965). On the elastic moduli of some heterogeneous materials. *Journal of the Mechanics and Physics of Solids, 13*, 223–227.

Budiansky, B., & Fleck, N. A. (1993). Compressive failure of fiber composites. *Journal of the Mechanics and Physics of Solids, 41*, 183–211.

Budiansky, B., & Fleck, N. A. (1994). Compressive kinking of fiber composites: A topic review. *Applied Mechanics Reviews, Part 2, 47*(6): 246–270.

Budiansky, B., & Kimmel, E. (1987). Elastic moduli of lungs. *ASME Journal of Applied Mechanics, 54*, 351–358.

Budiansky, B., & O'Connell, R. J. (1976). Elastic moduli of a cracked solid. *International Journal of Solids and Structures, 12*, 81–97.

Budiansky, B., & Wu, T. T. (1962). Theoretical prediction of plastic strains of polycrystals. In *Proceedings of the Fourth U. S. National Congress of Applied Mechanics* (pp. 1175–1185). New York: ASME.

Bufon, G. (1777). Essai d'arithmétique morale. *Supplément à l'Historie Naturelle.*

Buryachenko, V. (2007). *Micromechanics of heterogeneous materials*. New York: Springer Science.

Callegari, A. J., Norris, A. N., & Sheng, P. (1985). A generalized differential effective medium theory. *Journal of the Mechanics and Physics of Solids, 33*, 525–543.

Cammarata, R. C., Trimble, T. M., & Srolovitz, D. J. (2000a). Surface stress model for intrinsic stresses in thin films. *Journal of Materials Research*, *15*, 2468–2474.

Chaboche, J.-L. (1989). Constitutive equations for cyclic plasticity and visco-plasticity. *International Journal of Plasticity, 5*, 274–302.

Chaboche, J. L., Kruch, S., & Pottier, T. (1998). Micromechanics versus macromechanics: A combined approach for the metal matrix composites constitutive modelling. *European Journal of Mechanics – A/Solids, 17*, 885–908.

Chaboche, J. L., Kruch, S., Maire, J. F., & Pottier, T. (2001). Towards a micromechanics based inelastic and damage modeling of composites. *International Journal of Plasticity, 17*, 411–439.

Chaboche, J. L., Kanoute, P., & Roos, A. (2005). On the capabilities of mean-field approaches for the description of plasticity in metal matrix composites. *International Journal of Plasticity, 21*, 1409–1434.

Chadwick, P., Vianello, M., & Cowin, S. C. (2001). A new proof that the number of linear elastic symmetries is eight. *Journal of the Mechanics and Physics of Solids, 49*, 2471–2492.

Chan, K. S., Lindholm, U. S., & Bodner, S. R. (1988). *Constitutive modeling for isotropic materials* (NASA CR 182132).

Chen, T. (1993a). Green's functions and the non-uniform transformation problem in a piezoelectric medium. *Mechanics Research Communications, 20*, 271–278.

Chen, T. (1993b). The rotation of a rigid ellipsoidal inclusion embedded in an anisotropic piezoelectric medium. *International Journal of Solids and Structures, 30*, 1983–1995.
Chen, T. (1993c). Interfacial discontinuities in thermal conductions. *International Journal of Engineering Science, 31*, 425–434.
Chen, T. (1993d). An invariant treatment of interfacial discontinuities in piezoelectric media. *International Journal of Engineering Science, 31*, 1061–1072.
Chen, T. (1994). Some exact relations of inclusions in piezoelectric media. *International Journal of Engineering Science, 32*, 533–556.
Chen, T., & Dvorak, G. J. (2006). Fibrous nanocomposites with interface stress: Hill's and Levin's connections for effective moduli. *Applied Physics Letters*, *88*(211912), 1–3.
Chen, T., & Lin, F. Z. (1993). Numerical evaluation of derivatives of the anisotropic piezoelectric Green's functions. *Mechanics Research Communications, 20*, 501–506.
Chen, T., & Zheng, Q. S. (2000). Universal connections of elastic fibrous composites: Some new results. *International Journal of Solids and Structures, 37*, 2591–2602.
Chen, T., Chiu, M. S., & Weng, C. N. (2006). Derivation of the generalized Young-Laplace equation of curved interfaces in nano-scaled solids. *Journal of Applied Physics, 100*, 1–5.
Chen, T., Dvorak, G. J., & Benveniste, Y. (1990). Stress fields in composites reinforced by coated cylindrically orthotropic fibers. *Mechanics of Materials, 9*, 17–32.
Chen, T., Dvorak, G. J., & Benveniste, Y. (1992). Mori-Tanaka estimates of the overall elastic moduli of certain composite materials. *ASME Journal of Applied Mechanics, 59*, 539–546.
Chen, T., Dvorak, G. J., & Yu, C. C. (2007a). Solids containing spherical nano-inclusions with interface stresses: Effective properties and thermal-mechanical connections. *International Journal of Solids and Structures, 44*, 941–955.
Chen, T., Dvorak, G. J., & Yu, C. C. (2007b). Size-dependent elastic properties of unidirectional nano-composites with interface stresses. *Acta Mechanica, 188*, 39–54.
Chen, W., & Ravichandran, G. (1996). Static and dynamic compressive behavior of aluminum nitride under moderate confinement. *Journal of the American Ceramic Society, 79*, 579–584.
Chen, W., & Ravichandran, G. (1997). Dynamic compressive behavior of a glass ceramic under lateral confinement. *Journal of the Mechanics and Physics of Solids, 45*, 1303–1328.
Chen, W., & Ravichandran, G. (2000). Failure mode transition in ceramics under dynamic multiaxial compression. *International Journal of Fracture*, *101*(1–2), 141–159.
Chen, W. F. (2000). Plasticity, limit analysis and structural design. *International Journal of Solids and Structures, 37*, 81–92.
Chen, W. W., Rajendran, A. M., Bo Song, & Xu Nie. (2007). Dynamic fracture of ceramics in armor applications. *Journal of the American Ceramic Society, 90*, 1005–1018.
Christensen, R. M. (1969). Viscoelastic properties of heterogeneous media. *Journal of the Mechanics and Physics of Solids, 17*, 23.
Christensen, R. M. (1979, 2005). *Mechanics of composite materials*. New York: Wiley; Mineola: Dover.
Christensen, R. M. (1982, 2003). *Theory of viscoelasticity* (2nd ed.). New York: Academic; New York: Dover.
Christensen, R. M. (1987). Sufficient symmetry conditions for isotropy of the elastic moduli tensor. *Journal of Applied Mechanics, 54*, 772–777.
Christensen, R. M. (1990). A critical evaluation for a class of micromechanics models. *Journal of the Mechanics and Physics of Solids, 38*, 379–404.
Christensen, R. M. (1995). The hierarchy of microstructures for low density materials. *Zeitschrift für Angewandte Mathematik und Physik, 46*(Special Issue), S506–S521.
Christensen, R. M. (1998). Two theoretical elasticity micromechanics models. *Journal of Elasticity, 50*, 15–25.
Christensen, R. M. (2003). Mechanics of cellular and other low density materials. *International Journal of Solids and Structures, 37*, 93–104.
Christensen, R. M., & DeTeresa, S. J. (1992). Elimination/minimization of edge-induced stress singularities in fiber composite laminates. *International Journal of Solids and Structures, 29*, 1221–1231.

Christensen, R. M., & DeTeresa, S. J. (1997). The kink band mechanism for the compressive failure of fiber composite materials. *ASME Journal of Applied Mechanics, 64*, 1–6.

Christensen, R. M., & Lo, K. H. (1979). Solutions for effective shear properties in three phase sphere and cylinder models. *Journal of the Mechanics and Physics of Solids, 27*, 315–330. Erratum *ibid. 34*, 639 (1986).

Christensen, R. M., & Waals, F. M. (1972). Effective stiffness of randomly oriented fiber composites. *Journal of Composite Materials, 6*, 518–532.

Christensen, R. M., & Zywicz, E. (1990). A three-dimensional constitutive theory for fiber composite laminated media. *ASME Journal of Applied Mechanics, 57*, 948–955.

Christensen, R. M., Schantz, H., & Schapiro, J. (1992). On the range of validity of the Mori-Tanaka method. *Journal of the Mechanics and Physics of Solids, 40*, 69–73.

Clark, A. L. (1933). Buffon's needle problem. *Canadian Journal of Research 9*, 402, and *11*, 438.

Cleary, M. P., Chen, I. W., & Lee, S. M. (1980). Self-consistent techniques for heterogeneous solids. *ASCE Journal of Engineering Mechanics, 106*, 861–867.

Clyne, T. W., & Withers, P. J. (1993). *An introduction to metal matrix composites*. Cambridge: Cambridge University Press.

Cowin, S., & Doty, S. (2007). *Tissue mechanics*. New York: Springer.

Cowin, S. C., & Mehrabadi, M. M. (1987). On the identification of material symmetry for anisotropic materials. *Quarterly Journal of Mechanics and Applied Mathematics, 40*, 451–476.

Cowin, S. C., & Mehrabadi, M. M. (1989). Identification of the elastic symmetry of bone and other materials. *Journal of Biomechanics, 22*, 503–515.

Cowin, S. C., & Mehrabadi, M. M. (1995). Anisotropic symmetries of linear elasticity. *Applied Mechanics Reviews, 48*, 247–285.

Craft, W. J., & Christensen, R. M. (1981). Coefficient of thermal expansion for composites with randomly oriented fibers. *Journal of Composite Materials, 15*, 2–20.

Cribb, J. L. (1968). Shrinkage and thermal expansion of a two-phase material. *Nature, 220*, 576–577.

Crossman, F. W., & Wang, A. S. D. (1982). The dependence of transverse cracking and delamination on ply thickness in graphite/epoxy laminates. *American Society for Testing and Materials – Special Technical Publication, 775*, 118.

Dafalias, Y. F., & Popov, E. P. (1976). Plastic internal variables formalism of cyclic plasticity. *Journal of Applied Mechanics, 98*, 645–651.

Daniel, I. M., & Ishai, O. (2006). *Engineering mechanics of composite materials* (2nd ed.). New York: Oxford University Press.

Dawson, P. R. (2000). Computational crystal plasticity. *International Journal of Solids and Structures, 37*, 115–130.

deBotton, G., & Ponte Castañeda, P. (1993). Elastoplastic constitutive relations for fiber-reinforced solids. *International Journal of Solids and Structures, 30*, 1865–1890.

Debye, P., Anderson, H. R., & Brumberger, H. (1957). Scattering by an inhomogeneous solid. II. The correlation function and its applications. *Journal of Applied Physics, 28*, 679–683.

Deeg, W. F. (1980). *The analysis of dislocation, crack, and inclusion problems in piezoelectric solids*. Ph.D. dissertation. Stanford University.

Delale, F., & Erdogan, F. (1979). Bonded orthotropic strips with cracks. *International Journal of Fracture, 15*, 343–364.

Dionne, P. J., Ozisik, R., & Picu, R. C. (2005). Structure and dynamics of polyethylene nanocomposites. *Macromolecules, 38*, 9351–9358.

Dionne, P. J., Picu, R. C., & Ozisik, R. (2006). Adsorption and desorption dynamics of linear polymer chains to spherical nanoparticles: A Monte Carlo investigation. *Macromolecules, 39*, 3098–3092.

Drucker, D. C. (1950). Some implications of work hardening and ideal plasticity. *Quarterly of Applied Mathematics, 7*, 411–418.

Drucker, D. C. (1951). A more fundamental approach to plastic stress-strain relations. *Proceedings of the 1st U. S. National Congress of Applied Mechanics.* New York: ASME, pp. 487–491.

Drucker, D. C. (1967). *Introduction to mechanics of deformable solids*. New York: McGraw-Hill Book Co.

Drugan, W. J. (2000). Micromechanics-based variational estimates for a higher-order nonlocal constitutive equation and optimal choice of effective moduli of elastic composites. *Journal of the Mechanics and Physics of Solids, 48*, 1359–1387.

Drugan, W. J., & Willis, J. R. (1996). A micromechanics-based nonlocal constituive equation and estimates of representative volume element size for elastic composites. *Journal of the Mechanics and Physics of Solids, 44*, 497–524.

Duan, H. L., Wang, J., Huang, Z. P., & Karihaloo, B. L. (2005a). Size-dependent effective elastic constants of solids containing nano-inhomogeneities with interface stress. *Journal of the Mechanics and Physics of Solids*, *53*, 1574–1596.

Duan, H. L., Wang, J., Huang, Z. P., & Karihaloo, B. L. (2005b). Eshelby formalism for nano-inhomogeneities. *Proceedings of the Royal Society London, A 461*, 3335–3353.

Dunn, M. L. (1994). Electroelastic Green's functions for transversely isotropic piezo-electric media and their applications to the solutions of inclusion and inhomogeneity problems. *International Journal of Engineering Science, 32*, 119–131.

Dunn, M., & Ledbetter, H. (2000). Micromechanically based acoustic characterization of the fiber orientation distribution of morphologically textured short fiber composites: Prediction of thermomechanical and physical properties. *Materials Science and Engineering A, 285*, 56–61.

Dunn, M. L., & Taya, M. (1993). Analysis of piezoelectric composite materials containing ellipsoidal inhomogeneities. *Proceedings of the Royal Society London A, 443*, 265–287.

Dvorak, G. J. (1983). Metal matrix composites: Plasticity and fatigue. In Z. Hashin & C. T. Herakovich (Eds.), *Mechanics of composite materials: Recent advances* (pp. 73–91). New York: Pergamon Press.

Dvorak, G. J. (1986). Thermal expansion of elastic-plastic composite materials. *ASME Journal of Applied Mechanics, 53*, 737–743.

Dvorak, G. J. (1990). On uniform fields in heterogeneous media. *Proceedings of the Royal Society London A, 431*, 89–110.

Dvorak, G. J. (1992). Transformation field analysis of inelastic composite materials. *Proceedings of the Royal Society London, A, 437*, 311–327.

Dvorak, G. J. (1993). Micromechanics of inelastic composite materials: Theory and experiment. *ASME Journal of Engineering Materials and Technology, 115*, 327–338.

Dvorak, G. J. (1997). Thermomechanics of heterogeneous media. *Journal of Thermal Stresses, 20*, 799–817.

Dvorak, G. J. (Ed.) (1999). *Research trends in solid mechanics, a Report from the U.S. National Committee on Theoretical and Applied Mechanics.* Oxford: Elsevier Science Ltd. Also in *International Journal of Solids and Structures 37*(1&2) (2000).

Dvorak, G J (2001). Damage evolution and prevention in composite materials. In H. Aref & J. W. Phillips (Eds), *Mechanics for the New Millenium Proceedings of ICTAM 2000, the 20th International Congress of Theoretical and Applied Mechanics* (pp. 197–210). Kluver Academic Publishers.

Dvorak, G, J., & Bahei-El-Din, Y. A. (1979). Elastic-plastic behavior of fibrous composites, *Journal of the Mechanics and Physics of Solids, 27*, 5l–72.

Dvorak, G. J., & Bahei-El-Din, Y. A. (1980). Plastic deformation of a laminated plate with a hole. *ASME Journal of Applied Mechanics, 47*, 827–835.

Dvorak, G, J., & Bahei-El-Din, Y. A. (1982). Plasticity analysis of fibrous composites. *ASME Journal of Applied Mechanics, 49*, 327–335.

Dvorak, G. J., & Bahei-El-Din, Y. A. (1987). A bimodal plasticity of theory of fibrous composite materials. *Acta Mechanica, 69*, 219–241.

Dvorak, G. J., & Bahei-El-Din (2000). Micromechanics of inelastic composite materials. In A. Kelly & C. Zweben (Eds), *Comprehensive Composite Materials*, Vol. I: *Fiber Reinforcement and General Theory of Composites* (pp. 403 – 430). Elsevier Science.

Dvorak, G. J., & Benveniste, Y. (1992). On transformation strains and uniform fields in heterogeneous media. *Proceedings of the Royal Society London A, 437*, 291–310.

Dvorak, G. J., & Benveniste, Y. (1997). On micromechanics of inelastic and piezoelectric composites. In T. Tatsumi, E. Watanabe, & T. Kambe (Eds), *Theoretical and Applied Mechanics* 1996 (pp. 217–237). Elsevier Science B.V.

Dvorak, G. J., & Chen, T. (1989). Thermal expansion of three-phase composite materials. *ASME Journal of Applied Mechanics, 56*, 418–422.

Dvorak, G. J., & Johnson, W. S. (1980). Fatigue of metal matrix composites. *International Journal of Fracture, 16*, 585–607.

Dvorak, G. J., & Laws, N. (1987). Analysis of progressive matrix cracking in composite laminates. II. First ply failure. *Journal of Composite Materials, 21*, 309–329.

Dvorak, G. J., & Prochazka, P. (1996). Thick-walled composite cylinders with optimal fiber prestress, *Composites*, *27B*, 643–649.

Dvorak, G, J., & Rao, M.S.M. (1976a). Axisymmetric plasticity theory of fibrous composites. *International Journal of Engineering Science, 14*, 36l–373.

Dvorak, G, J., & Rao, M.S.M. (1976b). Thermal stresses in heat-treated fibrous composites. *ASME Journal of Applied Mechanics. 43*, 6l9–624.

Dvorak, G. J., & Sejnoha, M. (1995). Initial failure maps for fibrous CMC laminates. *Journal of the American Ceramic Society. 78*, 205–210.

Dvorak, G. J., & Sejnoha, M. (1996). Initial failure maps for ceramic and metal matrix composite laminates. *Modeling and Simulation in Materials Science and Engineering, 4*, 553–580.

Dvorak, G. J., & Suvorov, A. P. (2000). Effect of fiber prestress on residual stresses and onset of damage in symmetric laminates. *Composites Science and Technology, 60*, 1929–1939.

Dvorak, G. J., & Suvorov, A. P. (2006). Anti-plane shear cracks approaching a bi-material interface. *International Journal of Fracture, 137*, 275–294.

Dvorak, G. J., & Teply, J. (1985). Periodic hexagonal array models for plasticity analysis of composite materials. In A. Sawczuk & V. Bianchi (Eds.), *Plasticity today: Modeling, methods and applications* (W. Olszak memorial volume, pp. 623–642). Amsterdam: Elsevier Scientific Publishing Company.

Dvorak, G. J., & Zhang, J. (2001). Transformation field analysis of damage evolution in composite materials. *Journal of the Mechanics and Physics Solids, 49*, 2517–2541.

Dvorak, G. J., Bahei-El-Din, Y. A., Macheret, Y., & Liu, C. H. (1988). An experimental study of elastic-plastic behavior of fibrous boron-aluminum composites. *Journal of the Mechanics and Physics of Solids, 36*, 665–687.

Dvorak, G. J., Bahei-El-Din, Y. A., & Bank, L. C. (1989). Fracture of fibrous metal matrix composites – I. Experimental results. *Engineering Fracture Mechanics, 34*, 87–104.

Dvorak, G. J., Bahei-El-Din, Y. A., Shah, R., & Nigam, H. (1991). Experiments and modeling in plasticity of fibrous composites. In G. J. Dvorak (Ed.), *Inelastic deformation of composite materials* (pp. 270–293). New York: Springer.

Dvorak, G. J., Bahei-El-Din, Y. A., & Wafa, A. M. (1994). Implementation of the transformation field analysis for inelastic composite materials. *Computational Mechanics, 14*, 201–228.

Dvorak, G. J., Lagoudas, D. C., & Huang, C.-M. (1994). Fatigue damage and shakedown in metal matrix composite laminates. *Mechanics of Composite Materials and Structures, 1*, 171–202.

Dvorak, G. J., Lagoudas. D. C., & Huang, C-M. (2000). Shakedown and fatigue damage in metal matrix composites. In D. Weichert & G. Maier (Eds), *Inelastic Analysis of Structures under Variable Repeated Loads* (pp. 183 – 196). Kluver Academic Publishers.

Dvorak, G. J., Laws, N., & Hejazi, M. (1985). Analysis of progressive matrix cracking in composite laminates I. Thermoelastic properties of a ply with cracks. *Journal of Composite Materials, 19*, 216–234.

Dvorak, G. J., Prochazka, P., & Srinivas, M. V. (1999). Design and fabrication of submerged cylindrical laminates I. *International Journal of Solids and Structures, 36*, 3917–3943.

Dvorak, G. J., Rao, M.S.M., & Tarn, J. Q. (1973). Yielding in unidirectional composites under external loads and temperature changes. *Journal of Composite Materials, 7*, l94–216.

Dvorak, G. J., Rao, M. S. M., & Tarn, J. Q. (1974). Generalized yield surfaces for unidirectional composites. *Journal of Applied Mechanics, 41*, 249–253.

Einstein, A. (1905). Eine neue Berechnung der Moleküldimensionen. *Annales de Physique, 19*, 289–306.

Ellyin, F. (1989). An anisotropic hardening rule for elastoplastic solids based on experimental observations. *ASME Journal of Applied Mechanics, 56*, 489–507.

Elvin, A. A. (1996). Number of grains required to homogenize elastic properties of polycrystalline ice. *Mechanics of Materials, 22*, 51–64.

Entchev, P. B., & Lagudas, D. C. (2002). Modeling porous shape memory alloys using micromechanical averaging techniques. *Mechanics of Materials, 34*, 1–24.

Eshelby, J. D. (1956). The continuum theory of lattice defects. In F. Seitz & D. Turnbull (Eds.), *Progress in solid state physics* (Vol. 3, pp. 79–144). New York: Academic.

Eshelby, J. D. (1957). The determination of the elastic field of an ellipsoidal inclusion, and related problems. *Proceedings of the Royal Society London A, 241*, 376–396.

Eshelby, J. D. (1961). Elastic inclusions and inhomogeneities. In I. N. Sneddon, & R. Hill (Eds.), *Progress in solid mechanics* (Vol. 2, Ch. III). Amsterdam: North-Holland, pp. 89–140.

Eshelby, J. D., Read, W. T., & Shockley, W. (1953). Anisotropic elasticity with applications to dislocation theory. *Acta Metallurgica, 1*, 251–259.

Evans, K. E. (1991). Auxetic polymers: A new range of materials. *Endeavour, New Series, 15*, 170–174.

Evans, K. E., Nkansah, M. A., Hutchinson, I. J., & Rogers, S. C. (1991). Molecular network design. *Nature, 353*, 124.

Farez, N., & Dvorak, G. J. (1989). Large elastic-plastic deformations of fibrous metal matrix composites. *Journal of the Mechanics and Physics of Solids, 39*, 725–744.

Farez, N., & Dvorak, G. J. (1993). Finite deformation constitutive relations for elastic-plastic fibrous metal matrix composites. *Journal of Applied Mechanics, 60*, 619–625.

Feibig, M. (2005). Revival of the magnetoelectric effect (Topical review). *Journal of Physics D-Applied Physics, 38*, R123–152.

Ferrante, J., Smith, J. R., & Rose, J. H. (1982). Universal binding energy relations in metallic adhesion. In J. M. Georges (Ed.), *Microscopic aspects of adhesion and lubrication* (pp. 19–30). Amsterdam: Elsevier.

Ferrari, M., & Johnson, G. C. (1989). Effective elasticities of short-fiber composites with arbitrary orientation distribution. *Mechanics of Materials, 8*, 67–73.

Findley, W. N., Lai, J. S., & Onaran, K. (1976). *Creep and relaxation of nonlinear viscoelastic materials*. Amsterdam: North Holland Publishing Co.

Finot, M., & Suresh, S. (1996). Small and large deformation of thick and thin-film multi-layers: Effects of layer geometry, plasticity and compositional gradients. *Journal of the Mechanics and Physics of Solids, 44*, 683–722.

Fish, J., & Shek, K. L. (1999). Finite deformation plasticity of composite structures: Computational models and adaptive strategies. *Computer Methods in Applied Mechanics and Engineering, 172*, 145–174.

Fish, J., Shek, K. L., Shephard, M. S., & Pandheeradi, M. (1997). Computational plasticity for composite structures based on mathematical homogenization: Theory and practice. *Computer Methods in Applied Mechanics and Engineering, 157*, 69–94.

Fish, J., Yu, Q., & Shek, K. L. (1999). Computational damage mechanics for composite materials based on mathematical homogenization. *International Journal for Numerical Methods in Engineering, 45*, 1657–1679.

Flanagan, G. (1994). An efficient stress function approximation for the free-edge stresses in laminates. *International Journal of Solids and Structures, 31*, 941–952.

Fleck, N. A. (1997). Compressive failure of fiber composites. In J. W. Hutchinson, & T. Y. Wu (Eds.), *Advances in applied mechanics* (Vol. 33). New York: Academic Press.

Franciosi, P., & Berberinni, S. (2007). Heterogeneous crystal and poly-crystal plasticity modeling from a transformation field analysis with a regularized Schmid law. *Journal of the Mechanics and Physics of Solids, 55*, 2265–2299.

Fredholm, I. (1900). Sur les equations de l'equilibre d'un corps solidi elastique. *Acta Mathematica, 23*, 1–42.

Freed, A. D., & Walker, K. P. (1993). Viscoplasticity with creep and plasticity bounds. *International Journal of Plasticity, 9*, 213–242.

Freed, A. D., Chaboche, J.-L., & Walker, K. P. (1991). A viscoplastic theory with thermodynamic considerations. *Acta Mechanica, 90*, 155–174.

Fukui, Y., Takashima, K., & Ponton, C. B. (1994). Measurement of Young's modulus and internal friction of an *in situ* Al-Al/Ni functionally gradient material. *Journal of Materials Science, 29*, 2281–2288.

Fung, Y. C. (1965). *Foundations of solid mechanics*. Englewood Cliffs: Prentice Hall, Inc.

Garrett, K. W., & Bailey, J. E. (1977). Multiple transverse fracture in cross-ply laminates of glass fibre-reinforced polyester. *Journal of Materials Science, 12*, 157–168.

Gavazzi, A. C., & Lagoudas, D. C. (1990). On the numerical evaluation of Eshelby's tensor and its application to elastoplastic fibrous composites. *Computational Mechanics, 7*, 13–19.

Ghahremani, F. (1977). Numerical evaluation of the stresses and strains in ellipsoidalinclusions in an anisotropic elastic material. *Mechanics Research Communications, 4*, 89–91.

Ghosh, S., Lee, K., Raghavan, P. (2001). A multi-level computational model for multi-scale damage analysis in composite and porous materials. *International Journal of Solids and Structures*, *38*, 2335–2385.

Giannakopoulos, A. E., Suresh, S., Finot, M., & Olsson, M. (1995). Elastoplastic analysis of thermal cycling: Layered materials with compositional gradients. *Acta Metallurgica et Materialia, 43*, 1335–1354.

Gibbs, J. W. (1928). *The collected works of J.W. Gibbs* (Vol. 1, p. 315). New York: Londmans.

Gibson, L. J., & Ashby, M. F. (1997). *Cellular solids, structure and properties* (2nd ed.). Cambridge: Cambridge University Press.

Gooch, W. (2010). 2011 overview of the development of ceramic armor technology: Past, present and future. *35th International Conference on Advanced Ceramics & Composites.* American Ceramic Society.

Green, A. E., & Atkins, J. E. (1960). *Large elastic deformations and non-linear continuum mechanics.* Oxford: Clarendon Press.

Gudmundson, P., & Zhang, W. (1993). An analytical model for thermoelastic properties of composite laminates containing transverse cracks. *International Journal of Solids and Structures, 30*, 3211–3231.

Guo, C. Y., & Wheeler, L. (2006). Extreme Poisson's ratios and related elastic crystal properties. *Journal of the Mechanics and Physics of Solids, 54*, 690–707.

Gupta, V., Argon, A. S., & Suo, Z. (1992). Crack deflection at an interface between two orthotropic media. *ASME Journal of Applied Mechanics, 59*, S79–S87.

Gurtin, M. E., & Murdoch, A. I. (1975). A continuum theory of elastic material surfaces. *Archive of Rational Mechanics and Analysis*, *57*, 291–323, and *59*, 389–390.

Gurtin, M. E., Weissmuller, J., & Larche, F. (1998). A general theory of curved deformable interfaces in solids at equilibrium. *Philosophical Magazine, A 78*, 1093–1109.

Gusev, A. A. (1997). Representative volume element size for elastic composites: A numerical study. *Journal of the Mechanics and Physics of Solids, 45*, 1449–1459.

Ha, K., & Schapery, R. A. (1998). A three-dimensional viscoelastic constitutive model for particulate composites with growing damage and its experimental validation. *International Journal of Solids and Structures, 35*, 3497–3517.

Hadamard, J. (1903). *Leçons sur la propagation des ondes et les équations de l'hydro- dynamique*. Paris: Hermann Press.

Hashin, Z. (1962). The elastic moduli of heterogenous materials. *ASME Journal of Applied Mechanics, 29*, 143–150.

Hashin, Z. (1964). Theory of mechanical behavior of heterogeneous media. *Applied Mechanics Reviews, 17*, 1–9.

Hashin, Z. (1965). On elastic behavior of fiber reinforced materials of arbitrary transverse phase geometry. *Journal of the Mechanics and Physics of Solids, 13*, 119–134.

Hashin, Z. (1967). Variational principles in elasticity in terms of the elastic polarization tensor. *International Journal of Engineering Science, 5*, 213–223.

Hashin, Z. (1970). Complex moduli of viscoelastic composites I. General theory and applications to particulate composites. *International Journal of Solids and Structures, 6*, 539–552.
Hashin, Z. (1972). *Theory of fiber reinforced materials* (NASA CR-1974). Washington, DC: National Aeronautics and Space Administration, p. 690.
Hashin, Z. (1979). Analysis of properties of fiber composites with anisotropic constituents. *Journal of Applied Mechanics, 46*, 543–550.
Hashin, Z. (1984). Thermal expansion of polycrystalline aggregates: I. Exact analysis. *Journal of the Mechanics and Physics of Solids, 32*, 149–157.
Hashin, Z. (1985). Analysis of cracked laminates: A variational approach. *Mechanics of Materials, 4*, 121–136.
Hashin, Z. (1988). The differential scheme and its application to cracked materials. *Journal of the Mechanics and Physics of Solids, 36*, 719–734.
Hashin, Z. (1990). Thermoelastic properties of fiber composites with imperfect interface. *Mechanics of Materials, 8*, 333–348.
Hashin, Z. (1991). The spherical inclusion with imperfect interface. *Journal of Applied Mechanics, 58*, 444–449.
Hashin, Z. (2002). Thin interphase/imperfect interface in elasticity with application to coated fiber composites. *Journal of the Mechanics and Physics of Solids, 50*, 2509–2537.
Hashin, Z., & Rosen, B. W. (1964). The elastic moduli of fiber reinforced materials. *ASME Journal of Applied Mechanics 31E*, 223–232. Errata, 1965, *ibid., 32E*, 219.
Hashin, Z., & Shtrikman, S. (1962a). On some variational principles in anisotropic and nonhomogeneous elasticity. *Journal of the Mechanics and Physics of Solids, 10*, 335–342.
Hashin, Z., & Shtrikman, S. (1962b). A variational approach to the theory of the elastic behaviour of polycrystals. *Journal of the Mechanics and Physics of Solids, 10*, 343–352.
Hashin, Z., & Shtrikman, S. (1963). A variational approach to the theory of the elastic behaviour of multiphase materials. *Journal of the Mechanics and Physics of Solids, 11*, 127–140.
Hatami-Marbini, H., & Picu, R. C. (2009). Heterogeneous long-range correlated deformation of semiflexible random fiber networks. *Physics Reviews E, 80*(046703), 1–11.
Hatta, H., & Taya, M. (1986). Equivalent inclusion method for steady state heat conduction in composites. *International Journal of Engineering Science, 24*, 1159–1172.
Hauver, G. E., Rapacki, E. J., Netherwood, P. H., & Benck, R. F. (2005). *Interface defeat of long-rod projectiles by ceramic armor* (Report ARL-TR-3950), U.S. Army Research Laboratory.
Hayashi, T. (1967). Analytical study of interlaminar shear stresses in a laminate composite plate. Transactions. *Japan Society for Aeronautical and Space Sciences, 10*, 43–48.
Hayes, M., & Shuvalov, A. (1998). On the extreme values of Young's modulus, the shear modulus, and Poisson's ratio for cubic materials. *Journal of Applied Mechanics, 65*, 786–787.
Hazanov, S., & Huet, C. (1994). Order relationships for boundary condition effects in heterogeneous bodies smaller than representative volume. *Journal of the Mechanics and Physics of Solids, 42*, 1995–2011.
He, Q.-C. (1999). Uniform strain fields and microstructure-independent relations in nonlinear elastic fibrous composites. *Journal of the Mechanics and Physics of Solids, 47*, 1781–1793.
Hearmon, R. F. S. (1961). *Introduction to applied anisotropic elasticity*. Oxford: Clarendon Press.
Herakovich, C. T. (1998). *Mechanics of fibrous composites*. New York: Wiley.
Hershey, A. V. (1954). The elasticity of an isotropic aggregate of anisotropic cubic crystals. *ASME Journal of Applied Mechanics, 21*, 236–240.
Hervé, E., & Zaoui, A. (1995). Elastic behaviour of multiply coated fibre-reinforced composites. *International Journal of Engineering Science, 33*, 1419–1433.
Highsmith, A. L., & Reifsnider, K. L. (1982). Stiffness reduction mechanisms in composite laminates. *Damage in Composite Materials, American Society for Testing and Materials Special Technical Publication, 775*, 103–117.
Hill, R. (1948). A theory of the yielding and plastic flow of anisotropic metals. *Proceedings of the Royal Society London, A, 193*, 281–297.
Hill, R. (1950). *The mathematical theory of plasticity*. New York: Oxford University Press.

Hill, R. (1961). Discontinuity relations in mechanics of solids. In I. N. Sneddon & R. Hill (Eds.), *Progress in solid mechanics* (Vol. II, pp. 245–276). Amsterdam: North Holland Publications.

Hill, R. (1963a). Elastic properties of reinforced solids: Some theoretical principles. *Journal of the Mechanics and Physics of Solids, 11*, 357–372 [1].

Hill, R. (1963b). New derivations of some elastic extremum principles. In *Progress in applied mechanics. W. Prager 60th anniversary volume*. London: McMillan & Co., pp. 99–106.

Hill, R. (1964). Theory of mechanical properties of fibre-strengthened materials: I. Elastic behavior. *Journal of the Mechanics and Physics of Solids, 12*, 199–212.

Hill, R. (1965a). Continuum micromechanics of elastic-plastic polycrystals. *Journal of the Mechanics and Physics of Solids, 13*, 89–101.

Hill, R. (1965b). Theory of mechanical properties of fibre-strengthened materials – III. Self-consistent model. *Journal of the Mechanics and Physics of Solids, 13*, 189–198.

Hill, R. (1965c). A self-consistent mechanics of composite materials. *Journal of the Mechanics and Physics of Solids, 13*, 213–222.

Hill, R. (1967). The essential structure of constitutive laws for metal composites and polycrystals. *Journal of the Mechanics and Physics of Solids, 15*, 79–95.

Hill, R. (1971). On macroscopic measures of plastic work and deformation in micro-heterogeneous media. *Prikladnaya Matematika i Mekhanika, 35*, 31–39.

Hill, R. (1972). An invariant treatment of interfacial discontinuities in elastic composites. In L. I. Sedov (Ed.), *Continuum mechanics and related problems of analysis, N. I. Muskhelishvili 80th anniversary volume* (pp. 597–604). Moscow: Acad. Sciences.

Hill, R. (1983). Interfacial operators in the mechanics of composite media. *Journal of the Mechanics and Physics of Solids, 31*, 247–357.

Hirose, Y., Mura, T., & Shodja, H. M. (1996). Inclusion problems. *Applied Mechanics Reviews, 49*, S118–S127.

Ho, S., & Suo, Z. (1993). Tunneling cracks in constrained layers. *ASME Journal of Applied Mechanics, 69*, 890–894.

Hori, M., & Nemat-Nasser, S. (1993). Double-inclusion model and overall moduli of multi-phase composites. *Mechanics of Materials, 14*, 189–206.

Horii, H., & Nemat-Nasser, S. (1983). Overall moduli of solids with microcracks: Load-induced anisotropy. *Journal of the Mechanics and Physics of Solids, 31*, 155–171.

Hu, G. K., & Weng, G. J. (2000). The connections between the double inclusion model and the Ponte Castaneda-Willis, Mori Tanaka, and Kuster-Toksoz models. *Mechanics of Materials, 32*, 495–503.

Huang, J. H., & Yu, J. S. (1994). Electroelastic Eshelby tensors for an ellipsoidal piezoelectric inclusion. *Composites Engineering, 4*, 1169–1182.

Huet, C. (1990). Application of variational concepts to size effects in elastic hetero-geneous bodies. *Journal of the Mechanics and Physics of Solids, 38*, 813–841.

Hughes, T. J. R., & Pister, K. S. (1978). Consistent linearization in mechanics of solids and structures. *Computers and Structures, 9*, 391–397.

Hughes, T. J. R., & Taylor, R. L. (1978). Unconditionally stable algorithms for quasistatic elasto/viscoplastic finite element analysis. *Computers and Structures, 8*, 169–173.

Hutchinson, J. W. (1970). Elastic-plastic behaviour of polyrystalline metals and composites. *Proceedings of the Royal Society London, A, 319*, 247–272.

Hutchinson, J. W. (2000). Plasticity at the micron scale. *International Journal of Solids and Structures, 37*, 25–238.

Hutchinson, J. W., & Suo, Z. (1992). Mixed-mode cracking in layered materials. *Advances in Applied Mechanics, 29*, 63–191.

Indenbom, V. L., & Orlov, S. S. (1968). Construction of Green's function in terms of Green's function of lower dimension. *ASME Journal of Applied Mechanics, 32*, 414–420.

Jasiuk, I., Mura, T., & Tsuchida, E. (1988). Thermal stresses and thermal expansion coefficient of short fiber composites with sliding interfaces. *Journal of Engineering Materials and Technology, 110*, 96–110.

Jasiuk, I., & Kouider, M. W. (1993). The effect of an inhomogeneous interphase on elastic constants of transversely isotropic composites.

Jefferson, G., Haritos, G. K and McMeeking, R. M. (2002) The elastic response of a cohesive aggregate – a discrete element model with coupled particle interactions. *J. Mech. Phys. Solids, 50*, 2539–2575.

Jirasek, M., & Bazant, Z. P. (2002). *Inelastic analysis of structures*. Chichester: Wiley.

Ju, J. W., & Zhang, X. D. (1998). Micromechanics and effective transverse elastic moduli of composites with randomly located aligned circular fibers. *International Journal of Solids and Structures, 35*, 941–960.

Kachanov, M. (1992). Effective elastic properties of cracked solids. *Applied Mechanics Reviews, 45*, 305–336.

Kanoute, P., Boso, D. P., Chaboche, J. L., & Schrefler, B. A. (2009). Multiscale methods for composites: A review. *Archives of Computational Methods in Engineering, 16*, 31–75.

Kardomateas, G. A., & Philobox, M. S. (1995). Buckling of thick orthotropic cylindrical shells under combined external pressure and axial compression. *AIAA Journal, 33*, 1946–1953.

Kassapoglou, C., & Lagace, P. A. (1986). An efficient method for the calculation of interlaminar stresses in composite materials. *ASME Journal of Applied Mechanics, 53*, 744–750.

Kattan, P., & Voyiadjis, G. (1993). Overall damage and elastoplastic deformation in fibrous metal matrix composites. *International Journal of Plasticity, 9*, 931–949.

Kawashita, M., & Nozaki, H. (2001). Eshelby tensor of a polygonal inclusion and its special properties. *Journal of Elasticity, 64*, 71–84.

Kendal, M. G., & Moran, P. A. P. (1962). *Geometrical probability*. London: Charles Griffin & Co. Ltd.

Kerner, E. H. (1956). The elastic and thermo-elastic properties of composite media. *Proceedings of the Royal Society London, B, 69*, 808–813.

Kim, T., & Atluri, S. N. (1995a). Analysis of edge stresses in composite laminates under combined thermo-mechanical loading, using a complementary energy approach. *Computational Mechanics, 16*, 83–97.

Kim, T., & Atluri, S. N. (1995b). Optimal through-thickness temperature gradients for control of interlaminar stresses in composites. *AIAA Journal, 33*, 730–738.

Kinoshita, N., & Mura, T. (1971). Elastic fields of inclusions in anisotropic media. *Physica Status Solidi, 5*, 759–768.

Knauss, W. G., & Emri, I. J. (1981). Non-linear viscoelasticity based on free volume consideration. *Computers and Structures, 13*, 123–128.

Knauss, W. G., & Zhu, W. (2002a). Nonlinearly viscoelastic behavior of polycarbonate. Response under pure shear. *Mechanics of Time Dependent Materials, 6*, 231–269.

Knauss, W. G., & Zhu, W. (2002b). Nonlinearly viscoelastic behavior of polycarbonate. The role of volumetric strain. *Mechanics of Time Dependent Materials, 6*, 301–322.

Kouris, D. A., & Mura, T. (1989). The elastic field of a hemispherical inhomogeneity at the free surface of an elastic half space. *Journal of the Mechanics and Physics of Solids, 37*, 365–379.

Kovarik, V. (1989). *Stresses in layered shells of revolution*. Prague: Academia.

Krempl, E. (1985). Inelastic work and thermomechanical coupling in viscoplasticity. In A. Sawczuk and V. Bianchi (Eds), *Plasticity Today: Modeling Methods and Applications*. Elsevier Scientific Publishing Company, Amsterdam, The Netherlands.

Krempl, E. (2000). Visoplastic models for high temperature applications. *International Journal of Solids and Structures, 37*, 279–291.

Krempl, E., & Ruggles, M. B. (1990). The interaction of cyclic hardening and rachetting for AISI Type 304 stainless steel – II. Modeling with viscoplasticity theory based on overstress. *Journal of the Mechanics and Physics of Solids, 38*, 363–375.

Kröner, E. (1953). Das fundamental Integral der anisotropen elastischen Differential-gleichungen. *Zeitschrift für Physik, 136*, 402–410.

Kröner, E. (1958). Berechnung der elastischen Konstanten der Vielkristalls aus den Konstanten der Einkristalls. *Zeitschrift für Physik, 151*, 504–518.

Kroner, E. (1961). Zur plastischen Verformung des Vielkristalls. *Acta Metallurgica. 9*, 155–161.

Kröner, E., Datta, B. K., & Kessel, D. (1966). On the bounds of the shear modulus of macroscopically isotropic aggregates of cubic crystals. *Journal of the Mechanics and Physics of Solids, 14*, 21–24.

Kuhn, H. W., & Tucker, A. W. (1951). Nonlinear programming. In J. Neyman (Ed.), *Proceeidngs of the second Berkeley symposium on mathematical statistics and probability* (pp. 481–192). Berkeley: University of California Press.

Kuhn, R., Michelitsch, T., Levin, V. M., & Vakulennko, A. A. (2002). The analogue of the Eshelby tensor for a piezoelectric spheroidal inclusion in the hexagonal electroelastic medium. *Zeitschrift für Angewandte Mathematik und Physik, 53*, 584–602.

Kunin, I. A. (1982). *Elastic Media with Microstructure I. One-Dimensional Models*. Springer-Verlag. Berlin.

Kunin, I. A. (1983). *Elastic Media with Microstructure II. Three-Dimensional Models.* Springer-Verlag. Berlin.

Kunin, I. A., & Sosnina, E. G. (1973). Stress concentration on an ellipsoidal inhomogeneity in an anisotropic elastic medium. *Prikladnaya Matematika i Mekhanika, 37*, 306–315.

Kyriakides, S., Arseculeratne, R., Perry, E. J., & Liechti, K. M. (1995). On the compressive failure of fiber reinforced composites. *International Journal of Solids and Structures*, *32*, 689–738.

Lagoudas, D. C., Gavazzi, A. C., & Nigam, H. (1991). Elastoplastic behavior of metal matrix composites based on incremental plasticity and the Mori-Tanaka averaging scheme. *Computational Mechanics, 8*. 193–203.

Lagoudas, D.C., & Entchev, P., (2004). Modeling of transformation-induced plasticity and its effect on the behavior of porous shape memory alloys. Part I: Constitutive model for fully dense SMAs. *Mechanics of Materials, 36*, 865–892.

Lakes, R. (1987). Foam structures with a negative Poisson's ratio. *Science, 235*, 1038–1040.

Lakes, R. (1993). Advances in negative Poisson's ratio materials. *Advanced Materials, 5*, 293–296.

Lakes, R. (2000). Deformations in extreme matter. *Science, 288*, 1976–1977.

Landau, L. D., & Lifshitz, E. M. (1987). *Fluid mechanics* (2nd ed.). Oxford: Pergamon Press.

Laws, N. (1973). On thermostatics of composite materials. *Journal of the Mechanics and Physics of Solids, 21*, 9–17.

Laws, N. (1974). The overall thermoelastic moduli of transversely isotropic composites according to the self-consistent method. *International Journal of Engineering Science, 12*, 79–87.

Laws, N. (1975). On interfacial discontinuities in elastic composites. *Journal of Elasticity, 5*, 227–235.

Laws, N. (1977). The determination of stress and strain concentrations in an ellipsoidal inclusion in an anisotropic material. *Journal of Elasticity, 7*, 91–97.

Laws, N. (1980). The elastic response of composite materials. *Physics of Modern Materials, I.* International Atomic Energy Agency, Vienna, IAEA-SMR 46/107, pp. 465–520.

Laws, N. (1985). A note on penny-shaped cracks in transversely isotropic materials. *Mechanics of Materials, 4*, 209–212.

Laws, N., & Dvorak, G. J. (1987). The effect of fiber breaks and penny shaped cracks on the stiffness and energy release in unidirectional composites. *International Journal of Solids and Structures, 23*, 1269–1283.

Laws, N., & Dvorak, G. J. (1988). Progressive transverse cracking in composite laminates. *Journal of Composite Materials*. *22*, 900–916.

Laws, N., & McLaughlin, R. (1978). Self-consistent estimates for viscoelastic creep compliances of composite materials. *Proceedings of the Royal Society of London, A, 359*, 251–273.

Laws, N., & McLaughlin, R. (1979). The effect of fiber length on the overall moduli of composite materials. *Journal of the Mechanics and Physics of Solids, 27*, 1–13.

Laws, N., Dvorak, G. J., & Hejazi, M. (1983). Stiffness changes in composites caused by crack systems. *Mechanics of Materials, 2*, 123–137.

Lee, V. G. (2002). Evaluation of the three dimensional elastic Green's function in anisotropic cubic media. *International Journal of Engineering Science, 40*, 1349–1361.

Lee, Y.-D., & Erdogan, F. (1994/1995). Residual thermal stresses in FGM and laminated thermal barrier coatings. *International Journal of Fracture, 69*, 145–165.

Lekhnitskii, S. G. (1950). *Theory of elasticity of an anisotropic body*, Gostekhizdat Moscow (English translation published by Holden-Day, San Francisco, 1963).
Lekhnitskii, S. G. (1968). *Anisotropic plates* (Translated from 2nd Russian edition by S. W. Tsai, & T. Cheron, Gordon and Breach).
Lemaitre, J., & Chaboche, J.-L. (1995). *Mechanics of solid materials*. Cambridge: Cambridge University Press.
Levin, V. M. (1967). On the coefficients of thermal expansion of heterogeneous materials (in Russian). *Mekhanika Tverdogo Tela, 2*, 88–94.
Levitas, V. I., & Javanbakh, M. (2011). Phase-field approach to martensitic phase transformations: Effect of martensite-martensite interface energy. *International Journal of Materials Research* (formerly Z. Metallkd.) *102,* 652–665.
Levy, A. J. (2001). A finite strain analysis of cavity formation at a rigid inhomogeneity. *Journal of Elasticity, 64*, 131–156.
Levy, A. J. (2003). Bifurcation phenomena in the rigid inclusion power law matrix composite sphere. *International Journal of Solids and Structures, 40*, 2535–2561.
Li, Y. (1976). The anisotropic behavior of Poisson's ratio, Young's modulus, and shear modulus in hexagonal materials. *Physica Status Solidi, 38*, 171–175.
Liang, H. Y., Upmanyu, M., & Huang, H. (2005). Size dependent elasticity of nanowires: Non-linear effects. *Physical Review B 71*(241403R), 1–4.
Librescu, L. (1975). *Elastostatics and kinetics of anisotropic and heterogeneous shell-type structures*. Leyden: Noordhoff.
Lifshitz, I. M., & Rozenzweig, L. N. (1947). On the construction of the Green's tensor for the basic equation of the theory of elasticity of an anisotropic infinite medium. *Zhurnal Experimentalnoy i Teoreticheskoy Fiziki, 17*, 783–791.
Lindholm, U. S., Chan, K. S., Bodner, S. R., Walker, K. P., & Cassenti, B. N. (1984). *Constitutive modeling for isotropic materials.* NASA Lewis Research Center, NAS3-23925.
Lissenden, C. J. (2010). Experimental investigation of initial and subsequent yield surfaces for laminated metal matrix composites. *International Journal of Plasticity, 26*, 1606–1628.
Liu, C. H. (1988). *The elastic-plastic behavior of composite materials*. Ph.D. dissertation, Yale University.
Liu, L. P. (2009). Solutions to the Eshelby conjectures. *Proceedings of the Royal Society of London, A, 464*, 573–594.
Liu, L. P., James, R. D., & Leo, P. H. (2006). Magnetostrictive composites in the dilute limit. *Journal of the Mechanics and Physics of Solids, 54*, 951–974.
Losi, G. U., & Knauss, W. G. (1992a). Thermal stresses in nonlinearly viscoelastic solids. *Journal of Applied Mechanics, 59*, S43–S49.
Losi, G. U., & Knauss, W. G. (1992b). Free volume theory and nonlinea Thermoviscoelasticity. *Polymer Engineering and Science, 32*, 542–557.
Love, A. E. H. (1944). *A treatise on the mathematical theory of elasticity* (4th ed.). New York: Dover.
Lu, B., & Torquato, S. (1990). Local volume fraction fluctuations in heterogeneous media. *The Journal of Chemical Physics, 93*, 3452–3459.
Lu, M.-C., & Erdogan, F. (1983). Stress intensity factors in two bonded elastic layers containing cracks perpendicular to an interface, I. Analysis, II. Solution and results. *Engineering Fracture Mechanics, 18*, 491–528.
Lubarda, V. A., & Markenscoff, X. (1998). On the absence of Eshelby property for non-ellipsoidal inclusions. *International Journal of Solids and Structures, 35*, 3405–3411.
Lubliner, J. (1990). *Plasticity theory*. New York: Macmillan Publication & Co.
Luo, J., & Sun, C. T. (1991). Global-local methods for thermoelastic analysis of thick fiber-wound cylinders. *Journal of Composite Materials*, *25*, 453–468.
Maier, G. (1969). Shakedown theory in perfect elastoplasticity with associated and nonassociated flow laws: A finite element linear programing approach. *Meccanica. 4*, 250–260.

Maier, G. (1973). A shakedown matrix theory allowing for workhardening and second order geometric effects. In A. Sawczuck (Ed.), *Foundations of Plasticity* (Vol. 1, pp. 417–433). Noordoff: Leyden.

Malaise, F., Tranchet, J.-Y., & Collombet, F. (2000). Effects of dynamic confinement on the penetration resistance of ceramics against long rods. In M. D. Furnish, L. C., Chhabildas, & R. S. Hixson (Eds.), *Shock compression of condensed matter-1999* (pp. 1121–1140). New York: AP Press.

Malvern, L. E. (1969). *Introduction to the mechanics of a continuous medium*. Englewood Cliffs: Prentice Hall, Inc.

Markenscoff, X. (1998). Inclusions with constant eigenstress. *Journal of the Mechanics and Physics of Solids, 46*, 2297–2301.

Markworth, A. J., & Saunders, J. H. (1995). A model of structure optimization for a functionally graded material. *Materials Letters, 22*, 103–107.

Markworth, A. J., Parks, W. P., & Ramesh, K. S. (1995). Review: Modelling studies applied to functionally graded materials. *Journal of Materials Science, 30*, 2183–2193.

Masson, R. (2008). New explicit expressions of the Hill polarization tensor for general anisotropic elastic solids. *International Journal of Solids and Structures, 45*, 757–769.

McCartney, L. N., & Schoeppner, G. N. (2002) Predicting the effect of non-uniform ply cracking on the thermoelastic properties of cross-ply laminates. *Composites Science and Technology, 62*, 1841–1856.

McDowell, D. L. (2000). Modeling and experiments in plasticity. *International Journal of Solids and Structures, 37*, 293–309.

McLaughlin, R. (1977). A study of the differential scheme for composite materials. *International Journal of Engineering Science, 15*, 237–244.

Michel, J. C., & Suquet, P. (2003). Nonuniform transformation field analysis. *International Journal of Solids and Structures, 40*, 6937–6955.

Michel, J. C., Moulinec, H., & Suquet, P. (1999). Effective properties of composite materials with periodic microstructure: a computational approach. *Computer Methods in Applied Mechanics and Engineering, 172*, 109–143.

Michel, J. C., & Suquet, P. (2004). Computational analysis of nonlinear composite structures using the nonuniform transformation field analysis. *Computer Methods in Applied Mechanics and Engineering, 193*, 5477–5502.

Michelitsch, T., & Levin, V. M. (2000). Inclusions and inhomogeneities in electroelastic media with hexagonal symmetry. *European Physical Journal, B14*, 527–533.

Mikata, Y. (2000). Determination of piezoelectric Eshelby tensor in transversely isotropic solids. *International Journal of Engineering Science, 38*, 605–641.

Mikata, Y., & Taya, M. (1986). Thermal stresses in a coated short fiber composite. *Journal of Applied Mechanics, 53*, 681–689.

Milgrom, M., & Shtrikman, S. (1992). The energy of inclusions in linear media: Exact shape independent relations. *Journal of the Mechanics and Physics of Solids, 40*, 927–937.

Miller, M. F., Christian, J. L., & Wennhold, W. F. (1973). *Design, manufacture, development, test and evaluation of boron/aluminum structural components for Space Shuttle.* General Dynamics/Convair Aerospace (Contract No. NAS 8-27738).

Miller, R. E., & Shenoy, V. B. (2000). Size-dependent elastic properties of nanosized structural elements. *Nanotechnology, 11*, 139–147.

Milton, G. W. (1985). The coherent potential approximation is a realizable effective medium scheme. *Communications in Mathematical Physics, 99*, 463–500.

Milton, G. W. (2002). *The theory of composites*. Cambridge: Cambridge University Press.

Moon, H., & Phillips, A. (1977). An experimental investigation concerning yield surfaces and loading surfaces. *Acta Mechanica, 27*, 91–102.

Mori, T., & Tanaka, K. (1973). Average stress in matrix and average elastic energy of materials with misfitting inclusions. *Acta Metallurgica, 21*, 571–574.

Moschovidis, Z. A., & Mura, T. (1975). Two ellipsoidal inhomogeneities by the equivalent inclusion method. *Journal of Applied Mechanics, 42*, 847–852.

Moulinec, H., & Suquet, P. (1994). A fast numerical method for computing the linear and nonlinear mechanical properties of composites. *Comptes Rendus de I'Academie des Sciences Paris, 318*(Ser. II), 1417–1423.

Mulhern, J. F., Rogers, T. G., & Spencer, A. J. M. (1967). A continuum model for fibre-reinforced plastic materials. *Proceedings of the Royal Society London, A, 301*, 473–492.

Mulhern, J. F., Rogers, T. G., & Spencer, A. J. M. (1969). A continuum theory of a plastic-elastic fibre-reinforced material. *International Journal of Engineering Science, 7*, 129–152.

Mura, T. (1987). *Micromechanics of defects in solids* (2nd ed.). Dordrecht: Martinus Nijhoff.

Mura, T. (1988). Inclusion problems. *Applied Mechanics Reviews, 41*, 15–20.

Mura, T., & Kinoshita, N. (1971). Green's functions for anisotropic elasticity. *Physica Status Solidi, 47*, 607–618.

Nairn, J. A. (2006). On the calculation of energy release rates for cracked laminates with residual stress. *International Journal of Fracture, 139*, 267–293.

Needleman, A. (1987). A continuum model for void nucleation by inclusion debonding. *ASME Journal of Applied Mechanics, 54*, 525–531.

Needleman, A. (1990). An analysis of decohesion along an imperfect interface. *International Journal of Fracture, 42*, 21–40.

Nemat-Nasser, S. (1992). Phenomenological theories of elastoplasticity and strain localization at high strain rates. *Applied Mechanics Reviews, 45*, 519–545.

Nemat-Nasser, S. (2004). *Plasticity: A treatise on finite deformation of heterogeneous inelastic materials*. Cambridge: Cambridge University Press.

Nemat-Nasser, S., & Hori, M. (1995). Universal bounds for overall properties of linear and nonlinear heterogeneous solids. *Journal of Engineering Materials and Technology, 117*, 412–432.

Nemat-Nasser, S., & Hori, M. (1999). *Micromechanics: Overall properties of hetero-geneous materials* (2nd ed.). Amsterdam: Elsevier.

Nemat-Nasser, S., Iwakuma, T., & Hejazi, M. (1982). On composites with periodic structure. *Mechanics of Materials, 1*, 239–267.

Nigam, H., Dvorak, G. J., & Bahei-El-Din, Y. A. (1994). An experimental investigation of elastic-plastic behavior of a fibrous boron-aluminum composite: I. Matrix-dominated mode. II. Fiber dominated mode. *International Journal of Plasticity, 10*, 23–62.

Nix, W. D., & Gao, H. (1998). An atomistic interpretation of interface stress. *Scripta Materialia, 39*, 1653–1661.

Noor, A. K., & Burton, W. S. (1989). Assessment of shear deformation theories for multilayer composite plates. *Applied Mechanics Reviews, 42*, 1–13.

Norris, A. N. (1985). A differential scheme for effective moduli of composites. *Mechanics of Materials, 4*, 1–16.

Norris, A. N. (1989). An examination of the Mori-Tanaka effective medium approximation for multiphase composites. *ASME Journal of Applied Mechanics, 56*, 83–88.

Norris, A. N., Callegari, A. J., & Sheng, P. (1985). A generalized differential effective medium theory. *Journal of the Mechanics and Physics of Solids, 33*(6), 525–543.

Nozaki, H., & Taya, M. (1997). Elastic fields in a polygon-shaped inclusion with uniform eigenstrains. *ASME Journal of Applied Mechanics, 64*, 495–502.

Nye, J. F. (1957, 1985). *Physical properties of crystals. Their representation by tensors and matrices.* Oxford: Oxford University Press.

Nygårds, M. (2003). Number of grains necessary to homogenize elastic materials with cubic symmetry. *Mechanics of Materials, 35*, 1049–1053.

Ochoa, O. O., & Reddy, J. N. (1992). *Finite element analysis of composite laminates*. Dordrecht: Kluwer.

Oskay, C., & Fish, J. (2007). Eigendeformation-based reduced order homogenization for failure analysis of heterogeneous materials. *Computer Methods in Applied Mechanics and Engineering, 196*, 1216–1243.

Ostoja-Starzewski, M. (1998). Random field models of heterogeneous materials. *International Journal of Solids and Structures, 35*, 2429–2455.

Ozisik, M. N. (1968). *Boundary value problems of heat conduction*. Scranton: International Textbook Co.

Ozmusul, M. S., & Picu, R. C. (2002). Elastic moduli for particulate composites with graded filler-matrix interfaces. *Polymer Composites, 23*, 110–119.

Ozmusul, M. S., & Picu, R. C. (2003). Structure of linear polymeric chains confined between spherical impenetrable walls. *Journal of Chemical Physics*, *118*, 11239–11248.

Ozmusul, M. S., Picu, R. C., Sternstein, S. S., & Kumar, S. (2005). Lattice Monte Carlo simulations of chain conformations in polymer nanocomposites. *Macromolecules*, *38*, 4495–4500.

Pagano, N. J. (1969). Exact solutions for composite laminates in cylindrical bending. *Journal of Composite Materials, 3*, 398–411.

Pagano, N. J. (1978a). Stress fields in composite laminates. *International Journal of Solids and Structures, 14*, 385–400.

Pagano, N. J. (1978b). Free edge stress fields in composite laminates. *International Journal of Solids and Structures, 14*, 401–406.

Pagano, N. J., & Pipes, R. B. (1970). Interlaminar stresses in composite laminates under uniform axial extension. *Journal of Composite Materials, 4*, 538–548.

Pan, Y. C., & Chou, T. W. (1976). Point force solution for an infinite transversely isotropic solid. *ASME Journal of Applied Mechanics, 43*, 608–612.

Pan, Y. C., & Chou, T. W. (2000). Three-dimensional Green's functions in anisotropic bimaterials. *International Journal Solids and Structures, 37*, 5329–5351.

Panc, V. (1975). *Theories of elastic plates*. Leyden: Noordhoff.

Park, H. S., Klein, P. A., & Wagner, G. J. (2006). A surface Cauchy-Born model for nanoscale materials. *International Journal for Numerical Methods in Engineering, 68*, 1072–1095.

Parker, D. F., & England, A. H. (Eds.). (1995). *Anisotropy, inhomogeneity and nonlinearity is solid mechanics*. Dordrecht: Kluwer Academic.

Paul, B. (1960). Prediction of elastic constants of multiphase materials. *Transactions of the Metallurgy Society of AIME, 218*, 36–41.

Pecullan, S., Gibiansky, L. V., & Torquato, S. (1999). Scale effects on the elastic behavior of periodic and hierarchical two-dimensional composites. *Journal of the Mechanics and Physics of Solids, 47*, 1509–1542.

Percus, J. K., & Yevick, G. J. (1958). Analysis of classical statistical mechanics by means of collective coordinates. *Physical Review, 110*, 1–13.

Phillips, A. (1986). A review of quasistatic experimental plasticity and viscoplasticity. *International Journal of Plasticity, 2*, 315–328.

Phillips, A., & Lee, C. W. (1979). Yield surfaces and loading surfaces: Experiments and recommendations. *International Journal of Solids and Structures, 15*, 715–729.

Phillips, A., & Weng, G. J. (1975). An analytical study of an experimentally verified hardening law. *Journal of Applied Mechanics, 42*, 375–378.

Phillips, A., Liu, C. S., & Justusson, J. W. (1972). An experimental investigation of yield surfaces at elevated temperatures. *Acta Mechanica, 14*, 119–146.

Phillips, A., Ricciuti, M., & Tang, J. L. (1974). Some new observations on yield surfaces. *Acta Mechanica, 20*, 23–39.

Picu, R. C. (2009). Multiscale approach to predicting the mechanical behavior of polymeric melts, Ch. 10. In B. Farahmand (Ed.), *Virtual testing and predictive modeling: Fatigue and fracture allowances*. Springer Science.

Picu, R. C., Sarvestani, A., & Ozmusul, M. S. (2004). Elastic moduli of polymer nanocomposites derived from their molecular structure. In V. M. Harik (Ed.), *Trends in nanoscale mechanics: Analysis of nanostructured materials and multiscale modeling* (pp. 61–88). Dordrecht: Kluwer Academic Press.

Ponte Castaneda, P. (1991). The effective mechanical properties of nonlinear isotropic composites. *Journal of the Mechanics and Physics of Solids, 39*, 45–71.

Ponte Castaneda, P. (1996). A second-order theory for nonlinear composite materials. *Computes Rendus de I'Academie des Sciences Paris, 322*(Série II b), 3–10.

Ponte Castaneda, P., & Suquet, P. (1998). Nonlinear composites. *Advances in Applied Mechanics, 34*, 171–302.

Ponte Castaneda, P., & Willis, J. R. (1995). The effect of spatial distribution on the effective behavior of composite materials and cracked media. *Journal of the Mechanics and Physics of Solids, 43*, 1919–1951.

Postma, G. W. (1955). Wave propagation in a stratified medium. *Geophysics, 20*, 780–806.

Povstenko, Y. Z. (1993). Theoretical investigation of phenomena caused by heterogeneous surface tension in solids. *Journal of the Mechanics and Physics of Solids, 41*, 1499–1514.

Prager, W. (1956). A new method of analyzing stresses and strains in work-hardening plastic solids. *ASME Journal of Applied Mechanics, 23*, 493–496.

Praveen, G. N., & Reddy, J. N. (1998). Transverse matrix cracks in cross-ply laminates: Stress transfer, stiffness reduction and crack opening profiles. *Acta Mechanica*, *130*, 227–248.

Press, W. H., Flannery, B. P., Teukolsky, S. A., & Vetterling, W. T. (1989). *Numerical recipes*. New York: Cambridge University Press.

Prochazka, P. (1997). Slope optimization using transformation field analysis. *Engineering Analysis with Boundary Elements, 20*, 179–184.

Qu, J. (1993). The effect of slightly weakened interface on the overall elastic properties of composite materials. *Mechanics of Materials, 14*, 269–281.

Quintanilla, J., & Torquato, S. (1997). Local volume fraction fluctuations in random media. *The Journal of Chemical Physics, 106*, 2741–2751.

Ramanathan, T., Liu, H., & Brinson, L. C. (2005). Functionalized SWNT polymer nanocomposites for dramatic property improvement. *Journal of Polymer Science: Polymer Physics, 43*, 2269–2279.

Ramanathan, T., Abdala, A. A., Stankovich, S., et al. (2008). Functionalized graphene sheets for polymer nanocomposites. *Nature Nanotechnology, 3*(6), 327–331.

Rayleigh, L. (1873). Some general theorems relating to vibrations. *Proceedings of the London Mathematical Society, 4*, 357–368.

Rayleigh, L. (1877). *Theory of sound*. New York: Dover. 1945.

Reddy, J. N. (1997). *Mechanics of laminated composite plates: Theory and analysis*. New York: CRC Press.

Reissner, E. (1950). On a variational theorem in elasticity. *Journal of Mathematics and Physics, 29*, 90–95.

Reiter, T., & Dvorak, G. J. (1998). Micromechanical models for graded composite materials: II Thermomechanical loading. *Journal of the Mechanics of Physics of Solids, 46*, 1655–1673.

Reiter, T., Dvorak, G. J., & Tvergaard, V. (1997). Micromechanical models for graded composite materials. *Journal of the Mechanics and Physics of Solids, 45*, 1281–1302.

Ren, Z.-Y., & Zheng, Q.-S. (2002). A quantitative study on minimum sizes of representative volume elements of cubic polycrystals-numerical experiments. *Journal of the Mechanics and Physics of Solids, 50*, 881–893.

Ren, Z.-Y., & Zheng, Q.-S. (2004). Effects of grain sizes, shapes, and distribution on minimum sizes of representative volume elements of cubic polycrystals. *Mechanics of Materials, 36*, 1217–1229.

Reuss, A. (1929). Berechnung der Fliessgrenze von Mischkristallen auf Grund der Plastizitätsbedingung für Einkristalle. *Zeitschrift für Angewandte Mathematik und Mechanik, 9*, 49–58.

Rice, J. R. (1970). On the structure of stress-strain relations for time-dependent plastic deformation of metals. *ASME Journal of Applied Mechanics, 37*, 728–737.

Rice, J. R., & Cleary, M. P. (1976). Some basic stress-diffusion solutions for fluid-saturated elastic porous media with compressible constituents. *Reviews of Geophysics and Space Physics, 14*, 227–241.

Roach, G. F. (1982). *Green's functions*. New York: Cambridge University Press.

Rodin, G. (1996). Eshelby's inclusion problem for polygons and polyhedral. *Journal of the Mechanics and Physics of Solids, 44*, 1977–1995.

Roscoe, R. (1952). The viscosity of suspensions of rigid spheres. *British Journal of Applied Physics, 3*, 267–269.
Rose, C. A., & Herakovich, C. T. (1993). An approximate solution for interlaminar stresses in composite laminates. *Composites Engineering, 3*, 271–285.
Rose, J. H., Ferrante, J., & Smith, J. R. (1981). Universal binding energy curves for metals and bimetallic interfaces. *Physical Review Letters, 47*, 675–678.
Rosen, B. W., & Hashin, Z. (1970). Effective thermal expansion coefficients and specific heats of composite materials. *International Journal of Engineering Science, 8*, 157–173.
Russel, W. B. (1973). On the effective moduli of composite materials: Effect of fiber length and geometry at dilute concentrations. *Zeitschrift für Angewandte Mathematik und Physik, 24*, 581.
Sacco, E. (2009). A nonlinear homogenization procedure for periodic masonry. *European Journal of Mechanics A/Solids, 28*, 2090–2222.
Sanchez-Palencia, E. (1980). *Homogenization techniques and vibration theory*. Lecture Notes in Physics No. 127. Berlin: Springer.
Sarva, S., Nemat-Nasser, S., McGee, J., & Isaacs, J. (2007). The effect of thin membrane restraint on the ballistic performance of armor grade ceramic tiles. *Intlernational Journal of Impact Engineering*, *34*, 277–302.
Sasaki, M., & Hirai, T. (1991). Fabrication and properties of functionally gradient materials. *Journal of the Ceramic Society of Japan, 99*, 1002–1013.
Sayers, C. M. (1992). Elastic anisotropy of short-fibre reinforced composites. *Journal of the Mechanics and Physics of Solids, 29*, 2933–2944.
Schapery, R. A. (1968). Thermal expansion coefficients of composite materials based on energy pinciples. *Journal of Composite Materials, 2*, 380–404.
Schapery, R. A. (1997). Nonlinear viscoelastic and viscoplastic constitutive equations based on thermodynamics. *Mechanics of Time-Dependent Materials, 1*, 209–240.
Schulgasser, K. (1987). Thermal expansion of polycrystalline aggregates with texture. *Journal of the Mechanics and Physics of Solids, 35*, 35–42.
Shah, R. S. (1991). *Modeling and analysis of high temperature inelastic deformation in metal matrix composites.* Ph.D. dissertation, Rensselaer Polytechnic Institute.
Sharma, P., & Ganti, S. (2004). Size-dependent Eshelby's tensor for embedded nano-inclusions incorporating surface/interface energies. *ASME Journal of Applied Mechanics, 71*, 663–671.
Sharma, P., Ganti, S., & Bhate, N. (2003). Effect of surfaces on the size-dependent elastic state of nano-inhomogeneities. *Applied Physics Letters, 82*, 535–537.
Shield, R. T., & Ziegler, H. (1958). On Prager's hardening rule. *Zeitschrift für Angewandte Mathematik und Physik, 9*, 260–276.
Shim, H. W., Zhou, L. G., Huang, H., & Cale, T. S. (2005). Nanoplate elasticity under surface reconstruction. *Applied Physics Letters, 86*(151912), 1–3.
Sigmund, O., & Torquato, S. (1999). Design of smart composite materials using topology optimization. *Smart Materials and Structures, 8*, 365–379.
Simo, J. C., & Hughes, J. T. R. (1998). *Computational inelasticity*. New York: Springer.
Sirotin, Y. I., & Shakol'skaya, M. P. (1982). *Fundamentals of crystal physics*. Moscow: MIR Publishers.
Smith, G. F., & Rivlin, R. (1958). The strain-energy function for anisotropic elastic materials. *Transactions of the American Mathematical Society, 88*, 175–193.
Smith, G. E., & Spencer, A. J. M. (1970). A continuum theory of a plastic-rigid solid reinforced by two families of inextensible fibres. *Quarterly Journal of Mechanics and Applied Mathematics, 23*, 489–504.
Sneddon, N. I. (1974). *The linear theory of thermoelasticity*. Berlin/Heidelberg/New York: Springer.
Sokolnikoff, I. S. (1956). *Mathematical theory of elasticity*. New York: Mc Graw-Hill Book Co.
Spaepen, F. (2000). Interfaces and stresses in thin films. *Acta Materialia 48*, 31–42.
Spencer, A. J. M. (1972). *Deformation of fibre-reinforced materials*. London: Oxford University Press.
Spencer, A. J. M. (1980). *Continuum mechanics*. London/New York: Longman.

Spencer, A. J. M. (1987). Kinematic constraints, constitutive equations and failure rules for anisotropic materials. In J. P. Boehler (Ed.), Chapter 10 of *Applications of tensor functions in continuum mechanics, CISM Courses and Lectures* (No. 292, pp. 187–201). Wien: Springer.

Spencer, A. J. M. (1992). Plasticity theory for fibre-reinforced composites. *Journal of Engineering Mathematics, 26*, 107–118.

Srinivas, M. V., Dvorak, G. J., & Prochazka, P. (1999). Design and fabrication of submerged cylindrical laminates-II: Effect of fiber prestress. *International Journal of Solids and Structures*, *36*, 3945–3976.

Srinivasan, T. P., & Nigam, S. D. (1969). Invariant elastic constants for crystals. *Journal of Mathematics and Mechanics, 19*, 411–420.

Sternberg, E. (1958). Three-dimensional stress concentrations in the theory of elasticity. *Applied Mechanics Reviews, 11*, 1–4.

Stroh, A. N. (1958). Dislocations and cracks in anisotropic elasticity. *Philosophical Magazine, 3*, 625–646.

Sun, C. T., & Li, S. (1988). Three-dimensional effective elastic constants for thick laminates. *Journal of Composite Materials, 22*, 629–639.

Suquet, P. (1987). Elements of homogenization for inelastic solid mechanics. In E. Sanchez-Palencia & A. Zaoui (Eds.), *Homogenization techniques for composite media*. New York: Springer.

Suquet, P. (1997). Effective properties of nonlinear composites. In P. Suquet (Ed.), *Continuum micromechanics* (Vol. 337 of CISM Lecture Notes, pp. 197–264). New York: Springer.

Suvorov, A. P., & Dvorak, G. J. (2001a). Optimized fiber prestress for reduction of free edge stresses in composite laminates. *International Journal of Solids and Structures, 38*, 6751–6786.

Suvorov, A. P., & Dvorak, G. J. (2001b). Optimal design of prestressed laminate/ceramic plate assemblies, *Meccanica 36*, 87–109. (Special issue for the 70th birthday of Professor Giulio Maier).

Suvorov, A. P., & Dvorak, G. J. (2002a). Rate form of the Eshelby and Hill tensors. *International Journal of Solids and Structures, 39*, 5659–5678.

Suvorov, A. P., & Dvorak, G. J. (2002b). Stress relaxation in prestressed composite laminates. *ASME Journal of Applied Mechanics, 69*, 459–469.

Suvorov, A. S., & Selvadurai, A. P. S. (2010). Macroscopic constitutive equations of thermo-poroviscoelasticity derived using eigenstrains. *Journal of the Mechanics and Physics of Solids, 58*, 1461–1473.

Synge, J. L. (1957). *The hypercircle in mathematical physics*. New York: Cambridge University Press.

Takao, Y., & Taya, M. (1985). Thermal expansion coefficients and thermal stresses in a n aligned short fiber composite with application to a short carbon fiber/aluminum. *Journal of Applied Mechanics, 52*, 806–810.

Talbot, D. R. S., & Willis, J. R. (1985). Variational principles for inhomogeneous nonlinear media. *Journal of Applied Mathematics, 35*, 39–54.

Talbot, D. R. S., & Willis, J. R. (1992). Some simple explicit bounds for the overall behaviour of nonlinear composites. *International Journal of Solids and Structures, 29*, 1981–1987.

Talbot, D. R. S., & Willis, J. R. (1997). Bounds of third order for the overall response of nonlinear composites. *Journal of the Mechanics and Physics of Solids, 45*, 87–111.

Tanaka, K., & Mori, M. (1972). Note on volume integrals of the elastic field around an ellipsoidal inclusion. *Journal of Elasticity, 2*, 199–200.

Tanaka, K., & Mura, T. (1982). A theory of fatigue crack initiation at inclusions. *Metallurgical Transactions, 13A*, 117–123.

Tanaka, K., Tanaka, Y., Enomoto, K., Poterasu, V. F., & Sugano, Y. (1993a). Design of thermoelastic materials using direct sensitivity and optimization methods: Reduction of thermal stresses in functionally gradient materials. *Computer Methods in Applied Mechanics and Engineering, 106*, 271–284.

Tanaka, K., Tanaka, Y., Watanabe, H., Poterasu, V. F., & Sugano, Y. (1993b). An improved solution to thermoelastic material design infunctionally gradient materials: Scheme to reduce thermal stresses. *Computer Methods in Applied Mechanics and Engineering, 109*, 377–389.

Tarn, J. Q., Dvorak, G, J., & Rao, M.S.M. (1975). Shakedown of unidirectional composites. *International Journal of Solids and Structures, 6*, 751–764.

Teply, J. L., & Dvorak, G. J. (1987). Dual estimates of instantaneous properties of elastic-plastic composites. In A. J. M. Spencer (Ed.), *Continuum models of discrete systems* (pp. 205–2l6). Rotterdam: A. A. Balkema Press.

Teply, J. L., & Dvorak, G. J. (1988). Bounds on overall instantaneous properties of elastic-plastic composites. *Journal of the Mechanics and Physics of Solids, 36*, 29–58.

Teply, J. L., & Reddy, J. N. (1990). A unified formulation of micromechanics models of fiber-reinforced composites. In G. J. Dvorak (Ed.), *Inelastic deformation of composite materials* (pp. 341–372). New York: Springer.

Teply, J. L., Reddy, J. N., & Brockenbrough, J. R. (1992). A unified formulation of micromechanics models of fiber-reinforced composites. In J. N. Reddy & A. V. Krishna Murty (Eds.), *Composite structures* (pp. 294–325). New Delhi: Narosa Publication House.

Ting, T. C. T. (1987). Invariants of anisotropic elastic constants. *Quarterly Journal of Mechanics and Applied Mathematics, 40*, 431–438.

Ting, T. C. T. (1996). *Anisotropic elasticity: Theory and applications*. Oxford: Oxford University Press.

Ting, T. C. T. (2000). Recent developments in anisotropic elasticity. *International Journal of Solids and Structures, 37*, 401–409.

Ting, T. C. T. (2003). Generalization of Cowin-Mehrabadi theorems and direct proof that the number of linear elastic symmetries is eight. *International Journal of Solids and Structures, 40*, 7129–7142.

Ting, T. C. T. (2004). Very large Poisson's ratio with a bounded transverse strain in anisotropic elastic materials. *Journal of Elasticity, 77*, 163–176.

Ting, T. C. T. (2005a). The stationary values of Young's modulus for monoclinic and triclinic materials. *Journal of Mechanics, 21*, 249–253.

Ting, T. C. T. (2005b). Explicit expression of the stationary values of Young's modulus and the shear modulus for anistropic elastic materials. *Journal of Mechanics, 21*, 255–266.

Ting, T. C. T., & Barnett, D. M. (2005). Negative Poisson's ratios in anisotropic linear elastic media. *ASME Journal of Applied Mechanics, 72*, 929–931.

Ting, T. C. T., & Chen, T. (2005). Poisson's ratio for anisotropic elastic materials can have no bounds. *Quarterly Journal of Mechanics and Applied Mathematics, 58*, 73–82.

Ting, T. C. T., & He, Q. C. (2006). Decomposition of elasticity tensors and tensors that are structurally invariant in three dimensions. *Quarterly Journal of Mechanics and Applied Mathematics, 59*, 323–341.

Ting, T. C. T., & Lee, V. G. (1997). The three-dimensional elastostatic Green's function for general anisotropic linear elastic solids. *Quarterly Journal of Mechanics and Applied Mathematics, 50*, 407–426.

Tobochnik, J., & Chapin, P. M. (1988). Monte Carlo simulation of hard spheres near random closest packing using spherical boundary conditions. *The Journal of Chemical Physics, 88*, 5824–5830.

Torquato, S. (1997). Effective stiffness tensor of composite media-I. Exact series expansion. *Journal of the Mechanics and Physics of Solids, 45*, 1421–1448.

Torquato, S. (2002). *Random heterogeneous materials: Microstructure and macroscopic properties*. New York: Springer.

Torquato, S., & Stell, G. (1985). Microstructure of two-phase random media: V. The n-point matrix probability functions for impenetrable spheres. *The Journal of Chemical Physics, 82*, 980–987.

Tsai, S. W., & Wu, E. M. (1971). A general theory of strength for anisotropic materials. *Journal of Composite Materials, 5*, 58–80.

Turley, J., & Sines, G. (1971). The anisotropy of Young's modulus, shear modulus and Poisson's ratio in cubic materials. *Journal of Physics, 4*, 264–271.

Tvergaard, V. (1991). Micromechanical modeling of fiber debonding in a metal reinforced by short fibers. In G. J. Dvorak (Ed.), *Inelastic deformation of composite materials* (pp. 99–111). New York: Springer.

Tvergaard, V., (2003). Debonding of short fibers among particulates in metal matrix composites. *International Journal of Solids and Structures, 40*, 6957–6967.

Vel, S. S, & Batra, R.C. (1999). Analytical solutions for rectangular thick laminated plates subjected to arbitrary boundary conditions, *AIAA Jnl.*, *37*, 1464–1473.

Vel, S. S., & Batra, R.C. (2000a). The generalized plane strain deformations of thick anisotropic composite laminated plates. *International Journal of Solids and Structures, 37*, 715–733.

Vel, S. S., & Batra, R.C. (2000b). Three-dimensional analytical solutions for hybrid multilayered piezoelectric plates, *ASME Journal of Applied Mechanics, 67* , 558–567.

Vel, S. S., & Batra, R.C. (2001a). Closure to the generalized plane strain deformations of thick anisotropic composite laminated plates, *International Journal of Solids and Structures, 38*, 483–489.

Vel, S. S., & Batra, R.C. (2001b). Generalized plane strain thermoelastic deformation of laminated anisotropic thick plates, *International Journal of Solids and Structures, 38*, 1395–1414.

Vel, S. S, Mewer, R., & Batra, R. C. (2004). Analytical solution for the cylindrical bending vibration of piezoelectric composite plates, *International Journal of Solids and Structures, 41*, 1625–1643.

Verlet, L. (1972). Perturbation theory for the thermodynamic properties of simple liquids. *Molecular Physics, 24*, 1013–1024.

Visscher, W. M., & Bolstrelli, M. (1972). Random packing of equal and unequal spheres in two and three dimensions. *Nature, 239*, 504–507.

Voigt, W. (1889). Űber die Berechnung zwischen den beiden Elastizitätsconstanten isotroper Körper. *Wiedemanns Annalen der Physik und Chemie, 38*, 573–578.

Voigt, W. (1910). *Lehrbuch der Kristallphysik*. Leipzig: B. G. Teubner.

von Mises, R. (1928). Mechanik der plasticschen Formanderung in Kristallen. *Zeitschrift für Angewandte Mathematik und Mechanik, 8*, 161–185.

Walker, K. P. (1993). Fourier integral representation of the Green function for anisotropic elastic half-space. *Proceedings of the Royal Society London*, *A433*, 367–389.

Walpole, L. J. (1966). On bounds for the overall elastic moduli of inhomogeneous systems I. *Journal of the Mechanics and Physics of Solids, 14*, 151–162. 1966b II. *ibid., 14*, 289–301.

Walpole, L. J. (1969). On the overall elastic moduli of composite materials. *Journal of the Mechanics and Physics of Solids, 17*, 235–251.

Walpole, L. J. (1977). The determination of the elastic field of an ellipsoidal inclusion in an anisotropic medium. *Mathematical Proceedings of the Cambridge Philosophical Society, 81*, 283–289.

Walpole, L. J. (1980). Evaluation of overall reaction of a composite solid with inclusions of any shape. *Continuum models of discrete systems*. Waterloo: University of Waterloo Press.

Walpole, L. J. (1981). Elastic behavior of composite materials: Theoretical foundations. In *Advances in applied mechanics* (Vol. 21, pp. 169–242). New York: Academic.

Walpole, L. J. (1984). Fourth-rank tensors of the thirty-two crystal classes; multiplication tables. *Proceedings of the Royal Society London, A391*, 149–179.

Walpole, L. J. (1985a). The stress-strain law of a textured aggregate of cubic crystals. *Journal of the Mechanics and Physics of Solids, 33*, 363–370.

Walpole, L. J. (1985b). Evaluation of the elastic moduli of a transversely isotropic aggregate of cubic crystals. *Journal of the Mechanics and Physics of Solids, 33*(6), 623–636.

Walpole, L. J. (1985c). The analysis of the overall elastic properties of composite materials. In B. A. Bilby, K. J. Miller, & J. R. Willis (Eds.), *Fundamentals of deformation and fracture: Eshelby memorial symposium* (pp. 91–107). Cambridge: Cambridge University Press.

Walpole, L. J. (1986). The elastic shear moduli of a cubic crystal. *Journal of Physics, 19*, 457–462.

Walpole, L. J. (1987). Orthotropically textured elastic aggregates of cubic crystals. *Journal of the Mechanics and Physics of Solids, 35*, 497–517.

Walsh, J. B. (1965). The effect of cracks on the compressibility of rock. *Journal of Geophysical Research, 70*, 381.

Wang, A. D. S. (1984). Fracture mechanics of sublaminate cracks in composite materials. *Composite Technology Review, 6*, 45.

Wang, S. S., & Choi, I. (1982). Boundary-layer effects in composite laminates: Part I – Free-edge stress singularities. *ASME Journal of Applied Mechanics, 49*, 541–548.

Watcharotone, S., Wood, C. D., Friedrich, R., Chen, X., Qiao, R., Putz, K. W., & Brinson, L. C. (2011). Revealing the effects of interphase, interface and substrate on mechanical properties of polymers using coupled experiments and modeling of nanoindentation. *Advanced Engineering Materials, 13*, 400–404.

Weng, G. J. (1984). Some elastic properties of reinforced solids, with special reference to isotropic ones containing spherical inclusions. *International Journal of Engineering Science, 22*, 845–856.

Weng, G. J. (1990). The theoretical connection between Mori-Tanaka's theory and the Hashin-Shtrikman-Walpole bounds. *International Journal of Engineering Science, 28*, 1111–1120.

Weng, G. J. (1992). Explicit evaluation of Willis' bounds with ellipsoidal inclusions. *International Journal of Engineering Science, 30*, 83–92.

Wertheim, M. S. (1963). Exact solution of the Percus-Yevick integral equation for hard spheres. *Physical Review Letters, 10*, 321–323.

Whitney, J. M. (1987). *Structural analysis of laminated anisotropic plates*. Lancaster: Technomic Publications Co.

Williamson, R. L., Rabin, B. H., & Drake, J. T. (1993). Finite element analysis of thermal residual stresses at graded ceramic-metal interfaces. Part 1. Model description and geometrical effects. *Journal of Applied Physics, 74*, 1311–1320.

Willis, J. R. (1964). Anisotropic elastic inclusion problems. *Quarterly Journal of Mechanics and Applied Mathematics, 17*, 157–174.

Willis, J. R. (1965). The elastic interaction energy of dislocation loops in anisotropic media. *Quarterly Journal of Mechanics and Applied Mathematics, 18*, 419–433.

Willis, J. R. (1970). Stress fields produced by dislocations in anisotropic media. *Philosophical Magazine, 21*, 931–949.

Willis, J.R. (1975). The interaction of gas bubbles in an anisotropic elastic solid. *Journal of the Mechanics and Physics of Solid, 23*, 129–138.

Willis, J. R. (1977). Bounds and self-consistent estimates for the overall moduli of anisotropic composites. *Journal of the Mechanics and Physics of Solids, 25*, 185–202.

Willis, J. R. (1978). In J. W. Provan (Ed.), *Continuum models of discrete systems* (pp. 185–215). Waterloo: University of Waterloo Press.

Willis, J. R. (1980). A polarization approach to the scattering of elastic waves – I. Scattering by a single inclusion. II. Multiple scattering from inclusions. *Journal of the Mechanics and Physics of Solids, 28*, 287–327.

Willis, J. R. (1981). Variational and related method for the overall properties of composites. In *Advances in applied mechanics* (Vol. 21, pp. 1–78). Academic Press.

Willis, J. R. (1991). On methods for bounding the overall properties of nonlinear composites. *Journal of the Mechanics and Physics of Solids, 39*, 73–86. Errata *ibid. 40*, (1992) 441–445.

Withers, P. J. (1989). The determination of the elastic field of an ellipsoidal inclusion in a transversely isotropic medium, and its relevance to composite materials. *Philosophical Magazine, 59*, 759–781.

Wu, J. F., Shephard, M. S., Dvorak, G. J., & Bahei-El-Din, Y. A. (1989). A material Model for the finite element analysis of metal matrix composites. *Composites Science and Technology, 35*, 347–366.

Wu, T. T. (1966). The effect of inclusion shape on the elastic moduli of a two-phase material. *International Journal of Solids and Structures, 2*, 1–8.

Yang, F. Q. (2004). Size-dependent effective modulus of elastic composite materials: Spherical nanocavities at dilute concentrations. *Journal of Applied Physics, 95*, 3516–3520.

Ye, L. (1990). Some characteristics of distributions of free-edge interlaminar stresses in composite laminates. *International Journal of Solids and Structures, 26*, 331–351.

Yin, W. L. (1994a). Free-edge effects in anisotropic laminates under extension, bending and twisting, Part I: A stress-function-based variational approach. *Journal of Applied Mechanics, 61*, 410–415.

Yin, W. L. (1994b). Free-edge effects in anisotropic laminates under extension, bending and twisting, Part II: Eigenfunction analysis and the results for symmetric laminates. *Journal of Applied Mechanics, 61*, 416–421.

Zaoui, A., & Masson, R. (1998). Modelling stress-dependent transformation strains of heterogeneous materials. In Y. A. Bahei-El-Din & G. J. Dvorak (Eds.), *IUTAM symposium on transformation problems in composite and active materials* (pp. 3–16). Dordrecht: Kluwer Academic.

Zaverl, J. R., & Lee, D. (1978). Constitutive relations for nuclear reactor core materials. *Journal of Nuclear Materials, 75*, 14.

Zener, C. (1948). *Elasticity and anelasticity of metals*. Chicago: University of Chicago Press.

Zhang, D., Ye, J., & Lam, D. (2007). Properties degradation induced by transverse cracks in general symmetric laminates. *International Journal of Solids and Structures, 44*, 5499–5517.

Zhao, Y. H., Tandon, G. P., & Weng, G. J. (1989). Elastic moduli for a class of porous materials. *Acta Mechanica, 76*, 105–130.

Zheng, Q. S., & Chen, T. (2001). New perspective on Poisson's ratios of elastic solids. *Acta Mechanica, 150*, 191–195.

Zhou, L. G., & Huang, H. (2004). Are surfaces elastically softer or stiffer? *Applied Physics Letters, 84*, 1940–1942.

Ziegler, H. (1959). A modification of Prager's hardening rule. *Quarterly of Applied Mathematics, 17*, 55–65.

Zohdi, T. I., & Wriggers, P. (2005). *An introduction to computational micromechanics*. Berlin: Springer.

Zohdi, T. I., Oden, J. T., & Rodin, G. J. (1996). Hierarchical modeling of heterogeneous bodies. *Computer Merthods in Applied Mechanics and Engineering, 138*, 273–298.

Zuiker, J. R., & Dvorak, G. J. (1994). The effective properties of functionally graded composites-I. Extension of the Mori-Tanaka method to linearly varying fields. *Composites Engineering, 4*, 19–35.

Index

G.J. Dvorak, *Micromechanics of Composite Materials*, Solid Mechanics and Its Applications 186, DOI 10.1007/978-94-007-4101-0,